

ELECTRODIALYSIS OF SALTS, ACIDS AND BASES

Jakob Johannes Schoeman

A thesis submitted in partial fulfilment of the prerequisites for the degree of Doctor of Philosophy in the Faculty of Science, University of Pretoria, Pretoria.

(March 1992)

ELECTRODIALYSIS OF SALTS, ACIDS AND BASES BY ELECTRO-OSMOTIC PUMPING

Jakob Johannes Schoeman

Promoter: Professor Jacobus F van Staden

Department of Chemistry, University of Pretoria

Degree: Doctor of Philosophy

SYNOPSIS

Salts, acids and bases frequently occur in industrial effluents and usually have considerable pollution potential. Preliminary work has indicated that electro-osmotic pumping electro dialysis (EOP-ED) has the potential to recover chemicals and water for reuse and to reduce effluent volumes significantly. However, with respect to this technology, the following needs were identified:

- a) consider and fully document the relevant EOP-ED and ED theory;
- b) study the EOP-ED characteristics (transport numbers, brine concentration, current efficiency, current density, electro-osmotic coefficients, etc.) of commercially available and other membranes in a single cell pair (cp) with the aim of identifying membranes suitable for EOP-ED;
- c) evaluate a simple method and existing models with which membrane performance for concentration by EOP-ED can be predicted and described;
- d) evaluate EOP-ED for industrial effluent treatment in a conventional ED and in a sealed-cell ED (SCED) membrane stack.

A conventional ED membrane stack which was converted into an EOP-ED stack performed satisfactorily for concentration/desalination of sodium chloride, hydrochloric acid and caustic soda solutions. Dialysate concentrations of less than 500 mg/l could be obtained in the feed water and cell pair voltage ranges from 1 000 to 10 000 mg/l and 0,5 to 4,0 V/cp. Small brine volumes were obtained. Brine volume varied between 1,5 and 4,0%; 2,4 and 7,8%; and between 2,3 and 7,3% in the case of sodium chloride, hydrochloric acid and caustic soda solutions (1 000 to 5 000 mg/l feed). Current efficiency was high. Current efficiency varied between 75,2 and 93,6%; 29,2 and 46,3%; and between 68,9 and 81,2% when sodium chloride, hydrochloric acid and caustic soda solutions were electro dialyzed, respectively. Low electrical energy consumptions were obtained. Electrical energy consumption was less than 2,5 kWh/m³ product for sodium chloride solutions in the 1 000 to

3 000 mg/ℓ feed concentration range; between 0,2 and 3,2 kWh/m³ product at 1 000 mg/ℓ hydrochloric acid feed concentration; and between 0,4 and 2,2 kWh/m³ product for caustic soda in the 1 000 to 3 000 mg/ℓ feed concentration range. Water yield increased with increasing cell pair voltage and increasing linear flow velocity through the stack and decreased with decreasing feed water concentration. It would be advantageous to operate an EOP-ED stack at the highest possible linear flow velocity.

Sealed-cell ED should be very effectively applied for concentration/desalination of relatively dilute (500 to 3 000 mg/ℓ TDS) non-scale-forming salt solutions. Product water with a TDS of less than 300 mg/ℓ could be produced in the feed water concentration range from 500 to 10 000 mg/ℓ TDS. Electrical energy consumption of 0,27 to 5,9 kWh/m³ product was obtained (500 to 3 000 mg/ℓ feed water concentration range). Brine volume comprised approximately 2% of the initial feed water volume. Therefore, brine disposal cost should be reduced significantly with this technology. Sealed-cell ED became less efficient in the 5 000 to 10 000 mg/ℓ TDS feed water concentration range due to high electrical energy consumption (3,3 to 13,0 kWh/m³ product). However, SCED may be applied in this TDS range depending on the value of the product that can be recovered.

A relatively concentrated ammonium nitrate effluent (TDS 3 600 mg/ℓ) could be successfully treated with SCED. Brine volume comprised only 2,8% of the treated water volume. Electrical energy consumption was determined at 2,7 kWh/m³ product. It should be possible to reuse the brine and the treated water in the process. Membrane fouling, however, may affect the process adversely and this matter needs further investigation. Treatment of scale forming waters will affect the process adversely because scale will precipitate in the membrane bags, which cannot be opened for cleaning. Membrane scaling may be removed by current reversal or with cleaning solutions. However, this matter needs further investigation. Scale forming waters, however, should be avoided or treated with ion-exchange or nanofiltration prior to SCED treatment.

Sealed-cell ED has potential for treatment of relatively dilute (< 3 000 mg/ℓ TDS) non-scaling waters for chemical and water recovery for reuse. However, high TDS waters (up to approximately 16 000 mg/ℓ) may also be worth treating, depending on the value of the product that can be recovered. The successful application of SCED technology seems to depend on the need to apply this technology in preference to conventional ED for specific applications where high brine concentrations and small brine volumes are required. Capital cost of SCED equipment should be less than that of conventional ED due to the simpler design of the SCED stack. The membrane utilization factor of 95% is much higher than in conventional ED (approximately 80%).

Electro-osmotic pumping studies in a single cell pair have shown the following:

Brine concentration increased with increasing current density and increasing feed water concentration and levels off at high current density dependent on the electro-osmotic coefficients of the membranes. Current efficiency was nearly constant in a wide range of current densities and feed water concentrations in the case of the *Selemion* (salt and acid concentration) and *Raipore* membranes (salt concentration). However, all the other membranes showed a slight decrease in current efficiency indicating that the limiting current density was exceeded. Water flow through the membranes (salt and base concentration) increased with increasing current density and increasing feed water concentration. Increasing water flow increased current efficiency significantly, especially in the case of the more porous heterogeneous membranes. It will therefore not be necessary for membranes to have very high permselectivities ($> 0,9$) for use in EOP-ED because efficiency will be increased by water flow through the membranes. Consequently, water flow through ED membranes also has a positive effect in ED and this effect is often neglected. The electro-osmotic coefficients decreased with increasing feed water concentration until a constant value was obtained at high current density. Osmotic flow in EOP-ED decreased relative to the total flow with increasing current density while the electro-osmotic flow increased relative to the osmotic flow. Osmotic flow contributes significantly to the total water flow in EOP-ED. Membrane permselectivity decreased with increasing brine and feed concentration and increasing concentration gradient across the membranes.

Selemion AMV and CMV and *Ionac* membranes; *Selemion* AAV and CHV and the newly developed Israeli ABM membranes; and *Selemion* AMV and CMV, *Selemion* AMP and CMV and *Ionac* membranes performed well for salt, acid and base concentration, respectively. Current efficiencies varied between 62 and 91% (*Selemion* AMV and CMV); 34 and 60% (ABM-3 and *Selemion* CHV); and between 47 and 76% (*Selemion* AMV and CMV) for salt, acid and base concentration, respectively, in the feed water concentration range from 0,05 to 1,0 mol/l.

A simple membrane potential measurement has been demonstrated to function satisfactory to predict membrane performance for salt, acid and base concentration. Membrane performance could be predicted with an accuracy of 10; 20 and 20% and better for salt, acid and base concentration, respectively. Brine concentration could be predicted satisfactorily from apparent transport numbers and water flows. Maximum brine concentration, c_b^{\max} , could be predicted satisfactorily from two simple models.

The correct Onsager relationships to be used for potential measurements and for the transport number are at zero current and zero volume flow, and at zero concentration gradient and zero volume flow, respectively. In practical ED, measurements are conducted at zero pressure and in the presence of concentration gradients and volume flows. These factors will influence the results considerably in all systems in which volume flow is important and where the concentration factor is high as encountered

in EOP-ED. In measurement of membrane potential, the volume flow is against the concentration potential and in general will decrease potential. In ED water flow helps to increase current efficiency, but the concentration gradient is against current efficiency.

Models describe the system satisfactorily for concentration of salt, acid and base solutions. Brine concentration approached a limiting value (plateau) at high current density dependent on the electro-osmotic coefficients of the membranes. A constant slope (electro-osmotic coefficient) was obtained when water flow was plotted against current density. Straight lines were obtained when cell pair resistance was plotted against the specific resistance of the dialysate. Current efficiency increased with increasing flow of water through the membranes, decreased when the concentration gradient was high and the apparent transport numbers were low.

ELEKTRODIALISE VAN SOUTE, SURE EN BASISSE DEUR MIDDEL VAN ELEKTRO-OSMOTIESE POMPING

deur

Jakob Johannes Schoeman

Promoter: Professor Jacobus F van Staden

Departement Chemie, Universiteit van Pretoria

Graad: Philosophia Doctor

SAMEVATTING

Soute, sure en basisse kom dikwels in industriële uitvloeiels voor en het gewoonlik 'n aansienlike besoedelingspotensiaal. Voorlopige werk het aangedui dat elektro-osmotiese pomping elektrodialise (EOP-ED) die potensiaal het om chemikalieë en water vir hergebruik te herwin en om uitvloeielsvolumes betekenisvol te verminder. Daar is egter geïdentifiseer dat behoeftes bestaan om:

- a) EOP-ED- en ED-teorie deeglik in oënskou te neem en om die relevante teorie ten volle te dokumenteer;
- b) EOP-ED eienskappe (transportgetalle, loogkonsentrasie, stroomdoeltreffendheid, stroomdigtheid, elektro-osmotiese koëffisiënte, ens.) van kommersieël beskikbare en ander membrane in 'n enkelselpaar (sp) te bestudeer met die doel om membrane wat vir EOP-ED geskik is, te identifiseer;
- c) 'n eenvoudige metode en bestaande modelle te evalueer waarmee membraanwerkverrigting vir konsentrasie met EOP-ED voorspel en beskryf kan word;
- d) EOP-ED vir industriële uitvloeielsbehandeling in 'n konvensionele ED en in 'n geseëlde ED (GSED) membraanpak te evalueer.

'n Konvensionele ED-membraanpak wat na 'n EOP-ED membraanpak omgeskakel is, het bevredigende werkverrigting vir die konsentring/ontsouting van natriumchloried-, soutsuur- en bytsodaoplossings gelewer. Produkwaterkonsentrasies van minder as 500 mg/ℓ kon in die toevoerwater- en selpaarspanninggebiede van 1 000 tot 10 000 mg/ℓ en 0,5 tot 4,0 V/sp verkry word. Klein loogvolumes is verkry. Loogvolumes het tussen 1,5 en 4,0%; 2,4 en 7,8%; en 2,3 en 7,3% in die geval van natriumchloried-, soutsuur- en bytsodaoplossings, gewissel. Stroomdoeltreffendhede was hoog. Stroomdoeltreffendhede het tussen 75,2 en 93,6%; 28,2 en 46,3%; en tussen 68,9 en 81,2% gewissel toe natriumchloried-, soutsuur- en bytsodaoplossings respektiewelik, geëlektrodialiseer

is. Lae elektriese energieverbruik is verkry. Elektriese energieverbruik was minder as $2,5 \text{ kWh/m}^3$ produk vir natriumchloriedoplossings in die 1 000 tot 3 000 mg/l toevoerwaterkonsentrasiegebied; tussen 0,2 en $3,2 \text{ kWh/m}^3$ produk vir soutuur by 1 000 mg/l toevoerkonsentrasie; en tussen 0,4 en $2,2 \text{ kWh/m}^3$ produk vir bytsodaoplossings in die 1 000 tot 3 000 mg/l toevoerwaterkonsentrasiegebied. Wateropbrengs het met toenemende selpaarspanning en toenemende liniêre vloeisnelheid deur die membraanpak toegeneem en met afnemende toevoerkonsentrasie afgeneem. Dit sal dus voordelig wees om 'n EOP-ED membraanpak by die hoogste moontlike liniêre vloeisnelheid te bedryf.

Geseëldeselektrodialise behoort effektief vir die konsentrering/ontsouting van relatief verdunde (500 tot 3 000 mg/l TOVS) nie-skaalvormende soutoplossings toegepas te kan word. Produkwater met 'n TOVS inhoud van minder as 300 mg/l kan geproduseer word in die toevoerwaterkonsentrasiegebied van 500 tot 10 000 mg/l TOVS. Elektriese energieverbruik van 0,29 tot $5,9 \text{ kWh/m}^3$ produkwater is verkry (500 tot 3 000 mg/l toevoerwaterkonsentrasiegebied). Loogvolume het ongeveer 2% van die aanvanklike toevoervolume beslaan. Loogwegdoenkoste behoort dus betekenisvol met hierdie tegnologie verminder te kan word. Geseëldeselektrodialise het minder doeltreffend in die 5 000 tot 10 000 mg/l TOVS toevoerkonsentrasiegebied geword as gevolg van hoë elektriese energieverbruik ($3,3$ tot $13,0 \text{ kWh/m}^3$). Geseëldeselektrodialise kan egter in hierdie TOVS gebied toegepas word afhangende van die waarde van die produk wat herwin kan word.

'n Relatief gekonsentreerde ammoniumnitraatoplossing (TOVS 3 600 mg/l) kon suksesvol met GSED behandel word. Loogvolume het slegs 2,8% van die behandelde water volume beslaan. Elektriese energieverbruik is as $2,7 \text{ kWh/m}^3$ produk bepaal. Beide die loog- en die behandelde water behoort in die proses hergebruik te kan word. Membraanbevulling mag egter die proses nadelig affekteer en hierdie saak behoort verdere aandag te geniet. Behandeling van skaalvormende waters sal die proses nadelig beïnvloed omdat skalie in die membraansakkies kan neerslaan wat nie vir skoonmaakdoeleindes oopgemaak kan word nie. Skalie kan met stroomruiling of met skoonmaakmiddels verwyder word. Hierdie saak vereis egter verdere ondersoek. Skaalvormende waters behoort egter vermy te word of met ionuitruiing of nanofiltrasie voor GSED behandel te word.

Geseëldeselektrodialise het potensiaal om vir die behandeling van relatief verdunde ($< 3 000 \text{ mg/l}$ TOVS) nie-skaalvormende waters vir chemiekalieë- en waterherwinning vir hergebruik aangewend te word. Waters met hoë TOVS-vlakke (tot ongeveer 16 000 mg/l) behoort egter ook behandel te kan word afhangende van die waarde van die produk wat herwin kan word. Die suksesvolle toepassing van GSED-tegnologie blyk om van die behoefte af te hang om hierdie tegnologie in voorkeur bo konvensionele ED vir spesifieke toepassings aan te wend waar hoë loogkonsentrasies en klein loogvolumes vereis word. Kapitaalkoste van GSED-toerusting behoort minder te wees as die van konvensionele ED as gevolg van 'n meer eenvoudige ontwerp van die GSED-membraanpak. Die membraanbenuttingsfaktor van 95%

in GSED is baie hoër as wat in konvensionele ED verkry word (ongeveer 80%).

Elektro-osmotiese pumpingstudies in 'n enkelselpaar het die volgende aangetoon:

Loogkonsentrasie neem met toenemende stroomdigtheid en toenemende toevoerwaterkonsentrasie toe en plat af by hoë stroomdigthede afhanklik van die elektro-osmotiese koeffisiënte van die membrane. Stroomdoeltreffendheid was bykans konstant oor 'n groot gebied van stroomdigthede en toevoerwaterkonsentrasies in die geval van *Selemion*- (sout- en suurkonsentrasie) en *Raipore* membrane (soutkonsentrasie). Al die ander membrane het egter 'n geringe afname in stroomdoeltreffendheid getoon wat daarop dui dat die beperkende stroomdigtheid oorskry is. Watervloei deur die membrane (sout- en basiskonsentrasie) het met toenemende stroomdigtheid en toenemende toevoerwaterkonsentrasie toegeneem. Toenemende watervloei het stroomdoeltreffendheid aansienlik laat toeneem veral in die geval van die meer poreuse heterogene membrane. Dit sal dus nie nodig vir membrane wees om 'n baie hoë permselektiwiteit ($> 0,9$) vir gebruik in EOP-ED te hê nie omdat watervloei deur die membrane doeltreffend sal verhoog. Watervloei deur ED-membrane het gevolglik ook 'n positiewe effek, wat dikwels nie in ag geneem word nie. Die elektro-osmotiese koeffisiënte van die membrane neem met toenemende toevoerkonsentrasie af totdat 'n konstante waarde by hoë stroomdigtheid verkry word. Osmotiese vloei in EOP-ED neem met toenemende stroomdigtheid relatief tot die totale vloei af terwyl die elektro-osmotiese vloei relatief tot die osmotiese vloei toeneem. Osmotiese vloei dra betekenisvol by tot die totale watervloei in EOP-ED. Membraanpermselektiwiteit neem met toenemende loog-, toevoerkonsentrasie en toenemende konsentrasiegradiënt oor die membrane af.

Selemion AMV- en CMV- en *Ionac*-membrane; *Selemion* AAV- en CHV- en die nuut ontwikkelde Israeli ABM membrane; *Selemion* AMV- en CMV-, *Selemion* AMP- en CMV- en *Ionac* membrane het respektiewelik goeie werkverrigting vir sout-, suur- en basiskonsentrasie gelewer. Stroomdoeltreffendhede het tussen 62 en 91% (*Selemion* AMV en CMV); 34 en 60% (ABM-3 en *Selemion* CHV); en tussen 47 en 76% (*Selemion* AMV en CMV) respektiewelik vir sout-, suur- en basiskonsentrasie in die toevoerwaterkonsentrasiegebied van 0,05 tot 1 mol/l, gewissel.

Daar is gedemonstreer dat 'n eenvoudige membraanpotensiaalmeting suksesvol gebruik kan word om membraanwerkverrigting vir sout-, suur- en basiskonsentrasie te voorspel. Membraanwerkverrigting kan met 'n akkuraatheid van respektiewelik 10, 20 en 20% en beter voorspel word vir sout-, suur- en basiskonsentrasie. Loogkonsentrasie kan bevredigend met oënskynlike transportgetalle en watervloei voorspel word. Maksimum loogkonsentrasie; c_0^{mak} , kan bevredigend met twee eenvoudige modelle voorspel word.

Die korrekte Onsager verwantskappe wat respektiewelik vir potensiaalmetings en vir transportgetalle gebruik moet word is by zero stroom en zero volumevloeï, en by zero konsentrasiegradiënt en zero volumevloeï. In praktiese ED word metings egter by zero druk in die teenwoordigheid van konsentrasiegradiënte en volumevloeïe uitgevoer. Hierdie faktore sal die resultate aansienlik beïnvloed in alle sisteme waar volumevloeïe belangrik is en waar die konsentrasiefaktor hoog is soos wat in EOP-ED aangetref word. In die meting van membraanpotensiaal werk volumevloeï teen die konsentrasiepotensiaal en sal in die algemeen die potensiaal verlaag. In ED help watervloeï om die stroomdoeltreffendheid te verhoog maar die konsentrasiegradiënt sal die stroomdoeltreffendheid verlaag.

Modelle beskryf die sisteem vir konsentrering van sout-, suur- en basisoplossings bevredigend. Loogkonsentrasie bereik 'n limietwaarde (plato) by hoë stroomdigtheid afhanklik van die elektro-osmotiese koëffisiënte van die membrane. 'n Konstante helling (elektro-osmotiese koëffisiënt) is verkry toe watervloeï teen stroomdigtheid geplot is. Reguit lyne is verkry toe sel-paarweerstand teen die spesifieke weerstand van die produkwater geplot is. Stroomdoeltreffendheid het met toenemende watervloeï deur die membrane toegeneem, afgeneem toe die konsentrasie-gradiënt hoog en die oënskynlike transportgetalle laag was.



To my wife Deliana

ACKNOWLEDGEMENTS

This study was undertaken at the Division of Water Technology of the CSIR.

I would like to thank:

- the Water Research Commission for their financial support
- the Steering Committee of the Water Research Commission under the chairmanship of Dr H M Saayman for their assistance and enthusiasm throughout the project
- Dr B M van Vliet for the role he played to make a visit to the Weizmann Institute of Science in Israel possible
- Professor O. Kedem of the Weizmann Institute of Science in Israel for her valuable advice and fruitful discussions during visits to Israel and abroad
- Professor J F van Staden, my promoter, for his assistance and enthusiasm throughout the project
- Mrs G M Enslin, Mrs H MacLeod, Mrs E Hill and Mr A Steyn for their valuable technical assistance
- Mrs R P van de Venter for typing of this manuscript.

CONTENTS

	Page
SYNOPSIS	i
SAMEVATTING	v
ACKNOWLEDGEMENTS	x
1. INTRODUCTION	1
2. LITERATURE SURVEY	3
2.1 Electro-Osmotic Pumping of Salt Solutions with Homogeneous Ion-Exchange Membranes	3
2.2 Electro-Osmotic Pumping of Saline Solutions in a Unit-Cell Stack	5
2.3 Electro-Osmotic and Osmotic Flows	9
2.4 Structural Properties of Membrane Ionomers	13
2.5 Measurement of Transport Number	16
2.6 Transport Properties of Anion-Exchange Membranes in Contact with Hydrochloric Acid Solutions. Membranes for Acid Recovery by Electrodialysis	17
2.7 Electrodialysis Applications	18
3. THEORY	21
3.1 Theories of Membrane Transport	21
3.2 Conductance and Transport Number	34
3.3 Ion Coupling from Conventional Transport Coefficients	38
3.4 Transport Processes Occurring During Electrodialysis	49
3.5 Current Efficiency and Transport Phenomena in Systems with Charged Membranes	50
3.6 Efficiency of Energy Conversion in Electrodialysis	57
3.7 Conversion of Osmotic into Mechanical Energy in Systems with Charged Membranes	65
3.8 Donnan Exclusion	71
3.9 Relationship Between True and Apparent Transport Numbers	72
3.10 Electro-Osmotic Pumping - The Stationary State - Brine Concentration and Volume Flow	77
3.11 Flux Equations, Membrane Potentials and Current Efficiency	87
3.12 Electrodialysis Theory	92
4. ELECTRODIALYSIS IN PRACTICE	117
4.1 Electrodialysis Processes and Stacks	117
4.2 Ion-Exchange Membranes	120
4.3 Fouling	123
4.4 Pretreatment	124
4.5 Post-treatment	125

4.6	Seawater Desalination	125
4.7	Brackish Water Desalination for Drinking-Water Purposes	126
4.8	Energy Consumption	126
4.9	Treatment of a High Scaling, High TDS Water with EDR	127
4.10	Brackish Water Desalination for Industrial Purposes	128
4.11	ED/IX System	128
4.12	Industrial Wastewater Desalination for Water Reuse, Chemical Recovery and Effluent Volume Reduction	129
4.13	Other Possible Industrial Applications	131
4.14	Polarisation	132
4.15	Cell Stack	133
4.16	Process Design	135
5.	EXPERIMENTAL	136
5.1	Membranes	136
5.2	Membrane Preparation	136
5.3	Unit-Cell Construction	137
5.4	Determination of Brine Concentration, Current Efficiency and Water Flow as a Function of Feed Concentration and Current Density	138
5.5	Determination of Membrane Characteristics	140
5.6	Determination of Salt and Acid Diffusion Rate through Membranes	141
5.7	Bench-Scale EOP-ED Stack	142
5.8	Sealed-Cell ED Stack	146
6.	ELECTRO-OSMOTIC PUMPING OF SODIUM CHLORIDE SOLUTIONS WITH DIFFERENT ION-EXCHANGE MEMBRANES	148
6.1	Brine Concentration	148
6.2	Current Efficiency	184
6.3	Water Flow	207
6.4	Membrane Permselectivity	223
6.5	Membrane Characteristics	227
7.	ELECTRO-OSMOTIC PUMPING OF HYDROCHLORIC ACID SOLUTIONS WITH DIFFERENT ION-EXCHANGE MEMBRANES	229
7.1	Brine Concentration	229
7.2	Current Efficiency	253
7.3	Water Flow	270
7.4	Membrane Permselectivity	283
7.5	Acid and Salt Diffusion through Membranes	286
7.6	Membrane Characteristics	287
8.	ELECTRO-OSMOTIC PUMPING OF CAUSTIC SODA SOLUTIONS WITH DIFFERENT ION-EXCHANGE MEMBRANES	289
8.1	Brine Concentration	289

8.2	Current Efficiency	306
8.3	Water Flow	319
8.4	Membrane Permselectivity	328
8.5	Membrane Characteristics	330
9.	ELECTRO-OSMOTIC PUMPING OF SODIUM CHLORIDE-, HYDROCHLORIC ACID AND CAUSTIC SODA SOLUTIONS IN A CONVENTIONAL ELECTRODIALYSIS STACK	332
9.1	Concentration/Desalination of Sodium Chloride Solutions with Ionac MA-3475 and MC-3470 Membranes	332
9.2	Concentration/Desalination of Hydrochloric Acid Solutions with Selemion AAV and CHV Membranes	342
9.3	Concentration/Desalination of Caustic Soda Solutions with Selemion AMV and CMV Membranes	351
10.	CONCENTRATION/DESALINATION OF SALT SOLUTIONS AND INDUSTRIAL EFFLUENTS WITH SCED	360
10.1	Concentration of Salt Solutions	360
10.2	Concentration/Desalination of Industrial Effluents	369
11.	GENERAL DISCUSSION	376
11.1	Requirements for ED Membranes	376
11.2	Permselectivity with Acids and Bases	377
11.3	Brine Concentration, Electro-Osmotic and Osmotic Flows	377
11.4	Discrepancy between Transport Numbers Derived from Potential Measurements and Current Efficiency Actually Obtained	378
11.5	Current Efficiency and Energy Conversion in ED	380
11.6	Water Flow, Concentration Gradient and Permselectivity	381
11.7	Prediction of Brine Concentration	382
11.8	Membranes for Sodium Chloride, Hydrochloric Acid and Caustic Soda Concentration	383
11.9	Conventional EOP-ED Stack	384
11.10	Sealed-Cell Electrodialysis	384
12.	SUMMARY AND CONCLUSIONS	386
13.	NOMECLATURE	393
14.	LITERATURE	404
	APPENDIX A	
	APPENDIX B	
	APPENDIX C	
	APPENDIX D	

1. INTRODUCTION

Electro-osmotic pumping (EOP) is a variant of conventional electrodialysis (ED) that should be suitable for concentration/desalination of saline waters⁽¹⁾. In EOP, brine is not circulated through the brine compartments, but is evolved in a closed cell. Brine enters the cell as electro-osmotic and osmotic water and leaves the cell by electro-osmotic pumping. This leads to very high concentration factors (high brine concentration) and thus high recovery of product water and small volume of brine to be disposed of. The relatively simple design of an EOP-ED stack, the possibility that an EOP-ED stack may be cheaper than conventional ED and the small brine volume produced, are the major advantages of EOP-ED⁽¹⁾.

Electro-osmotic pumping of sodium chloride solutions has been described by Garza⁽¹⁾; Garza and Kedem⁽²⁾; Kedem *et al.*⁽³⁾; Kedem and Cohen⁽⁴⁾ and Kedem and Bar-On⁽⁵⁾. Water and salt fluxes were studied through ion-exchange membranes as a function of current density and feed concentration and mathematical models were developed to describe the experimental data⁽¹⁾. Kedem has reported that current efficiency determined in EOP experiments was close to the value expected from transport number determinations when sodium chloride solutions were electrodialyzed⁽⁵⁾. Kedem has also reported that apparent transport numbers gave a lower estimate of current efficiency in ED⁽²⁾. However, only results for sodium chloride solutions and one commercially available ion-exchange membrane, viz. *Selemion* AMV and CMV were reported. It would be very useful if membrane performance for concentration/desalination applications could be accurately predicted from transport numbers obtained from simple potential measurements. Information in this regard for ion-exchange membranes to be used for saline, acidic and basic effluent treatment, is limited.

A sealed-cell ED (SCED - membranes are sealed together at the edges) laboratory stack (EOP-ED stack) was also developed for evaluation of desalination/concentration of sodium chloride solutions^(3, 4, 5). However, only one membrane type that is presently not commercially available, viz., polysulphone based membranes, have been used in the SCED studies. Only desalination/concentration of sodium chloride solutions has been reported in the studies. Saline, acidic and alkaline effluents frequently occur in industry. These effluents have the potential to be treated with EOP-ED for water and chemical recovery and effluent volume reduction. No information, however, could be found in the literature regarding EOP characteristics (brine volume, current efficiency, electro-osmotic coefficients, etc.) of membranes suitable for EOP-ED of acidic and alkaline solutions. In addition, little information is available in the literature regarding EOP characteristics of membrane types to be used for EOP-ED of saline solutions. Consequently, information regarding EOP characteristics of commercially

available ion-exchange membranes suitable for saline, acidic and basic solution treatment is insufficient and information in this regard will be necessary to select membranes suitable for EOP-ED of saline, acidic and basic effluents. In addition, no information exists regarding the performance of an EOP-ED stack for industrial effluent treatment. Information on the theory of EOP-ED and ED is scattered throughout the literature^(1 - 5, 6 - 19) and is not well documented in any single publication.

Much information, on the other hand, is available in the literature regarding electro-osmosis in general and factors affecting water transport through ion-exchange membranes^(5, 20 - 32). Much information is also available in the literature regarding concentration/desalination of saline solutions and saline industrial effluents with conventional ED^(6, 7, 33 - 37) and electro dialysis reversal (EDR)⁽⁸⁾. Conventional ED and EDR, however, are established processes for brackish water desalination and to a lesser extent for wastewater treatment. These processes are applied with success, especially for brackish water treatment for potable use^(6, 8, 38, 39). Conventional ED and EDR, however, have the potential to be applied more for industrial effluent treatment.

The objectives of this study were therefore to:

- Consider and document the relevant EOP-ED theory properly;
- Study the EOP-ED characteristics (transport numbers, brine concentration, current density, current efficiency, electro-osmotic coefficients, etc.) of commercially available ion-exchange and other membranes in a single cell pair with the aim to identify membranes suitable for saline, acidic and alkaline effluent treatment;
- Determine whether membrane performance can be predicted effectively from simple transport number determinations and existing models;
- Study EOP-ED of saline solutions in a conventional ED stack;
- Study EOP-ED of saline solutions and industrial effluents in a SCED stack.

2. LITERATURE SURVEY

2.1 Electro-osmotic Pumping of Salt Solutions with Homogeneous Ion-Exchange Membranes

Garza⁽¹⁾ and Garza and Kedem⁽²⁾ have described electro-osmotic pumping of salt solutions with homogeneous membranes in a single cell pair. Brine concentrations, volume flows and current efficiencies were determined at different current densities (0 - 60 mA/cm²) for three different sodium chloride feed water concentrations (0,01; 0,1 and 0,5 mol/l). *Selemion* AMV and CMV and polyethylene-based membranes, however, were the only membranes used.

It was found that model calculations described the system in an appropriate way. The results predicted important results such as:

- a) approaching of a limiting (plateau) value of the maximum brine concentration (c_b^{\max}) as the current density is increased;
- b) dependence of c_b^{\max} on the electro-osmotic coefficient (EOC) of the membranes;
- c) approaching of a limiting value (plateau) of current efficiency (ϵ_p) at high current density (below its limiting value);
- d) approaching of a constant slope for curves of volume flow (J) through the membranes versus effective current density (I_{eff}).

It was experimentally found ^(1, 2) that graphs of brine concentration (c_b) versus current density levelled off at high values of current and that c_b approached a maximum plateau, c_b^{\max} , which depended only on the electro-osmotic coefficients (β) of the membrane pair ($c_b^{\max} = \frac{1}{2} F \beta$). The smaller the ratio between the osmotic and electro-osmotic water flows, the smaller the current necessary to reach this plateau.

Graphs of volume flow versus effective current density became straight lines at high values of the current. The electro-osmotic and osmotic coefficients could be determined from the slope and the intercept of the lines, respectively. The results have agreed quite well with values obtained from a standard method⁽¹⁾ which is very time consuming.

The average value of the apparent transport number for the different membrane pairs

($\bar{\Delta t}$'s) was determined from the membrane potential for a concentration difference similar to that obtained in the EOP experiments at high current densities⁽²⁾. It was found to give a good (lower) estimate of the actual Coulomb efficiency of the process at a salt concentration of 0,1 mol/l. However, no results at higher or lower concentrations were reported. *Selemon* AMV and CMV ion-exchange membranes were the only commercially available membranes used.

The maximum brine concentration, c_b^{\max} , was predicted from the following two relationships⁽²⁾:

$$a) \quad c_b^{\max} = \frac{1}{2\beta F} \quad \text{and} \quad (2.1)$$

$$b) \quad c_b^{\max} = c_b (1 + J_{\text{osm}}/J_{\text{elosm}}) \quad (2.2)$$

(Note: $J = J_{\text{osm}} + J_{\text{elosm}}$).

Good correlations between the two methods were obtained with the membranes and the salt solutions used.

The EOP results have shown that with appropriate membranes and control of polarization, EOP may be used as a good alternative to conventional ED for desalination/concentration of saline solutions. Laboratory scale EOP experiments may also be conducted as an alternative and convenient way of determining osmotic and electro-osmotic coefficients.

Experimental results were obtained for non-porous membranes. Current efficiencies were in the range of 60 - 85%. It was suggested by Garza⁽¹⁾ that a current efficiency of 90% could be obtained with a porous ion-exchange membrane. However, no other results were reported.

Most of the energy consumption in the EOP system will take place in the dialysate compartments⁽¹⁾. Therefore, to reduce it and to suppress concentration polarization, it would be advisable to combine the membranes with open dialysate compartments containing ion-conducting spacers.

It was suggested by Garza⁽¹⁾ that EOP would have the following advantages in relation to conventional ED when used for desalination:

- a) the capital cost of the equipment would be decreased due to the simpler

- construction of the unit-cell stack compared to the conventional plate-and-frame stack;
- b) the membrane utilization factor in the membrane bags could be about 95% compared to about 70 to 75% for membranes in conventional ED stacks;
 - c) higher current densities would be possible in unit-cell stacks because of the higher linear flow velocities that could be obtained. These higher current densities would result in higher production rates;
 - d) there would be a decrease in brine volume, and as a consequence, less brine disposal problems.

The only disadvantages could be the fact that more electrical energy per unit of product water would be experienced in the unit-cell stack because higher current densities were used. However, the increased cost for electrical energy would be more than off-set by the decrease in the cost of membrane replacement and amortization of the capital investment, according to Garza⁽¹⁾.

No information could be found in the literature regarding EOP characteristics (brine concentration, current efficiency, electro-osmotic coefficient, etc.) of membranes for acid and alkaline solution treatment in a single cell pair similar to that described for saline solutions.

2.2 **Electro-Osmotic Pumping of Saline Solutions in a Unit-Cell Stack**

The so-called unit-cell stack was described by Nishiwaki⁽⁶⁾ for the production of concentrated brine from seawater by ED. It consisted of envelope bags formed of cation- and anion-exchange membranes sealed at the edges and provided with an outlet, alternated with feed channels. The direction of volume flow through the stack was such to cause ionic flow into the membrane bags. The only water entering the bags was the electro-osmotic water drawn along with the ions plus the osmotic flow caused by the higher pressure of the brine compared to the feed. This variant of ED is called electro-osmotic pumping (EOP) and is used for production of concentrated brine from seawater for salt production.

A simple sealed-cell ED stack (SCED) was described by Kedem *et al.*⁽³⁾ in 1978. This cell consisted of thermally sealed polyethylene based membranes (21 bags, 5 x 9 cm). The membranes were not very selective at high salt concentration. It was found that smooth continuous operation was obtained with stable voltage and pH in the

concentration range from 0,01 to 0,04 mol/l and current densities from 5 to 20 mA/cm².

Kedem and Cohen⁽⁴⁾ have described the performance of a laboratory SCED unit for desalination/concentration of sodium chloride solutions. Heterogeneous ion-exchange membranes were used. The selectivity of these membranes, however, were lower than that of commercially available membranes. Nevertheless, it was demonstrated that various sodium chloride feed concentrations could be desalinated effectively. The results are shown in Table 2.1.

Table 2.1: Desalination of sodium chloride solutions at various cell pair voltages.

c_{feed}	c_{product}	Output	Energy Consumption	c_{brine}	Recovery	V_{cp}	d_{eff}
mg/l	mg/l	$\frac{\text{m}^3}{\text{m}^2\text{day}}$	$\frac{\text{kWh}}{\text{m}^3}$	mg/l	%	Volt	mm
2 670	810	3,25	1,55	82 780	98	1	1,13
1 910	320	1,86	1,33	60 610	97,3	1	1,13
1 570	570	2 60	0,56	45 800	97,8	0,72	1,07
1 910	540	1,62	0,54	46 040	97	0,5	0,82

c_f : feed concentration
 c_p : product concentration
 c_b : brine concentration
 V_{cp} : cell pair voltage
 d_{eff} : effective thickness of dialysate compartment (polarization factor).

Product water yield (output), electrical energy consumption, brine concentration, c_b , water recovery, cell pair voltage, V_{cp} , and the polarization factor (d_{eff}) are also shown in Table 2.1.

Kedem and Bar-on⁽⁵⁾ have reported results on the desalination of sodium chloride solutions with a SCED stack using heterogeneous ion-exchange membranes. The results are shown in Table 2.2.

Table 2.2: Desalination of sodium chloride solutions at a linear flow velocity of 14,4 cm/s.

V_{cp}	c_f mg/l	c_p mg/l	Energy consumption kWhr/m ³	Output m ³ /day	n_c %	c_b mg/l	d_{eff} mm
0,9	2 200	100	1,01	1,41	77,0	68 390	1,24
	1 500	500	0,51	3,68	76,5		1,10
	1 000	300	0,35	3,62	79,5		0,85
0,7	2 100	100	0,80	1,16	78	59 620	0,97
	1 500	500	0,39	3,06	78,5		0,83
	1 000	300	0,27	3,05	77		0,80
0,5	2 500	500	0,53	1,22	80	60 200	0,88
	1 500	500	0,27	1,95	80		0,71
	1 000	300	0,19	2,62	80		0,60

V_{cp} : cell pair voltage
 c_f : feed concentration
 c_p : product concentration
 n_c : current efficiency
 c_b : brine concentration
 d_{eff} : effective thickness of dialysate compartment (polarization factor).

The current efficiency (n_c) is shown for varying cell pair voltages and feed water concentrations. It was mentioned by Kedem and Bar-on⁽⁵⁾ that the permselectivity of the ion-exchange membranes that were used decreased substantially at high salt concentration. This, however, is not reflected in the data on the current efficiency that was obtained in the SCED stack (Table 2.2). It appears therefore, according to Kedem and Bar-on, that electro-osmosis contributes to salt transfer and helps to maintain current efficiency.

At constant cell pair voltage (V_{cp}), polarization is nearly constant and plots of cell pair resistance (R_{cp}) versus specific resistance of the dialysate (ρ) give straight lines in a rather wide concentration range⁽⁵⁾. As shown in Figure 2.1, this is not true for the whole range covered. Polarization decreases slightly with increasing current. For the estimated effective thickness of the dialysate compartment, d_{eff} , this is approximated by straight lines for parts of this range.

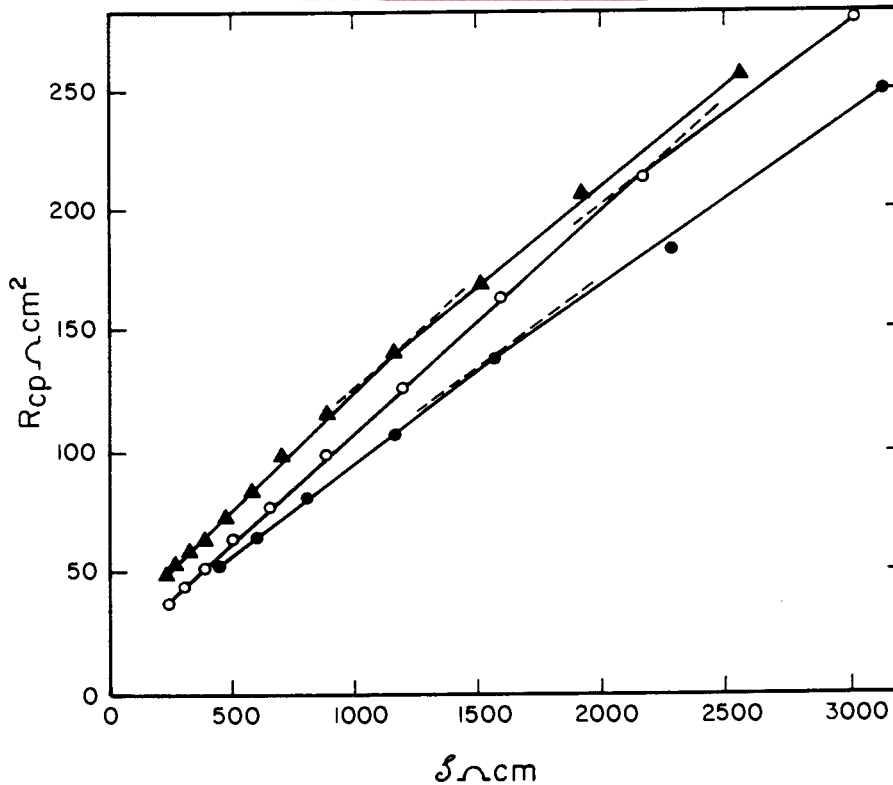


Figure 2.1: Apparent resistance per cell pair as a function of the specific resistance of the dialysate solution. $V_{cp} = 0,7 \text{ V}$.

Membrane potentials and ohmic resistance for a pair of membranes are shown in Table 2.3. Membrane potentials were measured with calomel electrodes between stirred cells. Column 4 shows the potentials for ideal permselectivity (absolute values). Membrane resistance (ΩC) was measured in 0,5 and 0,1 mol/l sodium chloride solutions.

Table 2.3: Membrane potential and ohmic resistance of a heterogeneous cation-exchange membrane (c) and a similar anion-exchange membrane (a)

Solutions	Membrane Potential				Solution Concentration	Membrane Resistance	
	$\Delta\psi_m^c$	$\Delta\psi_m^a$	$\Delta\psi_m^0$	$\frac{\Delta\psi_m^c + \Delta\psi_m^a }{2\Delta\psi_m^0}$		C	A
NaCl mol/l	mV	mV	mV	%	mol/l	Ωcm^2	Ωcm^2
0,02/0,04	15,6	14,9	16,7	91	0,5	9,5	9,8
0,1/0,2	14,8	14,4	16,3	89	0,1	37,1	26,6
0,5/1,0	13,2	11,9	16,8	75			
1,0/2,0	12,4	11,1	18,2	64			
0,02/1,0	80,0	72,6	93,0	82			

$\Delta\psi_m^c$: membrane potential of cationic membrane
 $\Delta\psi_m^a$: membrane potential of anionic membrane
 $\Delta\psi_m^0$: membrane potential for ideal permselectivity.

2.3 Electro-Osmotic and Osmotic Flows

Electro-osmosis of different salt, acid and alkaline solutions have been studied extensively through a wide variety of membranes^(5, 20 - 27, 28 -32, 40, 41).

Brydges and Lorimer⁽²⁰⁾ showed that when current density is varied, water transport number can:

- a) increase at low current density because osmotic water flow has been superimposed on water transport by the electric field;
- b) decrease at higher current density because of accumulation of salt in the membrane;
- c) decrease more at current densities near or above the limiting value because of an increased contribution of hydrogen and hydroxide ions to transport. These phenomena arise from a combination of diffusion (film) at both the membrane-solution interface and from the dependence of counter-ions and water transport numbers on external salt concentration.

Kruissink⁽²¹⁾ has showed that with *Nafion* 170 membranes under practical conditions (concentrated alkali (≥ 10 mol/l) and 5 mol/l sodium chloride), that electro-osmotic water transport caused the maximum current efficiency to increase from 0,45 (electro-osmotic water transport number zero) to about 0,75 to 0,80 (at electro-osmotic water transport number of 1).

Hidalgo-Alvarez *et al.*⁽²²⁾ have found that at low electric current, the electro-osmotic coefficient undergoes a sharp elevation. This effect was very similar to that found by Lakshminarayanaiah⁽⁴⁰⁾. At high electric current the electro-osmotic coefficient tends toward a constant value. This value depends on the concentration of the solution. When the concentration increases, the electro-osmotic permeability decreases.

Ceynowa⁽²³⁾ has indicated that the water transport number depends on many factors, such as experimental conditions (current density, stirring, difference in the concentration which occurs in the course of electrolysis on both sides of a membrane) as well as membrane parameters such as cross-linking, water content, ion-exchange capacity. Consequently, the resulting water transport number may sometimes be questionable and its properties complex.

The decrease of the water transport number with an increase in concentration of the external solution is usually given as the main non-controversial property⁽²³⁾. However, Tombalakian *et al.*⁽²⁴⁾ found constant values of the water transport number for the homogeneous sulphonic acid membranes of high cross-linking and low water content in hydrochloric acid solution. Demarty *et al.*⁽⁴¹⁾ stated the same for the heterogeneous *Ionac* MC 3470 XL membrane in hydrochloric acid solutions. Similarly Oda and Yawataya⁽²⁷⁾ reported that in some membranes in the presence of hydrochloric acid solution the water transport number remained constant at about 1,0 and the hydrogen ion transfer number only drops from 1,0 to 0,99. They also suggested that membranes deswell with increasing electrolyte concentration.

Ceynowa⁽²³⁾ found that the water and ion transport numbers at low sulphuric acid concentrations were in a wide range (5 - 70 mA/cm²) independent of current density in the case of the heterogeneous MRF-26 ion-exchange membrane. However, at high concentration (2,26 mol/kg water) the increase in water transport number with current density was remarkable. It was also found that the water transport number in the MRF membrane decreased with increasing concentration (0,5 to 2,0 mol/kg water). With Nafion-120 membrane the water transport number remained almost constant with increasing feed concentration.

Rueda *et al.*⁽²⁵⁾ stated that the decrease of water transport number with increase in external salt concentration could be attributed to the decrease of the selectivity of the membrane. At very dilute solutions, the current is carried by the cations because the anions are almost completely excluded from the cationic cellulose acetate membrane. As the external solution concentration increases, the permselectivity of the membrane decreases. Anions are now present in the membrane and cations and anions participate in the transport of current across the membrane in opposite directions. Obviously, water transport will be reduced. An increase of external salt concentration leads to an increase of charge concentration in the neighbourhood of the matrix and consequently a decreasing of the electro-osmotic permeability.

Electro-osmotic permeability of several cellulose acetate membranes have been determined using solutions of alkali-chlorides⁽²⁵⁾. The electro-osmotic permeability has been studied as a function of the external electrolyte concentration (0,001 to 0,1 mol/l) and of current density applied. The results showed that the electro-osmotic permeability depended on the thickness of the membranes and the nature of the cations. The electro-osmotic permeability has been found to be strongly dependent

on the external salt concentration. However, the electro-osmotic permeability was not significantly affected by current density.

Tasaka *et al.*⁽⁶⁶⁾ have also studied electro-osmosis in charged membranes. At low electrolytic concentrations the direction of electro-osmosis is the same as that of counter-ion flow, because most of the movable ions in the membrane are counter-ions. With increasing external salt concentration the concentration of co-ions in the membrane increases, and then electro-osmosis decreases. In many instances electro-osmosis tends towards zero at the limit of high electrolyte concentrations.

Oda and Yawataya⁽²⁷⁾ have found that the electro-osmotic coefficient of hydrochloric acid through a cation-exchange membrane remains almost constant over the concentration range from 0,5 to 4,0 mol/l. In hydrochloric acid solutions the electro-osmotic water transference is merely about one mole water per Faraday through a membrane.

Narebska *et al.*⁽²⁸⁾ have investigated the isothermal transport of ions and water across the perfluorinated Nafion 120 membrane in contact with sodium chloride solutions at a concentration of 0,05 up to 4 mol/l based on irreversible thermodynamics of transport. It was found that the specific conductivity of the membrane increased at low external electrolyte concentration. The apparent transport number of the cation decreased significantly at higher external electrolyte concentration. The electro-osmotic coefficient also decreased significantly at higher external electrolytic concentration. The osmotic volume flux, and salt diffusion flux increased with increasing electrolyte concentration while the hydrodynamic volume flow decreased with increasing electrolytic concentration. The membrane also deswelled significantly with increasing electrolyte concentration.

Narebska and Koter⁽²⁹⁾ have studied the conductivity of ion-exchange membranes on the grounds of irreversible thermodynamics of transport. They have found that convection conductivity covers 50 to 55% of the total membrane conductivity and even more at increased temperature. This means that the flowing water doubles the ability of the membrane to transport the ionic current. This confirms the substantial role that water plays in the transport behaviour of a membrane.

Narebska *et al.*,⁽³⁰⁾ have performed a detailed analysis of membrane phenomena in the system Nafion 120/NaOH_{aq}. They have determined the phenomenological resistance -

($r_{i,k}$) and friction coefficient ($f_{i,k}$). They have found that the resistance imposed by the membrane on the permeating OH^- ions is much lower than that for Cl^- ions. The three factors contributing to this effect - i.e. the frictions imposed by the cation (f_{21}), water (f_{2w}) and the polymer matrix (f_{2m}) - influence the flow of OH^- and Cl^- to a different degree. Chloride ions are hindered mainly by water, especially at increasing sorption. The flow of OH^- ions in diluted solution is hindered by the matrix and, at a higher concentration, by the cation and then by water.

Considering these results, it is apparent that the easy flow of NaOH results not only from the high mobility of OH^- ions, but also from the low osmotic flux (2 to 3 times less than in NaCl solutions) opposing the stream of electrolyte and the very low friction of the OH^- ions with water.

The water transport number decreased from 10 mol/Faraday to 2 mol/Faraday over the concentration range of 0,05 to 4 mol/l. The apparent transport number (Δt^c) also decreased significantly with increasing caustic soda concentration.

The transport of aqueous NaCl solutions across the perfluorinated Nafion 120 membrane have been studied on the basis of irreversible thermodynamics by Narebska *et al.*⁽³¹⁾. The straight resistance coefficients r_{ij} , partial frictions f_{ik} and diffusion indexes have been determined.

Since the Donnan equilibrium and TMS theory were published, it is a well known and documented fact that co-ions are rejected from a charged polymer by the high potential of the polymer network. It was found by Narebska *et al.*, that friction of this co-ion with the charged polymer was not the main force which resisted the flow of negative ions in the negatively charged polymer network. Except at 289 K and $m_{\text{ext}} = 0,5$, the anion-polymer frictional force ($2m$) was below the friction with water ($2w$) and it decreases with increasing electrolyte concentration and temperature. As a result, at high temperature and m_{ext} , the resistance against flowing anions is imposed by water; the lower the amount of water in the membrane, the higher this resistance.

Koter and Narebska⁽³²⁾ have investigated the mobilities of Na^+ , Cl^- and OH^- ions and water in Nafion 120 membranes. They have found that the interactions of Na^+ and Cl^- ions running in opposite directions are negligible in the whole concentration range (0,05 to 4 mol/l) studied. However, hydroxide ions impede cations, particularly at higher external concentrations (high sorption). This fact can be attributed to the higher

partial friction between Na^+ and OH^- ions caused by the phenomenon called "local hydrolysis".

The mobility of hydroxide ions exceeds that of chloride ions even more in the membrane than in the free solution. The mobility of hydroxide ions is much more sensitive to concentration than that of chloride ions. The mobility of the hydroxide ions declines much more rapidly than the mobility of the chloride ions. This reflects the dehydration of the membrane with increasing sorption of an electrolyte.

Kedem and Bar-on⁽⁵⁾ have mentioned that the current efficiency (n_c) for a single membrane pair was sometimes equal to and even higher than the apparent transport number of the membrane pair (\bar{t}) measured with calomel electrodes. According to them, this is due to the substantial influence of electro-osmotic and osmotic flow into the brine cells during ED which increase the current efficiency. Both osmotic and electro-osmotic water flow enters the brine cell through both membranes. It increases the flows of counter-ions leaving the brine. The total effect of volume flow into a brine cell is increased salt flow. There will also be a slight influence of osmotic flow on the potential measurements. This will decrease the potential measurement and therefore the apparent transport number⁽⁵⁾.

2.4 Structural Properties of Membrane Ionomers

Mauritz and Hopfinger⁽⁴²⁾ have described structural properties of ion-exchange membranes. Common functionalities of ion-exchange membranes are: $-\text{SO}_3^-$; $-\text{COO}^-$; $-\text{NH}_3^+$; $=\text{NH}_2^+$. These hydrophilic groups are responsible for the swelling of the hydrophobic network of ion-exchange membranes on exposure to water. Swelling of ion-exchange membranes may be inhibited by the presence of crystalline domains within the membrane matrix.

The approach to equilibrium for an initially dry ion-exchange membrane (in a given counter-ion salt form and containing no co-ions) that is subsequently immersed in pure water, can be visualized in the following way: Although the interaction between the organic polymer backbone is endothermic and may influence the rate of swelling, the strongly exothermic tendency of the counter-ions and ionogenic side chains to hydrate results in having the initially arrived water molecules strongly bound in ionic solvation shells resulting in little or no volume expansion of the network. In the truly dry state, the counter-ions are strongly bound by electrostatic forces in contact ion pairs. Further

uptake of water beyond that which is barely required for maximum occupancy of all the hydration shells results in moving the association - dissociation equilibrium between bound and unbound counter-ions toward increased counter-ion mobility. The driving force for swelling is the tendency for the water to dilute the polymer network. Stated in precise thermodynamic formalism, the difference between the water activity in the interior ($\bar{a}_w < 1$) and exterior ($a_w = 1$) of the membrane gives rise to a membrane internal osmotic pressure, Π , that results in a deformation of the polymer chain network:

$$\Pi v_w = RT \ln \bar{a}_w \quad (2.4.1)$$

This equation is a statement of the free energy balance across the membrane - water interface at equilibrium and that v_w the partial molar volume of the internal water component may, in reality, not be the same as for the bulk water, nor be of a uniform value throughout the polymer because of local structuring effects.

As the water uptake proceeds, the increased side-chain counter-ion dissociation allows for more complete ionic hydration. The deformation of the polymer chain network upon further incorporation of water molecules also proceeds by a shift in the distribution of rotational isomers to higher energy conformations and changes in other intra-molecular, as well as inter-molecular interactions. Consequently, the increased overall energy state, for a given membrane water content of n moles, per equivalent of resin, is manifested by polymer chain retractive forces that resist expansion of the network. Accordingly, the configurational entropy decreases as less conformations become available within the matrix. Eventually, an equilibrium water content, n_o , is reached at which the osmotic swelling pressure is balanced by the cohesive energy density.

A qualitative set of rules that describe the equilibrium water swelling of polymeric ion-exchangers are as follows according to Mauritz and Hopfinger:

- a) Increasing the cross-link density reduces the swelling by decreasing the average inter-chain separation;
- b) Swelling will greatly depend on the pK of the ionogenic groups as well as their number per unit volume. For example, the equilibrium water uptake for strong acid resins exceeds that of resins containing the less hydrophilic weak acid groups;

- c) The nature of the counter-ion can influence swelling in a number of ways. Firstly, water uptake naturally increases with increasing hydrative capacity of the counter-ion. In general, for alkali counter-ion forms, the following progression is noted: $\text{Li}^+ > \text{Na}^+ > \text{K}^+ > \text{Rb}^+ > \text{Cs}^+$. Increased valence reduces swelling by: (i) reducing the number of counter-ions in the resin through the electroneutrality requirement; (ii) forming ionic cross-links; and (iii) reducing the hydrative capacities by the formation of triplet associations such as: $-\text{SO}_3^- \cdots \text{Ca}^{2+} \cdots \text{SO}_3^-$;
- d) The internal resin osmotic pressure is enhanced as the association - dissociation equilibrium between bound and unbound counter-ions shifts to greater dissociation by allowing for more complete hydration shell formation.

Narebska and Wodzki⁽⁴³⁾ have investigated water and electrolyte sorption (sulphuric acid) in perfluorosulphonic and polyethylene-poly (styrene sulphonic acid) membranes of different cross-linking in the temperature range of 293 to 333 K and a concentration of external electrolyte up to 5,7 mol/kg H_2O . As the hydration of the membranes is an exothermic process, a decrease of swelling with increasing temperature could be predicted. Also due to the nature of sulphuric acid one could expect dehydration of the membranes with an increasing concentration of acid. It was found that an increase of both variables, i.e. temperature and concentration, caused deswelling of the membranes in a higher degree when the cross-linking is lower. Only for the membranes with a low degree of cross-linking (2 and 5% DVB) equilibrated with diluted solutions of sulphuric acid, a small increase of swelling is visible at a temperature range of 293 to 303 K.

Narebska *et al.*,⁽⁴⁴⁾ have studied swelling and sorption equilibria for Nafion membranes in concentrated solutions of sodium chloride (0 to 6 mol/kg H_2O), and sodium hydroxide (0 to 18 mol/kg H_2O), at 293 to 363 K. It was found that significant deswelling of the membranes took place with increasing electrolyte concentration. Increasing temperature (above 333 K), also caused a loss of water. Narebska *et al.*, have stated that deswelling of a membrane depends on the kind of membrane, temperature and the nature of the external electrolyte.

2.5 Measurement of Transport Number

The efficiency with which a membrane transport selectively any particular ionic species may be inferred by measuring the transport number of the species in the membrane. Two methods are normally used to determine membrane transport number. They are:

- a) the emf method⁽⁴⁵⁾ and;
- b) the Hittorf's method⁽⁴⁵⁾. In these methods different concentrations of electrolyte exist on either side of the membrane, even though in the Hittorf's method one might start initially with the same concentration. Therefore, the transport number values derived by these methods cannot be directly related to a definite concentration of the external solution.

Membrane potentials measured using concentrations c' and c'' on either side of the membrane may be used in the following equation to derive an average transport number:

$$E/E_{\max} = 2\bar{t}_+ - 1; \quad \bar{t}_+ = (E/E_{\max}) + 0,5 \quad (2.5.1)$$

If Ag-AgCl electrodes immersed in two chloride solutions are used, \bar{t}_+ is derived from⁽⁴⁵⁾:

$$E = 2\bar{t}_{+(app)} \frac{RT}{F} \ln \frac{a'}{a''} \quad (2.5.2)$$

The derived transport number value has been called the apparent transport number because in this type of measurement water transport has not been taken into account. This apparent value will be close to the true value when very dilute solutions are used.

In the Hittorf's method a known quantity of electricity is passed through the membrane cell containing two chambers filled with the same electrolyte separated by a membrane. Cations migrate to the cathode and anions migrate to the anode. The concentration change brought about in the two chambers, which is not more than about 10%, is estimated by the usual analytical methods. The transport number is calculated from $t_i = FJ/l$.

The determination of meaningful transport numbers for any membrane-electrolyte system calls for careful control of a number of factors. The important factors for the

control of the concentration of the donating or receiving side are⁽⁴⁵⁾:

- a) external concentration;
- b) current density; and
- c) difference in concentration on either side of the membrane.

The effect of current density on the values of \bar{t}_i has been demonstrated by Kressman and Tye⁽⁴⁶⁾ using multi-compartment cells and by Lakshminarayanan and Subrahmanyam⁽⁴⁷⁾ using simple cells. When external concentrations are small ($< 0,1$ mol/l) an increase of current density decreases \bar{t}_i values. This is attributed to polarization effects at the membrane-solution interface facing the anode.

The amount of polarization decreases as the concentration is increased. When the external concentration is $0,1$ mol/l, \bar{t}_i exhibits a maximum at a certain current density below which the \bar{t}_i values decrease as the current density is decreased and above which also \bar{t}_i values decreased as the current density is increased. The decrease as the current density is lowered is attributed to back diffusion of the electrolyte⁽⁴⁷⁾.

When external concentrations $> 0,1$ mol/l are used, polarization effects are negligible but back diffusion becomes dominant. As the quality of back flux due to diffusion is determined by the concentration differences allowed to build-up during electro dialysis, it should be made as small as possible to derive meaningful values for \bar{t}_i .

2.6 Transport Properties of Anion Exchange membranes in contact with Hydrochloric Acid Solutions. Membranes for Acid recovery by Electrodialysis

Boudet-Dumy *et al.*⁽⁴⁸⁾ have recently investigated chloride ion fluxes through *Selemion* AAV and ARA Morgane membranes specially designed for the recovery of acids by ED. In addition, measurement of the electrical conductance of the membranes and of the amount of sorbed electrolyte (HCl), at equilibrium, have been carried out. The analysis of the results suggested a low dissociation degree of acid present in the membrane. The lower dissociation of sorbed acid is a factor which decreases the proton leakage of the anion-exchange membrane. It was also shown that the flux of chloride ions from the anode to the cathode steadily increased as the amount of sorbed electrolyte increased. This result means that chloride ions are associated with the movement of positively charged species. This fact may be due to the formation of an aggregate form such as $(H_4OCl)^+$ resulting from the solvation of a proton by a water

molecule and an HCl molecule - ion association inside the membrane overcoming the state of a neutral HCl molecule. This result confirms the role of ion association in the membrane.

2.7 Electrodialysis Applications

Electrodialysis applications and potential applications^(6 - 8, 33 - 39, 49 - 62) are widely discussed in the literature. Electrodialysis is a membrane based separation technique that is appealing because of its capability to deionize one stream while concentrating the electrolytes in another stream. Thus, ED produces a purified stream that can either be discharged or reused, and a concentrated electrolyte stream that can be disposed of or processed for reclamation of the dissolved salt. Some applications of ED include desalination of brackish waters⁽⁵⁶⁾, desalting of whey and stabilization of wine⁽⁵⁷⁾, purification of protein solutions⁽⁵⁸⁾, recovery of metals from plating rinse waters⁽³⁸⁾, recovery of acids⁽⁵⁹⁾, recovery of heavy metals from mining mill process⁽⁶⁰⁾, and the treatment of cooling-tower blowdown for water recovery and effluent volume reduction⁽⁶¹⁾.

When concentration polarization is absent in ED, there are two main causes of the decrease in current efficiency⁽⁶²⁾: Co-ion intrusion and counter-ion backdiffusion. Co-ion intrusion is the passage of co-ions through an ion-exchange membrane from the concentrate to the diluate, and is due to the electrical potential and concentration gradients across the membrane. Counter-ion backdiffusion is the backward passage of counter-ions through an ion-exchange membrane from the concentrate to the diluate due to a high concentration gradient across the membrane. The effects of counter-ion backdiffusion can be decreased by increasing stack voltage, that is, increasing the electrical potential driving force. However, such an increase in stack voltage is limited by the limiting current density and high energy costs. Co-ion intrusion can be reduced by using ion-exchange membranes that exclude co-ions to a greater degree.

Kononov *et al.*⁽³³⁾ have described the removal of hydrochloric acid from waste waters containing organic products. The possibility was demonstrated of concentrating hydrochloric acid by ED. The model effluent contained 4,4 g/l hydrochloric acid, 58 g/l sofolene-3 and 20 g/l chlorohydrin. At a current density of 10 mA/cm² a brine was obtained containing 51 g/l acid with a current efficiency of 35%. The low current efficiency is explained by diffusion of acid from the brine into the dialysate and the decrease in the selectivity of the membranes in contact with concentrated hydrochloric

acid solution (50 g/l).

Korngold⁽³⁴⁾ has described the recovery of sulphuric acid from rinsing waters used in a pickling process. Sulphuric acid was concentrated from 9 100 mg/l to 34 300 mg/l while the diluate contained 3 700 mg/l sulphuric acid. Approximately 70% of the sulphuric acid in the rinsing water could be recovered by ED treatment.

Urano *et al.*⁽³⁷⁾ have described concentration/desalination of model hydrochloric and sulphuric acid solutions in a laboratory scale conventional electro-dialyzer. Newly developed Selemion AAV anion-exchange membrane were used. The transport number for hydrogen ions of this membrane is much smaller than that of conventional anion-exchange membranes with the result that the acid could be efficiently concentrated. However, no acid feed and brine concentrations were given.

The concentration of carbonate solutions by ED was reported by Laskorin *et al.*⁽³⁵⁾. The feed solution had the following composition: sodium carbonate (4 to 7 g/l); sodium bicarbonate (4 - 7 g/l) and sodium sulphate (2 to 3 g/l). The total salt content of the solution did not exceed 15 g/l. The first series of experiments was carried out with liquid circulation in both the diluting and concentrating compartments. A linear liquid velocity and a current density of 5 to 6 cm/s and 20 mA/cm² was used, respectively. The duration of the desalting cycle was 1,5 to 2,0 hour. A fresh portion of feed was introduced after each desalting cycle. The portion of concentrate remained unchanged for 10 cycles. MKK cation- and MAK anion selective membranes were used. The brine concentration was increased from 22,9 g/l at the end of the first cycle to 87, 8 g/l at the end of the 10th cycle at a current efficiency of 81%. The diluate concentration at the end of the cycles varied between 0,16 and 0,47 g/l.

A second series of experiments was conducted without circulation of liquid through the brine compartments. The solvent entered the brine compartments as a result of electro-osmotic transport through the membranes. The brine salt content reached a value of 182,8 g/l after 3 cycles. The current efficiency varied between 70 and 75% and the electrical energy consumption was approximately 2,7 kWh/kg salt. A higher brine concentration was obtained without circulation of brine through the brine compartments.

Smagnin and Chukkin⁽³⁶⁾ have described concentration of caustic soda and sodium

chloride with ED. Caustic soda and sodium chloride concentrations of 0,07 and 1,07 mol/l, respectively, were chosen as the feed solutions. No circulation of brine was used in a conventional ED stack. The change of brine concentration in relation to the current density was determined. MA-40 and MK-40 ion-exchange membranes were used. Maximum brine concentrations of 346 g/l caustic soda and 365 g/l sodium chloride were obtained at current densities of 249 and 117 mA/cm², respectively.

3. THEORY

3.1 Theories of Membrane Transport

3.1.1 Nernst-Planck and Pseudo-Thermodynamic Treatments

Theories of membrane transport and the application of non-equilibrium thermodynamics to transport processes have been described by Meares *et al.*⁽⁹⁾.

Many of the earlier treatments of membrane transport use the Nernst-Planck equations to describe the relationships between the flows of the permeating species and the forces acting on the system^(10, 63) according to Meares *et al.* According to these equations the flux J_i of species i at any point is equal to the product of the local concentration c_i of i , the absolute mobility u_i of i , and the force acting on i . This force has been identified with the negative of the local gradient of the electrochemical potential μ_i of i . Thus, at a distance x from a reference plane at right angles to the direction of unidimensional flow through a membrane

$$J_i = -c_i u_i d\mu_i/dx \quad (3.1.1.1)$$

The electrochemical potential of i can be divided into its constituent parts giving in place of equation eq. (3.1.1.1)

$$J_i = -c_i u_i (RT d \ln c_i/dx + RT d \ln \gamma_i/dx + \bar{V}_i dp/dx + z_i F d\psi/dx) \quad (3.1.1.2)$$

where γ_i , \bar{V}_i , z_i , p , and ψ represent the activity coefficient, the partial molar volume, the valence charge on i , the hydrostatic pressure, and the electrical potential, respectively. R is the gas constant, T the absolute temperature, and F the Faraday. It is apparent from eq. (3.1.1.2) that the Nernst-Planck equations make use of the Nernst-Einstein relation between the absolute mobility u_i and the diffusion coefficient D_i of species i . This is

$$D_i = u_i RT \quad (3.1.1.3)$$

On replacing the electrochemical mobility in eq. (3.1.1.2) by the diffusion coefficient, the more usual form of the Nernst-Planck flux equation is obtained according to Meares *et al.*

$$J_i = -D_i \left(\frac{dc_i}{dx} + c_i \frac{d \ln \gamma_i}{dx} + \frac{c_i \bar{V}_i}{RT} \frac{dp}{dx} + \frac{c_i z_i F}{RT} \frac{d\psi}{dx} \right) \quad (3.1.1.4)$$

On the basis of the Nernst-Planck equations, the flow of species *i* is regarded as unaffected by the presence of any other permeating species except in so far as the other species either influences the force acting on *i* by, for example, affecting the values of γ_i or ψ , or alters the state of the membrane and hence alters the value of D_i .

To obtain relationships between the flows of the permeating species and the observable macroscopic differences in concentration, electrical potential, and hydrostatic pressure between the solutions on the two sides of the membrane, it is necessary to integrate the Nernst-Planck equation (eq. 3.1.1.4) for each mobile component across the membrane and the membrane/solution boundaries. In order to carry out this integration an additional assumption has to be made. The differences between the various treatments derived from the Nernst-Planck equations lie in the different assumptions used. For example, in the theory of Goldman⁽⁶³⁾, which is widely applied to biological membranes, it is assumed that the gradient of electrical potential $d\psi/dx$ is constant throughout the membrane. It is usually assumed also that thermodynamic equilibrium holds across the membrane/solution interfaces and that the system is in a steady state so that the flows J_i are constant throughout the membrane. Generally these integrations do not lead to linear relationships between the flows and the macroscopic differences of electrochemical potential between the two bathing solutions.

The main disadvantage of the Nernst-Planck approach according to Meares⁽⁹⁾ is that it fails to allow for interactions between the flows of different permeating species. Such interactions are most obvious when a substantial flow of solvent, usually water, occurs at the same time as a flow of solute. For example, during the passage of an electric current across a cation-exchange membrane, the permeating cations and anions both impart momentum to the water molecules with which they collide. Since the number of cations is greater than the number of anions, the momentum imparted to the water by the cations is normally greater than the momentum imparted by the anions and an electro-osmotic flow of water is set up in the direction of the cation current. The

resultant bulk flow of the water has the effect of reducing the resistance to the flow of cations and increasing the resistance to the flow of anions. This flow of water occurs under the difference of electrical potential and in the absence of a concentration gradient of water. The appropriate Nernst-Planck equation would predict no flow of water under these conditions according to Meares *et al.* Furthermore the flows of cations and anions differ from those which would be predicted from the respective Nernst-Planck equations on account of the effect of the water flow on the resistances to ionic flow.

This effect of solvent flow on the flows of solute molecules or ions can be allowed for by adding a correction term to the Nernst-Planck equations⁽⁹⁾. Thus, it can be written

$$J_i = -c_i u_i \, d\mu/dx + c_i v \quad (3.1.1.5)$$

where v is the velocity of the local centre of mass of all the species⁽¹¹⁾. The term $c_i v$ is often called the convective contribution to the flow of i and some authors have preferred to define v as the velocity of the local centre of volume.

The addition of this convection term to the Nernst-Planck equation for the flow of a solute is probably a sufficient correction in most cases involving only the transport of solvent and nonelectrolyte solutes across a membrane in which the solvent is driven by osmotic or hydrostatic pressure according to Meares *et al.* The situation is much more complex when electrolyte solutes are considered according to Meares *et al.* Even at low concentrations the flows of cations and anions may interact strongly with each other. Interactions between the different ion flows may be of similar size to their interactions with the solvent flow. Under these circumstances the convection-corrected Nernst-Planck equations may still not give a good description of the experimental situation regarding the ion flows.

The theoretical difficulties arising from interacting flows can be formally overcome by the use of theories of transport based on nonequilibrium thermodynamics. Such theories are described in the next section.

3.1.2 Treatments based on Nonequilibrium Thermodynamics

Since the original papers of Staverman⁽¹²⁾ and Kirkwood⁽⁶⁴⁾, many papers have appeared on the application of nonequilibrium thermodynamics to transport across synthetic and biological membranes. In particular, major contributions have been

made by Katchalsky, Kedem, and co-workers. In view of the appearance of extensive texts^(13, 14), this account is intended only as a brief summary of the general principles.

3.1.2.1 The Phenomenological Equations

The theory of nonequilibrium thermodynamics allows that, in a system where a number of flows are occurring and a number of forces are operating, each flow may depend upon every force. Also, if the system is not too far from equilibrium, the relationships between the flows and forces are linear. Therefore, the flow J_i may be written as follows

$$J_i = \sum_{\text{all } k} L_{ik} X_k \quad (3.1.1.6)$$

where the X_k are the various forces acting on the system and the L_{ik} are the phenomenological coefficients which do not depend on the sizes of the fluxes or forces. The flow J_i may be a flow of a chemical species, a volume flow, a flow of electric current, or a flow of heat. The forces X_k may be expressed in the form of local gradients or macroscopic differences across the membrane of the chemical potentials, electric potential, hydrostatic pressure, or temperature. If a discontinuous formulation is used so that the macroscopic differences in these quantities across the membrane are chosen as the forces, then the L_{ik} coefficients in eq. (3.1.1.6) are average values over the membrane interposed between a particular pair of solutions.

Equation (3.1.1.6) imply, for example, that the flow of a chemical species i is dependent not only on its conjugate force X_i , i.e., the difference or negative gradient of its own chemical or electrochemical potentials but also on the gradients or differences of the electrochemical potentials of the other permeating species. Hence eq. (3.1.1.6) imply that a difference of electrical potential may cause a flow of an uncharged species, a fact which, as previously indicated, the Nernst-Planck equations do not recognize according to Meares *et al.* In general, eq. (3.1.1.6) allow that any type of vectorial force can, under suitable conditions, give rise to any type of vectorial flow.

In a system where n flows are occurring and n forces are operating, a total of n^2 phenomenological coefficients L_{ik} are required to describe fully the transport properties of the system. This must be compared with the n mobilities used in the Nernst-Planck description of the system. A corresponding number n^2 experimental transport measurements would have to be made to permit the evaluation of all the L_{ik} coefficients.

Fortunately a simplification can be made with the help of Onsager's reciprocal relationship⁽¹³⁾. This states that under certain conditions

$$L_{ik} = L_{ki} \quad (3.1.1.7)$$

The conditions required for eq. (3.1.1.7) to be valid are that the flows be linearly related to the forces and that the flows and forces be chosen such that

$$T\sigma = \sum_i J_i X_i \quad (3.1.1.8)$$

where σ is the local rate of production of entropy in the system when the X_i are the local potential gradients. The quantity $T\sigma$ is often represented by the symbol Φ and called the dissipation function because it represents the rate at which free energy is dissipated by the irreversible processes. In fact there is no completely general proof of eq. (3.1.1.7) but its validity has been shown for a large number of situations⁽¹⁴⁾.

With the help of the reciprocal relationship the number of separate L_{ik} coefficients required to describe a system of n flows and n forces is reduced from n^2 to $\frac{1}{2}n(n + 1)$.

This nonequilibrium thermodynamic theory holds only close to thermodynamic equilibrium. The size of the departure from equilibrium for which the linear relationship between flow and force, eq. (3.1.1.6), and the reciprocal relationship, eq. (3.1.1.7), are valid, depends upon the type of flow considered. Strictly, the range of validity must be tested experimentally for each type of flow process. In the case of molecular flow processes, electronic conduction, and heat conduction the linear and reciprocal relationships have been found to be valid for flows of the order of magnitude commonly encountered in membranes⁽⁶⁵⁾. In describing the progress of chemical reactions the relationships are valid only very close to equilibrium. Systems in which chemical reactions are taking place will be excluded from this discussion.

3.1.2.2 The Choice of Flows and Forces

In an isothermal membrane system the most obvious choice of flows is the set of flows of the permeating species--solvent, nonelectrolyte solutes, and ions. The conjugate forces are then the differences or local gradients of the electrochemical potentials of these species. To accord with eq. (3.1.1.8), in which $T\sigma$ must be positive, increasing potentials in the direction of positive fluxes constitute negative forces. A set of

phenomenological equations corresponding to eq. (3.1.1.6) can be written relating the flows to the forces. The values of the L_{ik} coefficients appearing in these equations depend on the interactions occurring in the membrane, i.e., on the chemical nature of the permeating species and of the membrane, on the detailed microstructure of the membrane, and on the local concentrations of the permeating species.

In principle it should be possible to obtain values for the $\frac{1}{2}n(n + 1)$ L_{ik} coefficients by carrying out a suitable set of $\frac{1}{2}n(n + 1)$ independent experiments. For example, if all the forces except one, X_a , were held at zero and the flows J_i , J_j , etc. of all the n species were measured, then the values of the coefficients L_{ia} , L_{ja} etc. could be obtained directly. Similar experiments would give the values for the remaining L_{ik} coefficients. Other sets of experiments may be used, and one may combine experiments where some of the forces are kept at zero, experiments where some of the flows are kept at zero, and experiments where some forces and some flows are kept at zero⁽¹⁴⁾.

Although the set of flows and conjugate forces outlined above may seem to be convenient for the molecular interpretation of the interactions occurring in a membrane system, the equations written in terms of these flows and forces are not convenient for the design of experiments for the evaluation of the L_{ik} coefficients. For example, the forces which are usually controlled experimentally are not differences of electrochemical potential, but differences of concentration, electrical potential, and hydrostatic pressure. Also, it may be more convenient to measure the total volume of the flows across a membrane rather than the flow of solvent, or to measure the electric current and one ionic flow rather than two ionic flows. For these reasons, sets of practical flows and forces are often chosen to describe membrane transport⁽¹⁴⁾. These practical sets of flows and their conjugate forces must satisfy the relationship of eq. (3.1.1.8), which gives the dissipation function.

A system involving the transport of water and a nonelectrolyte solute across a membrane can be described by giving the flows of water J_w and of solute J_s . The conjugate forces are then the differences, or the local gradients, of the chemical potentials of water μ_w and solute μ_s . The transport properties of this system are described by the following equations:

$$J_w = L_w \Delta \mu_w + L_{ws} \Delta \mu_s \quad (3.1.1.9)$$

$$J_s = L_{sw} \Delta \mu_w + L_s \Delta \mu_s$$

where according to the reciprocal relationship $L_{sw} = L_{ws}$ and the dissipation function of the system is given by the expression

$$\Phi = J_w \Delta \mu_w + J_s \Delta \mu_s \quad (3.1.1.10)$$

When considering ideal external solutions the forces $\Delta \mu_w$ and $\Delta \mu_s$ are often expanded into separate terms giving the contributions of the concentration differences and pressure difference to the total driving forces. Thus

$$\Delta \mu_w = (RT/c_w) \Delta \bar{c}_w \Delta c_w + V_w \Delta p$$

Here V_w is an average partial molar volume of water and \bar{c}_w is an average concentration of water. When $\Delta \mu_w$ and $\Delta \mu_s$ in eq. (3.1.1.10) are expanded in this way and the resulting concentration and pressure terms are grouped separately the expression for the dissipation function becomes⁽⁵⁰⁾

$$\Phi = J_v \Delta p + J_D RT \Delta c_s \quad (3.1.1.11)$$

where J_v the total volume flow is equal to $(\bar{V}_w J_w + \bar{V}_s J_s)$ and J_D is equal to $(J_s/\bar{c}_s - J_w/\bar{c}_w)$. J_D is sometimes called the exchange flow and represents the apparent mean velocity of the solute relative to the water. According to eq. (3.1.1.11) the system can be described in terms of J_v and J_D as flows and Δp and $RT \Delta c_s$ (or $\Delta \pi_s$) as their conjugate forces. Thus

$$J_v = L_p \Delta p + L_{pD} \Delta \pi_s \quad (3.1.1.12)$$

$$J_D = L_{Dp} \Delta p + L_D \Delta \pi_s$$

where L_{Dp} equals L_{pD} and $\Delta \pi_s$ is the difference in osmotic pressure between the solutions. Experimentally it is easier to control the values of the forces appearing in eq. (3.1.1.12) than those appearing in eq. (3.1.1.9).

Similarly a system involving flows of water and a salt dissociated into a cationic species and an anionic species can be described in terms of the flows J_w , J_1 , and J_2 of these molecular species or by the set comprising the total volume flow, the electric current, and the defined flow of salt, i.e., J_v , I and J_s ⁽¹⁴⁾. In the former case the conjugate forces are the differences of the electrochemical potentials of the species across the membrane, in the latter case the conjugate forces are the pressure difference minus the osmotic pressure difference, the electrical potential difference, and the difference of the pressure-independent part of the chemical potential of the salt. Care must be taken in the precise definition of these forces, particularly of the electrical potential difference⁽⁶⁷⁾.

Since the choice of flows and forces is to some extent open as long as the flows and forces satisfy eq. (3.1.1.8) a set can be chosen primarily for ease of theoretical interpretation of L_{ik} coefficients or for ease of experimental evaluation of the L_{ik} coefficients. Furthermore, given values of the L_{ik} coefficients relevant to one set of flows and forces, it is a straightforward operation to calculate the values of L_{ik} coefficients relevant to another set of flows and forces⁽⁶⁷⁾.

It is of course possible and often convenient to describe the transport properties of a system in terms of flows and forces which are not conjugate and which do not obey eq. (3.1.1.8). The system where the membrane is permeated by a flow of water and a flow of a solute can be described in terms of the flow of water J_w , the flow of solute J_s , the pressure difference Δp , and the difference in concentration of the solute $RT\Delta c_s$ or $\Delta\pi_s$. These flows and forces are interrelated by the equations

$$J_v = L_p \Delta p - \sigma L_p \Delta \pi_s \quad (3.1.1.13)$$

$$J_s = \bar{c}_s (1 - \sigma) J_v + \omega \Delta \pi_s$$

Here L_p has the same significance as in eq. (3.1.1.12). σ is called the reflection coefficient of the solute and is equal to $\Delta p / \Delta \pi_s$ at zero J_v , ω is the solute permeability $J_s / \Delta \pi_s$ at zero J_v , and \bar{c}_s is the average concentration of the solute in the two solutions⁽⁶⁷⁾.

In practice eq. (3.1.1.13) may be easier to use than eq. (3.1.1.12) because the flows generally measured are J_v and J_s rather than J_w and J_D . However, eq. (3.1.1.13) are not

a proper set of phenomenological equations in the sense of eq. (3.1.1.6). Neither are σ and ω phenomenological coefficients in the sense used so far. They are related to the L_{ik} coefficients of eq. (3.1.1.12) by the relationships⁽⁶⁶⁾.

$$\sigma = -L_{pD}/L_p \text{ and } \omega = \bar{c}_s(L_p L_D - L_{pD}^2)/L_p$$

3.1.2.3 Uses and Limitations of the Theory

The theory of nonequilibrium thermodynamics has been applied to membranes in a number of papers where the aim has been to obtain general relationships between observable macroscopic flows and forces. Topics investigated in this way have included: isotopic tracer flows and flux ratios^(68, 69), electrokinetic phenomena⁽⁷⁰⁾, the transport properties of complex membranes⁽¹⁴⁾, and the coupling of transport processes with chemical reactions, so-called active transport⁽¹³⁾. However, the main concern of these investigations has been the transport of non-electrolyte solutes and ions across charged and uncharged membranes^(12, 13, 46).

The L_{ik} coefficients obtained from experimental measurements of transport phenomena under one set of conditions can either be used to predict values of flows and forces under other sets of conditions or they can be analyzed for the purpose of interpreting, at a molecular level, the various interactions which occur between the permeating molecules and ions and the membrane material. This second use of the L_{ik} coefficients is especially interesting but it is by no means simple.

An inspection of any of the sets of phenomenological equations [(3.1.1.6), (3.1.1.9), (3.1.1.12), and (3.1.1.13)] shows that nowhere is any direct reference made to the membrane or its properties. The L_{ik} coefficients relate the flows of the permeating species to the gross thermodynamic forces acting on these species and, in general, no particular coefficient represents only the interaction of a permeating species with the membrane. Instead the properties of the membrane material affect the values of each of the L_{ik} coefficients to a greater or lesser extent.

The physical interpretation of measurements of transport properties is made more straightforward by inverting the matrix of the phenomenological equations [eq. (3.1.1.6)] to give the set of eqs. (3.1.1.14)

$$X_i = \sum_{\text{all } k} R_{ik} J_k \quad (3.1.1.14)$$

These represent the forces as linear functions of the flows. The R_{ik} and L_{ik} coefficients of eq's. (3.1.1.14) and (3.1.1.6) are related by the expression

$$R_{ik} = A_{ik} / |L| \quad (3.1.1.15)$$

where A_{ik} is the minor of L_{ik} and $|L|$ is the determinant of the L_{ik} coefficients. If the reciprocal relation is valid for the L_{ik} coefficients, it is valid also for the R_{ik} coefficients. Whereas the L_{ik} coefficients have the dimensions of conductance (i.e., flow per unit force), the R_{ik} coefficients have the dimensions of resistance (i.e., force per unit flow) and are frequently called resistance coefficients.

The R_{ik} coefficients are easier to interpret at the molecular level than the L_{ik} coefficients. A non-zero R_{ik} ($i \neq k$) implies a direct interaction between i and k , that is, the molecular flow of k directly causes a force to act on species i . On the other hand, a non-zero L_{ik} ($i \neq k$) does not necessarily imply a direct molecular interaction between species i and k , it means that the force acting on k affects the flow of i , perhaps directly or indirectly.

In effect eq. (3.1.1.14) means that, in the steady state, the gross thermodynamic force X_i acting on species i is balanced by the forces $R_{ik}J_k$ summed over all species k , including i . The term $R_{ii}J_i$ is the drag force per mole which would act on i when moving at a rate J_i/c_i through a medium where there was no net flow of any other species. Thus the R_{ii} coefficients are still complex quantities including contributions from the interactions between i and all other species present, including the membrane. However, each R_{ik} ($i \neq k$) coefficient represents only the single interaction between the flows of i and k . The R_{ii} coefficients, like the L_{ii} , must always be positive but R_{ik} ($i \neq k$) and the L_{ik} coefficients may be positive, negative, or zero.

3.1.3 The Frictional Model of Membrane Transport

The frictional model of membrane transport has been described by Meares *et al.*⁽⁹⁾. The idea of describing steady-state transport processes in a membrane as balances between the gross thermodynamic forces acting on the system and frictional interactions between the components of the system is one of long standing. More recently, the term molecular friction coefficient has been applied to the coefficient which relates the frictional force between two components to the difference between their

velocities. This approach has been used to describe transport processes across membranes by several authors. The precise treatment that will be considered here is the frictional model as proposed by Spiegler⁽⁷¹⁾.

The fundamental statement of the frictional model is that when the velocity of a permeating species has reached a constant value, the gross thermodynamic force X_i acting on one mole of that species must be balanced by the interactive forces, F_{ik} , acting between one mole of the same species and the other species present. Mathematically this is expressed by

$$X_i = - \sum_{k \neq i} F_{ik} \quad (3.1.3.1)$$

Furthermore, these interactions are assumed to be frictional in character so that each force F_{ik} is equal to a friction coefficient f_{ik} multiplied by the difference between the velocities v_i and v_k of the two species. Thus

$$F_{ik} = -f_{ik}(v_i - v_k) \quad (3.1.3.2)$$

and

$$X_i = \sum_{k \neq i} f_{ik}(v_i - v_k) \quad (3.1.3.3)$$

It should be noted that f_{ik} is the force acting on one mole of i owing to its interaction with the amount of k normally in the environment of i and under unit difference between the mean velocities of i and k . In general the concentrations of i and k are not equal and consequently the coefficients f_{ik} and f_{ki} are not equal. When the balance of forces is taken over unit volume of the system it is readily seen that

$$c_i f_{ik} = c_k f_{ki} \quad (3.1.3.4)$$

The quantity f_{ik}/c_k or f_{ki}/c_i represents the force acting between one mole of i and one mole of k at unit velocity difference. Its value obviously depends on the chemical types of the two species.

Besides containing a term such as $f_{ik}(v_i - v_k)$ for the interactions between i and each of the other permeating species, the right-hand side of eq. (3.1.3.3) also includes a term

$f_{im}(v_i - v_m)$ which allows for the interaction between i and the membrane. Usually the membrane is taken as the velocity reference so that v_m is zero.

With the help of the relationship

$$J_i = c_i v_i \quad (3.1.3.5)$$

eq. (3.1.3.3) can be rearranged to

$$X_i = (J_i/c_i) \frac{\sum_{K \neq i} f_{ik}}{K \neq i} - \frac{\sum_{K \neq i} (J_K f_{ik}/c_K)}{K \neq i} \quad (3.1.3.6)$$

Equation (3.1.3.6) has the same form as eq. (3.1.1.14) which relate the forces to the flows via the R_{ik} coefficients. Each R_{ik} coefficient can be equated to the corresponding $\sum f_{ik}/c_i$. This illustrates the complex nature of the R_{ik} coefficient. Each R_{ik} ($i=k$) coefficient is equivalent to the corresponding $-f_{ik}/c_k$.

In a system with n flows, $(n - 1)$ friction coefficients are required to describe the interactions of any one permeating species with the other permeating species. One further coefficient is required to describe its interaction with the membrane. A total of n^2 friction coefficients is thus required to describe the transport properties of the system but with the use of eq. (3.1.3.4) this number is reduced to $\frac{1}{2}n(n + 1)$, i.e., the same as the minimum number of independent L_{ik} or R_{ik} coefficients. Hence the minimum number of experimental measurements required to characterize the system fully is the same whether it is described in terms of the L_{ik} coefficients, the R_{ik} coefficients, or the f_{ik} coefficients. The most convenient set of experimental parameters to be measured may depend on which set of coefficients is chosen to represent the properties of the system.

The choice of coefficients can be made mainly on the basis of experimental convenience because, having obtained values of one set of coefficients, it is no problem to obtain values for the other sets from these. The relationships between the R_{ik} and L_{ik} coefficients, and between these and the friction coefficients have already been given briefly above and are discussed in more detail elsewhere⁽⁹⁾. Direct relationships between the friction coefficients and experimentally measurable quantities have also been discussed in several papers⁽⁹⁾. The method of obtaining one such relationship is mentioned here as an illustration of Spiegler's treatment.

In a system consisting of a membrane, water, one species of univalent cation and one species of univalent anion, the electrical conductivity k is given by the expression

$$k = F(J'_1 - J'_2) \quad (3.1.3.7)$$

where J'_1 and J'_2 are the flows of univalent cations and anions per unit area, respectively, under an electrical potential gradient of 1 V cm^{-1} . Under these conditions the forces acting on the cations, anions and water are F , $-F$, and $0 \text{ J cm}^{-1} \text{ mole}^{-1}$, respectively. On substituting these forces into the set of eqs. (3.1.3.6) describing the system, the equations can be solved for the flows J'_1 and J'_2 in terms of the friction coefficients and the concentrations of the ions and water. These expressions for J'_1 and J'_2 can then be substituted into eq. (3.1.3.7) to give an expression for k in terms of the friction coefficients operating in the system and the concentrations of the permeating species.

It is possible to obtain expressions for other transport parameters, such as the electro-osmotic permeability, transport numbers of the ions, and the self-diffusion coefficients of the permeating species in terms of the friction coefficients in a somewhat similar manner. A set of such expressions can then be solved to give the individual friction coefficients in terms of the transport parameters and the concentrations.

The procedure outlined above becomes rather tedious as the expressions giving the individual transport parameters in terms of the friction coefficients may be very complicated. Under certain circumstances a simpler procedure can be used to obtain values for the friction coefficients⁽⁹⁾.

The main advantage claimed for the use of the frictional model to describe transport processes in membranes, is that each friction coefficient represents the interaction between a particular pair of flows. They are not complex combinations of several interactions as are the L_{ik} and R_{ij} coefficients. The model also permits a direct evaluation of the interactions between the various permeating species and the membrane, interactions which are hidden in treatments which use only the L_{ik} and R_{ik} coefficients.

It may be possible under favourable conditions to neglect some of the frictional interactions on the basis of previous knowledge of the properties of the membrane and permeants. A smaller number of experimental measurements is then necessary to describe the system. For example Spiegler⁽⁷¹⁾ suggested that, in a system where a

cation-exchange membrane is in equilibrium with a dilute electrolyte solution, the friction coefficient f_{12} (where 1 represents cations and 2 represents anions) can be set equal to zero because of the low concentration of diffusible anions.

Simplifications such as that described above should be made only with great care. It is possible that even though f_{ik} may be negligibly small f_{ki} may be quite large because the ratio c_k/c_i [c.f. eq. (3.1.3.4)] may be large. In such a case the full number of experimental measurements must still be made.

The quantitative application of the frictional model to biological membrane systems is restricted by the difficulty of measuring or estimating values for the average or local concentrations of the permeating species in the membrane. These values are required for the calculation of the friction coefficients from the measured experimental parameters. Thus, although values for sets of L_{ik} coefficients (particularly L_p , σ , and ω) have been obtained for some biological systems, it has been possible to interpret these in terms of the friction coefficients in only a qualitative manner⁽⁹⁾. With homogeneous synthetic resin membranes the situation seems to be simpler. Some limited measurements of friction coefficients for such systems have been reported⁽⁹⁾.

3.2 Conductance and Transport Number

3.2.1 Conductance and Transport Number and their Relation to Flows and Forces in Electrodialysis

The author has derived the following relationships for conductance and transport number and their relation to flows and forces in electrodialysis

Consider a system consisting of two aqueous solutions containing only one permeable electrolyte separated by a membrane⁽¹⁴⁾. Different concentrations, pressures, and electrical potentials are allowed on both sides of the membrane. Envisage further the operation of two forces with two conjugated flows which may pass from one side of the membrane to the other. The simplest choice of flows and forces would be the flow of cation J_1 , driven by the difference in electrochemical potential $\Delta\hat{\mu}_1$, and the flow of anion J_2 , driven by the corresponding force $\Delta\hat{\mu}_2$. The following simple phenomenological equations can then be set-up⁽¹³⁾. (see eq. 3.1.1.6)

$$J_1 = L_1 \Delta \hat{\mu}_1 \quad (3.2.1)$$

$$J_2 = L_2 \Delta \hat{\mu}_2 \quad (3.2.2)$$

where L_1 and L_2 are the phenomenological coefficients which characterize the system.

The chemical potential of the electrolyte, $\Delta \mu_s$, is equal to the electrochemical potentials of the cation and the anion⁽¹⁴⁾.

$$\Delta \mu_s = \Delta \hat{\mu}_1 + \Delta \hat{\mu}_2 \quad (3.2.3)$$

The electrical current, I , through a membrane is related to the ionic flows by the relationship⁽¹³⁾.

$$I = (z_1 J_1 + z_2 J_2) F \quad (3.2.4)$$

where z_1 = valence of cation; z_2 = valence of anion; F = Faraday's constant.

When $I = 0$, then $J_1 = J_2$

The electromotive force, E , acting on the system can be determined by introducing a pair of electrodes reversible to one of the ions, say ion 2, and measuring the potential difference. The value of E is related thermodynamically to the difference in electrochemical potential of ion 2⁽¹⁴⁾:

$$E = \frac{\Delta \hat{\mu}_2}{z_2 F} \quad (3.2.5)$$

for NaCl, $z_2 = -1$

$$\text{and } E = \frac{\Delta \hat{\mu}_2}{-F} \quad (3.2.6)$$

$$\text{or } EF = -\Delta \hat{\mu}_2 \quad (3.2.7)$$

Membrane conductance is usually carried out under isothermal, isobaric conditions with constant salt concentrations across the membrane.

$$\text{when } \Delta\mu_s = 0, \text{ then } \Delta\tilde{\mu}_1 = -\Delta\tilde{\mu}_2 \quad (3.2.8)$$

The electric current, I , through the membrane is:

$$I = F(J_1 - J_2) \quad (3.2.9)$$

Substituting eq. (3.2.1) and (3.2.2) into eq. (3.2.9), gives

$$I = F(L_1\Delta\tilde{\mu}_1 - L_2\Delta\tilde{\mu}_2) \quad (3.2.10)$$

$$\text{But, } \Delta\tilde{\mu}_1 = -\Delta\tilde{\mu}_2 \quad (\text{see eq. 3.2.8})$$

$$\therefore I = F(-L_1\Delta\tilde{\mu}_2 - L_2\Delta\tilde{\mu}_2) \quad (3.2.11)$$

$$= -F\Delta\tilde{\mu}_2(L_1 + L_2) \quad (3.2.12)$$

$$\text{But } EF = -\Delta\tilde{\mu}_2 \quad (\text{see eq. 3.2.7})$$

$$\therefore I = F^2E(L_1 + L_2)$$

$$\therefore \left[\frac{I}{E} \right]_{\Delta\mu_s = 0, J_v = 0} = F^2(L_1 + L_2) = \text{Conductance} \quad (3.2.13)$$

when $I = 0$, then

$$J_1 - J_2 = 0 \quad (3.2.14)$$

Substituting eqs. (3.2.1) and (3.2.2) into eq. (3.2.14) gives

$$L_1\Delta\tilde{\mu}_1 - L_2\Delta\tilde{\mu}_2 = 0 \quad (3.2.15)$$

$$\text{But } \Delta\tilde{\mu}_1 = \Delta\mu_s - \Delta\tilde{\mu}_2 \quad (\text{see eq. 3.2.3})$$

$$L_1 (\Delta \mu_s - \Delta \tilde{\mu}_2) - L_2 \Delta \tilde{\mu}_2 = 0 \quad (3.2.16)$$

$$\text{and } \Delta \tilde{\mu}_2 = \frac{L_1}{L_1 + L_2} \Delta \mu_s \quad (3.2.17)$$

$$\text{or } -EF = \frac{L_1}{L_1 + L_2} \Delta \mu_s \quad (3.2.18)$$

$$\therefore \left[\frac{EF}{\Delta \mu_s} \right]_{I=0, J_v=0} = - \frac{L_1}{L_1 + L_2} \quad (3.2.19)$$

$$\text{Consider } \left[\frac{J_1/I}{\Delta \mu_s} \right]_{\Delta \mu_s = 0} = \frac{L_1 \Delta \tilde{\mu}_1}{F^2 E (L_1 + L_2)} \quad (3.2.20)$$

But $\Delta \tilde{\mu}_1 = -\Delta \tilde{\mu}_2$ and $EF = -\Delta \tilde{\mu}_2$

$$\therefore \left(\frac{J_1/I}{\Delta \mu_s} \right)_{\Delta \mu_s = 0} = \frac{L_1 (-\Delta \tilde{\mu}_2)}{-\Delta \tilde{\mu}_2 (L_1 + L_2) \cdot F} \quad (3.2.21)$$

$$= \frac{1}{F} \cdot \frac{L_1}{L_1 + L_2} \quad (3.2.22)$$

$$\therefore \left[\frac{JF/I}{\Delta \mu_s} \right]_{\Delta \mu_s = 0; J_v = 0} = \frac{L_1}{L_1 + L_2} \quad (3.2.23)$$

$$= \Delta t \text{ (transport number)} \quad (3.2.23)$$

$$= - \left(\frac{EF}{\Delta \mu_s} \right)_{I=0; J_v=0} \quad (3.2.24)$$

Note: The membrane potential $\Delta \Psi$ is related to the electromotive force measured between reversible electrodes by the expression⁽¹³⁾:

$$\Delta \Psi = E - \frac{\Delta \tilde{\mu}_2}{z_2 F}$$

3.3 Ion Coupling from Conventional Transport Coefficients

3.3.1 Ion Association and the Coupling of Flows

Kedem⁽¹⁵⁾ has described ion association and coupling of flows, charged hydrophobic membranes and the association model, transport properties and transport coefficients in the absence of volume flows and transport coefficients in the absence of a pressure gradient.

Anions and cations will exist in part as neutral ion pairs or molecules when the dielectric constant of the membrane is low. Three mobile species can be identified in the membrane phase according to Kedem: free anion, free cation and ion pair (only a univalent electrolyte will be considered). The dissipation function for ion flows, in this case, can be expressed either in terms of the two stoichiometric ion flows, J_1 and J_2 , or in terms of three species: free ion, J_1^* and J_2^* , and neutral molecule, J_s . Assuming dissociation equilibrium, the thermodynamic potential of the molecule is equal to that of the sum of the ions:

$$X_s = X_1 + X_2 \quad (3.3.1)$$

The relation between J_1 and J_1^* is:

$$J_1 = J_1^* + J_s \quad (3.3.2)$$

$$J_2 = J_2^* + J_s$$

and thus the two species dissipation function

$$\phi = J_1 X_1 + J_2 X_2$$

is equal to the three flow expression

$$\phi = J_1^* X_1 + J_2^* X_2 + J_s X_s = (J_1 - J_s) X_1 + (J_2 - J_s) X_2 + (X_1 + X_2) J_s$$

Assuming that no frictional interactions exist between the free ions and the neutral molecule and that volume flow is either negligible or absent, a linear relationship between flows and forces can be described by the following set of equations:

$$X_1 = R_{11}^* J_1^*; \quad X_2 = R_{22}^* J_2^*; \quad X_s = R_s J_s \quad (3.3.3)$$

Equations (3.3.1), (3.3.2) and (3.3.3) give:

$$R_{11}^*(J_1 - J_s) + R_{22}^*(J_2 - J_s) = R_s J_s \quad (3.3.4a)$$

from which J_s is expressed in terms of individual resistance coefficients of the three mobile species and the flow of the free ions,

$$J_s = \frac{R_{11}^* J_1^* + R_{22}^* J_2^*}{\Sigma R} \quad (3.3.4b)$$

where $\Sigma R = R_s + R_{11}^* + R_{22}^*$.

From the relations one obtains the phenomenological equations which describe the total stoichiometric ionic flows and forces by means of the individual resistance coefficients of the free and associated mobile species:

$$X_1 = R_{11}^* \left(1 - \frac{R_{11}^*}{\Sigma R} \right) J_1 - \frac{R_{11}^* R_{22}^*}{\Sigma R} J_2 \quad (3.3.5)$$

$$X_2 = - \frac{R_{11}^* R_{22}^*}{\Sigma R} J_1 + R_{22}^* \left(1 - \frac{R_{22}^*}{\Sigma R} \right) J_2$$

The corresponding resistance coefficients are:

$$R_{11} = R_{11}^* \frac{R_{22}^* + R_s}{R_{11}^* + R_{22}^* + R_s}$$

$$R_{22} = R_{22}^* \frac{R_{11}^* + R_s}{R_{11}^* + R_{22}^* + R_s} \quad (3.3.6)$$

$$R_{12} = - \frac{R_{11}^* R_{22}^*}{R_{11}^* + R_{22}^* + R_s}$$

The relative importance of the ion-coupling, according to Kedem, is best expressed in terms of the degree of coupling, $q^2 = R_{12}^2 / R_{11} R_{22}$, where $q^2 = 1$ means that the coupling between the flows is complete, and $q^2 = 0$ indicates absence of coupling⁽⁷²⁾.

For the case of ion association, this coefficient is given by:

$$q^2 = \frac{R_{11}^* R_{22}^*}{(R_s + R_{11}^*)(R_s + R_{22}^*)} \quad (3.3.7)$$

If $R_s \gg R_{11}^*$ and $R_s \gg R_{22}^*$ then $R_{11} \approx R_{11}^*$, $R_{22} \approx R_{22}^*$ and $q^2 \rightarrow 0$; i.e. there is no significant coupling. If, on the other hand, R_s is much smaller than the R_i^* terms, coupling can be practically complete.

The physical significance of these limits becomes clear if we introduce concentration and friction coefficients for the R's, $R_{ii} = f_i / c_i$.

To discuss the orders of magnitude, let us take all f_i 's approximately equal; then

$$q^2 \approx \frac{c_s^2}{(c_s + c_1^*)(c_s + c_2^*)} \quad (3.3.8)$$

Negligible coupling, i.e. $q^2 \rightarrow 0$, is found when the concentration of the free ion are much larger than the concentrations of associated molecules; on the other hand, strong association leads to a high degree of coupling, that is $q^2 \rightarrow 1$. In other words, the degree of coupling and degree of association are closely related.

Consider first a matrix, which does not carry fixed charges, i.e. $c_1^* = c_2^* = c^*$. The expression for the coupling coefficient will be given by

$$q^2 \cong \frac{c_s^2}{(c_s + c^*)^2} \quad (3.3.9)$$

For slight association expected in high dielectric media, $c_s \ll c^*$ and:

$$q^2 \cong \frac{c_s^2}{2c_s c^* + c^{*2}} = \frac{(c_s/c^*)^2}{1 + 2 c_s/c^*} \rightarrow 0 \quad (3.3.10)$$

No coupling will thus be observed.

In these media q^2 also remains small in the presence of fixed charges, i.e.

$$c_1^* \neq c_2^*$$

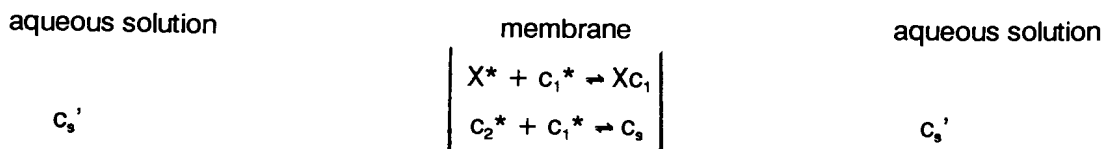
For slight dissociation, as is to be expected in hydrophobic membranes, $c_s \gg c^*$, and:

$$q^2 \cong \frac{1}{(1 + c^*/c_s)^2} \rightarrow 1 \quad (3.3.11)$$

The presence of fixed charges in hydrophobic membranes complicates the analysis of coupling effects, according to Kedem and requires a detailed consideration of a model.

3.3.2 Charged Hydrophobic Membranes - The Association Model

Consider a polymeric membrane matrix with chemically bound ionizable groups at a total concentration of X_t , and low water content⁽⁷³⁾. Several ion-exchange and dissociation equilibria are established when immersing such a membrane in an aqueous salt solution with a concentration c_s' .



Assuming ideality in the aqueous solutions, dissolution equilibria of the free counter-ion c_1^* and free co-ion c_2^* between the membrane and the aqueous solution are obtained

by equating the electrochemical potentials in the two phases:

$$\begin{aligned}\tilde{\mu}_1' &= \mu_1^{\circ'} + RT \ln c_1' + z_1 F \psi' = \mu_1^{\circ} + RT \ln c_1^* + z_1 F \psi = \tilde{\mu}_1 \\ \tilde{\mu}_2' &= \mu_2^{\circ'} + RT \ln c_2' + z_2 F \psi' = \mu_2^{\circ} + RT \ln c_2^* + z_2 F \psi = \tilde{\mu}_2.\end{aligned}\quad (3.3.12)$$

Adding the respective terms and applying the condition for ion pair formation reaction in the membrane: $\mu_s = \tilde{\mu}_1 + \tilde{\mu}_2$, we obtain after rearrangement:

$$c_s = k c_s'^2 \quad (3.3.13)$$

where c_s' is the concentration of the fully dissociated salt in water; c_s is the concentration of the undissociated salt in the membrane phase; c_1^* , c_2^* are the concentrations of free ions in the membrane; and $k = \exp [(\mu_s^{\circ} - \mu_1^{\circ'} - \mu_2^{\circ'})/RT]$.

Ion pair formation between the small ions is expressed by:

$$\frac{c_1^* c_2^*}{c_s} = K_d^s \quad c_s = c_2^t - c_2^* \quad (3.3.14)$$

where c_2^t , c_s indicate the concentration of the total and the undissociated salt in the membrane phase. Ion pair formation at the fixed ionic sites is given by:

$$\frac{c_1^* X^*}{(X_t - X^*)} = K_d^f \quad (3.3.15)$$

where X_t is the total concentration of fixed groups and X^* is its free fraction. Introducing electroneutrality for the dissociated species, $c_1^* = c_2^* + X^*$, into the above expressions and rearranging the equations for the modified Donnan equilibrium for non-aqueous membranes, we obtain a polynomial of 3rd degree with respect to c_2^* :

$$K_d^f c_2^{*3} + (K_d^f X_t + \alpha) c_2^{*2} - K_d^f \alpha c_2^* - \alpha^2 = 0 \quad (3.3.16)$$

$$\text{where } \alpha = K_d^s k c_s'^2$$

The adsorption isotherm of the co-ions, c_2^t , is given from the above relations by

$$c_2^t = c_2^* + c_s = c_2^* + \alpha/K_d^s \quad (3.3.17)$$

For analysis of the coupling coefficient, explicit expressions for the concentrations of the co-ion or counter-ion are obtained from eqs. (3.3.14) and (3.3.15) and the

electroneutrality condition:

for free co-ions:

$$c_2^* = \frac{K_d^s}{K_d^f} \left[\frac{c_2^t - c_2^*}{X_t - X^*} \right] X^* \quad (3.3.18)$$

for free counter-ions:

$$c_1^* = \left(\frac{K_d^s}{K_d^f} \left[\frac{c_2^t - c_2^*}{X_t - X^*} \right] + 1 \right) X^* \quad (3.3.19)$$

for small dissociation:

$$c_2^* \ll c_2^t \cong c_s \text{ and } X^* \ll X_t$$

At these conditions, free co-ion concentration becomes

$$c_2^* \cong m c_2^t a \quad (3.3.20)$$

where

$$m = K_d^s/K_d^f \text{ and } a = X^*/X_t \ll 1$$

Free counter-ion concentration is given by

$$c_1^* \cong m c_2^t a + X^* = a(m c_2^t + X_t) \quad (3.3.21)$$

Coupling coefficient is thus given by

$$q^2 = \frac{1}{(1 + c_1^*/c_s) (1 + c_2^*/c_s)} \cong \frac{1}{(1 + c_1^*/c_2^t) (1 + c_2^*/c_2^t)} \cong \frac{1}{1 + c_1^*/c_2^t} \quad (3.3.22)$$

High coupling $q^2 \rightarrow 1$ is obtained when $c_1^*/c_2^t \ll 1$;

$$\frac{c_1^*}{c_2^t} = a \frac{(m c_2^t + X_t)}{c_2^t} = a(m + X_t/c_2^t) \quad (3.3.23)$$

According to Kedem, high coupling will be observed in non-charged hydrophobic membranes with small salt dissociation constants; in charged hydrophobic membranes a high degree of coupling will be observed only in the case of large salt invasion.

3.3.3 Transport Properties and Transport Coefficients in the Absence of Volume Flow

Phenomenological equations for two stoichiometric ionic flows in the absence of volume flow is given by:

$$X_1 = R_{11}J_1 + R_{12}J_2 \quad (3.3.24)$$

$$X_2 = R_{21}J_1 + R_{22}J_2$$

with $R_{12} = R_{21}$

Electric current, electric potential and concentration are measured in practice and the conventional transport coefficients are defined accordingly. The relation between the driving forces and the R_{ij} 's are obtained from the constraints imposed for each measurement. The expression for driving force for ion transport, i.e. the difference in the electrochemical potential for equal concentrations on both sides of the membrane, is given by:

$$X_i = \Delta \tilde{\mu}_i = -z_i F E \quad (3.3.25)$$

So that

$$X_1 + X_2 = 0 \quad (3.3.26)$$

3.3.3.1 Electric conductance

Membrane conductance, κ , is:

$$\kappa = \left(\frac{I}{E} \right)_{\Delta\mu = 0; J_v = 0} \quad (\text{see eq. 3.2.13})$$

where the electric current, I , is given by

$$I = F(z_1 J_1 + z_2 J_2) \quad (\text{see eq. 3.2.4})$$

The current I can be expressed in terms of resistance coefficients and two driving forces by substituting eq. (3.3.24) into eq. (3.3.26).

$$\therefore J_2 = - \frac{R_{11} + R_{12}}{R_{22} + R_{12}} J_1 \quad (3.3.27)$$

Introducing J_2 from eq. (3.3.27) into eq. (3.3.24), and rearranging, gives:-

$$X_1 = R_{11} J_1 - \frac{R_{12}(R_{11} + R_{12})J_1}{R_{22} + R_{12}} = \frac{R_{11}R_{22} - R_{12}^2}{R_{22} + R_{12}} J_1 \quad (3.3.28)$$

From eqs. (3.2.4), (3.3.27) and (3.3.28), the current is

$$I = (J_1 - J_2) = \frac{R_{11} + R_{22} + 2R_{12}}{R_{11}R_{22} - R_{12}^2} X_1 \quad (3.3.29)$$

and the conductance, κ , is

$$\frac{\kappa}{F^2} = \left(\frac{I}{E} \right) \frac{1}{F^2} = \frac{J_1 - J_2}{X_1} = \frac{R_{11} + R_{22} + 2R_{12}}{R_{11}R_{22} - R_{12}^2} \quad (3.3.30)$$

3.3.3.2 Transport numbers

Transport numbers $t_{1,2}$ are defined as the fraction of the electric current carried by each of the ions, without concentration gradients. In practice, membrane potentials are measured assuming Onsager's symmetry.

The transport numbers in terms of the R_{ij} 's are:

$$t_1 = \frac{J_1}{J_1 - J_2} = \frac{R_{22} + R_{12}}{R_{11} + R_{22} + 2R_{12}} \quad (3.3.31)$$

$$t_2 = 1 - t_1 = \frac{R_{11} + R_{12}}{R_{11} + R_{22} + 2R_{12}} \quad (3.3.32)$$

The product of t_1 and t_2 is

$$t_1 t_2 = \frac{(R_{11} + R_{12})(R_{22} + R_{12})}{(R_{11} + R_{22} + 2R_{12})^2} \quad (3.3.33)$$

3.3.3.3 Salt permeability

Salt permeability or salt "leak", ω_s , is measured in the absence of electric current, so that

$$J_1 = J_2 = J_s \quad (3.3.34)$$

The driving force for salt flow is the gradient of its thermodynamic potential:

$$X_s = X_1 + X_2 \quad (3.3.35)$$

Adding the respective terms from eq. (3.3.24) gives:

$$X_s = (R_{11} + R_{22} + 2R_{12}) J_s \quad (3.3.36)$$

and

$$\frac{J_s}{X_s} = \omega_s c_s^{\text{av}} = \frac{1}{R_{11} + R_{22} + 2R_{12}} \quad (3.3.37)$$

where c_s^{av} is mean salt concentration on the two membrane sides.

3.3.3.4 Correlation between $\kappa_1, t_{1,2}$ and ω_s

In aqueous charged ion-exchange membranes where the total amount of co-ions is very small compared to that of the counter-ions, the electro-neutral salt leak will become a very small fraction of total membrane conductance. Comparing the expression for the leak-conductance (LC) ratio obtained from eqs. (3.3.30) and (3.3.37), the following equation is obtained:

$$\frac{\omega_s c_s^{av}}{\kappa/F^2} = \frac{R_{11} R_{22} - R_{12}^2}{(R_{11} + R_{22} + 2R_{12})^2} \quad (3.3.38)$$

This and the expression for the product of the transport numbers, eq. (3.3.33), shows that

$$\frac{\omega_s c_s^{av}}{\kappa/F^2} = t_1 t_2 - \frac{R_{12}}{R_{11} + R_{22} + 2R_{12}} = t_1 t_2 - R_{12} \omega_s c_s^{av} \quad (3.3.39)$$

In the case of zero volume flow and no coupling between the co- and counter-ions $R_{12} = 0$; a plot of the permeability ratio vs. the product of the two transport numbers should give a straight line with slope of 1, intersecting the origin:

$$\frac{\omega_s c_s^{av}}{\kappa/F^2} = t_1 t_2 \quad (3.3.40)$$

In general, $R_{12} \neq 0$ should lead to a substantial deviation from this curve which will depend on the type and the extent of coupling.

Mutual drag reflects positive coupling between ion flows by any type of mechanism and is represented by a negative value of R_{12} . In this case the relation between the LC ratio and the product of the two transport numbers will be characterized by an inequality.

$$\frac{\omega_s c_s^{av}}{\kappa/F^2} > t_1 t_2 \quad (3.3.41)$$

An estimate of R_{12} is readily obtained from measured values of salt leak, membrane conductance and transport numbers as is shown in eq. (3.3.42).

$$- R_{12} = \frac{1}{\kappa/F^2} - \frac{t_1 t_2}{\omega_s c_s^{av}} \quad (3.3.42)$$

3.3.4 Transport Coefficients in the Absence of a Pressure Gradient

In practice, membrane conductance is usually measured in open cells with atmospheric pressure on both sides of the membrane and with equal salt concentrations. Under these conditions, volume flow is in general not zero. Thus in charged membranes, electro-osmotic volume flow is to be expected.

The electric conductance $(I/E)_{\Delta p = 0} \equiv \kappa'$ is related to κ by⁽¹⁴⁾

$$\kappa' \equiv \frac{\kappa}{1 + P_E \beta} \quad (3.3.43)$$

where κ and P_E are the electric conductance and the electro-osmotic pressure respectively, measured under conditions of zero volume flow and salt gradient, and β is the electro-osmotic permeability, measured at zero pressure and salt gradient.

For a homogeneous charged membrane has β and P_E opposite signs⁽¹⁴⁾, and

$$\beta = - \frac{P_E L_p}{\kappa} \quad (3.3.44)$$

L_p and κ are straight coefficients and therefore always positive. This implies that $\kappa' > \kappa$, i.e. electro-osmosis enhances membrane conductivity as a consequence of water-ion frictional drag; its direction is that of counter-ion flow. Similarly salt permeability is usually measured at zero pressure and osmotic flow is allowed to take place. In this case, however, volume flow is opposed to the direction of salt diffusion and therefore,

$$\frac{J_s}{X_j/c_s} \equiv \omega_s'' < \omega_s \quad (3.3.44)$$

where (*) is used for measurement at $\Delta p = 0$. From eqs. (3.3.30), (3.3.43) and (3.3.44), the interaction between water flow and ion flows leads to the inequality.



$$\left(\frac{J_s}{X_s/c_s} \sqrt{\frac{J_1 - J_2}{X_1}} \right)_{\Delta p = 0} < \left(\frac{J_s}{X_s/c_s} \sqrt{\frac{J_1 - J_2}{X_1}} \right)_{J_v = 0} \quad (3.3.45)$$

Therefore, salt diffusion in the presence of volume flow is less than salt diffusion in the absence of volume flow. The membrane potential at $\Delta p = 0$ in practice would also differ from that measured in the absence of water flow. In general, existence of volume flow would result in the flattening of the concentration difference between the two membrane-solution interfaces. In charged ion-exchange membranes, this will mostly affect the counter-ions, and therefore the observed membrane potential would be lowered by water flow, even with ideal stirring which would give in effect no unstirred layers. In real measurement, the existence of unstirred layers would make this effect even larger. Maximum values of $t_1 t_2 = 0,25$ is obtained in completely non-permselective membranes, i.e. $t_1 = t_2 = 0,5$; in highly permselective membranes this product will approach zero. Volume flow will thus result in a smaller membrane potential of which will shift the measured data towards larger $t_1 t_2$ values.

In general, ion-water coupling, causes the experimental data to be shifted in the opposite direction to that affected by ion-ion coupling, according to Kedem.

Correlations (3.3.42) and (3.3.45) show that from customary measurements of conductance and membrane potential plus salt permeation, one gets a sharp distinction between ion-water coupling as found in usual ion-exchange membranes on the one hand, and ion-ion coupling as expected in hydrophobic membranes on the other hand. Zero coupling in the absence of volume flow was given by eq. (3.3.40).

3.4 Transport Processes Occurring During Electrodialysis

A number of transport processes occur simultaneously during ED, and these are illustrated in Figure 3.4.1⁽⁷⁾.

Counter-ion transport constitutes the major electrical movement in the process; the counter-ions transport with them by electro-osmosis a certain quantity of water. Co-ion transport is comparatively small and is dependent upon the quality of the ion-selective membrane and upon the brine concentration. Water is also transported electro-osmotically with the co-ions. Diffusion of electrolyte occurs from the brine to the dialysate compartment because in the ED process the brine stream is usually more concentrated than the dialysate stream. Water transport is also associated with

electrolyte diffusion. Water transport due to osmosis takes place from the low concentration dialysate compartment into the higher concentration brine compartment.

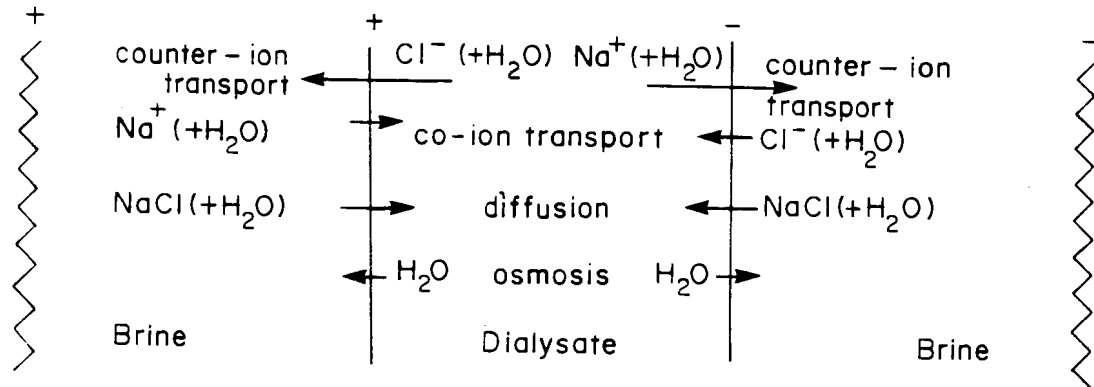


Figure 3.4.1: Illustration of transport processes which can occur simultaneously during the electro dialysis process.

The efficiency of demineralization of the liquid in the dialysate compartment may be considerably reduced by the counter effects of co-ion transport, diffusion, water transport associated with counter-ion movement and osmosis. The effect of these unwanted transfer processes can, however, be reduced by the correct selection of membranes and by the selection of the optimum operational procedure for a particular application⁽⁷⁾. Osmosis and electro-osmosis are effects which limit the usefulness of ED as a method of concentrating electrolyte solutions.

3.5 Current Efficiency and Transport Phenomena in Systems with Charged Membranes

The interaction between the current efficiency of electro dialytic separation with ion-exchange membranes and all the fluxes depressing selectivity, i.e., electric transport of co-ions, electro-osmotic flow of water, diffusion and osmosis have been described and experimentally examined by Koter and Narebska⁽¹⁷⁾. They have presented a simple definition of the current efficiency (CE) for a single ion-exchange membrane system. It allows for the estimation of CE from a determination of concentration changes in

cathode and anode solutions. With the proposed definition, CE can be expressed as a simple function of different kinds of transport taking place in the system. This fact makes it possible to examine the effects of these transports on current efficiency, that is to calculate the losses of CE due to:

- a) electric transport of co-ions;
- b) electro-osmotic flow of water;
- c) diffusion of a salt; and
- d) osmotic transport of water.

Thus, the full characteristics of a single ion-exchange membrane (cation- or anion-exchange) for a separation process like ED can be obtained. The mathematical solution has been examined for computing the current efficiency and its losses for the system $\text{NaCl}_{\text{aq}}/\text{Nafion 120 membrane}$ and $\text{NaOH}_{\text{aq}}/\text{Nafion 120 membrane}$ based on the experimental results published earlier⁽¹⁷⁾.

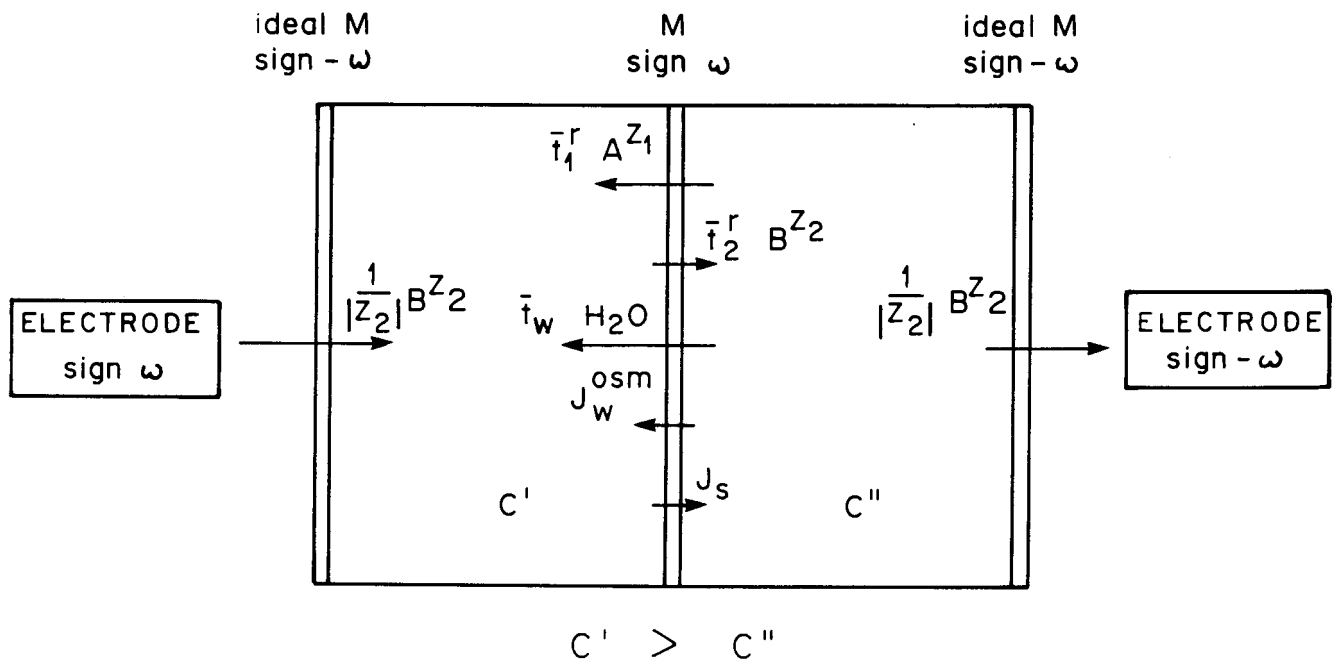
3.5.1 Current Efficiency of a Membrane System - A Definition

Consider the one membrane system as shown in Figure 3.5.1. The ion-exchange membrane (M) separates two solutions of an Av_1Bv_2 electrolyte differing in concentrations. For the cation-exchange membrane (sign $W = -1$) the cathode is on the more concentrated side whereas for the anion-exchange membrane ($W = +1$) it is on the diluted side. The electrodes and electrode reactions do not belong to the system. They are separated from the system by ideal membranes of reverse sign to the investigated membrane.

At $t = 0$, the concentration difference across the membrane is $\Delta c^0 = c^{0'} - c^{0''}$. After passing an electric current through the membrane for time t , the concentration difference changes to Δc^t . The ratio of $(\Delta c^t - \Delta c^0)$ for the real membrane to $(\Delta c^t - \Delta c^0)$ for the ideal membrane system ($t_2, t_w, J_s, J_w^{\text{os}} = 0$) is a measure of the current efficiency:

$$\text{CE} = \frac{(\Delta c^t - \Delta c^0)}{(\Delta c^t - \Delta c^0)_{\text{ideal}}} \quad (3.5.1)$$

Rearrangement of this formula⁽¹⁷⁾ leads to the following equation relating the current efficiency to the total counter-ions (J_1) and water (J_w) fluxes (see Appendix B).



A – counter-ion
B – co-ion

Figure 3.5.1: Standard system for defining the current efficiency of an ion-exchange membrane in the isobaric condition ($\Delta p = 0$). The transport processes caused by the passage of 1 Faraday of electric charge (\bar{t}_1 and \bar{t}_2 are the electric transport of counter-ions and co-ions, respectively; \bar{t}_w is the electro-osmotic transport of water) and by the concentration difference (J_s - diffusion of a salt, J_w^{osm} = osmotic flux of water) are shown.

$$CE = \omega z_1 v_1 (J_1/v_1 - 0,018\bar{m}J_w)/I \quad (3.5.2)$$

Consider that the counter-ions are driven by the constant electric field and the chemical potential gradient, and that the same holds for water, eq. (3.5.2) can be rearranged to:

$$CE = z_1 v_1 (\bar{t}_1^r/v_1 - 0,018\bar{m}\bar{t}_w - \omega(J_s - 0,018\bar{m}J_w^{osm})F/I \quad (3.5.3)$$

where

- \bar{t}_1^r = reduced transport number of counter-ions (eq. A2, Appendix B)
- \bar{t}_w = transport number of water
- \bar{m} = mean molality (eq. B17, Appendix B)
- J_s, J_w^{osm} = diffusion and osmotic fluxes
- I = electric current
- ω = -1 for cation-exchange membrane
- = +1 for anion-exchange membrane

The formula indicating the fluxes that decrease current efficiency, is as follows:

	Electrical transport of co-ions	Electro-osmotic transport of water	Diffusion of salt	Osmotic flux of water
CE = 1 -	$\bar{i}_2 - z_1$	$z_1 v_1 0,018 \tilde{m} \bar{i}_w -$	$z_1 v_1 \omega (J_s -$	$0,018 \tilde{m} J_w^{os}) F/l$

(3.5.3a)

With the help of the transport equations of irreversible thermodynamics and the Gibbs - Duhem equation, the diffusion and osmotic fluxes, J , and J_w^{os} , can be expressed as a function of the difference of the chemical potential of a solute, $\Delta \mu_s$ ⁽⁹⁾.

$$J_s - 0,018 \tilde{m} J_w^{os} = \left[\left(\frac{J_s}{\Delta \mu_s} \right) - 0,018 \tilde{m} \left(\frac{J_w^{os}}{\Delta \mu_s} \right) \right] \Delta \mu_s$$

$$= f(L_{ik}, \tilde{m}) \Delta \mu_s \quad (3.5.4)$$

Here $f(L_{ik}, \tilde{m})$ represents a combination of the phenomenological conductance coefficients L_{ik} and the mean molality, \tilde{m} , of a solute. Equation (3.5.3) and (3.5.4) clearly show that losses of selectivity due to osmotic and diffusion fluxes are dependent on the ratio of the chemical potential difference of solute and the current $\Delta \mu_s/l$.

3.5.2 Determination of Current Efficiency in a System with Electrode Reactions

Substituting the concentration changes for the system with ideal membrane, $(\Delta c^t - \Delta c^o)_{ideal}$ (eq. B15, Appendix B), and the equation

$$\Delta c^t - \Delta c^o = \omega (\Delta c_o^t - \Delta c_c^t) \quad (3.5.5)$$

Into eq. (3.5.1), eq (3.5.6) is obtained:

$$CE = \frac{z_1 v_1 V^o F (\Delta c_c^t - \Delta c_a^t)}{2(1 - v_s c^o) I \Delta t} \quad (3.5.6)$$

where $\Delta c_a^t, \Delta c_c^t$ = concentration changes of anolyte and catholyte after time Δt
 c^o = mean concentration of anolyte and catholyte at time $t = 0$,
 $c^o = (c_a^o + c_k^o)/2$.

Equation (3.5.6) can only be applied to the standard system (Fig. 3.5.1) without any other effect but transport, i.e., without the electrode reactions. Actually, the experimentally determined variations of the concentrations of the cathodic and anodic solutions are produced by both the transport phenomena and the electrode reaction.

For computing the current efficiency related to the transport phenomena only, the concentration/volume effects of the electrode reactions should be accounted for. The use of electrodes makes it necessary to correct the numerator of eq. (3.5.6), i.e., the difference $\Delta c_c - \Delta c_a$. In the general form the formula for the membrane current efficiency determined in the practical system can be written as:

$$CE = \frac{z_1 v_1}{2(1 - \bar{v}_s \bar{c}^o)} \left[\frac{FV^o}{I} \left(\frac{\Delta c_c^t}{\Delta t} - \frac{\Delta c_a^t}{\Delta t} \right)_{\text{pract}} + \text{correction} \right] \quad (3.5.7)$$

Some electrodes and the formulas for corrections are given by Koter and Narebska⁽¹⁷⁾.

3.5.3 Relation Between Current Efficiency and Efficiency of Energy Conversion

Regarding the general formula for efficiency of energy conversion given by Kedem and Caplan⁽⁷²⁾, the efficiency of energy conversion, η_E , for the system studied here, takes the form

$$\eta_E = \omega \frac{J_1^w}{I} \frac{\Delta \mu_s}{\Delta E} \quad (3.5.8)$$

where $J_1^w = J_1/v_1 - 0,018 \bar{m} J_w$ (3.5.9)
 $\Delta E =$ is the difference of electrical potential measured with electrodes reversible to co-ions.

$$\Delta E = \Delta \tilde{\mu}_2 / z_2 F \quad (3.5.10)$$

By comparing eq. (3.5.8) for J_1^w and eq. (3.5.3) for the current efficiency, it can be seen that η_E can be written as the product of current efficiency and the force-to-force ratio $\Delta \mu_s / \Delta E$:

$$\eta_E = \omega \frac{1}{z_1 v_1} CE \frac{\Delta \mu_s}{\Delta E} \quad (3.5.11)$$

3.5.4 The Losses of Current Efficiency

To determine losses of current efficiency due to different kinds of transport (eq. 3.5.3a), four experiments can be performed. Results are here presented for the systems $\text{NaCl}_{\text{aq}}/\text{Nafion 120}$ and $\text{NaOH}_{\text{aq}}/\text{Nafion 120}$. All the experimental results used for computing CE have been published elsewhere⁽¹⁷⁾.

Figures 3.5.2(a) and 3.5.2(b) present the effects of the conjugated fluxes on efficiency of electric transport of counter-ions across the cation-exchange membrane (Nafion 120) for two different values of concentration ratio; m'/m'' and current density, i : $m'/m'' = 5$, $i = 100 \text{ A/m}^2$, and $m'/m'' = 10$, $i = 500 \text{ A/m}^2$.

On both figures the current efficiency corresponds to the abscissa (see eq. 3.5.3a)

$$CE = 1 - \Sigma \text{ losses}$$

and is dependent on the mean concentration \bar{m} (eq. B17, Appendix A). The effects which diminish current efficiency are⁽¹⁷⁾:

- Electric transport of co-ions, i.e., imperfect membrane permselectivity (\bar{t}_2)
- Diffusion of solute (J_s)
- Electro-osmotic flow (\bar{t}_w)
- Osmotic water fluxes (J_w^{os})

The following conclusions can be drawn from the figures⁽¹⁷⁾:

The imperfect selectivity (\bar{t}_2), assumed to be one of the most important characteristics of a membrane, produces up to 8% (NaCl) and 35% (NaOH) of the CE losses at $\bar{m} = 2$. Similar to \bar{t}_2 , the effect of electro-osmotic flow of water (\bar{t}_w) increases with m . It plays a significant role in the system with NaCl where it diminishes CE up to 30%.

Depending on the working conditions, i.e., on the concentration ratio m'/m'' and current density, the decrease of CE due to osmotic and diffusion flows can be larger than that caused by electric transport of co-ions and water. This effect is especially

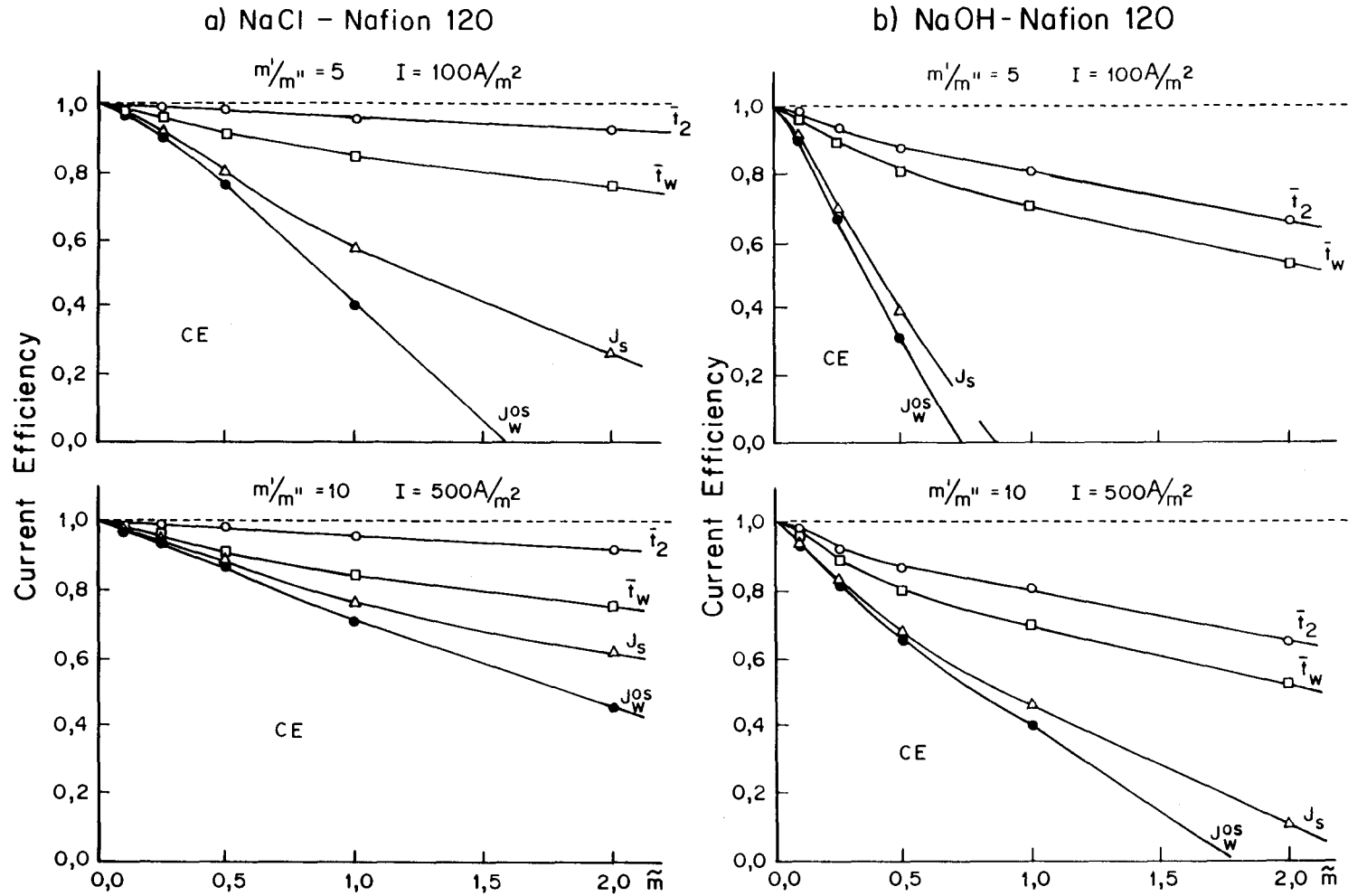


Figure 3.5.2: Losses of current efficiency due to imperfect selectivity of a membrane (\bar{t}_2), diffusion of a solute (J_s) and electro-osmotic flow (\bar{t}_w) and osmotic (J_w^{os}) fluxes. $T = 298\text{K}$.

seen at higher mean concentrations where the current efficiency can even be reduced to zero.

3.6 Efficiency of Energy Conversion in Electrodialysis

Efficiency of energy conversion in separation processes with Nafion 120 membranes from phenomenological transport coefficients has been described by Narebska and Koter⁽¹⁸⁾.

In systems devised for desalination/concentration processes with ion-exchange membranes separating single electrolyte solutions of different concentrations, electrical energy is used to drive a solute against its concentration gradient. In these processes, the electrical energy is converted into free energy of mixing and in that way it is stored in the system. The efficiency of energy conversion (η) depends both on the degree of coupling between the driving process and the driven flow (q), as well as the operating conditions.

Kedem and Caplan⁽⁷²⁾ have defined η and q in terms of irreversible thermodynamics and outlined the methods available to access both parameters for thermocouples, fuel cells, osmotic batteries and desalination stacks by treating the system as a two-flow process. Later, Caplan⁽⁷⁴⁾ published some data on the overall degree of coupling q and η_{\max} for hyperfiltration, concentration cells and ED, taking for the calculations the experimental results for a few points in dilute solutions.

Narebska and Koter⁽¹⁸⁾ have presented results for the degree of coupling and efficiency of energy conversion calculated for the system composed of a perfluorinated Nafion 120 membrane and sodium chloride solutions of different concentrations. Their aim have been to conduct a detailed analysis of input-output relations by treating the system and the transport involved as a three-flow process and describing quantitatively the transport of water which consumes energy unprofitably.

The system consisted of a cation exchange membrane and aqueous solutions of 1 : 1 electrolyte of different concentrations in the adjacent compartments. Sodium are driven by the applied electrical potential difference opposite the concentration difference of NaCl.

3.6.1 Mathematical Formulation

3.6.1.1 The degree of coupling and the efficiency of energy conversion in the two-flow system (basic definitions)

The efficiency of energy conversion η is based in the dissipation function ϕ which for the two-flow system takes the general form:

$$\phi = J_1 X_1 + J_2 X_2 \geq 0 \quad (3.6.1)$$

According to Kedem and Caplan⁽⁷²⁾, with one flow producing entropy ($J_2 X_2$), which is always positive and the other flow consuming entropy, being negative ($J_1 X_1$), the efficiency of energy conversion can be expressed as:

$$\eta = - \frac{J_1 X_1}{J_2 X_2} \quad (3.6.2)$$

Denoting the force ratio as X_1/X_2 and the ratio of the straight conductance coefficients L_{ij} appearing in the flow equations

$$J_1 = L_{11} X_1 + L_{12} X_2 \quad (3.6.3)$$

$$J_2 = L_{21} X_1 + L_{22} X_2$$

as $Z^2 = L_{11}/L_{22}$, the efficiency function can be calculated with the equation:

$$\eta = - \frac{q + Zx}{q + 1/Zx} \quad (3.6.4)$$

q is the degree of coupling of the flows satisfying the relation $|q| \leq 1$.

The conversion of energy of process 2 to process 1 is only possible when the two flows are coupled, therefore, the degree of coupling can be defined as:

$$q^2 = 1 - \frac{(J_2)_{J_1=0}}{(J_2)_{X_1=0}} = 1 - \frac{(J_1)_{J_2=0}}{(J_1)_{X_2=0}} = \frac{L_{12}^2}{L_{11} L_{22}} \quad (3.6.5)$$

For electrodialysis, the dissipation function can be written in the form:

$$\phi = J_1 \Delta \mu_s + IE \quad (3.6.6)$$

where J_1 is the flux of counterions, $\Delta \mu_s$ the difference of chemical potential of an electrolyte, I the electric current and E the potential difference between the solutions on opposite sides of the membrane measured with electrodes reversible to the anions.

Kedem and Caplan have presented the general solution for the degree of coupling in ED. They admitted, however, that in their solution the contribution of water flow was neglected. This means that they have treated the process as a two-flow system.

3.6.1.2 Three-flow System

In any real system with a single electrolyte and the ion-exchange membrane separating solutions of different concentrations, the flow of water is another process which participates in the entropy production. Consequently, the equation describing the dissipation function should contain the third component, $J_w \Delta \mu_w$:

$$\phi = J_1 \Delta \mu_s + J_w \Delta \mu_w + IE \geq 0 \quad (3.6.7)$$

Thus, the efficiency of energy conversion for multiple-flow system can be defined as⁽⁷⁴⁾:

$$\eta = - \frac{\sum_{i=1}^{n-1} J_i X_i}{J_n X_n} \quad (3.6.8)$$

In eq. (3.6.8) $J_n X_n$ represents the driving process and $J_i X_i$ represents the driven flow.

As for ED $J_n X_n = IE$ and $\sum_i^{n-1} J_i X_i = J_1 \Delta \mu_s + J_w \Delta \mu_w$, one gets:

$$\eta = \left(- \frac{J_1 \Delta \mu_s}{IE} \right) + \left(- \frac{J_w \Delta \mu_w}{IE} \right) = \eta_{IE} + \eta_{wE} \quad (3.6.9)$$

The first term of eq. (3.6.9) is the same as before, i.e. it expresses the storage of energy in producing a concentration difference in the permeant. The second term corresponds to the transport of water which acts opposite to the separation of the components. It causes a waste of energy by decreasing the concentration difference.

To find the degrees of coupling in both processes, the equations for transport of ions (J_1), water (J_w) and current (I) should be used in a general formula:

$$J_1 = L_{11}\Delta\mu_s + L_{1w}\Delta\mu_w + L_{1E}E$$

$$J_w = L_{1w}\Delta\mu_s + L_{ww}\Delta\mu_w + L_{wE}E \quad (3.6.10)$$

$$I = L_{1E}\Delta\mu_s + L_{wE}\Delta\mu_w + L_E E$$

3.6.1.3 Degrees of coupling for the three-flow system

Defining the degree of coupling according to Kedem and Caplan, three coefficients for the three-flow system are obtained which denote sodium ion-current coupling (q_{1E}), water-current coupling (q_{wE}) and sodium ion-water coupling (q_{1w}).

$$q_{ik}^2 = 1 - \left[\frac{(J_i)_{J_k=0}}{(J_i)_{X_k=0}} \right]_{X_j=0} = \frac{L_{ik}^2}{L_{ii}L_{kk}} \quad i,k = 1,w,E, \quad i \neq k \quad (3.6.11)$$

All the degrees of coupling were calculated according to eq. (3.6.11) using conductance coefficients L_{ik} , of eq. (3.6.10).

For the more practical discussion of the input-output relation, such as finding the maximum output or the driven region for ED, the overall degree of coupling q_E is also helpful. This can be derived from the general formula

$$\bar{q}^2 = 1 - \frac{(J_n)_{J_{i \neq n} = 0}}{(J_n)_{X_{i \neq n} = 0}} \quad (3.6.12)$$

For the system with three forces operating (ΔC , Δp , E , eq. (3.6.10), \bar{q}_E takes the form:

$$\bar{q}_E^2 = 1 - \frac{(I)_{J_1, J_w = 0}}{(I)_{\Delta\mu_s, \Delta\mu_w = 0}} = \frac{q_{1E}^2 + q_{wE}^2 - 2q_{1E}q_{wE}q_{1w}}{1 - q_{1w}^2} \quad (3.6.13)$$

At $\Delta p = 0$, which corresponds to operating conditions in ED, and applying the Gibbs-Duhem equation $c_s d\mu_s + c_w d\mu_w = 0$, the flow equations can be written in the form:

$$J_1 - \frac{c_s}{c_w} J_w = J_1^w = L'_{11} \Delta \mu_s + L'_{TE} E \quad (3.6.14)$$

$$I = L'_{TE} \Delta \mu_s + L_E E$$

where

$$L'_{11} = L_{11} - 2 \frac{c_s}{c_w} L_{1w} + \frac{c_s^2}{c_w^2} L_{ww} \quad (3.6.15)$$

$$L'_{TE} = L_{TE} - \frac{c_s}{c_w} L_{wE}$$

For these equations the formula for the overall degree of coupling takes the form:

$$q_E^2 = 1 - \frac{(I)_{J_1^w = 0}}{(I)_{\Delta \mu_s = 0}} = \frac{L_{TE}^2}{L'_{11} L_E} \quad (3.6.16)$$

3.6.1.4 Efficiency of Energy Conversion

Introducing eq. (3.6.10) into eq. (3.6.9) and assuming that $\Delta p = 0$, it is possible to derive the equations for both components of η (eq. 3.6.9), i.e. η_{IE} and η_{wE}

$$\eta_{IE} = - \frac{\left[Z_{TE} - \frac{c_s}{c_w} Z_{wE} q_{1w} \right] X + q_{IE}}{q_{IE} - \frac{c_s}{c_w} Z_{w1} q_{wE} + \frac{1}{Z_{wE} X}} \quad (3.6.17)$$

$$\eta_{wE} = \frac{c_s}{c_w} \frac{\left[Z_{TE} q_{1w} - \frac{c_s}{c_w} Z_{wE} \right] X + q_{wE}}{Z_{1w} q_{1w} - \frac{c_s}{c_w} q_{wE} + \frac{1}{Z_{wE}} X} \quad (3.6.18)$$

The meaning of q_{ik} is as before eq. (3.6.11), $x = \Delta \mu_s / E$ and $Z_{ik} = \sqrt{L_{ij} / L_{kk}}$ where $i, k = 1, \omega, E, i \neq k$. These equations are appropriate for calculating η for ED.

3.6.2 The Two-Flow and Overall Degrees of Coupling

Model calculations have shown the following⁽¹⁸⁾:

Tight coupling, ranging up to 0.98, was found between the ion and current flows (q_{IE}) for solutions up to 0,5 mol/l. (Fig 3.6.1).

The sodium transport number \bar{t}_1 was in the range 1,0 to 0,98 over this concentration range. The sodium transport number (\bar{t}_1) and q_{IE} decreased at higher concentrations.

The coupling of water-current flows (q_{wE}) was close to 0,5 at approximately 0,1 to 0,5 mol/l (Fig. 3.6.1). In that region $q_{wE} \approx q_{1w}$ implying that q_{wE} represents the coupling of water to ion flow; known as electro-osmosis. In more concentrated solutions q_{wE} and q_{1w} diverge. Water-ion coupling becomes higher and water-current coupling becomes lower. At higher concentrations ($> 0,5$ mol/l) the amount of "free" water in the membrane, the transport number of water \bar{t}_w and the osmotic flow, decrease. Effects originating in the deswelling of the membrane at high external concentration may result in the observed decrease of the electro-osmotic flow and the increased coupling between ions and the amount of water crossing the membrane. The overall coupling coefficient q_E slightly exceeds q_{IE} and changes with external concentration similar to q_{IE} .

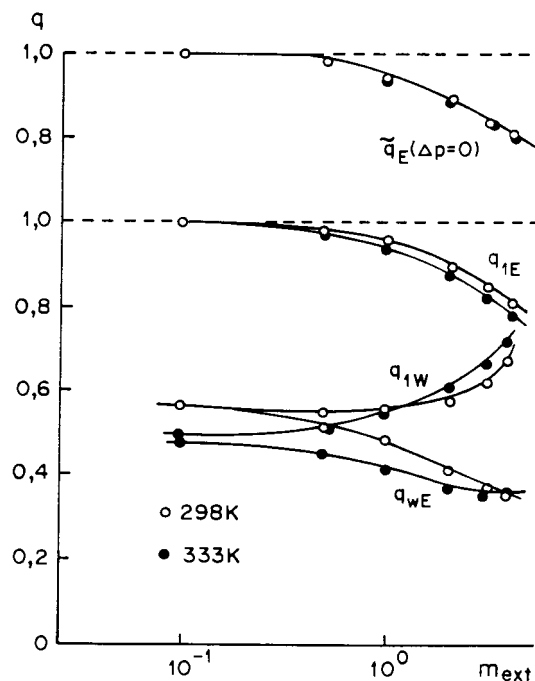


Figure 3.6.1: The concentration dependence of the degrees of coupling: sodium ions-current (q_{IE}), sodium ions-water (q_{1w}), water-current (q_{wE}), and the overall degree of coupling (\bar{q}_E) for the system NaCl_{aq} /Nafion 120 membrane.

3.6.3 Total Efficiency of Energy Conversion and its Components

The component efficiencies of energy conversion are not only of different meaning but of different sign (Fig. 3.6.2). The positive term η_{IE} indicates the fraction of the free energy of mixing produced by the driving process IE and stored in the system by the uphill transport of ions $J_1 \Delta \mu_s$, against their spontaneous flow. The negative term η_{wE} means that the transport of water proceeds in the direction of the conjugated force $\Delta \mu_w$ (downhill). The energy input increases the rate of flow. Thus, this term causes the entropy of the system to increase and the energy supplied to the system to be wasted.

Both η_{IE} and η_{wE} change with the ratio $\Delta \mu_s/FE$ and with the concentration of electrolyte. The maximum in the η_{IE} curve means that for any concentration range of NaCl solutions there is an optimal concentration difference for which the efficiency of energy conversion is at a maximum. There is no such maximum in the η_{wE} curve. The waste of energy due to water flow becomes much higher as the electrolyte becomes more concentrated and the concentration difference between the NaCl solutions in the adjacent compartments is higher.

The sum of η_{IE} and η_{wE} gives the total efficiency as η . The total efficiency, η , decreases with increasing concentration. The degree of coupling, \bar{q}_E , also decreases with increasing concentration.

Computations of q (coupling) and η (efficiency) employing the derived equations and phenomenological conductance coefficients determined for the system Nafion 120 membrane/sodium chloride solutions led to the following conclusions⁽¹⁸⁾:

- Coupling of the current to the flow of sodium ions (q_{IE}), of importance for the efficiency of energy conversion, is close to unity when the membrane is in contact with dilute solutions and is going down with increasing external concentration.
- Coupling of the current to the flow of water (q_{wE}), which is achieved by water-cation coupling (q_{lw}), reaches a value as high as half that of q_{IE} , pointing to the unavoidable loss of energy during ED.

- The total efficiency of energy conversion (η) depends both on the concentration of separated electrolytes and on the ratio of thermodynamic forces ($\Delta\mu_s/FE$) acting in the system. The maximum of efficiency depends on the force ratio and decreases with increasing external concentration.
- The total efficiency of energy conversion is a complex quantity composed of a positive component (η_{IE}) related to the transport of cations and a negative one (η_{WE}) related to the transport of water; both components change with the external concentration to a different degree. The measure of the loss of energy (η_{WE}) may reach a value of as much as 70% of η_{max} in the more concentrated solutions.

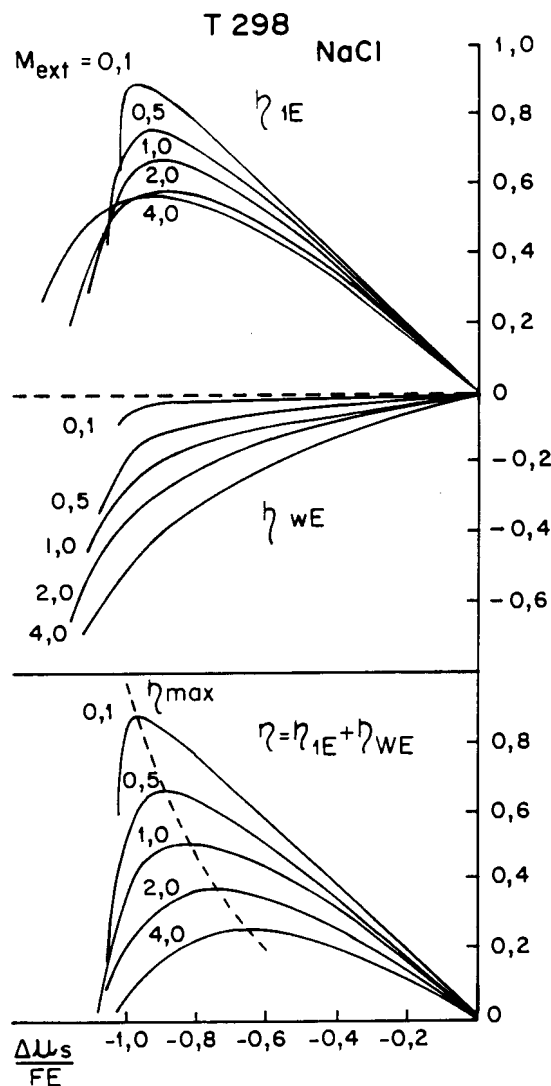


Figure 3.6.2: The efficiency of energy conversion η and the component efficiencies η_{IE} , η_{WE} and force ratio $\Delta\mu_s/FE$, at different concentrations NaCl in the external solution ($T = 333\text{ K}$).

3.7 Conversion of Osmotic into Mechanical Energy in Systems with Charged Membranes

Narebska *et al.*,⁽¹⁹⁾ have described the problem of conversion of osmotic energy into mechanical energy within the framework of irreversible thermodynamics. Using the numerical results for the conductance coefficients for the system Nafion 120 membrane/single salt and alkali solutions, the couplings between the volume and the osmotic fluxes, q , and the efficiency of osmotic into mechanical energy conversion, η , have been computed.

The standard application of membrane systems is for separation of suspensions and molecular mixtures, gaseous or liquid, into components on an expense of supplied energy. Mechanical, thermal or electric energy can be used. More than twenty membrane separation techniques are known. In each of these systems, however, the difference in concentration of components on both sides of a membrane presents the effective source of osmotic energy, generating the spontaneous osmotic flux affecting the separation. For example, in ED, the osmotic flow of water dilutes the brine, thus lowering the energetic efficiency of desalination. In reverse osmosis, the osmotic pressure is a powerful force to overcome. Osmotic energy is thereby a native energy of a membrane system affecting both the income of energy and the separation process itself.

Conversion of osmotic energy into electric energy was postulated and theoretically described by Kedem and Caplan⁽⁷²⁾. Systems converting osmotic energy into mechanical energy called "osmotic pumps" were proposed by Lee *et al.*,⁽⁷⁵⁾. The energetic efficiency of the process, however, still seems to be a problem.

The work by Narebska *et al.*,⁽¹⁹⁾ has been aimed at a theoretical analysis of osmotic into mechanical energy conversion, using irreversible thermodynamics as the underlying theory.

3.7.1 Theoretical

The system consists of an ion-exchange membrane separating electrolyte solutions of different molalities. Assuming ideal membrane permselectivity (totally impermeable to a solute) and the zero current condition, the only flow in the system should be the osmotic flow of water which is driven to the more concentrated side. However, for real

polymer membranes and particularly when they are in contact with concentrated solutions, diffusion of a solute across the membrane should be admitted as an additional phenomenon. The solute permeates the membrane towards the dilute solution side, that is, opposite to the osmotic flow.

In terms of irreversible thermodynamics the two flows

- the osmotic flow of water J_w and
- the diffusional flow of the solute J_s are described by the following equations:

$$J_s = L_s \Delta \mu_s + L_{sw} \Delta \mu_w \quad (3.7.1a)$$

$$J_w = L_{ws} \Delta \mu_s + L_w \Delta \mu_w \quad (3.7.1b)$$

$\Delta \mu_s$, $\Delta \mu_w$ are the differences of chemical potential of a solute and water, respectively. L_{ik} denotes the phenomenological conductance coefficients.

It is convenient to transform eq. (3.7.1a) and (3.7.1b) into another set of equations.

$$J_w' = L_w' \Delta \mu_w^c + L_{wp}' \Delta p \quad (3.7.2a)$$

$$J_v = L_{pv}' \Delta \mu_w^c + L_p' \Delta p \quad (3.7.2b)$$

Here J_w' denotes the flow of water against the flow of a solute conjugated to the concentration part of the chemical potential difference of water, $\Delta \mu_w^c$:

$$J_w' = J_w - \bar{c}_w / \bar{c}_s * J_s \quad (3.7.3)$$

$$\Delta \mu_w^c = RT \ln (a_w' / a_w'') \quad (3.7.4)$$

J_v of equation (3.7.2b) denotes the total volume flow conjugated to the difference of pressure in the compartments on the opposite sides of the membrane, Δp .

$$J_v = \bar{v}_s J_s + \bar{v}_w J_w \quad (3.7.5)$$

The relation between the fluxes and forces of equations (3.7.1a and 3.7.1b) and of equations (3.7.2a and 3.7.2b) can be expressed in a matrix form

$$\begin{pmatrix} J_w' \\ J_v' \end{pmatrix} = A * \begin{pmatrix} J_s \\ J_w \end{pmatrix}, \quad \begin{pmatrix} \Delta \mu_w^c \\ \Delta p \end{pmatrix} = A^{-1T} * \begin{pmatrix} \Delta \mu_s \\ \Delta \mu_w \end{pmatrix} \quad (3.7.6 \text{ and } 3.7.7)$$

$$L' = A * L * A^T \quad (3.7.8)$$

where

$$A = \begin{pmatrix} -\bar{c}_w/\bar{c}_s & 1 \\ \bar{v}_s & \bar{v}_w \end{pmatrix}, \quad L = \begin{pmatrix} L_s & L_{sw} \\ L_{ws} & L_w \end{pmatrix}$$

With the flows of equations (3.7.2a and 3.7.2b) the dissipation function Φ consists of two components:

$$\Phi = \begin{matrix} J_w' \Delta \mu_w^c & + & J_v \Delta p \\ \text{osmotic} & & \text{mechanical} \\ \text{energy} & & \text{energy} \\ \text{component} & & \text{component} \end{matrix} \quad (3.7.9)$$

The efficiency of energy conversion, η , as defined by Kedem and Caplan⁽⁷²⁾, can be written as follows:

$$\eta = - \frac{J_v \Delta p}{J_w' \Delta \mu_w^c} \quad (3.7.10)$$

$$0 < \eta < 1$$

For the system discussed here, η , means the output of mechanical energy produced by the input of unit osmotic energy. To acquire computational verification of various systems this equation should be transformed by substituting equations (3.7.2a and 3.7.2b) into equation (3.7.10) to give

$$\eta = - \frac{q + z * \Delta p / \Delta \mu_w^c}{q + 1 / (Z * \Delta p / \Delta \mu_w^c)} \quad (3.7.10 \text{ a})$$

Here

$$q = L'_{wp} / (L'_w L'_p)^{0.5}$$

$$Z = (L'_p/L'_w)^{0,5}$$

q is called a coupling coefficient. For energy conversion the size of q is fundamental. The value of q may vary between -1 and +1. A high value of q indicates tight coupling between the two processes involved in energy conversion. For the system discussed here, these are the spontaneous osmotic flow of water and the volume flow producing energy.

3.7.2 Transport Experiments and Computations

The perfluorinated cation-exchange membrane Nafion 120 (Du Pont de Nemours, USA), was used for measuring the membrane transport process as well as performing experiments with an osmotic unit. The measured membrane transport properties were the membrane electric conductivity, concentration potential, osmotic, electro-osmotic, diffusion and hydrodynamic flows. From these data the set of coefficients of equation (3.7.2), that is L'_w , L'_p , L'_{wp} was calculated and then the coupling coefficient q (eq (3.7.11)) and the efficiency of energy conversion, η (eq. 3.7.10(1)) were found.

The theory was experimentally verified in a simple osmotic unit⁽¹⁹⁾.

3.7.3 Osmotic and Diffusion Fluxes in Membrane Systems

For a given membrane, the flow of water and the diffusion of a solute, flowing in the opposite direction, depend strongly on the nature of the electrolyte. For the electrolytes used and the Nafion 120 membrane, the osmotic flow is low with sodium hydroxide solution, higher with sodium chloride and the highest with sulphuric acid solutions (Table 3.7.1). For the same system the diffusion fluxes change in the opposite direction. J_s of NaOH is about 25% of the osmotic flow; J_s of NaCl 4%; and J_s of H_2SO_4 is zero within the range of concentrations used.

Table 3.7.1: Osmotic and diffusion fluxes per unit of the chemical potential difference of a solute for systems with Nafion 120 membrane. $m = 1$, $T = 25^\circ C$.

Flows	NaOH	NaCl	H_2SO_4
	(* $10^{-10} \text{ mol}^2/\text{m}^3 \text{ Ns}$)		
Osmotic flow of water ($-J_w/\Delta\mu_s$)	4,7	8,0	17,7
Diffusion of solute ($-J_s/\Delta\mu_s$)	1,1	0,33	- 0,16

3.7.4 Osmotic Energy Conversion

The coupling coefficient, q , and the efficiency of energy conversion, η , have been calculated with equations (3.7.10a) and (3.7.11). The couplings between the spontaneous osmotic flow (J_w) driven by the difference of solvent activity ($\Delta\mu_w^o$) and the volume flow (J_v) producing the pressure (Δp) are shown as a function of the mean molalities of solutions bathing the membrane (Fig. 3.7.2). The coupling coefficient, q , is high for the system with sulphuric acid, ranging from 0,6 to 0,95 in 1 molar solution. For the other two electrolytes q does not exceed 0,4 (NaCl) or is even as low as 0,1 (NaOH). These results show the necessity of using membranes rejecting a solute almost perfectly. Even little diffusion as in the case of sodium chloride can disturb the coupling drastically.

This effect is even more pronounced as can be seen from the energy conversion, η (Fig. 3.7.3). Again, the η coefficient is the highest for the system with H_2SO_4 reaching 0,4. For this system the maximum of η is observed for the ratio of produced pressure to the osmotic one $\Delta p/\Delta\pi = 0,8$ (for ideal system it is one). In the case of the easily diffusing NaOH the energy conversion becomes negligible and decreased to 0,01 and the ratio $\Delta p/\Delta\pi$ for η_{max} is as low as 0,15.

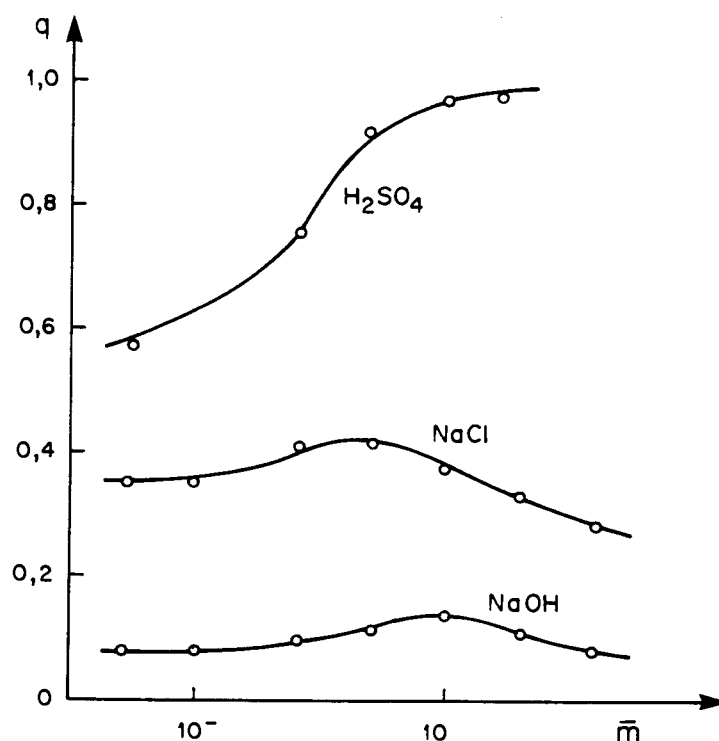


Figure 3.7.2: The concentration of coupling coefficient (eq. (3.7.11)) for various electrolyte solutions and Nafion 120 membrane; 298 K.

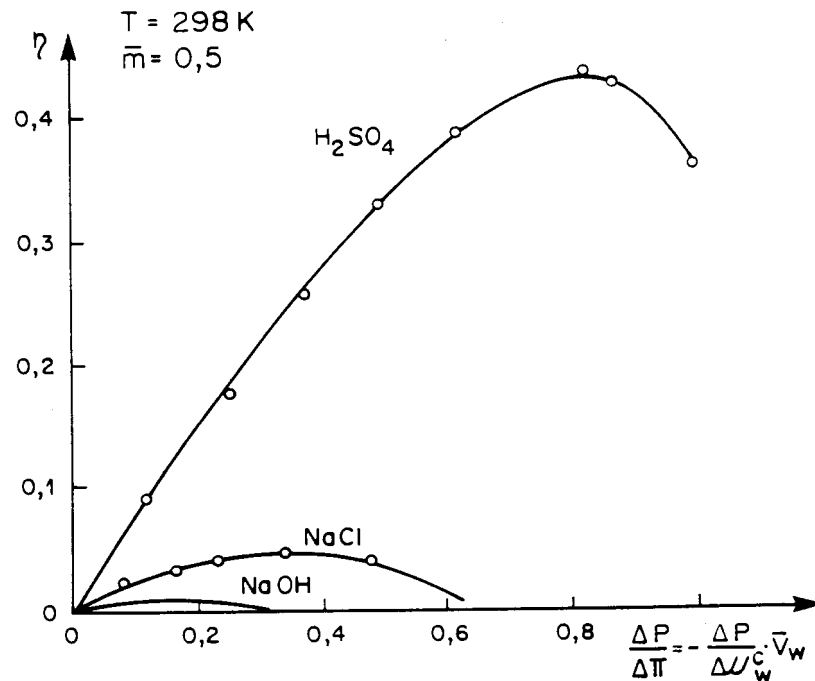


Figure 3.7.3: The dependence of the efficiency of osmotic into mechanical energy conversion (eq. 3.7.10) on the ratio $\Delta P/\Delta \Pi$; 298 K.

In order to examine the system further, the rate of fluxes for other electrolytes were measured (Table 3.7.2). These results confirm that only the solutes perfectly rejected by a membrane, like sulphuric acid, appears to be efficient in an osmotic pump. Only in the case of a membrane highly permselective to the given electrolyte, the free energy of mixing, which usually goes unexploited, can be put to effective use.

The following conclusions can be drawn⁽¹⁹⁾:

- A high degree of osmotic to mechanical energy conversion ranging from 0,4 to 0,5 can only be achieved in a system with a membrane, which rejects the solute almost entirely, that is with $\sigma \rightarrow 1$.
- A salt flux reaching even 4% of the osmotic flux of water (Table 3.7.1, NaCl) results in a vast decrease of the efficiency of energy conversion ($\eta < 0,1$).
- While in contact with an electrolyte which permeates Nafion 120 membrane more easily (like NaOH), the system cannot convert the osmotic energy to any remarkable degree ($\eta < 0,01$).

Table 3.7.2: Experimental volume fluxes in the systems with Nafion 120 membrane

ELECTROLYTE	J_v	$J_v/\Delta\pi$
	(* 10^{-8} m/s)	(* 10^{-8} m/s atm)
NaCl	10,8	0,236
Na ₂ SO ₄	4,59	0,145
HCl	36,7	0,70
H ₂ SO ₄	42,0	1,76
H ₃ PO ₄	6,72	0,60

3.8 Donnan Exclusion

If a resin is allowed to equilibrate in an electrolyte solution rather than in pure water, the water uptake is comparatively less due to the lowered external water activity, $a_w(< 1)$. Specifically, the osmotic swelling pressure becomes⁽¹¹⁾

$$\Pi = -(RT/v_w) \ln (\bar{a}_w/a_w) < -(RT/v_w) \ln \bar{a}_w \quad (3.8.1)$$

In addition to the water fraction, the dissolved ions will distribute themselves across the membrane-solution interface according to a condition of free energy balance. Qualitatively, the driving force for electrolyte uptake is the initial solute chemical potential gradient across the interface. Considering this solely, the equilibrium concentrations within and exterior to the membrane would be equal were it not for the presence of the ionizable side-chains that through the constant of electro-neutrality, resist the co-ion uptake. A simple theory that explains the overall features of electrolyte uptake by ion-exchangers was outlined by Donnan⁽⁷⁶⁾.

Assuming complete ionization, equivalent interdiffusion, electro-neutrality, and the equality of single-ion activities and concentrations, the theoretical result for the free energy balance across the interface between a 1 : 1 electrolyte solution of concentration C (mol per litre) and cation-exchange membrane, in which the ionogenic side-chain density is R , is

$$\bar{C}(\bar{C} + R) = C^2 \quad (3.8.2)$$

where \bar{C} is the internal equilibrium electrolyte concentration and the membrane was originally in the salt form. Immediately, it is seen that $\bar{C} < C$ and that co-ion exclusion is enhanced by increasing R . As C becomes very large, the Donnan exclusion

mechanism becomes increasingly less effective.

3.9 Relationship Between True and Apparent Transport Numbers

The relationship between true and apparent transport numbers has been described by Laskshminarayanaiah⁽⁴⁵⁾.

The emf of a cell of the type shown in Figure 3.9.1 is given by the following equation which cannot be integrated without knowledge of how \bar{t}_i and \bar{t}_w vary with external electrolyte concentration.

$$E = - (2 RT/F) \int_1^2 (\bar{t}_i - 10^{-3} m_{\pm} M \bar{t}_w) d \ln a_{\pm} \quad (3.9.1)$$

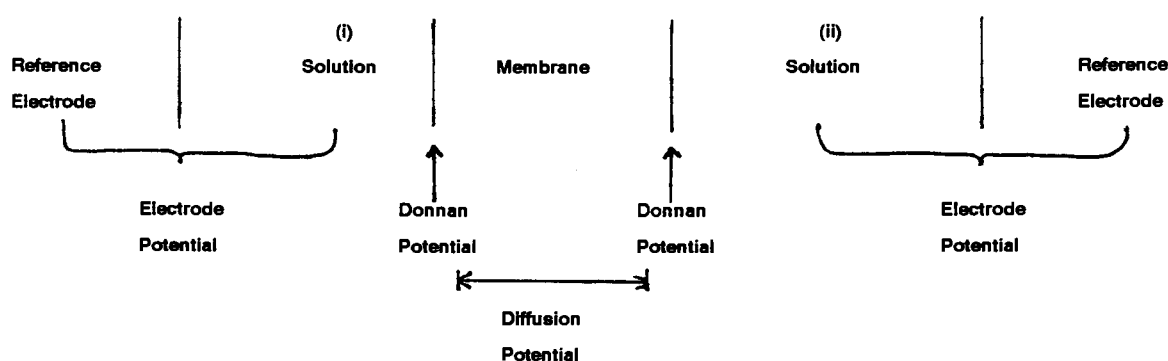


Figure 3.9.1: Electric potentials across an ionic membrane separating different salt solutions.

\bar{t}_i and \bar{t}_w must be found by separate experiments and their values must be unambiguous without being influenced by factors such as current density and back diffusion. Even then, what relation these experimental values bear to \bar{t}_i and \bar{t}_w of eq. (3.9.1) is not clearly known.

However, an approximate approach can be made by integrating eq. (3.9.1) within narrow limits a_{\pm}' and a_{\pm}'' . On integration, eq. (3.9.1) takes the form:

$$E = - \frac{2RT}{F} (\bar{t}_i - 10^{-3} m_{\pm} M \bar{t}_w) \ln \frac{a_{\pm}'}{a_{\pm}''} \quad (3.9.2)$$

The emf of a cell of the type shown in Figure 3.9.1 can be calculated from the modified Nernst equation.

$$E = 2\bar{t}_{+(app)} \frac{RT}{F} \ln \frac{a'}{a''} \quad (3.9.3)$$

which can be equated to eq. (3.9.3) to give⁽⁷⁷⁾:

$$\bar{t}_+ = t_{+(app)} + 0,018m_{\pm} \bar{t}_w \quad (3.9.4)$$

Hale and McCouley tested eq. (3.9.4) using different heterogeneous membranes and found good agreement between true \bar{t}_+ measured directly and \bar{t}_+ calculated using eq. (3.9.4). Their measurements although confined to a number of different membranes, were made with one set of electrolyte solutions only (0,667 and 1,333 mol/l NaCl). Lakshminarayanaiah⁽⁷⁸⁾ checked eq. (3.9.4) over a wide concentration range. He found that the \bar{t}_+ values calculated from eq. (3.9.4) were higher than the measured values particularly in high electrolyte concentrations. This discrepancy existing in the case of strong solutions is difficult to reconcile in view of the fact that Lakshminarayanaiah and Subrahmanyas⁽⁴⁷⁾ showed that eq. (3.9.1) is able to generate values for E (however from measured values of t_+ and t_w) agreeing with observed values. A more recent evaluation by Lakshminarayanaiah⁽⁷⁹⁾ has shown that eq. (3.9.4) is able to give values for \bar{t}_+ agreeing with those measured directly.

The relationship of $\bar{t}_{+(app)}$ obtained from emf measurements to \bar{t}_+ measured directly, unlike eq. (3.9.4), has been approached from a different standpoint by Oda and Yawataya⁽⁸⁰⁾. The apparent transport number ($\bar{t}_{+(app)}$) calculated from emf data was related to the concentration of the external solution by an "interpolation technique". This consists in measuring E using two solutions, c' and c'' , in the cell shown in Figure 3.9.1. In the first measurement of membrane potential, solution (") is so chosen that c'' is less than c' and in the second measurement c' is held constant and c'' is so chosen that it is now greater than c' . Each of the two values of $\bar{t}_{+(app)}$ calculated from the two measurements is now referred to that particular concentration of c' used in the experiment and plotted. The value of $\bar{t}_{+(app)}$ pertaining to c' which is kept constant in the two experiments is obtained by interpolation. Usually, $\bar{t}_{+(app)}$ is related to the mean external electrolyte concentration, i.e. $(c' + c'')/2$.

True values of \bar{t}_+ and \bar{t}_w were determined by Oda and Yawataya from the same experiment by the mass method which consisted in estimating the mass changes in

both the salt and the water in the cathode chamber following the passage of a known quantity of current through the system, electrolyte solution (c) \rightleftharpoons membrane \rightleftharpoons electrolyte solution (c). The relationship between \bar{t}_+ and $\bar{t}_{+(app)}$ was derived in the following manner⁽⁸⁰⁾.

A selective membrane of fixed charge density \bar{X} (equivalent per unit volume of swollen membrane) in equilibrium with an external electrolyte solution contains $\bar{X}(1 - \bar{s})$ equivalents of counter-ions and $\bar{X}\bar{s}$ equivalents of co-ions where \bar{s} is the equivalent of co-ions per equivalent of fixed group present in the membrane. This arises from the Donnan absorption of the electrolyte by the membrane.

When an electric field is applied, ions and water move. In a membrane in which interactions between different membrane components, viz., counter-ion, co-ion, water and membrane, matrix, are absent, one may assume that the fixed water in the membrane is negligible and that all mobile water moves with the same velocity and in the same direction as the counter-ion. As a result, counter-ions move faster and co-ions move slower than they would otherwise if water stood still. Consequently, the mobilities (u 's) of the counter-ion and co-ion may be written as:

$$\bar{u}'_+ = \bar{u}_+ + \bar{u}_w \quad (3.9.5)$$

$$\bar{u}'_- = \bar{u}_- - \bar{u}_w \quad (3.9.6)$$

where +, -, and w stand for cation, anion and water, respectively. \bar{u}'_+ and \bar{u}'_- are the increased and decreased mobilities due to the transport of water.

Due to water transport, the specific conductance of the membrane is increased. If k' is the membrane specific conductance, then

$$\bar{k}' = F[\bar{X}(1 + \bar{s})\bar{u}'_+ + \bar{X}\bar{s}\bar{u}'_-] \quad (3.9.7)$$

On substituting from eqs. (3.9.5) and (3.9.6), eq. (3.9.7) becomes

$$\bar{k}' = F\bar{X}[(1 + \bar{s})\bar{u}_+ + \bar{s}\bar{u}_- + \bar{u}_w] \quad (3.9.8)$$

If water transport is absent, the membrane conductance k is given by

$$\bar{k}' = Fx[(1 + \bar{s})\bar{u}_+ + \bar{s}\bar{u}_-] \quad (3.9.9)$$

It follows from eqs. (3.9.8) and (3.9.9) that the increase in conductance due to water transport is given by

$$\bar{k}' - \bar{k} = F\bar{X}\bar{u}_w \quad (3.9.10)$$

Transport numbers by definition are given by

$$t_+ = \frac{(1 + \bar{s})\bar{u}'_+}{(1 + \bar{s})\bar{u}_+ + \bar{s}\bar{u}'_-} \quad (3.9.11)$$

$$t_{+(app)} = \frac{(1 + \bar{s})\bar{u}_+}{(1 + \bar{s})\bar{u}_+ + \bar{s}\bar{u}'_-} \quad (3.9.12)$$

Substituting from eqs. (3.9.5) - (3.9.10) into eqs. (3.9.11) and (3.9.12) and remembering that $\bar{t}_{+(app)} + \bar{t}_{-(app)} = 1$, it can be shown that⁽⁸⁰⁾:

$$\bar{t}_+ - \bar{t}_{+(app)} = (\bar{t}_{-(app)} + \bar{s})[(\bar{k}' - \bar{k})/\bar{k}'] \quad (3.9.13)$$

Substituting from eq. (3.9.10), eq. (3.9.13) becomes

$$\bar{t}_+ - \bar{t}_{+(app)} = [\bar{t}_{-(app)} + \bar{s}][F\bar{X}\bar{u}_w/\bar{k}'] \quad (3.9.14)$$

When a potential of E volts acts along length λ cm of a membrane capillary, the water in the pore moves with a mobility, u_w cm/s (i.e., E/ℓ is unity). The volume (millilitres) of water flowing per second through a membrane subject to unit potential gradient is given by β_E and is equal to $(u_w A)$ where A is the pore area. But β , the volume of water flowing per Coulomb is given by:

$$\beta = V/i \quad (3.9.15)$$

where V is millilitres of water flowing per second and i is the current in amperes. But $i = k_p A$ per unit potential gradient and k_p is the specific conductance of the pore liquid of an infinitely swollen membrane (k_p is really a modified membrane conductance). Consequently, it follows that

$$\beta_E = \bar{u}_w A = \bar{k}_i A \beta \quad (3.9.16)$$

Equation (3.9.16) differs from the original equation of Oda and Yawataya which is dimensionally incorrect⁽⁴⁵⁾.

Substitution of eq. (3.9.16) into eq. (3.9.14) gives

$$\bar{t}_+ = t_{+(app)} + (\bar{t}_{-(app)} + \bar{s}) F \bar{X}_1 \bar{k}_i \beta / k' \quad (3.9.17)$$

But k' may be equated to $\varphi_w \bar{k}_i$ where φ_w is the volume fraction of water in the membrane. Equation (3.9.17), therefore, becomes

$$\bar{t}_+ = \bar{t}_{+(app)} + [\bar{t}_{-(app)} + \bar{s}] F \bar{X}_v \beta \quad (3.9.18)$$

where $\bar{X}_v = \bar{X} / \varphi_w$, equivalent of fixed groups per unit volume of interstitial water.

Since the method usually used to measure the transport number of water \bar{t}_w which is equal to (F6/18), depends on following volume changes in the anode and cathode chambers, the observed volume changes, which measures only solution flow, have to be corrected for both salt transport and electrode reactions to give values for water flow only. If reversible Ag-AgCl electrodes are used, the passage of a Faraday of current produces at the cathode, a mole of Ag and \bar{t}_+ moles of MCl (M = univalent cation) and in the same time a mole of AgCl disappears. The actual increase in volume ΔV_c , which is equal to the volume decrease at the anode, due to water transport, is given by

$$\Delta V_c = \Delta V_o + \bar{V}_{AgCl} - \bar{V}_{Ag} - \bar{t}_+ \bar{V}_{MCl} \quad (3.9.19)$$

where the \bar{V} 's are partial molar volumes and ΔV_o is the observed volume change. As $V_{AgCl} = 25,77$ and $V_{Ag} = 10,28$, eq. (3.9.19) becomes

$$\Delta V_c = \Delta V_o + 15,5 - \bar{t}_+ \bar{V}_{MCl}$$

\bar{V}_{MCl} values can be evaluated using the usual equations⁽⁶¹⁾ and \bar{t}_+ values must be obtained by experiment using the appropriate concentration. Then

$$\bar{t}_w = \Delta V / \bar{V}_{H_2O} = \Delta V / 18 \quad (3.9.20)$$

$F\bar{X}_v\beta$ may be written as \bar{t}_w/\bar{W}_e

where $\bar{t}_w = F\beta/18$ and $\bar{W}_e = 1/18\bar{X}_v$; i.e., moles of water per equivalent of ion-exchange site. Substitution of these values in eq. (3.9.18) gives

$$t_+ = \begin{cases} \bar{t}_{+(app)} + [\bar{t}_{-(app)} + \bar{s}](\bar{t}_w/\bar{W}_e) \\ \text{or} \\ (\bar{t}_w/\bar{W}_e)(1 + \bar{s}) + \bar{t}_{+(app)}(1 - (\bar{t}_w/\bar{W}_e)) \end{cases} \quad (3.9.21)$$

Oda and Yawataya computed \bar{t}_+ values from eq. (3.9.18) by measuring $\bar{t}_{+(app)}$, \bar{s} , \bar{X}_v and β . Although these values were lower than the observed values of \bar{t}_+ , they considered the agreement good since the divergence of the calculated values from the observed values was within the limits of experimental error.

3.10 Electro-Osmotic Pumping - The Stationary State - Brine Concentration and Volume Flow

3.10.1 Ion Fluxes and Volume Flow

In the unit cell flow regime ED becomes a three-port system like reverse osmosis. The feed solution is introduced between the concentrating cells, passes between the cells and leaves the system. The permeate composition is completely determined by membrane performance under the conditions of the process. A schematic diagram of a unit cell showing ion and water fluxes in the system is shown in Figure 3.10.1⁽¹⁾. For a uni-univalent salt-like sodium chloride, the current density through a cation-exchange membrane is related to the ion fluxes according to Garza⁽¹⁾ by:

$$I = F(z_1 j_1^c + z_2 j_2^c) \quad (3.10.1)$$

$$= F(j_1^c - j_2^c) \quad (3.10.2)$$

$$= F(|j_1^c| + |j_2^c|) \quad (3.10.3)$$

where $z_1 = 1$ (cation)

and $z_2 = -1$ (anion)

and j_1^c and j_2^c are the cation and anion fluxes through the cation-exchange membrane respectively.

Effective transport numbers are defined as follows^(1, 2):

$$\bar{t}_1^c = \frac{|j_1^c|}{(|j_1^c| + |j_2^c|)} = (1 + \Delta t^c)/2 \quad (3.10.4)$$

$$\bar{t}_2^c = \frac{|j_2^c|}{(|j_1^c| + |j_2^c|)} = (1 - \Delta t^c)/2 \quad (3.10.5)$$

$$\text{where } \Delta t^c = \bar{t}_1^c - \bar{t}_2^c \quad (3.10.6)$$

$$\text{and } \bar{t}_1^c + \bar{t}_2^c = 1 \quad (3.10.7)$$

Δt^c = difference between counter- and co-ion transport number or membrane permselectivity.

\bar{t}_1^c = cation transport number through cation membrane

\bar{t}_2^c = anion transport number through cation membrane

and the bar refers to the membrane phase.

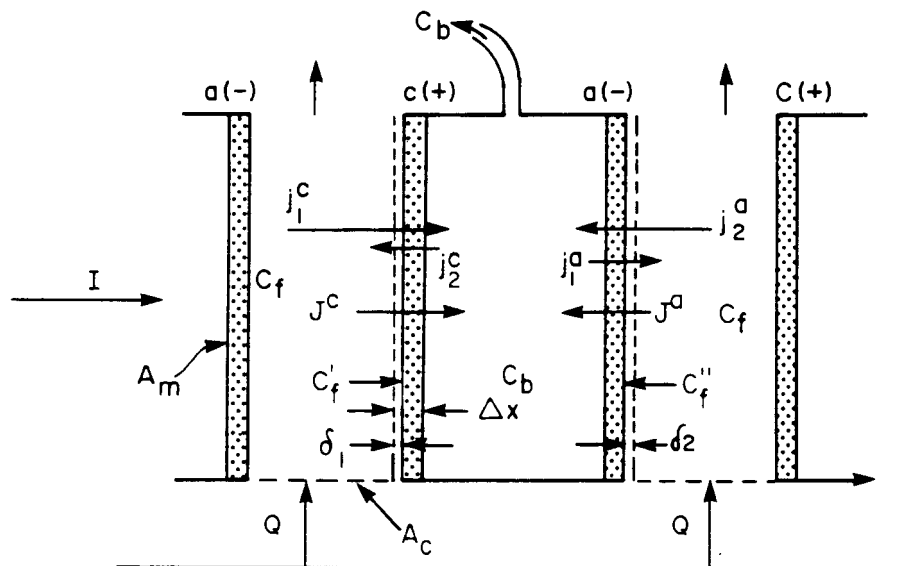


Figure 3.10.1: Representation of fluxes in the ED unit-cell system.

c and a indicate the cation- and anion-exchange membranes and subscripts 1 and 2 refer to the cations and anions, respectively (uni-univalent salts); Δx : membrane thickness; δ 's: effective Nernst layers; c_f 's: feed concentration; c_b : brine concentration; J^c and J^a : water fluxes; j^c and j^a anion and cation currents. A_m : effective membrane area; A_c : transversal area of the dialysate compartment; Q : flow of dialysate. The arrows show the direction of the fluxes.

Further,

$$j_1^c = \bar{t}_1^c (|j_1^c| + |j_2^c|) = \bar{t}_1^c I/F = (1 + \Delta t^c) I/2F \quad (3.10.8)$$

$$j_2^c = \bar{t}_2^c (|j_1^c| + |j_2^c|) = \bar{t}_2^c I/F = (1 - \Delta t^c) I/2F \quad (3.10.9)$$

(Note: Effective transport numbers are to be distinguished from the usual transport numbers which refer to the above ratio's in the absence of concentration gradients).

The brine concentration, c_b , can be obtained from the following material balance (Figure 3.10.1):

$$c_b = \frac{|j_1^c| - |j_1^a|}{|J^c| + |J^a|} = \frac{|j_2^a| - |j_2^c|}{|J^c| + |J^a|} \quad (3.10.10)$$

where J^c and J^a are the water fluxes (flows) through the cation and anion membranes, respectively.

Consider,

$$c_b = \frac{|J^c| - |j_1^a|}{|J^c| + |J^a|} \quad (3.10.11)$$

Substitute eq. (3.10.8) into eq. (3.10.11)

$$\therefore c_b = \frac{(\bar{t}_1^c I/F) - (\bar{t}_1^a I/F)}{|J^c| + |J^a|} \quad (3.10.12)$$

$$= \frac{(1 + \Delta t^c) I/2F - (1 - \Delta t^a) I/2F}{|J^c| + |J^a|} \quad (3.10.13)$$

$$= \frac{I/2F [(1 + \Delta t^c) - (1 - \Delta t^a)]}{|J^c| + |J^a|} \quad (3.10.14)$$

$$= \frac{I (\Delta t^c + \Delta t^a)}{2F (|J^c| + |J^a|)} \quad (3.10.15)$$

$$c_b = \frac{I \Delta \bar{t}}{F (|J^c| + |J^a|)} \quad (3.10.16)$$

$$= \frac{I \Delta \bar{t}}{2FJ} \quad (3.10.17)$$

$$\Delta \bar{t} = \frac{\Delta t^c + \Delta t^a}{2} \quad (3.10.18)$$

$$\text{and } 2J = |J^c| + |J^a| \quad (3.10.19)$$

The volume flow through every membrane is equal to the sum of the electro-osmotic and osmotic contributions⁽²⁾.

$$\text{Therefore } J = J_{\text{elosm}} + J_{\text{osm}} \quad (3.10.20)$$

The electro-osmotic water flow for the cation and anion membrane is given by⁽²⁾:

$$J_{\text{elosm}}^c = (\beta_1^c t_1^c - \beta_2^c t_2^c) I \quad (3.10.21)$$

$$J_{\text{elosm}}^a = (\beta_2^a t_2^a - \beta_1^a t_1^a) I \quad (3.10.22)$$

The assumption here according to Garza & Kedem⁽²⁾ is that the electro-osmotic water flow is governed by the drag exerted by the ions. The β 's are 'drag' coefficients. They represent the amount of water dragged along with every type of ion by electro-osmosis. For tight membranes, the value of the β 's should not be very different from the primary hydration water associated with the ions. For porous membranes, however, the value of the β 's may be several ten folds larger.

The osmotic contribution is given by⁽²⁾:

$$J_{\text{osm}} = 2RT \sigma L_p \Delta(g c_s) \quad (3.10.23)$$

where R is the universal gas constant, T the absolute temperature, g the osmotic coefficient, σ the reflection coefficient and L_p the hydraulic permeability.

Therefore,

$$J_{\text{osm}}^c + J_{\text{osm}}^a = 2RT(g_b c_b - g_f c_f) (\sigma^c L_p^c + \sigma^a L_p^a) \quad (3.10.24)$$

Introduction of equations (3.10.20); (3.10.21); (3.10.22) into equation (3.10.16) and neglecting the terms $(\beta_1^c - \beta_2^c) \bar{t}_2^c$ and $(\beta_2^a - \beta_1^a) \bar{t}_1^a$ in comparison with $\beta_1^c \Delta t^c$ and $\beta_2^a \Delta t^a$, gives: (note: use was made of eq.(3.10.6)

$$c_b = \frac{l(\Delta t^c + \Delta t^a)2}{F(\beta_1^c \Delta t^c + \beta_2^a \Delta t^a) + 2RT(g_b c_b - g_f c_f) \sigma^c L_p^c + \sigma^a L_p^a} \quad (3.10.25)$$

$$= \frac{(\Delta t^c + \Delta t^a)/2}{F(\beta_1^c \Delta t^c + \beta_2^a \Delta t^a) + 2FRT(g_b c_b - g_f c_f) \sigma^c L_p^c + \sigma^a L_p^a / l} \quad (3.10.26)$$

Equation (3.10.26) is justified for very permselective membranes where t_2^c and t_1^a are small, or where $\beta_1^c \approx \beta_2^a$ and $\beta_2^c \approx \beta_1^a$.

For high current densities, the second term (osmotic contribution) in the denominator of equation (3.10.26) may be neglected.

Therefore,

$$c_b^{\max} = \frac{(\Delta t^c + \Delta t^a)/2}{F(\beta_1^c \Delta t^c + \beta_2^a \Delta t^a)} \quad (3.10.27)$$

For $\beta^c \approx \beta^a$ and $\Delta t^c \approx \Delta t^a$ (symmetric membranes), equation (3.10.27) becomes

$$c_b^{\max} = \frac{1}{F(\beta_1^c + \beta_2^a)} = \frac{1}{2FB} \quad (3.10.28)$$

where $2B = \beta_1^c + \beta_2^a$.

β_1^c and β_2^a are the drag coefficients associated with the counterions. These coefficients are identical with the electro-osmotic coefficient, $\beta = (J/l)_{\Delta P = \Delta T = 0}$ measured at low concentration where co-ion exclusion is practically complete, i.e.

$$t_{\text{counter-ion}} \approx 1, t_{\text{co-ion}} \approx 0.$$

The cases for which equation (3.10.28) applies (i.e. for very permselective and/or for approximately symmetric membranes, at high current densities) are of considerable interest and importance according to Garza and Kedem⁽²⁾ since the brine concentration depends only on the electro-osmotic coefficients, β_1^c and β_2^a . c_b^{\max} can also be determined from equations (3.10.26); (3.10.27) and (3.10.28)

$$c_b = \frac{l \Delta \bar{t}}{F(J_{\text{elosm}} + J_{\text{osm}})} \quad (3.10.29)$$

$$= \frac{l \Delta \bar{t}}{F J_{\text{elosm}} (1 + J_{\text{osm}} / J_{\text{elosm}})} \quad (3.10.30)$$

$$= \frac{C_b^{\max}}{1 + J_{osm}/J_{elosm}} \quad (3.10.31)$$

3.10.2 Symmetric cells

The theory of EOP in general leads to difficult computations which must be carried out numerically according to Garza⁽¹⁾. However, there is one case in which results can be given in terms of simple closed formula. This case depends on the assumption of a symmetric cell⁽¹⁾. In a symmetric cell the cation- and anion-exchange membranes have identical physical properties in all regards except for the sign of their fixed charges. Because of cell symmetry, the magnitudes of the counter-ion fluxes through both membranes are the same. When a symmetric salt is chosen like potassium chloride, the anion and cation have equal mobilities. In other words, the magnitude of the cation flux through the cation exchange membrane is the same as the magnitude of the anion flux through the anion-exchange membrane. Also the magnitudes of the co-ion fluxes through both membranes are the same, i.e., the magnitude of the anion flux through the cation-exchange membrane is the same as the magnitude of the cation flux through the anion-exchange membrane.

$$|j_1^c| = |j_2^a|; |j_1^a| = |j_2^c| \quad (3.10.32)$$

and thus

$$\bar{i}_1^c = \bar{i}_2^a; \bar{i}_1^a = \bar{i}_2^c; \Delta t^c = \Delta t^a = \Delta \bar{t} \quad (3.10.33)$$

Water flows also are of equal magnitude and opposite direction:

$$|J^c| = |J^a| = J \text{ or } J^c = -J^a = J \quad (3.10.34)$$

The amount of salt leaving through the brine outlet per unit time and membrane area, $2J c_b$, is related to the cation flows by (eqs. 3.10.10 and 3.10.19):

$$2Jc_b = |j_1^c| - |j_1^a| \quad (3.10.35)$$

and in the symmetric system is :

$$J = |\Delta \bar{t}| / 2c_b F \quad (3.10.36)$$

3.10.2.1 Current Efficiency

The amount of salt transferred per Faraday of current passed through a symmetric unit cell is given from equation 3.10.36 by

$$\varepsilon_p = \frac{2Jc_b}{I/F} = \Delta \bar{t} \quad (3.10.37)$$

The overall efficiency, ε , is, however, somewhat smaller than ε_p , since water is also lost with the salt. The effective current density, i.e. the purification of the product achieved, is given by⁽¹⁾:

$$I_{\text{eff}} = F \left(\frac{Q}{A_m} - 2J \right) (c_f - c_p) = F \left(\frac{Q}{A_m} - 2J \right) (\Delta c_f) \quad (3.10.38)$$

where Q is the amount of feed solution entering a channel per unit time, A_m the effective membrane area (Figure 3.10.1), Δ the degree of mineralization given by:

$$\Delta = \frac{c_f - c_p}{c_f} \quad (3.10.39)$$

where

c_f is the concentration of the feed solution entering the stack, and c_p the concentration of the product leaving it.

The mass balance for the salt is:

$$\frac{Qc_f}{A_m} = \left(\frac{Q}{A_m} - 2J \right) c_p + 2Jc_b \quad (3.10.40)$$

Therefore

$$I_{\text{eff}}/F = \left(\frac{Q}{A_m} - 2J \right) (c_f - c_p) = 2J(c_b - c_f) \quad (3.10.41)$$

and

$$\varepsilon = \frac{I_{\text{eff}}}{I} = \Delta t \left(1 - \frac{c_f}{c_b} \right) = \varepsilon_p \times \varepsilon_w \quad (3.10.42)$$

where

$$\varepsilon_{\omega} = 1 - c_i/c_o \quad (3.10.43)$$

As is customary in ED, the overall efficiency is presented as the product of two terms, one due to the lack of ideal permselectivity in the membranes, ε_p , the other reflecting the loss of water to the brine, ε_w .

3.10.2.2 Electro-Osmotic Flow

Electro-osmotic flow is measured under the restrictions⁽¹⁾:

$$\Delta c = 0, \quad du_w/dx = 0$$

Under these conditions are :

$$J_{\text{elosm}} = (j_1 \beta_1 + j_2 \beta_2)F \quad (3.10.44)$$

Equation 3.10.44 can also be written as :

$$J_{\text{elosm}} = (\beta_1 t_1 - \beta_2 t_2)I \quad (3.10.45)$$

$$= [\beta_1(t_1 - t_2) + (\beta_1 - \beta_2) t_2]I \quad (3.10.46)$$

$$= [\beta_1 \Delta t + (\beta_1 - \beta_2) t_2]I \quad (3.10.47)$$

For small values of t_2 , or for $\beta_1 = \beta_2 = \beta$ equation (3.10.47) becomes :

$$J_{\text{elosm}} = \beta^{\circ} \Delta t I \quad (3.10.48)$$

where β° is the customary electro-osmotic coefficient measured at low ionic strength where co-ion exclusion is high and $\Delta t \approx 1$, i.e.:

$$\beta^{\circ} = (J/I)_{\Delta C = \Delta P = \Delta T = 0, \Delta t = 1} = (J_{\text{elosm}}/I)_{\Delta t = 1}$$

3.10.2.3 Osmotic Flow at High Co-Ion Exclusion

Osmotic flow is measured under the restrictions⁽¹⁾:

$$I = \Delta p = 0, \quad j_1 = j_2 = 0.$$

(absence of electric current, hydrostatic pressure and impermeable solutes). In this case is⁽¹⁾:

$$J_{osm} = L_p \sigma \Delta \pi \quad (3.10.49)$$

3.10.2.4 Volume Flow in Electro-Osmotic Pumping

The volume flow into the membrane concentrating cells in EOP is the sum of the electro-osmotic and osmotic water flows and is given by⁽¹⁾:

Therefore,

$$J = -L_p \sigma \Delta \Pi + \beta^\circ \Delta t I \quad (3.10.50)$$

3.10.3 Non-Symmetric Cell

3.10.3.1 Porous membranes

In the previous section a simplified theory of the electro-osmotic pumping process was given where only the symmetric cell case was treated. By 'symmetric cell' is meant that the cation- and anion-exchange membranes are assumed to have the same values for the physical properties of interest in the process, namely, absolute effective charge density, electro-osmotic coefficient, and hydraulic permeability. If this were not the case, the calculations would become much more complicated since Δt (difference between the effective transport numbers of counter- and co-ions) may have different values for the two types of membranes, and the expression for the brine concentration, c_b , will not be as simple as for the symmetric case⁽¹⁾. c_b may be found in the general case from material balance considerations to be equal to :-

$$c_b = \frac{|j_1^c| - |j_1^a|}{|J^c| + |J^a|} \quad (3.10.11)$$

From the definition of 'effective' transport numbers given before (eqs. 3.10.4 and 3.10.5), it can be written :

$$\begin{aligned} |j_1^c| - |j_1^a| &= |j_2^a| - |j_2^c| \\ &= (1 + \Delta t^c)I/2F - (1 - \Delta t^a)I/2F \end{aligned}$$

$$= (\Delta t^c + \Delta t^a)l/2F \quad (3.10.51)$$

The volume flow is given by the sums of electro-osmotic and osmotic terms, namely:

$$\begin{aligned} J &= J_{\text{elosm}} + J_{\text{osm}} \\ &= (\beta_1 t_1 - \beta_2 t_2)l + 2RT \sigma L_p \Delta(\phi_s c_s) \end{aligned} \quad (3.10.52)$$

Therefore,

$$\begin{aligned} &|J^c| + |J^a| \\ &= l(\beta_1^c t_1^c - \beta_2^c t_2^c + \beta_2^a t_2^a - \beta_1^a t_1^a) + 2RT (\phi_b c_b - \phi_f c_f) \times (\sigma^c L_p^c + \sigma^a L_p^a) \\ &= l[\beta_1^c (t_1^c - t_2^c) + (\beta_1^c - \beta_2^c) t_2^c + \beta_2^a (t_2^a - t_1^a) + (\beta_2^a - \beta_1^a) t_1^a] + \dots + 2RT (\phi_b c_b - \phi_f c_f) \\ &\times (\sigma^c L_p^c + \sigma^a L_p^a) \end{aligned} \quad (3.10.53)$$

for small values of t_2^c and t_1^a , or for $\beta_1^c = \beta_2^a = \beta_c^o$, and $\beta_2^c = \beta_1^a = \beta_a^o$; equation (3.10.53) becomes:

$$|J^c| + |J^a| = l(\beta_1^c \Delta t^c + \beta_2^a \Delta t^a) + 2RT (\phi_b c_b - \phi_f c_f) \times (\sigma^c L_p^c + \sigma^a L_p^a) \quad (3.10.54)$$

Substituting equations (3.10.51) and (3.10.54) into (3.10.11), gives:

$$c_b = \frac{(\Delta t^c + \Delta t^a)/2}{F(\beta_1^c \Delta t^c + \beta_2^a \Delta t^a) + 2RT(\phi_b c_b - \phi_f c_f)(\sigma^c L_p^c + \sigma^a L_p^a)l/F} \quad (3.10.55)$$

In the case of high current density, the second term in the denominator of equation (3.10.55) can be neglected. Therefore,

$$c_b^{\text{max}} = \frac{(\Delta t_{\text{max}}^c + \Delta t_{\text{max}}^a)/2}{F(\beta_1^c \Delta t_{\text{max}}^c + \beta_2^a \Delta t_{\text{max}}^a)} \quad (3.10.56)$$

Plots of Δt versus current density for every membrane are expected to have the same kind of behaviour as for the symmetric cell case, as no new elements have been added. The value of c_b , however, depends now on the properties of both membranes, and not on those of only one of them. Therefore, for high current densities the values of Δt become independent on l , and can be calculated⁽¹⁾. Since the values of Δt depends on c_b , which in its turn depends on Δt^c and Δt^a , trial and error calculations are necessary according to Garza.

In conclusion, for the non-symmetric-cell case (as for the symmetric cell) the following is expected⁽¹⁾:

- The Coulomb efficiency of the concentrating cell will reach a maximum (plateau) value at high current densities (below the limiting value of the current)

$$\begin{aligned}\varepsilon &= \Delta t = t_1^c - t_1^a = (1 + \Delta t^c)/2 - (1 - \Delta t^a)/2 \\ &= (\Delta t^c + \Delta t^a)/2\end{aligned}\quad (3.10.57)$$

- The brine concentration, c_b , to reach a maximum value (also at high current densities below the limiting value) independent of I and of the feed concentration;
- The volume flow (3.10.54) versus $I\Delta t$ plots will become straight lines at high current densities since the osmotic contribution becomes almost independent of current density when the latter is sufficiently high (because c_b becomes constant and c' - the concentration at the feed interface (Fig. 3.10.1) may be kept within certain limits by controlling concentration polarization); and the electro-osmotic contribution is directly proportional to $I\Delta \bar{t}$ ($\Delta \bar{t} = (\Delta \bar{t}^c + \Delta \bar{t}^a)/2$, when either $\Delta t^c = \Delta t^a$ or $\beta_1^c = \beta_2^a$).

3.11 Flux Equations, Membrane Potentials and Current Efficiency

Flux equations, membrane potentials and current efficiency relevant to EOP-ED have been described by Kedem and Bar-On⁽⁵⁾. The total ED process comprises three independent flows and forces; electric current and potential; volume flow and pressure/osmotic pressure; salt flow and concentration difference. For small flows and gradients linear equations can be written for each of the flows, including the influence of all gradients⁽¹⁴⁾.

In practical ED, especially in EOP, flows and forces are large and one can not expect linear equations to hold, even if the usually defined membrane transport coefficients are constant, according to Kedem and Bar-on. In fact, transport coefficients may vary considerably in the concentration range between feed and brine. For an adequate discussion of flows under these conditions, Kedem and Bar-On have followed the analysis given previously for reverse osmosis⁽⁸²⁾.

In the schematic presentation shown in Figure 3.11.1, the membrane is broken down into differential elements, separated by uniform solution segments which are in equilibrium with the two contiguous membrane faces. All fluxes going from left to right are counted positive. The gradient of a scalar y , dy/dx , is taken as the value of the scalar on the right (double prime) minus the value on the left (single prime), divided by the distance. On the other hand, the operator Δ is defined with the opposite sign, in order to bring the notation used by Kedem and Bar-On in line with that of previous publications⁽⁶⁾:

$$\Delta c = c' - c'' \text{ and}$$

$$y = \int dy$$

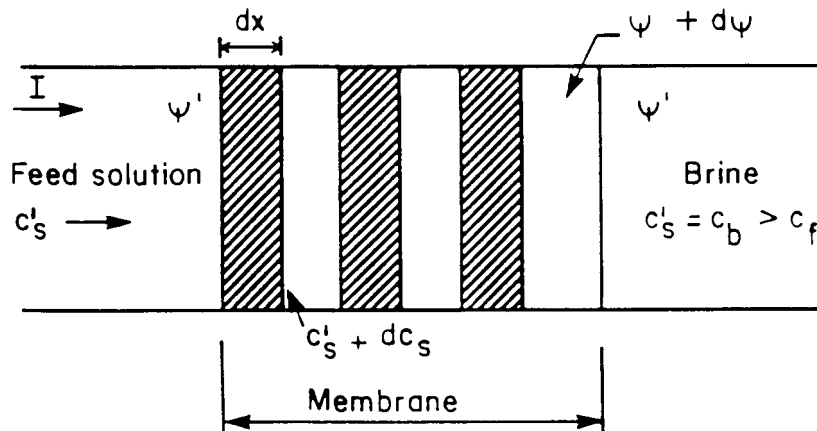


Figure 3.11.1: Schematic representation of cation-exchange membrane.

Salt flow across a differential layer of cation-exchange membrane can be written as a function of electric current, volume flow and concentration gradient according to Kedem and Katchalsky⁽¹⁴⁾:

$$S^c = \frac{J_1^c + J_2^c}{2} = c_s (1 - \sigma^c) J_v^c + \bar{P} \Delta c + \frac{\Delta t}{2} \frac{I}{F} \quad (3.11.1)$$

where

$$\Delta t^c = t_1^c - t_2^c = 2t_1^c - 1 \quad (3.11.2)$$

Equation (3.11.1) can be derived as follows according to Kedem and Bar-On⁽⁵⁾:

In a discontinuous system containing water and one uni-valent salt in the absence of hydrostatic pressure, the rate of free energy dissipation is :

$$\phi = j_1 \Delta \tilde{\mu}_1 + j_2 \Delta \tilde{\mu}_2 + j_w \Delta \mu_w \quad (A1)$$

where the μ_i 's are the electro-chemical potentials of ions 1 and 2.

$$\Delta \tilde{\mu}_1 + \Delta \tilde{\mu}_2 = \Delta \mu_s \quad (A2)$$

$$\Delta \tilde{\mu}_1 + \Delta \tilde{\mu}_2 = 2F\Delta\Psi (\Delta p = 0) \quad (A3)$$

$$I = F(J_1 - J_2) \quad (A4)$$

$$\Delta \mu_w = -\bar{V}_w \Delta \Pi_s \quad (A5)$$

$$J_v = \bar{V}_w J_w \quad (A6)$$

Equation (A1) can be transformed to :

$$\phi = \frac{(J_1^c + J_2^c)}{2} \Delta \mu_s + I \Delta \Psi - J_v \Delta \pi_s \quad (A7)$$

because

$$\begin{aligned} & \frac{J_1 + J_2}{2} (\Delta \tilde{\mu}_1 + \Delta \tilde{\mu}_2) + (J_1 - J_2) \frac{(\Delta \tilde{\mu}_1 - \Delta \tilde{\mu}_2)}{2} - J_v \Delta \pi_s \\ &= \frac{J_1}{2} \Delta \tilde{\mu}_1 + \frac{J_2}{2} \Delta \tilde{\mu}_1 + \frac{J_1}{2} \Delta \tilde{\mu}_2 + \frac{J_2}{2} \Delta \tilde{\mu}_2 + \frac{J_1}{2} \Delta \tilde{\mu}_1 - \frac{J_2}{2} \Delta \tilde{\mu}_1 - \frac{J_1}{2} \Delta \tilde{\mu}_2 + \frac{J_2}{2} \Delta \tilde{\mu}_2 - J_v \Delta \pi_s \\ &= J_1 \Delta \tilde{\mu}_1 + J_2 \Delta \tilde{\mu}_2 + J_w \Delta \mu_w \end{aligned}$$

The salt flow was identified with J_1 (uni-valent cation). Therefore

$$J_2 = J_1 - I/F \quad (3.11.3)$$

The expressions for the ion fluxes in terms of the practical coefficients are⁽¹⁴⁾:

$$J_1 = \omega \Delta \Pi_s + c_s (1 - \sigma) J_v + t_1 I/F \quad (3.11.4)$$

and

$$J_2 = \omega \Delta \Pi_s + c_s (1 - \sigma) J_v - (1 - t_1) I/F \quad (3.11.5)$$

Therefore, the salt flow

$$\frac{J_1 + J_2}{2} = c_s(1-\sigma)J_v + \omega \Delta \pi_s + \frac{\Delta t}{2}I/F \quad (3.11.6)$$

where ω = solute permeability

and $\Delta \pi_s$ = difference in osmotic pressure of permeable solute

Equation (3.11.1) is identical with equation (3.11.6).

\bar{P} in equation (3.11.1) is the specific salt permeability, Δc the concentration difference and σ the reflection coefficient. In an ideally permselective cation-exchange membrane will $\Delta t^c \rightarrow 1$, $P \rightarrow 0$, $\sigma \rightarrow 1$, so that $S^c = 1/2F$. Similarly, in an ideal anion-exchange membrane will $\Delta t^a \rightarrow 0$, $P \rightarrow 0$, $\sigma \rightarrow 1$, and $-S^a = 1/2F$ and $\eta_c = 1$.

Consider now a cation-exchange membrane in which salt exclusion is not complete with co-ions carrying a significant fraction of the current⁽⁵⁾. In this case Δt will be smaller than 1 and will decrease with increasing c_s (salt concentration) as salt invasion becomes pronounced. Salt permeability will increase when c_s increases. If the influence of volume flow is negligible, a constant stationary value of S^c is possible only if the concentration profile is concave, i.e. dc/dx decreases from the feed to the brine surface⁽⁵⁾. A region of constant c_s may then develop near the brine surface at high current density. The upper limit of the partial current efficiency η_c^c is then determined by Δt^c characterizing the membrane equilibrated with the brine solution. The same argument holds for the anion-exchange membrane. Therefore, according to Kedem and Bar-on, without the influence of volume flow

$$\eta_c < \frac{\Delta t^c(c_b) + \Delta t^a(c_b)}{2} \quad (3.11.7)$$

when back diffusion is overcome by high current density.

The conventional method for determination of transport numbers is the measurement of membrane potential, i.e. $\Delta \Psi$ between two solutions separated by the examined membrane without electric current. The potential across a differential layer is given by the expression⁽⁵⁾:

$$-F \frac{d\Psi}{dx} = \Delta t \frac{1}{2} \frac{d\mu_s}{dx} - F \frac{\beta}{L_p^R} J_v \quad (3.11.8)$$

where β is the electro-osmotic coefficient and L_p is the hydraulic permeability. The last

term represents a streaming potential. If this can be neglected, the potential between feed and brine solution is given by :

$$\Delta \Psi_m = \frac{RT}{F} \int_{c_i}^{c_b} \Delta t \left(1 + \frac{d \ln \gamma^\pm}{d \ln c_s} \right) d \ln c_s \quad (3.11.9)$$

for an ideal membrane is $\Delta t = 1$

$$\Delta \Psi_i = \frac{RT}{F} \ln \frac{(c_s \gamma^\pm)_b}{(c_s \gamma^\pm)_i} \quad (3.11.10)$$

where γ^\pm is an activity coefficient and the average transport number is

$$\bar{\Delta t} = \frac{\Delta \Psi_m}{\Delta \Psi_i} \quad (3.11.11)$$

This average transport number, according to Kedem and Bar-on, is closer to the value for c_i than for c_b . The conclusion from equations (3.11.7), (3.11.9) and (3.11.11) is that for concentration dependent transport numbers, the actual current efficiency is expected to be less than predicted from membrane potentials, i.e.

$$\eta < \frac{\Delta \Psi_m^c + |\Delta \Psi_m^a|}{|2\Delta \Psi_i|} \quad (3.11.12)$$

The correlation given by equation (3.11.12) is valid only if the influence of volume flow is negligible.

The potential per cell pair, V_{cp} (in volt), at a given current density ($i = l/cm^2$, mA/cm²), is the sum of several terms⁽⁴⁾:

$$V_{cp} = V_n + i (R_m + R_p + R_d + R_b) \quad (3.11.13)$$

where V_n is the concentration potential, a counter driving force built up by the concentration process. Its magnitude depends on the concentration ratio between the brine and dialysate and the permselectivity of the membrane at the given conditions. V_n is measured during interruption of the current for a few seconds - long enough to disperse concentration gradients near the membranes, short enough to avoid changes of bulk concentration.

$\frac{V_{cp} - V_n}{i}$ is the resistance of the cell pair; R_m membrane resistance;

R_b , brine compartment resistance; R_d , dialysate compartment resistance; and R_p , the ohmic resistance and additional counter potential due to polarization layers adjacent to the membrane surface facing the dialysate. In this system, R_b is negligible, since the brine is always more concentrated than the dialysate. For the simplest characterization of the system, it can be written⁽⁴⁾:

$$R_{cp} = \frac{V_{cp} - V_n}{i} = R_m + \rho d_{eff} \quad (3.11.14)$$

where ρ is the specific resistance of the dialysate solution, and d_{eff} is the effective thickness of the dialysate compartment. In this simple representation the shadow effect of the spacer, polarization layers and any other possible disturbances are lumped into d_{eff} .

The measurement of voltage and current during desalination at a given circulating flow velocity gives the stack resistance as a function of concentration. If desalination is carried out at constant voltage, straight lines are obtained for a plot of cell pair resistance (R_{cp}) as a function of specific resistance of the bulk dialysate solution (ρ) in a wide range of currents and concentrations (c). This is due to nearly constant i/c , which determines, at given bulk flow, the polarization. Straight lines show not only that R_d , but also that the contribution of polarization, is an approximately linear function of bulk dialysate resistance.

3.12 Electro dialysis Theory

3.12.1 Basic Principles

An ED cell is shown in Figure 3.12.1. It comprises of a driven electrochemical cell containing electrodes at each end and a series of compartments or channels of typically 1 mm width, separated by membranes⁽⁶⁾. Alternate membranes are "anion permeable" ("A" in Fig. 3.12.1) and "cation-permeable" ("C" in Fig. 3.12.1). The membranes are thin sheets of polymer which have been treated with cationic and anionic groups to impart selective permeability. Under the influence of an applied potential between the electrodes, current flows within the ED cell, being carried by cations - which tend to migrate towards the negatively charged electrode (cathode) - and anions - which tend to move in the direction of the positively charged electrode (anode).

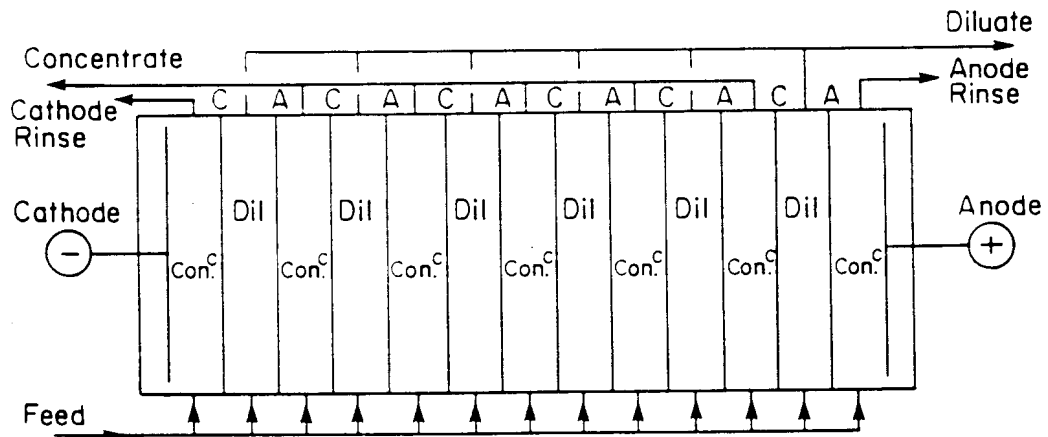
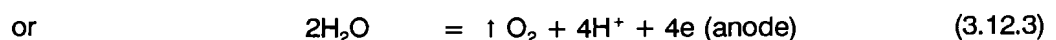
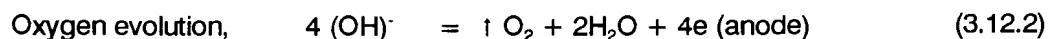
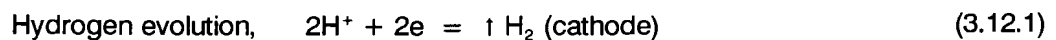


Figure 3.12.1: General layout of an ED stack. Dil = diluting compartments; Con.^c = concentrating compartments.

To see how water purification can occur in such a cell, consider the smaller set-up shown in Figure 3.12.2 and, in particular, the events in the compartment marked D₂. The various cations present in the water (say Na⁺, Ca²⁺, etc.) can pass freely through the cation-permeable membrane at one end of the compartment and the anions can pass through the anion-permeable membrane at the opposite end. However, neither the cations nor the anions can move out of the adjacent compartments F because the membranes towards which they move (under the influence of the applied potential) are of the wrong type (electrical charge) to allow passage of the ions. Ions, however, can escape from compartments D₂. The result of all this, in a multi-compartment cell, is that water is diluted and concentrated in alternate compartments (as noted in Fig. 3.12.1) - thus enabling the collection of the purer water from the so-called diluate channels.

During ED of a natural water, several electrode reactions are possible, but the most generally observed ones are⁽⁶³⁾:



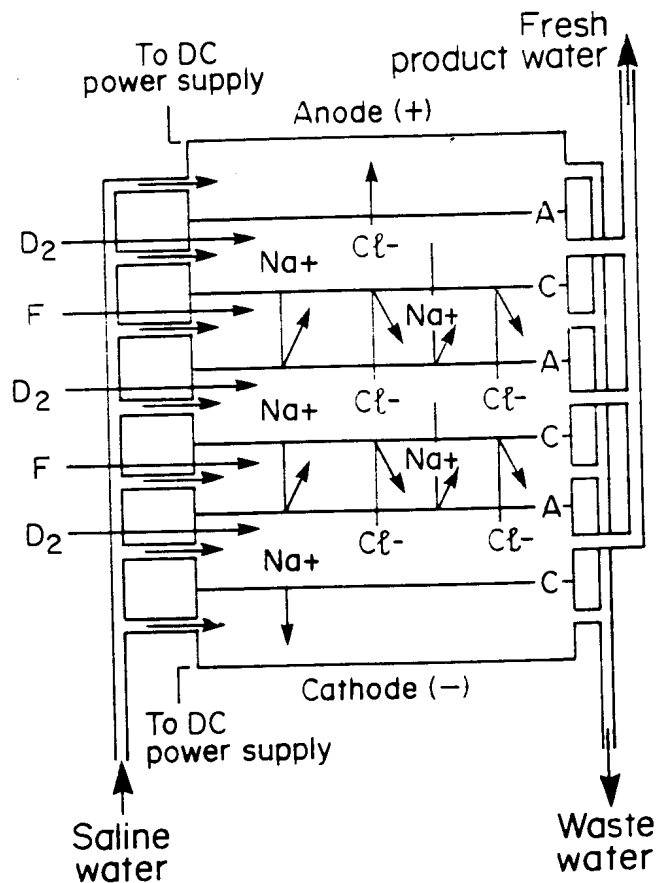


Figure 3.12.2: Ion movement during ED.

3.12.2 Desalting Rate

An important factor in any desalination process is the rate at which desalination occurs. In order to determine the factors which control the desalination rate in an ED unit, it is necessary to examine in some detail the ion-transport processes occurring in the cell⁽¹⁰⁾ (and particularly within and around the membranes). This is done by considering the ion-transport numbers (i.e. the fraction of the current carried by the different kinds of ions in the cell), in particular, it is necessary to compare the transport numbers in the bulk solution and in the membranes. Consider, therefore, desalination of a solution of sodium chloride. In the bulk solution, away from the membranes, the current is carried by the opposite drift of Na⁺ and Cl⁻ ions, in fact, 60% of the current is carried by the Cl⁻ ions and 40% by Na⁺ ions, i.e. the transport numbers in the bulk solution are $t_1 = 0,4$ and $t_2 = 0,6$. In perfect membranes, however, only one type of ion can pass through a membrane and the total current is carried by that ion. The characteristics of perfect and practical ion-exchange membranes are shown in Table 3.12.1.

Table 3.12.1: Characteristics of perfect and practical ion-exchange membranes.

Membrane Type	Cation-permeable membrane (CPM)	Anion-permeable membrane (APM)
Perfect membrane	$\bar{t}_1^c = 1,0; \bar{t}_2^c = 0$	$\bar{t}_1^a = 0; \bar{t}_2^a = 1,0$
"Practical" membrane	$\bar{t}_1^c \approx 1,0; \bar{t}_2^c \ll 1$	$\bar{t}_1^a \ll 1; \bar{t}_2^a \approx 1,0$

where \bar{t}_1^c = transport number of cations (Na^+) in CPM

\bar{t}_2^c = transport number of anions (Cl^-) in CPM

\bar{t}_1^a = transport number of cations in APM

\bar{t}_2^a = transport number of anions in APM

The efficiency with which a membrane excludes a particular ion is expressed by the permselectivity of the membrane with respect to that ion. The permselectivity is defined as follows⁽⁷⁾:

For cation permeable membranes:

$$P^c = \frac{t_2 - \bar{t}_2}{t_2} = \frac{\bar{t}_1 - t_1}{1 - t_1} \quad (3.12.4)$$

For anion permeable membranes:

$$P^a = \frac{t_1 - \bar{t}_1}{t_1} = \frac{\bar{t}_2 - t_2}{1 - t_2} \quad (3.12.5)$$

Consider now the ion transport processes occurring within an ED unit and it is useful to begin with a simple cell containing sodium chloride solution with just one perfect membrane (a CPM) inserted (Fig. 3.12.3). In the situation depicted in Figure 3.12.3, chloride ions are drifting to the right and sodium ions to the left. At the membrane the sodium ion flux is proportional to the current I . Thus, as indicated in the magnified sketch of the membrane region (Fig. 3.12.3a),

$$\bar{t}_{\text{Na}^+} = 1,0; \bar{t}_{\text{Cl}^-} = 0,0$$

i.e. the Na^+ migration rate is I/F equiv/s where I is the current and F is Faraday's constant. In the bulk solution on either side of, but away from, the membrane,

$$t_{\text{Na}^+} = 0,4 \text{ and } t_{\text{Cl}^-} = 0,6$$

i.e. migration rates in equiv/s are $0,4 I/F$ of Na^+ and $0,6 I/F$ of Cl^- .

Consider now the two boundary-layer regions on either side of the membrane. The

ion flow due to the electrical current will produce the following mass balance for the passage of each Faraday of current.

R.H.S. Sodium

Inflow from solution	Outflow through membrane
0,4	1,0
Sodium depletion	= 0,6 (equiv)

Chloride

Inflow from membrane	Outflow to solution
0,0	0,6
Chloride depletion	= 0,6 (equiv)

Consequently, it appears that there is a deficiency in the salt mass balance on the R.H.S. of the membrane, when account is taken only of the electrical flow of ions. However, the nett efflux of salt from this region will reduce the concentration at the membrane surface and this will trigger an additional migration process, namely a diffusive flux of salt from the bulk solution into the depleted boundary region. In the steady state, the mass flux due to diffusion must be equivalent to sodium and chloride depletion rates of 0,6 (caused by the electrical flux) in order to maintain the salt concentrations in the boundary region.

L.H.S. Sodium

Inflow from membrane	Outflow to solution	Accumulation Rate
1,0	0,4	0,6 (equiv)

Chloride

Inflow from solution	Outflow to membrane	Accumulation Rate
0,6	0,0	0,6 (equiv)

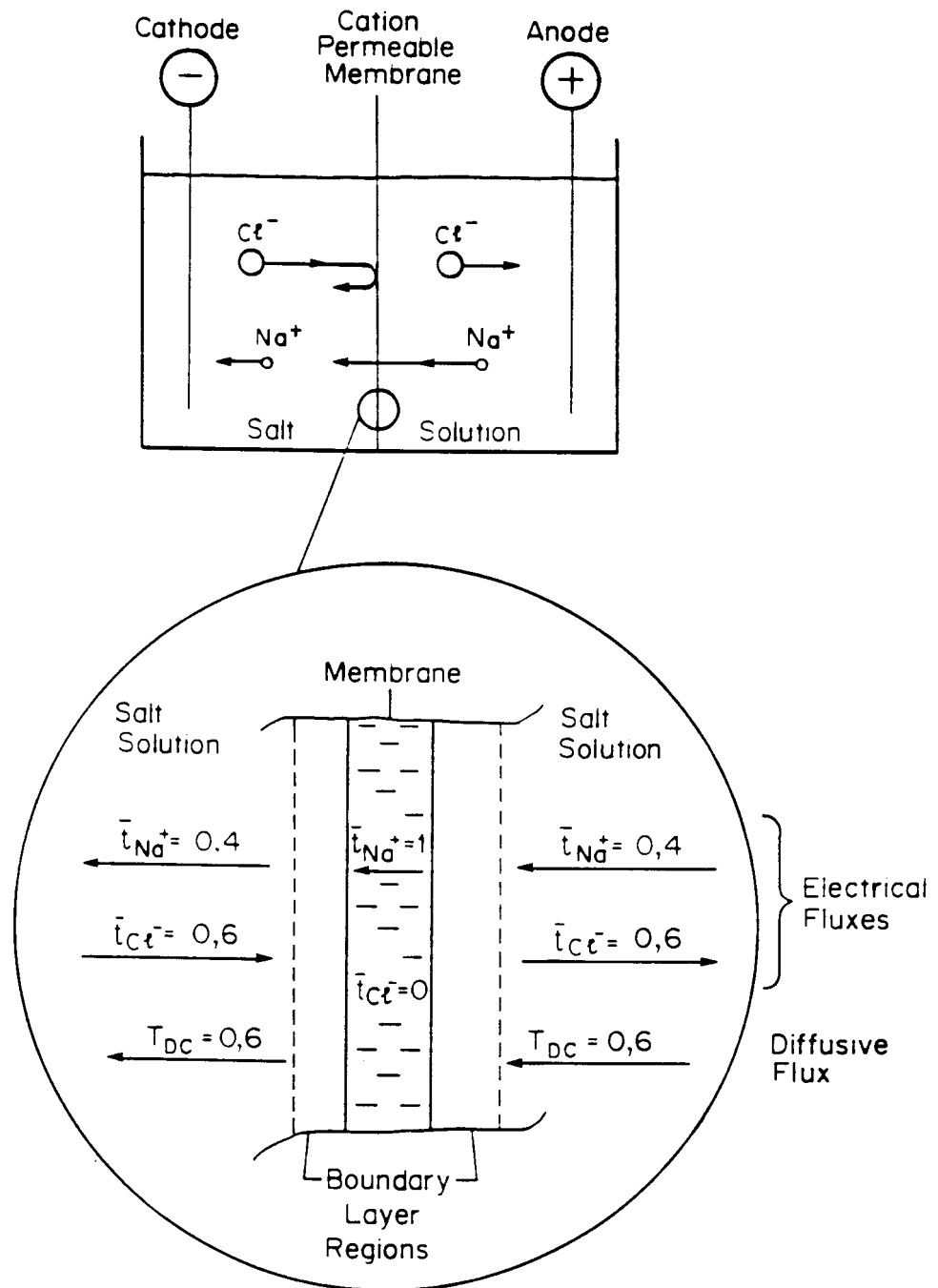


Figure 3.12.3 (Upper) and Figure 3.12.3(a) (Lower).

Processes occurring within and around a cation-permeable membrane in an electrochemical cell containing NaCl solution.

In a similar manner to the salt deficiency on the R.H.S. of the membrane as a result of Coulombic migration, there appears to be an accumulation of salt on the L.H.S. of the membrane equivalent to a transport number of 0,6. This imbalance of mass flow is again in the steady state, counted by a diffusive flow of salt. This time the salt concentration is increased at the membrane surface by the electrical migration and the salt therefore diffuses away into the bulk of the solution. Comparing this situation with

the straightforward electrolysis process without the membrane, the nett effect of inserting the membrane is to produce an apparent diffusion of salt from right to left across the membrane. The rate (in equivs per Faraday) of this apparent diffusion transport number, T_{DC} may be expressed in terms of the transport numbers. For the present case, it is clear that $T_{DC} = 0,6$ equiv/Faraday, i.e. $T_{DC} = t_2$. However, in the general case for imperfect membranes, a similar analysis as that above leads to:

$$T_{DC} = t_2 - \bar{t}_2^c$$

A similar analysis and argument may be set up for an anion-permeable membrane. In this case, if the membrane was perfect (i.e. $\bar{t}_1^a = 0$ and $\bar{t}_2^a = 1,0$), there would appear to be a salt depletion on the L.H.S. To balance these there would have to be an apparent diffusion of salt from left to right across the membrane. In this case for an imperfect membrane, $T_{DA} = t_1 - \bar{t}_1^a$ which reduces to $T_{DA} = 0,4$ for the case of a perfect APM in a NaCl solution.

Consider now what will happen if an anion-permeable membrane is inserted on the right hand side of the cation permeable membrane in Figure 3.12.3. Such a set up is depicted in Figure 3.12.4. Passage of current through this system will produce an apparent effect of salt diffusion out of the space between the two membranes. For the simple example of perfect membranes in NaCl solution, the rates of these apparent diffusions will be

$$\text{To the left across the C.P.M., } T_{DC} = 0,6$$

$$\text{To the right across the A.P.M., } T_{DA} = 0,4$$

But, for the general case with imperfect membranes $T_{DC} = t_2 - \bar{t}_2^c$ and $T_{DA} = t_1 - \bar{t}_1^a$.

Therefore, the total apparent diffusive flux out of the central compartment of a set-up like Figure 3.12.4 is:

$$T_D = T_{DC} + T_{DA} = t_2 - \bar{t}_2^c + t_1 - \bar{t}_1^a \quad (3.12.6)$$

$$= 1 - \bar{t}_2^c - \bar{t}_1^a \text{ equiv per Faraday} \quad (3.12.7)$$

$$= 1 \text{ for perfect membranes.} \quad (3.12.8)$$

T_D , the salt flux out of the central compartment, is clearly a measure of the desalting rate, i.e. for a current flow of I amp,

$$\text{Desalting rate} = I/F (T_{DC} + T_{DA}) \text{ equiv/s} \quad (3.12.9)$$

$$= I/F \text{ equiv/s (for perfect membranes).} \quad (3.12.10)$$

Hence, for a system with perfect membranes, the salt removal from the space between the membranes is exactly equivalent to the charge that is passed through the system. This is exactly equivalent to the decrease in salt concentration in sodium chloride in a simple electrolytic cell in which the electrode reactions involved sodium deposition (cathodic) and chlorine evolution (anodic). (Note: If the membranes been the other way round in Figure 3.12.4, the APM on the left and the CPM on the right, then the effect would be to concentrate rather than dilute the solution between the membranes).

Thus, the desalting rate increases with cell current. Another important factor is the number of membranes. As mentioned earlier, the above expressions apply to a simple ED cell containing just one pair of membranes. The system can be greatly improved by inserting many pairs of membranes because each pair produces an equivalent amount of desalination. Thus, the total desalination achieved per unit charge flow is

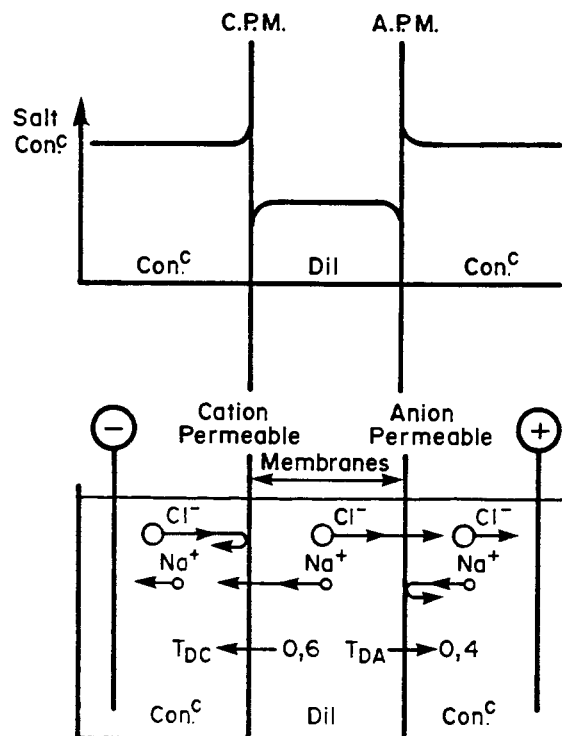


Figure 3.12.4: Cell containing a pair of membranes.

N times that in a one-pair set-up, where N is the number of membrane pairs, i.e.

$$\text{Desalting rate} = \frac{NI}{F} (T_{DC} + T_{DA}) \quad (3.12.11)$$

Note that, in Figure 3.12.2, there are 6 membrane pairs giving a desalting rate of $6I/F$ equiv/s for perfect membranes.

3.12.3 Energy Requirements for Electrodialysis

In order to estimate the energy requirements for ED all the potential differences (or IR drops) in the cell must be investigated. The required applied voltage for ED comprises several elements⁽¹⁶⁾:

- i) a voltage necessary to drive the electrode reactions;
- ii) a voltage required to overcome the aqueous solution resistances in the ED cell;
- iii) a voltage necessary to overcome the membrane potentials;

The first of these is determined from the electrode potentials for the particular electrode reaction and increases with cell current due to polarisation of the electrode reactions. However, in commercial units, this component of the required applied voltage is usually small in comparison to those arising from (ii) and (iii). Therefore, the latter factors will be considered in more detail.

3.12.3.1 Solution Resistances

The resistivity of an aqueous electrolyte decreases with increasing ionic concentration. Therefore, IR drops through the diluate channels are considerably greater than those through the concentrate channels. A further complication, with consequences for ED energy requirements, is concerned with concentration changes which occur in the regions immediately adjacent to the membranes. These are summarized in Figure 3.12.5 which illustrates that salt depletion occurring in the boundary regions adjacent to the membranes in the diluate channels and enrichment occurring in the boundary layers on the concentrate side of the membranes. For a cation-permeable membrane,

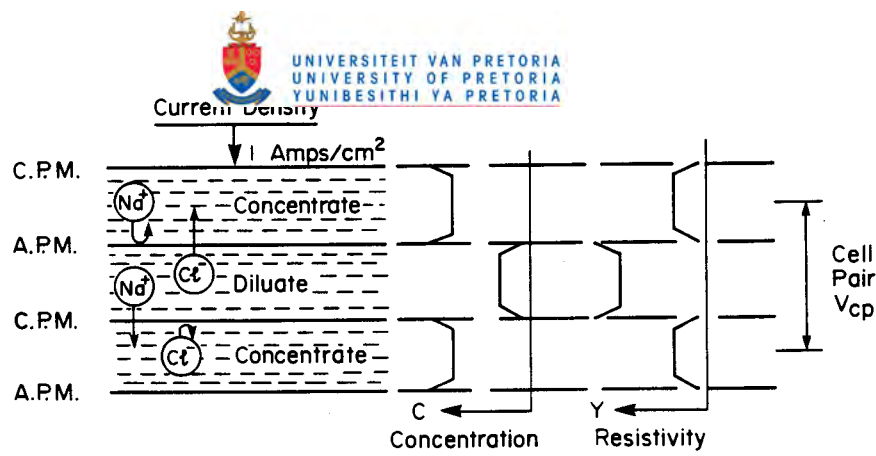


Figure 3.12.5: The cell pair showing salt depletion occurring in the boundary regions adjacent to the membranes in the diluate channels and salt enrichment occurring in the boundary layers on the concentrate side of the membrane.

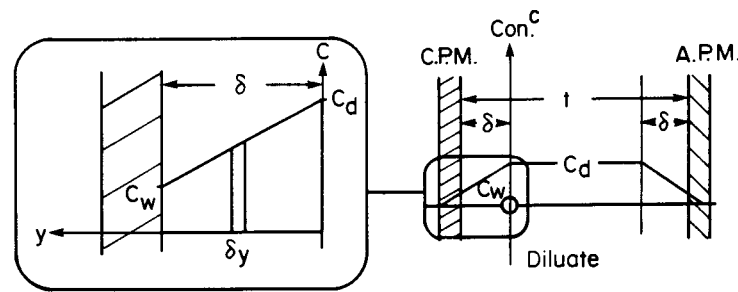


Figure 3.12.6: Concentration changes in boundary layers around membranes.

the concentration of salt in the "diluate boundary layer" is lower than the concentration of salt in the "main diluate stream", but the salt concentration is relatively enriched in the "concentrate boundary layer". Both these effects are clear on the concentration profiles shown in Figure 3.12.5. This phenomenon is very similar to concentration polarization processes which can occur around electrodes in electrochemical cells except that, in the present context, there is an unbalanced Faradaic transport in and around membranes which promotes additional diffusion fluxes to establish the steady-state concentration profile. Thus, these concentration-polarization phenomena around membranes in ED cells are a natural and inevitable result of the desalting mechanism i.e. of the change in electrical transport numbers at the membrane interface upon which the ED desalination process relies.

One important practical consequence of concentration polarization around membranes in ED units, indicated in Figure 3.12.5, is that the resistance of the diluate boundary layers is significantly greater than in the bulk diluate stream. Therefore, the occurrence

of concentration polarization increases the energy requirements for ED.

3.12.3.2 Membrane Potentials

When an ion-selective membrane separates two solutions of a salt at different concentrations, a potential difference is set-up across the membrane. This happens because, in the absence of any applied potentials, Na⁺ ions will tend to migrate across the cation-exchange membrane from the concentrated solution to the diluate solution. This will lead to a charge imbalance across the membrane with the diluate side becoming positively charged relative to the concentrated side. Eventually this potential difference across the membrane will build up to such a level that further ion transfer is discouraged and the value of the potential difference at this equilibrium condition is known as the membrane potential. For a salt consisting of single-charged ions, and assuming that activities can be equated to concentrations, the magnitude of the membrane potential is given by

$$E_m = - (\bar{t}_1 - \bar{t}_2) \frac{RT}{F} \ln \left(\frac{C_{w1}}{C_{w2}} \right) \quad (3.12.12)$$

where C_{w1} and C_{w2} are the concentrations of the salt in the concentrated and dilute solutions respectively.

The important point about the above is that natural flow across a membrane is from concentrate to diluate (i.e. the opposite to that required in desalination) and, to reverse this natural flow direction requires the application of a potential of magnitude greater than E_m , i.e. the membrane potential represents a potential drop which has to be overcome by the external applied voltage in order for desalination to occur. However, this is not the whole story. The magnitude of the membrane potential indicated by the above equation only applies to the equilibrium (i.e. infinitely-low current) state. As previously discussed, an inevitable consequence of desalination at finite currents is the occurrence of concentration polarization. The consequent concentrate enrichment and diluate depletions at the membrane/solution interface means that C_{w1} will be greater than the bulk concentrate composition and C_{w2} will be less than the bulk diluate concentrations. Therefore, another important effect of concentration polarization is to increase the membrane potential and hence the energy requirements for desalination.

3.12.3.3 The Cell-Pair Potential

The major part of the energy requirements for ED comprises the voltage necessary to overcome the solution resistances and membrane potentials. Estimation of the voltage is conveniently done by considering one cell pair which, as shown in Figure 3.12.5, encompasses a pair of membranes. The cell pair potential V_{cp} , is the sum of all the potential drops across the membranes and solutions comprising one cell pair.

Consider the basic conflict between attempts to maximise desalting rate and to minimize energy requirements. The flux of salts from the diluate channel is given by

$$T_D = 1 - \bar{t}_2^c - \bar{t}_1^a \quad (3.12.13)$$

and that the desalting rate, d , is given by:

$$d = \frac{IT_D}{F} \text{ equiv cm}^{-2} \text{ s}^{-1} \quad (3.12.14)$$

(using current density, i , instead of current I). The power required to drive a cell pair is:

$$P = V_{cp} i \text{ watts cm}^{-2} \quad (3.12.15)$$

Therefore, increases in i , whilst raising the desalting rate, also lead to higher energy consumption - not only directly but also by increasing V_{cp} due to higher IR drops and concentration-polarization effects.

3.12.3.4 Resistances

The major contributor to V_{cp} is the resistance of the diluate stream. It is normal practice to keep the concentration of the concentrate high enough for its resistance to be negligible in comparison to that of the diluate. Modern membranes have, however, negligible small resistances. As a first approximation, it can be considered that the diluate stream is providing all the resistance. To calculate the resistance, the main stream and the boundary layers must be considered separately.

Considering the total thickness (including boundary layers) of the diluate stream to be ' t ' cm (typically 0,1 cm) (see Fig. 3.12.6). Let the thickness of the boundary layers (adjacent to the membranes) be δ (determined by hydrodynamic conditions and typically 0,01 cm).

3.12.3.5 Main stream of diluate

The resistance of 1 cm² cross section, d, is given by:

$$R_d = \frac{t - 2\delta}{\kappa} \text{ ohm} \quad (3.12.16)$$

with the conductivity, κ , expressed in units of (ohm/cm)⁻¹.

But the conductivity, κ , depends on the concentration C_d (equiv/cm³) of the diluate stream via $\kappa = \Lambda C_d$ (3.12.17)

where Λ = equivalent conductivity in cm²/ohm equiv.

$$\therefore R_d = \frac{t - 2\delta}{\Lambda C_d} \quad (3.12.18)$$

3.12.3.6 Boundary layers of diluate

Faradaic transport (i.e. under the influence of the applied electric field) of ions, across the membranes out of the diluate compartment, leads to a depletion of salt in the boundary layers which, in turn, causes a diffusion flux from the bulk diluate. The concentration gradient across the boundary layer stabilises (i.e. steady-state conditions are established) when the two fluxes are equal.

Consider the CPM boundary layer (left diagram on Fig. 3.12.6).

$$\text{Faradaic Flux} = i/F (t_2 - \bar{t}_2^0) \approx (it_2/F) \quad (3.12.19)$$

$$\text{Diffusion flux} = -D \frac{dc}{dy} \quad (3.12.20)$$

Therefore, at steady state,

$$-D \frac{dc}{dy} = t_2 i/F \quad (3.12.21)$$

Conductivity (and hence resistance) is concentration dependent. Therefore, to find the

boundary-layer resistance, R_{BC} , integration must be carried out across the layer.

$$\text{Resistance of element } \delta y = \frac{\delta y}{\kappa} = \frac{\delta y}{\Delta C} \quad (3.12.22)$$

(see Fig. 3.12.6)

Therefore, resistance of boundary layer,

$$R_{BC} = \int_0^\delta \frac{dy}{\Delta C} \quad (3.12.23)$$

Concentration gradient (assumed linear - see Figure 3.12.6) is:-

$$\frac{dc}{dy} = \frac{C_w - C_d}{\delta} \quad (3.12.24)$$

Changing the integration variable limits:-

$$R_{BC} = \int_{C_d}^{C_w} \frac{\delta}{\left(\frac{C_w - C_d}{\Delta C}\right)} dc = \frac{\delta}{(C_w - C_d)\Delta} \ln \left(\frac{C_w}{C_d}\right) \quad (3.12.25)$$

$$R_{BC} = \frac{\delta}{(C_d - C_w)\Delta} \ln \left(\frac{C_d}{C_w}\right) \quad (3.12.26)$$

(since $C_d - C_w = -(C_w - C_d)$ and $\ln x = -\ln 1/x$)

An alternative expression for R_{BC} can be produced by using the previously formulated steady-state relation.

$$-D \frac{dc}{dy} = t_2 \frac{i}{F} = -D \frac{(C_w - C_d)}{\delta} = \frac{D(C_d - C_w)}{\delta} \quad (3.12.27)$$

$$\therefore C_d - C_w = \frac{t_2 \delta i}{FD} \quad (3.12.28) \text{ (A)}$$

$$\therefore R_{BC} = \frac{\delta FD}{t_2 \delta i \Delta} \ln \left[\frac{C_d}{\frac{C_d - \left(\frac{t_2 \delta i}{FD}\right)}{1}} \right] \quad (3.12.29)$$

$$= - \frac{FD}{t_2 i \Delta} \ln \left(1 - \frac{t_2 \delta i}{FDC_d} \right) \quad (3.12.30)$$

A similar analysis can be carried out to obtain an expression for the resistance, R_{BA} , of the diluate boundary layer at the APM (right hand side of Figure 3.12.6). This leads to the following expression:-

$$R_{BA} = -\frac{FD}{t_1 i \Lambda} \ln \left(1 - \frac{t_1 \delta i}{FDC_d} \right) \quad (3.12.31)$$

The depletion of solute in the boundary layers arises from the rapid flux of solute species through the membranes - this flux being directly proportional to the current flowing in the cell. In other words, as i increases from zero, the concentration gradient in the boundary layer increases (C_w decreases as i increases). It follows, therefore, that there are limits to the current that can be carried by the solute ions in an ED system - this limit being reached when C_w approaches zero.

As C_w approaches 0, equation (A) becomes:

$$C_d = \frac{t_2 \delta i_{\max}}{FD} \quad (3.12.32)$$

and

$$i_{\max} = \frac{C_d FD}{t_2 \delta} \quad (3.12.33) \quad (B)$$

which in turn, defines, for any given ED unit, a definite limit to the desalting rate -

$$\frac{Ni_{\max}}{F}$$

Another aspect of this "limiting current density phenomenon concerns the transport of H^+ and OH^- ions across CPM and APM membranes, respectively. At low current densities, the current is carried almost exclusively by solute ions rather than by H^+ and OH^- . This is because of the very low concentrations of H^+ and OH^- in neutral solution (10^{-7} mol/l) - and is despite the approximately ten times higher mobilities of H^+ and OH^- compared with solute ions. But, as i increases, the flux of H^+ and OH^- across the membranes increases until, as i_{\max} is approached, the flux of H^+ at the CPM and of OH^- at the APM becomes a substantial fraction of the total current. In rather more precise

terms, because of their tenfold higher mobilities, an appreciable fraction of the current will be carried by H⁺ and OH⁻, present at concentrations of 10⁻⁷ mol/l, when the solute concentration at the membrane/diluate interface C_w, falls towards a value of about 5 x 10⁻⁶ mol/l. Such a situation not only results in an obvious decreased efficiency of desalination but also in highly undesirable pH changes in the solutions. One consequence of such pH changes is that they can lead to an increased tendency towards scale precipitation if the pH increases significantly in any local region.

3.12.3.7 Membrane Potentials

The contribution of membrane potentials to the cell-pair potential is most conveniently predicted by considering ED of a solution of a single salt comprising of univalent ions. As was noted earlier, for this case the membrane potential was given by:

$$E_m = - (\bar{t}_1 - \bar{t}_2) \frac{RT}{F} \ln \frac{C_{w1}}{C_{w2}} \quad (3.12.34)$$

where C_{w1} and C_{w2} now represent the bulk concentrations of the salt in the compartments on either side of the membrane. Note, though, that the membrane potential is determined by the salt concentrations at the membrane/salt interface. It was noted earlier that finite cell-current flow resulted in salt depletions and enrichments within the boundary region beside the membrane. In such circumstances, E_m will no longer be determined by the bulk-salt concentrations (C_{w1} and C_{w2}) but by the concentration-polarised membrane/boundary layer interfacial values (C_{wbc} and C_{wdc}, in the C.P.M. in Figure 3.12.7). Therefore, in order to obtain an expression for E_m in these practically-relevant conditions, it is necessary to estimate the concentrations C_{wbc} and C_{wdc} for C.P.M. and C_{wda} and C_{wba} for the A.P.M.. This exercise is considerably simplified if it is assumed (see Figure 3.12.7) that the four boundary layers have identical effective thickness, δ. If we assume a perfect cation permeable membrane (C.P.M.) and use the notation of Figure 3.12.7, the polarised C.P.M. membrane potential is given by:-

$$E_{mc} = -(1-0) \frac{RT}{F} \ln \frac{C_{wbc}}{C_{wdc}} \quad (3.12.35)$$

$$\text{Now } C_d - C_{wdc} = \frac{t_2 \cdot \delta \cdot i}{FD} \quad (\text{see A}) \quad (3.12.36)$$

$$\therefore C_{wdc} = C_d - \frac{t_2 \cdot \delta \cdot i}{FD} \quad (3.12.37)$$

$$\text{Similarly } C_{wbc} = C_c + \frac{t_2 \cdot \delta \cdot i}{FD} \quad (3.12.38)$$

$$\text{hence } E_{mc} = \frac{RT}{F} \ln \left[\frac{C_c + \frac{t_2 \cdot \delta \cdot i}{FDC_d}}{C_d - \frac{t_2 \cdot \delta \cdot i}{FDC_d}} \right] \quad (3.12.39)$$

Similarly for the AMP.

$$E_{ma} = \frac{RT}{F} \ln \left[\frac{C_c + \frac{t_1 \cdot \delta \cdot i}{FDC_d}}{C_d - \frac{t_1 \cdot \delta \cdot i}{FDC_d}} \right] \quad (3.12.40)$$

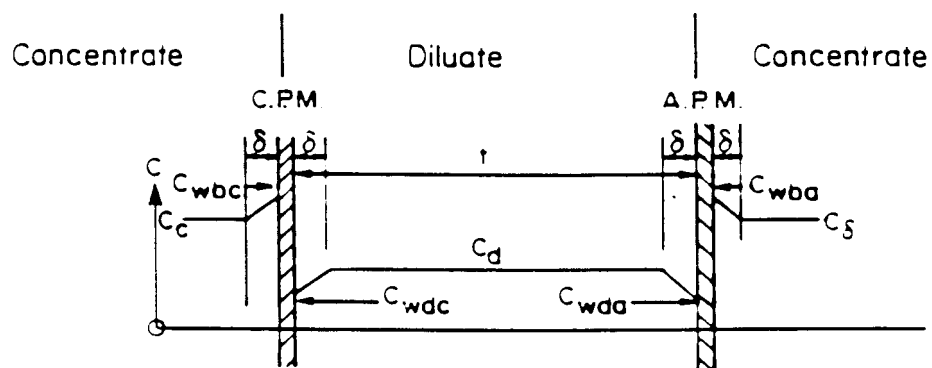


Figure 3.12.7: Concentration polarisation effects on membrane potential.

If the concentrate stream is several or more times as concentrated as the diluate stream, then

$$\frac{C_c}{C_d} > \frac{t_2 \delta i}{FDC_d} \quad (3.12.41)$$

$$\text{because } \frac{1}{i_{\max}} = \frac{t_2 \delta}{FDC_d} \quad (\text{see equation B}) \quad (3.12.42)$$

and $\frac{i}{i_{\max}}$ has a maximum value of 1

All the relevant terms have now been covered, which, to a first approximation, contribute to the cell pair potential V_{cp} .

Cell pair potential V_{cp} is given by:

$$\text{i.e. } V_{cp} = i (R_d + R_{BC} + R_{BA}) + E_{mc} + E_{ma} \quad (3.12.43)$$

$$\begin{aligned} \therefore V_{cp} &= \frac{i(t-2\delta)}{\Delta C_d} - \frac{FD}{t_2 \Lambda} \ln \left(1 - \frac{t_2 \delta i}{FDC_d} \right) - \frac{FD}{t_1 \Lambda} \ln \left(1 - \frac{t_1 \delta i}{FDC_d} \right) \\ &+ \frac{RT}{F} \ln \left(\frac{C_c}{C_d} + \frac{t_2 \delta i}{FDC_d} \right) - \frac{RT}{F} \ln \left(1 - \frac{t_2 \delta i}{FDC_d} \right) \\ &+ \frac{RT}{F} \ln \left(\frac{C_c}{C_d} + \frac{t_1 \delta i}{FDC_d} \right) - \frac{RT}{F} \ln \left(1 - \frac{t_1 \delta i}{FDC_d} \right) \end{aligned} \quad (3.12.44)$$

Rearranging:-

$$\begin{aligned} V_{cp} &= \frac{i(t-2\delta)}{\Delta C_d} - \left(\frac{FD}{t_2 \Lambda} + \frac{RT}{F} \right) \ln \left(1 - \frac{t_2 \delta i}{FDC_d} \right) \\ &- \left(\frac{FD}{t_1 \Lambda} + \frac{RT}{F} \right) \ln \left(1 - \frac{t_1 \delta i}{FDC_d} \right) \\ &+ \frac{RT}{F} \left[\ln \left(\frac{C_c}{C_d} + \frac{t_1 \delta i}{FDC_d} \right) + \ln \left(\frac{C_c}{C_d} + \frac{t_2 \delta i}{FDC_d} \right) \right] \end{aligned} \quad (3.12.45)$$

Further simplification of the bottom line of the above expression it is necessary to recall that:-

$$\frac{C_c}{C_d} \gg \frac{t_2 \delta i}{FDC_d} \quad \left(\text{and similarly } \gg \frac{t_1 \delta i}{FDC_d} \right)$$

$$V_{cp} = \frac{i(t - 2\delta)}{\Delta C_d} - \left(\frac{FD}{t_2 \Lambda} + \frac{RT}{F} \right) \ln \left(1 - \frac{t_2 \delta i}{FDC_d} \right) - \left(\frac{FD}{t_1 \Lambda} + \frac{RT}{F} \right) \ln \left(1 - \frac{t_1 \delta i}{FDC_d} \right) +$$

$$\frac{2RT}{F} \ln \frac{C_c}{C_d} \quad (3.12.46) \text{ (C)}$$

The order of magnitudes of some of the terms in the above relation is as follows by considering the desalination of sodium chloride:-

$$F = 96\,500 \text{ Coulomb/equiv}, t_2 = 0,6, R = 8,3 \text{ joule/}^\circ\text{K}$$

$$D \text{ (diffusion coefficient)} = 1,5 \times 10^5 \text{ cm}^2/\text{s}, t_1 = 0,4$$

$$\Lambda = 108,9 \text{ cm}^2 \text{ ohm}^{-1} \text{ equiv}^{-1}.$$

From which we can estimate the following terms:-

$$\frac{FD}{t_2 \Lambda} = \frac{96\,500 \times 1,5 \times 10^5}{0,6 \times 108,9} \left| \frac{\text{coulomb cm}^2 \text{ ohm equiv}}{\text{equiv s cm}^2} = \text{volts} \right|$$

$$= 0,02215 \text{ volt}$$

$$\frac{RT}{F} = \frac{8,3 \times 300}{96\,500} = 0,0258 \text{ volt}$$

In short $\frac{FD}{t_2 \Lambda}$ and $\frac{RT}{F}$ are of the same order

$$\text{Also } \frac{FD}{t_1 \Lambda} = 0,03323 \text{ volt}$$

Remember also that $\frac{t_2 \delta i}{FDC_d}$ and $\frac{t_1 \delta i}{FDC_d}$ have maximum values of 1.

Of the remaining terms in equation (C) t, δ and C_c may be considered as design parameters which may be chosen and fixed. Therefore, in estimating the energy requirement for V_{cp} , it remains to find the most suitable combination of variables in V_{cp} , i and C_d . A convenient way of doing this is too recast equation (C) in a non-dimensional form. This operation can be done in several steps:-

- (i) Multiply both sides of (C) by F/RT .

This makes the L.H.S of (C) $\frac{V_{cp}F}{RT}$ which is a (voltage) non-dimensional term,

which we call V .

- (ii) The first term on the RHS of (C) now becomes

$$\frac{i(t-2\delta) F}{C_d \Delta RT}$$

If we multiply this term by $\frac{i_{max}}{i_{max}} = \frac{C_d F D}{t_2 \delta} \times \frac{1}{i_{max}}$ (3.12.47)

we get $\frac{i}{i_{max}} \frac{t-2\delta}{\delta} \frac{F^2 D}{\Delta t_2 RT} = \beta \lambda I$ (3.12.48)

when it is separated into three non-dimensional terms

$$I = \frac{i}{i_{max}} \quad (3.12.49)$$

$$\lambda = \left(\frac{t-2\delta}{\delta} \right) \quad (3.12.50)$$

$$\beta = \frac{F^2 D}{\Delta t_2 RT} \quad (3.12.51)$$

- (iii) Replace C_o/C_d by C -another non-dimensional ("concentration ratio") term.

The substitution of the above non-dimensional terms into (C), together with some manipulation, gives the following non-dimensional equation:

Simple Resistance	Polarization	Useful
$V = \beta \lambda I$	$-(1 + \beta) \ln \left(1 - I \right) - \left(1 + \frac{t_2}{t_1} \beta \right) \ln \left(1 - \frac{t_1}{t_2} I \right)$	$+ 2 \ln C$ (3.12.52) (D)

Possible ranges of values for λ , I , and C

	Typical plant values
$0 < \lambda < \text{large}$	9
$0 < I < 1$	0,95
$10 < C < 200$	15 - 70

Equation (D) is divided into terms coming from simple resistive losses (since the $\beta\Delta I$ term is derived from the first term on the RHS of equation (C) which represents the bulk dilute resistance), and the work done against the membrane potentials (said to be "useful" because it represents the minimum energy without polarization effects), and the polarization-losses (all these terms being derived from all the terms in (C) except the first and the last (simple membrane potential). These contributions to the cell pair potential may be plotted separately as they are in Figure 3.12.8. The "useful" potential is only a function of C and the two "loss" potentials are both functions of I, the resistive loss being a function of λ as well. This graph then covers the total likely range of conditions to be found in practical ED stacks. Thus, the various curves for different values of λ are plots of the contributions of the resistance loss ($\beta\lambda I$) to the V term for different values of λ (the cell to boundary layer thickness ratio). Note that, as λ increases (i.e. as the cell size increases) the energy requirements increase. Note also, that, for the calculations of the value of β (used in the λ -plots and also in the polarization plot) that a temperature of 300 °K has been used.

3.12.4 Estimation of Effects of Flow of Solution through Stack on Desalting Process

No account of the effects of flow of solution through the compartments of the ED stack have been taken up to now. This matter can be estimated by investigating how conditions vary as the diluate passes along its channel⁽¹⁶⁾. This procedure can be started by carrying out a salt mass balance on an element, dx, in which the concentration changes from C_d by a small amount dC_d (See Figure 3.12.9).

Area of element = $1 \times t = t \text{ cm}^2$

Therefore, rate of salt flow into element is $C_d U_d t \text{ equiv s}^{-1}$.

Salt flux out of element along diluate channel is $(C_d + dC_d) t U_d \text{ equiv s}^{-1}$.

Flux of salt through membranes (= desalting rate)

$$= \frac{i}{F} \text{ equiv/cm}^2 \text{ s}$$

$$= \frac{i}{F} dx \text{ equiv/s (out of element dx of membrane area dx cm}^2\text{)}$$

∴ Mass balance on salt gives:-

$$C_d t U_d = (C_d + dC_d) t U_d + i dx / F \quad (3.12.52)$$

$$\text{or, } -dC_d t U_d = i dx / F \quad (3.12.53)$$

$$-dC_d = \frac{i}{t} \frac{dx}{F U_d} \quad (3.12.54)$$

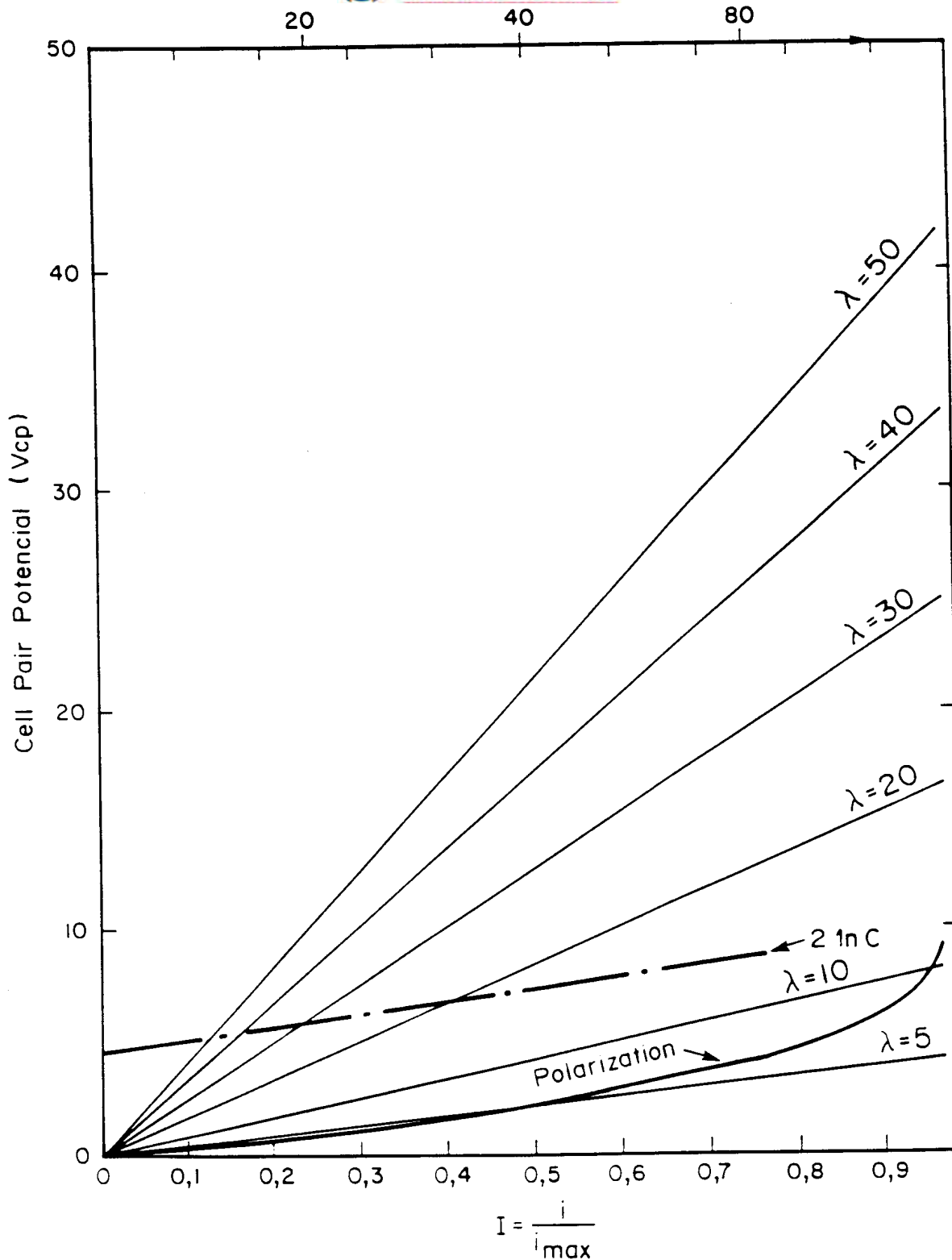


Figure 3.12.8: Effect of I on V_{cp} ($V_{cp} = \beta \lambda I$) at different cell to boundary layer thickness ratio's (λ) (simple resistive losses); effect of I on V_{cp} ($V_{cp} = -(1 + \beta) \ln(1 - I) - (1 + \frac{t_2}{t_1} \beta) \ln(1 - \frac{t_1}{t_2} I)$) (polarisation losses); effect of C (C_d/C_d) on V_{cp} ($V_{cp} = 2 \ln C$) (useful potential).

If i in the above equation is replaced by the dimensionless current term $I = i/i_{\max}$

$$\text{or } I = \frac{i t_2 \delta}{C_d F D} \quad (3.12.55)$$

i.e. using the expression (derived earlier) for i_{\max} :-

$$i_{\max} = \frac{C_d F D}{t_2 \delta} \quad (3.12.56)$$

one obtain:

$$-dC_d = \frac{I C_d D}{t_2 \delta} \times \frac{dx}{t U_d} \quad (3.12.57)$$

or:

$$dx = -\frac{t_2 \delta t U_d}{D I} \times \frac{dC_d}{C_d} \quad (3.12.58)$$

$$\int_0^x dx = -\frac{t_2 \delta t U_d}{D I} \int_{C_d(x=0)}^x \frac{dC_d}{C_d} \quad (3.12.59)$$

$$\therefore x = -\frac{t_2 \delta t U_d}{D I} [\ln C_d(x) - \ln C_d(x=0)] \quad (3.12.60)$$

$$= -\frac{t_2 \delta t U_d}{D I} \ln \frac{C_d(x)}{C_d(x=0)} \quad (3.12.61)$$

$$\text{and } C_d(x) = C_d(0) e^{-\left(\frac{D I}{t_2 \delta t U_d}\right) x} \quad (3.12.62)$$

$$= C_f e^{-\left(\frac{D I}{t_2 \delta t U_d}\right) x} \quad (3.12.63)$$

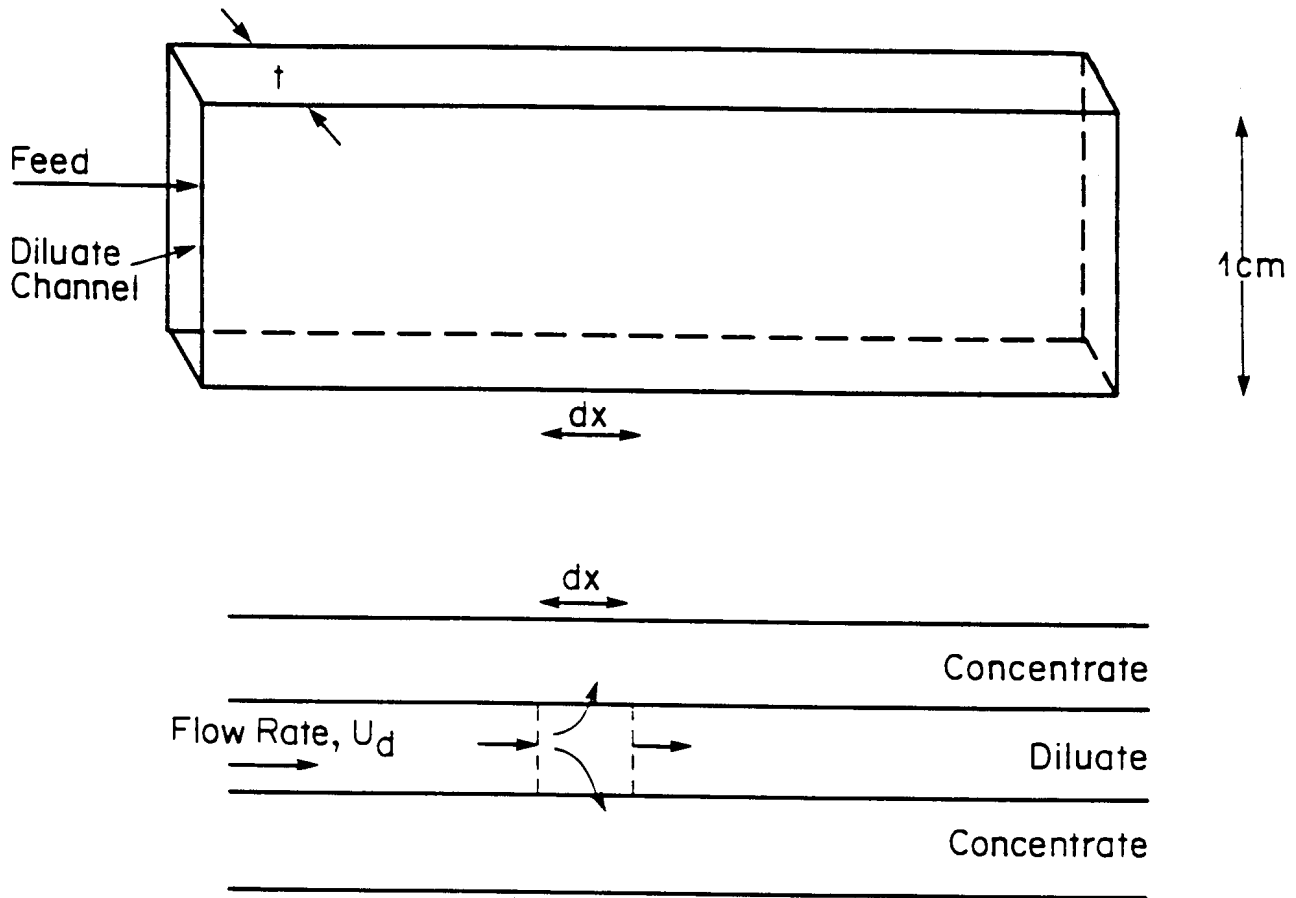


Figure 3.12.9: Flow through a diluate channel.

Now V_{cp} will be constant along the cell, but C_d and I will vary with x . Polarisation will be worse (i.e. highest value of I) at the stack entrance. Hence, if there is a "design" limit on polarisation it must be applied here (at $x = 0$). Hence, at this location $C_d = C_f$ (feed concentration) and $I = I_{max}$. It can therefore be worked out what the cell pair voltage will be at this point and this will be the value for the whole stack. Having settled on a value for V_{cp} , it can be examined how C_d and i (or I) vary with x . A typical result of such an analysis is shown in Figure 3.12.10.

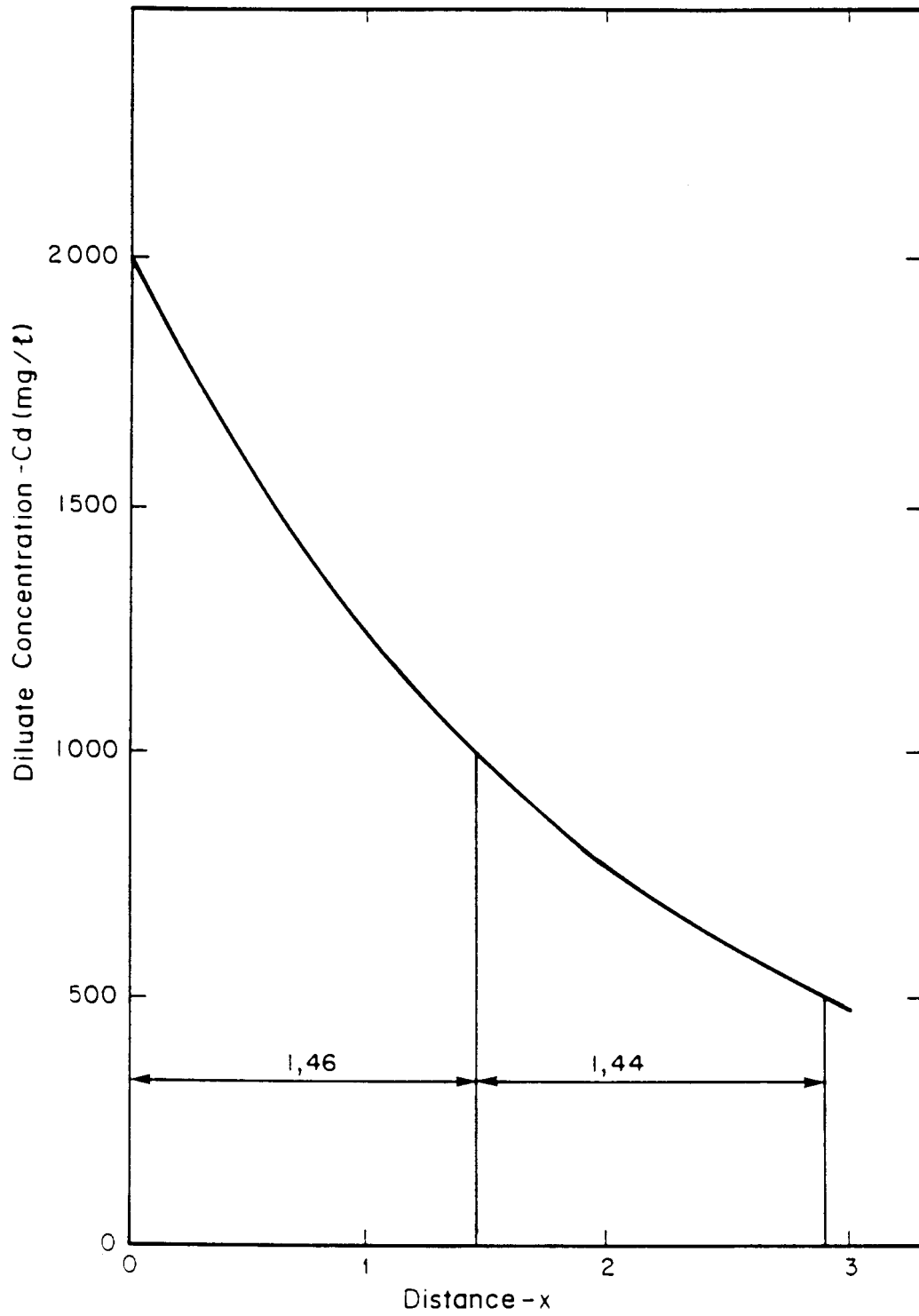


Figure 3.12.10: Variation of diluate concentration along cell pair.

4. ELECTRODIALYSIS IN PRACTICE

Electrodialysis technology has progressed significantly during the past 40 years since the introduction of synthetic ion-exchange membranes in 1949⁽⁵³⁾. The first two decades of this period saw the development of classical or unidirectional standard electrodialysis. However, during the past decade, the main feature has been the development of the polarity reversal process - the so-called electrodialysis reversal (EDR)⁽⁸⁴⁾. This form of electrodialysis desalination has virtually displaced unidirectional ED for most brackish water applications and is slowly gaining a significant share of this market.

EDR is at present mainly used for the desalination of brackish waters to produce fresh potable and industrial water. Unidirectional ED is used on a large scale in Japan for concentrating seawater to produce brine for salt production⁽⁸⁵⁾ and is also used on a small scale for seawater desalination⁽⁸⁶⁾ and for brackish water desalination⁽⁸⁷⁾.

Outside the water desalination field, ED is also being used on a large and increasing scale in North America and Europe to de-ash cheese whey to produce a nutritious high quality protein food supplement⁽⁵³⁾. It is also finding application in the treatment of industrial waste waters for water recovery, reuse and effluent volume reduction^(61, 88).

4.1 Electrodialysis Processes and Stacks

Different types of ED processes and stacks are used commercially for ED applications⁽⁶⁾. The filter-press- and the unit-cell stacks are the most familiar.

4.1.1 Filter-Press Stacks

The filter press stack configuration^(6, 9) in which alternate cation- and anion-exchange membranes are arranged between compartment frames in a plate-and-frame filter press assembly is shown in Figure 4.1.

Salt solution flows between the alternately placed cation and anion permeable membranes in the ED stack. Direct current (DC) provides the motive force for ion migration through the ion-exchange membranes and the ions are removed or concentrated in the alternate water passage by means of permselective ion-exchange membranes. This process is called the standard ED process.

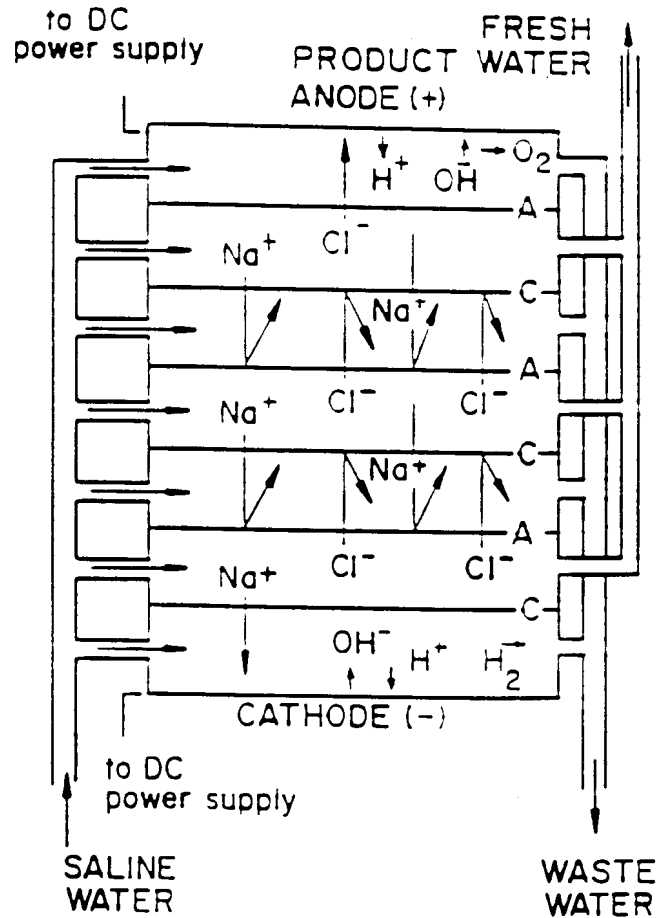


Figure 4.1: Plate-and-frame type EDR membrane stack.
C = cation membrane. A = anion membrane.

The standard ED process often requires the addition of acid and/or polyphosphate to the brine stream to inhibit the precipitation of sparsely soluble salts (such as CaCO_3 and CaSO_4) in the stack. To maintain performance, the membrane stack needs to be cleaned periodically to remove scale and other surface fouling matter. This can be done in two ways⁽⁶⁾ by cleaning in-place (CIP); and stack disassembly.

Special cleaning solutions (dilute acids or alkaline brine) are circulated through the membrane stacks for in-place cleaning, but at regular intervals the stacks need to be disassembled and mechanically cleaned to remove scale and other surface-fouling matter. Regular stack disassembly is a time-consuming operation and is a disadvantage of the standard ED process.

The electro dialysis reversal process (EDR) operates on the same basic principles as the standard ED process. In the EDR process, the polarity of the electrodes is automatically reversed periodically (about three to four times per hour) and, by means of motor operated valves, the 'fresh product water' and 'waste water' outlets from the membrane stack are interchanged. The ions are thus transferred in opposite directions across the membranes. This aids in breaking up and flushing out scale, slime and other deposits from the cells. The product water emerging from the previous brine cells is usually discharged to waste for a period of one to two minutes until the desired water quality is restored.

The automatic cleaning action of the EDR process usually eliminates the need to dose acid and/or polyphosphate, and scale formation in the electrode compartments is minimized due to the continuous change from basic to acidic conditions. Essentially, therefore, three methods of removing scale and other surface fouling matter are used in the EDR process⁽⁶⁾, viz., cleaning in place, stack disassembly as used in the standard ED process; and reversal of flow and polarity in the stacks. The polarity reversal system greatly extends the intervals between the rather time-consuming task of stack disassembly and reassembly, with an overall reduction in maintenance time.

The capability of EDR to control scale precipitation more effectively than standard ED is a major advantage of this process, especially for applications requiring high water recoveries. However, the more complicated operation and maintenance requirements of EDR equipment necessitate more labour and a greater skill level and may be a disadvantage of the process.

4.1.2 Unit-Cell Stack

A unit cell stack is shown in Figure 4.2. In this case the cation- and anion exchange membranes are sealed together at the edges to form a concentrating cell which has the shape of an envelope-like bag⁽⁶⁾. Many of these concentrating cells can be placed between electrodes in an ED stack.

The concentrating cells are separated by screen-like spacers. The feed flows between these concentrating cells and the direction of current through the stack is such as to cause ionic flow into the bags. Water flow into the cells is due to electro-osmosis (water is drawn along with the ions), and osmosis (water flows from the feed solution to the more concentrated brine). Small tubes are attached to each unit cell to allow

overflow of the brine. Because brine is pumped out of the cells mainly by the inflow of electro-osmotic water flow, this variant of ED is called electro-osmotic pumping ED.

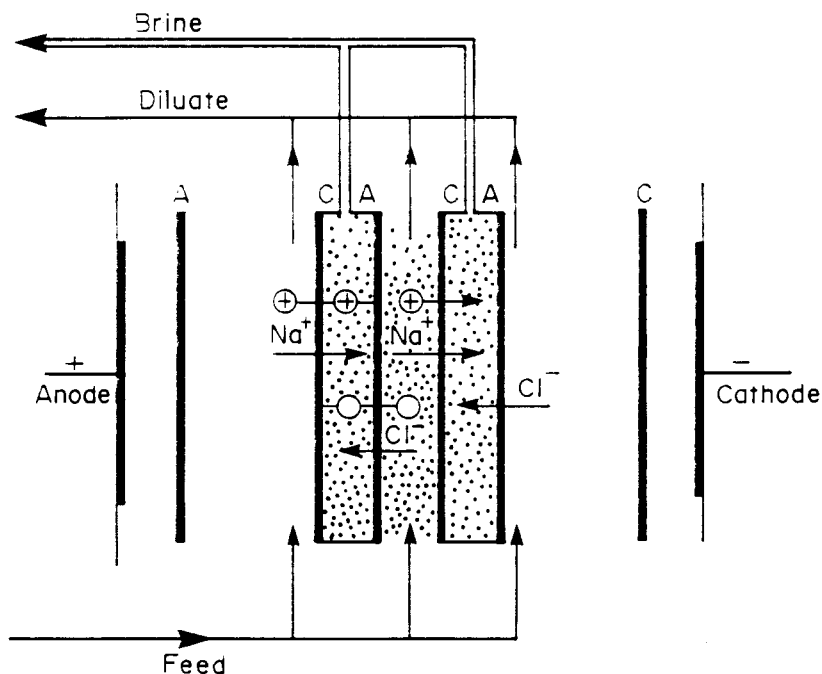


Figure 4.2: Schematic diagram of an ED unit cell stack.
C = cation membrane. A = anion membrane.

4.2 Ion-Exchange Membranes

Ion-exchange membranes are ion-exchangers in film form. There are two types: anion-exchange and cation-exchange membranes. Anion-exchange membranes contain cationic groups fixed to the resin matrix. The fixed cations are in electroneutrality with mobile anions in the interstices of the resin. When such a membrane is immersed in a solution of an electrolyte, the anions in solution can intrude into the resin matrix and replace the anions initially present, but the cations are prevented from entering the matrix by the repulsion of the cations affixed to the resin.

Cation-exchange membranes are similar. They contain fixed anionic groups that permit intrusion and exchange of cations from an external source, but exclude anions. This type of exclusion is called Donnan exclusion.

Details of methods for making ion-exchange membranes are presented in the literature^(89 - 91). Heterogeneous membranes have been made by incorporating ion-exchange particles into film-forming resins (a) by dry molding or calendaring mixtures of the ion-exchange and film-forming materials; (b) by dispersing the ion-exchange material in a solution of the film-forming polymer, then casting films from the solution and evaporating the solvent; and (c) by dispersing the ion-exchange material in a partially polymerized film-forming polymer, casting films, and completing the polymerization.

Heterogeneous membranes with usefully low electrical resistances contain more than 65% by weight of the cross-linked ion-exchange particles. Since these ion-exchange particles swell when immersed in water, it has been difficult to achieve adequate mechanical strength and freedom from distortion combined with low electrical resistance.

To overcome these and other difficulties with heterogeneous membranes, homogeneous membranes were developed in which the ion-exchange component forms a continuous phase throughout the resin matrix. The general methods of preparing homogeneous membranes are as follows⁽⁶⁾:

- Polymerization of mixtures of reactants (e.g., phenol, phenolsulfonic acid, and formaldehyde) that can undergo condensation polymerization. At least one of the reactants must contain a moiety that either is, or can be made, anionic or cationic.
- Polymerization of mixtures of reactants (e.g., styrene, vinylpyridine, and divinylbenzene) that can polymerize by additional polymerization. At least one of the reactants must contain an anionic or cationic moiety, or one that can be made so. Also, one of the reactants is usually a cross-linking agent to provide control of the solubility of the films in water.
- Introduction of anionic or cationic moieties into preformed films by techniques such as imbibing styrene into polyethylene films, polymerizing the imbibed monomer, and then sulfonating the styrene. A small amount of cross-linking agent (e.g., divinylbenzene) may be added to control leaching of the ion-exchange component. Other similar techniques, such as graft polymerization of imbibed monomers, have been used to attach ionized groups onto the molecular chains of preformed films.
- Casting films from a solution of a mixture of a linear film-forming polymer and

a linear polyelectrolyte, and then evaporating the solvent.

Membranes made by any of the above methods may be cast or formed around scrims or other reinforcing materials to improve their strength and dimensional stability.

The properties of some representative commercially available ion-exchange membranes as reported by the manufacturers are shown in Table 4.1⁽⁶⁾.

Table 4.1: Reported Properties of Ion-Exchange Membranes*

Manufacturer and Designation	Type of Membrane	Area Resistance (ohm-cm ²)	Transference Number of Counterion ^a	Strength	Approximate Thickness (mm)	Dimensional Changes on Wetting and Drying (%)	Size available
AMF^b		(0,6 N KCl)		Mullen burst (kPa)			
C-80	Cat-exch	5 ± 2	0,80 (0,5/1,0 N KCl)	310	0,30		
C-100	Cat-exch	7 ± 2	0,90 (0,5/1,0 N KCl)	414	0,22	10 - 13	1,1 m wide rolls
A-80	An-exch	6 ± 2	0,80 (0,5/1,0 N KCl)	310	0,30		
A-100	An-exch	8 ± 2	0,90 (0,5/1,0 N KCl)	379	0,23	12 - 15	1,1 m wide rolls
ACI^c		(0,5 N NaCl)		Tenstile strength (kg/mm ²)			
CK-1	Cat-exch	1,4	0,85 (0,25/0,5 N NaCl)		0,23		
DK-1	Cat-exch	1,8	0,85 (0,25/0,5 N NaCl)	2 to 2,4	0,23	15 - 23	1,1 x 1,1 m
CA-1	An-exch	2,1	0,92 (0,25/0,5 N NaCl)		0,23		
DA-1	An-exch	3,5	0,92 (0,25/0,5 N NaCl)	2 to 2,3	0,23	12 - 18	1,1 x 1,1 m
AGC^d		(0,5 N NaCl)		Mullen burst (kPa)			
CMV	Cat-exch	3	0,93 (0,5/1,0 N NaCl)	1 241	0,15		
CSV	Cat-exch	10	0,92 (0,5/1,0 N NaCl)	1 241	0,30	< 2	1,1 m wide rolls
AMV	An-exch	4	0,95 (0,5/1,0 N NaCl)	1 531	0,15		
ASV	An-exch	5	0,95 (0,5/1,0 N NaCl)	1 531	0,15		
IC^e		(0,1 N NaCl)		Mullen burst (kPa)			
MC-3142	Cat-exch	12	0,94 (0,5/1,0 N NaCl)	1 379	0,20		
MC-3235	Cat-exch	18	0,95 (0,1/0,2 N NaCl)	1 137	0,30	< 3 ^g	1 x 3 m
MC-3470	Cat-exch	35	0,96 (0,1/0,2 N NaCl)	1 379	0,20		
MA-3148	An-exch	20	0,90 (0,5/1,0 N NaCl)	1 379	0,20		
MA-3236	An-exch	120	0,93 (0,5/1,0 N NaCl)	1 137	0,30	< 3 ^g	1 x 3 m
IM-12	An-exch ^f	12	0,96 (0,1/0,2 N NaCl) ^g	999	0,15 ^g	Not given	
MA-3475R	An-exch	11	0,99 (0,5/1,0 N NaCl)	1 379	0,36	Not given	
II^h				Mullen burst (kPa)			
CR-61	Cat-exch	11	0,93 (0,2 N NaCl) ^b	793	0,58	Cracks on drying	
AR-111A	An-exch	11	0,93 (0,1/0,2 N NaCl) (by electrophoretic method in 0,5 N NaCl)	862	0,61		0,5 x 1 m
TSCⁱ				Mullen burst (kPa)			
CL-2,5T	Cat-exch	3	0,98	551	0,15		
CLS-25T	Cat-exch ^k	3	0,98	551	0,15	Not given	1 x 1,3 m
AV-4T	An-exch	4	0,98	1 034	0,18		
AVS-4T	An-exch ^k	5	0,98	965	0,18	Not given	1 x 1,3 m

- * Properties are those reported by manufacturer, except for those membranes designated with footnote g.
- a Calculated from concentration potentials measured between solutions of the two normalities listed.
- b American Machine and Foundry Co., Stamford, Connecticut.
- c Asahi Chemical Industry, Ltd. Tokyo, Japan.
- d Asahi Glass Co., Ltd., Tokyo, Japan.
- e Membranes that are selective for univalent (over multivalent) ions.
- f Ionac Chemical Co., Birmingham, New Jersey.
- g Measured at Southern Research Institute.
- h Special anion-exchange membrane that is highly diffusive to acids.
- i Ionics, Inc., Cambridge, Massachusetts.
- j Tokuyama Soda Co., Ltd., Tokyo, Japan.
- k Univalent selective membranes.

4.3 Fouling

Fouling of ED membranes by dissolved organic and inorganic compounds may be a serious problem in practical electro dialysis^(6, 92, 93) unless the necessary precautions (pretreatment) are taken. Organic fouling is caused by the precipitation of large negatively charged anions on the anion-permeable membranes in the dialysate compartments.

Organic fouling of anion permeable membranes takes place in a number of ways⁽⁹²⁾:

- a) The anion is small enough to pass through the membrane by electromigration but causes only a small increase in electrical resistance and a decrease in permselectivity of the membrane;
- b) The anion is small enough to penetrate the membrane, but its electromobility in the membrane is so low that its hold-up in the membrane causes a sharp increase in the electrical resistance and a decrease in the permselectivity of the membrane;
- c) The anion is too big to penetrate the membrane and accumulates on the surface (to some extent determined by the hydrodynamic conditions and also by a phase change which may be brought about by the surface pH). The decrease in electrical resistance and permselectivity of the membrane is slight. The accumulation can be removed by cleaning.

In case (c) the electro dialysis process will operate without serious internal membrane fouling and only mechanical (or chemical) cleaning will be necessary. Case (b) would make it almost impossible to operate the electro dialysis process. In case (a), the electro dialysis process can be used if the concentration of large anions in solution is low or if the product has a high enough value to cover the high electrical energy costs.

Inorganic fouling is caused by the precipitation (scaling) of slightly soluble inorganic compounds (such as CaSO_4 and CaCO_3) in the brine compartments and the fixation of multivalent cations (such as Fe and Mn) on the cation-permeable membranes. Organic anions or multivalent cations can neutralize or even reverse the fixed charge of the membranes, with a significant reduction in efficiency. Fouling also causes an increase in membrane stack resistance which, in turn, increases electrical consumption and adversely effects the economics of the process.

The following constituents are, to a greater or lesser extent, responsible for membrane fouling⁽⁹⁴⁾:

- Traces of heavy metals such as Fe, Mn and Cu.
- Dissolved gases such as O₂, CO₂ and H₂S.
- Silica in diverse polymeric and chemical forms.
- Organic and inorganic colloids.
- Fine particulates of a wide range of sizes and composition.
- Alkaline earths such as Ca, Ba and Sr.
- Dissolved organic materials of both natural and man-made origin in a wide variety of molecular weights and compositions⁽⁹²⁾.
- Biological materials - viruses, fungi, algae, bacteria - all in varying stages of reproduction and life cycles.

Many of these foulants may be controlled by pretreatment steps which usually stabilize the ED process. However, according to Katz⁽⁹⁴⁾, the development of the EDR process has helped to solve the pretreatment problem more readily in that it provides self-cleaning of the vital membrane surfaces as an integral part of the desalting process.

4.4 Pretreatment

Pretreatment techniques for ED are similar to those used for RO⁽⁶⁾. Suspended solids are removed by sand and cartridge filters ahead of the membranes. Suspended solids, however, must be reduced to a much lower level for RO than for ED. The precipitation of slightly soluble salts in the standard ED process may be minimized by ion-exchange softening and/or reducing the pH of the brine through acid addition and/or the addition of an inhibiting agent.

Organics are removed by carbon filters, and hydrogen sulphide by oxidation and filtration. Biological growths are prevented by a chlorination-dechlorination step. The dechlorination step is necessary to protect the membranes from oxidation. Iron and manganese are removed by green sand filters, aeration, or other standard water treatment methods. It has been suggested that multivalent metal and organic ions, and hydrogen sulphide, however, must be reduced to a lower level for EDR than for RO⁽⁹⁵⁾.

The overall requirements for pretreatment in ED, may be somewhat less rigorous than for RO due to the nature of the salt separation and the larger passages provided⁽⁶⁾.

In ED, the ions (impurities) move through the membranes, while in RO the water moves under a high pressure through the membranes while the salts are rejected. Salts with a low solubility can, therefore, more readily precipitate on spiral and hollow fine fibre RO membranes to cause fouling and to block the small water passages. Suspended solids can also more readily form a deposit. However, this might not be the case with tubular RO membranes. With the EDR process, precipitated salts in the brine compartments can be more readily dissolved and flushed out of the system using polarity reversal without the need for chemical pretreatment.

However, high removals of suspended solids, iron, manganese, organics and hydrogen sulphide are still critical to avoid fouling and suppliers of EDR equipment recommend pretreatment of the feed water⁽⁹⁾, if it contains the following ions: Fe > 0,3 mg/l; Mn > 0,1 mg/l; H₂S > 0,3 mg/l; free chlorine and turbidity > 2 NTU. In every case, of course, a careful examination of the prospective water would be necessary to determine suitability and pretreatment.

A certain degree of fouling is, however, unavoidable. Membranes should, therefore, be washed regularly with dilute acid and alkali solutions to restore performance.

4.5 Post-treatment

The EDR product water is usually less aggressive than the RO product because acid is usually not added in EDR for scale control⁽⁹⁵⁾. Post-pH adjustment may, therefore, not be required as with RO. Non-ionic matter in the feed such as silica, particulates, bacteria, viruses, pyrogens and organics will not be removed by the ED process and must, if necessary, be dealt with during post-treatment.

4.6 Seawater Desalination

There is limited application of ED for seawater desalination because of high costs⁽⁸⁾. A small batch system (120 m³/d) has been in operation in Japan since 1974 to produce water of potable quality at a power consumption of 16,2 kWh/m³ product water⁽⁹⁶⁾. A 200 m³/d seawater EDR unit was evaluated in China⁽⁹⁷⁾. This unit operated at 31°C; its performance was stable; total electric power consumption was 18,1 kWh/m³ product water and the product water quality of 500 mg/l TDS met all the requirements for potable water. When the stacks were disassembled for inspection, there were no signs of scale formation.

With the commercial ED units currently available, the energy usage for seawater desalination is relatively high compared with that of RO. However, work under the Office of Water Research and Technology (OWRT) programmes has indicated that high-temperature ED may possibly be competitive with RO⁽⁹⁸⁾. Results have shown that the power consumption can be reduced to the levels required for seawater RO (8 kWh/m³) and that a 50% water recovery can probably be attained.

4.7 **Brackish Water Desalination for Drinking-Water Purposes**

A considerable number of standard ED plants for the production of potable water from brackish water are in operation^(8, 87). These plants are operating successfully. However, after the introduction of the reversal process in the early 1970's, Ionics Incorporated shifted almost all their production to this process⁽⁹⁴⁾.

The major application of the EDR process is for the desalination of brackish water. The power consumption and, to some degree, the cost of equipment required is directly proportional to the TDS to be removed from the feed water⁽⁸⁾. Thus, as the feedwater TDS increases, the desalination costs also increase. In the case of the RO process, a cost: TDS removal relationship also exists, but it is not as pronounced. Often the variation in the scaling potential of the feed water and its effect on the percentage of product water recovery can be more important than the cost: TDS relationship.

Thus, for applications requiring low TDS removals, ED is often the most energy-efficient method, whereas with highly saline feed waters RO may be expected to use less energy and is preferred. The economic crossover point between ED and RO based on operating costs is, however, difficult to define precisely and needs to be determined on a site-specific basis. Apart from local power costs, other factors must also be considered in determining the overall economics. Among these, to the advantage of ED, are the high recoveries possible (up to 90%), the elimination of chemical dosing (with EDR), and the reliability of performance that is characteristic of the ED process.

4.8 **Energy Consumption**

The energy consumption of a typical EDR plant is as follows⁽⁸⁾:

Pump	:	0,5 to 1,1 kWh/m ³ product water
Membrane stack	:	0,7 kWh/m ³ product water/1 000 mg of TDS removed
Power losses	:	5% of total energy usage

The major energy requirement, therefore, is for pumping the water through the ED unit and for the transport of the ions through the membranes.

4.9 Treatment of a High Scaling, High TDS Water with EDR

The successful performance of EDR on high calcium sulphate waters has been reported⁽⁸⁴⁾. Brown⁽⁹⁹⁾ has described the performance of an EDR plant treating 300 m³/d of a high calcium sulphate water with a TDS of 9 700 mg/ℓ. The only pretreatment applied was iron removal on green sand. The quality of the feed, product and brine is shown in Table 4.2

The water recovery and energy consumption were 40% and 7,7 kWh/m³ of product water, respectively. No attempt was made to optimize water recovery. The stack resistance increased by only 3% after one year of operation, which clearly indicates the successful operation of the EDR unit in spite of the super saturated condition of the brine with respect to calcium sulphate. Membrane life times are estimated to be 10 years.

The main developments in EDR during the past few years have been the following:

- **EDR has achieved CaSO₄ saturation** in the brine stream of up to 440% without performance decline on tests of several hundred hours' duration⁽⁹⁹⁾.
- EDR has desalted a hard (Ca²⁺ approx. 150 mg/ℓ) brackish water of 4 000 mg/ℓ TDS at water recoveries of up to 93% without cumbersome and expensive pre-softening⁽⁹⁴⁾.
- An EDR test unit has achieved 95% or greater recovery of a limited 4 000 mg/ℓ TDS brackish water resource by substituting a more abundant 14 000 mg/ℓ saline water in the brine stream⁽¹⁰⁰⁾. The substitution of seawater in the brine stream would be freely available in coastal or island locations with limited high quality brackish water resources.
- The development, extensive field testing and subsequent large-scale commercial usage of a new family of thick (0,5 mm), rugged anti-fouling anion-permeable membranes in the USA with much higher current efficiencies and chlorine resistance than those formerly available⁽¹⁰⁰⁾.

Table 4.2: Water Quality Before and After EDR Treatment

Constituent	Feed (mg/l)	Product (mg/l)	Brine (mg/l)
Na ⁺	2 090	79	3 694
Ca ⁺⁺	652	4	1 390
Mg ⁺⁺	464	4	964
Cl ⁻	3 687	111	7 084
HCO ₃ ⁻	134	25	175
SO ₄ ⁼	2 672	19	5 000
TDS	9 727	242	18 307
pH	7,0	6,8	7,2

4.10 Brackish Water Desalination for Industrial Purposes

In the past most ED plants treated brackish waters of 1 000 to 10 000 mg/l TDS and produced general purpose industrial product water of 200 to 500 mg/l TDS. However, ED capital and construction costs have declined during recent years to the point where it is already feasible to treat water containing 200 to 1 000 mg/l TDS and produce product water containing as little as 3 to 5 mg/l TDS⁽¹⁰¹⁾. These low TDS levels are achieved by multistaging. The systems, which often employ ion-exchange (IX) units as 'polishers', are usually referred to as ED/IX systems.

4.11 ED/IX System

New and existing ion-exchange facilities can be converted to ED/IX systems by addition of ED units upstream of the ion-exchange units. The ED unit reduces chemical consumption, waste, service interruptions and resin replacement of the ion-exchanger in proportion to the degree of prior mineral removal achieved⁽¹⁰¹⁾. For small capacity systems (2 to 200 m³/d) the optimum ED demineralization will usually be 90% or greater; for larger installations, and particularly those where adequate ion-exchange capacity is already provided, the optimum demineralization via ED is more likely to be in the 60 to 80% range.

It must, however, be stressed that RO may also be used for the abovementioned application. RO may function better than ED because it removes silica and organic material better than ED. However, the choice of the treatment method (ED or RO) would be determined by the specific requirements and costs for a particular situation.

Honeywell in the USA, which manufactures printed circuit boards and does zinc plating and anodizing, used IX for the treatment of their process waters before they changed

over to an ED/IX system⁽¹⁰²⁾. ED was chosen instead of RO because of lower membrane replacement costs. Process waters of varying degrees of purity are required, dissolved solids being the primary concern. Water with a TDS of about 50 mg/l is suitable for zinc plating and anodizing and water with a TDS with a minimum specific resistance of 100 000 ohms is satisfactory for circuit board fabrication operations⁽¹⁰²⁾. The purity of the treated water (raw water TDS - 250 to 500 mg/l) after treatment with the ED/IX system was better than expected. Service runs have been up to ten times longer than before.

4.12 **Industrial Wastewater Desalination for Water Reuse, Chemical Recovery and Effluent Volume Reduction**

Large volumes of water containing varying amounts of salt, which are generated by washing and regenerating processes, blowdown from cooling towers, disposal of dilute chemical effluents, to name a few, present significant problems, particularly when zero effluent discharge is required. The problem is one of too much water carrying comparatively little salt, but still having a TDS content too great for acceptance to a receiving stream. Many industries face this problem today and have to consider the application of processes for concentrating salts or desalting water. The ED system for water recovery and brine concentration may be one of the best suited to alleviate the problem.

Some typical examples are given to illustrate this principle:

4.12.1 **Electrodialysis of nickel plating solutions**

During many plating operations, a substantial amount of bath solution adheres to plated work pieces as they leave the plating tank. In this manner valuable materials are lost as 'drag-out' into the subsequent rinse tank. This contaminated rinse solution can be passed through an ED system where these valuable materials can be recovered and returned to the plating tank.

One such opportunity of significant industrial importance is provided by nickel electroplating operations⁽¹⁰³⁾. Earlier work by Trivedi and Prober⁽¹⁰⁴⁾ demonstrated the successful application of ED to nickel solutions. Later, Eisenmann⁽¹⁰⁵⁾ and Itoi⁽¹⁰³⁾ reported the use of ED to recover nickel from electroplating rinse waters.

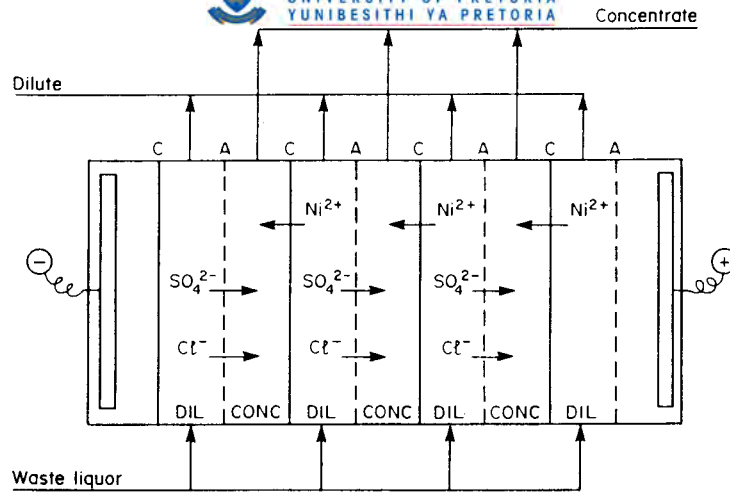


Figure 4.3: Electrodialysis of the washwater from a nickel galvanizing operation.

The wash water from a nickel galvanizing line is treated by ED as shown in Figure 4.3.

The results achieved in an existing facility are given in Table 4.3. The concentration ratio of the concentrated solution to the dilute solution is greater than 100. The concentrated solution is reused in the plating bath while the dilute solution is reused as wash water. The recovery of nickel discharged from the wash tank is approximately 90% or greater.

If organic electrolytes are present in the additives used in the galvanization bath, they must be removed prior to ED treatment to prevent organic fouling of the ED membranes.

Table 4.3: Electrodialysis of a Nickel Galvanization Effluent

Constituent	Effluent (g/l)	Concentrate (g/l)	Diluent (g/l)
NiSO ₄	12,47	133,4	1,27
NiCl ₂	1,81	29,1	0,039

4.12.2 Treatment of cooling tower blowdown for water recovery and effluent volume reduction

The range of TDS levels encountered in cooling tower blowdown waters usually varies from about 1 500 to 4 000- mg/l and higher levels at about 4 000 to 12 000- mg/l

have also been reported⁽¹⁰⁶⁾. The disposal of large volumes of this saline effluent can be a serious problem. The application of ED for the treatment of blowdown streams to recover good quality water for reuse and produce a small volume of concentrate promises to be the best prospective system available^(107,108).

Blowdown waters from cooling towers can be concentrated tenfold or more using ED, while recovering and recycling the desalted water to the cooling tower at one-half its original concentration⁽⁸⁸⁾. To accomplish this, blowdown is pretreated, filtered and passed through the ED system. By recirculation of the brine, it is possible to concentrate the salts into a small stream, while allowing for recovery of about 90% of the water.

The concentration of cooling blowdown waters in an EDR pilot plant at one of Eskom's power stations was evaluated⁽⁸¹⁾. Pretreatment of the blowdown water with lime softening, clarification, pH reduction, filtration and chlorination was found to be a basic precondition for successful operation. The operating experience on the EDR pilot plant was sufficiently positive to warrant full-scale application.

Detailed design studies and cost estimates for ED and several other alternative blowdown recovery/concentration systems have been reported⁽⁸⁸⁾. The side stream process design which utilizes ED results in the lowest capital costs for the conditions specified. According to Wirth and Westbrook⁽⁸⁸⁾, it is expected that if the cost comparison were made on overall annual operating costs, the same results would occur.

4.13 Other Possible Industrial Applications

4.13.1 Concentration of sodium sulphate and its conversion into caustic soda and sulphuric acid

A pilot study has demonstrated the feasibility of the concentration of a sodium sulphate solution with ED in a first stage and the subsequent conversion into caustic soda and sulphuric acid in a second stage⁽¹⁰⁹⁾. The sodium sulphate solution (20 to 40 g/l) was treated in a multi-compartment electro dialyzer to yield a brine (260 - 320 g/l, 10% of feed volume) and a product (2 g/l, 90% of feed volume) which could be used as reclaimed water.

The brine was treated further in a three-compartment electro dialyzer to produce caustic soda and sulphuric acid at a concentration of 17 to 19% by mass and a power consumption of approximately 3,1 to 3,3 kWh/kg sodium sulphate decomposed. The sodium sulphate content of both products was about 1%.

4.13.2 Recovery of acid and caustic soda from ion-exchange regeneration wastes

Laboratory results of an electro dialytic process for acid and caustic recovery from ion-exchange regenerant wastes have been described⁽¹¹⁰⁾. The object of the study was to minimize the discharge of dissolved salts from a water treatment plant producing boiler feed water while recovering some of the pollution abatement process costs from the savings in regenerant chemical costs.

It was shown that the electro dialytic process for recovery of sulphuric acid and sodium hydroxide from ion-exchange regenerant wastes, and substantially reducing the amount of salt discharged to drain, is technically feasible. The nett costs for acid and caustic waste treatment was estimated at US \$4,20 and \$3,00/m³ waste treated, respectively.

4.13.3 Concentration of dilute chemical effluents

Laboratory investigations have shown that dilute (approximately 2%) solutions of NH₄NO₃, Na₂SO₄, NaNO₃ and NaCl can be concentrated to approximately 20% by ED at an energy consumption of about 1 kWh/kg salt⁽¹¹¹⁾. The brine volumes were less than 10% of the original volume.

4.14 Polarisation

The current which is passed through an ED stack is carried almost exclusively by ions of the same sign. In the solution, all types of ions carry this current. The rate at which the current can pass through the solution is limited by the diffusion rate of ions to the membrane surface since there will inevitably be changes in the concentration of the solution close to the membrane surface. It is apparent that as the current density is increased, it becomes more difficult for the ions in the solution to carry the required current. This effect is known as concentration polarization⁽¹¹⁾. The greater the current density used the greater are these polarization effects. Polarization also becomes a problem the more dilute the solution becomes.

The main effects of polarization are⁽⁶⁾:

- i) the differences in concentration result in increased membrane potentials and so the power required per unit charge passed is increased.
- ii) The current efficiency can also be reduced which means that the current required per unit of output is also increased.
- iii) When it is attempted to carry current in excess of the ions available to be transported through the membrane, the water "splits" into hydroxide and hydrogen ions. At the anion membrane the current is carried by hydroxide ions through the membrane and hydrogen ions are rejected to the solution. At the cation membrane the opposite effect occurs: hydroxide ions are transported to the membrane and are rejected to the solution. This effect is to be avoided since, firstly, both the current and the voltage efficiency are reduced (some of the current serves to split the water instead of desalting it and there is an increased voltage requirement) and secondly, when the water splits the pH in the boundary layer on the membrane surface can change increasing the likelihood of scale formation.

4.15 Cell Stack

It has already been shown that the basic unit in an ED plant is the cell pair where cation and anion permeable membranes are alternately arranged so as to produce adjacent diluate and concentrate streams. A number of cell pairs are located between a pair of electrodes to form what is known as a cell stack. The number of cell pairs varies depending on the manufacturer but is usually about 300.

In any cell pair the membranes are separated by a spacer. The hydrodynamic design of the flow between the membranes is of extreme importance⁽⁶⁾. It is essential that as far as it is practicable turbulent flow exists in individual cell pairs. Streamline flow produces a relatively stagnant or slow moving layer on the membrane surface. Since the current carrying ions have to diffuse through this film at low solution concentration, polarization becomes more likely. There are a number of requirements a spacer must meet. The fluid should flow at the same rate across the whole active membrane area and should be turbulent within the limits of pressure drop. The manifold must supply each spacer equally. The spacer should support the membrane, this being particularly

important in the region between the manifolds. The spacer material should be inert, should possess physical properties so as to permit a hydraulic seal when pressurised and be dimensionally stable.

The spacers are usually perforated PVC nets and, depending on the design, are 0,5 mm to 1 mm thick⁽⁶⁾. The size of the spacer depends on the size of the membrane used. In general, large components tend to cost less per unit of effective membrane area. However, practical considerations such as the ease of handling and mechanical strength must be taken into account. Components which are thin result in lower operating costs but there are difficulties in providing good flow distribution. It is apparent that the presence of the spacer reduces the active membrane area since it also serves to support the membrane. There is an advantage in utilising as much of the membrane surface area as possible but this results in difficulties in supporting and sealing the membranes. A membrane of about 1,5 m² is probably the maximum practicable, usually the area is 0,5 m² to 1 m². The effective membrane area is about 85 % of the total membrane area.

Stack sealing is of importance to stack operation. The spacer should seal easily since the lower compression force required to seal the stack, the less likely will be the chance of damaging components. This aspect of design becomes most complex in the region of manifolds. This area should be as small as possible but should not cause a high pressure drop. Also, since a seal must be made round this area the support in this region must be able to withstand the compressive scaling forces of the stack.

The stack itself should be easy to maintain. It often occurs that only a few cell pairs in the stack require maintenance. In a large stack it is desirable to be able to open the stack at any section and remove a cell pair without disturbing any of the other cell pairs.

The electrodes must be made of a material which is corrosion resistant, since at the cathode the flow becomes alkaline while at the anode gaseous chlorine and oxygen are formed. It is normal to have separate feeds to the anode and cathode, the anode rinse going to a drain while the cathode rinse is treated with acid and then recirculated. The maximum voltage across a stack is 3 volts per cell pair and so a normal stack voltage will be about 900 volts.

4.16 Process Design

Since the amount of desalting depends directly on the current level it is a straightforward exercise to calculate the performance of a given stack at a particular current density. In order to achieve a given level of desalination the plant can either be run in a batch process or in a once-through process⁽⁶⁾.

In a batch process, the water to be desalinated is stored in a tank and then partially desalted by passing it through the stack to a second tank having been further desalted. After each pass the concentration is checked and the process is repeated until the required level of demineralization is achieved. This method is often used when the feed water is subject to changes in composition. For example, in a lot of cases brackish well water is liable to increase in salinity at high pumping rates.

In a once-through system, the required desalting is achieved by passing the diluate stream through successive stacks arranged hydraulically in series. This process tends to be used in the higher capacity plants and requires less control systems. Where possible (i.e. where the feed water salinity can be guaranteed) a continuous type of plant is always to be preferred. Since plant operation is simpler, the likelihood of breakdown is reduced and the capital cost is reduced.

In both systems the concentrate streams are recycled to minimize blow-down and possible use of chemicals. The flow of the concentrate stream is normally 25% or less than that of the diluate stream. To minimize the electrical resistance of the stack it is desirable to have the concentrate stream at the maximum concentration possible (this also minimizes the blow-down to waste). The normal limiting factor for the degree of concentration is the solubility of calcium sulphate.

In both systems the limiting current density controls the amount of desalination possible. The onset of polarization manifests itself in the change of chemical conditions in the plant and also in an increase in the voltage requirements maintaining the current. The lower the salt content in the water, the lower will be the limiting current density. Electrodialysis, therefore, is not applicable in the production of high purity waters.

5. EXPERIMENTAL

5.1 Membranes

The membrane and membrane types shown in Table 5.1 were selected for the EOP study of sodium chloride-, hydrochloric acid- and caustic soda solutions.

Table 5.1 Membrane and membrane types selected for EOP of Sodium Chloride-, Hydrochloric Acid- and Caustic Soda Solutions

Membranes	Anionic (A) Cationic (C)	Type	Salt	Acid	Base
Selemion AMV	A	Homogeneous	✓	✓	✓
Selemion CMV	C	Homogeneous	✓	✓	✓
Ionac MA 3470	A	Heterogeneous	✓	✓	✓
Ionac MC 3475	C	Heterogeneous	✓	✓	✓
Raipore R 4030	A	Homogeneous	✓		
Raipore R 4010	C	Homogeneous	✓		
Ionics A 204 UZL 386	A	Homogeneous	✓		
Ionics C 61 CZL 386	C	Homogeneous	✓		
WTPSA-1	A	Heterogeneous	✓		
WTPSC-1	C	Heterogeneous	✓		
WTPVCA-2	A	Heterogeneous	✓		
WTPVCC-2	C	Heterogeneous	✓		
WTPSTA-3	A	Heterogeneous	✓		
WTPSTC-3	C	Heterogeneous	✓		
Selemion AAV	A	Homogeneous		✓	
Selemion CHV	C	Homogeneous		✓	
ABM-1	A	Homogeneous		✓	
Selemion CHV	C	Homogeneous		✓	
ABM-2	A	Heterogeneous		✓	
Selemion CHV	C	Homogeneous		✓	
ABM-3	A	Heterogeneous		✓	
Selemion CHV	C	Homogeneous		✓	
Selemion AMP	A	Homogeneous			✓
Selemion CMV	C	Homogeneous			✓

5.2 Membrane Preparation

The WTA (WATERTEK anion) and WTC (WATERTEK cation) ion-exchange membranes were prepared as follows:

Resin (strong acid and strong base) with a particle size of less than 70 μm was suspended in appropriate swelling, base and casting solutions and the membranes were cast on polypropylene support material. The membranes were dried for approximately 1 hour in a convection oven at temperatures from 65 to 80°C before use. Polysulphone (for WTPSA-1; WTPSC-1 membranes), polyvinyl chloride (for

WTPVCA-2, WTPVCC-2 membranes) and polystyrene (for WTPSTA-3, WTPSTC-3 membranes) were used as base materials. N- methyl-2 pyrrolidone (NMP) was used as casting solution for the polysulphone (PS) based membranes while cyclohexanone was used as casting solution for the polyvinyl chloride and polystyrene based (PST) membranes.

The ABM membranes for acid EOP studies were supplied by the membrane research group of the Weizmann Institute of Science in Israel. The membranes used in the sealed-cell ED tests were also developed by the membrane research group of the Weizmann Institute of Science in Israel. The membranes were made from microbeads of styrene-divinylbenzene copolymer which were modified to cation- and anion-exchange particles. The cation-exchange particles were formed by chlorosulphonation with chlorosulphonic acid followed by hydrolysis to yield the sulphonated product. The anion-exchange particles were formed by chloromethylation followed by amination with triethylamine to yield the anion-exchange particles.

The ion-exchange membranes were formed by casting a suspension of the particles on a fabric. The suspension was evaporated to dryness to yield the dry membrane. The cation- and anion-exchange membranes were then heat-sealed to give the membrane bags.

5.3 Unit-Cell Construction

A unit cell can be constructed in the following number of ways : -

- a) glueing the membrane edges together with a suitable glue;
- b) glueing the membrane edges to either side of an injection moulded nylon ring (Figure 5.1) which has a brine exit within it⁽¹⁾; and
- c) mounting of the membranes between gaskets as in the filter press stack design.

For experiment, the volume, however, of the brine compartment must be kept to a minimum in order to minimize time for achieving the steady state and for beginning to measure water flow. An injection moulded nylon ring (Figure 5.1) was used in the EOP experiments as the unit cell.

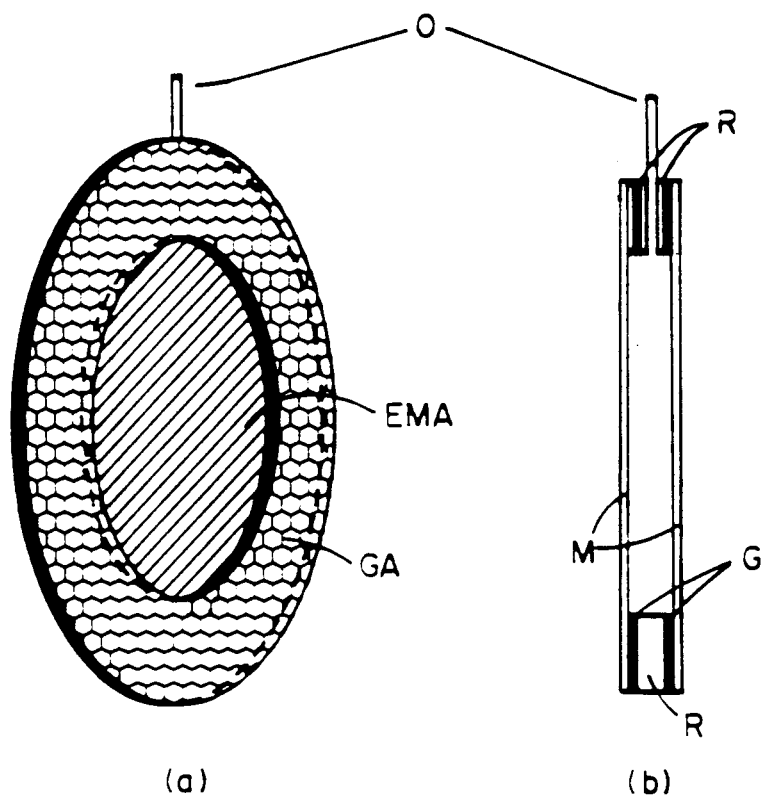


Figure 5.1: Schematic of injection moulded nylon ring that was used for construction of the membrane bag. The membranes are glued to both sides of the ring.

a : Front view	b : Lateral view
O : brine outlet	EMA : Effective membrane area
GA: Glueing area	M : Membrane
G : Glue	R : Nylon ring.

5.4 Determination of Brine Concentration, Current Efficiency and Water Flow as a Function of Feed Concentration and Current Density

The EOP cell used in the experiments was described by Oren and Litan⁽¹¹²⁾ and is shown in Figure 5.2. It consists of two symmetric units, each of which contains a separate electrode. A carbon slurry was circulated through the electrode compartments and was used as electrode rinse solution. The membranes were attached to the nylon ring with silicon sealant and the nylon ring (membrane bag) was placed between the two circulation cells and rubber rings were used to secure sealing. Approximately 40 litres of solution containing salt, acid or base was circulated through the cell renewing its content approximately 60 times per minute. In this way an approximately constant feed concentration was maintained during the experiments.

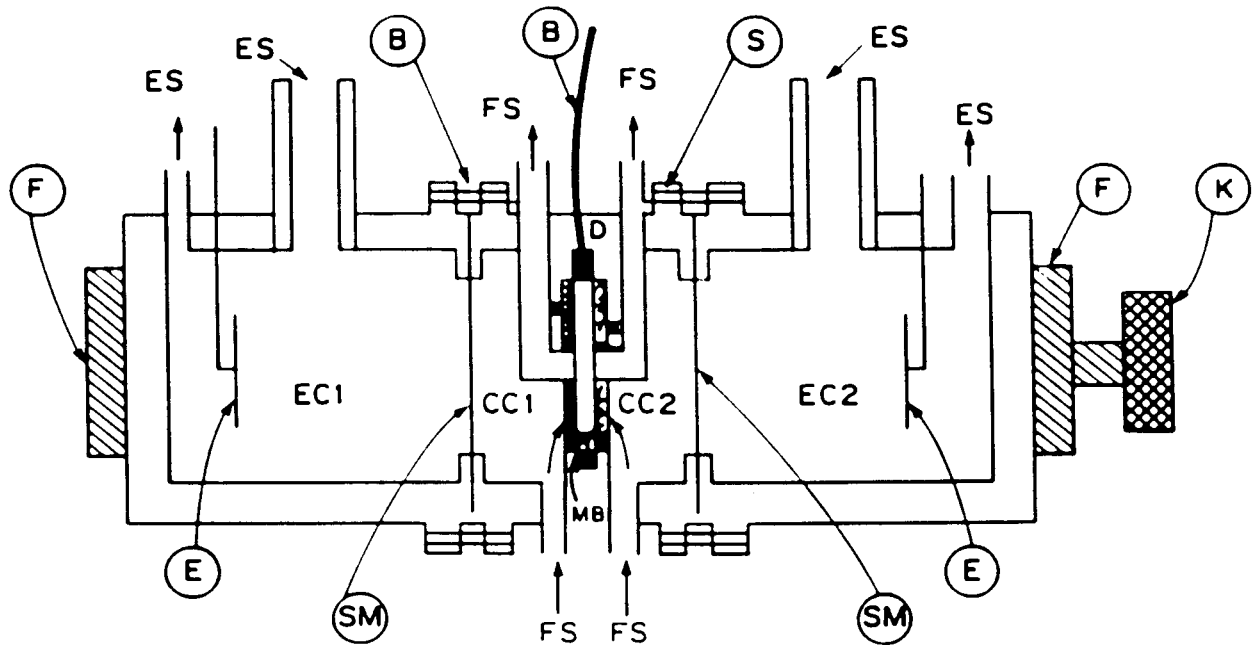


Figure 5.2: Schematic diagram of the apparatus used for the EOP experiments. EC1 and EC2: Electrode cells; CC1 and CC2: Circulation cells for the feed solution (FS); B: Brine outlet; MB: Membrane bag; SM: Membrane separating the electrode compartments from the feed solution; E: Electrodes; D: Perforated porous polypropylene disks; S: Stainless Steel Screws; F: Clamping frame; K: Tightening knob.

Efficient stirring and streaming of the solution in the cell were effected by the Mearns and Sutton's method of forcing the solution onto the membrane surface through perforated polypropylene discs⁽¹¹²⁾. This has been shown to be a very efficient way of stirring. Constant current was supplied to the cell by a Hewlett Packard constant current source. Current was measured with a Hewlett Packard digital multimeter. Brine samples were collected at certain intervals and their volume and concentration determined. Each point on the plots of c_b versus I , and of J versus I_{eff} was the average of 3 to 5 measurements after the system had reached the stationary state. Concentration changes in the feed solution during the time of the experiments were found to be negligible.

Current efficiency, ϵ_p , was calculated as follows⁽¹⁾:

$$\epsilon_p = \frac{2Jc_b}{I/F} = \frac{c_b(V/t)}{I/F} \equiv \Delta \bar{t} \quad (\text{see eq. 3.10.37})$$

where c_b represents the brine concentration, V the volume of the solution that enters the bag per unit area ($7,55 \text{ cm}^2$) in t seconds ($V/t = 2J$), I the applied current density (mA/cm^2) and F is Faraday's constant.

The maximum brine concentration, c_b^{max} , was determined from the following relation

$$c_b^{\text{max}} = \frac{1}{2BF} \quad (\text{see eq. 3.10.28})$$

where $2B$ is the electro-osmotic coefficient determined from the slope of the J versus I_{eff} plots and F is Faraday's constant.

5.5 Determination of Membrane Characteristics

5.5.1 Membrane potential

The difference between the counter- and co-ion transport number, Δt , which is called the apparent transport number or membrane permselectivity, was measured as follows:

The potential ($\Delta \Psi_m$) of a membrane is usually measured between 0,1/0,2 mol/l or 0,5/1,0 mol/l sodium chloride solutions in a specially designed cell with calomel electrodes. The theoretical potential, $\Delta \Psi_i$, is calculated from the activities of the two solutions. Membrane permselectivity, Δt , can then be calculated from these values where $\Delta \Psi_m$ is the measured potential and a_s^{11}/a_s^1 is the ratio of salt activities on both sides of the membrane.

$$\Delta t = \frac{\Delta \Psi_m}{\Delta \Psi_i} \quad (\text{see eq. 3.11.11})$$

where $\Delta t = 2t_1 - 1$ and

$$\Delta \Psi_i = \frac{RT}{F} \ln \frac{a_s^{11}}{a_s^1} \quad (\text{see eq. 3.11.10})$$

5.5.2 Ion-Exchange Capacity

Membrane capacity was determined as follows⁽¹¹³⁾:

Approximately 3 g dried membrane sample (weighed accurately) was equilibrated with 150 ml 1 mol/l hydrochloric acid for 16 hours at room temperature. The membrane

sample was rinsed free of chloride. The sample was then treated with 200 ml 4% sodium carbonate solution for 2 hours, neutralized to below pH 8,3 with 0,1 mol/l sulphuric acid, potassium chromate (2 ml) added and the sample titrated with standardized 0,1 mol/l silver nitrate and the total anion membrane exchange capacity calculated.

5.5.3 Gel Water Content

The gel water content of the membranes was determined as follows⁽¹¹³⁾:

Membrane samples (pretreated to their reference form⁽¹¹³⁾) were blotted dry with filter paper and mass recorded. The membrane sample was then dried at 105°C for 16 hours and the dried mass recorded. The gel water content (%) was calculated from the mass loss.

5.5.4 Membrane Resistance

Membrane resistance was measured between platinum electrodes coated with platinum black in a specially designed membrane resistance measurement cell with a resistance meter. Salt concentrations of 0,1 and 0,5 mol/l sodium chloride were used. Membrane resistance was expressed in ohm.cm².

5.6 Determination of Salt and Acid Diffusion Rate through Membranes

Salt and acid diffusion rate through *Selemion* AMV and AAV membranes was determined in the cell shown in Figure 5.3. The cell consists of two half-cells containing stirrers with a volume of approximately 200 ml per half-cell. A membrane with an exposed area of 2,55 cm² was clamped between the two half-cells and salt or acid solution with a concentration difference of 0,05/2 mol/l and 0,05/4 mol/l was placed in the two half-cells. Diffusion was allowed to take place and the rate of concentration change in the two cells was determined.

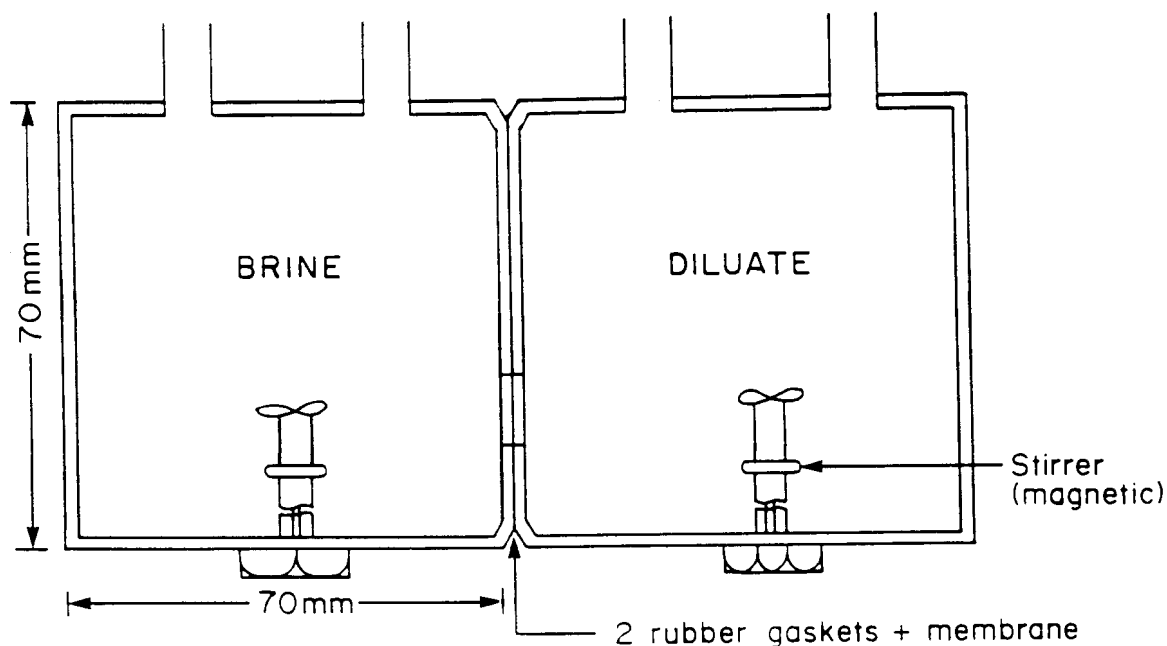


Figure 5.3: Diagram of cell used for determination of diffusion of hydrochloric acid and sodium chloride through membranes (membrane area = 2,55 cm²).

5.7 Bench-Scale EOP-ED Stack

A bench-scale EOP-ED stack has been designed and constructed from materials available in South Africa. A simplified diagram of the membrane configuration in the stack is shown in Figure 5.4. The stack is similar to a conventional filter-press type ED stack. The only difference is that brine is not circulated through the brine compartments as is the case in conventional ED. Water enters the brine compartments by means of electro-osmosis and runs out of these compartments in a groove in the spacer at the top of each brine cell. The stack contained 10 cell pairs with an effective membrane area of 169 cm².

The end plates were made from PVC. A diagram of the end plates is shown in Figure 5.5. Water flow through the stack into the diluting and brine compartments was directed by the manifold shown in Figure 5.5. Gaskets made from polycarbonate (2 mm) and teflon (2 mm) were used in the stack to separate the membranes from each other. A diagram of a gasket is shown in Figure 5.6. PVC spacers (0,3 mm) were used to separate the membranes from each other. Platinized titanium or graphite electrodes were used in the stack.

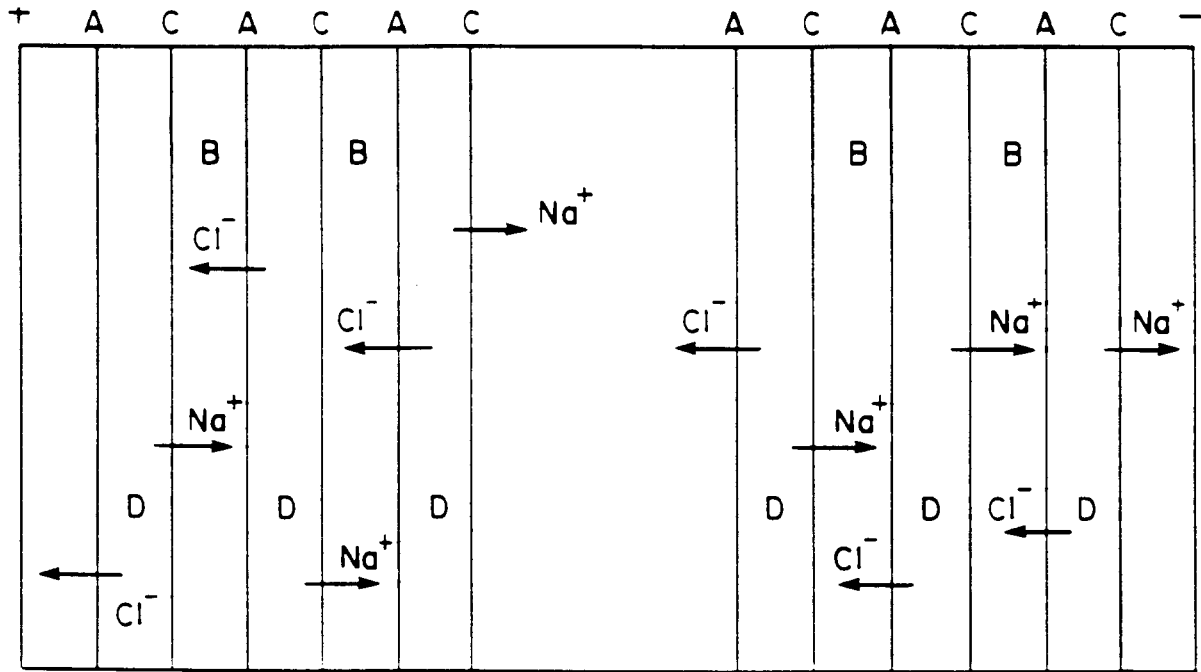


Figure 5.4: Simplified diagram of membrane configuration in EOP-ED stack.
B = brine compartment; D = diluting compartment.

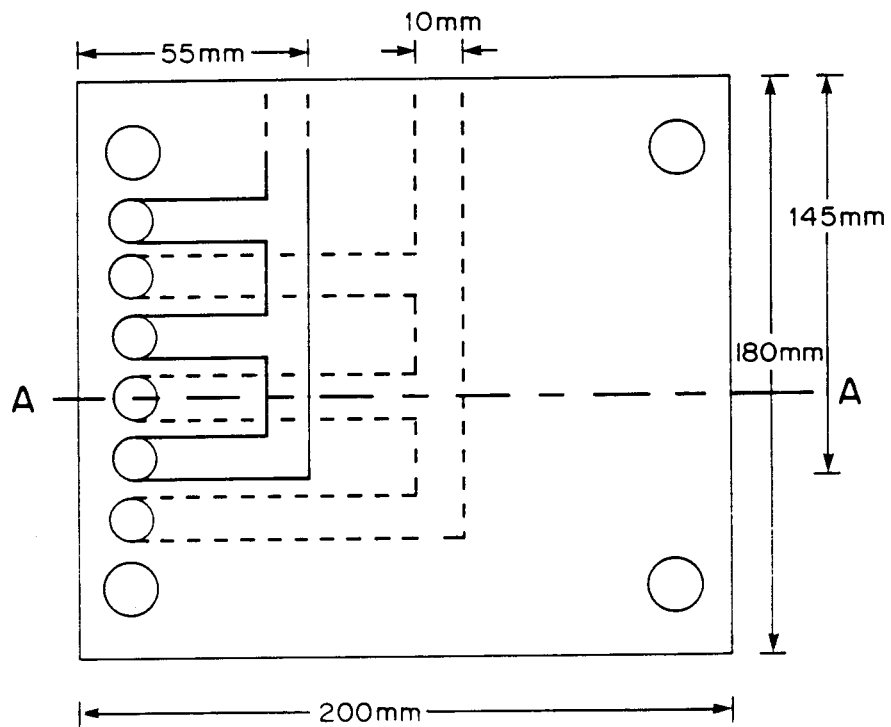


Figure 5.5: End plates of EOP-ED stack.

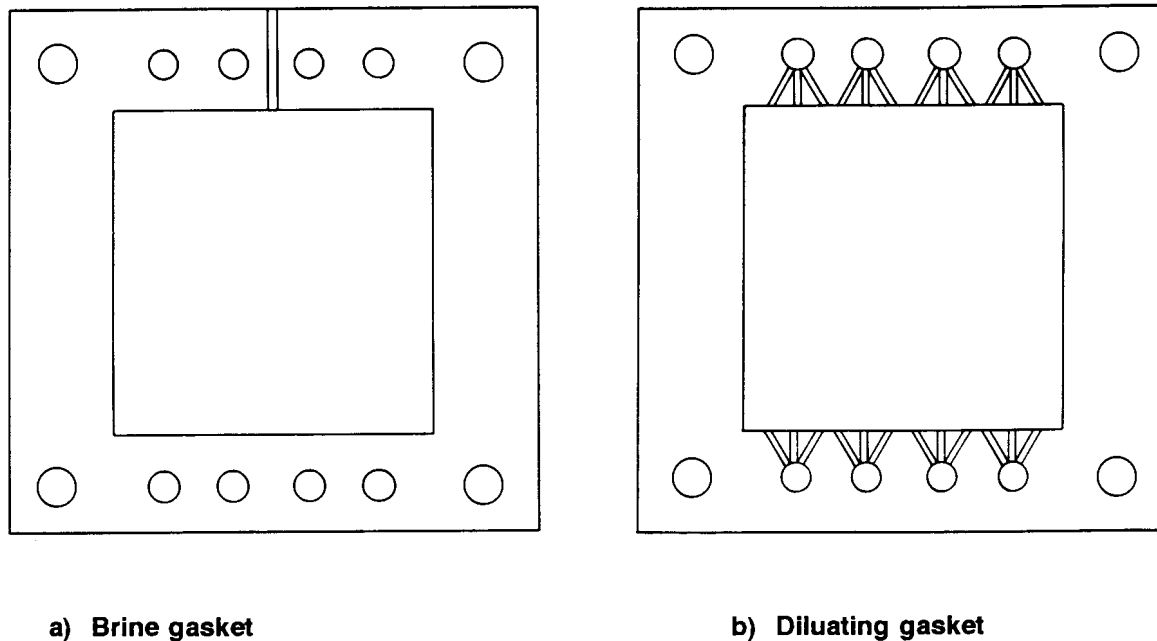


Figure 5.6: Gaskets used in EOP-ED stack.

Ionac MA-3475 and MC-3470 membranes were used for concentration/desalination of sodium chloride solutions while *Selemion* AAV and CHV and *Selemion* AMV and CMV membranes were used for hydrochloric acid and caustic soda concentration/desalination, respectively.

Solutions of sodium chloride, hydrochloric acid and caustic soda in deionized water of different initial concentrations were concentrated/desalinated at different cell pair voltages in the stack. The experimental set-up is shown in Figure 5.7. Feed (c_i), product (c_p) and brine (c_b) concentrations were determined from conductivity measurements.

A typical ED experiment was conducted as follows:

Feed solution (12 ℓ) was circulated at a linear flow velocity of 1 cm/s through the dialysate compartments. The electrode solution consisted of 2 litre of a 2% carbon slurry in 1 mol/ ℓ sodium chloride solution. The pH of this solution was adjusted to approximately 5 and circulated through the electrode compartments.

Direct current voltage of 0,5; 1,0; 1,5; 2,0; 3 and 4 volt was applied across a cell pair. Voltage between the cells was measured with platinum wire connected to a voltmeter. Platinum wire was inserted between the first and last brine cell. Current was recorded at 15 minute intervals and the concentration potential (V_n) was determined by interrupting the current for a few seconds. The final brine volume and the concentration of the desalinated feed (product water) and brine were determined at the end of the runs.

Current efficiency (CE), water recovery (WR), brine volume (BV), electrical energy consumption (EEC), concentration factor (CF), output (OP) (water yield), d_{eff} and R_{cp} were determined from the experimental data. Graphs were compiled of reduction in feed water concentration as a function of time and of cell pair resistance (V_{cp}) as a function of specific resistance (ρ) of the dialysate. An example of the calculations is shown in Appendix C.

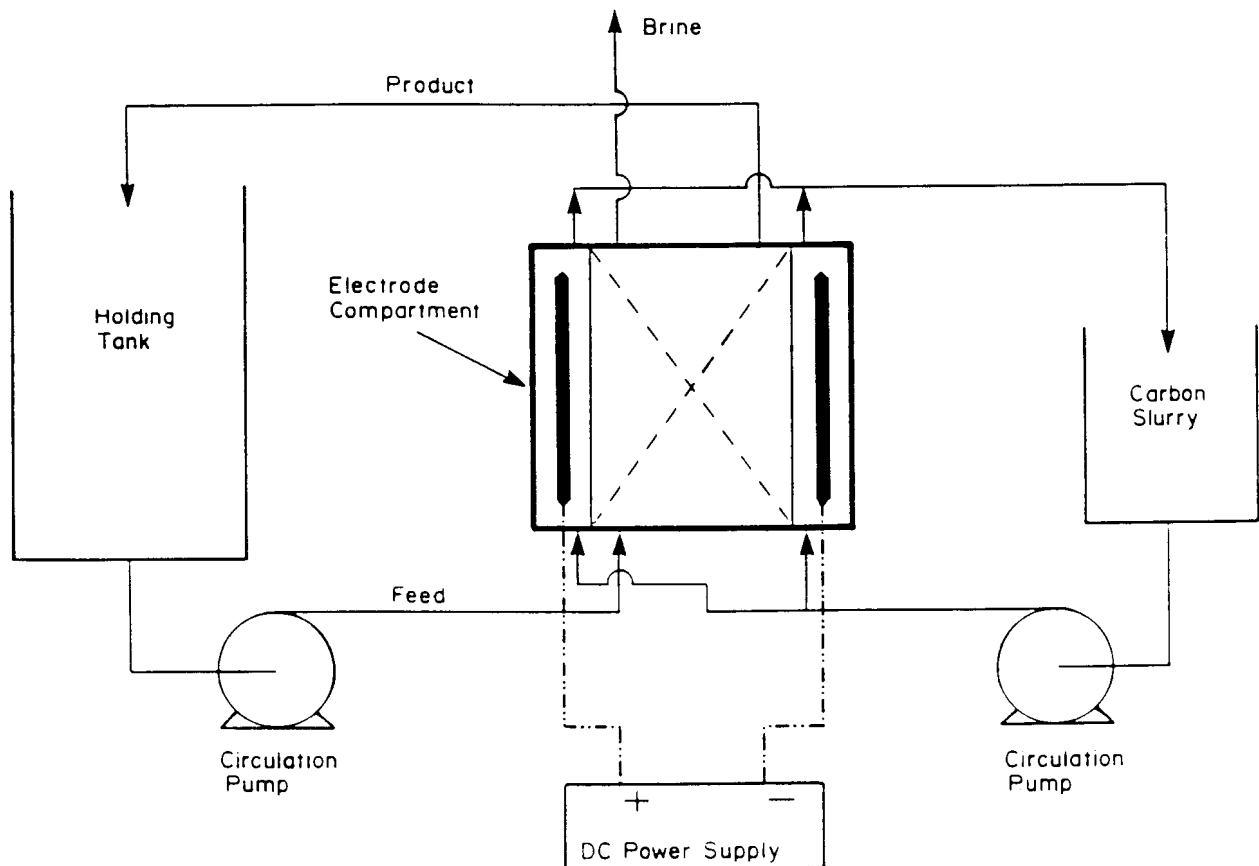


Figure 5.7: Experimental set-up for EOP-ED of sodium chloride, hydrochloric acid and caustic soda solutions.

5.8 Sealed-Cell ED Stack

A simplified diagram of the sealed-cell (SCED) membrane stack is shown in Figure 5.8. The brine sealed cells with outlets are arrayed in an open vessel, separated by spacers (0,3 mm). The dialysate enters through a suitable port at the bottom of the vessel and runs out through an overflow. Direct current is applied through carbon suspension electrodes⁽⁴⁾. The external dimensions of the sealed brine cells are 60 x 80 mm, giving an effective membrane area of 100 cm² per cell pair (cp).

Solutions of sodium chloride, ammonium nitrate, sodium sulphate, sodium nitrate and calcium chloride in deionized water of different initial concentrations were concentrated/desalinated at different cell pair voltages in the SCED unit. Feed (c_i), product (c_p) and brine (c_b) concentrations were determined from conductivity measurements. Various industrial effluents were also treated with SCED.

Feed solution (15 ℓ) was circulated at a linear flow velocity of 15 cm/s through the dialysate compartments. The electrode solution consisted of 2 ℓ of a 2 % carbon slurry in 1 mol/ℓ sodium chloride solution. The pH of the solution was adjusted to approximately 5 and circulated through the electrode compartments.

Electrodialysis was started by applying a DC voltage of approximately 0,5 Volt per cell pair across 17 membrane bags. Voltage between the membrane bags was measured with calomel electrodes connected to a salt bridge. Current was recorded at 10 or 20 minute intervals during ED and V_n was determined during interruption of the current for a short period. The final brine volume, concentration of the desalinated feed (product water) and brine were determined at the end of the runs.

Current efficiency (CE), water recovery (WR), brine volume (BV), electrical energy consumption (EEC), concentration factor (CF), output (OP) (water yield), effective thickness of dialysate compartment (d_{eff}), and membrane resistance (R_{cp}) were determined from the experimental data. Graphs were plotted of feed water concentration, brine concentration, current efficiency and electrical energy consumption as a function of time, and of cell pair voltage as a function of the specific resistance (ρ) of the dialysate.

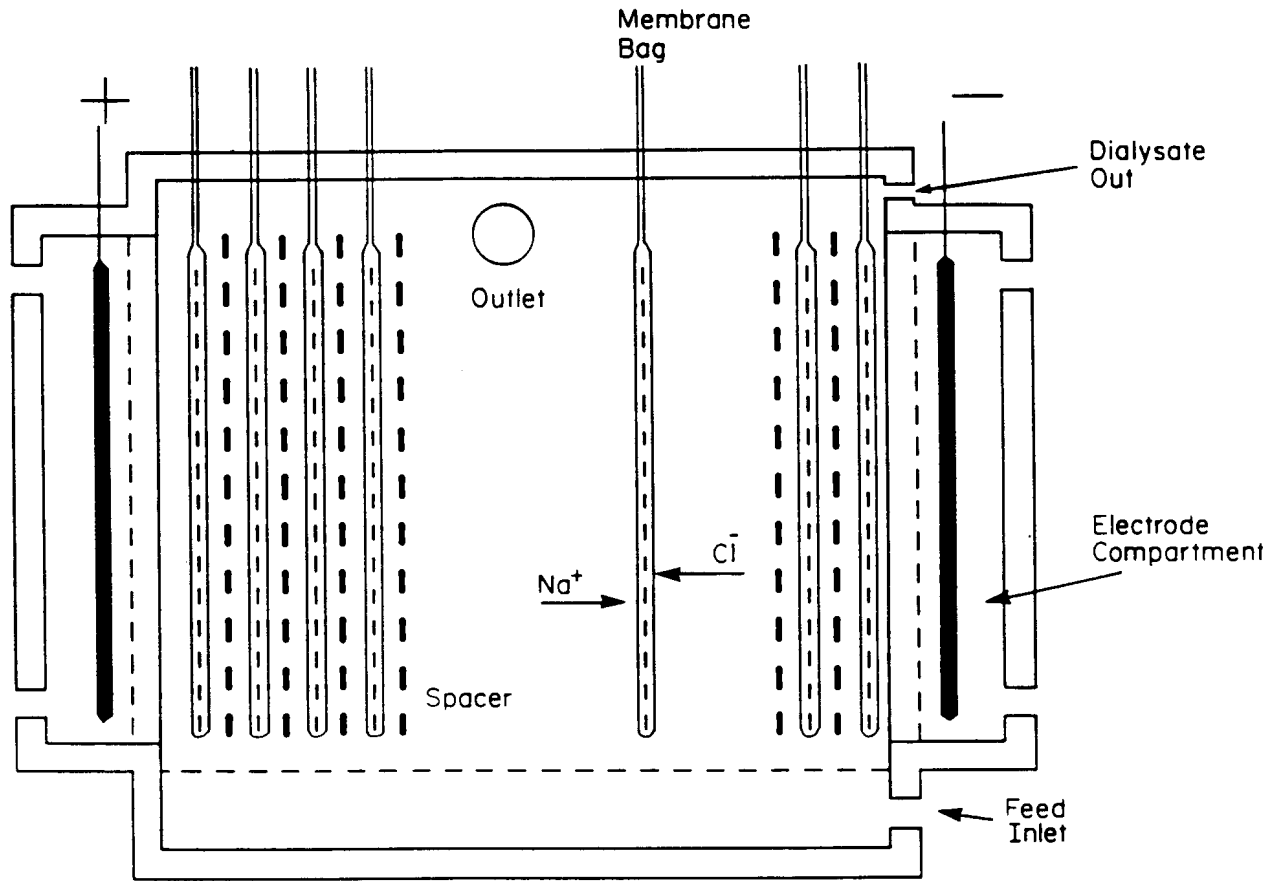


Figure 5.8: Simplified diagram of SCED membrane stack.

6. ELECTRO-OSMOTIC PUMPING OF SODIUM CHLORIDE SOLUTIONS WITH DIFFERENT ION-EXCHANGE MEMBRANES

Brine concentrations, water flows and current efficiencies were determined at different current densities for different sodium chloride feed water concentrations. Membrane permselectivities (apparent transport numbers - Δt 's) were measured at the same concentration differences as encountered during EOP experiments when brine concentration had reached the steady state. The EOP results are summarized in Tables 6.1 to 6.28 for the different membranes.

6.1 Brine Concentration

Brine concentration (c_b) as a function of current density (I) is shown in Figures 6.1 to 6.7. Initially brine concentration increases rapidly and then levels off at higher current densities. Brine concentration increases with increasing current density and increasing feed water concentration. Highest brine concentrations were obtained with *Selemion* and *Ionac* membranes (Table 6.29). Brine concentrations of 25,1 and 23,4% were obtained at high current density (0,1 mol/l feed) with *Selemion* and *Ionac* membranes, respectively. Lower brine concentrations were obtained with the *Ionics* and WTPS membranes (19,0 and 20,9%, respectively) while the lowest concentrations were obtained with the *Raipore*, WTPVC and WTPST membranes (14,4, 15,1 and 15,4%, respectively). The concentration performance of the WTPS membranes compares favourably with that of the commercially available membranes.

It appears that the brine concentration will reach a maximum value, c_b^{\max} . This was predicted from the flow equations⁽¹⁾. Maximum brine concentration was nearly reached in the case of the *Raipore*- (Fig. 6.3), WTPVC- (Fig. 6.6) and WTPST- (Fig. 6.7) membranes at 0,05 mol/l feed concentration at high current density. Maximum brine concentration was also nearly reached in the case of the *Selemion*- (Fig. 6.1), *Ionac*- (Fig. 6.2), *Raipore*- (Fig. 6.3), *Ionics*- (Fig. 6.4), WTPS- (Fig 6.5), WTPVC- (Fig. 6.6) and WTPST- (Fig. 6.7) membranes in the 0,1 to 1,0 mol/l feed concentration range at high current densities.

Maximum brine concentration, c_b^{\max} , was calculated from the following two relationships, viz.

$$c_b^{\max} = \frac{1}{2\beta F} \quad (\text{see eq. 3.10.28})$$

Table 6.1 : Electro-osmotic pumping experimental conditions and results for 0,05 mol/l sodium chloride (Selemon AMV and CMV)

Current Density i , mA/cm ²	Brine concentration c_b , mol/l		Water flow J , cm/h	Current Efficiency e_p , %	Effective Current Density i_{eff} , mA/cm ²	Transport Numbers				
	$c_{b, exp.}$	$c_{b, calc.}$				Δt^c	Δt^a	$\bar{\Delta}t$	\bar{i}_1^c	\bar{i}_2^a
5	1,62	1,59	0,102	62,37	3,12	0,91	0,82	0,87	0,96	0,91
10	2,15	2,76	0,115	66,22	6,62	0,88	0,82	0,85	0,94	0,91
15	2,65	3,35	0,137	64,79	9,72	0,85	0,78	0,82	0,93	0,89
20	2,81	3,54	0,170	64,93	12,99	0,86	0,75	0,81	0,93	0,88
30	3,31	4,05	0,217	64,15	19,25	0,84	0,73	0,79	0,92	0,86

Electro-osmotic coefficient (2β) = 0,219 μ F (slope = 0,008194 ml/mAh)

J_{osm} = y-intercept = 0,06023 cm/h

c_b^{max} = 4,55 mol/l

$\Delta t^c = t_1^c - t_2^c$

$\Delta t^a = t_2^a - t_1^a$

$\bar{\Delta}t$ = Average transport number of membrane pair

\bar{i}_1^c = Transport number of cation through cation membrane

\bar{i}_2^a = Transport number of anion through anion membrane.

Table 6.2 : Electro-osmotic pumping experimental conditions and results for 0,1 mol/l sodium chloride (Selemon AMV and CMV)

Current Density i , mA/cm ²	Brine concentration c_b , mol/l		Water flow J , cm/h	Current Efficiency e_p , %	Effective Current Density i_{eff} , mA/cm ²	Transport Numbers				
	$c_{b, exp.}$	$c_{b, calc.}$				Δt^c	Δt^a	$\bar{\Delta}t$	\bar{i}_1^c	\bar{i}_2^a
5	1,79	2,1	0,076	73,0	3,65	0,94	0,81	0,87	0,97	0,90
10	2,37	2,64	0,118	74,4	7,47	0,89	0,78	0,84	0,94	0,89
15	2,83	3,02	0,152	76,7	11,51	0,89	0,75	0,82	0,94	0,88
20	3,02	3,21	0,188	76,1	15,23	0,88	0,73	0,81	0,94	0,87
30	3,58	3,74	0,238	76,2	22,86	0,85	0,74	0,80	0,93	0,87
40	3,91	4,09	0,286	75,0	30,01	0,89	0,68	0,78	0,94	0,84
50	4,29	4,33	0,330	75,9	37,95	0,82	0,71	0,77	0,91	0,85

Electro-osmotic coefficient (2β) = 0,198 μ F (slope = 0,00739 ml/mAh)

J_{osm} = y-intercept 0,067696 cm/h

c_b^{max} = 5,05 mol/l

$\Delta t^c = t_1^c - t_2^c$

$\Delta t^a = t_2^a - t_1^a$

$\bar{\Delta}t$ = Average transport number of membrane pair

\bar{i}_1^c = Transport number of cation through cation membrane

\bar{i}_2^a = Transport number of anion through anion membrane.

Table 6.3 : Electro-osmotic pumping experimental conditions and results for 0,5 mol/l sodium chloride (Selemon AMV and CMV)

Current Density i , mA/cm ²	Brine concentration c_b , mol/l		Water flow J , cm/h	Current Efficiency e_p , %	Effective Current Density i_{eff} , mA/cm ²	Transport Numbers				
	$c_{b, exp.}$	$c_{b, calc.}$				Δt^c	Δt^a	$\bar{\Delta}t$	\bar{i}_1^c	\bar{i}_2^a
5	1,72	1,71	0,0895	82,5	4,13	0,92	0,71	0,82	0,96	0,86
10	2,74	2,33	0,122	89,66	8,96	0,86	0,67	0,76	0,93	0,83
20	3,54	2,82	0,190	91,72	18,34	0,81	0,63	0,72	0,91	0,81
30	3,94	3,27	0,248	87,35	26,21	0,86	0,59	0,72	0,93	0,80
40	4,20	3,26	0,323	90,89	36,36	0,81	0,60	0,71	0,90	0,80
50	4,50	3,51	0,378	91,23	45,62	0,84	0,58	0,71	0,92	0,79
60	4,66	3,62	0,440	91,46	54,88	0,85	0,57	0,71	0,93	0,79

Electro-osmotic coefficient (2β) = 0,187 μ F (slope = 0,006959 ml/mAh)

J_{osm} = y-intercept = 0,062409 cm/h

c_b^{max} = 5,36 mol/l

$\Delta t^c = t_1^c - t_2^c$

$\Delta t^a = t_2^a - t_1^a$

$\bar{\Delta}t$ = Average transport number of membrane pair

\bar{i}_1^c = Transport number of cation through cation membrane

\bar{i}_2^a = Transport number of anion through anion membrane.

Table 6.4: Electro-osmotic pumping experimental conditions and results for 1,0 mol/l sodium chloride (Salemion AMV and CMV)

Current Density I , mA/cm ²	Brine concentration c_b , mol/l		Water flow J , cm/h	Current Efficiency e_p , %	Effective Current Density I_{em} , mA/cm ²	Transport Numbers				
	$c_{b, exp}$	$c_{b, calc}$				Δt^c	Δt^a	$\bar{\Delta}t$	\bar{i}_c^c	\bar{i}_a^c
10	2,95	2,41	0,113	89,00	8,90	0,84	0,62	0,73	0,92	0,81
20	3,73	2,90	0,174	87,14	17,43	0,82	0,55	0,68	0,91	0,77
30	4,12	3,16	0,236	86,95	26,09	0,79	0,55	0,67	0,90	0,78
40	4,55	3,51	0,279	85,21	34,08	0,80	0,51	0,66	0,90	0,76
50	5,07	3,70	0,328	89,28	44,64	0,79	0,52	0,65	0,89	0,76
60	5,10	3,79	0,384	87,52	52,51	0,80	0,50	0,65	0,90	0,75

Electro-osmotic coefficient (2β) = 0,154 t/F (slope = 0.005757 ml/mAh)

J_{osm} = y-intercept = 0,078991 cm/h

c_b^{max} = 6,48 mol/l

$\Delta t^c = t_1^c - t_2^c$

$\Delta t^a = t_2^a - t_1^a$

$\bar{\Delta}t$ = Average transport number of membrane pair

\bar{i}_c^c = Transport number of cation through cation membrane

\bar{i}_a^c = Transport number of anion through anion membrane.

Table 6.5 : Electro-osmotic pumping experimental conditions and results for 0,05 mol/l sodium chloride (Ionac MA-3475 and MC-3470)

Current Density I , mA/cm ²	Brine concentration c_b , mol/l		Water flow J , cm/h	Current Efficiency e_p , %	Effective Current Density I_{em} , mA/cm ²	Transport Numbers				
	$c_{b, exp}$	$c_{b, calc}$				Δt^c	Δt^a	$\bar{\Delta}t$	\bar{i}_c^c	\bar{i}_a^c
5	1,50	1,82	0,0883	71,01	3,55	0,93	0,80	0,86	0,96	0,90
10	2,16	2,80	0,1112	64,41	6,44	0,91	0,76	0,83	0,95	0,88
15	2,60	3,45	0,1324	61,54	9,23	0,90	0,73	0,82	0,95	0,87
20	2,87	4,05	0,1456	56,04	11,21	0,83	0,74	0,79	0,92	0,87
25	3,25	4,60	0,1589	55,39	13,85	0,86	0,71	0,78	0,93	0,85

Electro-osmotic coefficient (2β) = 0,186 t/F (slope = 0.0069464 ml/mAh)

J_{osm} = y-intercept = 0,0657676 cm/h

c_b^{max} = 5,37 mol/l

$\Delta t^c = t_1^c - t_2^c$

$\Delta t^a = t_2^a - t_1^a$

$\bar{\Delta}t$ = Average transport number of membrane pair

\bar{i}_c^c = Transport number of cation through cation membrane

\bar{i}_a^c = Transport number of anion through anion membrane.

Table 6.6 : Electro-osmotic pumping experimental conditions and results for 0,1 mol/l sodium chloride (Ionac MA-3475 and MC-3470)

Current Density I , mA/cm ²	Brine concentration c_b , mol/l		Water flow J , cm/h	Current Efficiency e_p , %	Effective Current Density I_{em} , mA/cm ²	Transport Numbers				
	$c_{b, exp}$	$c_{b, calc}$				Δt^c	Δt^a	$\bar{\Delta}t$	\bar{i}_c^c	\bar{i}_a^c
5	1,92	2,29	0,0662	68,17	3,41	0,89	0,73	0,81	0,95	0,87
10	2,49	2,94	0,0997	64,19	6,42	0,88	0,70	0,79	0,94	0,85
15	2,89	3,65	0,1186	61,70	9,25	0,86	0,68	0,77	0,93	0,84
20	3,18	3,84	0,14834	63,23	12,65	0,86	0,67	0,76	0,93	0,83
30	3,4	4,27	0,1977	60,09	18,03	0,84	0,67	0,75	0,92	0,83
40	3,81	4,89	0,2295	58,62	23,45	0,84	0,66	0,75	0,92	0,83
50	4,00	5,32	0,2649	56,81	28,40	0,85	0,66	0,76	0,93	0,83

Electro-osmotic coefficient (2β) = 0,206 t/F (slope = 0.0076844 ml/mAh)

J_{osm} = y-intercept = 0,0503481 cm/h

c_b^{max} = 4,85 mol/l

$\Delta t^c = t_1^c - t_2^c$

$\Delta t^a = t_2^a - t_1^a$

$\bar{\Delta}t$ = Average transport number of membrane pair

\bar{i}_c^c = Transport number of cation through cation membrane

\bar{i}_a^c = Transport number of anion through anion membrane.

Table 6.7 : Electro-osmotic pumping experimental conditions and results for 0,5 mol/l sodium chloride (Ionac MA-3475 and MC-3470)

Current Density I , mA/cm ²	Brine concentration c_b , mol/l		Water flow J , cm/h	Current Efficiency e_p , %	Effective Current Density I_{eff} , mA/cm ²	Transport Numbers				
	$c_{b,exp}$	$c_{b,calc}$				Δt^*	Δt^*	$\bar{\Delta}t$	\bar{i}_1^*	\bar{i}_2^*
5	2,37	1,69	0,07568	96,17	4,81	0,80	0,57	0,69	0,90	0,79
10	2,95	2,57	0,097	76,81	7,68	0,80	0,54	0,67	0,90	0,77
20	3,69	3,03	0,1589	78,61	15,72	0,78	0,52	0,65	0,89	0,76
30	3,99		0,205	73,19	21,95					
40	4,05	3,84	0,2472	67,10	26,84	0,77	0,50	0,64	0,88	0,75
50	4,37	4,42	0,26136	61,23	30,62	0,75	0,49	0,62	0,87	0,75
60	4,51	4,91	0,2825	56,93	34,16	0,73	0,51	0,62	0,87	0,75
70	4,59	5,05	0,3178	55,87	39,11	0,73	0,50	0,61	0,86	0,75

Electro-osmotic coefficient (2β) = 0,190 μ /F (slope = 0,0070843 m/mAh)
 J_{osm} = y-intercept = 0,0454963 cm/h
 c_b^{max} = 5,26 mol/l
 $\Delta t^* = t_1^* - t_2^*$

$\Delta t^* = t_2^* - t_1^*$
 $\bar{\Delta}t$ = Average transport number of membrane pair
 \bar{i}_1^* = Transport number of cation through cation membrane
 \bar{i}_2^* = Transport number of anion through anion membrane.

Table 6.8: Electro-osmotic pumping experimental conditions and results for 1,0 mol/l sodium chloride (Ionac MA-3475 and MC-3470)

Current Density I , mA/cm ²	Brine concentration c_b , mol/l		Water flow J , cm/h	Current Efficiency e_p , %	Effective Current Density I_{eff} , mA/cm ²	Transport Numbers				
	$c_{b,exp}$	$c_{b,calc}$				Δt^*	Δt^*	$\bar{\Delta}t$	\bar{i}_1^*	\bar{i}_2^*
20	3,96	2,76	0,1766	93,73	18,75	0,76	0,54	0,65	0,88	0,77
40	4,47	3,36	0,286	85,70	34,28	0,75	0,54	0,64	0,88	0,77
60	4,56	3,62	0,411	83,648	50,19	0,78	0,55	0,67	0,89	0,78
80	4,91	3,68	0,5033	82,804	66,24	0,73	0,51	0,62	0,87	0,76

Electro-osmotic coefficient (2β) = 0,187 μ /F (Slope 0,0069749 m/mAh)
 J_{osm} = y-intercept = 0,0487359 cm/h
 c_b^{max} = 5,35 mol/l
 $\Delta t^* = t_1^* - t_2^*$

$\Delta t^* = t_2^* - t_1^*$
 $\bar{\Delta}t$ = Average transport number of membrane pair
 \bar{i}_1^* = Transport number of cation through cation membrane
 \bar{i}_2^* = Transport number of anion through anion membrane.

Table 6.9 : Electro-osmotic pumping experimental conditions and results for 0,05 mol/l sodium chloride (Ralpore R4030 anion and R4010 cation)

Current Density I , mA/cm ²	Brine concentration c_b , mol/l		Water flow J , cm/h	Current Efficiency e_p , %	Effective Current Density I_{eff} , mA/cm ²	Transport Numbers				
	$c_{b,exp}$	$c_{b,calc}$				Δt^*	Δt^*	$\bar{\Delta}t$	\bar{i}_1^*	\bar{i}_2^*
5	0,86	1,44	0,1059	48,85	2,44	0,79	0,84	0,82	0,90	0,92
10	1,19	1,84	0,1589	50,70	5,07	0,74	0,82	0,78	0,87	0,91
15	1,47	2,32	0,1827	48,02	7,20	0,71	0,81	0,76	0,85	0,90
20	1,55	2,50	0,2225	46,23	9,25	0,70	0,80	0,75	0,85	0,90
30	1,62	2,57	0,317	46,01	13,80	0,67	0,79	0,73	0,83	0,90

Electro-osmotic coefficient (2β) = 0,547 μ /F (slope = 0,0204201 m/mAh)
 J_{osm} = y-intercept = 0,0348506
 c_b^{max} = 1,83 mol/l
 $\Delta t^* = t_1^* - t_2^*$

$\Delta t^* = t_2^* - t_1^*$
 $\bar{\Delta}t$ = Average transport number of membrane pair
 \bar{i}_1^* = Transport number of cation through cation membrane
 \bar{i}_2^* = Transport number of anion through anion membrane.

Table 6.10: Electro-osmotic pumping experimental conditions and results for 0,1 mol/l sodium chloride (Raipore R4030 anion and R4010 cation)

Current Density i , mA/cm ²	Brine concentration c_b , mol/l		Water flow J , cm/h	Current Efficiency, e_p , %	Effective Current Density i_{eff} , mA/cm ²	Transport Numbers				
	$c_{b, exp.}$	$c_{b, calc.}$				Δt^c	Δt^a	$\bar{\Delta}t$	i_1^c	i_2^a
5	0,99	1,35	0,1148	60,62	3,03	0,83	0,83	0,83	0,92	0,92
10	1,37	1,72	0,172	63,23	6,32	0,78	0,80	0,79	0,89	0,90
20	1,86	2,28	0,251	62,74	12,55	0,75	0,77	0,76	0,88	0,89
30	2,16	2,57	0,3192	61,61	18,48	0,71	0,75	0,73	0,86	0,88
40	2,33	2,68	0,3973	62,04	24,82	0,71	0,72	0,71	0,85	0,86
50	2,47	2,86	0,467	61,97	30,99	0,70	0,73	0,72	0,85	0,86

Electro-osmotic coefficient (2β) = 0,320 μ F (slope = 0,0119546 ml/mAh)
 J_{osm} = y-intercept = 0,0985769 cm/h
 c_b^{max} = 3,13 mol/l
 $\Delta t^c = t_1^c - t_2^c$

$\Delta t^a = t_2^a - t_1^a$
 $\bar{\Delta}t$ = Average transport number of membrane pair
 i_1^c = Transport number of cation through cation membrane
 i_2^a = Transport number of anion through anion membrane.

Table 6.11 : Electro-osmotic pumping experimental conditions and results for 0,5 mol/l sodium chloride (Raipore R4030 anion and R4010 cation)

Current Density i , mA/cm ²	Brine concentration c_b , mol/l		Water flow J , cm/h	Current Efficiency e_p , %	Effective Current Density i_{eff} , mA/cm ²	Transport Numbers				
	$c_{b, exp.}$	$c_{b, calc.}$				Δt^c	Δt^a	$\bar{\Delta}t$	i_1^c	i_2^a
5	1,28	1,89	0,0894	61,11	3,05	0,98	0,83	0,90	0,99	0,91
10	1,65	2,21	0,1456	64,36	6,44	0,92	0,80	0,86	0,96	0,90
20	2,07	2,51	0,2384	66,14	13,23	0,86	0,75	0,80	0,93	0,87
30	2,38	2,67	0,3178	67,59	20,27	0,81	0,71	0,76	0,91	0,85
40	2,62	2,76	0,3947	69,30	27,72	0,78	0,68	0,73	0,89	0,84
50	2,92	2,96	0,4450	69,66	34,83	0,77	0,64	0,71	0,89	0,82
60	3,08	3,22	0,4760	65,61	39,36	0,74	0,64	0,69	0,87	0,82
70	3,32	3,10	0,5615	71,35	49,95	0,71	0,62	0,67	0,86	0,81
90	3,46	3,24	0,6880	70,97	63,87	0,72	0,61	0,66	0,86	0,81

Electro-osmotic coefficient (2β) = 0,251 μ F (slope 0,0093668 ml/mAh)
 J_{osm} = y-intercept = 0,1117984 cm/h
 c_b^{max} = 3,98 mol/l
 $\Delta t^c = t_1^c - t_2^c$

$\Delta t^a = t_2^a - t_1^a$
 $\bar{\Delta}t$ = Average transport number of membrane pair
 i_1^c = Transport number of cation through cation membrane
 i_2^a = Transport number of anion through anion membrane.

Table 6.12: Electro-osmotic pumping experimental conditions and results for 1,0 mol/l sodium chloride (Raipore R4030 anion and R4010 cation)

Current Density i , mA/cm ²	Brine concentration c_b , mol/l		Water flow J , cm/h	Current Efficiency e_p , %	Effective Current Density i_{eff} , mA/cm ²	Transport Numbers				
	$c_{b, exp.}$	$c_{b, calc.}$				Δt^c	Δt^a	$\bar{\Delta}t$	i_1^c	i_2^a
30	2,6	2,08	0,339	78,77	23,63	0,67	0,59	0,63	0,83	0,80
50	3,14	2,473	0,461	77,59	38,80	0,65	0,57	0,61	0,83	0,79
70	3,34	2,62	0,5934	75,89	53,13	0,64	0,56	0,60	0,82	0,78
90	3,48	2,96	0,7205	74,68	67,21	0,72	0,55	0,63	0,86	0,78

Electro-osmotic coefficient (2β) = 0,236 μ F (Slope = 0,0087973 ml/mAh)
 J_{osm} = y-intercept = 0,1265161 cm/h
 c_b^{max} = 4,24 mol/l
 $\Delta t^c = t_1^c - t_2^c$

$\Delta t^a = t_2^a - t_1^a$
 $\bar{\Delta}t$ = Average transport number of membrane pair
 i_1^c = Transport number of cation through cation membrane
 i_2^a = Transport number of anion through anion membrane.

Table 6.13: Electro-osmotic pumping experimental conditions and results for 0,05 mol/l sodium chloride (Ionics A-204-UZL-386 and C-61-CZL-386)

Current Density I , mA/cm ²	Brine concentration c_b , mol/l		Water flow J , cm/h	Current Efficiency ϵ_p , %	Effective Current Density I_{eff} , mA/cm ²	Transport Numbers				
	$c_{b, exp.}$	$c_{b, calc.}$				Δt^c	Δt^a	$\bar{\Delta}t$	\bar{i}_1^c	\bar{i}_2^a
5	1,51	2,26	0,0662	53,61	2,68	0,78	0,82	0,80	0,89	0,91
10	1,87	2,69	0,1059	53,11	5,31	0,74	0,79	0,76	0,87	0,89
15	2,19	3,13	0,1324	51,84	7,78	0,72	0,76	0,74	0,86	0,88
20	2,52	3,72	0,1456	48,92	9,78	0,70	0,75	0,73	0,85	0,88
30	2,80	4,53	0,1766	44,18	13,25	0,69	0,74	0,71	0,85	0,87

Electro-osmotic coefficient (2β) = 0,234 μ F (slope = 0,0087337 ml/mAh)
 $J_{osm} = y$ -intercept = 0,0612608 cm/h
 $C_c^{max} = 4,27$ mol/l
 $\Delta t^c = t_1^c - t_2^c$

$\Delta t^a = t_2^a - t_1^a$
 $\bar{\Delta}t$ = Average transport number of membrane pair
 \bar{i}_1^c = Transport number of cation through cation membrane
 \bar{i}_2^a = Transport number of anion through anion membrane.

Table 6.14: Electro-osmotic pumping experimental conditions and results for 0,1 mol/l sodium chloride (Ionics A-204-UZL-386 and C-61-CZL-386)

Current Density I , mA/cm ²	Brine concentration c_b , mol/l		Water flow J , cm/h	Current Efficiency ϵ_p , %	Effective Current Density I_{eff} , mA/cm ²	Transport Numbers				
	$c_{b, exp.}$	$c_{b, calc.}$				Δt^c	Δt^a	$\bar{\Delta}t$	\bar{i}_1^c	\bar{i}_2^a
5	1,55	1,97	0,0728	60,53	3,03	0,76	0,78	0,77	0,88	0,89
10	1,87	2,41	0,1165	58,43	5,84	0,74	0,76	0,75	0,87	0,88
15	2,24	2,81	0,1457	58,32	8,75	0,72	0,74	0,73	0,86	0,87
20	2,61	3,32	0,1589	55,60	11,11	0,70	0,72	0,71	0,85	0,86
30	3,00	3,95	0,1942	52,07	15,62	0,67	0,70	0,69	0,84	0,85
40	3,25	4,60	0,2207	48,07	19,23	0,66	0,70	0,68	0,83	0,85

Electro-osmotic coefficient (2β) = 0,204 μ F (slope = 0,0076266 ml/mAh)
 $J_{osm} = y$ -intercept = 0,0748388 cm/h
 $C_c^{max} = 4,89$ mol/l
 $\Delta t^c = t_1^c - t_2^c$

$\Delta t^a = t_2^a - t_1^a$
 $\bar{\Delta}t$ = Average transport number of membrane pair
 \bar{i}_1^c = Transport number of cation through cation membrane
 \bar{i}_2^a = Transport number of anion through anion membrane.

Table 6.15: Electro-osmotic pumping experimental conditions and results for 0,5 mol/l sodium chloride (Ionics A-204-UZL-386 and C-61-CZL-386)

Current Density I , mA/cm ²	Brine concentration c_b , mol/l		Water flow J , cm/h	Current Efficiency ϵ_p , %	Effective Current Density I_{eff} , mA/cm ²	Transport Numbers				
	$c_{b, exp.}$	$c_{b, calc.}$				Δt^c	Δt^a	$\bar{\Delta}t$	\bar{i}_1^c	\bar{i}_2^a
10	2,42	2,20	0,1059	68,74	6,87	0,61	0,63	0,62	0,81	0,82
20	2,75	2,60	0,1766	65,09	13,02	0,61	0,62	0,62	0,81	0,81
30	3,08	2,97	0,2260	62,21	18,67	0,60	0,60	0,60	0,79	0,80
40	3,28	3,20	0,2754	60,56	24,22	0,59	0,59	0,60	0,79	0,80
50	3,48	3,43	0,3178	59,31	29,65	0,58	0,59	0,58	0,79	0,79
60	3,77	3,44	0,3443	58,00	34,80	0,56	0,57	0,57	0,78	0,79
70	3,8	3,70	0,3973	57,82	40,47	0,56	0,57	0,56	0,78	0,78
80	3,91	3,94	0,4291	56,22	44,98	0,56	0,57	0,57	0,78	0,79
90	3,94	4,00	0,4768	55,95	50,36	0,56	0,57	0,57	0,78	0,79
100	3,98	4,20	0,5033	53,70	53,70	0,56	0,57	0,57	0,78	0,79

Electro-osmotic coefficient (2β) = 0,211 μ F (slope = 0,0078875 ml/mAh)
 $J_{osm} = y$ -intercept = 0,0780686 cm/h
 $C_c^{max} = 4,73$ mol/l
 $\Delta t^c = t_1^c - t_2^c$

$\Delta t^a = t_2^a - t_1^a$
 $\bar{\Delta}t$ = Average transport number of membrane pair
 \bar{i}_1^c = Transport number of cation through cation membrane
 \bar{i}_2^a = Transport number of anion through anion membrane.

Table 6.16: Electro-osmotic pumping experimental conditions and results for 1,0 mol/l sodium chloride (Ionics A-204-UZL-386 and C-61-CZL-386)

Current Density I , mA/cm ²	Brine concentration c_b , mol/l		Water flow J , cm/h	Current Efficiency e_p , %	Effective Current Density I_{eff} , mA/cm ²	Transport Numbers				
	$c_{b, exp}$	$c_{b, calc}$				Δt^c	Δt^a	$\bar{\Delta}t$	\bar{i}_1^c	\bar{i}_2^a
30	3,48	2,49	0,2472	76,88	23,06	0,58	0,52	0,55	0,79	0,76
50	3,72	2,72	0,3708	73,96	36,98	0,57	0,51	0,54	0,79	0,75
70	3,94	3,13	0,4450	67,15	47,00	0,57	0,50	0,53	0,78	0,75
90	4,08	3,46	0,5298	64,38	57,94	0,59	0,50	0,54	0,79	0,75

Electro-osmotic coefficient (2β) = 0,216 μ F (slope = 0,0080659 m μ /mAh)

J_{osm} = y-intercept = 0,0655084 cm/h

c_b^{max} = 4,63 mol/l

$\Delta t^c = t_1^c - t_2^c$

$\Delta t^a = t_2^a - t_1^a$

$\bar{\Delta}t$ = Average transport number of membrane pair

\bar{i}_1^c = Transport number of cation through cation membrane

\bar{i}_2^a = Transport number of anion through anion membrane.

Table 6.17: Electro-osmotic pumping experimental conditions and results for 0,05 mol/l sodium chloride (WTPSA-1, WTPSC-1)

Current Density I , mA/cm ²	Brine concentration c_b , mol/l		Water flow J , cm/h	Current Efficiency e_p , %	Effective Current Density I_{eff} , mA/cm ²	Transport Numbers				
	$c_{b, exp}$	$c_{b, calc}$				Δt^c	Δt^a	$\bar{\Delta}t$	\bar{i}_1^c	\bar{i}_2^a
5	1,66	2,20	0,0695	61,88	3,09	0,82	0,83	0,82	0,91	0,91
10	1,99	2,36	0,1280	60,78	6,08	0,81	0,81	0,81	0,90	0,90
15	2,4	3,16	0,1390	59,64	8,95	0,78	0,79	0,79	0,89	0,89
20	2,85	3,85	0,1456	55,65	11,13	0,72	0,77	0,75	0,86	0,88
25	3,32	4,45	0,1523	54,22	13,55	0,70	0,75	0,73	0,85	0,86

Electro-osmotic coefficient (2β) = 0,087 μ F (slope = 0,0032427 m μ /mAh)

J_{osm} = y-intercept = 0,1090328 cm/h

c_b^{max} = 11,50 mol/l

$\Delta t^c = t_1^c - t_2^c$

$\Delta t^a = t_2^a - t_1^a$

$\bar{\Delta}t$ = Average transport number of membrane pair

\bar{i}_1^c = Transport number of cation through cation membrane

\bar{i}_2^a = Transport number of anion through anion membrane.

Table 6.18: Electro-osmotic pumping experimental conditions and results for 0,1 mol/l sodium chloride (WTPSA-1, WTPSC-1)

Current Density I , mA/cm ²	Brine concentration c_b , mol/l		Water flow J , cm/h	Current Efficiency e_p , %	Effective Current Density I_{eff} , mA/cm ²	Transport Numbers				
	$c_{b, exp}$	$c_{b, calc}$				Δt^c	Δt^a	$\bar{\Delta}t$	\bar{i}_1^c	\bar{i}_2^a
5	1,68	2,06	0,0728	65,61	3,28	0,81	0,79	0,80	0,90	0,90
10	2,10	2,52	0,1165	65,46	6,55	0,79	0,78	0,79	0,89	0,89
15	2,53	3,07	0,1390	62,87	9,43	0,76	0,76	0,76	0,88	0,88
20	2,91	3,81	0,1456	56,82	11,36	0,74	0,74	0,74	0,87	0,87
30	3,42		0,1655	50,59	15,17					
40	3,58	5,74	0,1854	44,48	17,79	0,711	0,72	0,71	0,86	0,86

Electro-osmotic coefficient (2β) = 0,156 μ F (slope = 0,0058244 m μ /mAh)

J_{osm} = y-intercept = 0,0801568 cm/h

c_b^{max} = 6,41 mol/l

$\Delta t^c = t_1^c - t_2^c$

$\Delta t^a = t_2^a - t_1^a$

$\bar{\Delta}t$ = Average transport number of membrane pair

\bar{i}_1^c = Transport number of cation through cation membrane

\bar{i}_2^a = Transport number of anion through anion membrane.

Table 6.19: Electro-osmotic pumping experimental conditions and results for 0,5 mol/l sodium chloride (WTPSA-1, WTPSC-1)

Current Density i , mA/cm ²	Brine concentration c_b , mol/l		Water flow J , cm/h	Current Efficiency e_p , %	Effective Current Density i_{em} , mA/cm ²	Transport Numbers				
	$c_{b, exp.}$	$c_{b, calc.}$				Δt^c	Δt^a	$\bar{\Delta}t$	\bar{i}_1^c	\bar{i}_2^a
10	2,22	2,12	0,1218	72,51	7,25	0,72	0,66	0,69	0,86	0,83
20	3,17	3,034	0,1589	67,53	13,51	0,68	0,61	0,64	0,84	0,81
30	3,68	3,95	0,1766	58,06	17,42	0,65	0,60	0,62	0,82	0,80
40	3,77		0,2030	51,58	20,63					
50	3,90		0,2207	46,16	23,07					
60	4,01		0,2295	41,13	24,68					
80	4,1	6,951	0,2560	35,18	28,42	0,62	0,57	0,60	0,81	0,78
100	4,24	7,937	0,2825	32,11	32,11	0,63	0,57	0,60	0,81	0,78

Electro-osmotic coefficient (2θ) = 0,175 μ F (slope = 0,0065332 m/mAh)
 J_{osm} = y-intercept = 0,0699265 cm/h
 c_b^{max} = 5,71 mol/l
 $\Delta t^c = t_1^c - t_2^c$

$\Delta t^a = t_2^a - t_1^a$
 $\bar{\Delta}t$ = Average transport number of membrane pair
 \bar{i}_1^c = Transport number of cation through cation membrane
 \bar{i}_2^a = Transport number of anion through anion membrane.

Table 6.20: Electro-osmotic pumping experimental conditions and results for 1,0 mol/l sodium chloride (WTPSA-1, WTPSC-1)

Current Density i , mA/cm ²	Brine concentration c_b , mol/l		Water flow J , cm/h	Current Efficiency e_p , %	Effective Current Density i_{em} , mA/cm ²	Transport Numbers				
	$c_{b, exp.}$	$c_{b, calc.}$				Δt^c	Δt^a	$\bar{\Delta}t$	\bar{i}_1^c	\bar{i}_2^a
30	3,77	2,63	0,2225	74,96	22,49	0,54	0,51	0,52	0,77	0,75
50	4,06	3,50	0,2667	58,04	29,02	0,51	0,49	0,50	0,76	0,74
70	4,17	4,82	0,2790	44,56	31,19	0,53	0,50	0,51	0,76	0,75
90	4,27	5,78	0,2914	37,06	33,35	0,51	0,49	0,50	0,76	0,75

Electro-osmotic coefficient (2θ) = 0,175 μ F (slope = 0,0065210 m/mAh)
 J_{osm} = y-intercept = 0,0762254 cm/h
 c_b^{max} = 5,72 mol/l
 $\Delta t^c = t_1^c - t_2^c$

$\Delta t^a = t_2^a - t_1^a$
 $\bar{\Delta}t$ = Average transport number of membrane pair
 \bar{i}_1^c = Transport number of cation through cation membrane
 \bar{i}_2^a = Transport number of anion through anion membrane.

Table 6.21: Electro-osmotic pumping experimental conditions and results for 0,05 mol/l sodium chloride (WTPVCA-2, WTPVCC-2)

Current Density i , mA/cm ²	Brine concentration c_b , mol/l		Water flow J , cm/h	Current Efficiency e_p , %	Effective Current Density i_{em} , mA/cm ²	Transport Numbers				
	$c_{b, exp.}$	$c_{b, calc.}$				Δt^c	Δt^a	$\bar{\Delta}t$	\bar{i}_1^c	\bar{i}_2^a
5	0,99	1,36	0,1077	56,24	2,81	0,79	0,77	0,79	0,90	0,89
10	1,3	1,77	0,1562	54,46	5,44	0,75	0,74	0,74	0,87	0,87
15	1,64	2,18	0,1788	52,40	7,86	0,75	0,64	0,70	0,87	0,82
20	1,74	2,07	0,2119	49,42	9,88	0,68	0,49	0,59	0,84	0,75
30	1,85	2,7	0,2913	48,17	14,45	0,75	0,66	0,70	0,87	0,83

Electro-osmotic coefficient (2θ) = 0,412 μ F (slope = 0,0153695 m/mAh)
 J_{osm} = y-intercept = 0,0649212 cm/h
 c_b^{max} = 2,43 mol/l
 $\Delta t^c = t_1^c - t_2^c$

$\Delta t^a = t_2^a - t_1^a$
 $\bar{\Delta}t$ = Average transport number of membrane pair
 \bar{i}_1^c = Transport number of cation through cation membrane
 \bar{i}_2^a = Transport number of anion through anion membrane.

Table 6.22: Electro-osmotic pumping experimental conditions and results for 0,1 mol/l sodium chloride (WTPVCA-2, WTPVCC-2)

Current Density I , mA/cm ²	Brine concentration c_b , mol/l		Water flow J , cm/h	Current Efficiency e_p , %	Effective Current Density I_{eff} , mA/cm ²	Transport Numbers				
	$c_{b,exp.}$	$c_{b,calc.}$				Δt^c	Δt^a	$\bar{\Delta}t$	\bar{i}_1^c	\bar{i}_2^a
5	1,05	0,94	0,1509	59,65	2,98	0,79	0,74	0,76	0,89	0,87
10	1,47	1,80	0,1483	58,45	5,85	0,73	0,70	0,71	0,86	0,85
15	1,72	2,12	0,1854	56,99	8,55	0,72	0,68	0,70	0,86	0,84
20	1,92	2,17	0,2219	54,53	10,91	0,66	0,63	0,65	0,83	0,81
30	2,26	2,92	0,256	51,71	15,51	0,70	0,64	0,67	0,85	0,82
40	2,58	3,47	0,2825	48,853	19,54	0,68	0,64	0,66	0,84	0,82

Electro-osmotic coefficient (2β) = 0,261 t/F (slope = 0,0097235 ml/mAh)

J_{osm} = y-intercept = 0,0994504 cm/h

c_b^{max} = 3,84 mol/l

$\Delta t^c = t_1^c - t_2^c$

$\Delta t^a = t_2^a - t_1^a$

$\bar{\Delta}t$ = Average transport number of membrane pair

\bar{i}_1^c = Transport number of cation through cation membrane

\bar{i}_2^a = Transport number of anion through anion membrane.

Table 6.23: Electro-osmotic pumping experimental conditions and results for 0,5 mol/l sodium chloride (WTPVCA-2, WTPVCC-2)

Current Density I , mA/cm ²	Brine concentration c_b , mol/l		Water flow J , cm/h	Current Efficiency e_p , %	Effective Current Density I_{eff} , mA/cm ²	Transport Numbers				
	$c_{b,exp.}$	$c_{b,calc.}$				Δt^c	Δt^a	$\bar{\Delta}t$	\bar{i}_1^c	\bar{i}_2^a
5	1,43	1,23	0,0971	74,463	3,7231	0,6620	0,6148	0,6384	0,83	0,81
10	1,77		0,1562	74,153	7,4153					
15	2,08	1,70	0,1942	72,207	10,831	0,6128	0,5666	0,5897	0,81	0,78
20	2,26		0,2295	69,54	13,908					
30	2,58		0,2913	67,173	20,152					
40	2,81	2,33	0,3443	64,848	25,939	0,5696	0,5070	0,5383	0,78	0,75
60	3,02	2,581	0,429	57,9	34,74	0,5179	0,4715	0,4947	0,76	0,74

Electro-osmotic coefficient (2β) = 0,267 t/F (slope = 0,0099646 ml/mAh)

J_{osm} = y-intercept = 0,0869006 cm/h

c_b^{max} = 3,74 mol/l

$\Delta t^c = t_1^c - t_2^c$

$\Delta t^a = t_2^a - t_1^a$

$\bar{\Delta}t$ = Average transport number of membrane pair

\bar{i}_1^c = Transport number of cation through cation membrane

\bar{i}_2^a = Transport number of anion through anion membrane.

Table 6.24: Electro-osmotic pumping experimental conditions and results for 1,0 mol/l sodium chloride (WTPVCA-2, WTPVCC-2)

Current Density I , mA/cm ²	Brine concentration c_b , mol/l		Water flow J , cm/h	Current Efficiency e_p , %	Effective Current Density I_{eff} , mA/cm ²	Transport Numbers				
	$c_{b,exp.}$	$c_{b,calc.}$				Δt^c	Δt^a	$\bar{\Delta}t$	\bar{i}_1^c	\bar{i}_2^a
10	2,0	1,25	0,20	81,66	8,17	0,55	0,47	0,51	0,78	0,73
20	2,4	1,37	0,25	80,67	16,13	0,47	0,44	0,46	0,74	0,72
40	3,14	1,68	0,37	78,04	31,22	0,43	0,40	0,42	0,72	0,70
60	3,26	1,88	0,48	70,22	42,13	0,41	0,40	0,41	0,70	0,70

Electro-osmotic coefficient (2β) = 0,221 t/F (slope = 0,0082250 ml/mAh)

J_{osm} = y-intercept = 0,125719 cm/h

c_b^{max} = 4,54 mol/l

$\Delta t^c = t_1^c - t_2^c$

$\Delta t^a = t_2^a - t_1^a$

$\bar{\Delta}t$ = Average transport number of membrane pair

\bar{i}_1^c = Transport number of cation through cation membrane

\bar{i}_2^a = Transport number of anion through anion membrane.

Table 6.25: Electro-osmotic pumping experimental conditions and results for 0,05 mol/l sodium chloride (WTPSTA-3, WTPSTC-3)

Current Density I , mA/cm ²	Brine concentration c_b , mol/l		Water flow J , cm/h	Current Efficiency ϵ_p , %	Effective Current Density I_{eff} , mA/cm ²	Transport Numbers				
	$c_{b, exp.}$	$c_{b, calc.}$				Δt^*	Δt^*	$\bar{\Delta}t$	\bar{i}_1^*	\bar{i}_2^*
10	1,65	2,29	0,1368	60,53	6,05	0,87	0,81	0,84	0,93	0,90
15	1,92	2,65	0,1721	59,08	8,86	0,82	0,81	0,81	0,91	0,90
20	2,08	3,01	0,1960	54,65	10,93	0,81	0,78	0,80	0,90	0,90
25	2,11	3,20	0,2295	51,69	12,92	0,78	0,80	0,79	0,89	0,89
30	2,16	3,32	0,2649	51,13	15,34	0,79	0,78	0,79	0,89	0,89

Electro-osmotic coefficient (β) = 0,371 μ /F (slope = 0,0138276 m³/mAh)
 J_{osm} = y-intercept = 0,0502337 cm/h
 c_b^{max} = 2,69 mol/l
 $\Delta t^* = t_1^* - t_2^*$

$\Delta t^* = t_2^* - t_1^*$
 $\bar{\Delta}t$ = Average transport number of membrane pair
 \bar{i}_1^* = Transport number of cation through cation membrane
 \bar{i}_2^* = Transport number of anion through anion membrane.

Table 6.26: Electro-osmotic pumping experimental conditions and results for 0,1 mol/l sodium chloride (WTPSTA-3, WTPSTC-3)

Current Density I , mA/cm ²	Brine concentration c_b , mol/l		Water flow J , cm/h	Current Efficiency ϵ_p , %	Effective Current Density I_{eff} , mA/cm ²	Transport Numbers				
	$c_{b, exp.}$	$c_{b, calc.}$				Δt^*	Δt^*	$\bar{\Delta}t$	\bar{i}_1^*	\bar{i}_2^*
10	1,76	2,14	0,1404	66,24	6,62	0,83	0,77	0,80	0,92	0,89
15	1,87	2,31	0,1920	64,18	9,63	0,83	0,76	0,79	0,91	0,88
20	2,19	2,71	0,2154	63,24	12,65	0,82	0,75	0,78	0,91	0,88
30	2,35	2,90	0,2914	61,19	18,36	0,78	0,74	0,76	0,88	0,87
40	2,55	3,23	0,3496	59,75	23,90	0,78	0,74	0,76	0,89	0,87
50	2,64	2,96	0,4186	59,24	29,62	0,63	0,69	0,66	0,82	0,85

Electro-osmotic coefficient (β) = 0,317 μ /F (slope = 0,011834 m³/mAh)
 J_{osm} = y-intercept = 0,0691379 cm/h
 c_b^{max} = 3,15 mol/l
 $\Delta t^* = t_1^* - t_2^*$

$\Delta t^* = t_2^* - t_1^*$
 $\bar{\Delta}t$ = Average transport number of membrane pair
 \bar{i}_1^* = Transport number of cation through cation membrane
 \bar{i}_2^* = Transport number of anion through anion membrane.

Table 6.27: Electro-osmotic pumping experimental conditions and results for 0,5 mol/l sodium chloride (WTPSTA-3, WTPSTC-3)

Current Density I , mA/cm ²	Brine concentration c_b , mol/l		Water flow J , cm/h	Current Efficiency ϵ_p , %	Effective Current Density I_{eff} , mA/cm ²	Transport Numbers				
	$c_{b, exp.}$	$c_{b, calc.}$				Δt^*	Δt^*	$\bar{\Delta}t$	\bar{i}_1^*	\bar{i}_2^*
10	2,02	1,87	0,1377	74,96	7,50	0,74	0,65	0,69	0,87	0,82
20	2,45	2,23	0,2225	73,07	14,61	0,72	0,61	0,66	0,86	0,81
30	2,85	2,56	0,2826	71,96	21,59	0,70	0,59	0,65	0,85	0,80
40	2,91	2,56	0,3576	69,74	27,90	0,65	0,58	0,61	0,82	0,79
50	3,11	2,88	0,4026	67,13	33,57	0,67	0,57	0,62	0,83	0,79
70	3,29	2,75	0,5033	63,41	44,39	0,53	0,53	0,53	0,76	0,76
90	3,37	3,45	0,6093	61,15	55,04	0,65	0,60	0,63	0,82	0,80
110	3,41	3,59	0,7152	59,43	65,38	0,65	0,60	0,62	0,82	0,80

Electro-osmotic coefficient (β) = 0,259 μ /F (slope = 0,0096672 m³/mAh)
 J_{osm} = y-intercept = 0,0793991 cm/h
 c_b^{max} = 3,86 mol/l
 $\Delta t^* = t_1^* - t_2^*$

$\Delta t^* = t_2^* - t_1^*$
 $\bar{\Delta}t$ = Average transport number of membrane pair
 \bar{i}_1^* = Transport number of cation through cation membrane
 \bar{i}_2^* = Transport number of anion through anion membrane.

Table 6.28: Electro-osmotic pumping experimental conditions and results for 1,0 mol/l sodium chloride (WTPSTA-3, WPTSC-3)

Current Density i , mA/cm ²	Brine concentration c_b , mol/l		Water flow J , cm/h	Current Efficiency e_p , %	Effective Current Density i_{eff} , mA/cm ²	Transport Numbers				
	$c_{b, exp}$	$c_{b, calc}$				Δt^*	Δt^*	$\bar{\Delta}t$	i_1^*	i_2^*
30	2,94	2,02	0,3179	83,51	25,05	0,62	0,52	0,57	0,81	0,76
50	3,27	2,18	0,4715	82,67	41,33	0,61	0,49	0,55	0,81	0,75
70	3,41	2,45	0,5827	76,10	53,27	0,60	0,49	0,55	0,80	0,74
90	3,47	2,43	0,7159	73,92	66,53	0,54	0,49	0,52	0,77	0,75

Electro-osmotic coefficient (2β) = 0,257 t/F (slope = 0,0095674 m/mAh)
 J_{osm} = y-intercept = 0,0766808 cm/h
 c_b^{max} = 3,90 mol/l
 $\Delta t^* = t_1^* - t_2^*$

$\Delta t^* = t_2^* - t_1^*$
 $\bar{\Delta}t$ = Average transport number of membrane pair
 i_1^* = Transport number of cation through cation membrane
 i_2^* = Transport number of anion through anion membrane.

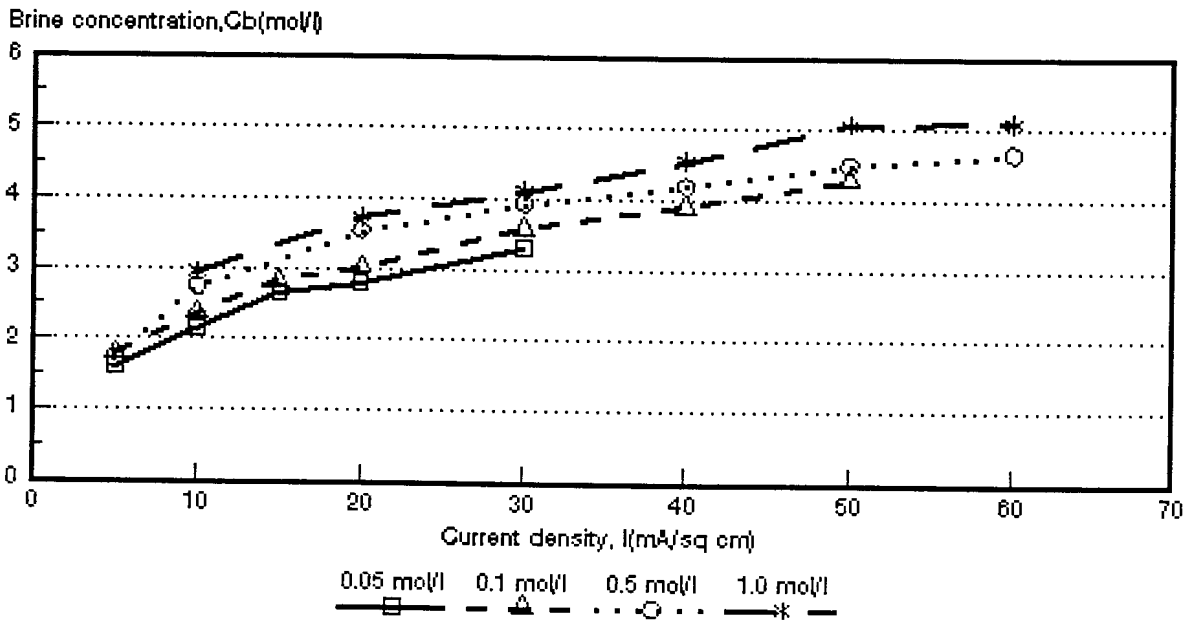


Figure 6.1: Brine concentration as a function of current density for 4 different NaCl feed concentrations. *Selmemion* AMV and CMV membranes.

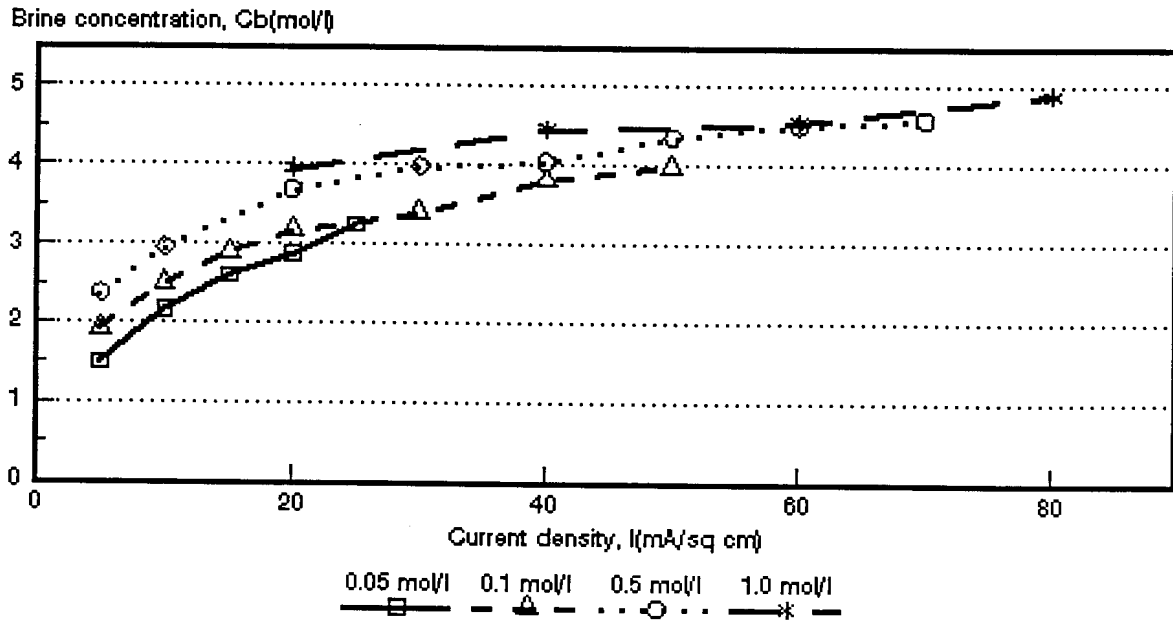


Figure 6.2: Brine concentration as a function of current density for 4 different NaCl feed concentrations. *Ionac* MA-3475 and MC-3470 membranes.

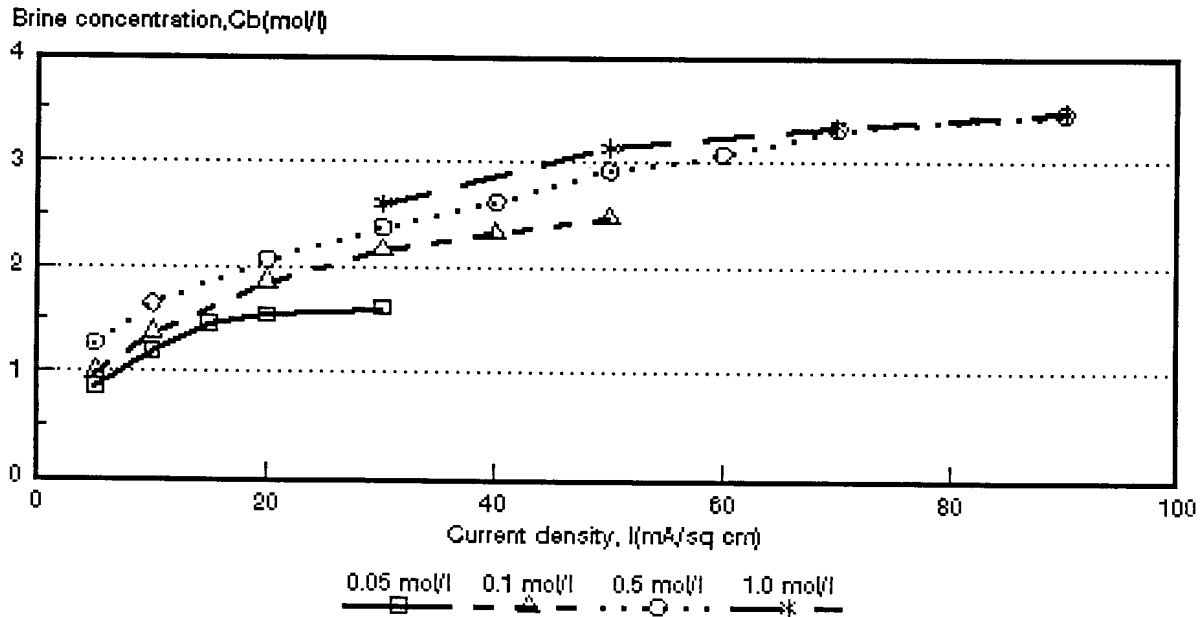


Figure 6.3: Brine concentration as a function of current density for 4 different NaCl feed concentrations. *Raipore* R4030 and R4010 membranes.

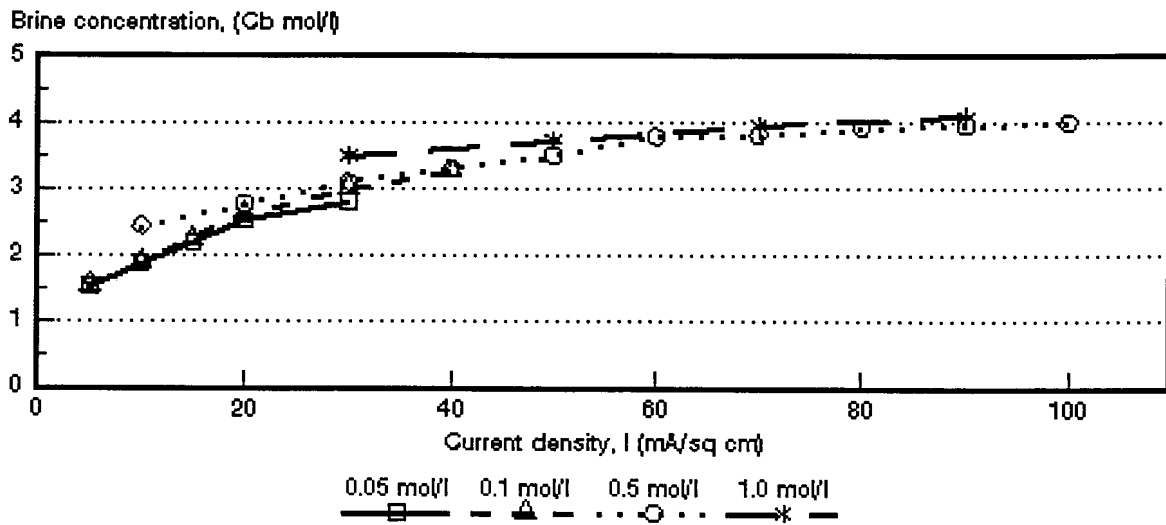


Figure 6.4: Brine concentration as a function of current density for 4 different NaCl feed concentrations. *Ionics*A-204-UZL-386 and C-61-CZL-386 membranes.

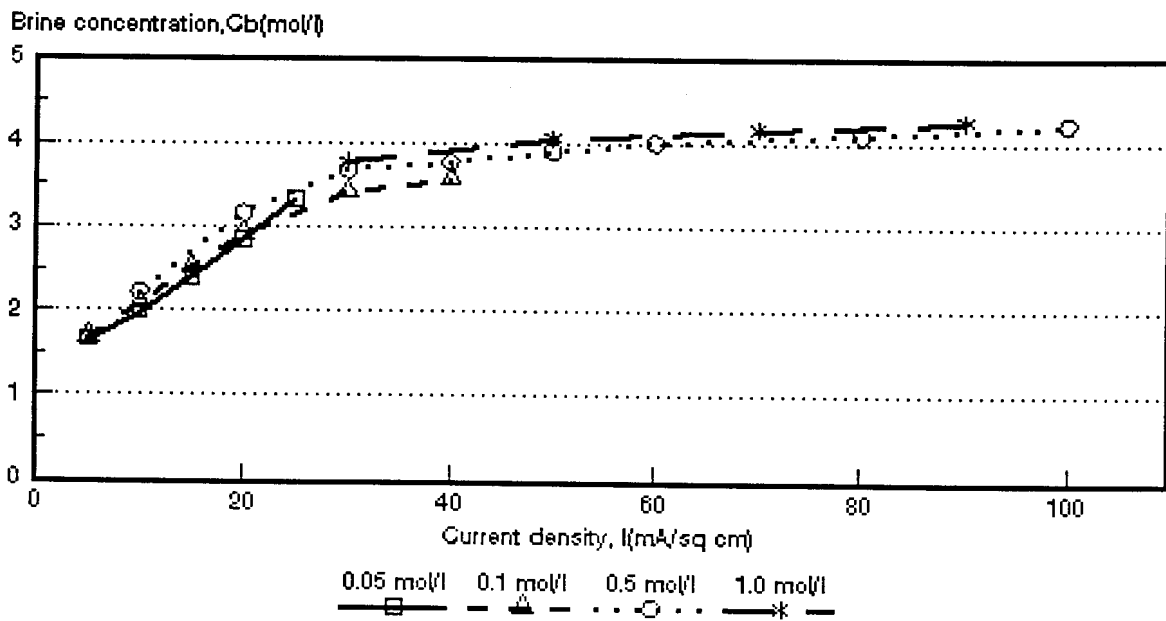


Figure 6.5: Brine concentration as a function of current density for 4 different NaCl feed concentrations. WTPSA-1 and WTPSC-1 membranes.

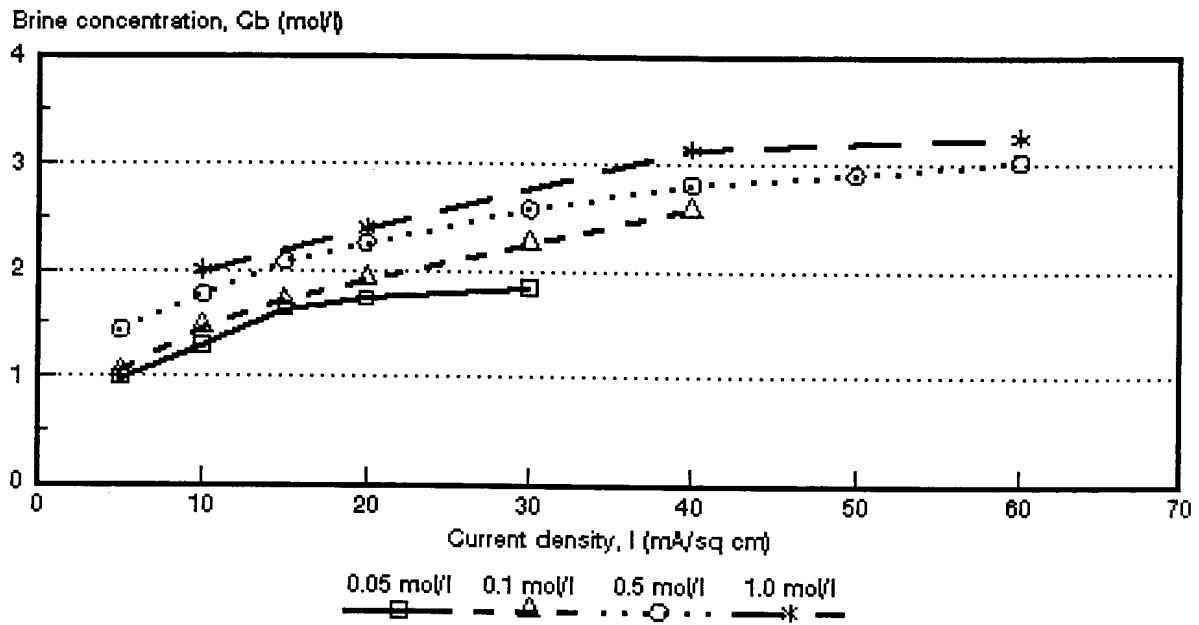


Figure 6.6: Brine concentration as a function of current density for 4 different NaCl feed concentrations. WTPVCA-2 and WTPVCC-2 membranes.

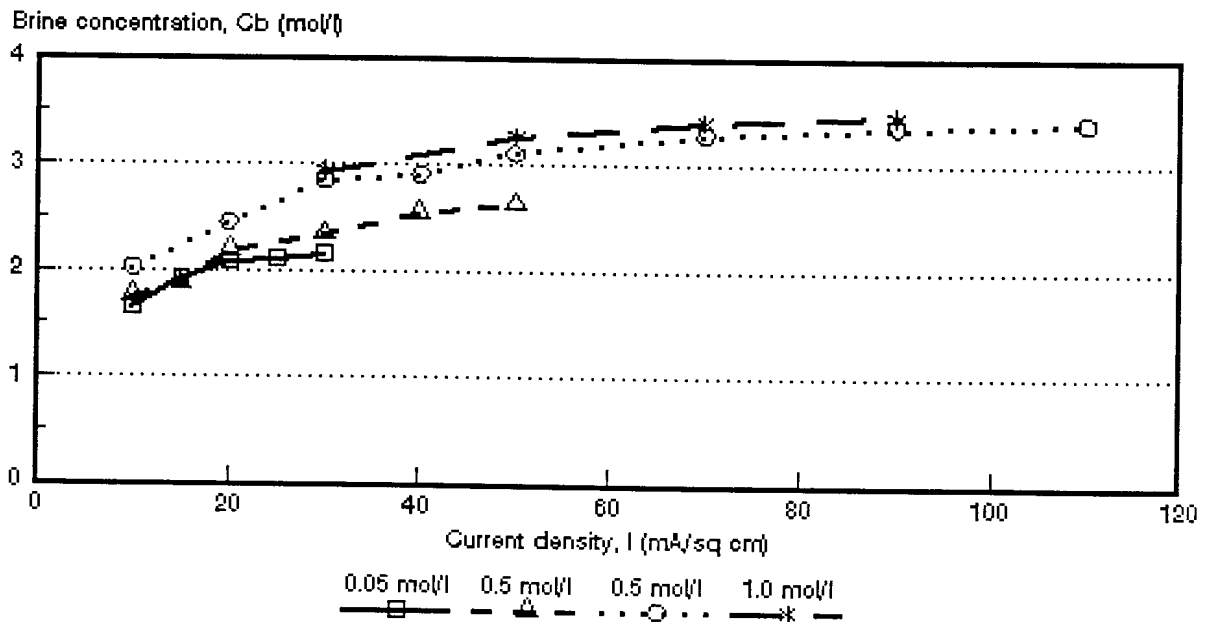


Figure 6.7: Brine concentration as a function of current density for 4 different NaCl feed concentrations. WTPSTA-3 and WTPSTC-3 membranes.

Table 6.29: Brine concentrations obtained at the highest current densities investigated for different sodium chloride feed concentrations

Feed Concentration mol/l	Brine Concentration* (%)						
	Selemion	Ionac	Raipore	Ionics	WTPS	WTPVC	WTPST
0,05	19,3	19,0	9,5	16,4	19,4	10,8	12,6
0,10	25,1	23,4	14,4	19,0	20,9	15,1	15,4
0,50	27,2	26,8	20,2	23,3	24,8	17,7	19,9
1,0	29,8	28,7	20,3	23,8	25,0	19,1	20,3

* Brine concentrations obtained from data in Tables 6.1 to 6.28.

$$\text{and } c_b^{\max} = c_b(1 + J_{\text{osm}}/J_{\text{el osm}}) \quad (\text{see eq. 3.10.31})$$

The results are shown in Tables 6.30 and Figures 6.8 to 6.14. Very good correlations were obtained with the above two relationships to determine c_b^{\max} . Consequently, any one of these two methods can be used to determine c_b^{\max} .

Maximum brine concentration seems to depend more on feed concentration in the case of the *Selemion*- (Fig. 6.8), *Raipore*- (Fig. 6.10), *WTPS*- (Fig. 6.12), *WTPVC*- (Fig. 6.13) and *WTPST*- (Fig. 6.14) membranes than has been experienced with the *Ionac*- (Fig. 6.9) and *Ionics*- (Fig. 6.11) membranes. This effect was especially pronounced for the *Selemion*-, *Raipore*- and *WTPS* membranes, and to a lesser extent for the *WTPVC*- and *WTPST* membranes. Much less change in maximum brine concentration as a function of feed concentration was experienced with the *Ionac*- (Fig. 6.9) and *Ionics* (Fig. 6.11) membranes. The *Ionac*- and *Ionics* membranes showed almost no dependence of maximum brine concentration on feed concentration in the feed concentration range of 0,05 to 1,0 mol/l. It is interesting to note that the calculated maximum brine concentration has been very high at 0,05 mol/l feed concentration in the case of the *WTPS* membranes (Fig. 6.12). The maximum brine concentration first declined very rapidly and then much slower to become almost independent of feed concentration in the 0,1 to 1,0 mol/l feed concentration range. This opposite behaviour encountered with the more hydrophobic *WTPS* membranes can be ascribed to membrane swelling when the membranes come into contact with water⁽⁴²⁾.

Brine concentrations at different current densities were predicted from measured transport numbers and volume flows (J) with the relationship:

$$c_b = \frac{I\bar{\Delta}t}{2FJ} \quad (\text{see eq. 3.10.17})$$

The experimental and calculated brine concentrations are shown in Tables 6.1 to 6.28 and Figures 6.15 to 6.42. The calculated brine concentrations were determined from the average value of the apparent transport numbers (Δt 's) of a membrane pair ($\bar{\Delta}t$) and from the water flows (J).

The correlation between the calculated and experimentally determined brine concentrations expressed as the ratio $c_{b\text{calc}}/c_{b\text{exp}}$ is shown in Table 6.31. The calculated brine concentrations were higher than the experimentally determined brine concentrations in the 0,05 to 0,1 mol/l feed concentration range in the case of the *Selemion*-, *lonac*-, *lonics*-, WTPS-, WTPVC- and WTPST membranes (Figs. 6.15 to 6.42 and Table 6.31). The calculated brine concentration was still higher than the experimentally determined brine concentration at 0,5 mol/l feed concentration for the *Raipore* membranes (Fig. 6.25). However, calculated brine concentrations became less than the experimentally determined brine concentrations in the 0,5 to 1,0 mol/l feed concentration range in the case of the *Selemion*- (Fig's. 6.17 and 6.18), *lonac*- (Fig's. 6.21 and 6.22), *lonics*- (Fig's. 6.29 and 6.30), WTPVC- (Fig's. 6.37 and 6.38) and WTPST (Fig's. 6.41 and 6.42) membranes. Calculated brine concentration became less than the experimentally determined brine concentration at 1,0 mol/l feed concentration for the *Raipore*- (Fig. 6.26) and WTPS- (Fig. 6.34) membranes.

Good correlations were obtained between the calculated and experimentally determined brine concentrations for all the membranes investigated depending on feed concentration and current density used (Table 6.31). For the *Selemion* membranes the ratio $c_{b\text{calc}}/c_{b\text{exp}}$ varied between 1,0 and 1,07 in the current density range from 15 to 50 mA/cm² (0,1 mol/l feed). In the case of the *lonac* membranes the ratio $c_{b\text{calc}}/c_{b\text{exp}}$ varied between 0,95 and 1,1 in the current density range from 40 to 70 mA/cm² (0,5 mol/l feed). The $c_{b\text{calc}}/c_{b\text{exp}}$ ratio for the *Raipore* membranes varied between 0,93 and 1,05 in the 40 to 90 mA/cm² current density range (0,5 mol/l feed). The correlation between $c_{b\text{calc}}/c_{b\text{exp}}$ for the *lonics* membranes varied between 0,91 and 1,06 in the current density range from 10 to 100 mA/cm² (0,5 mol/l feed). The WTPS membranes showed a very good correlation of 0,95 to 1,07 of $c_{b\text{calc}}/c_{b\text{exp}}$ in the current density range from 10 to 30 mA/cm² (0,5 mol/l feed). However, a poor correlation was obtained at high current densities. The WTPVC membranes showed a correlation of $c_{b\text{calc}}/c_{b\text{exp}}$ of 0,82 to 0,86 in the 5 to 60 mA/cm² current density range (0,5 mol/l

feed) while the WTPST membranes showed a correlation of 0,84 to 1,05 in the 10 to 110 mA/cm² current density range (0,5 mol/l feed). Therefore, brine concentration should be reasonably accurately predicted from simple transport number and water flow determinations depending on feed water concentration and current density used.

Table 6.30: Maximum brine concentration calculated from
 $c_b^{max} = 1/2 F\beta^*$ and $c_b^{max} = c_b (1 + J_{osm}/J_{elasm})^{**}$

Feed Concentration mol/l	Maximum Brine Concentration, c_b^{max} (mol/l)													
	Selemion		Ionac		Raipore		Ionics		WTPS		WTPVC		WTPST	
	1	2	1	2	1	2	1	2	1	2	1	2	1	2
0,05	4,55	4,54	5,37	5,31	1,83	1,83	4,27	4,29	11,5	11,38	2,43	2,44	2,69	2,71
0,10	5,05	5,06	4,85	4,80	3,13	3,12	4,89	4,83	6,41	6,42	3,84	3,71	3,15	3,11
0,50	5,36	5,31	5,26	5,29	3,98	4,02	4,73	4,74	5,71	5,76	3,74	3,77	3,86	3,85
1,00	6,48	6,49	5,35	5,44	4,24	4,22	4,63	4,63	5,72	5,74	4,54	4,66	3,90	3,89

1 : $c_b^{max} = 1/2 F\beta$

2 : $c_b^{max} = c_b (1 + J_{osm} / J_{elasm})$

* : Calculated from electro-osmotic coefficients (Tables 6.1 to 6.28)

** : Calculated from $J_{elasm} = J - J_{osm}$ (y-intercept and the corresponding c_b values) (Tables 6.1 to 6.28).

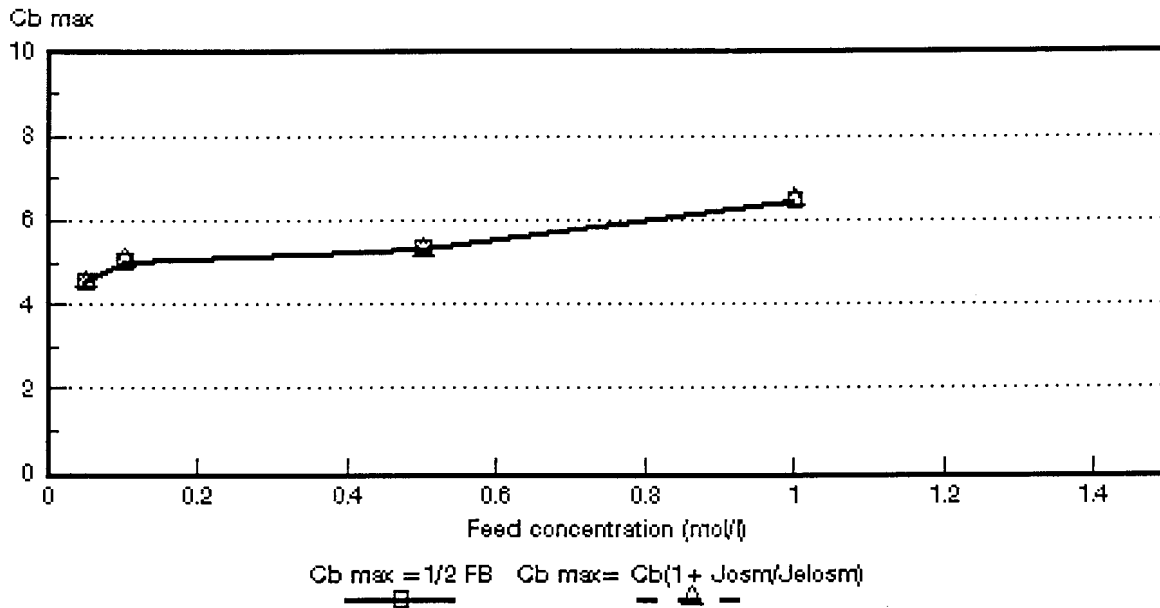


Figure 6.8: c_b^{\max} as a function of feed concentration for different NaCl feed concentrations. *Selemion* AMV and CMV membranes.

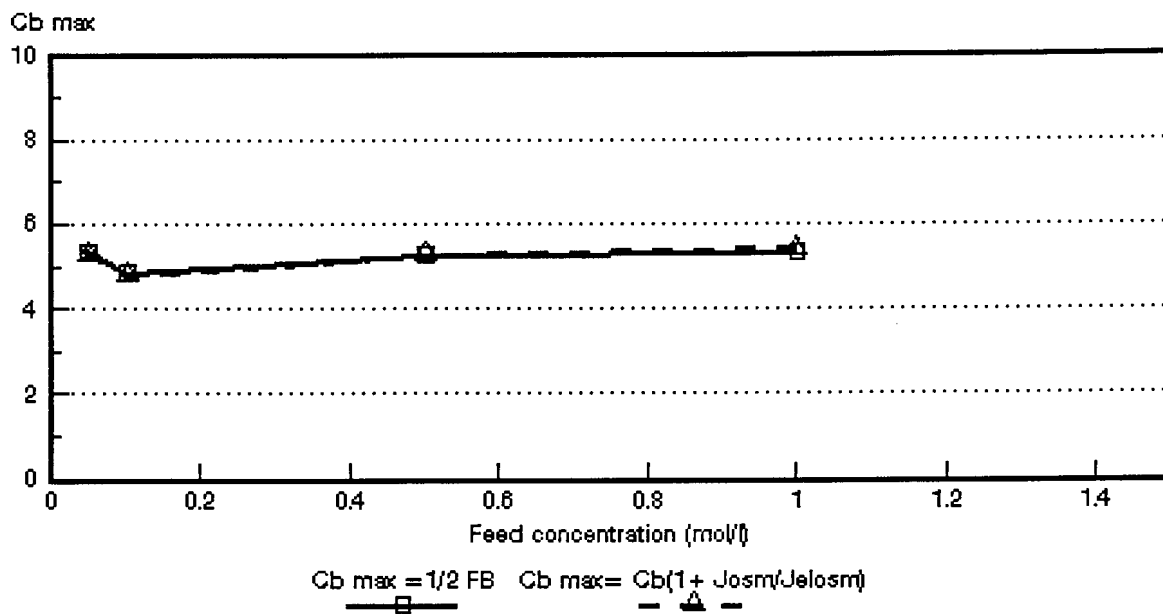


Figure 6.9: c_b^{\max} as a function of feed concentration for different NaCl feed concentrations. *Ionac* MA-3475 and MC-3470 membranes.

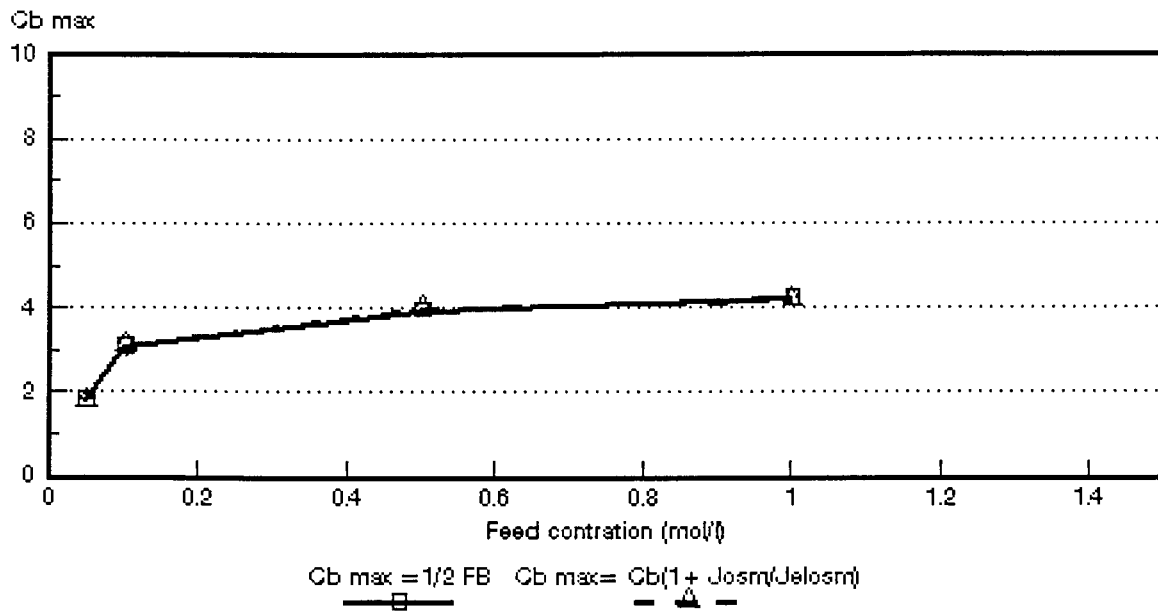


Figure 6.10: c_b^{\max} as a function of feed concentration for different NaCl feed concentrations. *Raipore R4030 and R4010 membranes.*

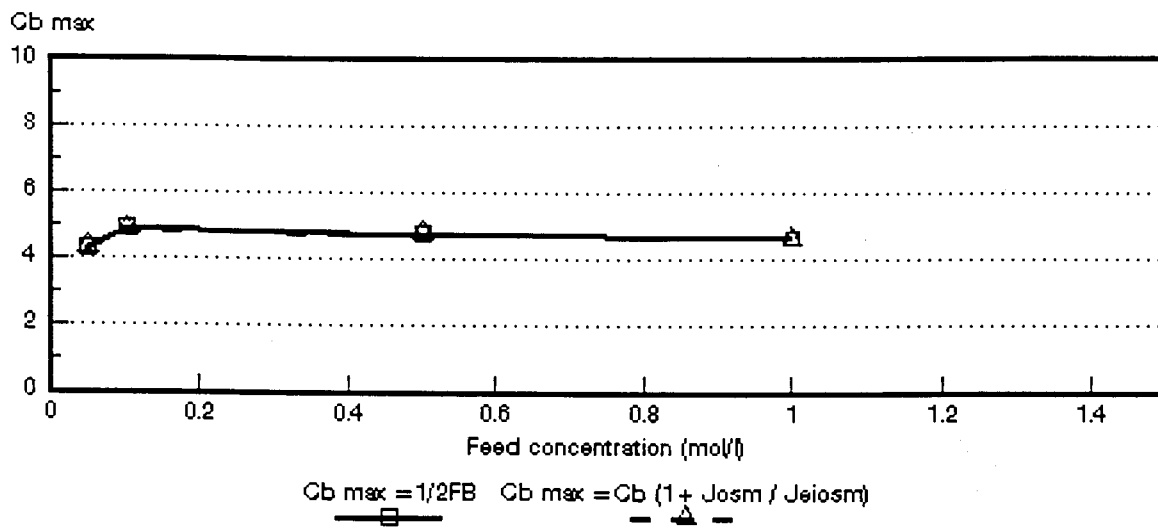


Figure 6.11: c_b^{\max} as a function of feed concentration for different NaCl feed concentrations. *Ionics A-204-UZL-386 and C-61-CZL-386 membranes.*

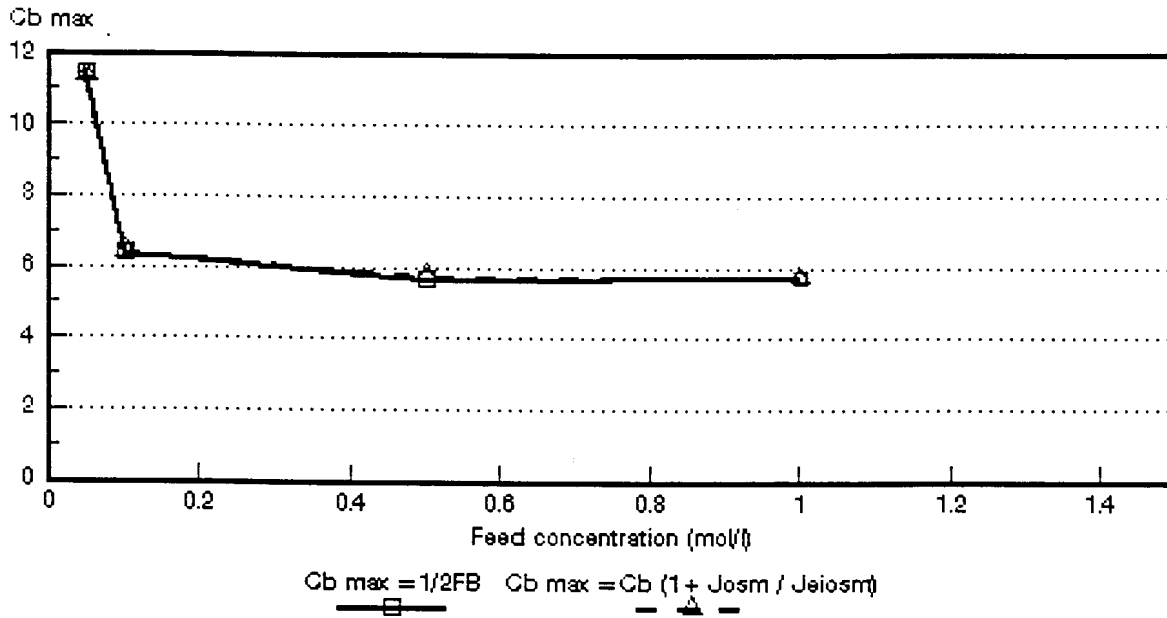


Figure 6.12: c_b^{max} as a function of feed concentration for different NaCl feed concentrations. WTPSA-1 and WTPSC-1 membranes.

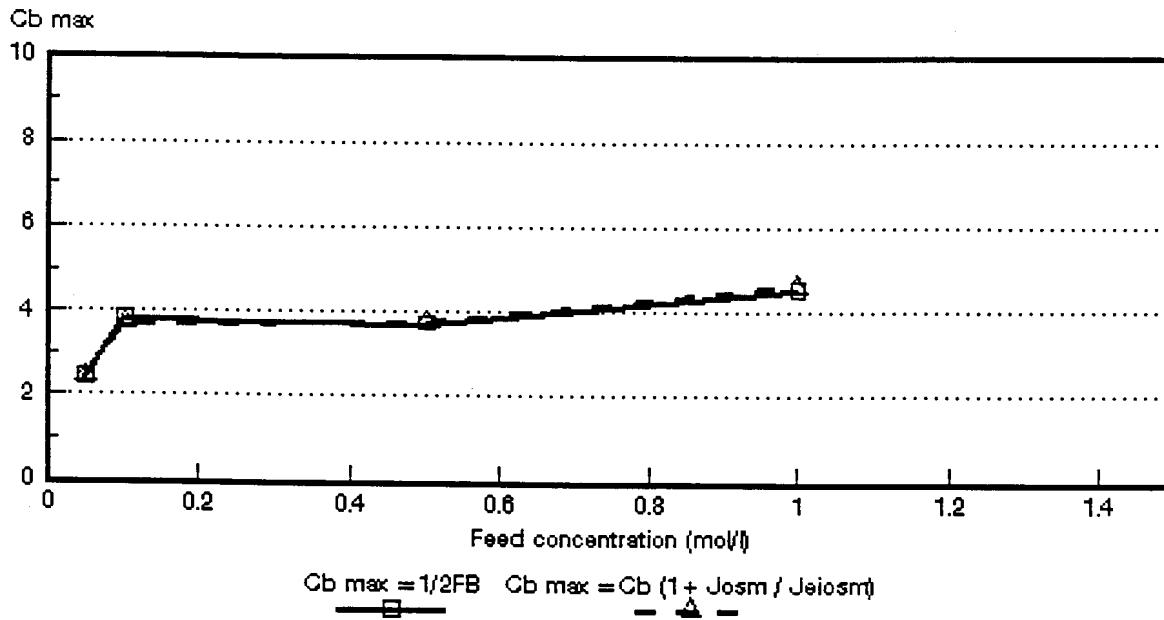


Figure 6.13: c_b^{max} as a function of feed concentration for different NaCl feed concentrations. WTPVCA-2 and WTPVCC-2 membranes.

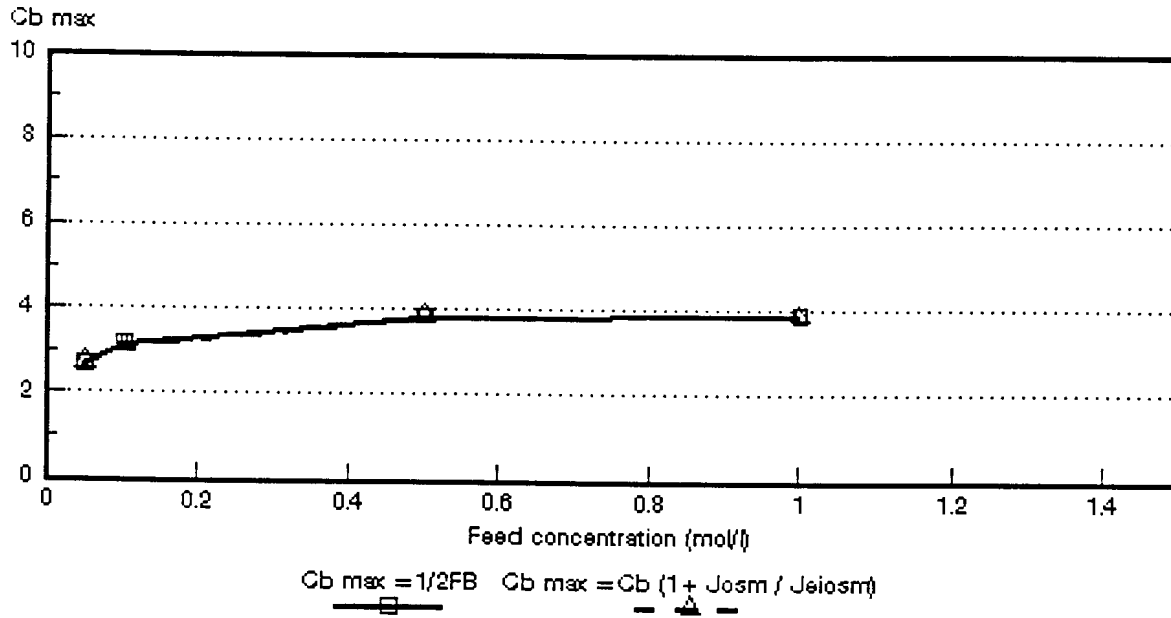


Figure 6.14: c_b^{max} as a function of feed concentration for different NaCl feed concentrations. WTPSTA-3 and WTPSTC-3 membranes.

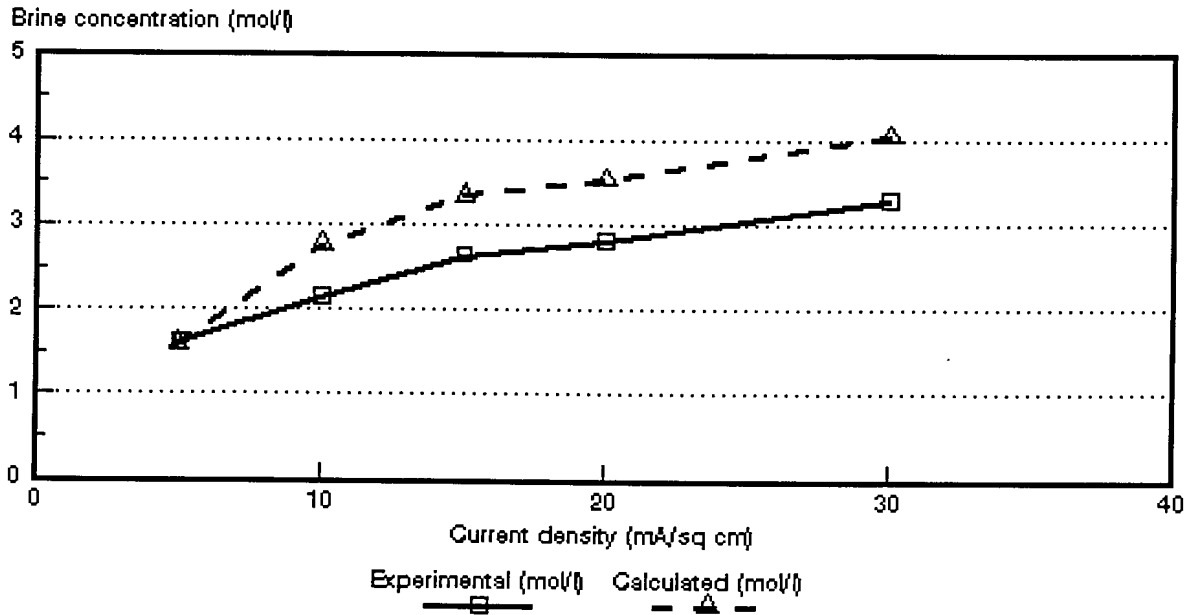


Figure 6.15: Experimental and calculated brine concentrations as a function of current density for 0,05 mol/l NaCl feed solution. Selemiom AMV and CMV membranes.

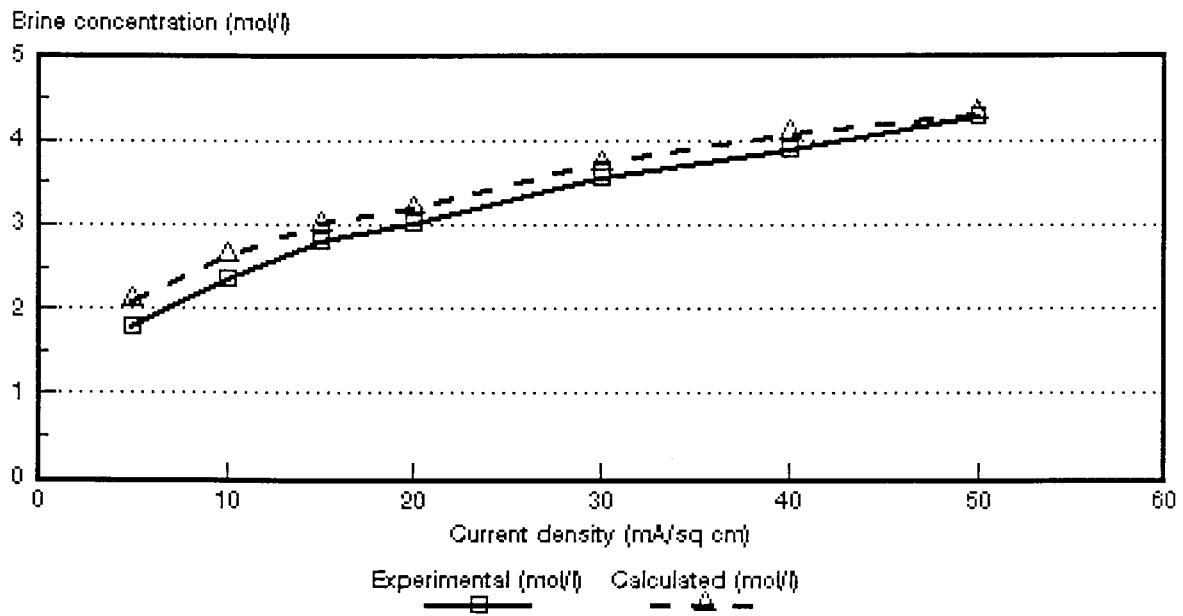


Figure 6.16: Experimental and calculated brine concentrations as a function of current density for 0,1 mol/l NaCl feed solution. *Selemion* AMV and CMV membranes.

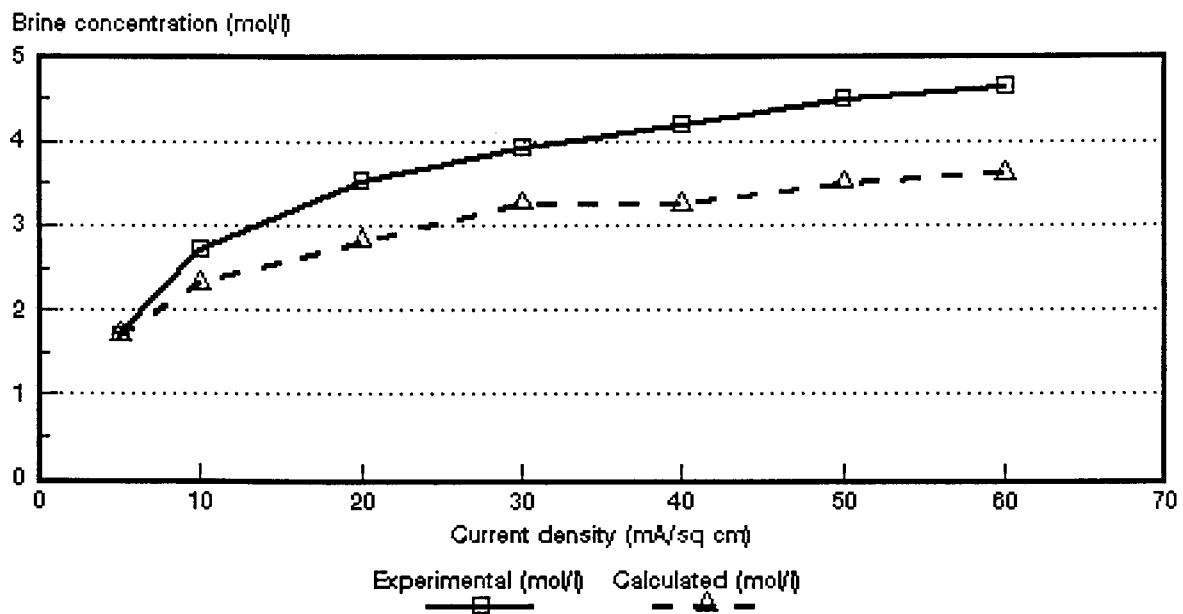


Figure 6.17: Experimental and calculated brine concentrations as a function of current density for 0,5 mol/l NaCl feed solution. *Selemion* AMV and CMV membranes.

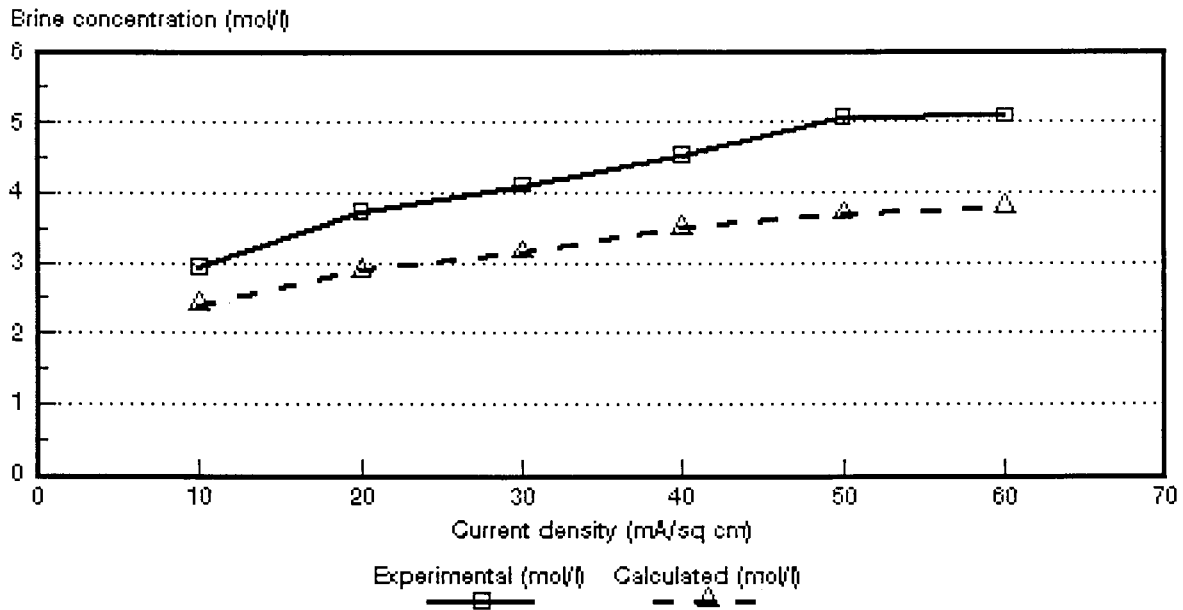


Figure 6.18: Experimental and calculated brine concentrations as a function of current density for 1,0 mol/l NaCl feed solution. *Selemion* AMV and CMV membranes.

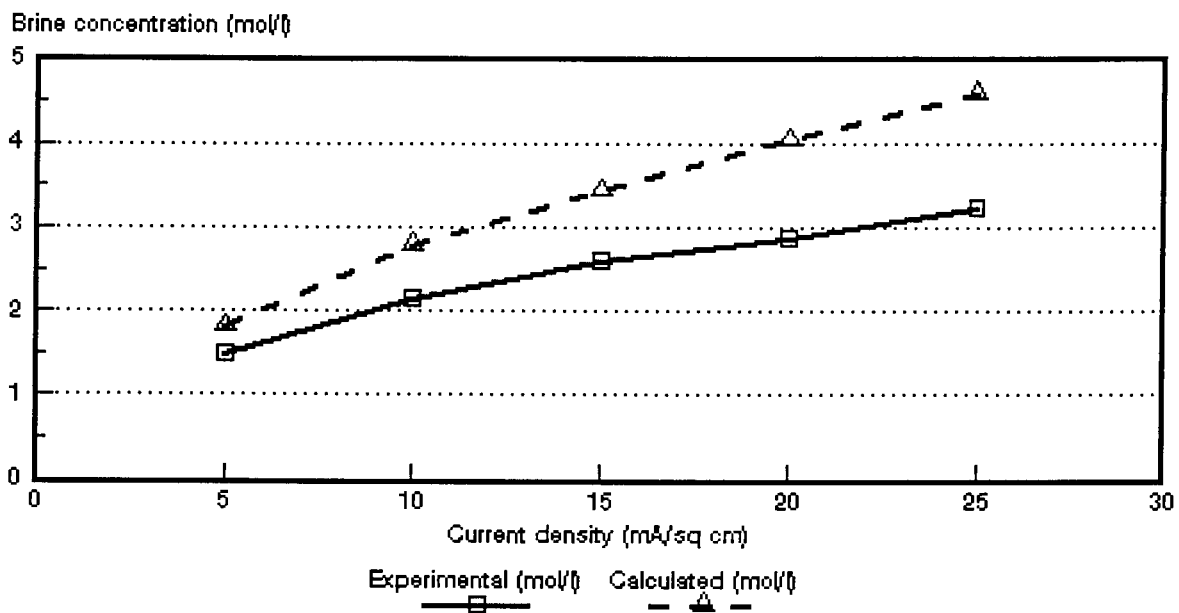


Figure 6.19: Experimental and calculated brine concentrations as a function of current density for 0,05 mol/l NaCl feed solution. *Ionac* MA-3475 and MC-3470 membranes.

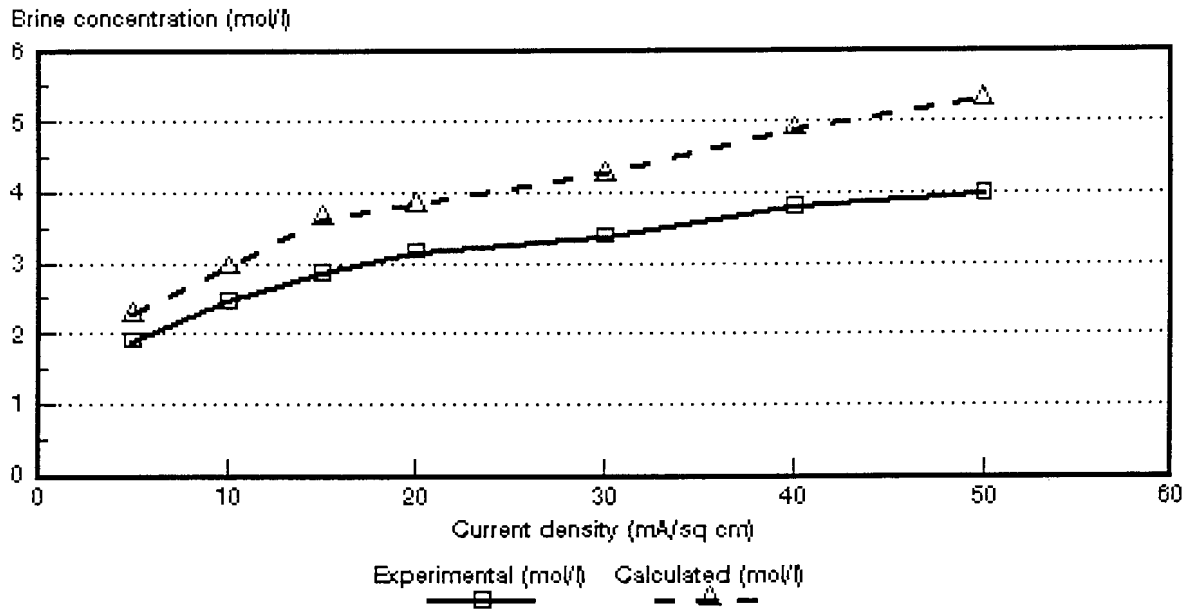


Figure 6.20: Experimental and calculated brine concentrations as a function of current density for 0,1 mol/l NaCl feed solution. *Ionac* MA-3475 and MC-3470 membranes.

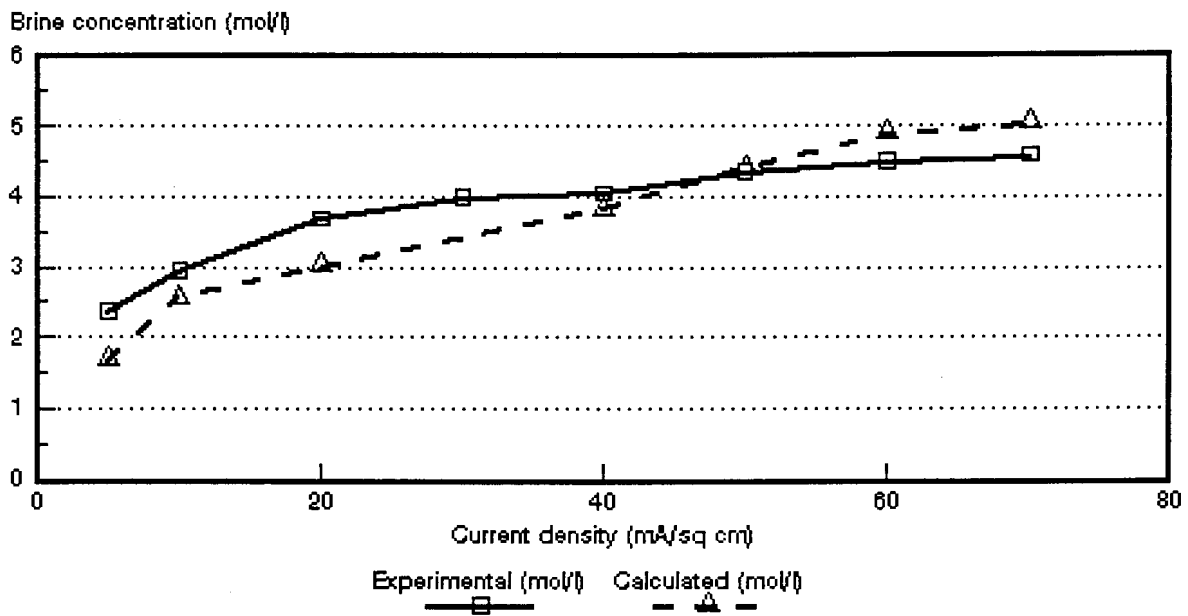


Figure 6.21: Experimental and calculated brine concentrations as a function of current density for 0,5 mol/l NaCl feed solution. *Ionac* MA-3475 and MC-3470 membranes.

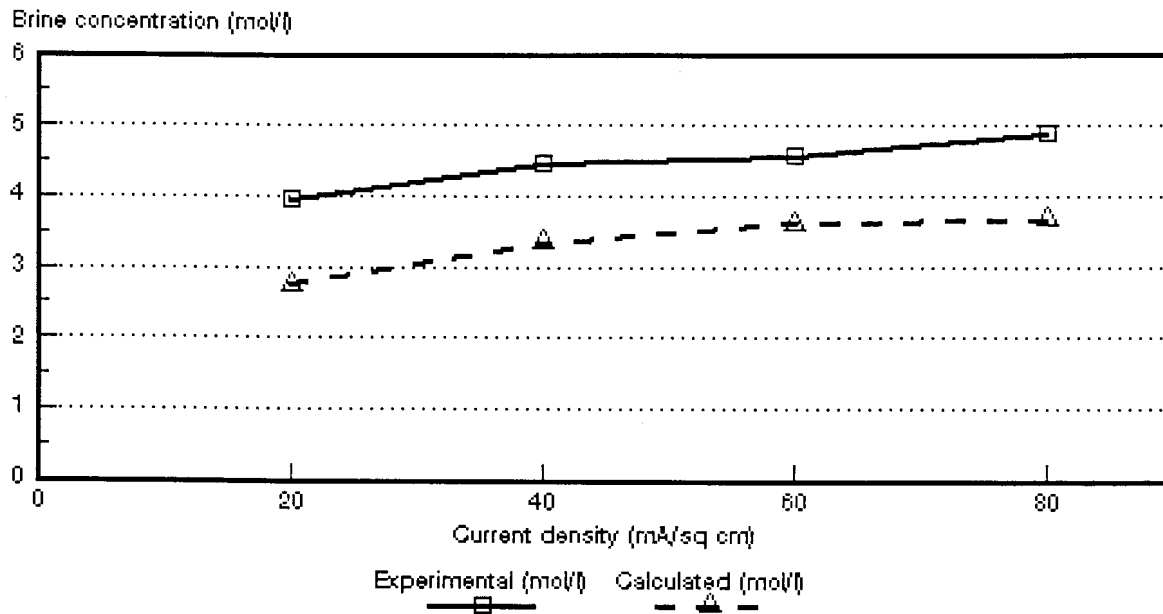


Figure 6.22: Experimental and calculated brine concentrations as a function of current density for 1,0 mol/l NaCl feed solution. *Ionac* MA-3475 and MC-3470 membranes.

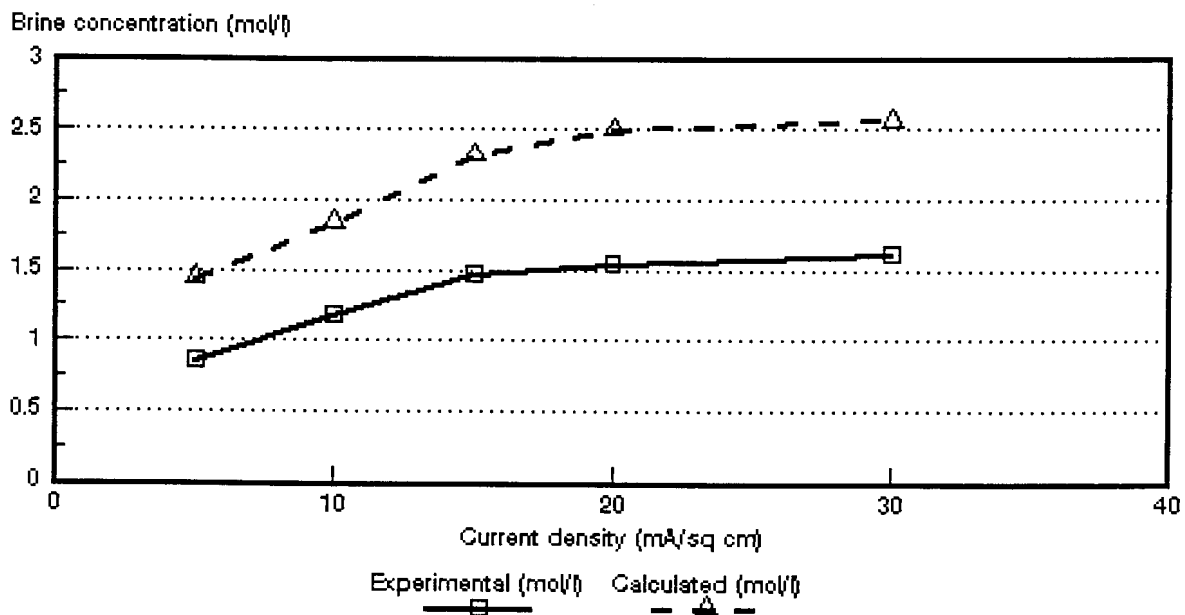


Figure 6.23: Experimental and calculated brine concentrations as a function of current density for 0,05 mol/l NaCl feed solution. *Raipore* R4030 and R4010 membranes.

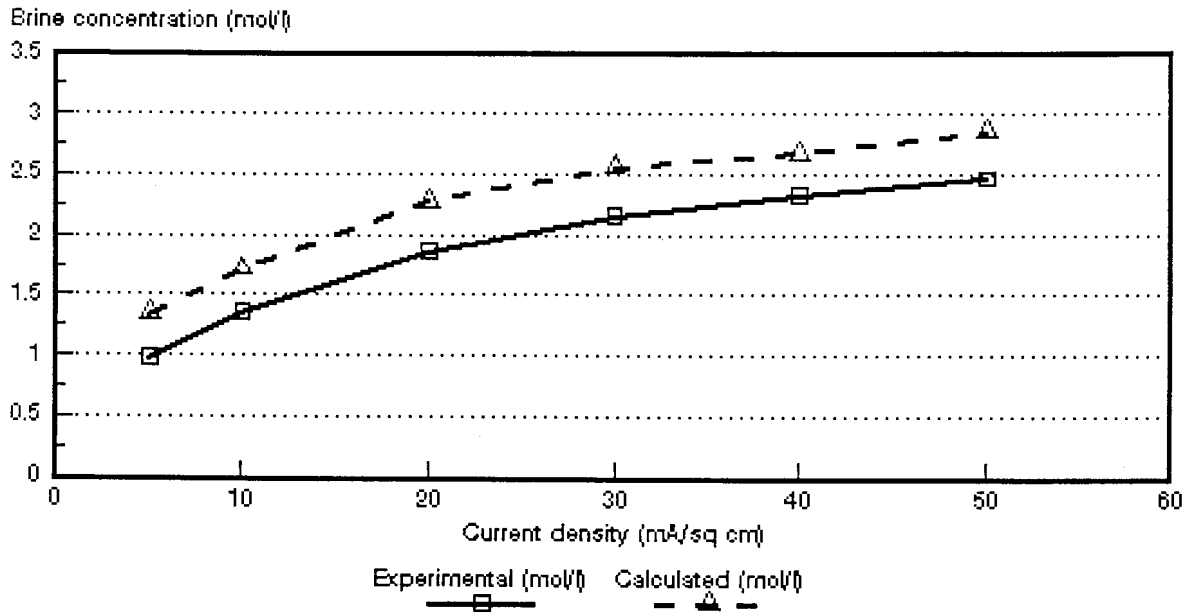


Figure 6.24: Experimental and calculated brine concentrations as a function of current density for 0,1 mol/l NaCl feed solution. *Raipore* R4030 and R4010 membranes.

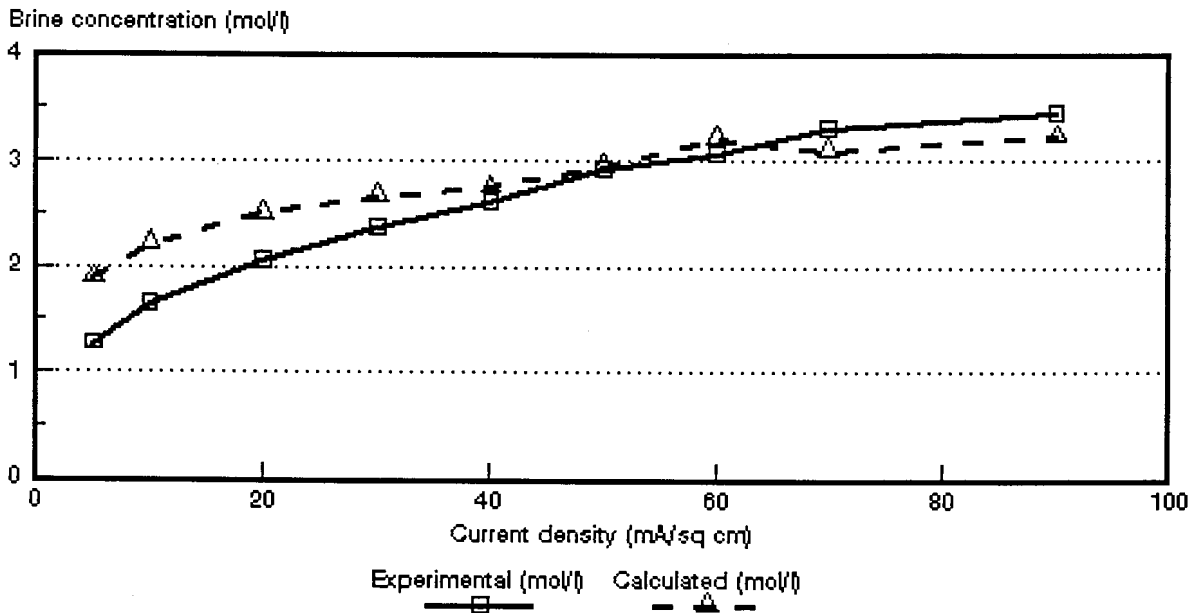


Figure 6.25: Experimental and calculated brine concentrations as a function of current density for 0,5 mol/l NaCl feed solution. *Raipore* R4030 and R4010 membranes.

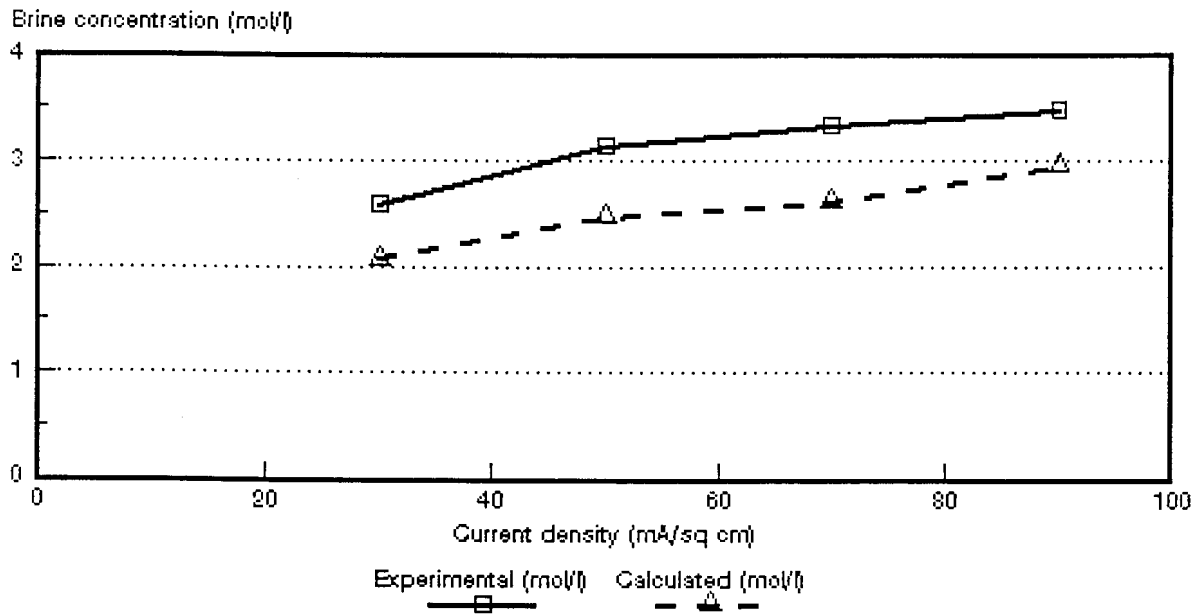


Figure 6.26: Experimental and calculated brine concentrations as a function of current density for 1,0 mol/l NaCl feed solution. *Raipore R4030 and R4010* membranes.

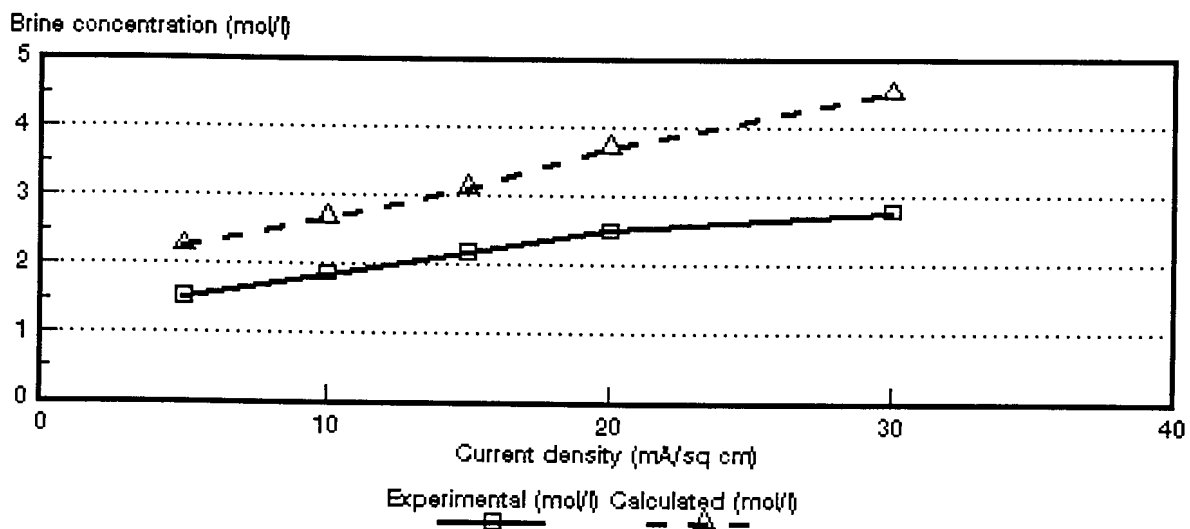


Figure 6.27: Experimental and calculated brine concentrations as a function of current density for 0,05 mol/l NaCl feed solution. *Ionics A-204-UZL-386 and C-61-CZL-386* membranes.

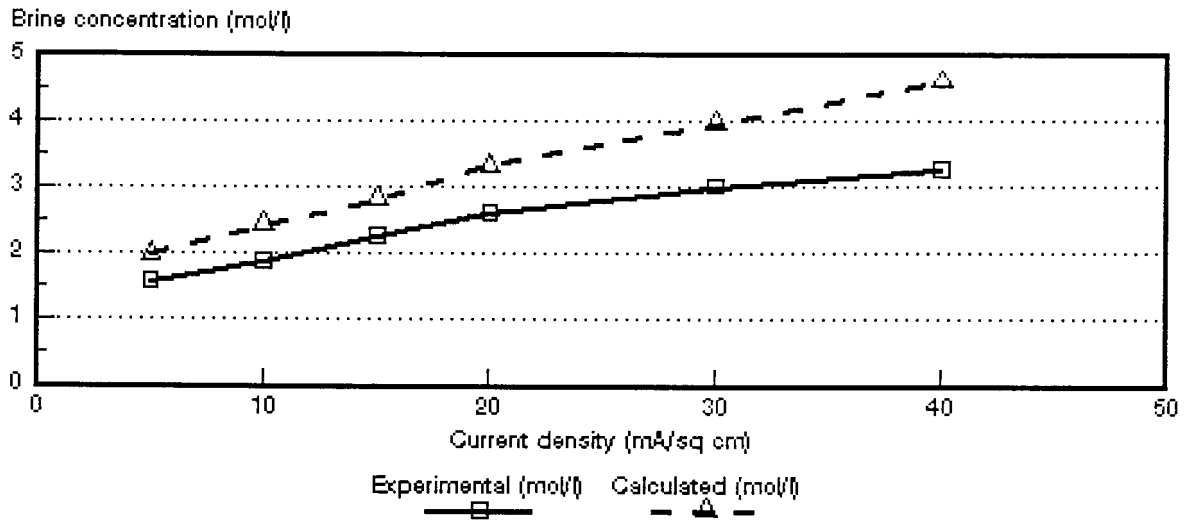


Figure 6.28: Experimental and calculated brine concentrations as a function of current density for 0,1 mol/l NaCl feed solution. *Ionics A-204-UZL-386* and *C-61-CZL-386* membranes.

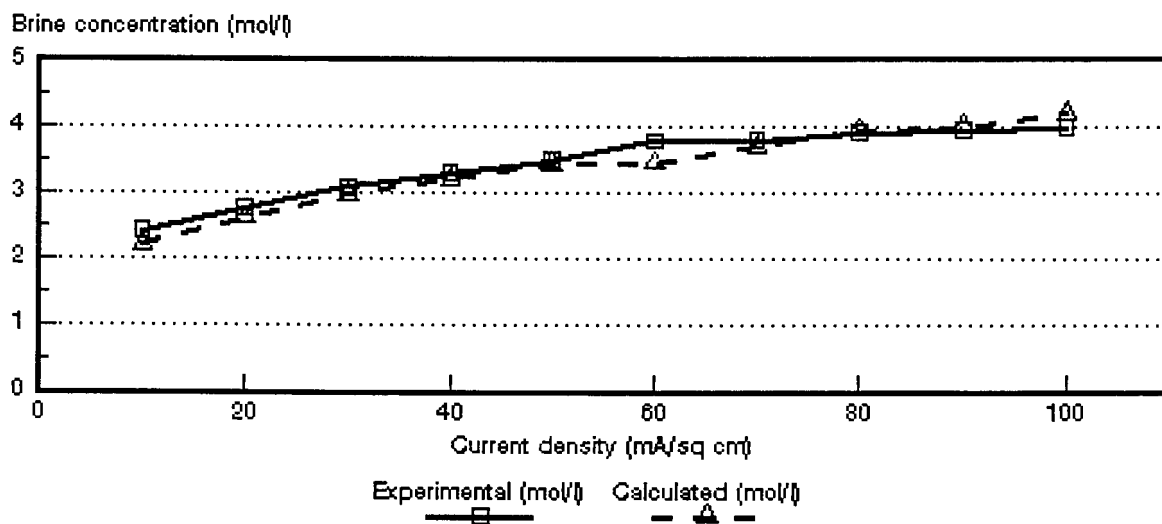


Figure 6.29: Experimental and calculated brine concentrations as a function of current density for 0,5 mol/l NaCl feed solution. *Ionics A-204-UZL-386* and *C-61-CZL-386* membranes.

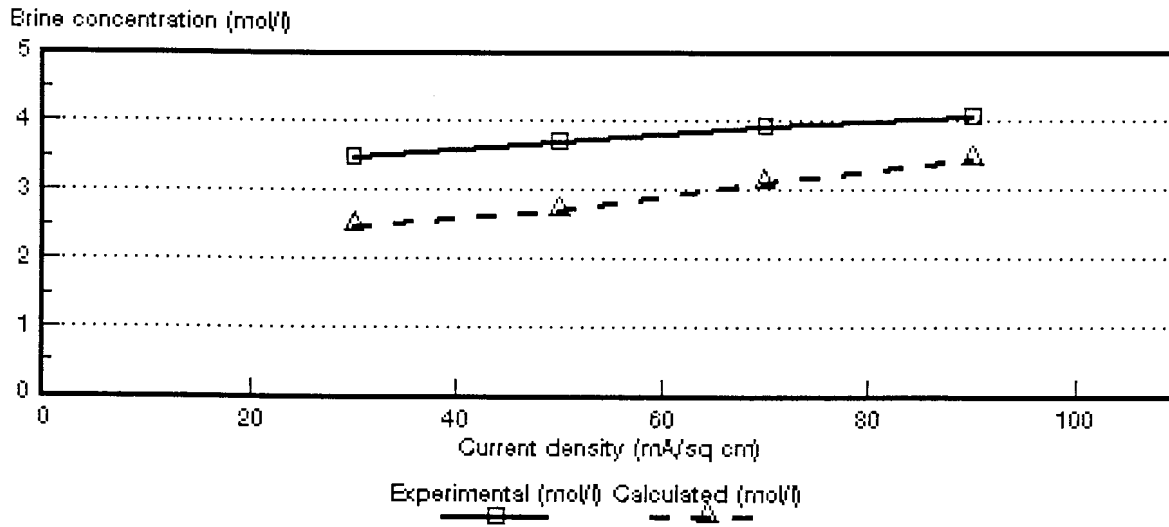


Figure 6.30: Experimental and calculated brine concentrations as a function of current density for 1,0 mol/l NaCl feed solution. *Ionics A-204-UZL-386* and *C-61-CZL-386* membranes.

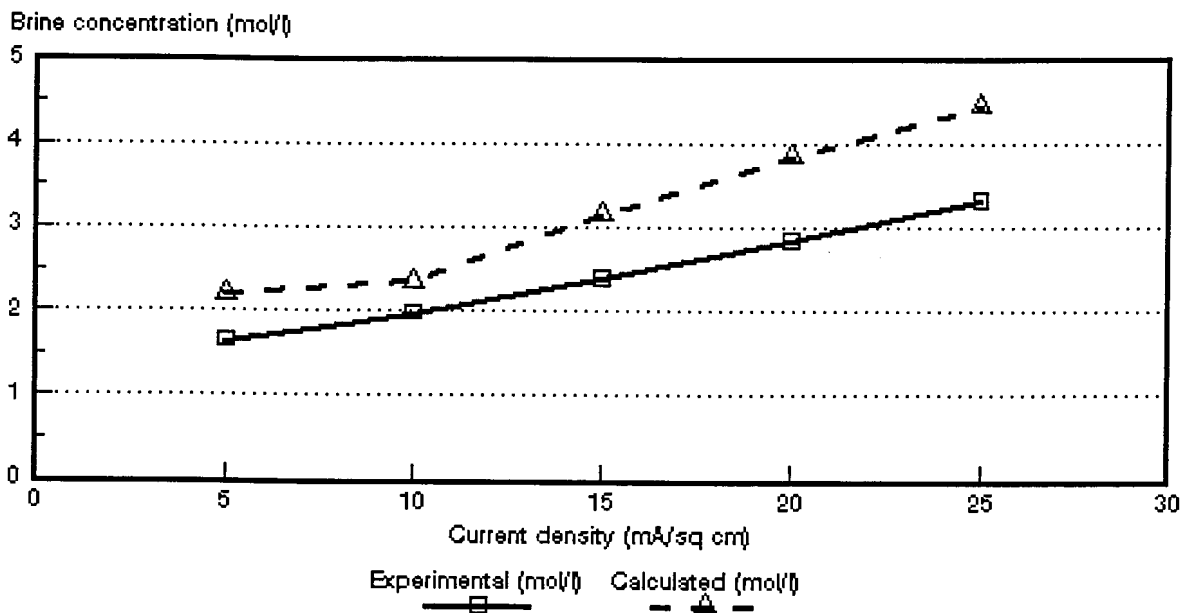


Figure 6.31: Experimental and calculated brine concentrations as a function of current density for 0,05 mol/l NaCl feed solution. *WTPSA-1* and *WTPSC-1* membranes.

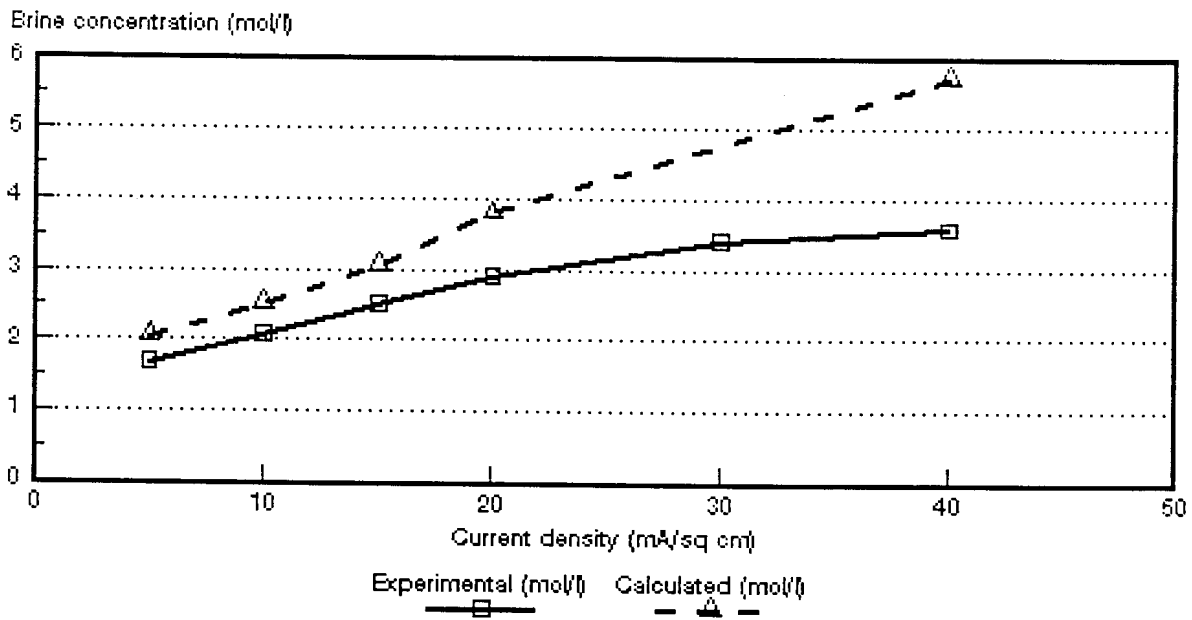


Figure 6.32: Experimental and calculated brine concentrations as a function of current density for 0,1 mol/l NaCl feed solution. WTPSA-1 and WTPSC-1 membranes.

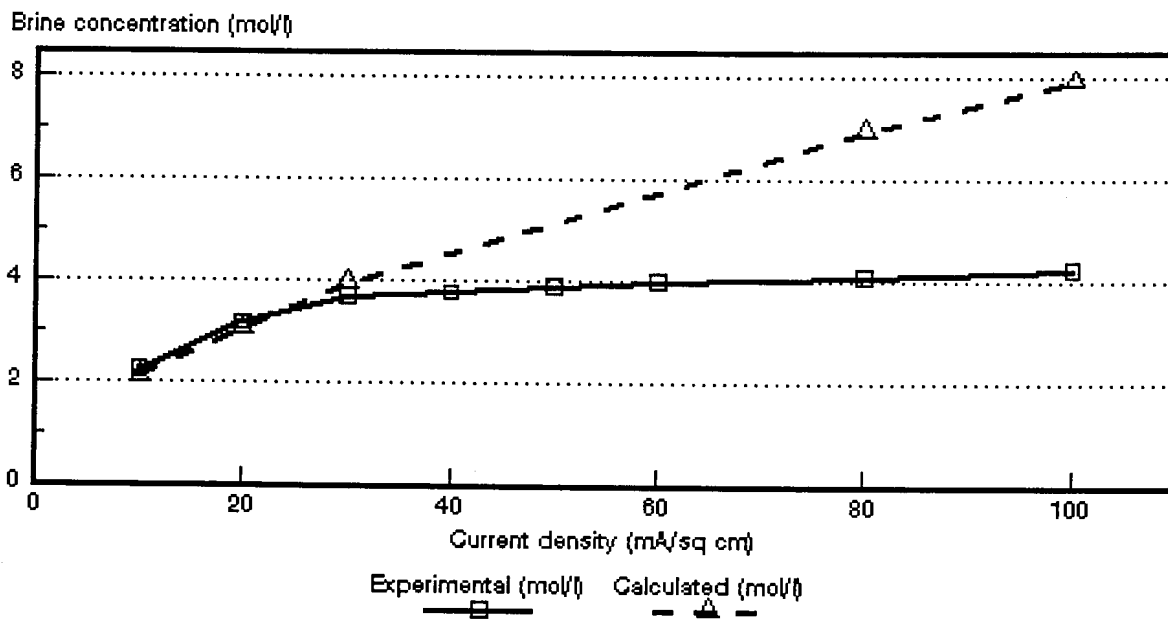


Figure 6.33: Experimental and calculated brine concentrations as a function of current density for 0,5 mol/l NaCl feed solution. WTPSA-1 and WTPSC-1 membranes.

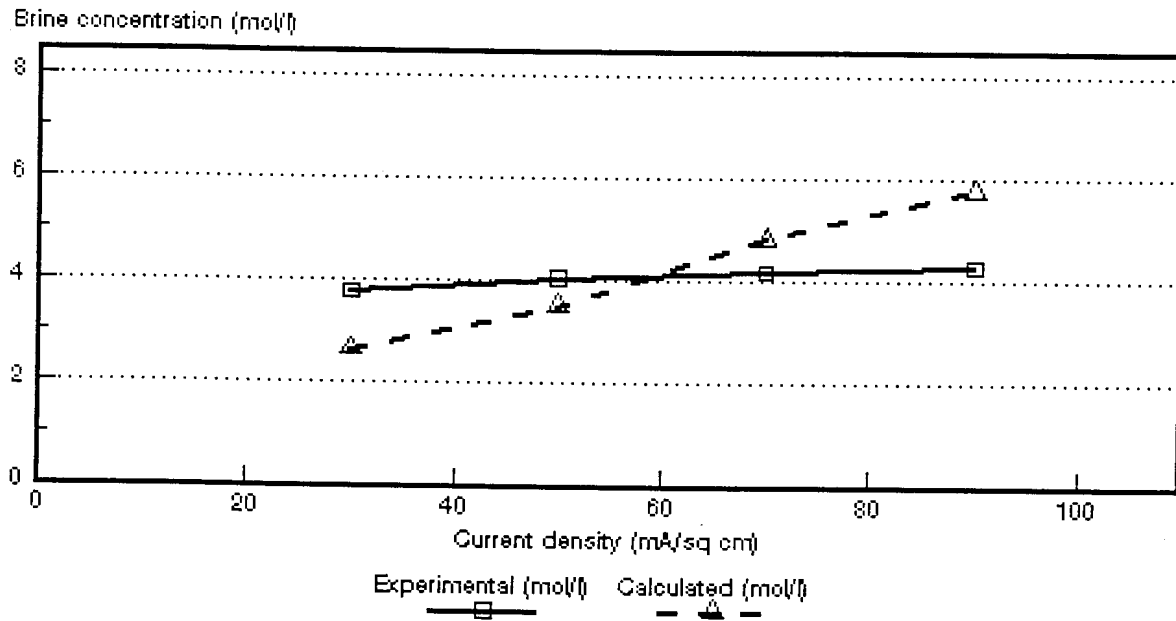


Figure 6.34: Experimental and calculated brine concentrations as a function of current density for 1,0 mol/l NaCl feed solution. WTPSA-1 and WTPSC-1

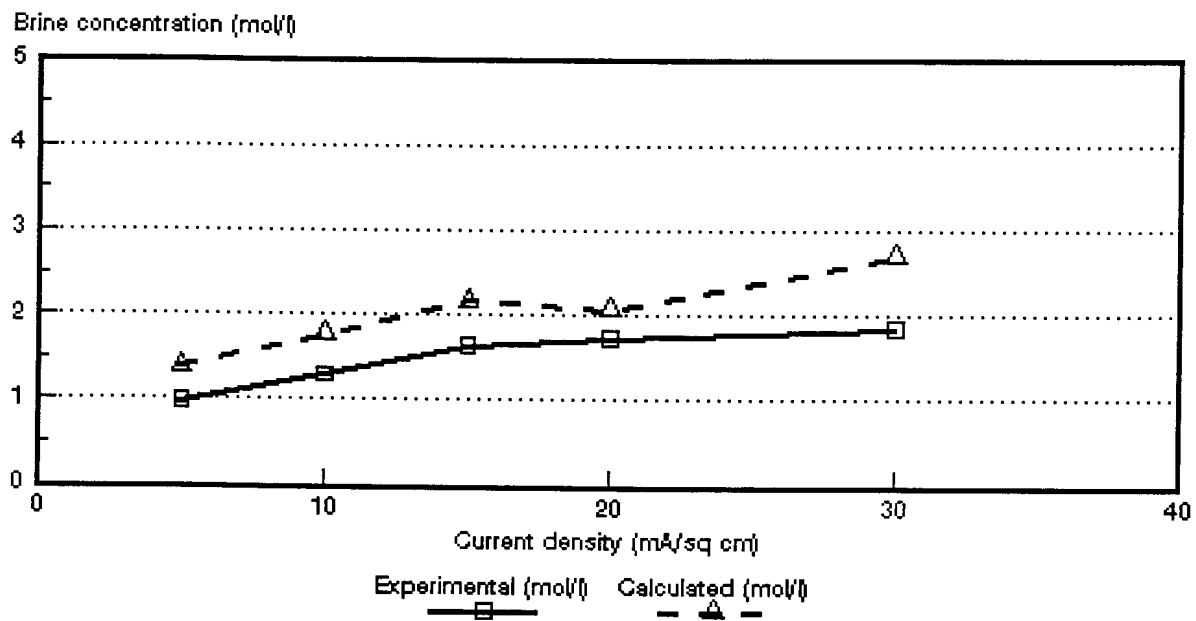


Figure 6.35: Experimental and calculated brine concentrations as a function of current density for 0,05 mol/l NaCl feed solution. WTPVCA-2 and WTPVCC-2 membranes.

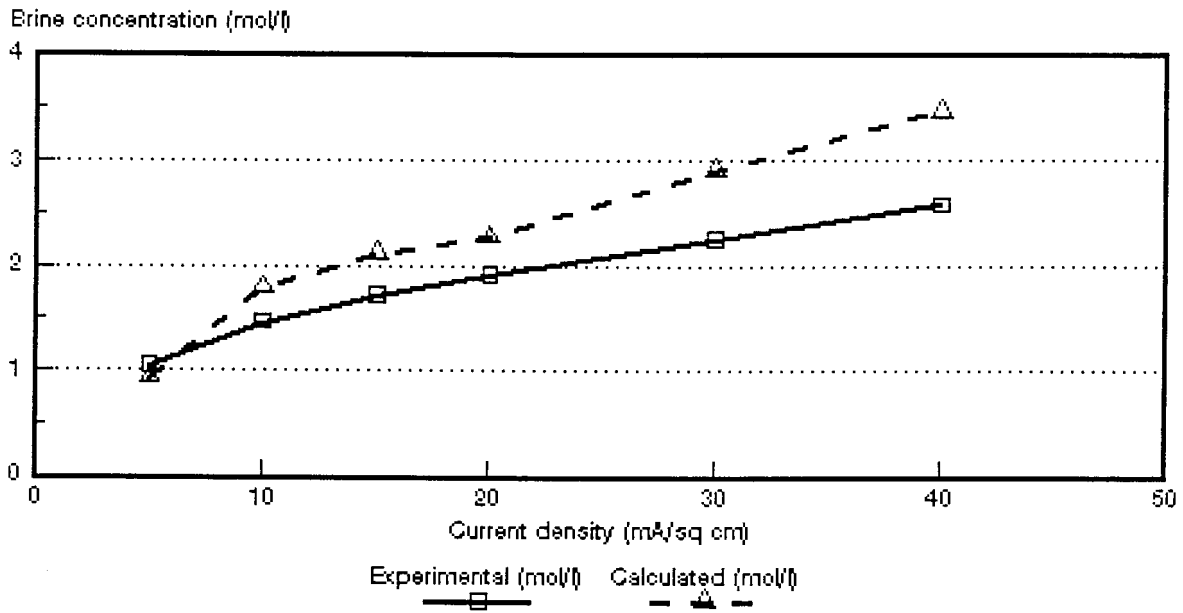


Figure 6.36: Experimental and calculated brine concentrations as a function of current density for 0,1 mol/l NaCl feed solution. WTPVCA-2 and WTPVCC-2 membranes.

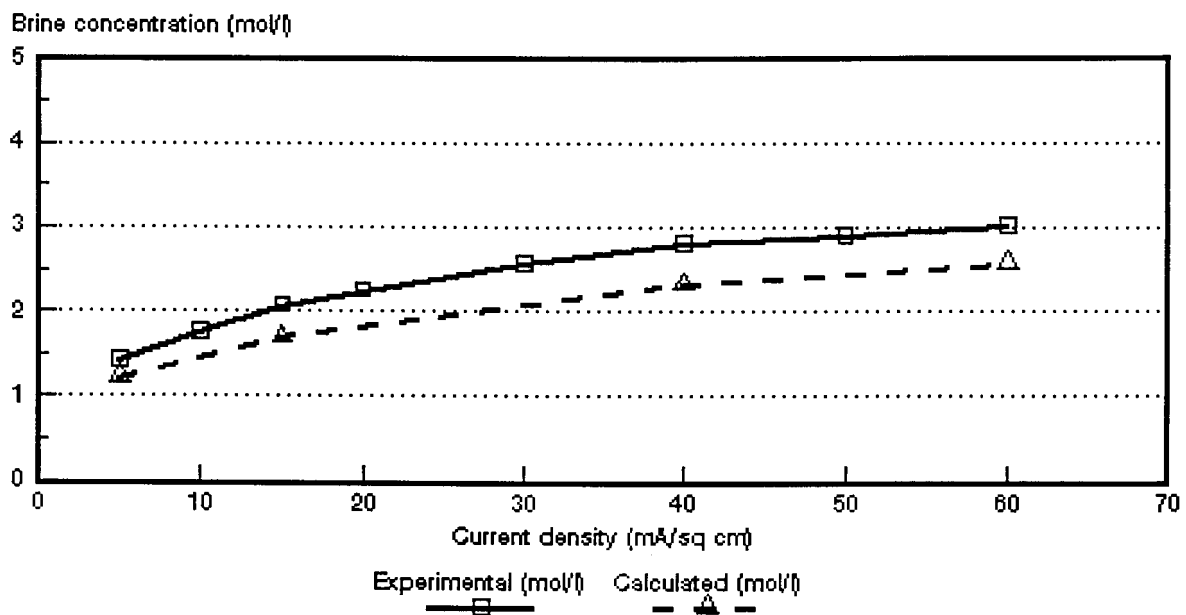


Figure 6.37: Experimental and calculated brine concentrations as a function of current density for 0,5 mol/l NaCl feed solution. WTPVCA-2 and WTPVCC-2 membranes.

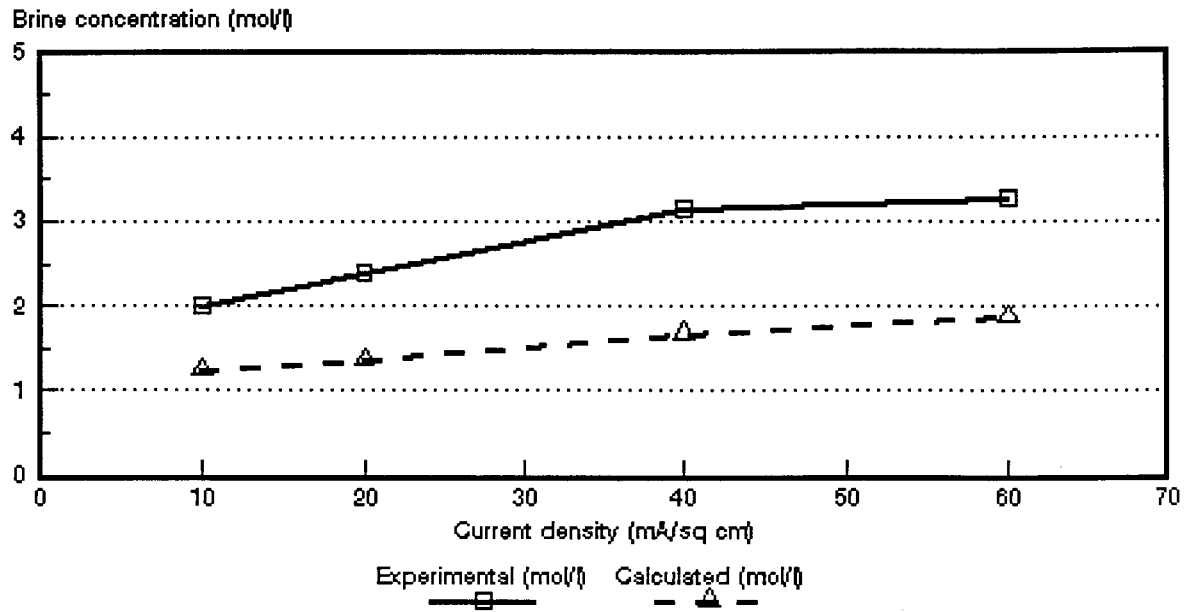


Figure 6.38: Experimental and calculated brine concentrations as a function of current density for 1,0 mol/l NaCl feed solution. WTPVCA-2 and WTPVCC-2 membranes.

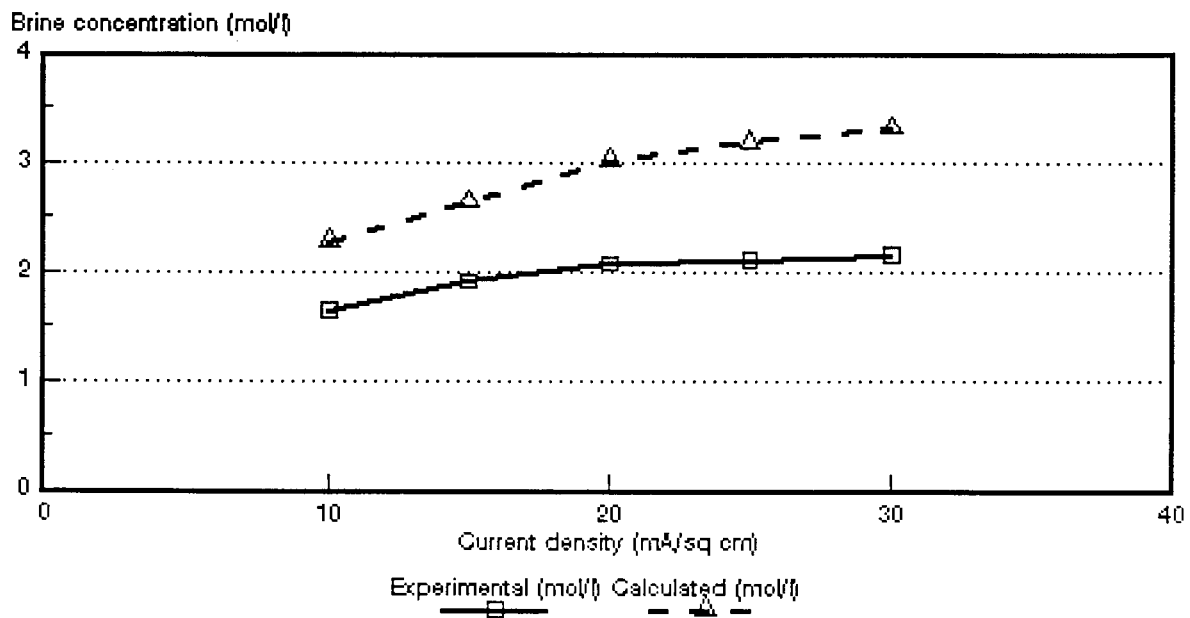


Figure 6.39: Experimental and calculated brine concentrations as a function of current density for 0,05 mol/l NaCl feed solution. WTPSTA-3 and WTPSTC-3 membranes.

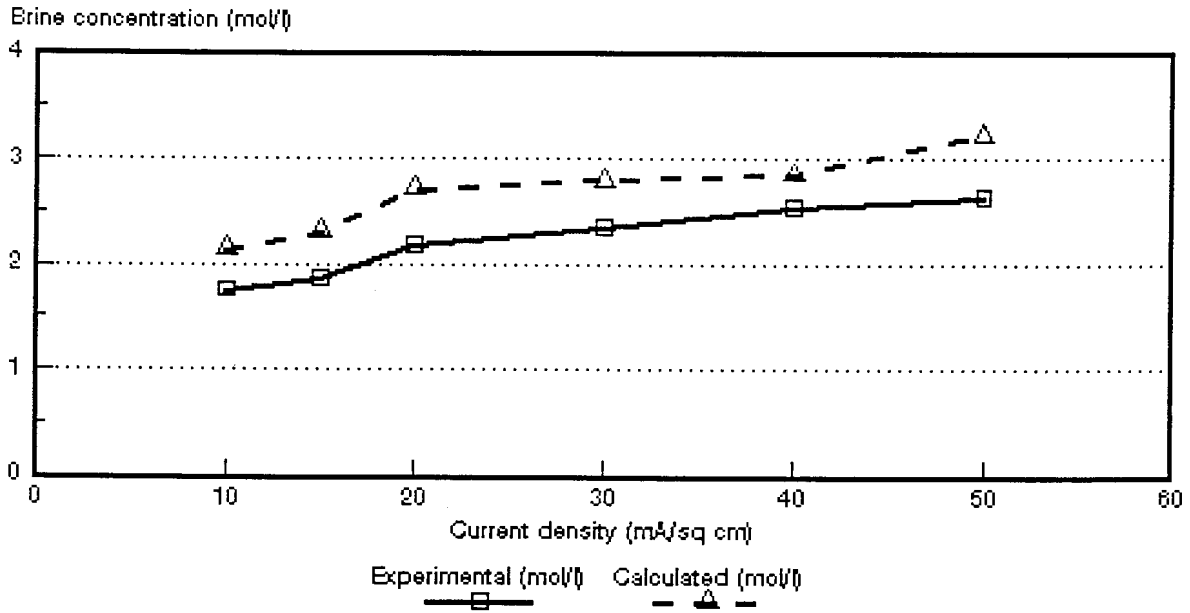


Figure 6.40: Experimental and calculated brine concentrations as a function of current density for 0,1 mol/l NaCl feed solution. WTPSTA-3 and WTPSTC-3 membranes.

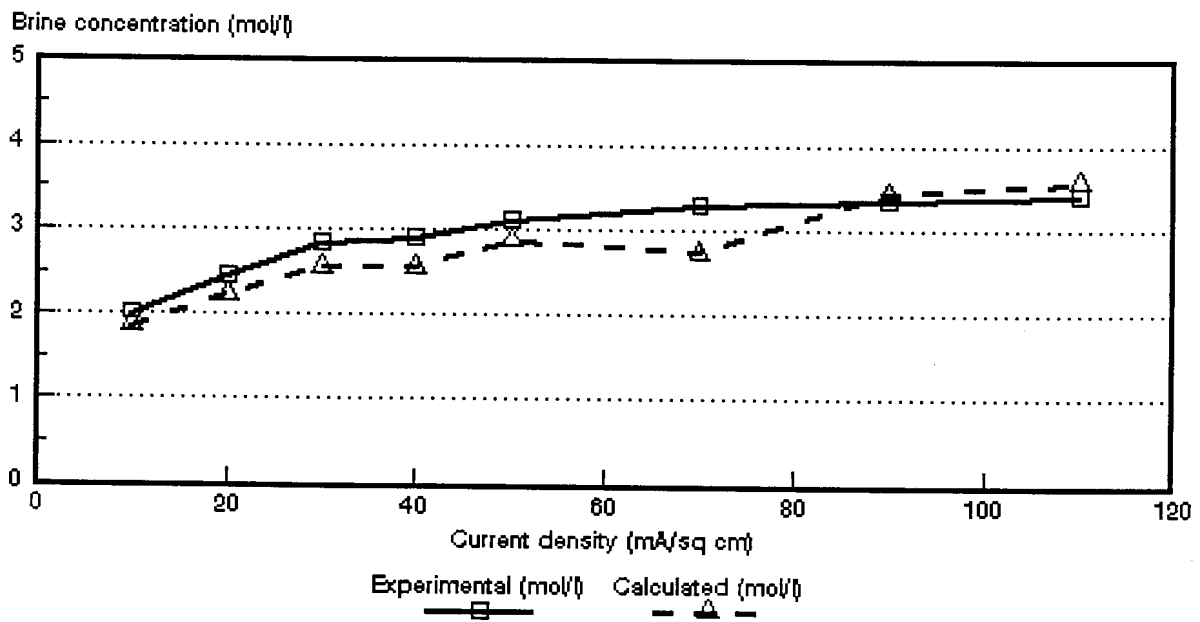


Figure 6.41: Experimental and calculated brine concentrations as a function of current density for 0,5 mol/l NaCl feed solution. WTPSTA-3 and WTPSTC-3 membranes.

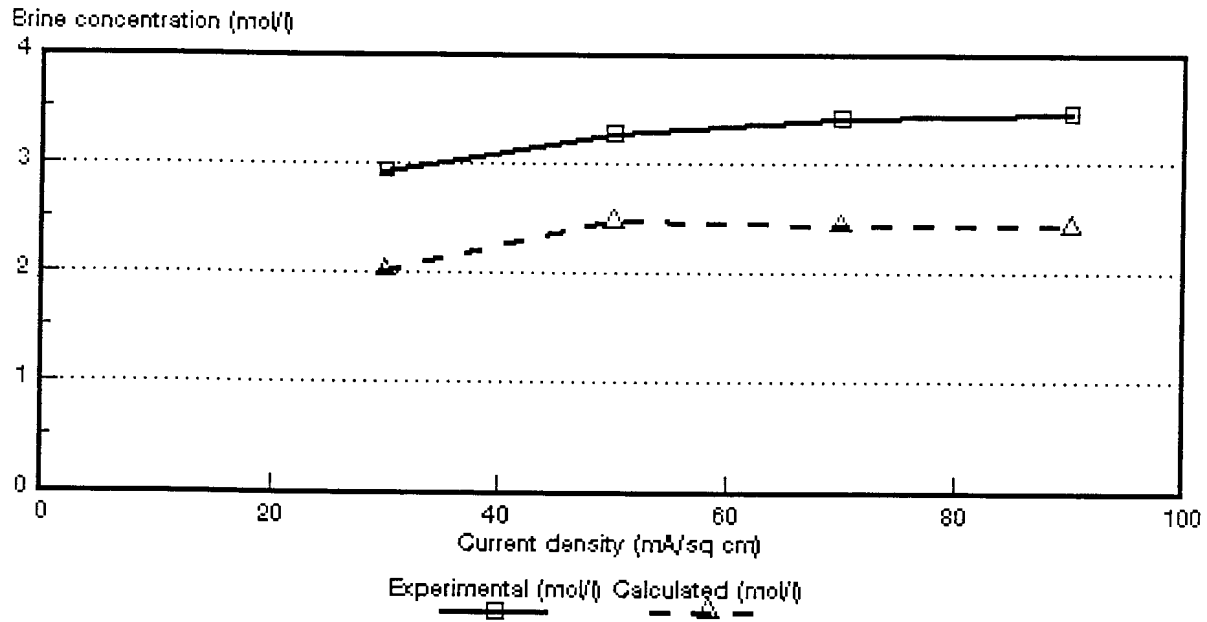


Figure 6.42: Experimental and calculated brine concentrations as a function of current density for 1,0 mol/l NaCl feed solution. WTPSTA-3 and WTPSTC-3 membranes.

Table 6.31: Correlation between calculated ($c_{b, calc}$) and experimentally ($c_{b, exp}$) determined brine concentrations.

Current Density mA/cm ²	$c_{b, calc}/c_{b, exp}$																															
	Selemion AMV & CMV Concentration, mol/t				Ionac MA-3475 & MC-3470 Concentration, mol/t				Raipore R4030 & R4010 Concentration, mol/t				Ionics A-204-UZL & C-61-CZL Concentration, mol/t				WTPS WTPSA & WTPSA Concentration, mol/t				WTPVC WTPVCA & WTPVCC Concentration, mol/t				WTPST WTPSTA & WTPSTC Concentration, mol/t							
	0,05	0,1	0,5	1,0	0,05	0,1	0,5	1,0	0,05	0,1	0,5	1,0	0,05	0,1	0,5	1,0	0,05	0,1	0,5	1,0	0,05	0,1	0,5	1,0	0,05	0,1	0,5	1,0				
5	0,98	1,17	0,99		1,21	1,19	0,71		1,67	1,36	1,48		1,50	1,27			1,33	1,22			1,37	0,90	0,86									
10	1,28	1,11	0,85	0,82	1,30	1,18	0,87		1,54	1,26	1,34		1,43	1,29	0,91		1,19	1,20	0,95		1,36	1,22		0,63	1,39	1,22	0,93					
15	1,26	1,07			1,33	1,26			1,57				1,43	1,25			1,32	1,21			1,33	1,23	0,82		1,38	1,23						
20	1,26	1,06	0,79	0,78	1,41	1,21	0,82	0,70	1,61	1,23	1,21		1,48	1,27	0,95		1,35	1,31	0,96		1,19	1,13		0,57	1,45	1,24	0,91					
25					1,42												1,34								1,52							
30	1,22	1,04	0,83	0,77		1,26			1,56	1,19	1,12	0,80	1,62	1,31	0,96	0,72			1,07	0,70	1,46	1,29			1,54	1,23	0,99	0,69				
40		1,05	0,77	0,77		1,28	0,95	0,75		1,15	1,05			1,42	0,98			1,60				1,34	0,83	0,54		1,27	0,88					
50		1,00	0,78	0,73		1,33	1,01			1,16	1,01	0,79			0,99	0,73				0,86						1,12	0,93	0,66				
60			0,77	0,74			1,09	0,79			1,05				0,91								0,85	0,57								
70							1,10				0,93	0,78			0,97	0,79				1,16							0,84	0,72				
80								0,75							1,01				1,70													
90											0,94	0,85			1,02	0,85				1,35							1,02	0,70				
100															1,06					1,67												
110																												1,05				

6.2 Current Efficiency

Current efficiency (ϵ_p) determined during the EOP experiments as a function of current density is shown in Figures 6.43 to 6.49 for the different membranes. Current efficiency increases with increasing feed water concentration in the concentration range from 0,05 to 1,0 mol/l. However, current efficiency was slightly lower at the highest feed concentration in the case of the *Selemion* membranes (Fig 6.43). It is interesting to note that current efficiency has been significantly higher at the higher feed concentrations in the case of the *Ionac*- (Fig. 6.44), *Raipore*- (Fig. 6.45), *Ionics*- (Fig. 6.46), WTPS- (Fig. 6.47), WTPVC- (Fig. 6.48) and WTPST- (Fig 6.49) membranes.

No significant change in current efficiency was observed as a function of current density in the case of the *Selemion* membranes in the feed concentration range studied (Fig 6.43). This showed that the limiting current density was not reached in the range of current densities and feed water concentrations used for these membranes. However, changes in current efficiency, especially at the lower feed concentration levels (0,05 to 0,5 mol/l), were experienced with the *Ionac*- (Fig. 6.44), *Raipore*- (Fig. 6.45, 0,05 mol/l), *Ionics*- (Fig. 6.46, 0,05 to 1,0 mol/l), WTPS- (Fig. 6.47, 0,05 to 1,0 mol/l), WTPVC- (Fig. 6.48, 0,05 to 1,0 mol/l) and WTPST- (Fig. 6.49, 0,05 to 1,0 mol/l) membranes. This showed that the limiting current density was exceeded with increasing current density. A significant reduction in current efficiency was experienced in the case of the WTPS membranes at the higher feed concentrations at relatively low current densities (Fig. 6.47). This showed that the limiting current density was exceeded and that polarization was taking place.

The apparent transport numbers for a membrane pair ($\bar{\Delta}t$), for the anion- (Δt^a) and cation- (Δt^c) membranes, determined from membrane potential measurements for a concentration difference similar to that obtained in the EOP experiments at the different current densities and feed water concentrations used, are shown in Figures 6.50 to 6.77. The current efficiencies (ϵ_p) as determined by the EOP method and shown in Figures 6.43 to 6.49 are also shown in Figures 6.50 to 6.77. The correlation between the apparent transport numbers ($\bar{\Delta}t$, Δt^a and Δt^c) and the current efficiency (ϵ_p) is shown in Tables 6.32 to 6.34.

The apparent transport numbers ($\bar{\Delta}t$, Δt^a , Δt^c) were higher than the current efficiencies at the lower feed water concentrations (0,05 to 0,1 mol/l) (Tables 6.32 to 6.34 and Figs. 6.50 to 6.77). However, the apparent transport numbers became smaller than the

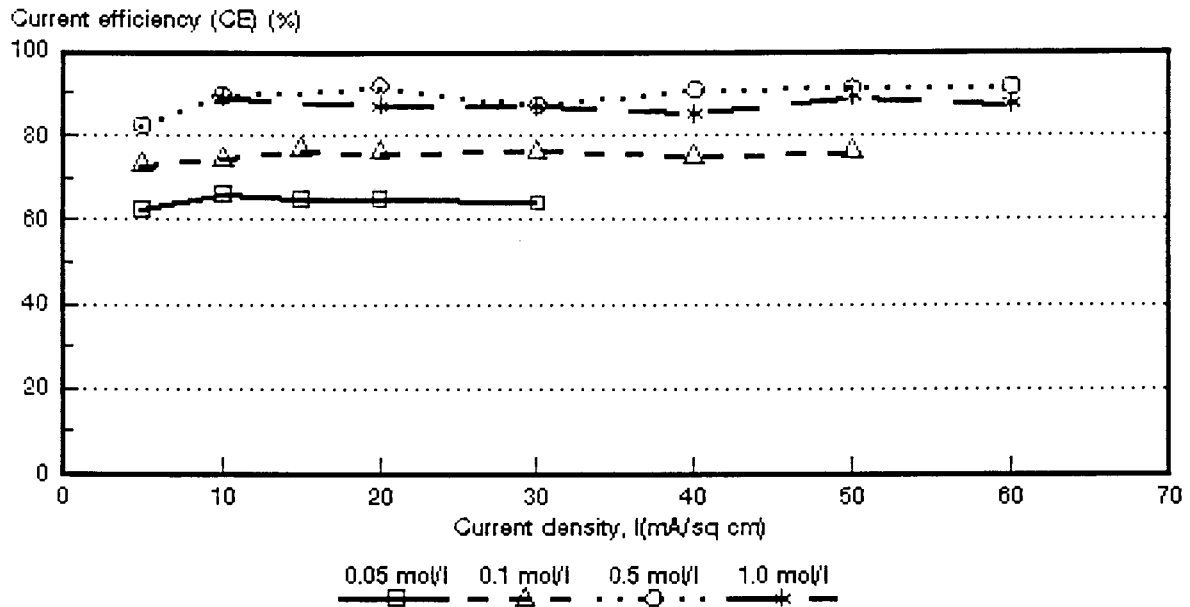


Figure 6.43: Current efficiency (e_p) as a function of current density for 4 different NaCl feed concentrations. *Selemion* AMV and CMV membranes.

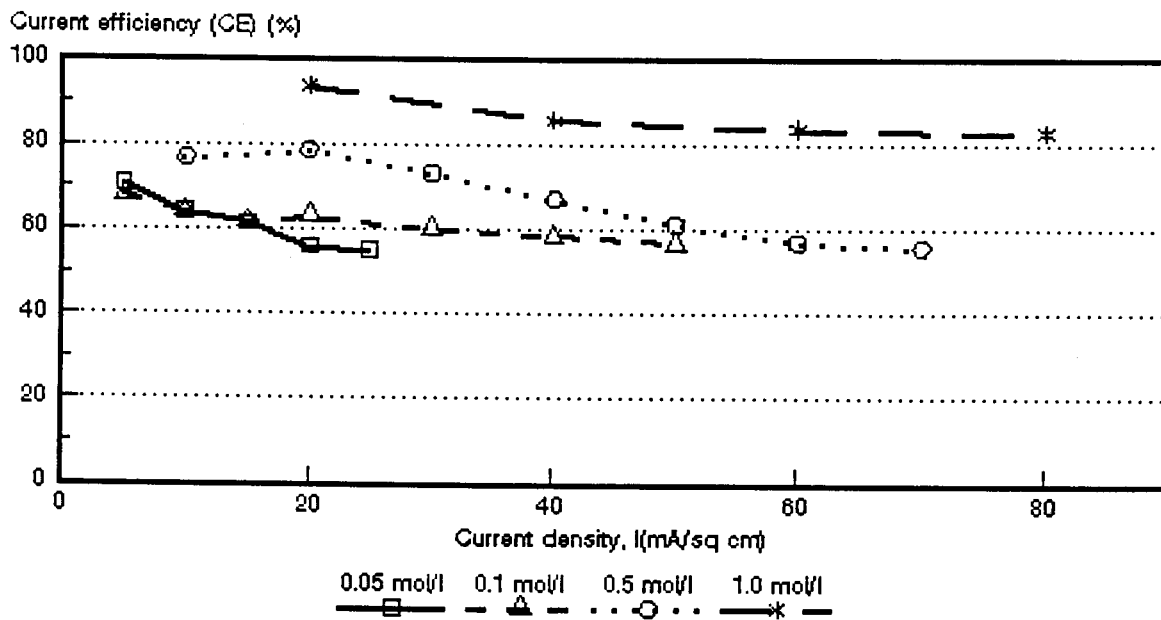


Figure 6.44: Current efficiency (e_p) as a function of current density for 4 different NaCl feed concentrations. Ionac MA-3475 and MC-3470 membranes.

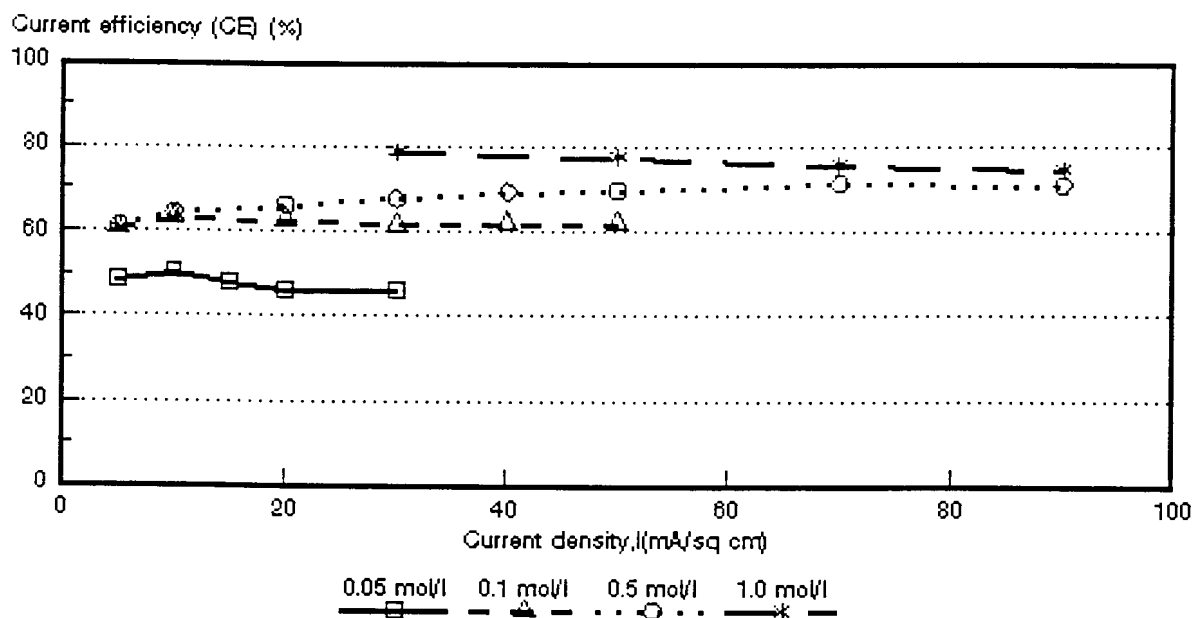


Figure 6.45: Current efficiency (e_p) as a function of current density for 4 different NaCl feed concentrations. *Raipore* R4030 and R4010 membranes.

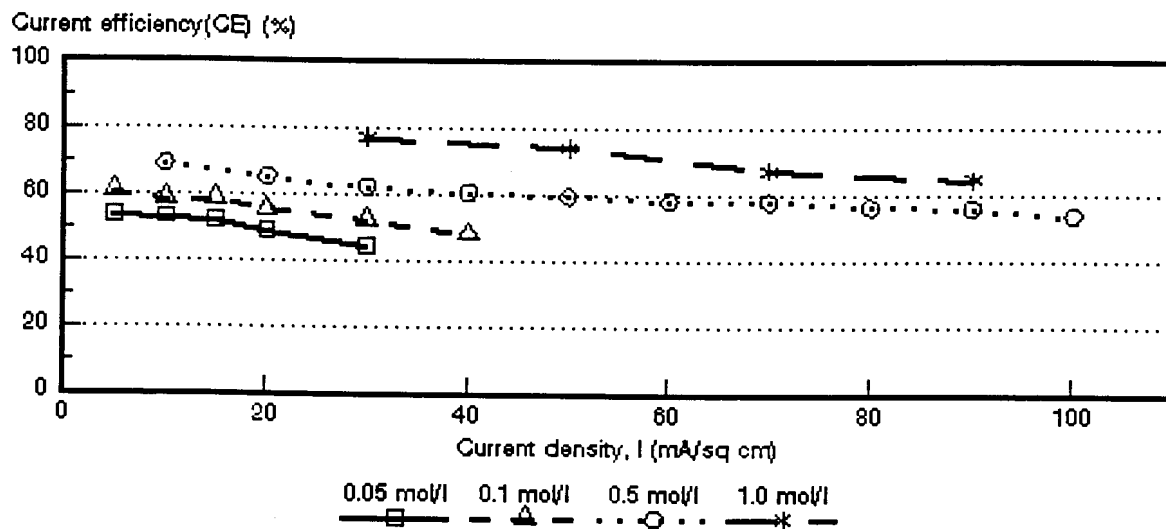


Figure 6.46: Current efficiency (e_p) as a function of current density for 4 different NaCl feed concentrations. *Ionics* A-204-UZL-386 and C-61-CZL-386 membranes.

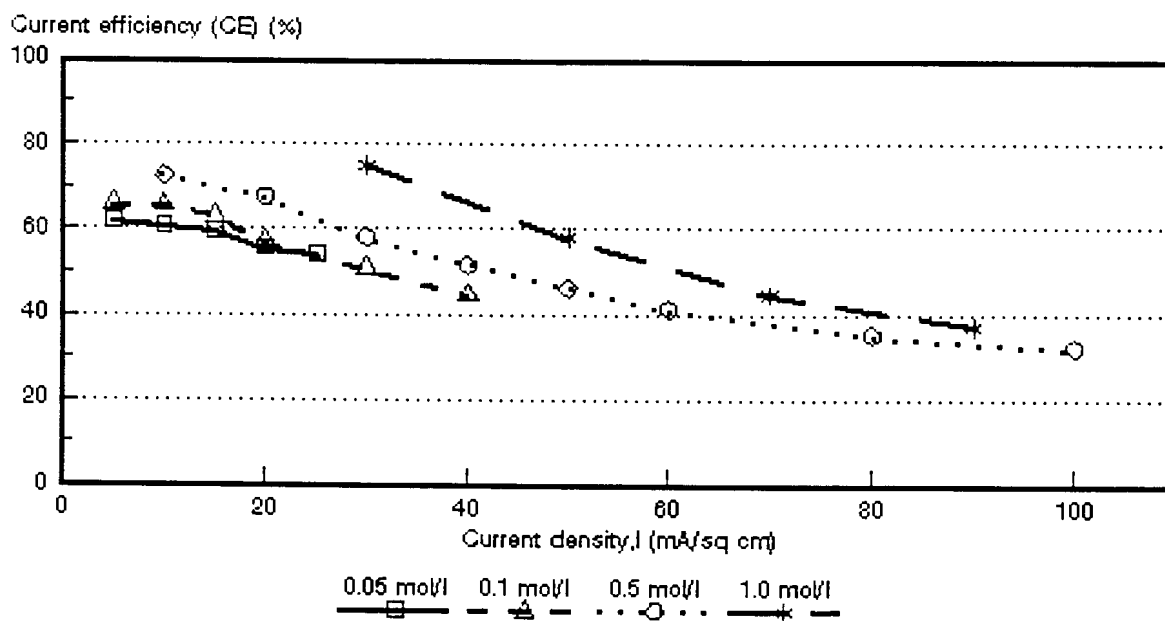


Figure 6.47: Current efficiency (ϵ_p) as a function of current density for 4 different NaCl feed concentrations. WTPSA-1 and WTPSC-1 membranes

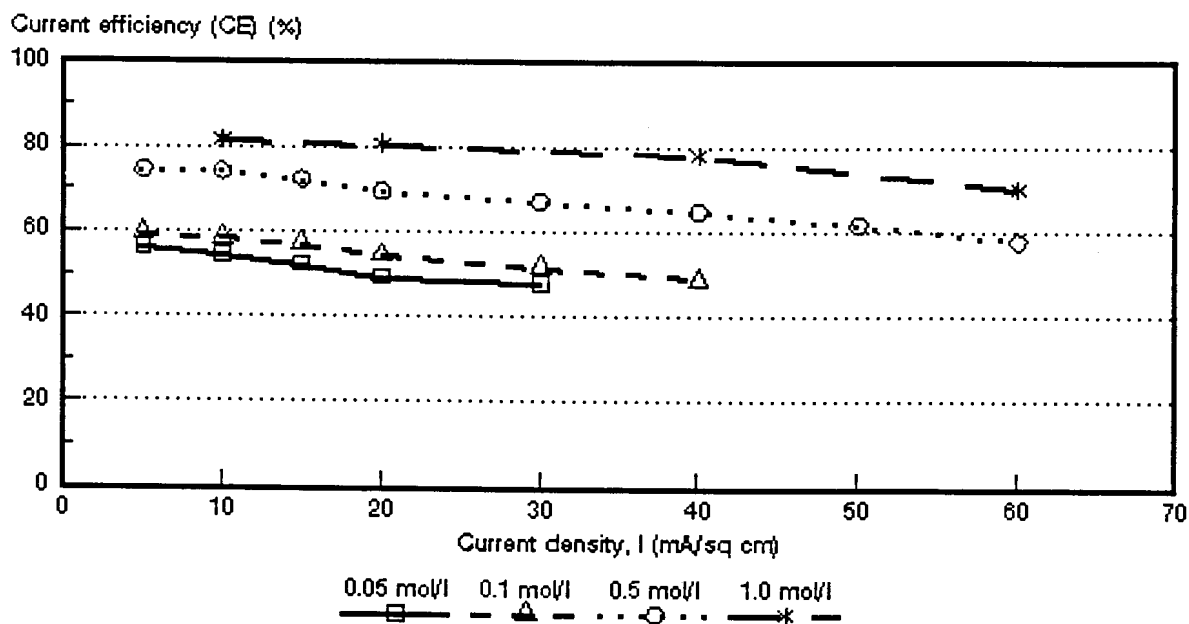


Figure 6.48: Current efficiency (ϵ_p) as a function of current density for 4 different NaCl feed concentrations. WTPVCA-2 and WTPVCC-2 membranes.

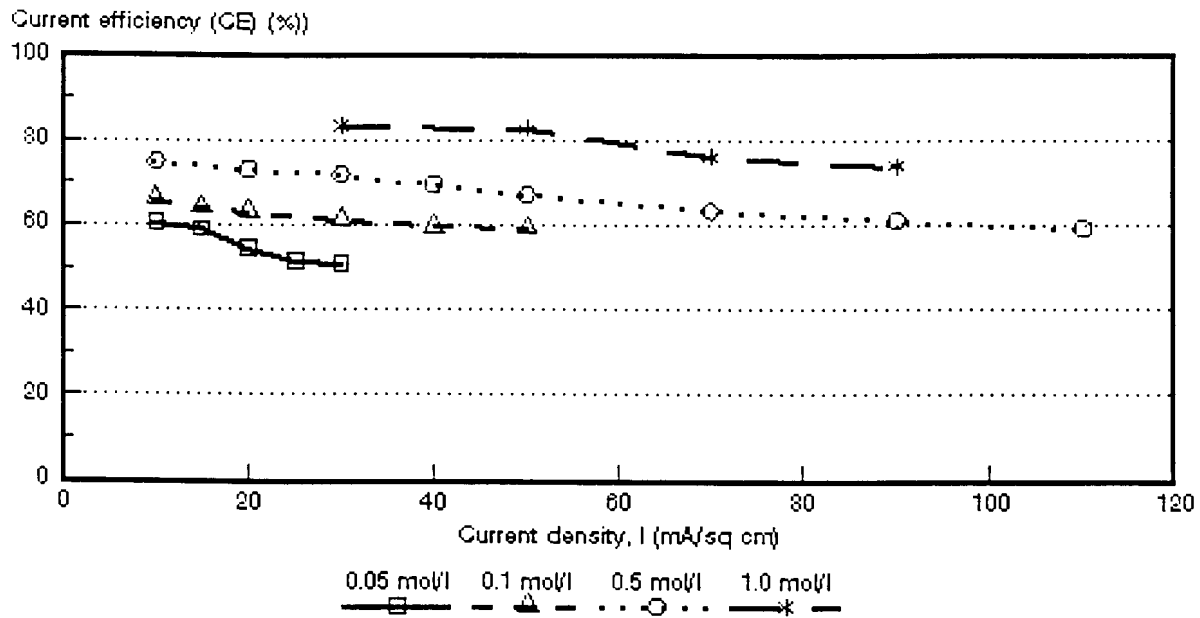


Figure 6.49: Current efficiency (e_p) as a function of current density for 4 different NaCl feed concentrations. WTPSTA-3 and WTPSTC-3 membranes.

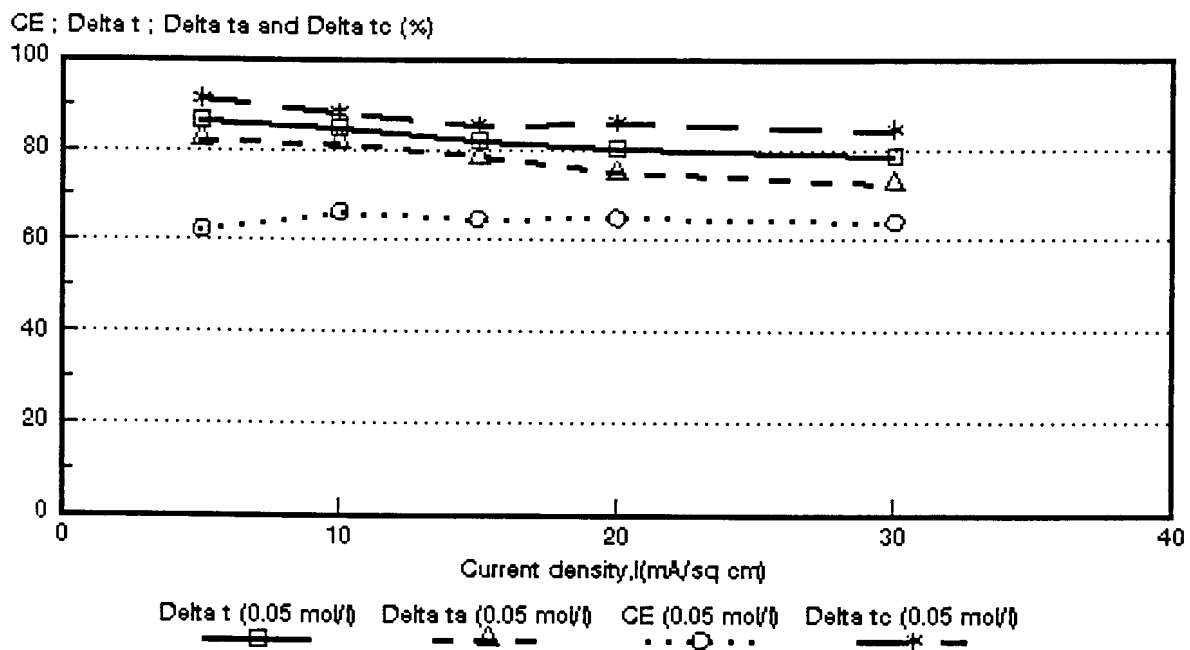


Figure 6.50: Current efficiency ($CE = e_p$) and apparent transport numbers as a function of current density for 0,05 mol/l NaCl feed. Selemion AMV and CMV membranes. $\Delta t = \bar{\Delta}t$; $\Delta t_a = \Delta t^*$; $\Delta t_c = \Delta t^*$.

CE ; Delta t ; Delta ta and Delta tc (%)

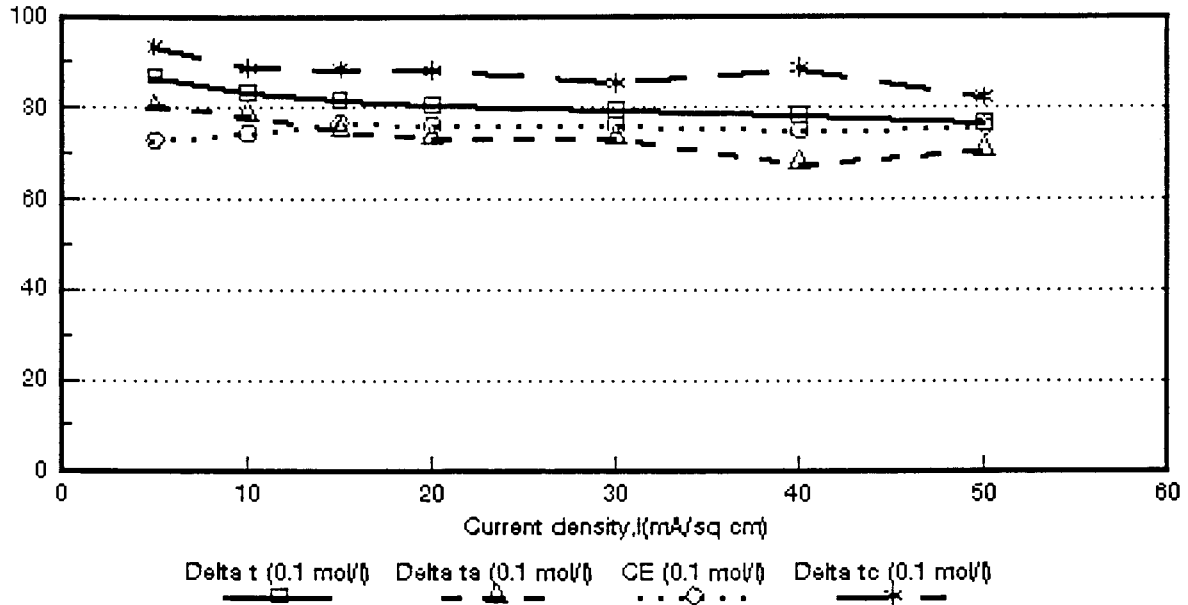


Figure 6.51: Current efficiency ($CE = e_p$) and apparent transport numbers as a function of current density for 0,1 mol/l NaCl feed. *Selemion AMV* and *CMV* membranes. $\Delta t = \bar{\Delta}t$; $\Delta t_a = t^*$; $\Delta t_c = \Delta t^c$.

CE ; Delta t ; Delta ta and Delta tc (%)

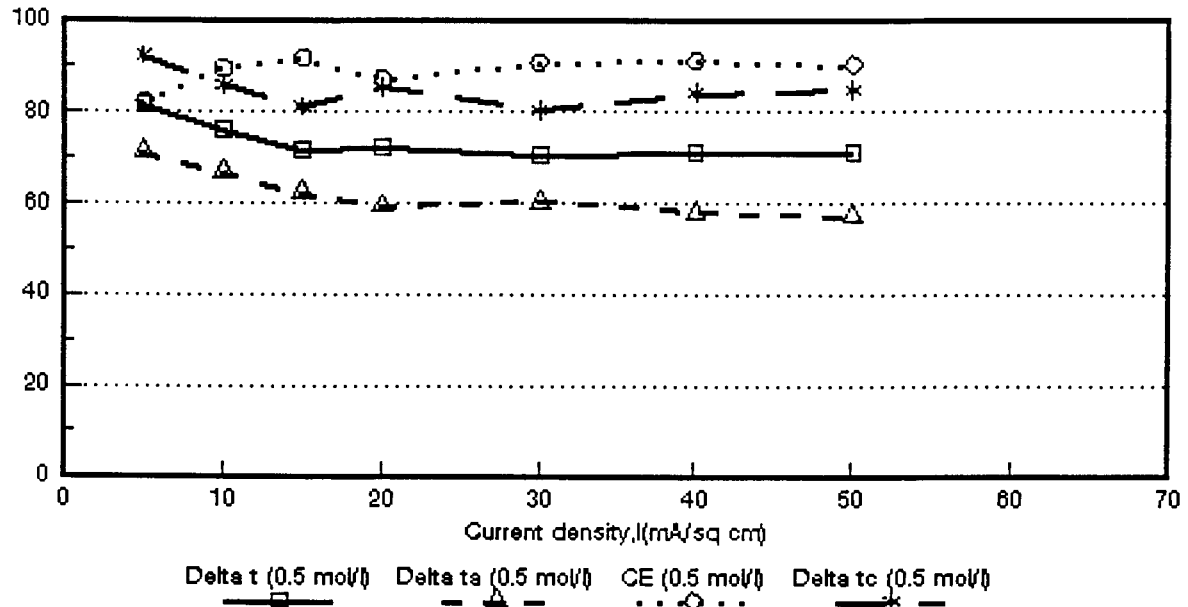


Figure 6.52: Current efficiency ($CE = e_p$) and apparent transport numbers as a function of current density for 0,5 mol/l NaCl feed. *Selemion AMV* and *CMV* membranes. $\Delta t = \bar{\Delta}t$; $\Delta t_a = \Delta t^*$; $\Delta t_c = \Delta t^c$.

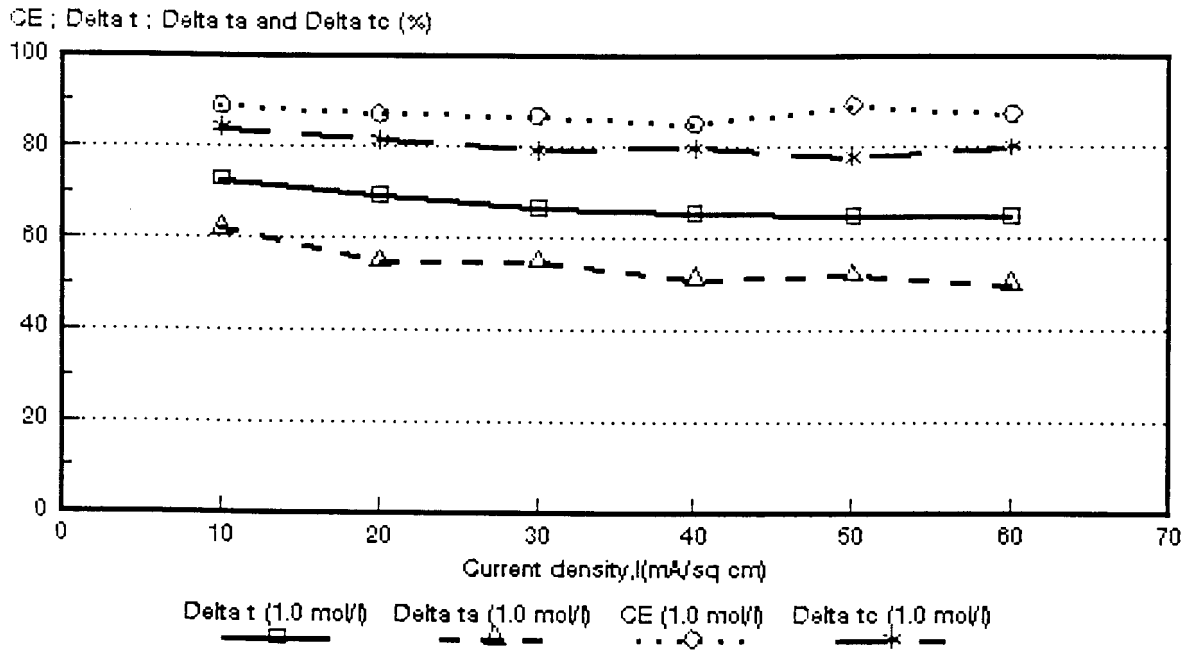


Figure 6.53: Current efficiency ($CE = e_p$) and apparent transport numbers as a function of current density for 1,0 mol/l NaCl feed. *Selemon AMV* and *CMV* membranes. $\Delta t = \bar{\Delta}t$; $\Delta t_a = \Delta t^a$; $\Delta t_c = \Delta t^c$.

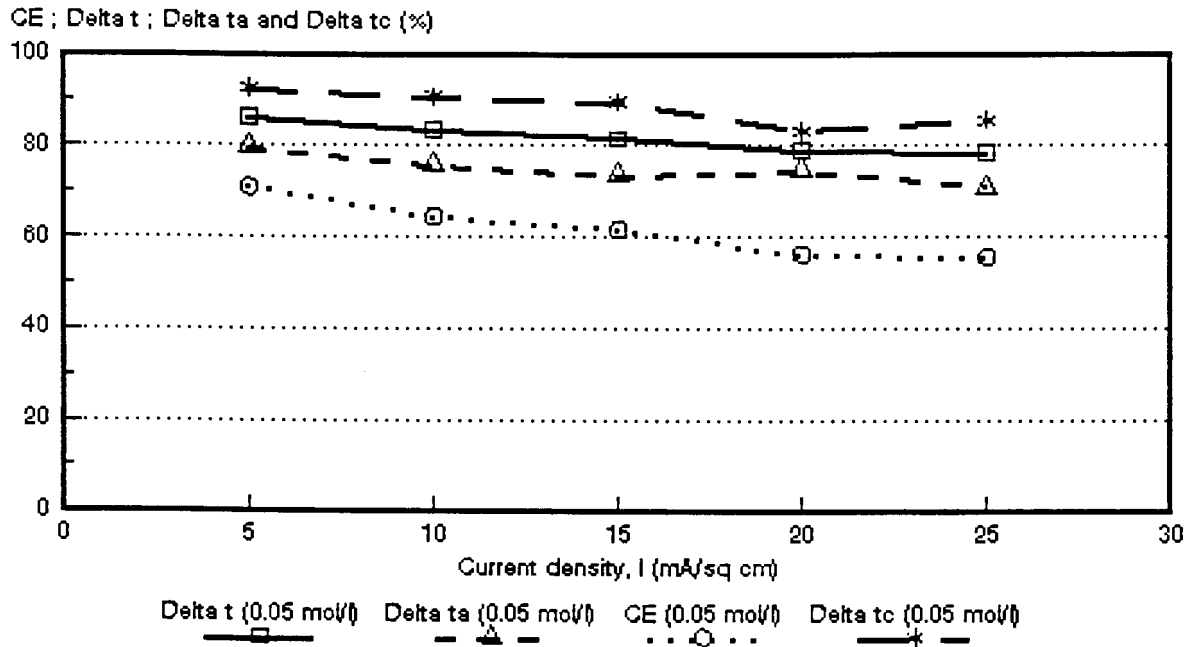


Figure 6.54: Current efficiency ($CE = e_p$) and apparent transport numbers as a function of current density for 0,05 mol/l NaCl feed. *Ionac MA-3475* and *MC-3470* membranes. $\Delta t = \bar{\Delta}t$; $\Delta t_a = \Delta t^a$; $\Delta t_c = \Delta t^c$.

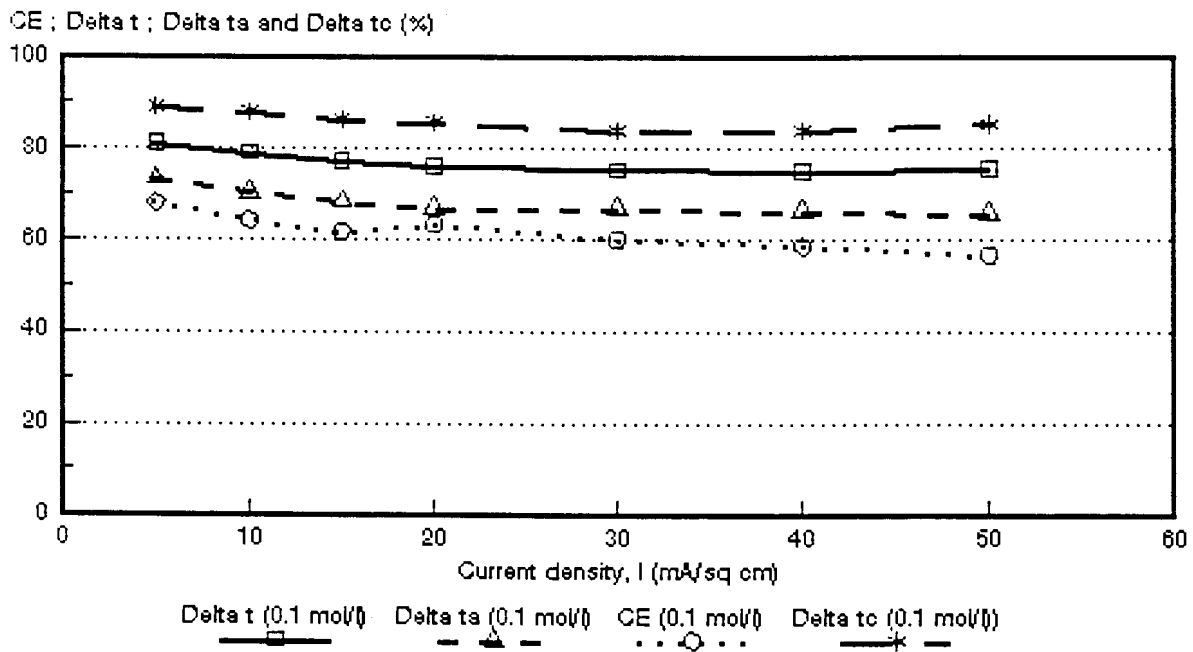


Figure 6.55: Current efficiency ($CE = e_p$) and apparent transport numbers as a function of current density for 0,1 mol/l NaCl feed. *Ionac* MA-3475 and MC-3470 membranes. $\Delta t = \bar{\Delta}t$; $\Delta ta = \Delta t^a$; $\Delta tc = \Delta t^c$.

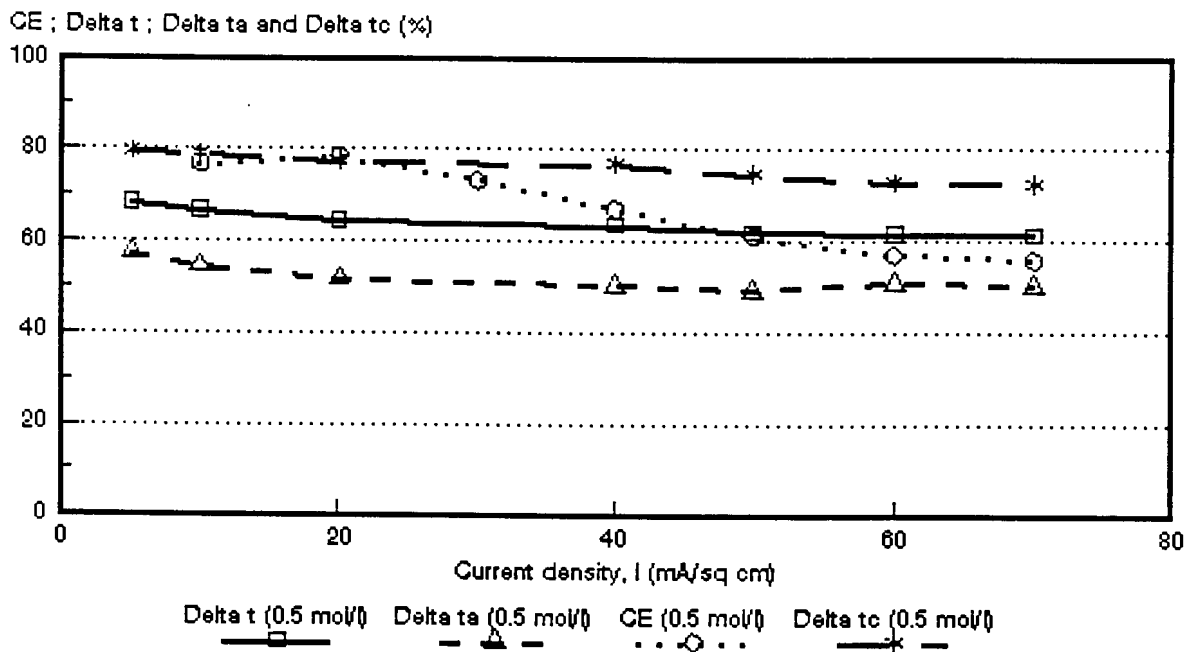


Figure 6.56: Current efficiency ($CE = e_p$) and apparent transport numbers as a function of current density for 0,5 mol/l NaCl feed. *Ionac* MA-3475 and MC-3470 membranes. $\Delta t = \bar{\Delta}t$; $\Delta ta = \Delta t^a$; $\Delta tc = \Delta t^c$.

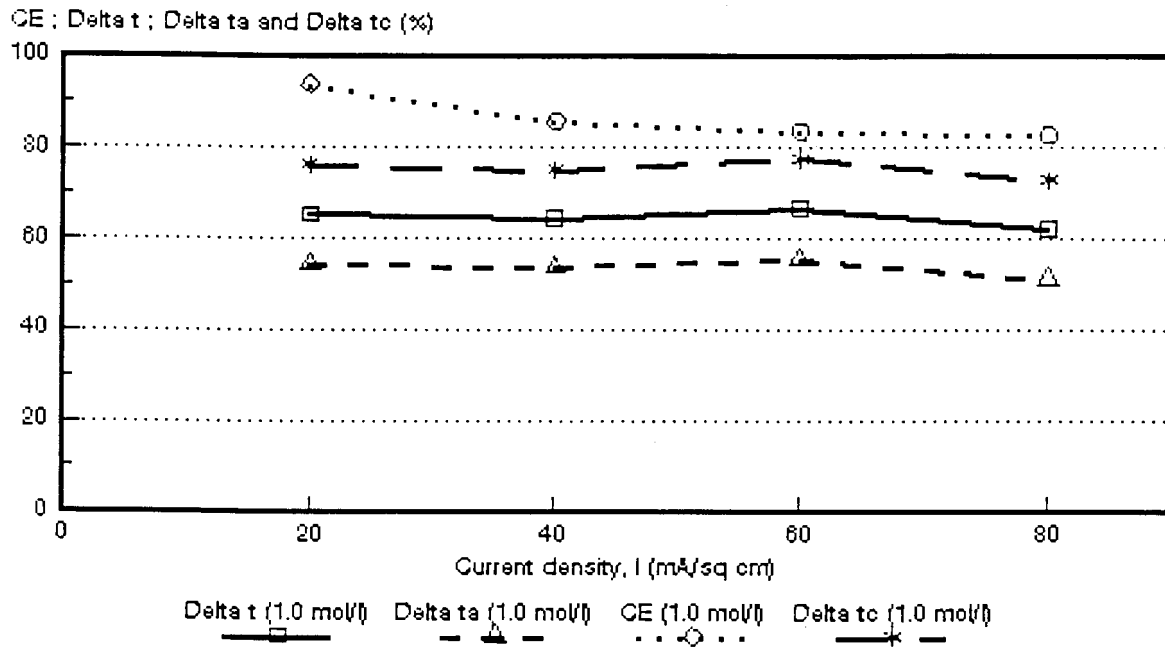


Figure 6.57: Current efficiency ($CE = \epsilon_p$) and apparent transport numbers as a function of current density for 1,0 mol/l NaCl feed. *Ionac* MA-3475 and MC-3470 membranes. $\Delta t = \bar{\Delta}t$; $\Delta t_a = \Delta t^*$; $\Delta t_c = \Delta t^c$.

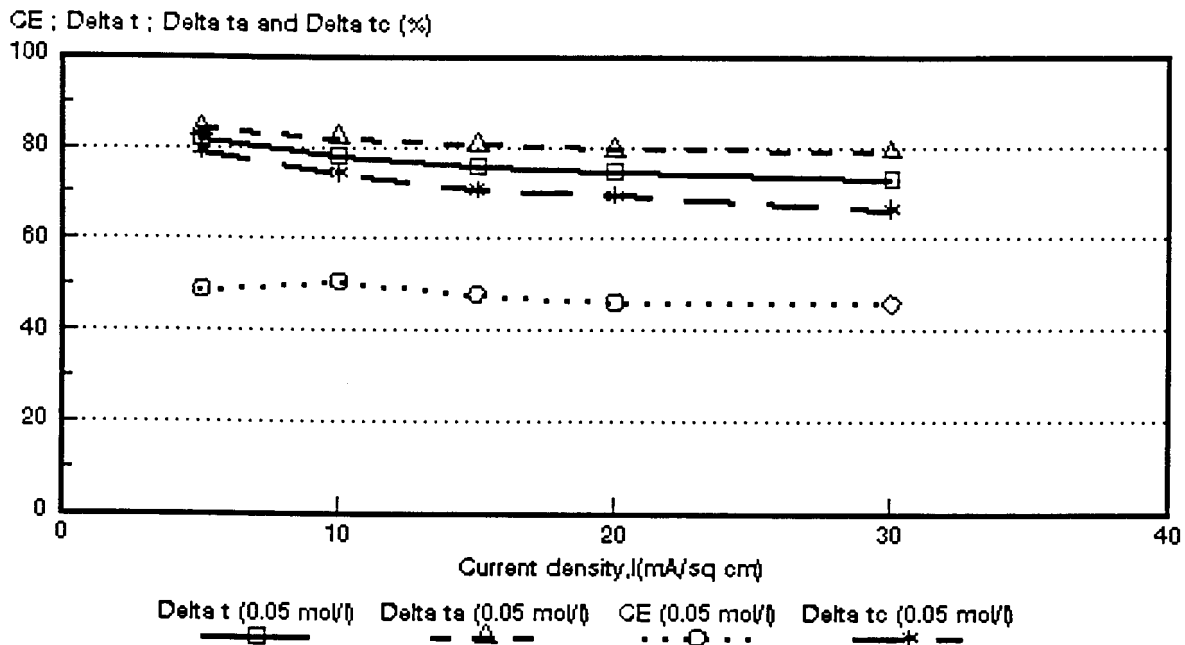


Figure 6.58: Current efficiency ($CE = \epsilon_p$) and apparent transport numbers as a function of current density for 0,05 mol/l NaCl feed. *Raipore* R4030 and R4010 membranes. $\Delta t = \bar{\Delta}t$; $\Delta t_a = \Delta t^*$; $\Delta t_c = \Delta t^c$.

CE ; Delta t ; Delta ta and Delta tc (%)

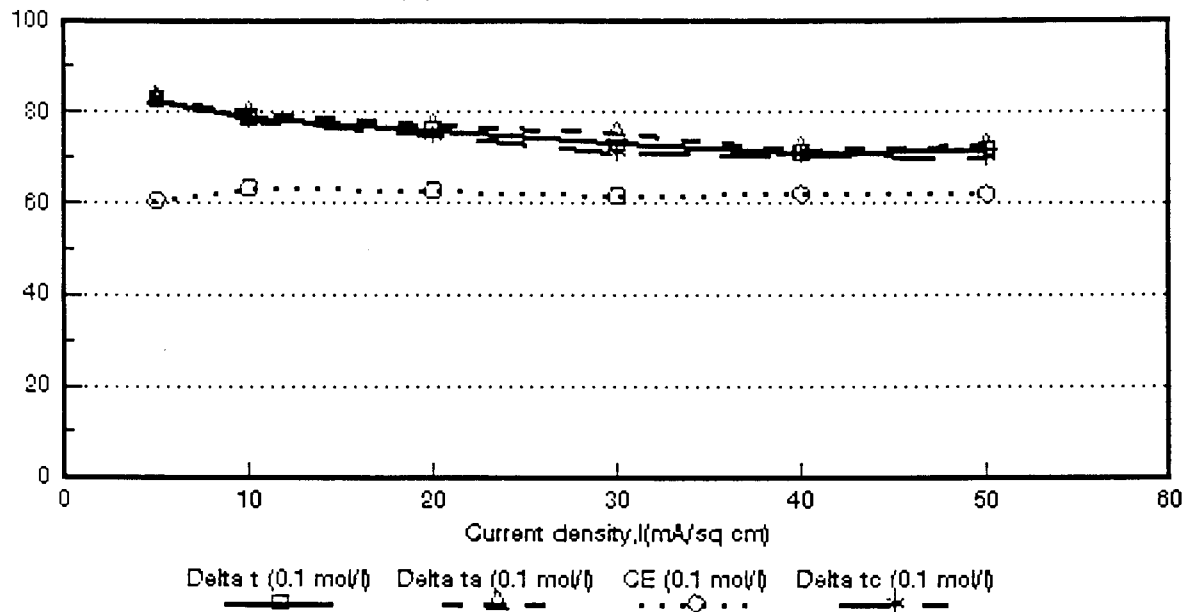


Figure 6.59: Current efficiency ($CE = e_p$) and apparent transport numbers as a function of current density for 0,1 mol/l NaCl feed. Raipore R4030 and R4010 membranes. $\Delta t = \bar{\Delta}t$; $\Delta t_a = \Delta t^a$; $\Delta t_c = \Delta t^c$.

CE ; Delta t ; Delta ta and Delta tc (%)

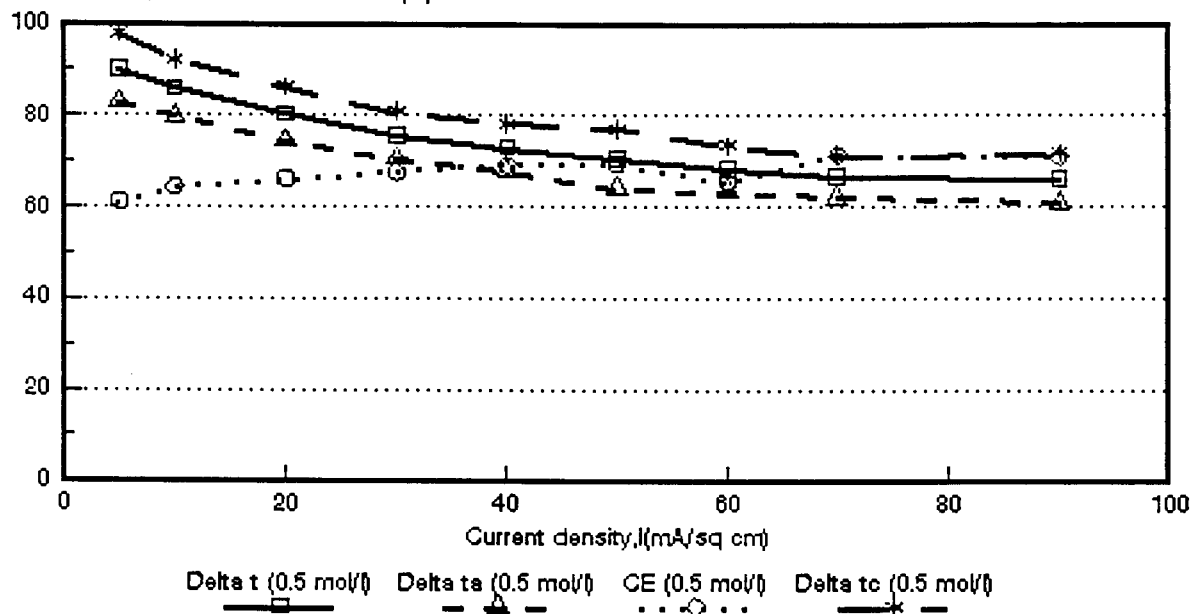


Figure 6.60: Current efficiency ($CE = e_p$) and apparent transport numbers as a function of current density for 0,5 mol/l NaCl feed. Raipore R4030 and R4010 membranes. $\Delta t = \hat{\Delta}t$; $\Delta t_a = \Delta t^a$; $\Delta t_c = \Delta t^c$.

CE ; Delta t ; Delta ta and Delta tc (%)

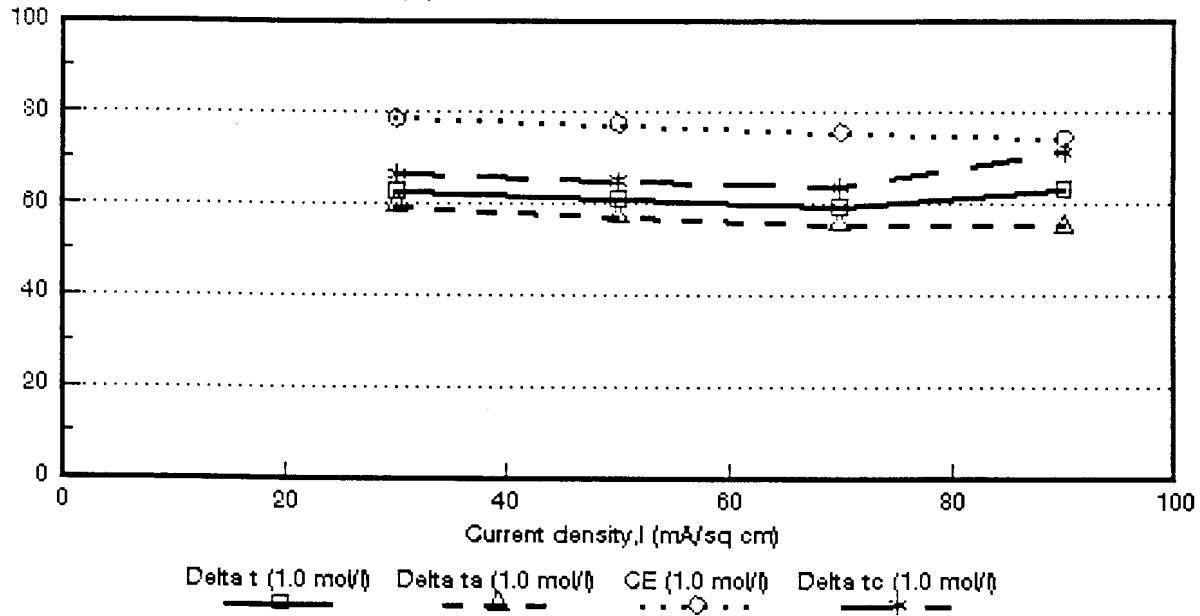


Figure 6.61: Current efficiency ($CE = e_p$) and apparent transport numbers as a function of current density for 1,0 mol/l NaCl feed. *Raipore* R4030 and R4010 membranes. $\Delta t = \bar{\Delta}t$; $\Delta t_a = \Delta t^*$; $\Delta t_c = \Delta t^c$.

CE ; Delta t ; Delta ta and Delta tc (%)

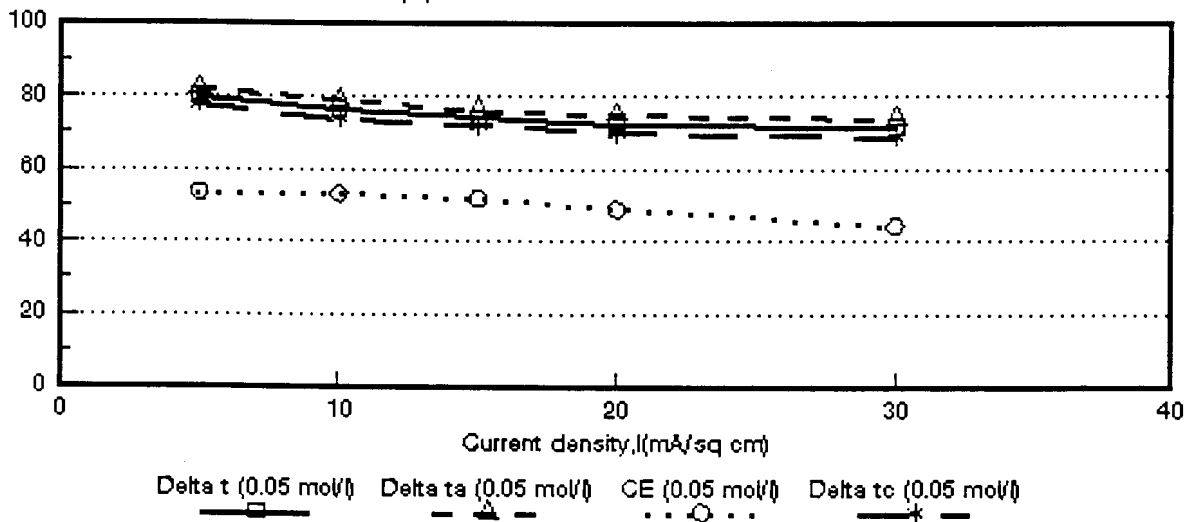


Figure 6.62: Current efficiency ($CE = e_p$) and apparent transport numbers as a function of current density for 0,05 mol/l NaCl feed. *Ionics* A-204-UZL-386 and C-61-CZL-386 membranes. $\Delta t = \bar{\Delta}t$; $\Delta t_a = \Delta t^*$; $\Delta t_c = \Delta t^c$.

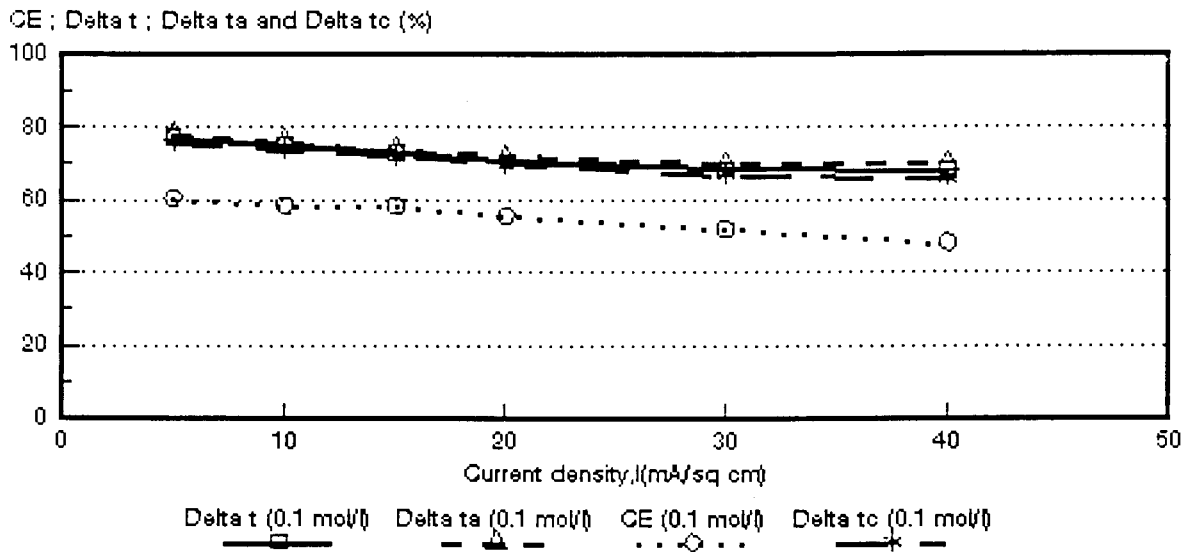


Figure 6.63: Current efficiency ($CE = e_p$) and apparent transport numbers as a function of current density for 0,1 mol/l NaCl feed. *Ionics A-204-UZL-386* and *C-61-CZL-386* membranes. $\Delta t = \bar{\Delta}t$; $\Delta t_a = \Delta t^a$; $\Delta t_c = \Delta t^c$.

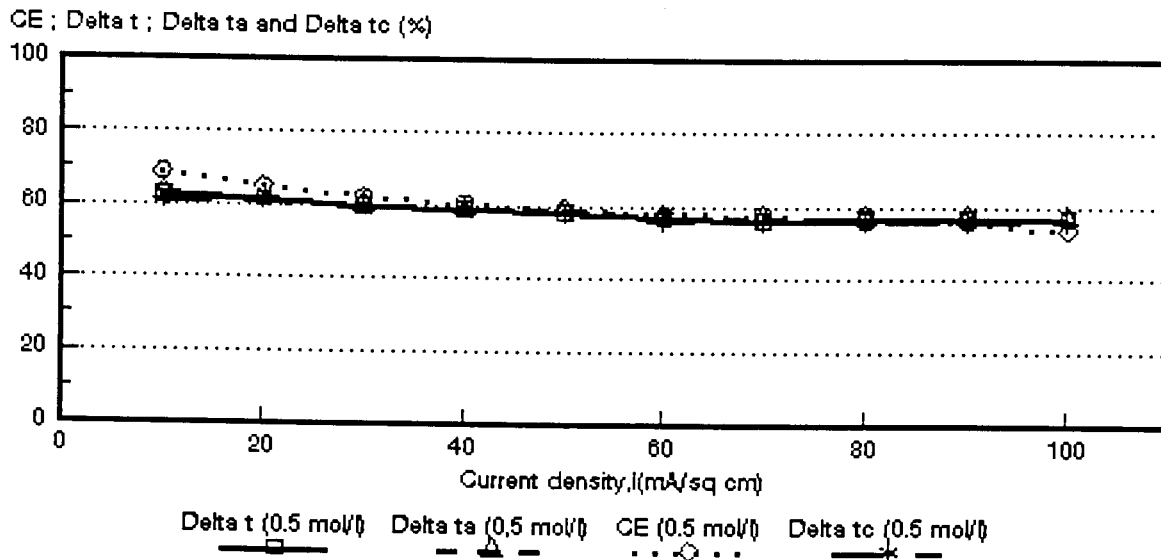


Figure 6.64: Current efficiency ($CE = e_p$) and apparent transport numbers as a function of current density for 0,5 mol/l NaCl feed. *Ionics A-204-UZL-386* and *C-61-CZL-386* membranes. $\Delta t = \bar{\Delta}t$; $\Delta t_a = \Delta t^a$; $\Delta t_c = \Delta t^c$.

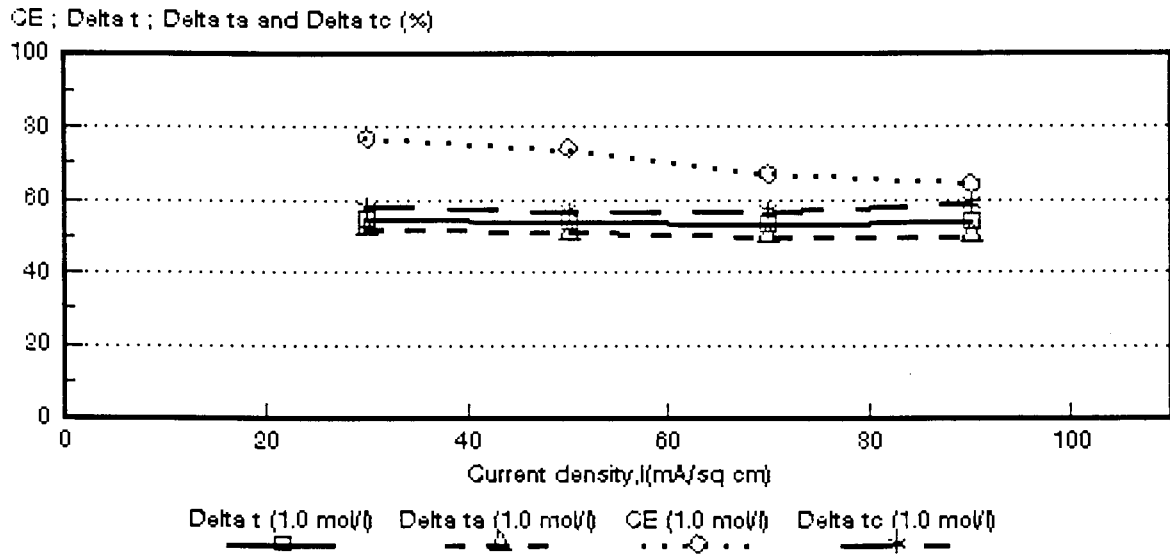


Figure 6.65: Current efficiency ($CE = e_p$) and apparent transport numbers as a function of current density for 1,0 mol/l NaCl feed. *Ionics A-204-UZL-386* and *C-61-CZL-386* membranes. $\Delta t = \bar{\Delta}t$; $\Delta t_a = \Delta t^a$; $\Delta t_c = \Delta t^c$.

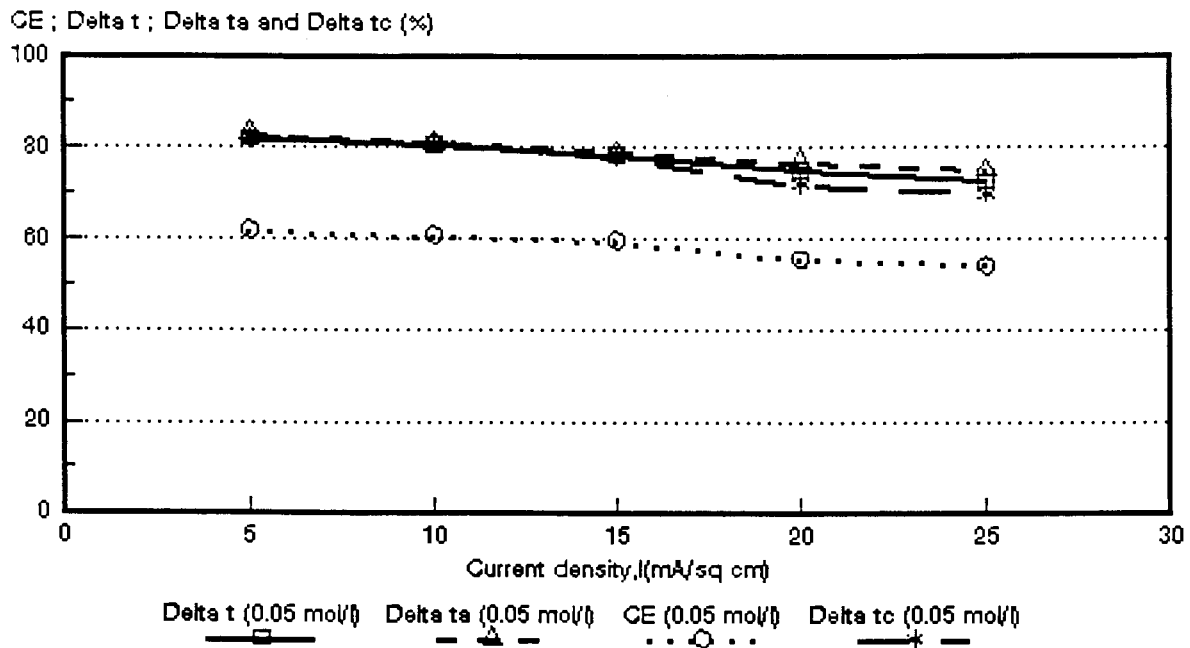


Figure 6.66: Current efficiency ($CE = e_p$) and apparent transport numbers as a function of current density for 0,05 mol/l NaCl feed. *WTPSA-1* and *WTPSC-1* membranes. $\Delta t = \bar{\Delta}t$; $\Delta t_a = \Delta t^a$; $\Delta t_c = \Delta t^c$.

CE ; Delta t ; Delta ta and Delta tc (%)

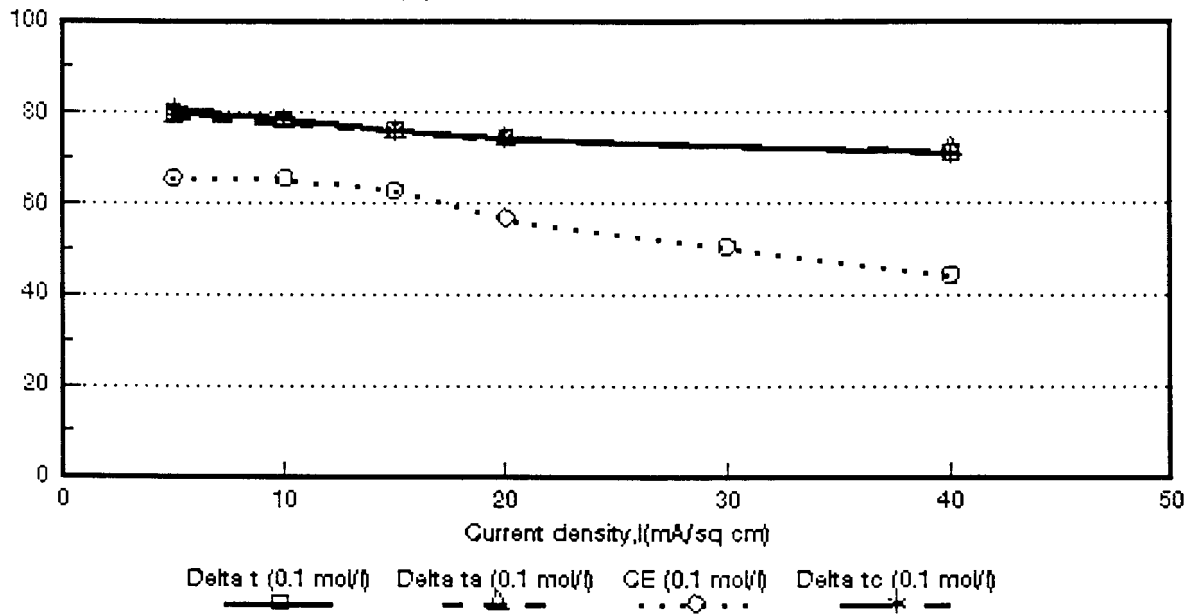


Figure 6.67: Current efficiency ($CE = \epsilon_p$) and apparent transport numbers as a function of current density for 0,1 mol/l NaCl feed. WTPSA-1 and WTPSC-1 membranes. $\Delta t = \bar{\Delta}t$; $\Delta t_a = \Delta t^*$; $\Delta t_c = \Delta t^c$.

CE ; Delta t ; Delta ta and Delta tc (%)

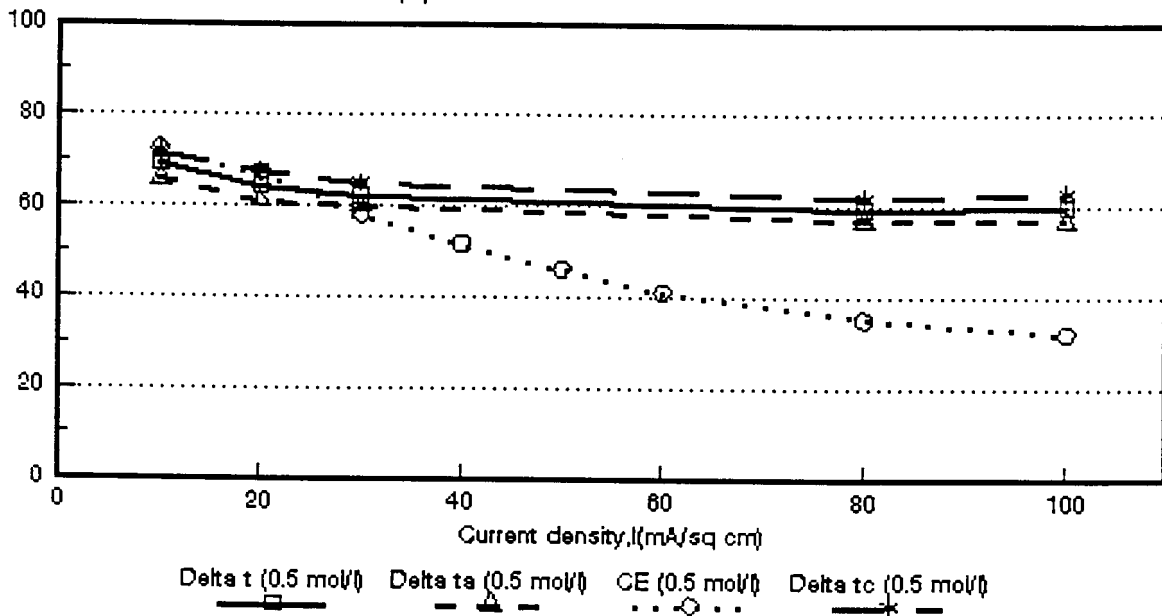


Figure 6.68: Current efficiency ($CE = \epsilon_p$) and apparent transport numbers as a function of current density for 0,5 mol/l NaCl feed. WTPSA-1 and WTPSC-1 membranes. $\Delta t = \bar{\Delta}t$; $\Delta t_a = \Delta t^*$; $\Delta t_c = \Delta t^c$.

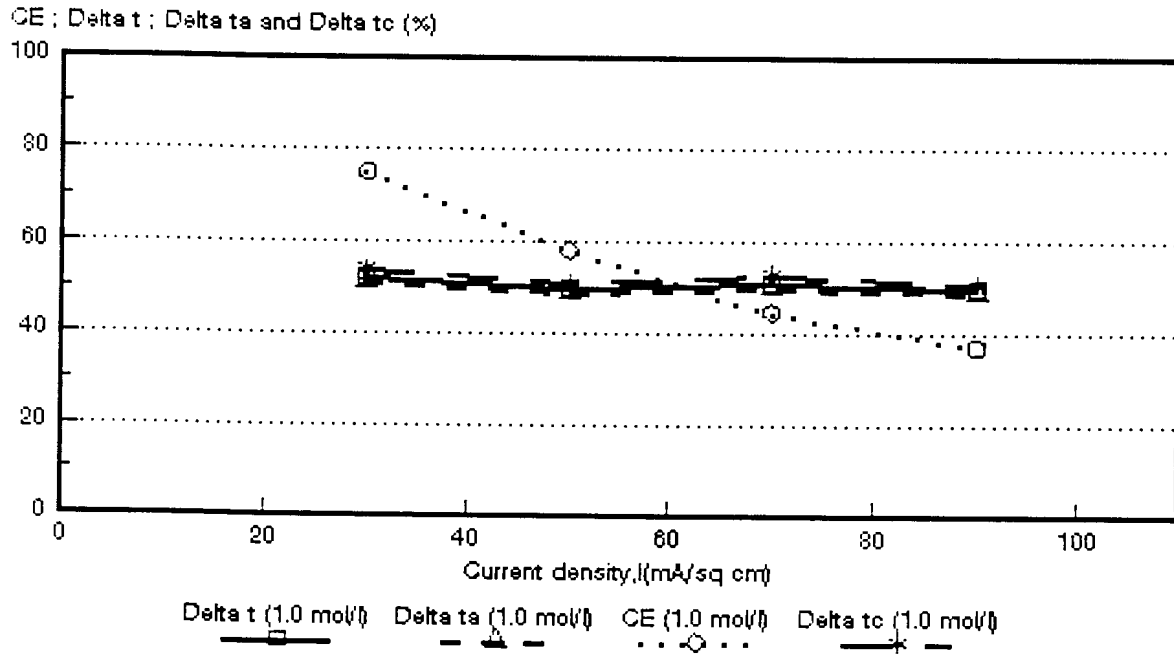


Figure 6.69: Current efficiency ($CE = e_p$) and apparent transport numbers as a function of current density for 1,0 mol/l NaCl feed. WTPSA-1 and WTPSC-1 membranes. $\Delta t = \bar{\Delta}t$; $\Delta ta = \Delta t^*$; $\Delta tc = \Delta t^*$.

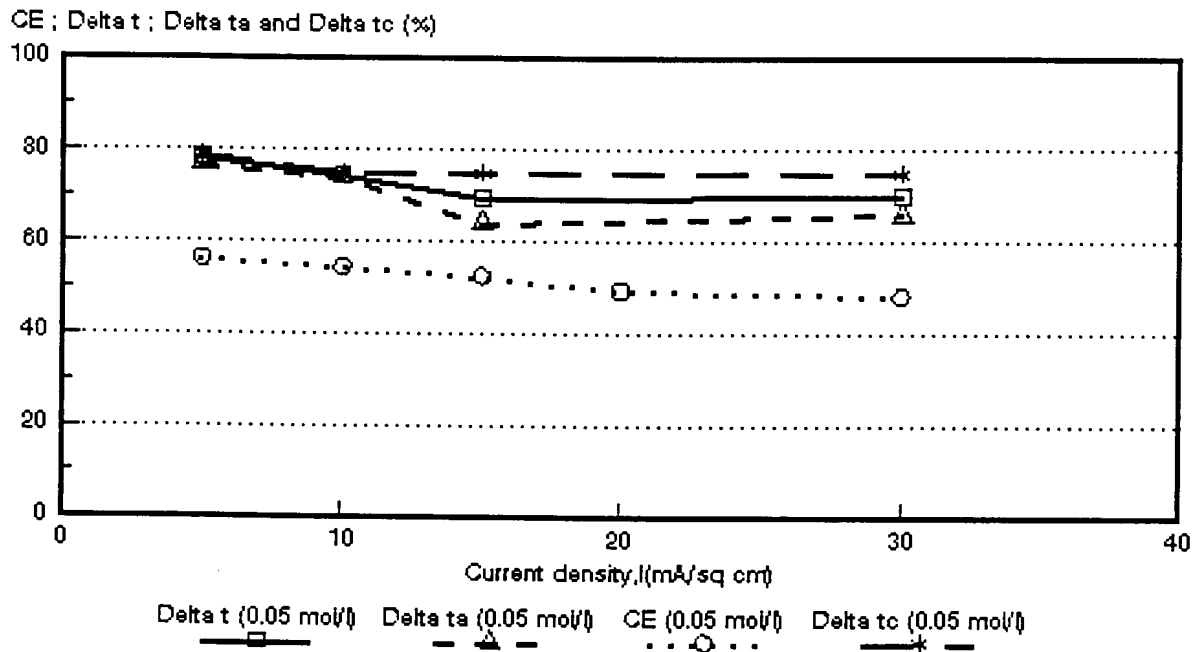


Figure 6.70: Current efficiency ($CE = e_p$) and apparent transport numbers as a function of current density for 0,05 mol/l NaCl feed. WTPVCA-2 and WTPVCC-2 membranes. $\Delta t = \bar{\Delta}t$; $\Delta ta = \Delta t^*$; $\Delta tc = \Delta t^*$.

CE ; Delta t ; Delta ta and Delta tc (%)

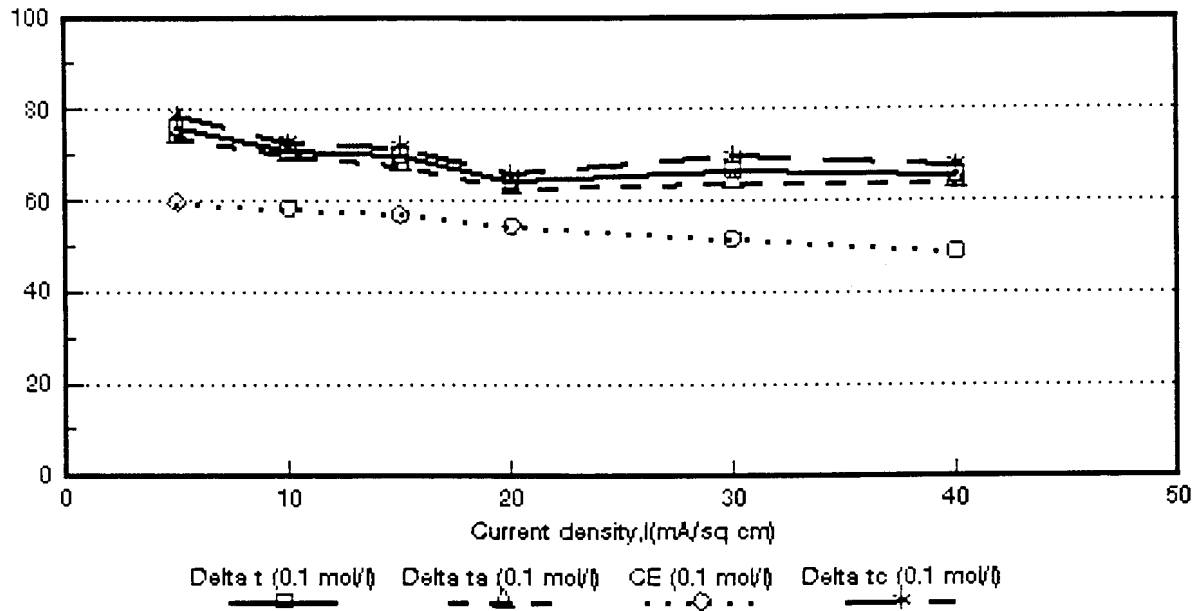


Figure 6.71: Current efficiency ($CE = e_p$) and apparent transport numbers as a function of current density for 0,1 mol/l NaCl feed. WTPVCA-2 and WTPVCC-2 membranes. $\Delta t = \bar{\Delta t}$; $\Delta ta = \Delta t^a$; $\Delta tc = \Delta t^c$.

CE ; Delta t ; Delta ta and Delta tc (%)

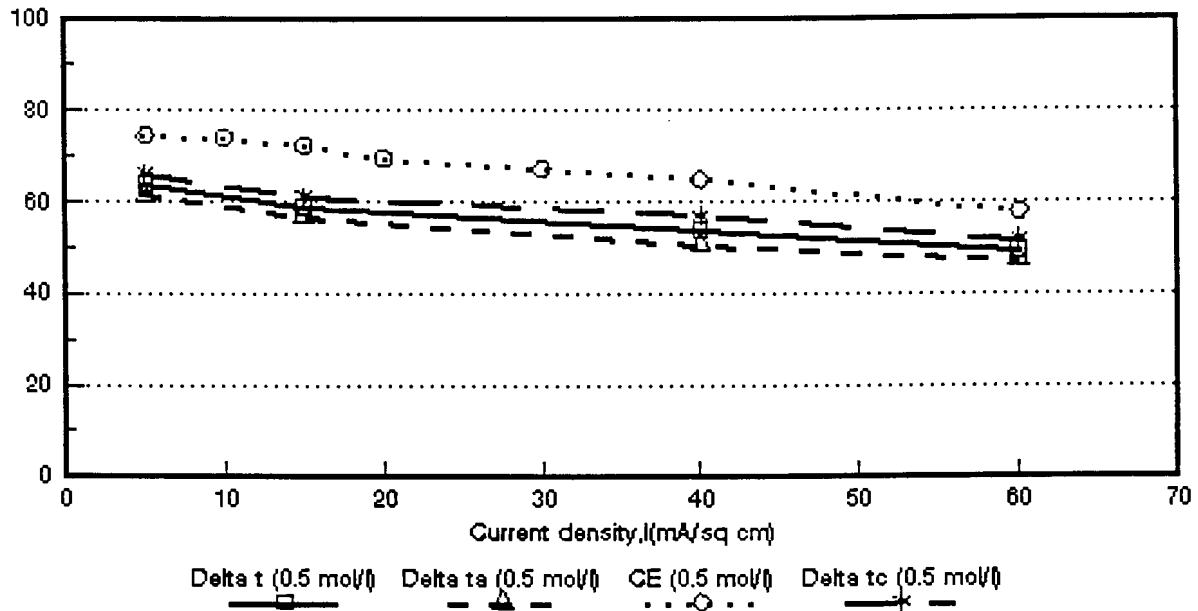


Figure 6.72: Current efficiency ($CE = e_p$) and apparent transport numbers as a function of current density for 0,5 mol/l NaCl feed. WTPVCA-2 and WTPVCC-2 membranes. $\Delta t = \bar{\Delta t}$; $\Delta ta = \Delta t^a$; $\Delta tc = \Delta t^c$.

CE ; Delta t ; Delta ta and Delta tc (%)

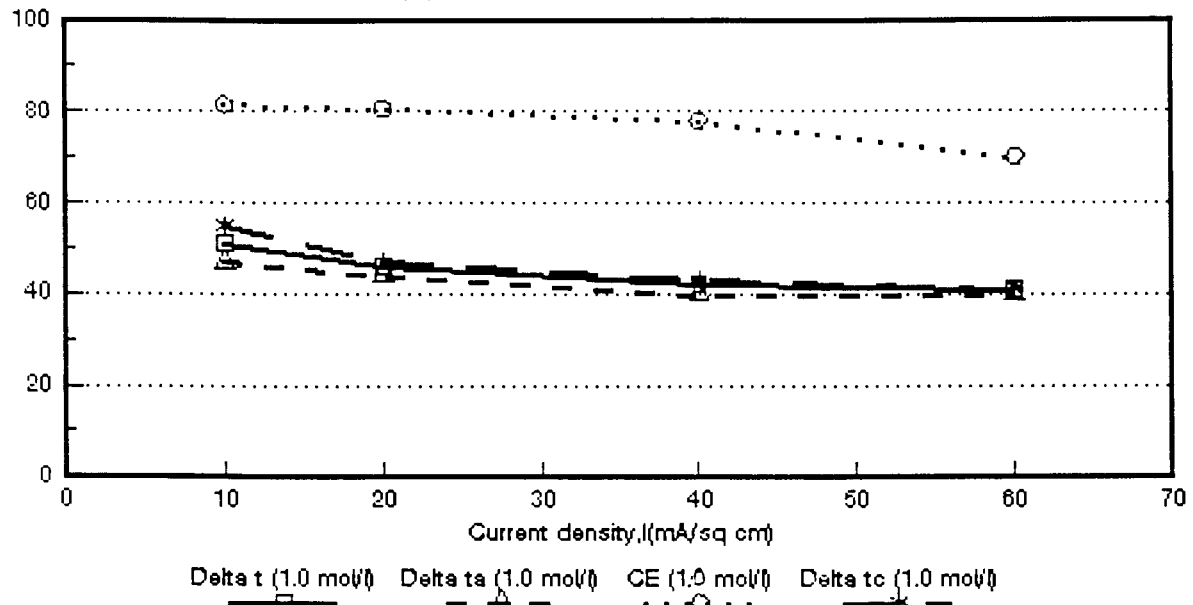


Figure 6.73: Current efficiency ($CE = e_p$) and apparent transport numbers as a function of current density for 1,0 mol/l NaCl feed. WTPVCA-2 and WTPVCC-2 membranes. $\Delta t = \bar{\Delta}t$; $\Delta t_a = \Delta t^a$; $\Delta t_c = \Delta t^c$.

CE ; Delta t ; Delta ta and Delta tc (%)

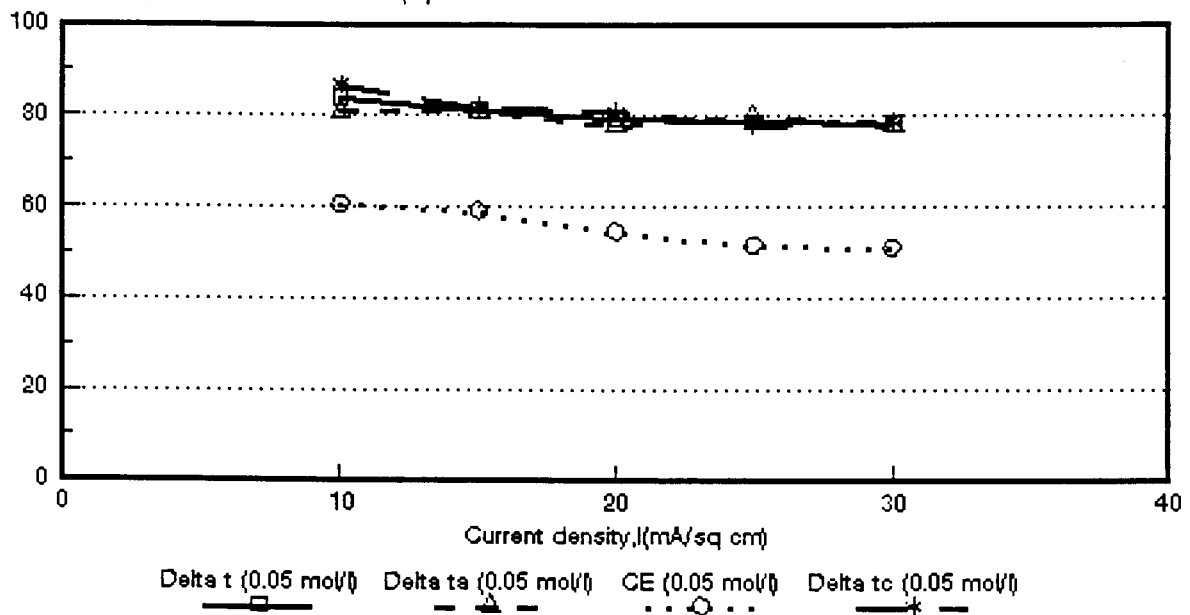


Figure 6.74: Current efficiency ($CE = e_p$) and apparent transport numbers as a function of current density for 0,05 mol/l NaCl feed. WTPSTA-3 and WTPSTC-3 membranes. $\Delta t = \bar{\Delta}t$; $\Delta t_a = \Delta t^a$; $\Delta t_c = \Delta t^c$.

CE ; Delta t ; Delta ta and Delta tc (%)

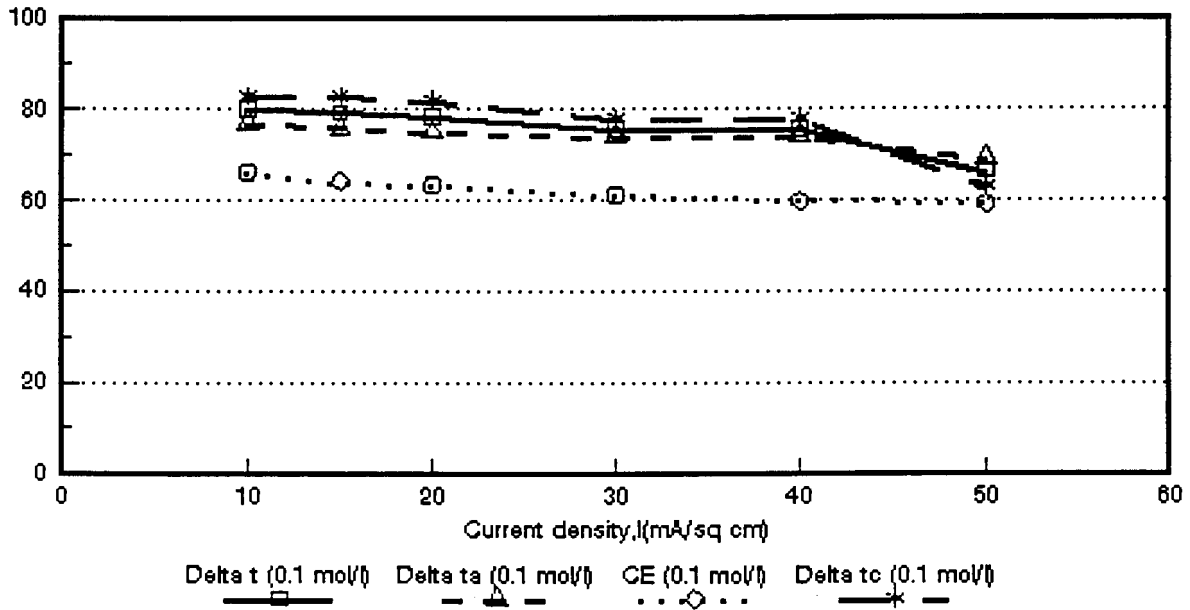


Figure 6.75: Current efficiency ($CE = e_p$) and apparent transport numbers as a function of current density for 0,1 mol/l NaCl feed. WTPSTA-3 and WTPSTC-3 membranes. $\Delta t = \bar{\Delta}t$; $\Delta t_a = \Delta t^a$; $\Delta t_c = \Delta t^c$.

CE ; Delta t ; Delta ta and Delta tc (%)

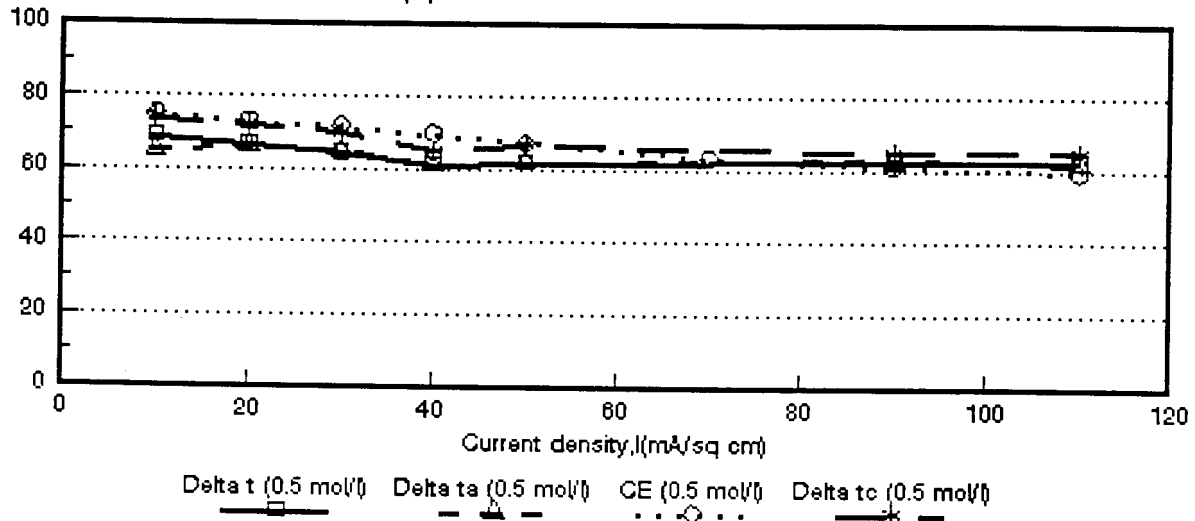


Figure 6.76: Current efficiency ($CE = e_p$) and apparent transport numbers as a function of current density for 0,5 mol/l NaCl feed. WTPSTA-3 and WTPSTC-3 membranes. $\Delta t = \bar{\Delta}t$; $\Delta t_a = \Delta t^a$; $\Delta t_c = \Delta t^c$.

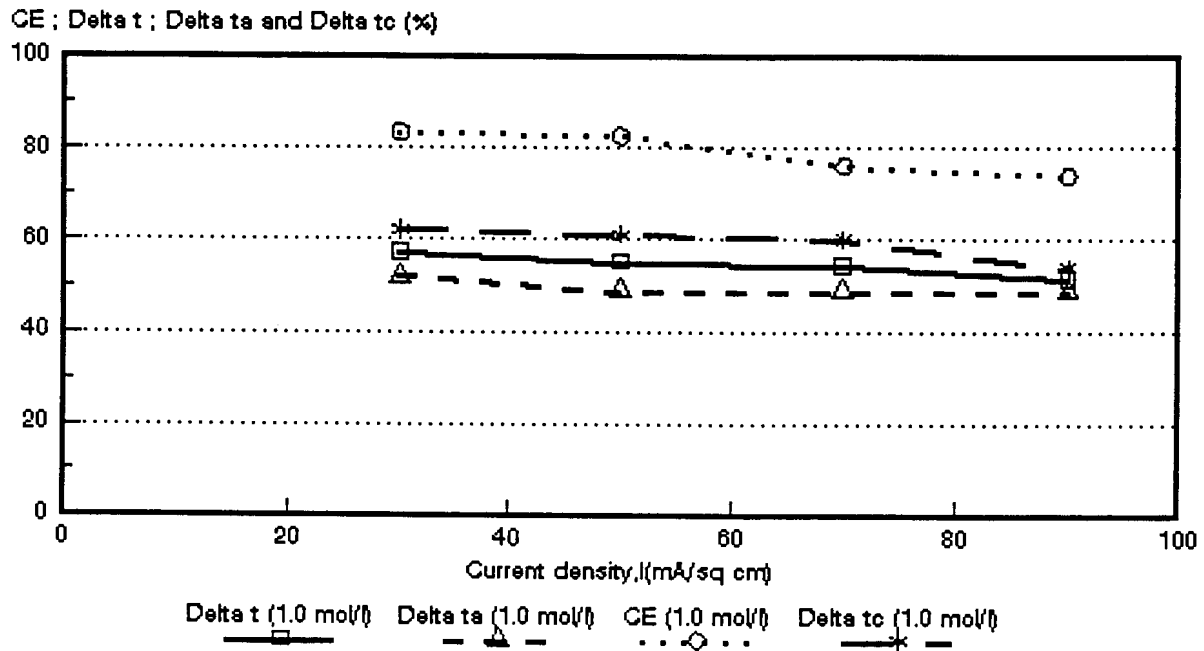


Figure 6.77: Current efficiency ($CE = e_p$) and apparent transport numbers as a function of current density for 1,0 mol/l NaCl feed. WTPSTA-3 and WTPSTC-3 membranes. $\Delta t = \bar{\Delta}t$; $\Delta t_a = \Delta t^a$; $\Delta t_c = \Delta t^c$.

current efficiencies at the higher feed water concentrations (0,5 to 1,0 mol/l). The only exception in this regard was obtained with the *Raipore* membranes where the apparent transport numbers became lower than the current efficiency at 1,0 mol/l feed concentration.

Good correlations were obtained between the apparent transport number of a membrane pair ($\bar{\Delta}t$) and current efficiency (e_p) for all the membranes investigated depending on the feed concentration and current density used (Table 6.32). The ratio between $\bar{\Delta}t/e_p$ for the *Selemion* membranes varied between 1,01 and 1,07 in the current density range from 15 to 50 mA/cm² (0,1 mol/l feed). This ratio for the *Ionac* membranes varied between 0,95 to 1,09 in the current density range from 40 to 70 mA/cm² (0,5 mol/l feed). For the *Raipore* membranes the ratio ($\bar{\Delta}t/e_p$) varied between 0,94 and 1,05 in the current density range from 40 to 90 mA/cm² (0,5 mol/l feed). For the *Ionics* membranes the ratio varied between 0,95 and 1,02 in the current density range from 20 to 90 mA/cm² (0,5 mol/l feed). A good correlation was obtained

between $\bar{\Delta}t$ and ϵ_p (0,95 to 1,07 at 0,5 mol/l feed) for the WTPS membranes in the current density range from 10 to 30 mA/cm². The correlations, however, at high current densities (Table 6.32, 80 mA/cm²) were not very good due to polarization that was taking place. Relatively good correlations were also obtained between $\bar{\Delta}t$ and ϵ_p for the WTPVC and WTPST membranes. The correlation varied between 0,82 to 0,86 (5 to 60 mA/cm², WTPVC) and between 0,88 and 1,04 (10 to 110 mA/cm², WTPST) at 0,5 mol/l feed concentration. The ratio between $\bar{\Delta}t/\epsilon_p$ varied between approximately 0,82 and 1,09 in the feed concentration range from 0,1 to 0,5 mol/l for the different membranes investigated. Therefore, it appears that apparent transport numbers determined from a simple membrane potential method should give a good approximate estimation of membrane performance for ED concentration/desalination applications. Membrane performance for concentration/desalination applications should be predicted with an accuracy of approximately 10% from membrane potential measurements depending on the feed concentration and current density used.

The apparent transport numbers of the anion- (Δt^a) and cation (Δt^c) membranes should also be used to predict membrane performance for concentration/desalination applications (Tables 6.33 and 6.34). However, the accuracy of the prediction will depend on the feed concentration and current density used.

Table 6.32: Correlation between apparent transport number for a membrane pair ($\bar{\Delta}t$) and current efficiency (e_p).

Current Density mA/cm ²	$\bar{\Delta}t/e_p$																															
	Selemion AMV & CMV Concentration, mol/t				Ionac MA-3475 & MC-3470 Concentration, mol/t				Raipore R4030 & R4010 Concentration, mol/t				Ionica A-204-UZL & C-61-CZL Concentration, mol/t				WTPS WTPSA & WTPSC Concentration, mol/t				WTPVC WTPVCA & WTPVCC Concentration, mol/t				WTPST WTPSTA & WTPSTC Concentration, mol/t							
	0,05	0,1	0,5	1,0	0,05	0,1	0,5	1,0	0,05	0,1	0,5	1,0	0,05	0,1	0,5	1,0	0,05	0,1	0,5	1,0	0,05	0,1	0,5	1,0	0,05	0,1	0,5	1,0				
5	1,39	1,19	0,99		1,21	1,19	0,72		1,68	1,37	1,47		1,49	1,27			1,32	1,22			1,41	1,27	0,86									
10	1,28	1,13	0,85	0,82	1,29	1,23	0,87		1,54	1,25	1,34		1,43	1,28	0,90		1,33	1,21	0,95		1,36	1,21		0,82	1,39	1,21	0,92					
15	1,27	1,07			1,33	1,25			1,58				1,43	1,25			1,32	1,21			1,34	1,23	0,82		1,37	1,23						
20	1,25	1,06	0,79	0,78	1,41	1,20	0,83	0,69	1,62	1,21	1,21		1,49	1,28	0,95		1,35	1,30	0,95		1,19	1,19		0,57	1,46	1,23	0,90					
25					1,41												1,35								1,52							
30	1,23	1,05	0,82	0,77		1,25			1,59	1,19	1,12	0,80	1,61	1,32	0,96	0,72			1,07	0,69	1,45	1,30			1,55	1,24	0,90	0,68				
40		1,04	0,78	0,77		1,28	0,95	0,75		1,15	1,05			1,41	0,99			1,60				1,35	0,83	0,54		1,27	0,88					
50		1,01	0,78	0,73		1,34	1,01			1,16	1,02	0,79			0,98	0,73				0,86						1,11	0,92	0,67				
60			0,78	0,74			1,09	0,80			1,05				0,98								0,85	0,58								
70							1,09				0,94	0,79			0,97	0,79				1,14						0,84	0,72					
80								0,75							1,01				1,70													
90											1,03	0,84			1,02	0,84				1,35							1,03	0,70				
100															1,06				1,87													
110																											1,04					

Table 6.33: Correlation between apparent transport number of the anion membrane (Δt^*) and current efficiency (ϵ_p).

Current Density mA/cm ²	$\Delta t^*/\epsilon_p$																											
	Selemion AMV & CMV Concentration, mol/t				Ionac MA-3475 & MC-3470 Concentration, mol/t				Raipore R4030 & R4010 Concentration, mol/t				Ionics A-204-UZL & C-61-CZL Concentration, mol/t				WTPS WTPSA & WTPSC Concentration, mol/t				WTPVC WTPVCA & WTPVCC Concentration, mol/t				WTPST WTPSTA & WTPSTC Concentration, mol/t			
	0,05	0,1	0,5	1,0	0,05	0,1	0,5	1,0	0,05	0,1	0,5	1,0	0,05	0,1	0,5	1,0	0,05	0,1	0,5	1,0	0,05	0,1	0,5	1,0	0,05	0,1	0,5	1,0
5	1,31	1,11	0,86		1,13	1,07	0,59		1,72	1,37	1,36		1,53	1,29			1,34	1,20			1,37	1,24	0,82					
10	1,24	1,04	0,75	0,70	1,18	1,09	0,70		1,62	1,27	1,24		1,49	1,30	0,92		1,33	1,19	0,91		1,36	1,20		0,58	1,34	1,16	0,87	
15	1,20	0,98			1,19	1,10			1,69				1,47	1,27			1,33	1,21			1,22	1,20	0,78		1,37	1,18		
20	1,16	0,96	0,69	0,63	1,32	1,06	0,66	0,58	1,73	1,23	1,13		1,53	1,29	0,95		1,38	1,30	0,90		0,99	1,18		0,55	1,43	1,19	0,83	
25					1,28												1,38								1,55			
30	1,14	0,97	0,68	0,61		1,11			1,72	1,22	1,05	0,75	1,67	1,34	0,96	0,68			1,03	0,68	1,37	1,24			1,53	1,21	0,82	0,62
40		0,91	0,66	0,60		1,13	0,75	0,63		1,16	0,98			1,46	0,97			1,62				1,31	0,77	0,51		1,24	0,83	
50		0,94	0,64	0,58		1,16	0,80			1,18	0,92	0,73			0,99	0,69				0,84						1,17	0,85	0,59
60			0,62	0,57			0,90	0,66			0,98				0,98								0,81	0,57				
70							0,89				0,87	0,74			0,99	0,74											0,84	0,64
80								0,62							1,01				1,62									
90											0,86	0,74			1,02	0,78											0,96	0,66
100															1,06					1,78								
110																											1,01	

Table 6.34: Correlation between apparent transport number of the cation membrane (Δt°) and current efficiency (ϵ_p).

Current Density mA/cm ²	$\Delta t^{\circ}/\epsilon_p$																												
	Selemion AMV & CMV Concentration, mol/l				Ionac MA-3475 & MC-3470 Concentration, mol/l				Raipore R4030 & R4010 Concentration, mol/l				Ionics A-204-UZL & C-61-CZL Concentration, mol/l				WTPS WTPSA & WTPSC Concentration, mol/l				WTPVC WTPVCA & WTPVCC Concentration, mol/l				WTPST WTPSTA & WTPSTC Concentration, mol/l				
	0,05	0,1	0,5	1,0	0,05	0,1	0,5	1,0	0,05	0,1	0,5	1,0	0,05	0,1	0,5	1,0	0,05	0,1	0,5	1,0	0,05	0,1	0,5	1,0	0,05	0,1	0,5	1,0	
5	1,46	1,29	1,12		1,31	1,30	0,83		1,62	1,37	1,60		1,46	1,26			1,32	1,23			1,41	1,32	0,89						
10	1,33	1,20	0,96	0,94	1,41	1,37	1,04		1,46	1,23	1,43		1,40	1,27	0,89		1,33	1,21	0,99		1,38	1,25		0,67	1,44	1,26	0,99		
15	1,31	1,16			1,46	1,39			1,48				1,39	1,23			1,31	1,21			1,43	1,27	0,84		1,39	1,29			
20	1,33	1,16	0,88	0,94	1,48	1,36	0,99	0,81	1,52	1,20	1,30		1,43	1,26	0,94		1,29	1,30	1,01		1,38	1,21		0,58	1,48	1,30	0,98		
25	1,31				1,55												1,29								1,51				
30		1,12	0,98	0,91		1,40			1,46	1,15	1,20	0,85	1,56	1,29	0,96	0,75			1,17	0,72	1,56	1,35			1,55	1,27	0,97	0,74	
40		1,19	0,89	0,94		1,43	1,15	0,88		1,15	1,13			1,37	0,97			1,60				1,39	0,86	0,55		1,30	0,93		
50		1,08	0,92	0,88		1,50	1,23			1,13	1,10	0,84			0,98	0,77				0,88						1,06	1,00	0,74	
60			0,93	0,91			1,28	0,93			1,13				0,97							0,88	0,58						
70						1,31					0,99	0,84			0,97	0,85				1,19							0,84	0,79	
80								0,88							1,00				1,76										
90											1,02	0,95			1,00	0,92				1,37							1,06	0,73	
100															1,04				1,96										
110																												1,09	

6.3 Water Flow

Water flow (J) through the membranes as a function of current density and feed water concentration is shown in Figures 6.78 to 6.84. Water flow (J) through the membranes relative to the flow at $J_{0,5 \text{ mol/l}}$ and $J_{0,1 \text{ mol/l}}$ is shown in Table 6.35. Water or volume flow through the membranes increases as a function of both current density and feed water concentration. All the membranes showed an increase in water flow with increasing feed water concentration except the *Selemion* membranes at 1,0 mol/l feed concentration (Table 6.35). It is further interesting to note that water flows are significantly higher at the highest feed concentration (1,0 mol/l) in the case of the *lonac*- (Fig 6.79), *Raipore*- (Fig. 6.80), *Ionics*- (Fig. 6.81), WTPS- (Fig. 6.82), WTPVC- (Fig. 6.83) and WTPST- (Fig. 6.84) membranes. Current efficiencies for these membranes were also the highest at the highest feed concentration when more water flowed through the membranes (see Figs. 6.43 to 6.49). Therefore, it appears that increasing current efficiency is caused by increasing water flow through the membranes. This effect was especially pronounced for the more porous heterogeneous *lonac*-, WTPS-, WTPVC- and WTPST membranes.

Water flow (J) through the membranes as a function of effective current density, I_{eff} , (actual current density times Coulomb efficiency) and feed water concentration for the different membranes are shown in Figures 6.85 to 6.91. Straight lines were obtained at higher values of I_{eff} . The slope of these lines corresponds to the combined electro-osmotic coefficient (2β) of a membrane pair. The electro-osmotic coefficients decreases significantly with increasing feed concentration in the case of the *Selemion*- (Fig. 6.85), *Raipore*- (Fig. 6.87), WTPS- (Fig. 6.89), WTPVC- (Fig. 6.90) and WTPST- (Fig. 6.91) membranes as can be seen from the slopes of the lines.

The electro-osmotic coefficients as a function of feed concentration are shown in Figures 6.92 to 6.98. The reduction in the electro-osmotic coefficients with increasing feed concentration can be ascribed to deswelling of the membranes at high feed concentration^(27, 28, 42 - 44) and/or a reduction in membrane permselectivity at high feed concentration⁽²⁵⁾. This effect was far less for the *lonac*- and *Ionics* membranes. The WTPS membranes, on the other hand, showed an increase in the electro-osmotic coefficient with increasing feed concentration (Fig. 6.96). Therefore, it appears that this hydrophobic membrane starts to swell with increasing feed concentration in the feed concentration range from 0,05 to 0,5 mol/l⁽⁴²⁾.

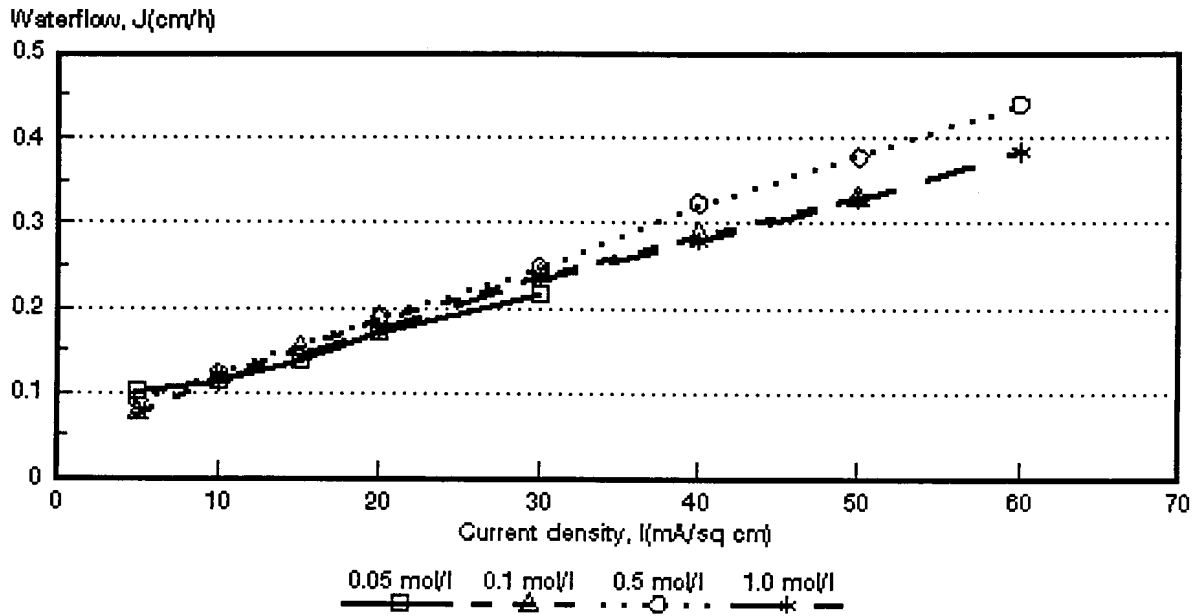


Figure 6.78: Water flow through the Selemion AMV and CMV membranes as a function of current density and feed water concentration.

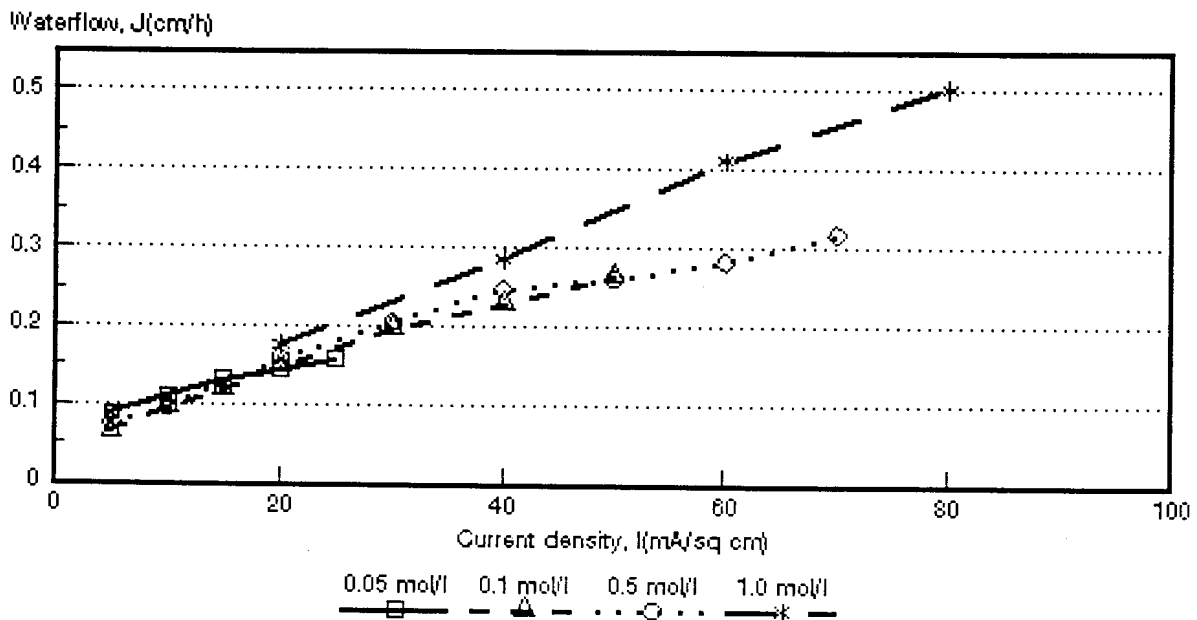


Figure 6.79: Water flow through the Ionac MA-3475 and MC-3470 membranes as a function of current density and feed water concentration.

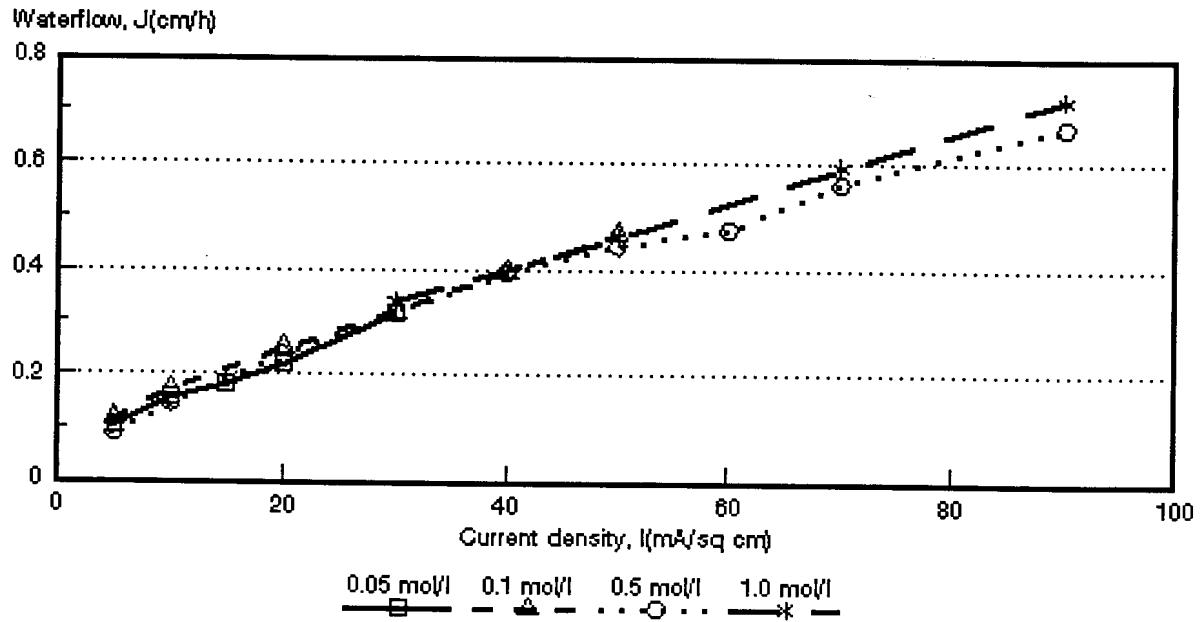


Figure 6.80: Water flow through the Raipore R4030 and R4010 membranes as a function of current density and feed water concentration.

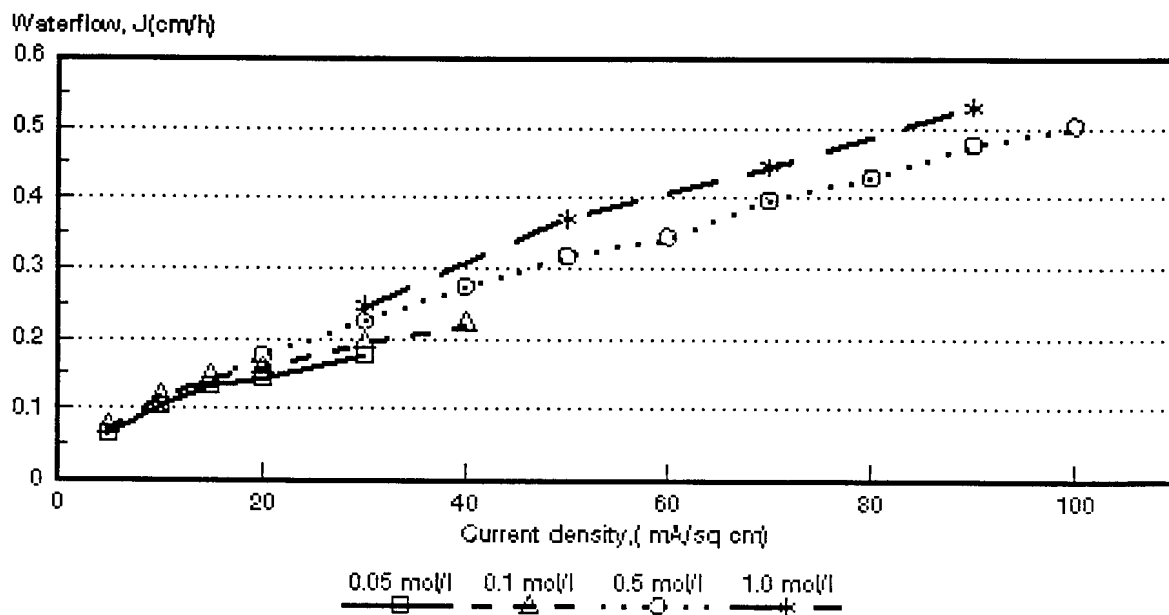


Figure 6.81: Water flow through the Ionics A-204-UZL-386 and C-61-CZL-386 membranes as a function of current density and feed water concentration.

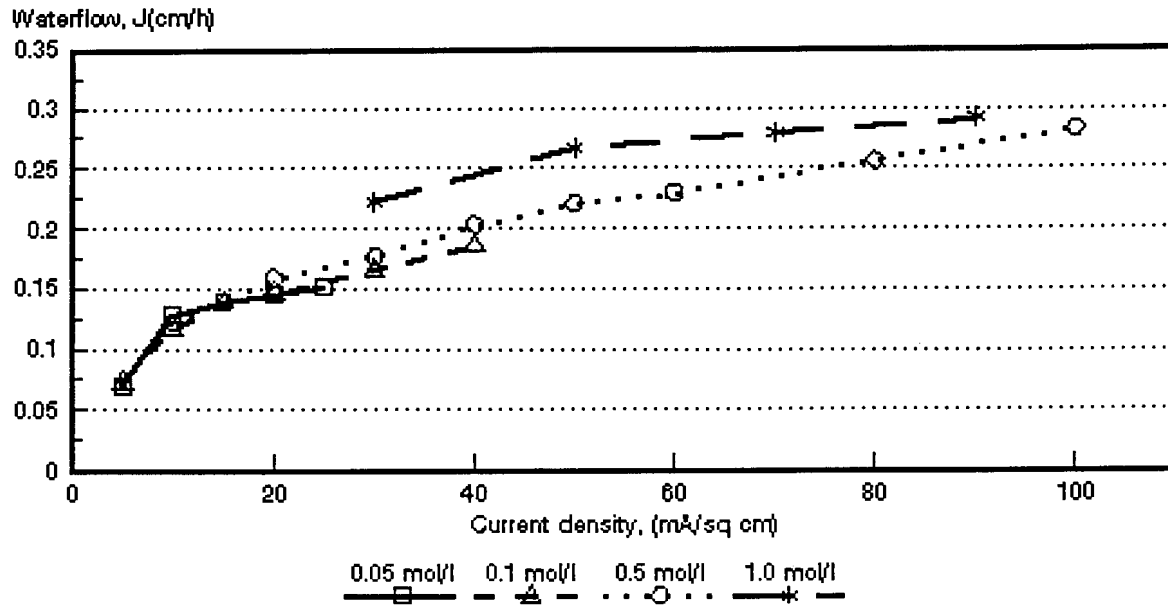


Figure 6.82: Water flow through the WTPSA-1 and WTPSC-1 membranes as a function of current density and feed water concentration.

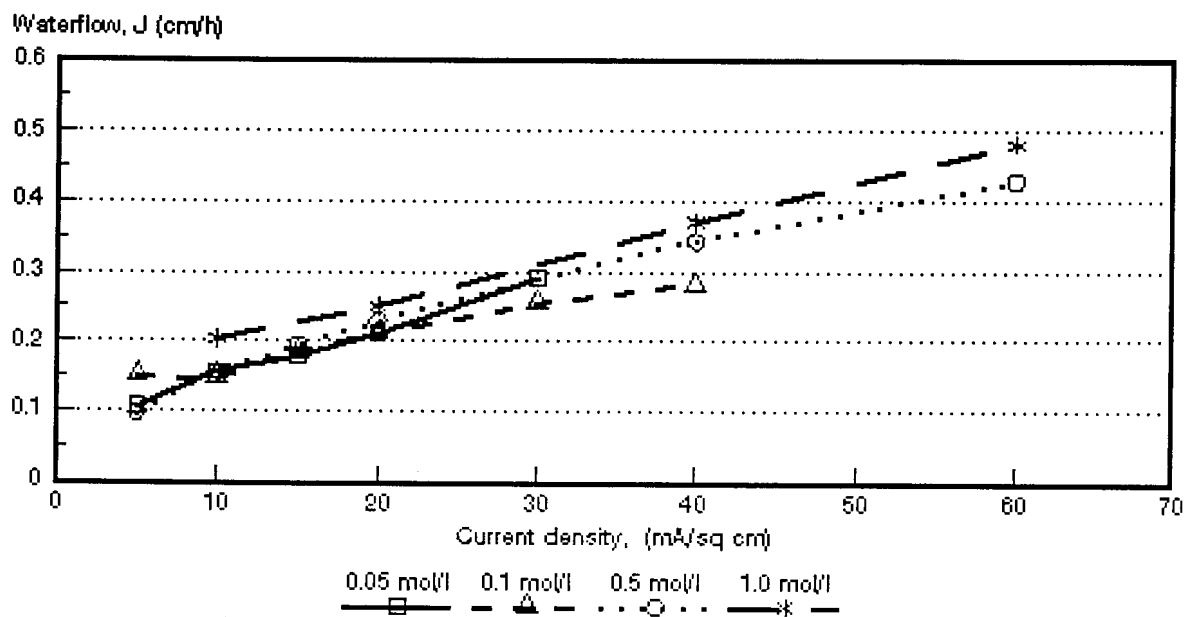


Figure 6.83: Water flow through the WTPVCA-2 and WTPVCC-2 membranes as a function of current density and feed water concentration.

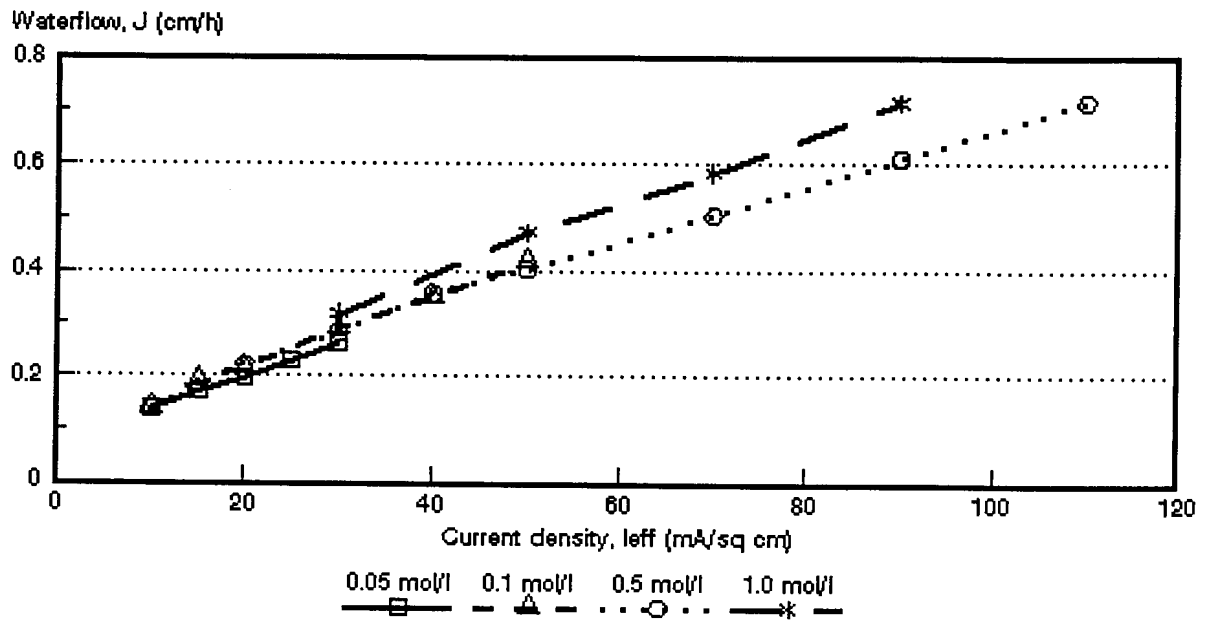


Figure 6.84: Water flow through the WTPSTA-3 and WTPSTC-3 membranes as a function of current density and feed water concentration.

Table 6.35: Water flow (J_i) through the membranes relative to the flow at $J_{0,5 \text{ mol/t}}$ or $J_{0,1 \text{ mol/t}}$

Current Density mA/cm ²	$J/J_{0,5 \text{ mol/t}}$																											
	Selenium AMV & CMV Concentration, mol/t				Ionac MA-3475 & MC-3470 Concentration, mol/t				Raipore R4030 & R4010 Concentration, mol/t				Ionics A-204-UZL & C-61-CZL Concentration, mol/t				WTPS WTPSA & WTPSC Concentration, mol/t				WTPVC WTPVCA & WTPVCC Concentration, mol/t				WTPST WTPSTA & WTPSTC Concentration, mol/t			
	0,05	0,1	0,5	1,0	0,05	0,1	0,5	1,0	0,05	0,1	0,5	1,0	0,05	0,1	0,5	1,0	0,05	0,1	0,5	1,0	0,05	0,1	0,5	1,0	0,05	0,1	0,5	1,0
5	1,14	0,85	1,0		1,17	0,87	1,0		1,18	1,28	1,0		1,0		1,0				1,0		1,11	1,55	1,0				1,0	
10	0,94	0,97	1,0	0,93	1,15	1,03	1,0		1,09	1,18	1,0		1,0	1,1	1,0		1,05	0,96	1,0		1,00	0,95	1,0	1,29	0,99	1,02	1,0	
15			1,0				1,0				1,0				1,0				1,0		0,92	0,95	1,0				1,0	
20	0,89	0,99	1,0	0,92	0,92	0,93	1,0	1,11	0,93	1,05	1,0		0,82	0,90	1,0		0,92	0,92	1,0		0,92	0,97	1,0	1,09	0,88	0,87	1,0	
25			1,0				1,0				1,0				1,0				1,0				1,0				1,0	
30	0,88	0,96	1,0	0,95		0,96	1,0		1,00	1,00	1,0	1,07	0,78	0,88	1,0	1,09		0,94	1,0	1,28	1,00	0,88	1,0		0,94	1,03	1,0	1,12
40		0,89	1,0	0,86		0,93	1,0	1,16		1,01	1,0			0,80	1,0			0,91	1,0			0,82	1,0	1,08		0,98	1,0	
50		0,87	1,0	0,87		1,01	1,0			1,05	1,0	1,04			1,0	1,17			1,0	1,21			1,0			1,04	1,0	1,17
60			1,0	0,87			1,0	1,45			1,0				1,0				1,0				1,0	1,12			1,0	
70 (5)*	(1,34)	(1,0)			(1,33)	(1,0)			(0,92)	(1,0)	1,0	1,06	(0,91)	(1,0)	1,0	1,12	(0,95)	(1,0)				1,0				1,0	1,0	1,18
80(10)*	(0,97)	(1,0)			(1,12)	(1,0)			(0,92)	(1,0)			(0,91)	(1,0)			(1,10)	(1,0)			(0,97)	(1,0)			(0,97)	(1,0)	1,0	
90(15)*	(0,90)	(1,0)			(1,11)	(1,0)			(0,89)	(1,0)	1,0	1,05	(0,91)	(1,0)	1,0	1,11	(1,00)	(1,0)			(0,90)	(1,0)			(0,90)	(1,0)	1,0	1,17
100(20)*	(0,90)	(1,0)			(0,98)	(1,0)			(0,89)	(1,0)			(0,91)	(1,0)			(1,00)	(1,0)			(0,91)	(1,0)			(0,91)	(1,0)	1,0	
110(30)*	(0,91)	(1,0)				(1,0)			(0,99)	(1,0)			(0,92)	(1,0)							(0,91)	(1,0)			(0,91)	(1,0)	1,0	

(*) : $J_{0,05} / J_{0,1}$

i = 0,05; 0,1; 0,5 and 1,0 mol/t

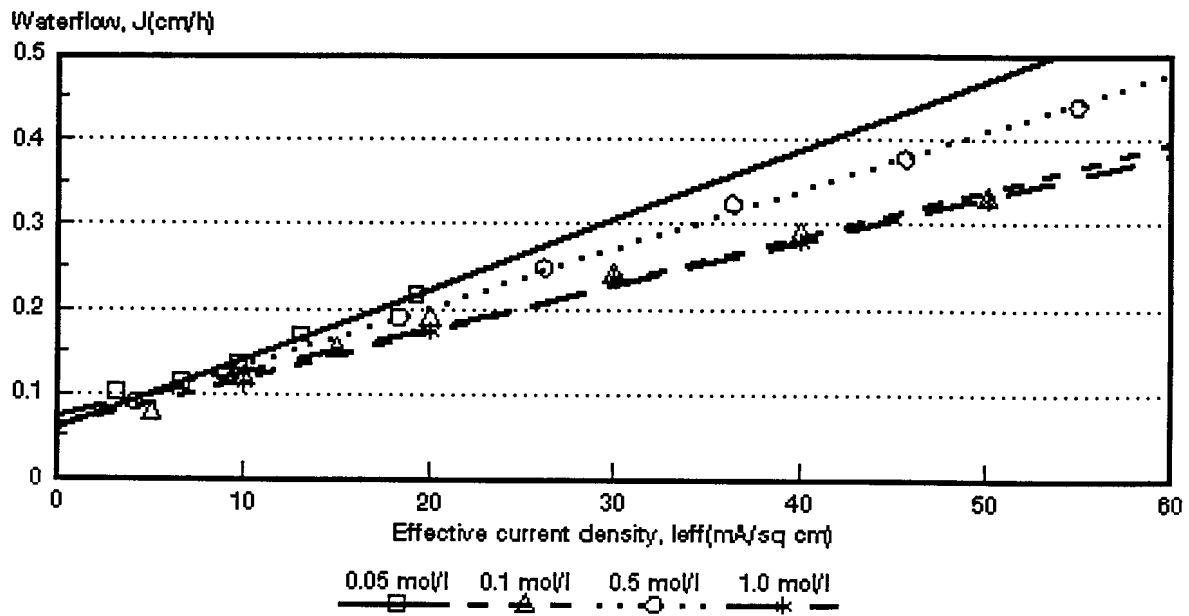


Figure 6.85: Water flow through the *Selemion* AMV and CMV membranes as a function of effective current density and feed water concentration.

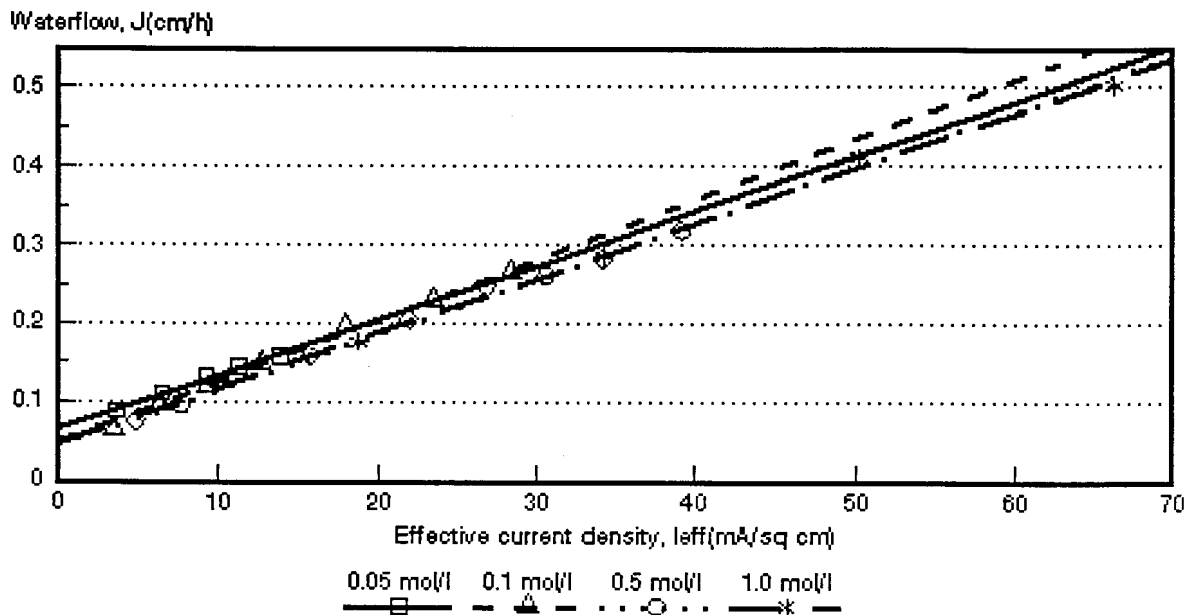


Figure 6.86: Water flow through the *Ionac* MA-3475 and MC-3470 membranes as a function of effective current density and feed water concentration.

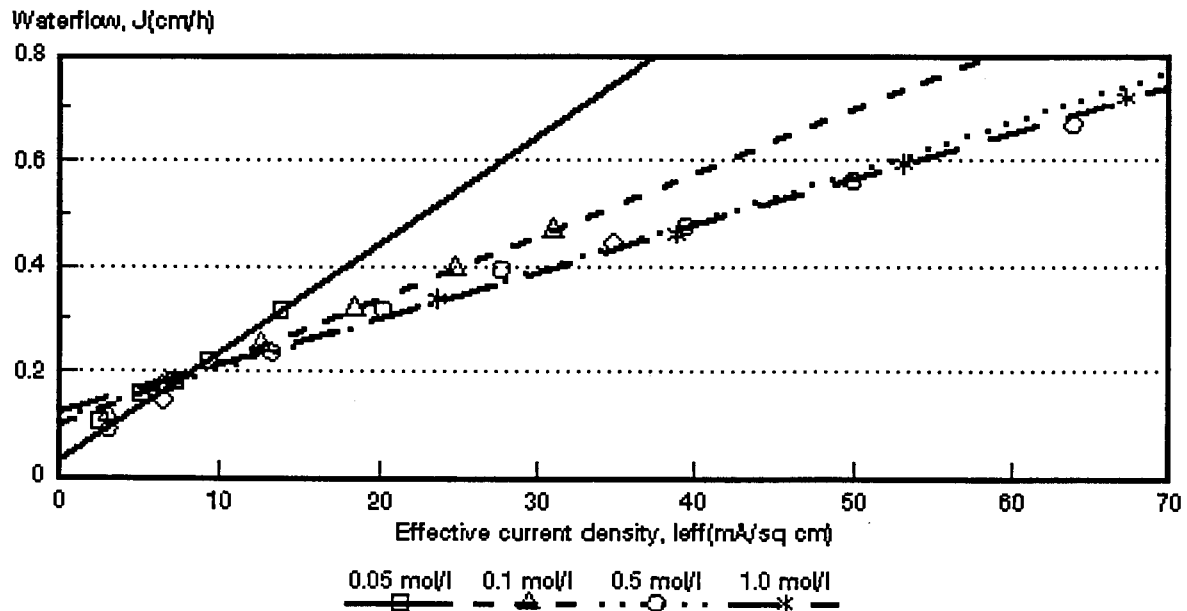


Figure 6.87: Water flow through the *Raipore* R4030 and R4010 membranes as a function of effective current density and feed water concentration.

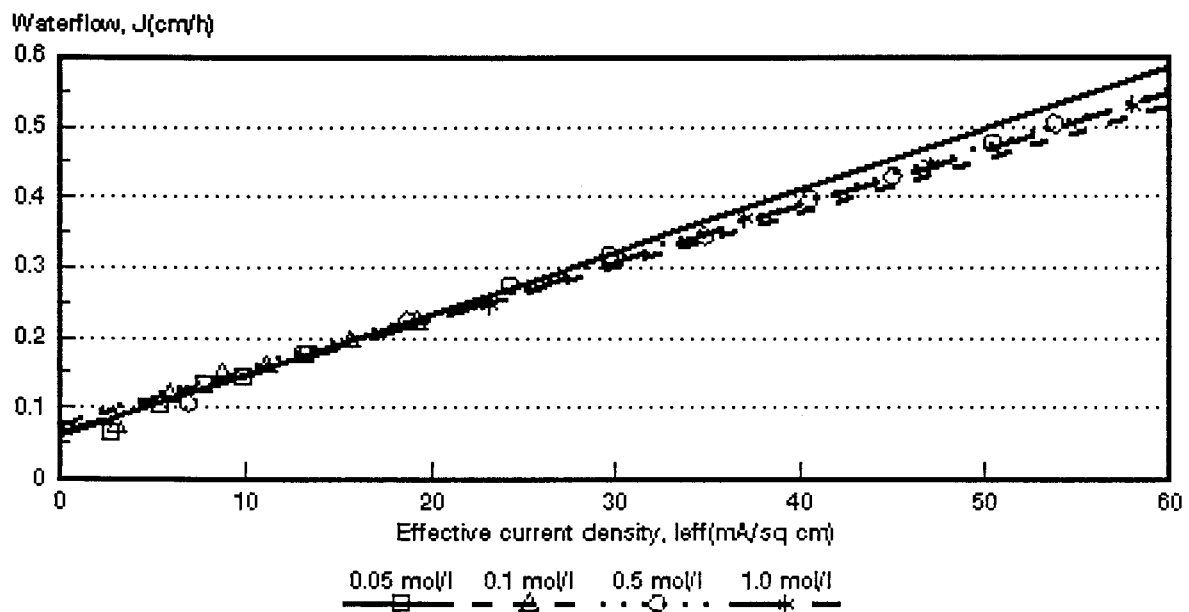


Figure 6.88: Water flow through the *Ionics* A-204-UZL-386 and C-61-CZL-386 membranes as a function of effective current density and feed water concentration.

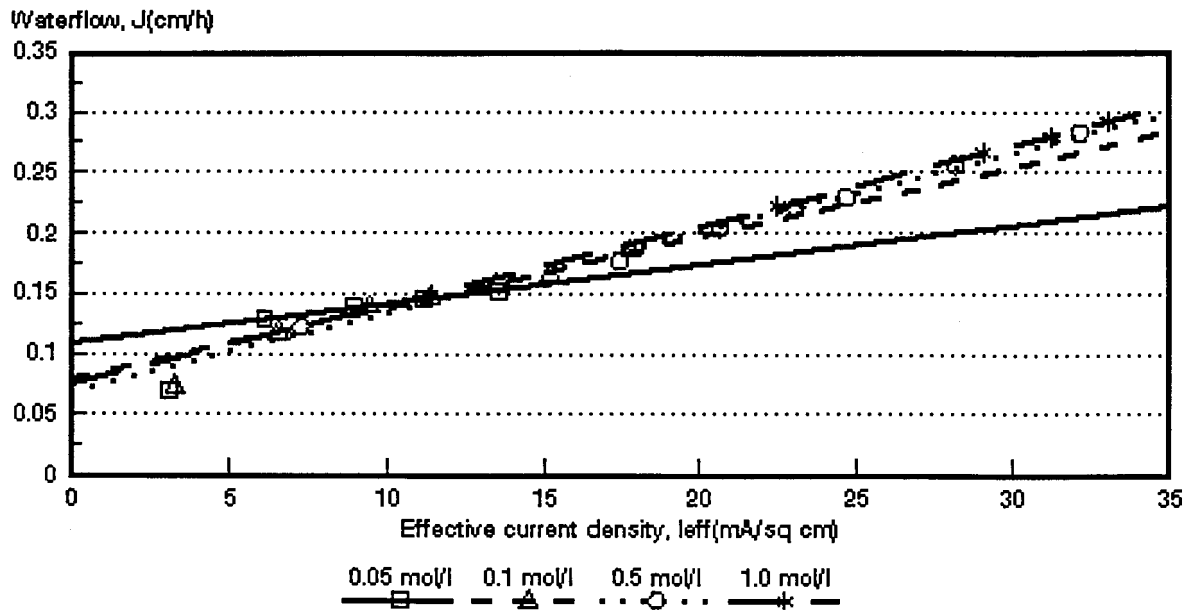


Figure 6.89: Water flow through the WTPSA-1 and WTPSC-1 membranes as a function of effective current density and feed water concentration.

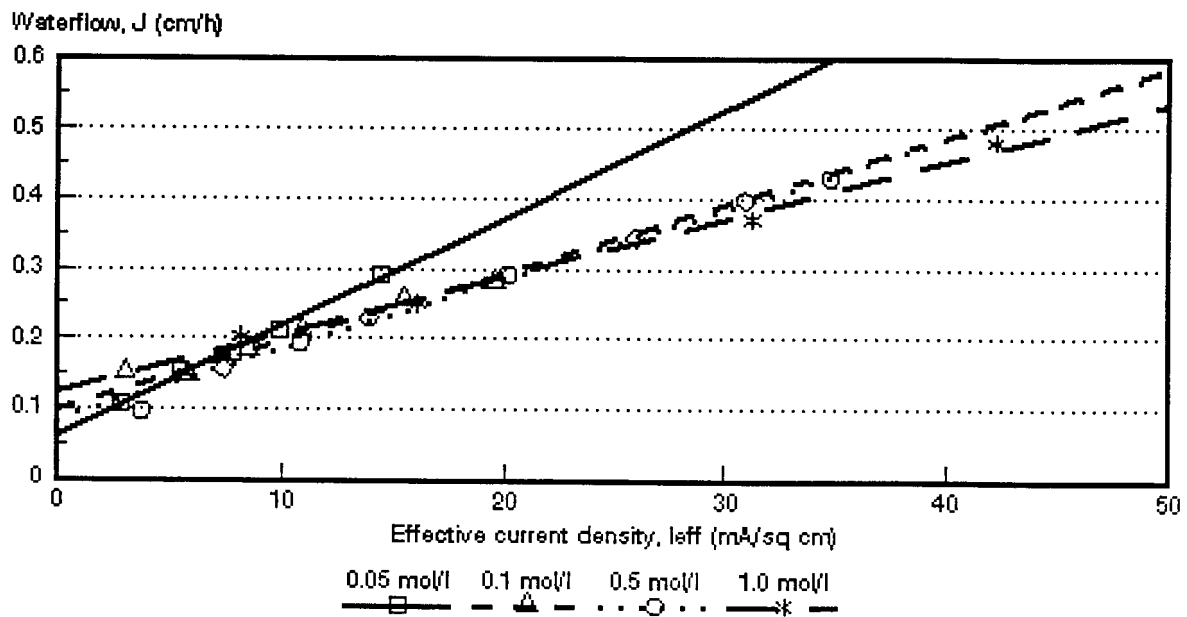


Figure 6.90: Water flow through the WTPVCA-2 and WTPVCC-2 membranes as a function of effective current density and feed water concentration.

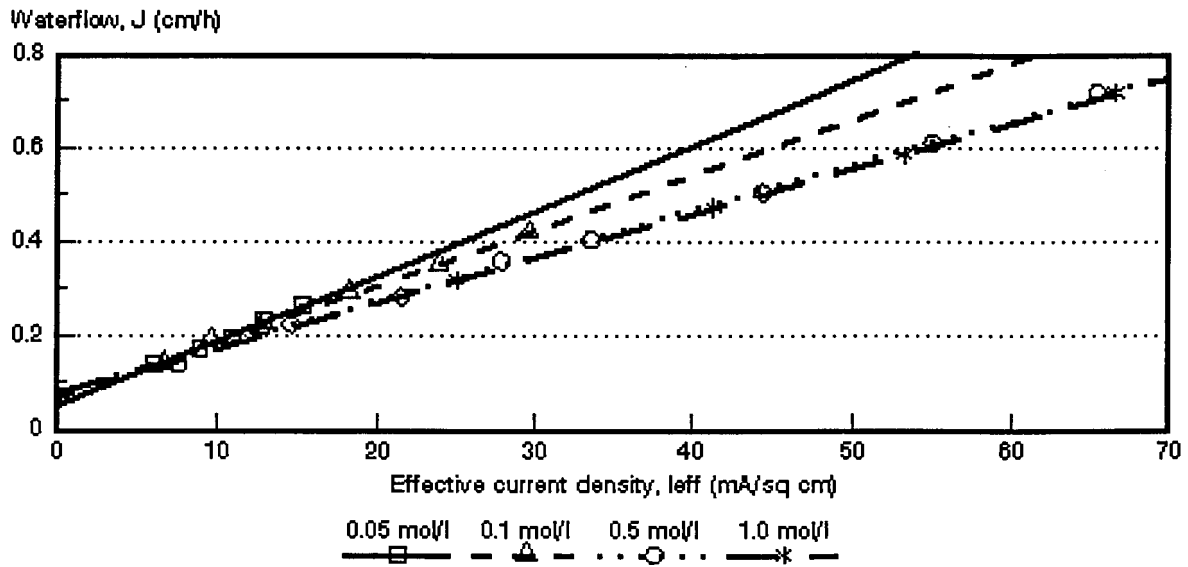


Figure 6.91: Water flow through the WTPSTA-3 and WTPSTC-3 membranes as a function of effective current density and feed water concentration.

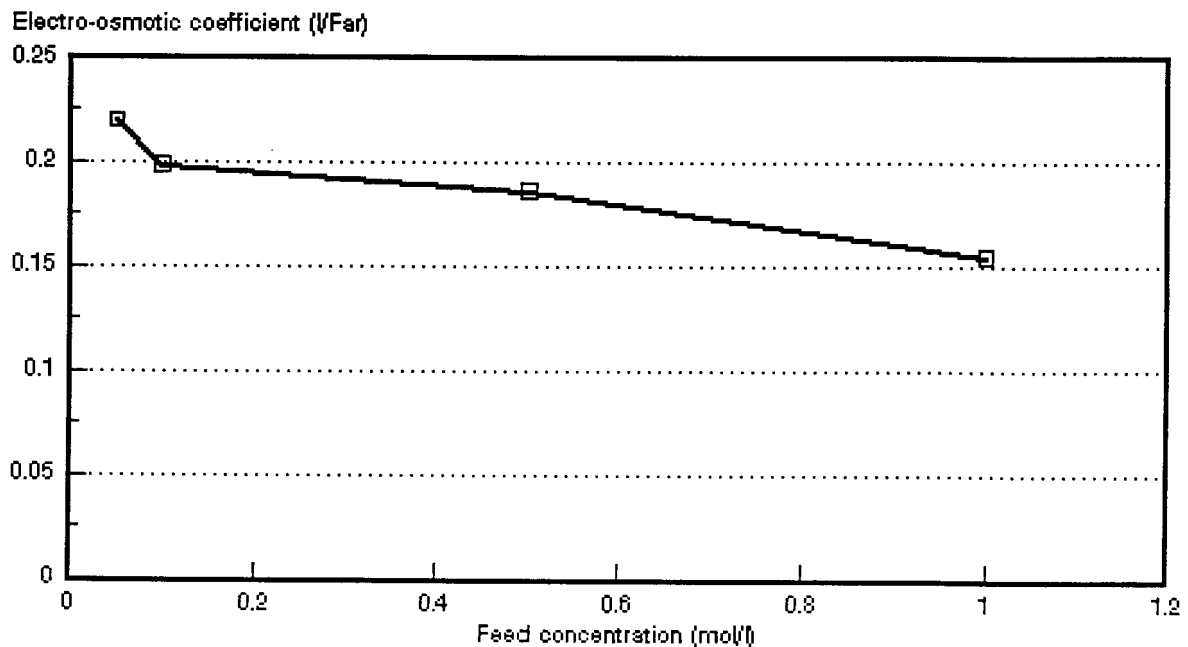


Figure 6.92: Electro-osmotic coefficient as a function of NaCl feed concentration. *Selemion* AMV and CMV membranes.

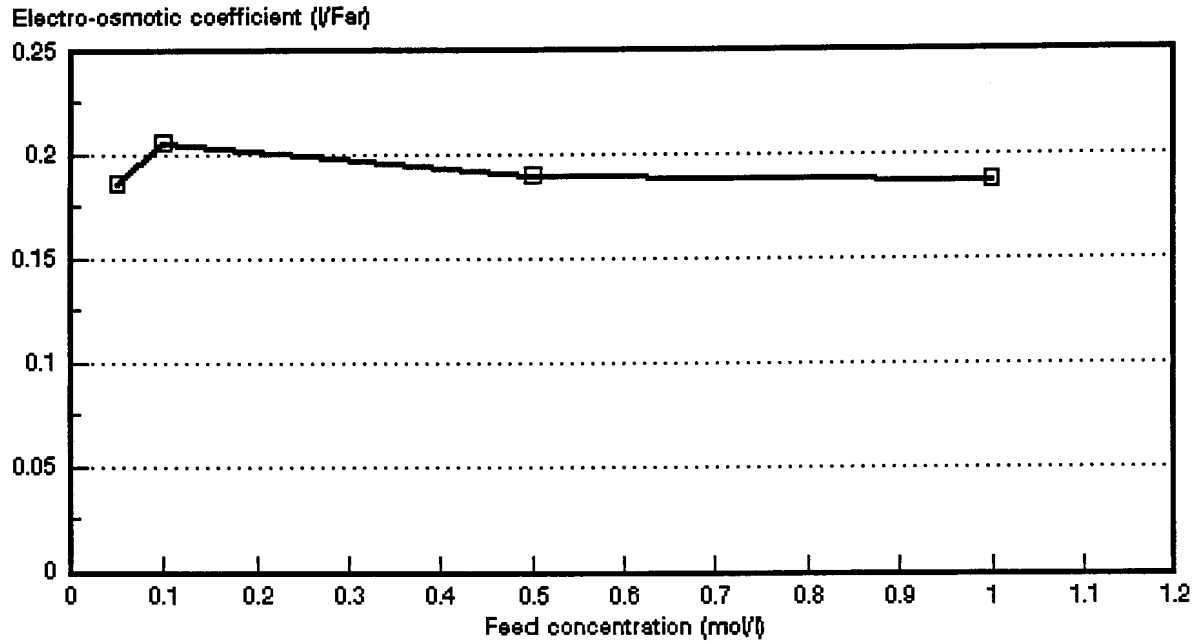


Figure 6.93: Electro-osmotic coefficient as a function of NaCl feed concentrations. *Ionac MA-3475 and MC-3470 membranes.*

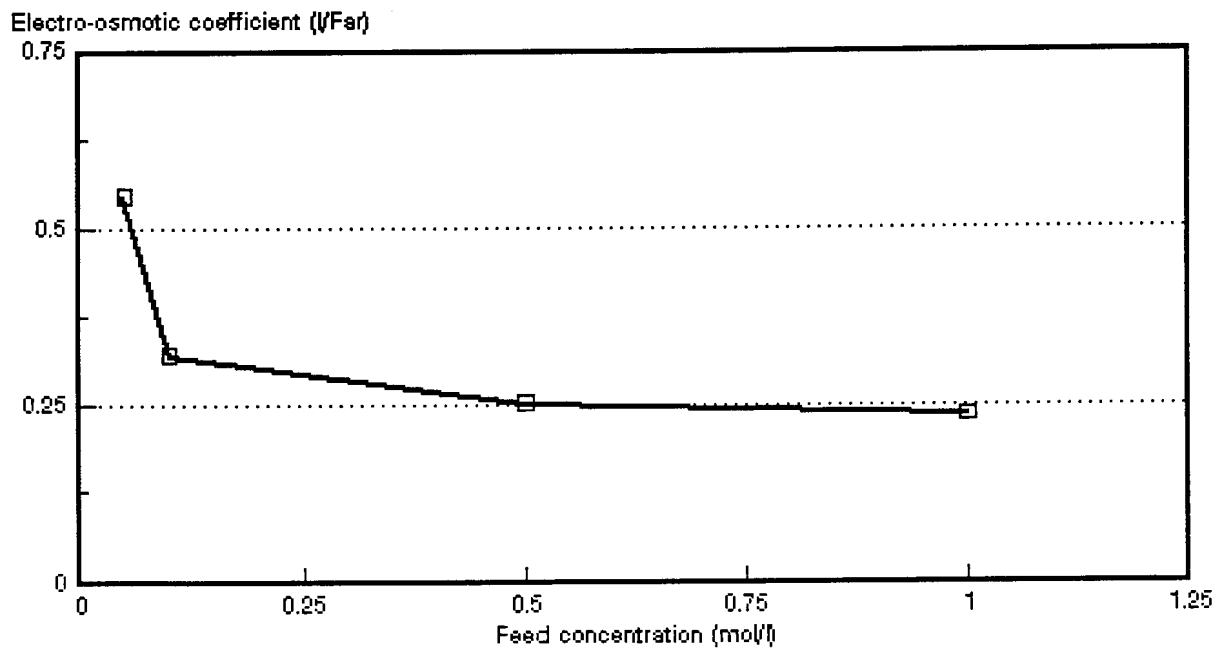


Figure 6.94 Electro-osmotic coefficient as a function of NaCl feed concentrations. *Raipore R4030 and R4010 membranes.*

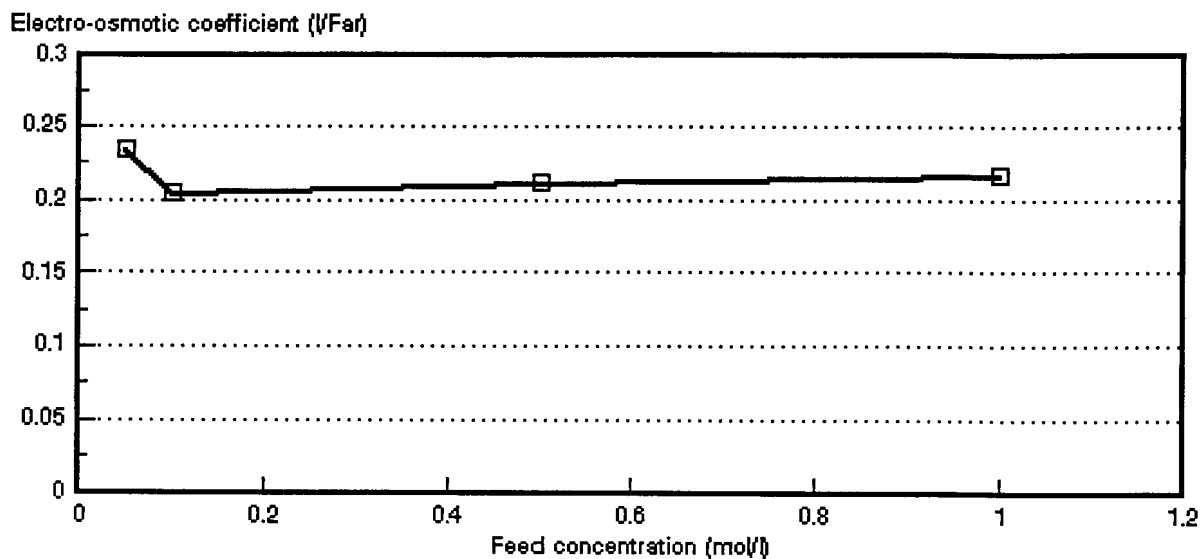


Figure 6.95: Electro-osmotic coefficient as a function of NaCl feed concentrations. *Ionics A-204-UZL-386 and C-61-CZL-386 membranes.*

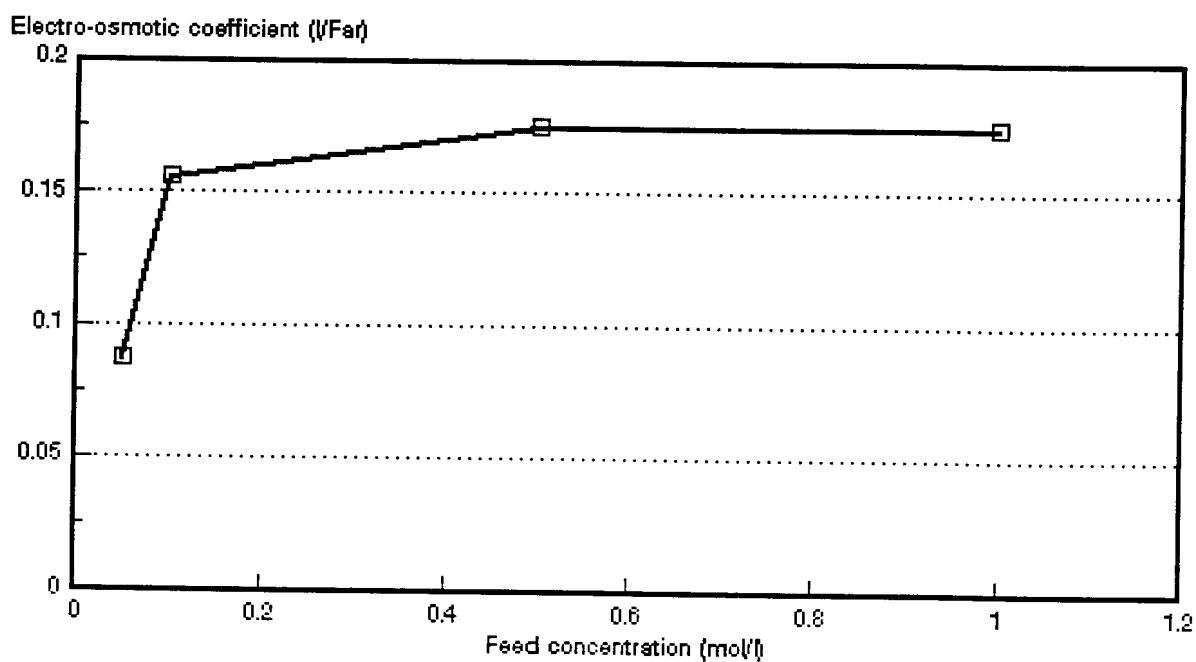


Figure 6.96: Electro-osmotic coefficient as a function of NaCl feed concentrations. *WTPSA-1 and WTPSC-1 membranes.*

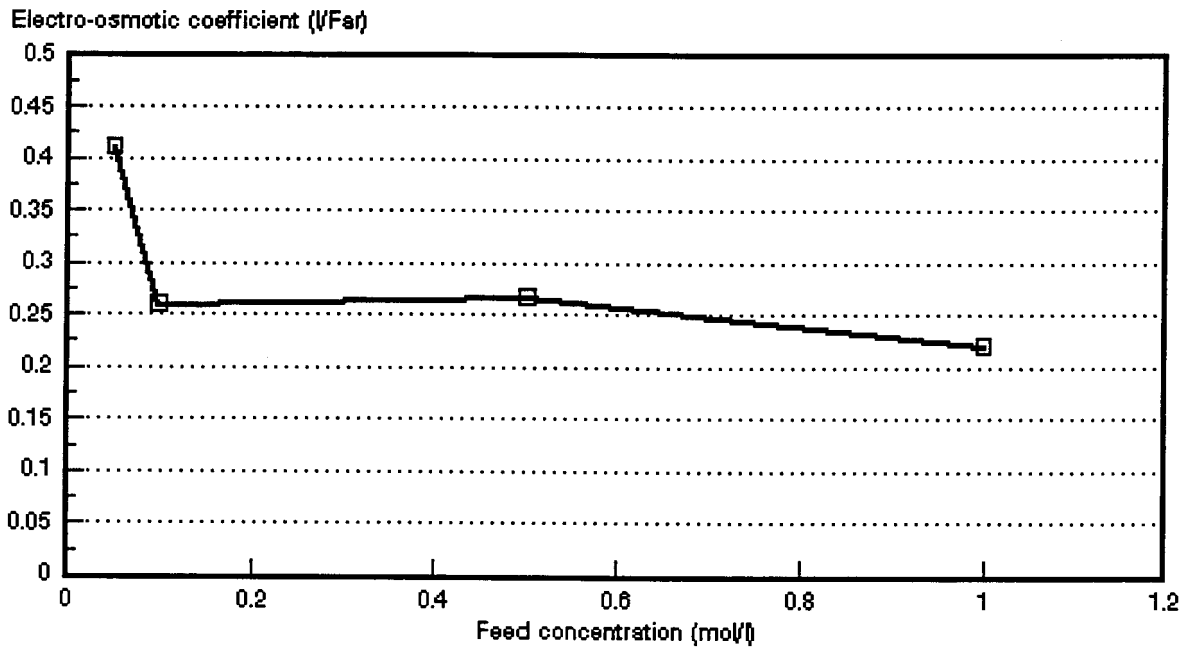


Figure 6.97: Electro-osmotic coefficient as a function of NaCl feed concentrations. WTPVCA-2 and WTPVCC-2 membranes.

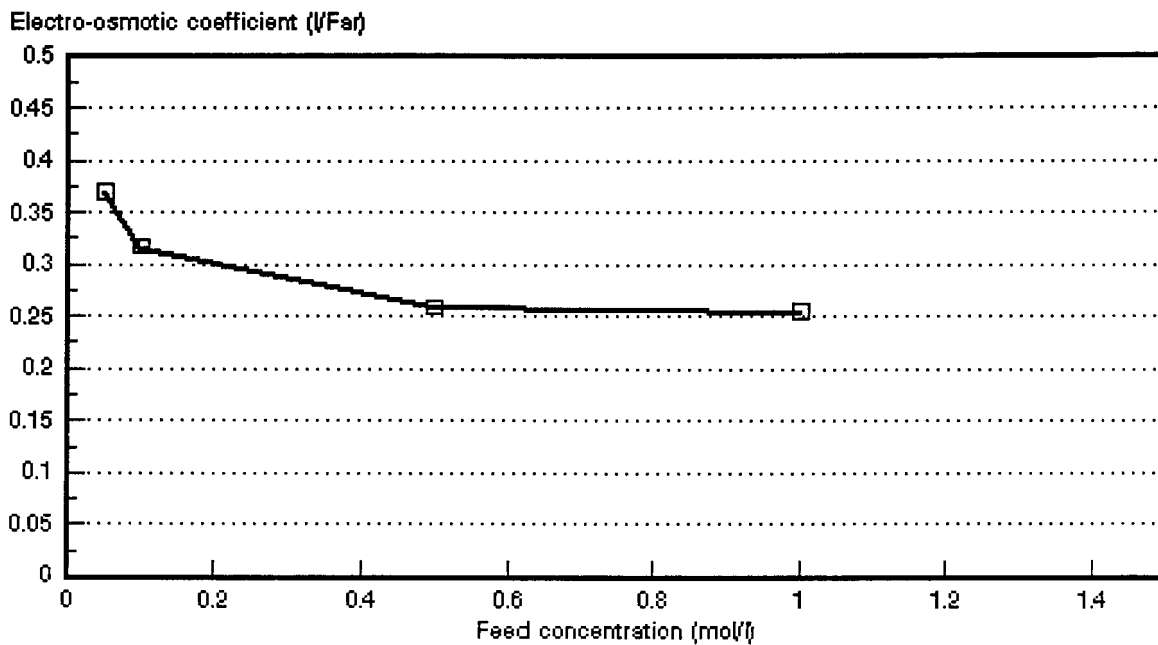


Figure 6.98: Electro-osmotic coefficient as a function of NaCl feed concentrations. WTPSTA-3 AND WTPSTC-3 membranes.

Table 6.36: Effect of the electro-osmotic coefficient (EOC)* on the maximum salt brine concentration, c_b^{\max} .

Membranes	Feed Concentration (mol/l)	EOC $\ell/\text{Faraday}$	C_b^{\max} mol/l	mol H ₂ O/Faraday
Selemion AMV & CMV	0,05	0,219	4,55	12,2
	0,10	0,198	5,05	11,0
	0,5	0,187	5,36	10,4
	1,0	0,154	6,48	8,6
Ionac MA-3475 & MC-3470	0,05	0,186	5,37	10,3
	0,10	0,206	4,85	11,4
	0,5	0,190	5,26	10,6
	1,0	0,187	5,35	10,4
Raipore R4030 & R4010	0,05	0,547	1,83	30,4
	0,10	0,320	3,13	17,8
	0,50	0,251	3,98	13,9
	1,0	0,236	4,24	13,1
Ionics A-204-UZL & C-61-CZL-386	0,05	0,234	4,27	13,0
	0,10	0,204	4,89	11,3
	0,5	0,211	4,73	11,7
	1,0	0,216	4,63	12,0
WTPS WTPSCA-1 & WTPSA-1	0,05	0,087	11,5	4,8
	0,10	0,156	6,41	8,7
	0,5	0,175	5,71	9,7
	1,0	0,175	5,72	9,7
WTPVC WTPVCA-2 & WTPVCC-2	0,05	0,412	2,43	22,8
	0,10	0,261	3,84	14,5
	0,5	0,267	3,74	14,8
	1,0	0,221	4,54	12,3
WTPST WTPSTA-3 & WTPSTC-3	0,05	0,371	2,69	20,6
	0,1	0,317	3,15	17,6
	0,5	0,259	3,86	14,4
	1,0	0,257	3,90	14,3

* Data from Tables 6.1 to 6.28.

The effect of the electro-osmotic coefficient on the maximum brine concentration, c_b^{\max} , is shown in Table 6.36. Maximum brine concentration increases with decreasing electro-osmotic coefficient. The electro-osmotic coefficients of the *Raipore* membranes were higher than the electro-osmotic coefficients of the other membranes. Consequently, lower brine concentrations were obtained with this membrane type. It is further interesting to note that the electro-osmotic coefficients of the WTPS membranes have been the lowest in the 0,05 to 0,5 mol/l feed concentration range. Therefore, high brine concentrations could be obtained (Table 6.36).

Approximately 10 to 11 mol H₂O/Faraday passed through the *Selemion*-, *Ionac*- and *Ionics* membranes in the 0,1 to 0,5 mol/l feed concentration range (Table 6.36).

Approximately 9 to 10 mol H₂O/Faraday passed through the WTPS membranes in this same feed concentration range. However, more water passed through the other membranes in this feed concentration range.

The osmotic flow (J_{osm}) relative to the total flow (J) through the membranes as a function of current density, is shown in Table 6.37. Osmotic flow decreases with increasing current density. The contribution of osmotic flow at a current density of 30 mA/cm² (0,1 mol/l feed) in the case of the *Selemion*-, *Ionac*-, *Raipore*-, *Ionics*-, WTPS-, WTPVC- and WTPST membranes were 28,4%; 25,5%; 30,8%; 38,5%; 48,4%; 38,8% and 23,7% of the total flow through the membranes, respectively. Consequently, osmosis contributes significantly to water flow through the membranes especially at relatively low current density. The osmotic flow contribution to total water flow through the membranes was much less at high current density. Osmotic flow contribution to total flow through the membranes at a current density of 50 mA/cm² (0,1 mol/l feed) was 20,5; 19,0; 21,1 and 16,5% for the *Selemion*-, *Ionac*-, *Raipore*- and WTPST membranes, respectively. Osmotic flow contribution was only 10,7% of total water flow in the case of the WTPST membranes at a current density of 110 mA/cm².

It is interesting to note that the water flow (J) versus the effective current density (i_{eff}) relationship becomes linear long before the maximum brine concentration, c_b^{max} , is reached.

Table 6.37: Osmotic flow* (J_{osm}) relative to the total flow (J) through the membranes as a function of current density.

Membranes	Current Density mA/cm ²	J_{osm}/J (%) Feed Concentration (mol/l)			
		0,05	0,1	0,5	1,0
Selemon AMV & CMV	10	52,3	57,4	51,2	69,9
	20	35,4	36,0	32,8	45,4
	30	27,7	28,4		33,5
	40			19,3	28,3
	50		20,5		
	60			14,1	20,6
Ionac MA-3475 & MC-3470	10	59,1	50,5	46,9	
	20	45,2	33,9	28,6	27,6
	30		25,5	22,2	17,0
	40		21,9	18,4	
	50		19,0		11,9
	60			16,1	9,7
Raipore R4030 & R4010	10	21,9	57,3	76,8	
	20	15,6	39,3	46,9	
	30	11,0	30,8	35,2	37,3
	40		24,8	28,3	
	50		21,1	25,1	27,4
	60		-	23,5	
	70			19,91	21,3
	90			16,2	17,6
Ionics A-204-UZL & C-61-CZL-386	10	57,8	64,2	73,7	
	20	42,1	47,1	44,2	
	30	34,7	38,5	34,5	26,5
	40		33,9	28,34	
	50			24,6	17,7
	60			22,7	
	80			18,2	
	90			16,4	12,3
	100			15,5	
WTPS WTPSA-1 & WTPSC-1	10	85,2	68,8	57,4	
	20	74,9	55,1	44,0	
	30		48,4	39,6	34,3
	40		43,2	34,4	
	50			31,7	28,5
	60			30,5	
	70				27,3
	80			27,3	
	90				26,2
100			24,7		
WTPVC WTPVCA-2 & WTPVCC-2	10	41,6	67,1	55,6	62,8
	20	30,6	44,8	37,9	50,2
	30	22,2	38,8	29,8	
	40		35,2	25,2	34,0
	60			20,3	26,2
WTPST WTPSTA-3 & WTPSTC-3	10	36,7	49,2	57,7	
	20	25,6	32,1	35,7	
	30	19,0	23,7	27,7	24,1
	40		19,8	22,2	
	50		16,5	19,7	16,3
	70			15,8	
	90			13,0	13,2
	110			11,1	10,7

* Data from Tables 6.1 to 6.28.

6.4 Membrane Permselectivity

Membrane permselectivity ($\bar{\Delta}t$) as a function of brine concentration for various initial feed concentrations, is shown in Figures 6.99 to 6.105. Membrane permselectivity decreased with increasing brine concentration for all the membranes investigated. Permselectivity decreased with increasing feed concentration in the case of the *Selemion*-, *lonac*-, WTPS-, WTPVC- and WTPST membranes. However, permselectivity was slightly higher at 1,0 mol/l feed concentration than at 0,5 mol/l feed concentration in the case of the *lonac* membranes (Fig. 6.100). Permselectivity showed an increase with increasing feed concentration in the case of the *Raipore* membrane (Fig. 6.101).

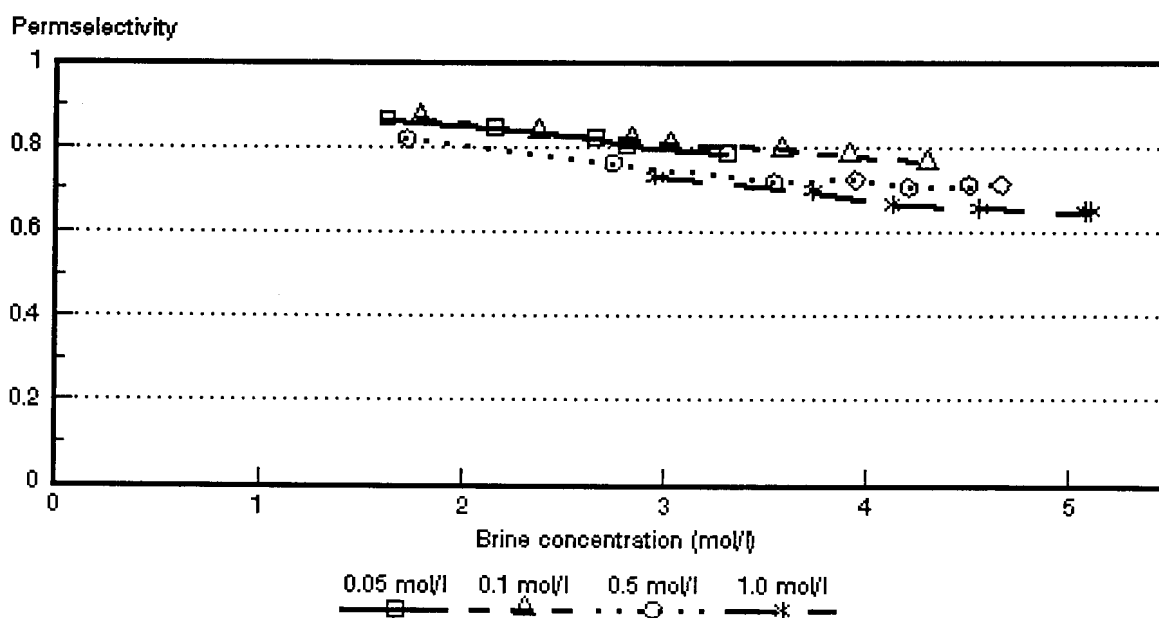


Figure 6.99: Membrane permselectivity ($\bar{\Delta}t$) as a function of brine concentration for different NaCl feed concentrations. *Selemion* AMV and CMV membranes.

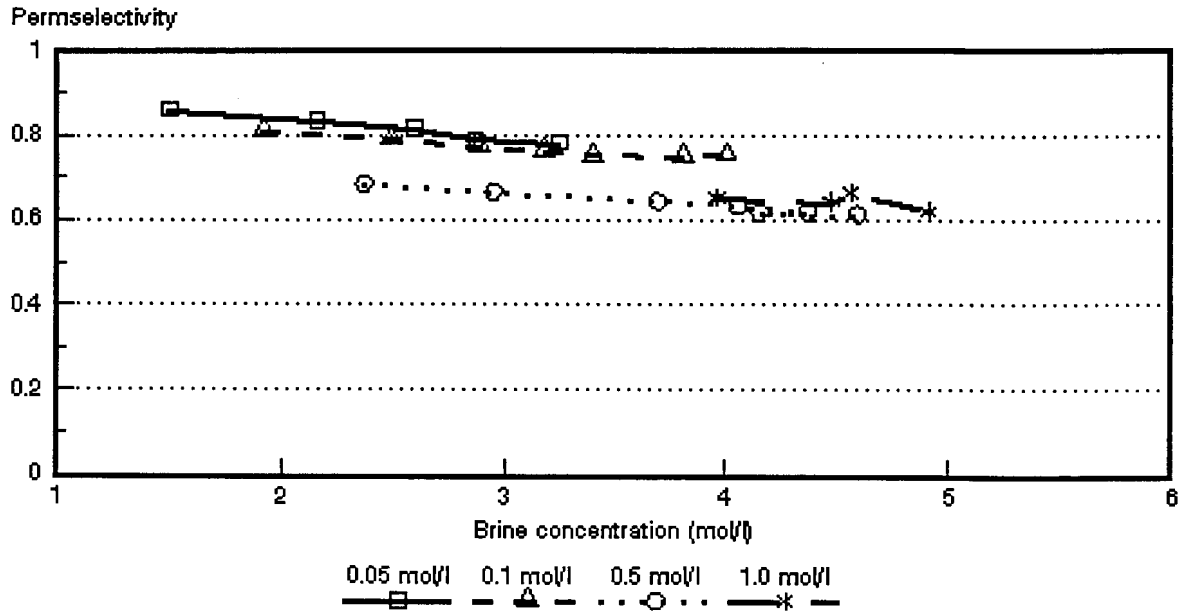


Figure 6.100: Membrane permselectivity ($\bar{\Delta}t$) as a function of brine concentration for different NaCl feed concentrations. *Ionac* MA-3475 and MC-3470 membranes.

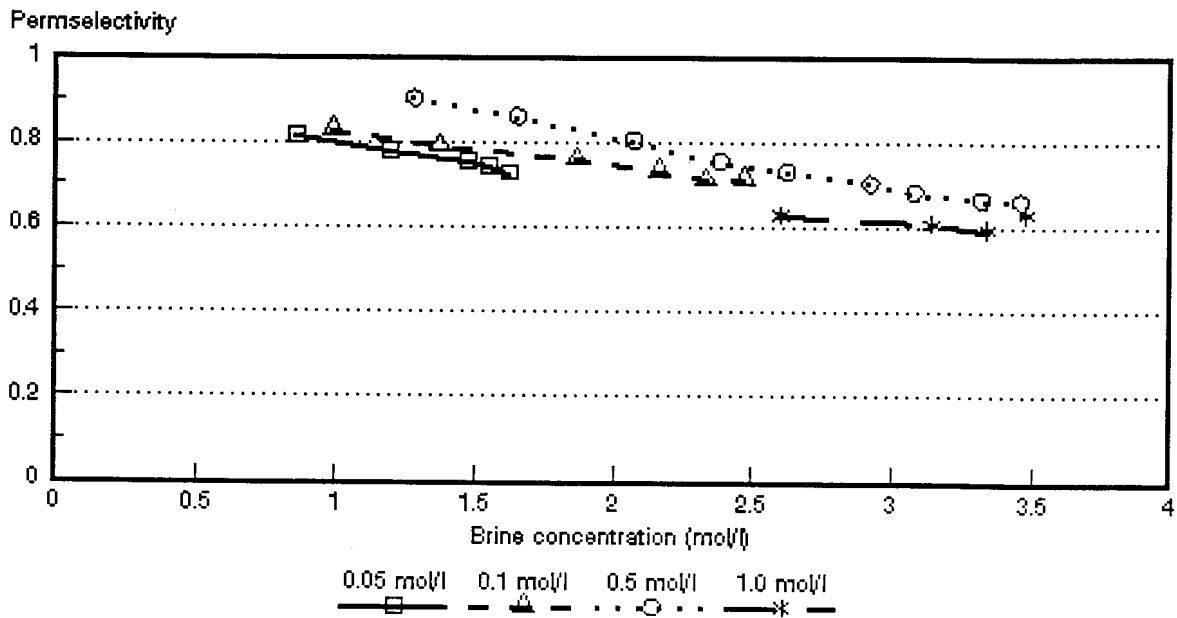


Figure 6.101: Membrane permselectivity ($\bar{\Delta}t$) as a function of brine concentration for different NaCl feed concentrations. *Raipore* R4030 and R4010 membranes.

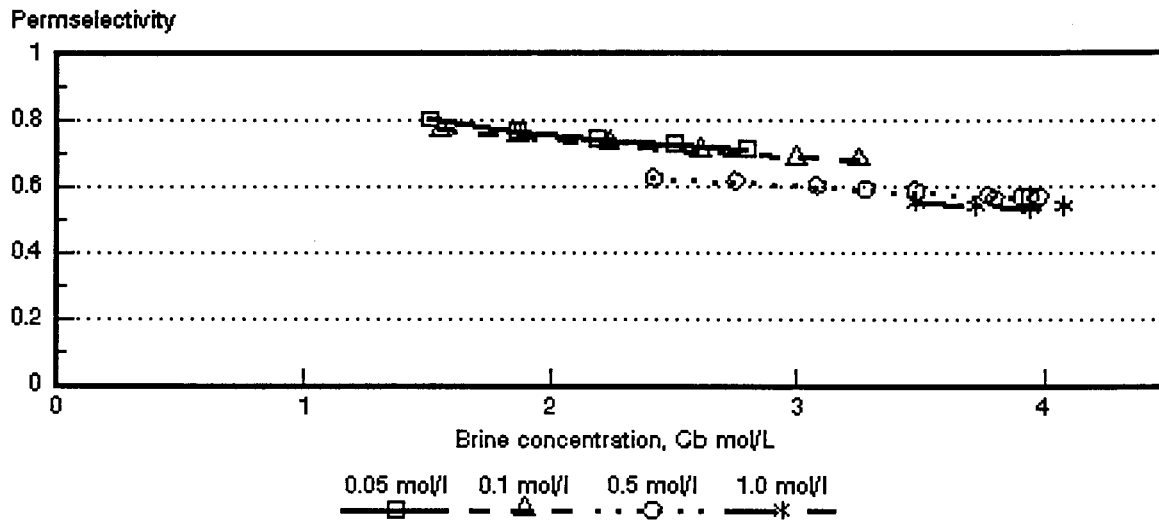


Figure 6.102: Membrane permselectivity ($\bar{\Delta}t$) as a function of brine concentration for different NaCl feed concentrations. *Ionics A-204-UZL-386* and *C-61-CZL-386* membranes.

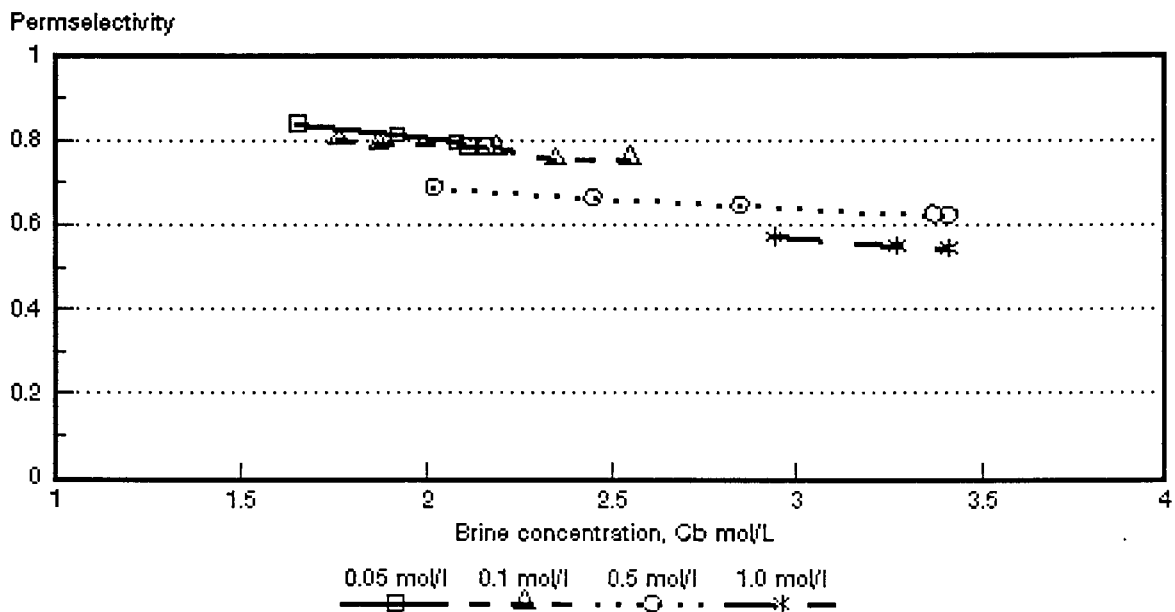


Figure 6.103: Membrane permselectivity ($\bar{\Delta}t$) as a function of brine concentration for different NaCl feed concentrations. *WTPSA-1* and *WTPSC-1* membranes.

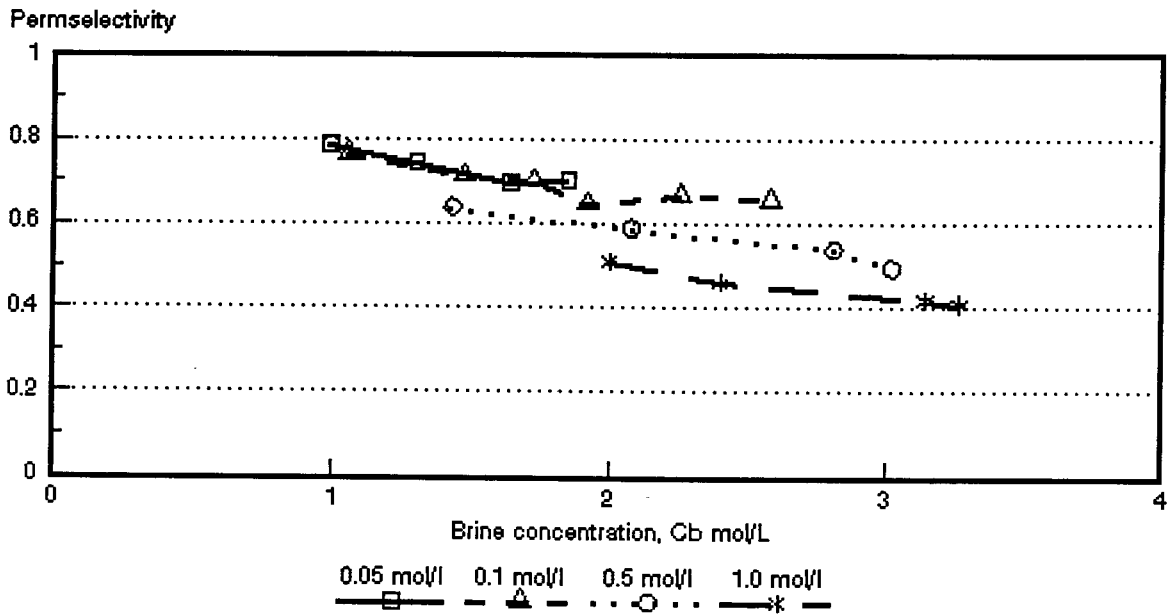


Figure 6.104: Membrane permselectivity ($\bar{\Delta}t$) as a function of brine concentration for different NaCl feed concentrations. WTPVCA-2 and WTPVCC-2 membranes.

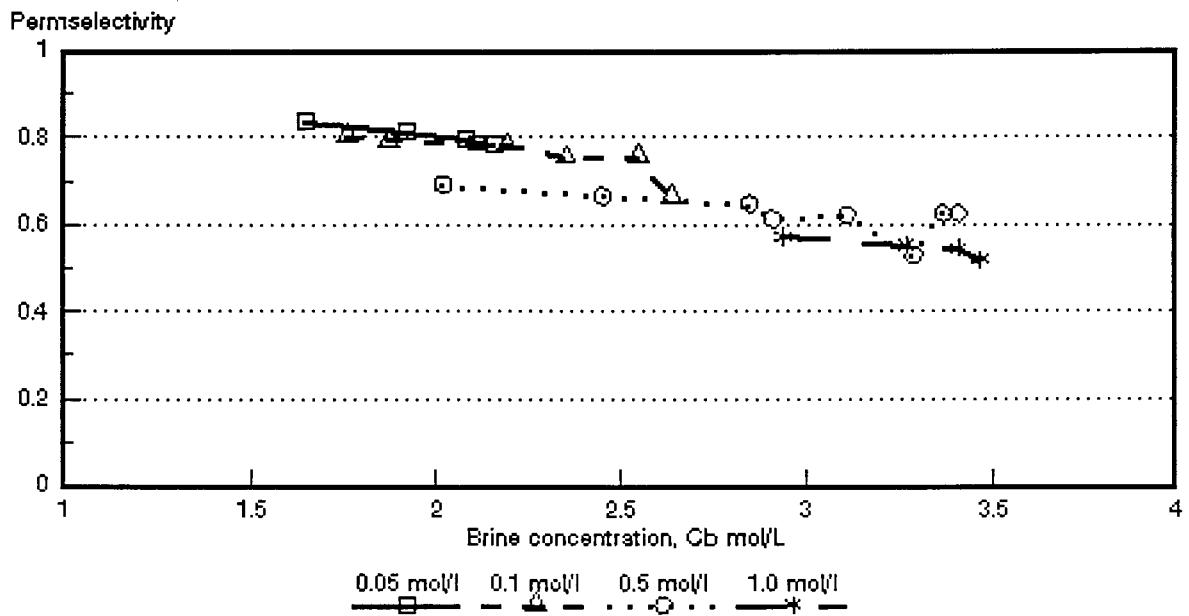


Figure 6.105: Membrane permselectivity ($\bar{\Delta}t$) as a function of brine concentration for different NaCl feed concentrations. WTPSTA-3 and WTPSTC-3 membranes.

6.5 Membrane Characteristics

6.5.1 Membrane resistance

Membrane resistances are summarized in Table 6.38.

Table 6.38: Membrane resistances of the membranes used for EOP of sodium chloride solutions

Membrane	Resistance - ohm cm ²	
	0,1 mol/l NaCl	0,5 mol/l NaCl
Selemion AMV	4,7	1,5
Selemion CMV	3,8	1,0
Ionac MA-3475	36,6	19,4
Ionac MC-3470	42,0	24,3
Raipore R4030	3,1	1,0
Raipore R4010	1,3	-
Ionics A-204-UZL-386	13,4	12,3
Ionics C-61-CZL-386	14,2	15,2
WTPSA-1	97,9	60,3
WTPSC-1	12,8	8,6
WTPVCA-2	21,1	11,1
WTPVCC-2	24,9	14,9
WTPSTA-3	83,3	49,3
WTPSTC-3	24,9	14,3

6.5.2 Gel water contents and ion-exchange capacities of the membranes used for EOP of sodium chloride solutions

The gel water contents and the ion-exchange capacities are summarized in Table 6.39.

Table 6.39: Gel water contents and ion-exchange capacities of the membranes used for the EOP of sodium chloride solutions.

Membrane	Gel Water Content (%)	Ion-exchange capacity me/dry g
Selemion AMV	18,4	1,26
Selemion CMV	22,7	2,4
Ionac MA-3475	17,8	1,06
Ionac MC-3470	18,5	1,82
Ionics A-204-UZL-386	22,9	1,49
Ionics C-61-CZL-386	23,7	1,51
WTPSA-1	26,4	0,54
WTPSC-1	43,4	1,75
WTPVCA-2	15,9	1,15
WTPVCC-2	29,8	0,76
WTPSTA-3	35,57	1,13
WTPSTC-3	31,44	0,61

6.5.3 Permselectivities of the membranes used for the EOP of sodium chloride solutions

The permselectivities of the membranes at different salt gradients are summarized in Table 6.40.

Table 6.40: Membrane permselectivities of the membranes used for EOP of sodium chloride solutions at different salt gradients

Membrane	$\Delta t(1)^*$	$\Delta t(2)^{**}$	$\Delta t(3)^{***}$
Selemion AMV	0,86	0,75	0,71
Selemion CMV	1,00	0,99	0,88
Ionac MA-3475	0,83	0,66	0,64
Ionac MC-3470	1,00	0,91	0,78
Raipore R4030	0,85	0,72	0,66
Raipore R4010	0,96	0,85	0,63
Ionics A-204-UZL-386	0,92	0,75	0,67
Ionics C-61-CZL-386	0,94	0,82	0,70
WTPSA-1	0,92	0,75	0,68
WTPSC-1	0,90	0,77	0,58
WTPVCA-2	0,86	0,65	0,50
WTPVCC-2	0,90	0,71	0,54
WTPSTA-3	0,91	0,73	0,65
WTPSTC-3	0,89	0,72	0,69

(1)* : 0,1/0,2 mol/l

(2)** : 0,5/1,0 mol/l

(3)*** : 0,1/4,0 mol/l NaCl

7. ELECTRO-OSMOTIC PUMPING OF HYDROCHLORIC ACID SOLUTIONS WITH DIFFERENT ION-EXCHANGE MEMBRANES

Acid brine concentrations, water flows and current efficiencies were determined at different current densities for different hydrochloric acid feed water concentrations. Membrane permselectivities (apparent transport numbers) were measured at concentration differences similar to those obtained during EOP experiments. The results are summarized in Tables 7.1 to 7.17.

7.1 Brine Concentration

Acid brine concentration (c_b) as a function of current density is shown in Figures 7.1 to 7.5. Acid concentration increases more rapidly in the beginning as has been experienced with the salt solutions and then starts to level off. The levelling off in acid concentration is more pronounced at the lower acid feed concentrations (0,05 mol/l, Figs. 7,3 and 7,5). The acid concentration curves were steeper than the curves obtained during sodium chloride concentration. Higher current densities could be obtained easier with the acid feed solutions.

Acid brine concentration increases with increasing current density and increasing acid feed water concentration as has been the case with sodium chloride solutions. The highest acid concentrations were obtained with the *Selemion* AAV and CHV membranes followed by the ABM-3 and CHV and ABM-2 and CHV membranes (Table 7.18). Acid brine concentrations of 25,0; 22,6 and 22,9% could be obtained from 0,5 mol/l feed solutions with *Selemion* AAV and CHV, ABM-3 and CHV and ABM-2 and CHV membranes, respectively. The ABM-1 and CHV membranes did not perform as well as the other membranes for acid concentration while very low acid brine concentrations were obtained with the *Selemion* AMV and CMV membranes. The reason for the low acid concentrations obtained with the *Selemion* AMV and CMV membranes compared to the other anion membranes could be ascribed to the very low permselectivity of the *Selemion* AMV membrane for chloride ions (Tables 7.1 to 7.17). The permselectivity (Δt^a) of the *Selemion* AMV membrane was only 0,2 at 0,1 mol/l hydrochloric acid feed (20 mA/cm²) compared to 0,64 for the *Selemion* AAV; 0,62 for the ABM-3; approximately 0,5 for the ABM-2 and 0,57 for the ABM-1 membranes (Tables 7.1; 7.5; 7.9; 7.13; 7.16). The concentration gradients across the *Selemion* AAV, ABM-3, ABM-2 and ABM-1 membranes were also much higher than the concentration gradient across the *Selemion* AMV membrane during determination

Table 7.1 : Electro-osmotic pumping experimental conditions and results for 0,1 mol/l hydrochloric acid (Selemion AMV and CMV)

Current Density i , mA/cm ²	Brine concentration c_b , mol/l		Water flow J , cm/h	Current Efficiency e_p , %	Effective Current Density i_{eff} , mA/cm ²	Transport Numbers				
	$c_{b, exp.}$	$c_{b, calc.}$				Δt^a	Δt^b	$\bar{\Delta}t$	\bar{i}_1^c	\bar{i}_2^d
10	0,88	4,36	0,0555	13,15	1,32	1,00	0,30	0,65	1,00	0,65
20	1,17	4,67	0,093	14,57	2,91	0,96	0,20	0,58	0,98	0,60
30	1,45	5,14	0,121	15,63	4,69	0,97	0,13	0,55	0,99	0,57
40	1,62	5,49	0,140	15,20	6,08	0,95	0,08	0,52	0,98	0,54
50	1,78	5,43	0,170	16,21	8,11	0,95	0,04	0,50	0,97	0,52
60	1,95	5,58	0,189	16,46	9,88	0,92	0,02	0,47	0,96	0,51

Electro-osmotic coefficient ($\bar{\alpha}$) = 0,357 μ /F (slope = 0,013304 ml/mAh)
 J_{osm} = y-intercept = 0,059376 cm/h
 c_b^{max} = 2,80 mol/l
 $\Delta t^c = t_1^c - t_2^c$

$\Delta t^a = t_2^a - t_1^a$
 Δt = Average transport number of membrane pair
 \bar{i}_1^c = Transport number of cation through cation membrane
 \bar{i}_2^d = Transport number of anion through anion membrane.

Table 7.2: Electro-osmotic pumping experimental conditions and results for 0,54 mol/l hydrochloric acid (Selemion AMV and CMV)

Current Density i , mA/cm ²	Brine concentration c_b , mol/l		Water flow J , cm/h	Current Efficiency e_p , %	Effective Current Density i_{eff} , mA/cm ²	Transport Numbers				
	$c_{b, exp.}$	$c_{b, calc.}$				Δt^a	Δt^b	$\bar{\Delta}t$	\bar{i}_1^c	\bar{i}_2^d
10	1,07	4,42	0,047	13,40	1,34	0,96	0,15	0,56	0,98	0,58
20	1,37	4,99	0,074	13,60	2,72	0,95	0,04	0,50	0,97	0,52
30	1,58	5,17	0,103	15,58	4,37	0,92	0,02	0,47	0,96	0,51
40	1,75	5,33	0,126	14,73	5,89	0,90	0,02	0,46	0,95	0,51
50	1,91	5,96	0,155	15,85	7,93	0,90	0,06	0,48	0,95	0,53
60	2,05	6,16	0,176	16,10	9,66	0,90	0,08	0,49	0,95	0,54

Electro-osmotic coefficient ($\bar{\alpha}$) = 0,371 μ /F (slope = 0,0138374 ml/mAh)
 J_{osm} = y-intercept = 0,0436566 cm/h
 c_b^{max} = 2,70 mol/l
 $\Delta t^c = t_1^c - t_2^c$

$\Delta t^a = t_2^a - t_1^a$
 Δt = Average transport number of membrane pair
 \bar{i}_1^c = Transport number of cation through cation membrane
 \bar{i}_2^d = Transport number of anion through anion membrane.

Table 7.3: Electro-osmotic pumping experimental conditions and results for 1,0 mol/l hydrochloric acid (Selemion AMV and CMV)

Current Density i , mA/cm ²	Brine concentration c_b , mol/l		Water flow J , cm/h	Current Efficiency e_p , %	Effective Current Density i_{eff} , mA/cm ²	Transport Numbers				
	$c_{b, exp.}$	$c_{b, calc.}$				Δt^c	Δt^d	$\bar{\Delta}t$	\bar{i}_1^e	\bar{i}_2^f
10	1,36	5,39	0,0336	12,40	1,24	0,88	0,09	0,49	0,94	0,55
20	1,62	5,63	0,0608	13,17	2,63	0,81	0,11	0,46	0,91	0,55
30	1,79	5,51	0,0940	15,03	4,51	0,82	0,11	0,46	0,91	0,55
40	1,97	7,03	0,1095	14,45	5,78	0,87	0,17	0,52	0,93	0,58
50	2,15	6,82	0,1280	14,69	7,35	0,81	0,13	0,47	0,90	0,57
60	2,29	7,65	0,1480	15,20	9,12	0,82	0,19	0,51	0,91	0,60
70	2,42	8,04	0,1630	15,10	10,57	0,82	0,18	0,50	0,91	0,59

Electro-osmotic coefficient ($\bar{\alpha}$) = 0,306 μ /F (slope = 0,011409 ml/mAh)
 J_{osm} = y-intercept = 0,043319 cm/h
 c_b^{max} = 3,27 mol/l
 $\Delta t^c = t_1^c - t_2^c$

$\Delta t^a = t_2^a - t_1^a$
 Δt = Average transport number of membrane pair
 \bar{i}_1^e = Transport number of cation through cation membrane
 \bar{i}_2^f = Transport number of anion through anion membrane.

Table 7.4: Electro-osmotic pumping experimental conditions and results for 0,05 mol/l hydrochloric acid (Selemion AAV and CHV)

Current Density I , mA/cm ²	Brine concentration c_b , mol/l		Water flow J , cm/h	Current Efficiency e_p , %	Effective Current Density I_{eff} , mA/cm ²	Transport Numbers				
	$c_{b, exp.}$	$c_{b, calc.}$				Δt^c	Δt^a	$\bar{\Delta}t$	\bar{i}_1^c	\bar{i}_2^a
10	2,59	4,88	0,062	42,91	4,29	0,95	0,67	0,81	0,98	0,83
20	3,25	6,13	0,093	40,38	8,08	0,91	0,61	0,76	0,96	0,81
30	3,69	6,83	0,123	40,66	12,20	0,91	0,59	0,75	0,95	0,80
40	4,12	7,66	0,141	39,01	15,60	0,90	0,55	0,72	0,95	0,77
50	4,45	8,27	0,160	38,16	19,08	0,89	0,53	0,71	0,94	0,76
60	4,70	9,64	0,178	37,41	22,45	0,88	0,49	0,69	0,94	0,75
70	5,01	9,04	0,196	37,52	26,26	0,87	0,49	0,68	0,93	0,74

Electro-osmotic coefficient (2β) = 0,140 μ F (slope = 0,00523 m/mAh)
 J_{osm} = y-intercept = 0,059609 cm/h
 c_b^{max} = 7,14 mol/l
 $\Delta t^c = t_1^c - t_2^c$

$\Delta t^a = t_2^a - t_1^a$
 $\bar{\Delta}t$ = Average transport number of membrane pair
 \bar{i}_1^c = Transport number of cation through cation membrane
 \bar{i}_2^a = Transport number of anion through anion membrane.

Table 7.5 : Electro-osmotic pumping experimental conditions and results for 0,1 mol/l hydrochloric acid (Selemion AAV and CHV)

Current Density I , mA/cm ²	Brine concentration c_b , mol/l		Water flow J , cm/h	Current Efficiency e_p , %	Effective Current Density I_{eff} , mA/cm ²	Transport Numbers				
	$c_{b, exp.}$	$c_{b, calc.}$				Δt^c	Δt^a	$\bar{\Delta}t$	\bar{i}_1^c	\bar{i}_2^a
10	2,68	5,12	0,060	43,4	4,34	0,94	0,71	0,83	0,97	0,85
20	3,36	6,76	0,086	38,88	7,78	0,91	0,64	0,78	0,96	0,82
30	3,84	7,17	0,117	40,05	12,02	0,90	0,59	0,75	0,95	0,80
40	4,41	7,86	0,140	41,36	16,54	0,89	0,59	0,74	0,94	0,79
50	4,63	8,47	0,157	38,95	19,48	0,88	0,54	0,71	0,94	0,77
60	4,87	8,67	0,180	39,05	23,43	0,88	0,51	0,70	0,94	0,76
70	5,12	8,64	0,211	41,29	28,90	0,88	0,51	0,70	0,94	0,76
80	5,33	9,03	0,225	40,18	32,14	0,87	0,51	0,69	0,94	0,76
100	5,73	9,62	0,264	40,48	40,48	0,88	0,48	0,68	0,94	0,74

Electro-osmotic coefficient (2β) = 0,141 μ F (slope = 0,005249 m/mAh)
 J_{osm} = y-intercept = 0,055129 cm/h
 c_b^{max} = 7,09 mol/l
 $\Delta t^c = t_1^c - t_2^c$

$\Delta t^a = t_2^a - t_1^a$
 $\bar{\Delta}t$ = Average transport number of membrane pair
 \bar{i}_1^c = Transport number of cation through cation membrane
 \bar{i}_2^a = Transport number of anion through anion membrane.

Table 7.6: Electro-osmotic pumping experimental conditions and results for 0,5 mol/l hydrochloric acid (Selemion AAV and CHV)

Current Density I , mA/cm ²	Brine concentration c_b , mol/l		Water flow J , cm/h	Current Efficiency e_p , %	Effective Current Density I_{eff} , mA/cm ²	Transport Numbers				
	$c_{b, exp.}$	$c_{b, calc.}$				Δt^c	Δt^a	$\bar{\Delta}t$	\bar{i}_1^c	\bar{i}_2^a
10	2,62	5,87	0,050	35,45	3,55	0,89	0,69	0,79	0,94	0,84
20	3,53		0,089	42,24	8,45	0,87	0,62	0,75	0,94	0,81
30	4,03	6,95	0,115	41,45	12,44	0,86	0,57	0,71	0,93	0,79
40	4,39		0,138	40,65	16,26	0,81	0,56	0,70	0,92	0,78
50	4,72	8,01	0,160	40,34	20,17	0,83	0,55	0,69	0,91	0,77
60	5,10		0,173	39,33	23,60	0,82	0,52	0,67	0,91	0,76
70	5,35	8,83	0,195	39,90	27,93	0,78	0,54	0,66	0,89	0,77
80	5,67		0,213	40,46	32,37	0,84	0,59	0,71	0,92	0,80
100	5,96	8,80	0,258	41,26	41,26	0,73	0,49	0,61	0,86	0,75
120	6,35		0,289	41,08	49,30	0,82	0,47	0,64	0,91	0,73
140	6,84	9,50	0,304	39,78	55,69	0,76	0,54	0,65	0,88	0,77

Electro-osmotic coefficient (2β) = 0,126 μ F (slope = 0,004688 m/mAh)
 J_{osm} = y-intercept = 0,061762 cm/h
 c_b^{max} = 7,93 mol/l
 $\Delta t^c = t_1^c - t_2^c$

$\Delta t^a = t_2^a - t_1^a$
 $\bar{\Delta}t$ = Average transport number of membrane pair
 \bar{i}_1^c = Transport number of cation through cation membrane
 \bar{i}_2^a = Transport number of anion through anion membrane.

Table 7.7: Electro-osmotic pumping experimental conditions and results for 1,0 mol/l hydrochloric acid (Selemion AAV and CHV)

Current Density I , mA/cm ²	Brine concentration c_b , mol/l		Water flow J , cm/h	Current Efficiency e_p , %	Effective Current Density i_{eff} , mA/cm ²	Transport Numbers				
	$c_{b, exp}$	$c_{b, calc}$				Δt^a	Δt^a	$\bar{\Delta}t$	\bar{i}_1^c	\bar{i}_2^a
10	2,87	5,47	0,051	39,30	3,93	0,91	0,59	0,75	0,96	0,79
20	3,58		0,085	40,89	8,18	0,82	0,56	0,69	0,91	0,78
30	4,10	6,69	0,111	40,60	12,18	0,82	0,50	0,66	0,91	0,75
40	4,63		0,135	42,00	16,80	0,80	0,50	0,65	0,90	0,75
50	5,01	7,95	0,149	40,13	20,07	0,80	0,47	0,64	0,90	0,73
60	5,31	8,08	0,172	40,85	24,51	0,81	0,44	0,62	0,90	0,72
80	5,86	8,69	0,209	40,96	32,77	0,76	0,46	0,61	0,88	0,73
100	6,19	9,50	0,245	40,73	40,73	0,75	0,50	0,62	0,88	0,75
140	7,00	10,40	0,299	40,08	56,11	0,71	0,48	0,60	0,86	0,74
180	7,44	11,42	0,351	38,94	70,09	0,70	0,49	0,60	0,85	0,75

Electro-osmotic coefficient (2β) = 0,125 μ /F (slope = 0,004674 ml/mAh)
 $J_{osm} = y$ -intercept = 0,055604 cm/h
 $c_b^{max} = 8,00$ mol/l
 $\Delta t^c = t_1^c - t_2^c$

$\Delta t^a = t_2^a - t_1^a$
 $\bar{\Delta}t$ = Average transport number of membrane pair
 \bar{i}_1^c = Transport number of cation through cation membrane
 \bar{i}_2^a = Transport number of anion through anion membrane.

Table 7.8: Electro-osmotic pumping experimental conditions and results for 0,05 mol/l hydrochloric acid (ABM-3 and Selemion CHV)

Current Density I , mA/cm ²	Brine concentration c_b , mol/l		Water flow J , cm/h	Current Efficiency e_p , %	Effective Current Density i_{eff} , mA/cm ²	Transport Numbers				
	$c_{b, exp}$	$c_{b, calc}$				Δt^c	Δt^a	$\bar{\Delta}t$	\bar{i}_1^c	\bar{i}_2^a
10	2,47	4,55	0,064	42,53	4,25	0,90	0,66	0,78	0,95	0,83
20	2,91	5,79	0,098	38,42	7,68	0,93	0,60	0,77	0,97	0,80
30	3,33	7,13	0,117	34,81	10,44	0,90	0,59	0,74	0,95	0,79
40	3,78	7,69	0,138	34,89	13,96	0,90	0,53	0,71	0,95	0,76
50	4,00	8,44	0,154	33,06	16,53	0,89	0,50	0,70	0,95	0,75
60	4,16	8,68	0,176	32,70	19,62	0,88	0,48	0,68	0,94	0,74

Electro-osmotic coefficient (2β) = 0,171 μ /F (slope = 0,0063924 ml/mAh)
 $J_{osm} = y$ -intercept = 0,0495041 cm/h
 $c_b^{max} = 5,85$ mol/l
 $t^c = t_1^c - t_2^c$

$t^a = t_2^a - t_1^a$
 $\bar{\Delta}t$ = Average transport number of membrane pair
 \bar{i}_1^c = Transport number of cation through cation membrane
 \bar{i}_2^a = Transport number of anion through anion membrane.

Table 7.9: Electro-osmotic pumping experimental conditions and results for 0,1 mol/l hydrochloric acid (ABM-3 and Selemion CHV)

Current Density I , mA/cm ²	Brine concentration c_b , mol/l		Water flow J , cm/h	Current Efficiency e_p , %	Effective Current Density i_{eff} , mA/cm ²	Transport Numbers				
	$c_{b, exp}$	$c_{b, calc}$				Δt^c	Δt^a	$\bar{\Delta}t$	\bar{i}_1^c	\bar{i}_2^a
10	2,27	4,76	0,0675	41,01	4,1	0,97	0,75	0,86	0,99	0,88
20	2,90	5,95	0,0976	37,80	7,56	0,94	0,62	0,78	0,97	0,81
30	3,41	6,80	0,119	36,32	10,90	0,92	0,52	0,72	0,96	0,76
40	3,78	7,09	0,147	37,31	14,92	0,92	0,48	0,70	0,96	0,74
50	3,99	7,46	0,166	35,42	17,71	0,90	0,43	0,66	0,95	0,71
60	4,38	9,00	0,178	34,99	20,99	0,89	0,55	0,72	0,94	0,77

Electro-osmotic coefficient (2β) = 0,166 μ /F (slope = 0,0061880 ml/mAh)
 $J_{osm} = y$ -intercept = 0,0523128 cm/h
 $c_b^{max} = 6,02$ mol/l
 $t^c = t_1^c - t_2^c$

$t^a = t_2^a - t_1^a$
 $\bar{\Delta}t$ = Average transport number of membrane pair
 \bar{i}_1^c = Transport number of cation through cation membrane
 \bar{i}_2^a = Transport number of anion through anion membrane.

Table 7.10 : Electro-osmotic pumping experimental conditions and results for 0,5 mol/l hydrochloric acid (ABM-3 and Selemion CHV)

Current Density, i , mA/cm ²	Brine concentration, c_b , mol/l		Water flow, J , cm/h	Current Efficiency, E_p , %	Effective Current Density, i_{eff} , mA/cm ²	Transport Numbers				
	$C_{b, exp.}$	$C_{b, calc.}$				Δt^c	Δt^a	$\bar{\Delta}t$	\bar{i}_1^c	\bar{i}_2^a
10	2,41	4,64	0,062	40,42	4,04	0,92	0,64	0,78	0,96	0,82
20	3,04	5,70	0,093	38,05	7,61	0,90	0,53	0,71	0,95	0,76
30	3,61	6,48	0,114	36,88	11,06	0,86	0,46	0,66	0,93	0,73
40	3,97		0,138	36,65	14,64	0,85	0,40	0,62	0,92	0,70
50	4,35	7,36	0,152	35,52	17,76	0,84	0,36	0,60	0,92	0,68
70	5,30	8,52	0,172	34,95	24,47	0,82	0,30	0,56	0,91	0,65
90	5,50	8,81	0,212	34,72	31,25	0,83	0,29	0,56	0,91	0,64
110	5,95	8,76	0,252	36,09	40,14	0,82	0,26	0,54	0,91	0,63
120	6,18	8,34	0,284	37,13	48,27	0,82	0,24	0,53	0,91	0,62

Electro-osmotic coefficient (2β) = 0,124 μ F (slope = 0,0046224 ml/mAh)
 J_{osm} = y-intercept = 0,0643752 cm/h
 c_b^{max} = 8,06 mol/l
 $t^c = t_1^c - t_2^c$

$t^a = t_2^a - t_1^a$
 $\bar{\Delta}t$ = Average transport number of membrane pair
 \bar{i}_1^c = Transport number of cation through cation membrane
 \bar{i}_2^a = Transport number of anion through anion membrane.

Table 7.11: Electro-osmotic pumping experimental conditions and results for 1,0 mol/l hydrochloric acid (ABM-3 and Selemion CHV)

Current Density i , mA/cm ²	Brine concentration c_b , mol/l		Water flow J , cm/h	Current Efficiency e_p , %	Effective Current Density i_{eff} , mA/cm ²	Transport Numbers				
	$C_{b, exp.}$	$C_{b, calc.}$				Δt^c	Δt^a	$\bar{\Delta}t$	\bar{i}_1^c	\bar{i}_2^a
20	3.05	4.07	0.145	59.558	11.911	1.00	0.57	0.79	1,00	0,78
40	4.19	5.81	0.184	51.694	20.678	0.93	0.50	0.72	0,97	0,75
60	4.66	6.41	0.238	49.634	29.780	0.93	0.44	0.68	0,96	0,71
80	5.4	7.87	0.261	47.291	37.833	0.91	0.47	0.69	0,95	0,73

Electro-osmotic coefficient (2β) = 0,125 μ F (slope = 0,0046471 ml/mAh)
 J_{osm} = y-intercept = cm/h
 c_b^{max} = 8,03 mol/l
 $\Delta t^c = t_1^c - t_2^c$

$\Delta t^a = t_2^a - t_1^a$
 $\bar{\Delta}t$ = Average transport number of membrane pair
 \bar{i}_1^c = Transport number of cation through cation membrane
 \bar{i}_2^a = Transport number of anion through anion membrane.

Table 7.12 : Electro-osmotic pumping experimental conditions and results for 0,05 mol/l hydrochloric acid (ABM-2 and Selemion CHV)

Current Density, i , mA/cm ²	Brine concentration, c_b , mol/l		Water flow, J , cm/h	Current Efficiency, E_p , %	Effective Current Density, i_{eff} , mA/cm ²	Transport Numbers				
	$C_{b, exp.}$	$C_{b, calc.}$				Δt^c	Δt^a	$\bar{\Delta}t$	\bar{i}_1^c	\bar{i}_2^a
10	3,15	5,2	0,050	42,87	4,29	0,90	0,51	0,71	0,95	0,76
20	3,92		0,076	40,01	8,00					
30	4,40	7,6	0,095	37,49	11,24	0,88	0,40	0,64	0,94	0,70
40	4,72		0,117	36,86	14,74					
50	4,80		0,143	36,81	18,40					
60	4,90	9,1	0,145	31,89	19,14	0,87	0,32	0,59	0,93	0,66

Electro-osmotic coefficient (2β) = 0,170 μ F (slope = 0,0063345 ml/mAh)
 J_{osm} = y-intercept = 0,0245486 cm/h
 c_b^{max} = 5,88 mol/l
 $t^c = t_1^c - t_2^c$

$t^a = t_2^a - t_1^a$
 $\bar{\Delta}t$ = Average transport number of membrane pair
 \bar{i}_1^c = Transport number of cation through cation membrane
 \bar{i}_2^a = Transport number of anion through anion membrane.

Table 7.13 : Electro-osmotic pumping experimental conditions and results for 0,1 mol/l hydrochloric acid (ABM-2 and Selemion CHV)

Current Density i , mA/cm ²	Brine concentration c_b , mol/l		Water flow J , cm/h	Current Efficiency e_p , %	Effective Current Density i_{eff} , mA/cm ²	Transport Numbers				
	$c_{b, exp.}$	$c_{b, calc.}$				Δt^c	Δt^a	$\bar{\Delta}t$	\bar{i}_1^c	\bar{i}_2^a
10	2,1	3,3	0,091	51,13	5,11	0,96	0,65	0,81	0,97	0,82
20	2,95		0,117	46,08	9,21					
30	3,40		0,132	40,24	12,07					
40	3,82	6,8	0,146	37,29	14,91	0,88	0,45	0,66	0,94	0,55
50	4,28		0,152	34,95	17,48					
60	4,42		0,172	34,00	20,40					
80	4,82		0,198	32,08	25,6					
100	5,18	10,02	0,230	31,87	31,87	0,87	0,36	0,62	0,93	0,68

Electro-osmotic coefficient (2β) = 0,133 μ F (slope = 0,0049643 m/mAh)
 J_{osm} = y-intercept = 0,0704871 cm/h
 c_b^{max} = 7,51 mol/l
 $t^c = t_1^c - t_2^c$

$t^a = t_2^a - t_1^a$
 Δt = Average transport number of membrane pair
 \bar{i}_1^c = Transport number of cation through cation membrane
 \bar{i}_2^a = Transport number of anion through anion membrane.

Table 7.14: Electro-osmotic pumping experimental conditions and results for 0,5 mol/l hydrochloric acid (ABM-2 and Selemion CHV)

Current Density i , mA/cm ²	Brine concentration c_b , mol/l		Water flow, J , cm/h	Current Efficiency, E_p , %	Effective Current Density, i_{eff} , mA/cm ²	Transport Numbers,				
	$c_{b, exp.}$	$c_{b, calc.}$				Δt^c	Δt^a	$\bar{\Delta}t$	t_1^c	t_2^a
10	2,88	4,3	0,0625	48,26	4,83	0,90	0,55	0,73	0,95	0,77
20	4,06		0,086	46,85	9,37					
30	4,44		0,1130	44,43	13,33					
40	5,02	6,3	0,127	42,81	17,12	0,82	0,25	0,53	0,90	0,62
60	5,30		0,1576	37,32	22,39					
80	5,70		0,194	37,1	29,68					
100	5,95	7,5	0,229	36,61	36,61	0,75	0,17	0,46	0,87	0,58
120	6,30		0,256	36,03	43,24					

Electro-osmotic coefficient (2β) = 0,131 μ F (slope = 0,0049116 m/mAh)
 J_{osm} = y-intercept = 0,0465110 cm/h
 c_b^{max} = 7,6 mol/l
 $\Delta t^c = t_1^c - t_2^c$

$\Delta t^a = t_2^a - t_1^a$
 Δt = Average transport number of membrane pair
 \bar{i}_1^c = Transport number of cation through cation membrane
 \bar{i}_2^a = Transport number of anion through anion membrane.

Table 7.15 Electro-osmotic pumping experimental conditions and results for 0,05 mol/l hydrochloric acid (ABM-1 and Selemion CHV)

Current Density i , mA/cm ²	Brine concentration c_b , mol/l		Water flow J , cm/h	Current Efficiency e_p , %	Effective Current Density i_{eff} , mA/cm ²	Transport Numbers				
	$c_{b, exp.}$	$c_{b, calc.}$				Δt^c	Δt^a	$\bar{\Delta}t$	\bar{i}_1^c	\bar{i}_2^a
10	2,00	4,24	0,0675	36,24	3,621	0,98	0,55	0,77	0,99	0,76
20	2,65	5,86	0,0927	32,93	6,586	0,96	0,50	0,73	0,98	0,75
30	3,1		0,1336	29,35	8,805					
40	3,1		0,1456	30,267	12,106					
50	3,7		0,1483	29,425	14,712					
60	3,95	10,15	0,1509	26,645	15,987	0,92	0,45	0,68	0,96	0,72
80	4,00		0,1854	24,852	19,882					

Electro-osmotic coefficient (2β) = 0,188 μ F (slope = 0,0070105 m/mAh)
 J_{osm} = y-intercept = 0,0465611 cm/h
 c_b^{max} = 5,32 mol/l
 $\Delta t^c = t_1^c - t_2^c$

$\Delta t^a = t_2^a - t_1^a$
 Δt = Average transport number of membrane pair
 \bar{i}_1^c = Transport number of cation through cation membrane
 \bar{i}_2^a = Transport number of anion through anion membrane.

Table 7.16 : Electro-osmotic pumping experimental conditions and results for 0,1 mol/l hydrochloric acid (ABM-1 and Selemion CHV)

Current Density i , mA/cm ²	Brine concentration c_b , mol/l		Water flow J , cm/h	Current Efficiency e_p , %	Effective Current Density i_{eff} , mA/cm ²	Transport Numbers				
	$c_{b, exp.}$	$c_{b, calc.}$				Δt^c	Δt^a	$\bar{\Delta t}$	\bar{i}_1^c	\bar{i}_2^a
10	2,2	3,00	0,0675	39,84	3,98	0,92	0,16	0,54	0,96	0,58
20	2,85	6,0	0,0927	35,42	7,08	0,91	0,57	0,74	0,95	0,79
30	3,3		0,1324	35,05	11,72					
40	3,5	6,6	0,1483	34,79	13,91	0,87	0,45	0,66	0,93	0,73
50	3,9		0,1655	34,62	17,31					
60	4,15	7,03	0,1942	36,02	21,6	0,86	0,35	0,61	0,93	0,68
80	4,5		0,211	31,95	25,56					
100	4,9	8,76	0,247	32,47	32,47	0,85	0,30	0,58	0,93	0,65

Electro-osmotic coefficient (2β) = 0,152 μ /F (slope = 0,0056523 ml/mAh)

J_{osm} = y-intercept = 0,0692712 cm/h

c_b^{max} = 6,58 mol/l

$\Delta t^c = t_1^c - t_2^c$

$\Delta t^a = t_2^a - t_1^a$

$\bar{\Delta t}$ = Average transport number of membrane pair

\bar{i}_1^c = Transport number of cation through cation membrane

\bar{i}_2^a = Transport number of anion through anion membrane.

Table 7.17 : Electro-osmotic pumping experimental conditions and results for 0,5 mol/l hydrochloric acid (ABM-1 and Selemion CHV)

Current Density i , mA/cm ²	Brine concentration c_b , mol/l		Water flow J , cm/h	Current Efficiency e_p , %	Effective Current Density i_{eff} , mA/cm ²	Transport Numbers				
	$c_{b, exp.}$	$c_{b, calc.}$				Δt^c	Δt^a	Δt	\bar{i}_1^c	\bar{i}_2^a
10	2,35		0,0635	40,05	4,00					
20	2,80	5,2	0,0971	36,45	7,29	0,87	0,46	0,67	0,94	0,73
30	3,3		0,1165	34,36	10,31					
40	3,62	6,2	0,1456	35,34	14,14	0,84	0,35	0,60	0,92	0,68
60	4,2	6,2	0,1854	34,79	20,88	0,83	0,18	0,51	0,92	0,59
80	4,65		0,2119	33,02	26,42					
100	5,1	7,8	0,2613	35,73	35,73	0,79	0,12	0,46	0,90	0,56
120	5,25		0,291	34,17	41,00					

Electro-osmotic coefficient (2β) = 0,149 μ /F (slope = 0,0055429 ml/mAh)

J_{osm} = y-intercept = 0,0647860 cm/h

c_b^{max} = 6,71 mol/l

$\Delta t^c = t_1^c - t_2^c$

$\Delta t^a = t_2^a - t_1^a$

Δt = Average transport number of membrane pair

\bar{i}_1^c = Transport number of cation through cation membrane

\bar{i}_2^a = Transport number of anion through anion membrane.

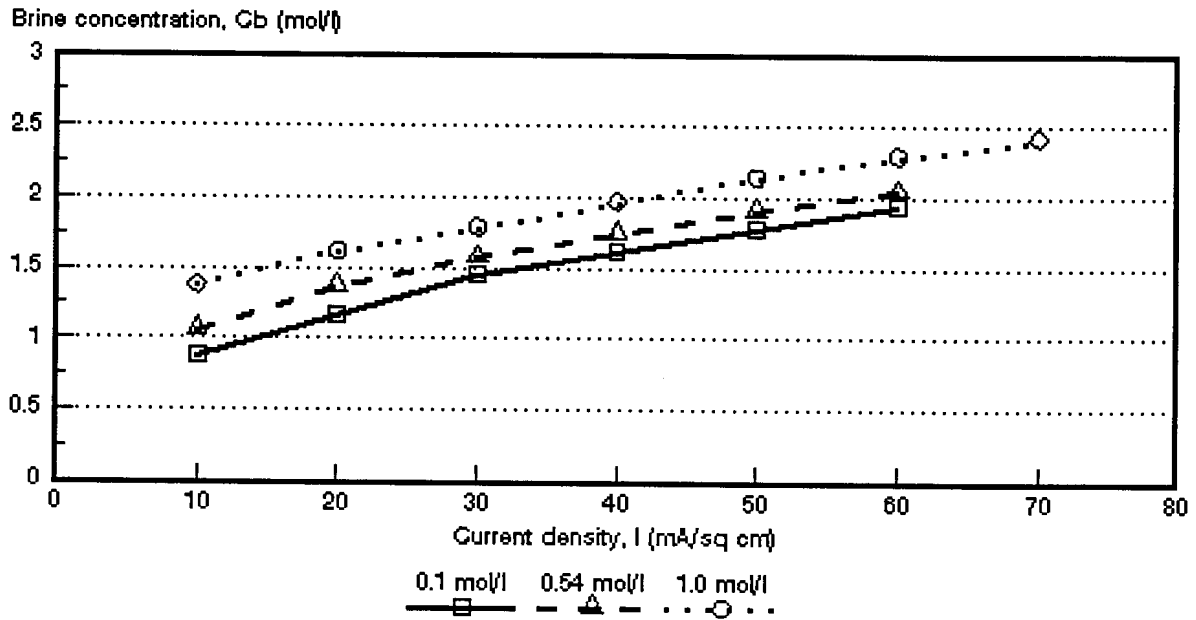


Figure 7.1: Acid concentration as a function of current density for 3 different HCl feed concentrations. *Selemion AMV and CMV membranes.*

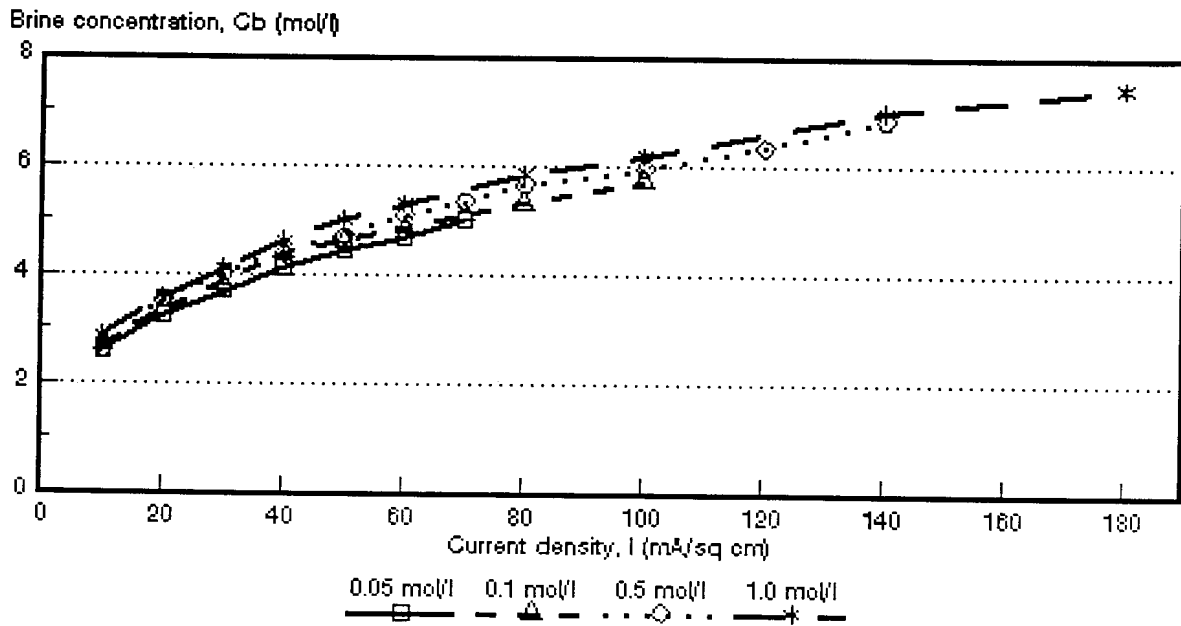


Figure 7.2: Acid concentration as a function of current density for 4 different HCl feed concentrations. *Selemion AAV and CHV membranes.*

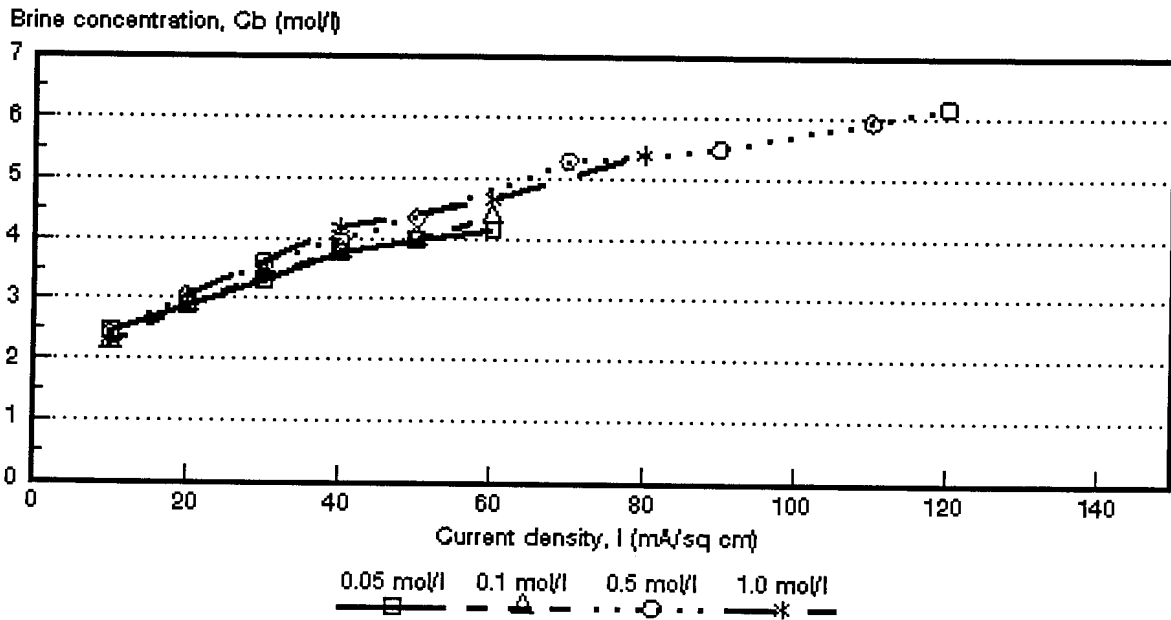


Figure 7.3: Acid concentration as a function of current density for 3 different HCl feed concentrations. *ABM-3* and *Selemion CHV* membranes.

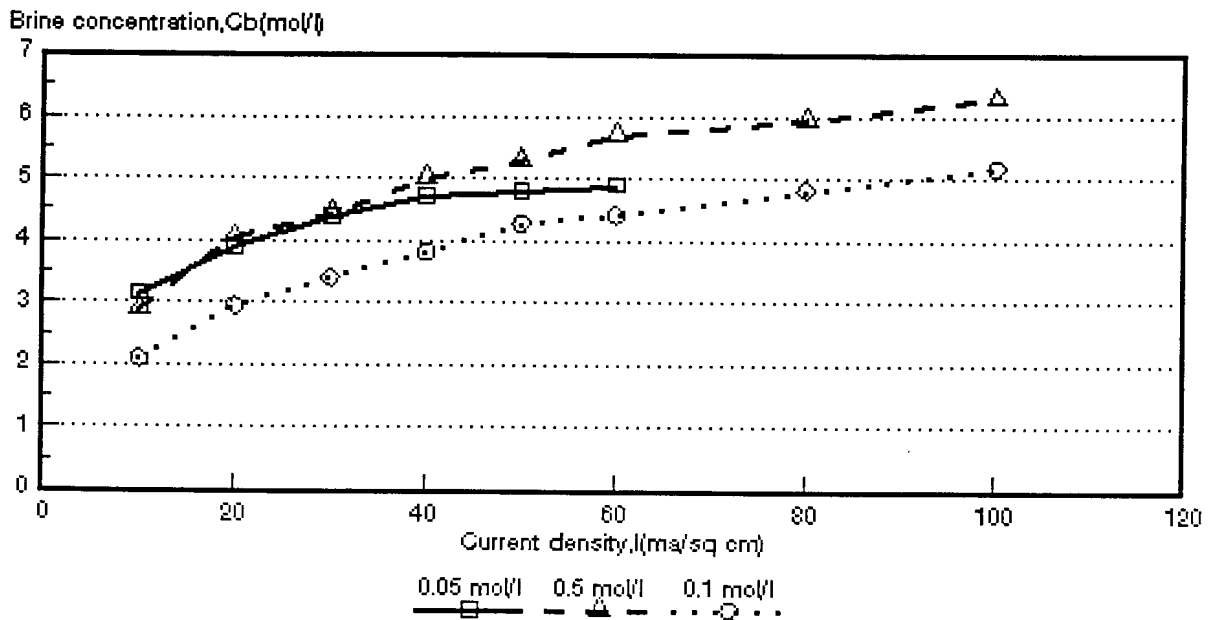


Figure 7.4 Acid concentration as a function of current density for 3 different HCl feed concentrations. *ABM-2* and *Selemion CHV* membranes.

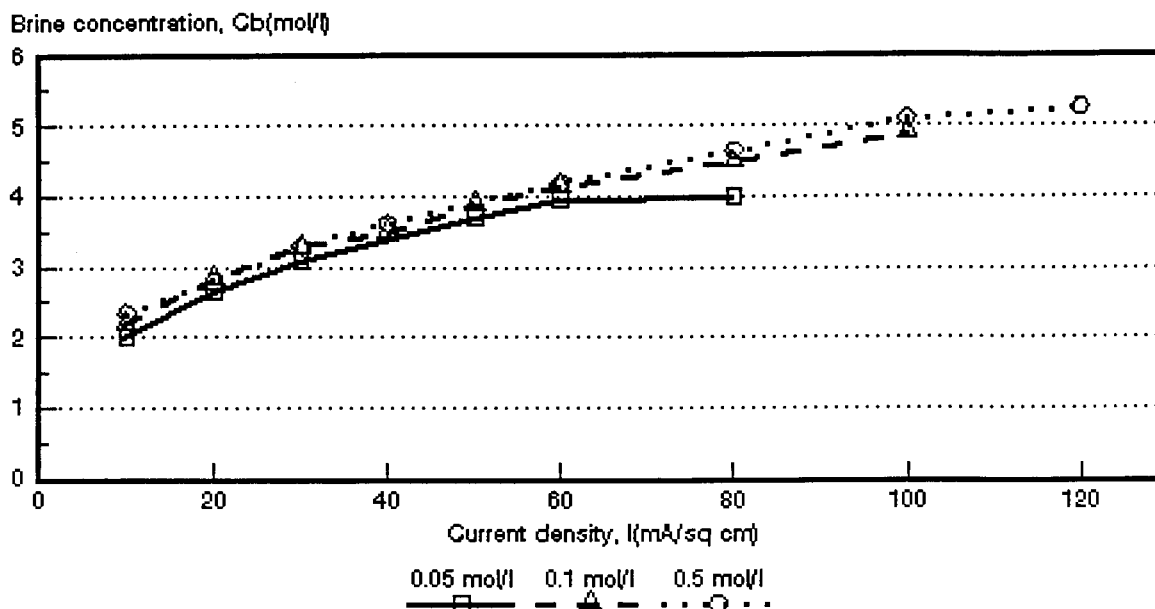


Figure 7.5: Acid concentration as a function of current density for 3 different HCl feed concentrations. ABM-1 and *Selemion* CHV membranes.

Table 7.18 Acid brine concentrations obtained at the highest current densities investigated for different hydrochloric acid feed concentrations.

Feed Concentration mol/l	Brine Concentration* (%)				
	Selemion	Selemion	Israeli & Selemion	Israeli & Selemion	Israeli & Selemion
	AMV & CMV	AAV & CHV	ABM-3 & CHV	ABM-2 & CHV	ABM-1 & CHV
0,05	-	18,3	15,2	17,9	14,6
0,10	7,1	20,9	16,0	18,9	17,9
0,50**	7,5	25,0	22,6	22,9	19,2
1,0	8,8	27,2	19,7***		

* Brine concentrations obtained from the data in Tables 7.1 to 7.17.

** 0,54 mol/l for AMV and CMV.

*** Lower current density.

of membrane permselectivity. Adsorbed hydrochloric acid and ion association are factors which decrease the proton leakage of anion exchange membranes⁽⁴⁸⁾.

It also appears as has been experienced with sodium chloride solutions that acid brine concentration will approach a maximum value, c_b^{\max} . The maximum brine concentration, c_b^{\max} , will be reached faster for the lower acid feed concentrations than for the higher acid feed concentrations (Figs. 7.3, 7.4 and 7.5). However, it appears that the maximum brine concentration for acid, especially at the higher acid feed concentrations, will be reached at much higher current densities than has been the case with the sodium chloride solutions. Maximum acid brine concentrations were calculated from the same relationships as used in 6.1. The results are shown in Table 7.19 and Figures 7.6 to 7.10. Very good correlations were obtained by the two methods.

The maximum acid brine concentration that can be obtained depends on the acid feed concentration. This was evident for all the membranes investigated. However, the maximum acid brine concentration remained almost constant in the case of the *Selemion* AAV and CHV membranes at 0,5 and 1,0 mol/l feed concentration (Table 7.19, Fig. 7.7). The same behaviour was observed for the ABM-3 and CHV membranes (Fig. 7.8). Maximum acid brine concentration for the ABM-2-, ABM-1- and CHV membranes remained constant at 0,1 and 0,5 mol/l feed concentration (Figs. 7.9 and 7.10).

Acid brine concentration at different current densities was predicted from measured transport numbers (Δt 's) and volume flows with the same relationship as used in 6.1. The experimental and calculated acid brine concentrations are shown in Tables 7.1 to 7.17 and Figures 7.11 to 7.27.

The calculated acid brine concentrations were determined from the average apparent transport number of a membrane pair ($\bar{\Delta t}$). The correlations between the calculated and the experimentally determined acid brine concentrations were not satisfactory as could be seen from Figures 7.11 to 7.27 and Table 7.20. The calculated acid brine concentrations were much higher than the experimentally determined concentrations. The calculated acid brine concentrations were approximately 3 to 4 times higher for the *Selemion* AMV and CMV membranes than the experimentally determined concentrations (Table 7.20). The calculated acid brine concentrations were approximately 1,5 to 2 times higher for the *Selemion* AAV and CHV membranes than

the experimentally determined values in the feed concentration and current density ranges studied. Approximately the same results were obtained for the ABM-3, ABM-2 and ABM-1 membranes. Therefore, it appears that simple membrane potential measurements for a membrane pair (Δt) cannot be applied effectively to predict acid brine concentration accurately. The reason for this may be ascribed to backdiffusion of acid during EOP experiments which reduces current efficiency and therefore acid brine concentration.

Table 7.19: Maximum acid brine concentration calculated from $c_b^{\max} = 1/2 F\beta^*$ and $c_b^{\max} = c_b (1 + J_{osm}/J_{elosem})^{}$**

Feed Concentration mol/l	Maximum Acid Brine Concentration, c_b^{\max} (mol/l)									
	Selemion		Selemion		Israeli & Selemion		Israeli & Selemion		Israeli & Selemion	
	AMV & CMV		AAV & CHV		ABM-3 & CHV		ABM-2 & CHV		ABM-1 & CHV	
	1	2	1	2	1	2	1	2	1	2
0,05			7,1	7,1	5,9	5,8	5,9	5,9	5,3	5,2
0,10	2,8	2,8	7,1	7,4	6,0	5,8	7,5	7,5	6,6	6,7
0,50	2,7	2,7	7,9	8,1	8,1	8,0	7,6	7,6	6,7	6,6
1,00	3,3	3,3	8,0	8,2	8,0	8,0				

- 1 : $c_b^{\max} = 1/2 F\beta$
 2 : $c_b^{\max} = c_b (1 + J_{osm}/J_{elosem})$
 * : calculated from electro-osmotic coefficients (Tables 7.1 to 7.17)
 ** : Calculated from $J_{elosem} = J - J_{osm}$ (y-intercept and the corresponding c_b values) (Tables 7.1 to 7.17)

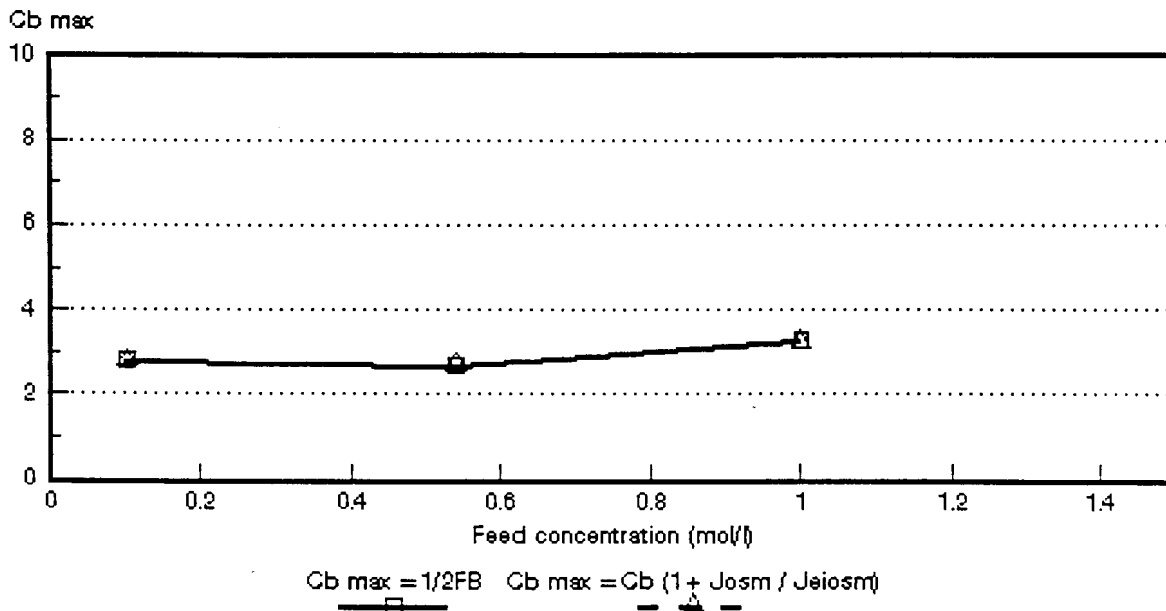


Figure 7.6: Maximum acid brine concentration as a function of feed concentration for different HCl feed concentrations. Selemion AMV and CMV membranes.

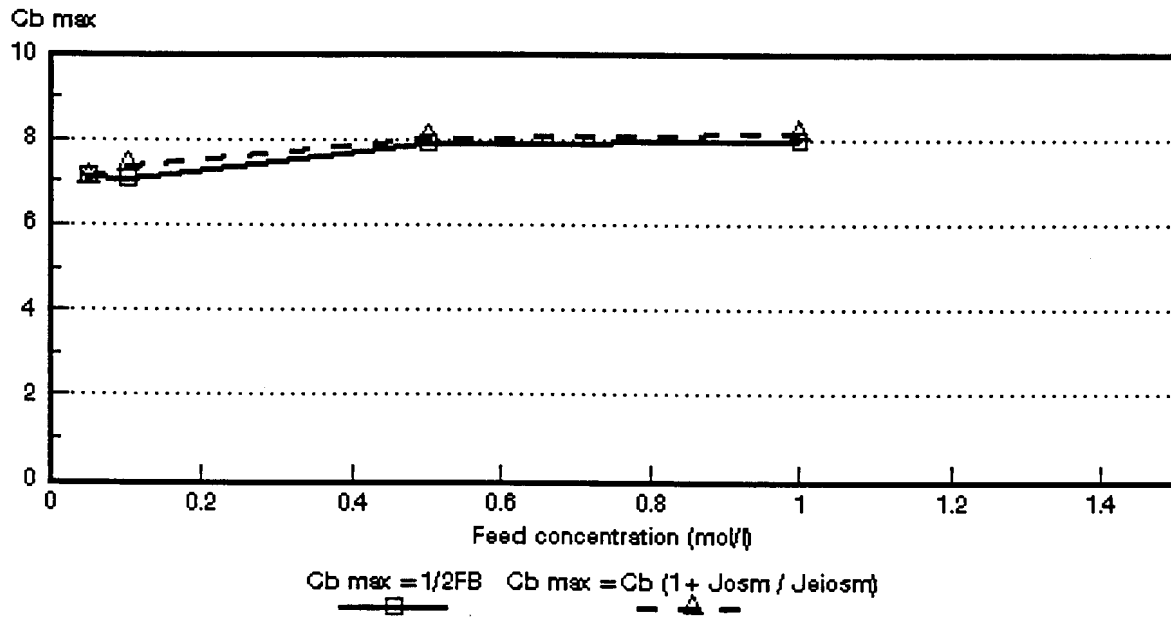


Figure 7.7: Maximum acid brine concentration as a function of feed concentration for different HCl feed concentrations. *Selemion AAV* and *CHV* membranes.

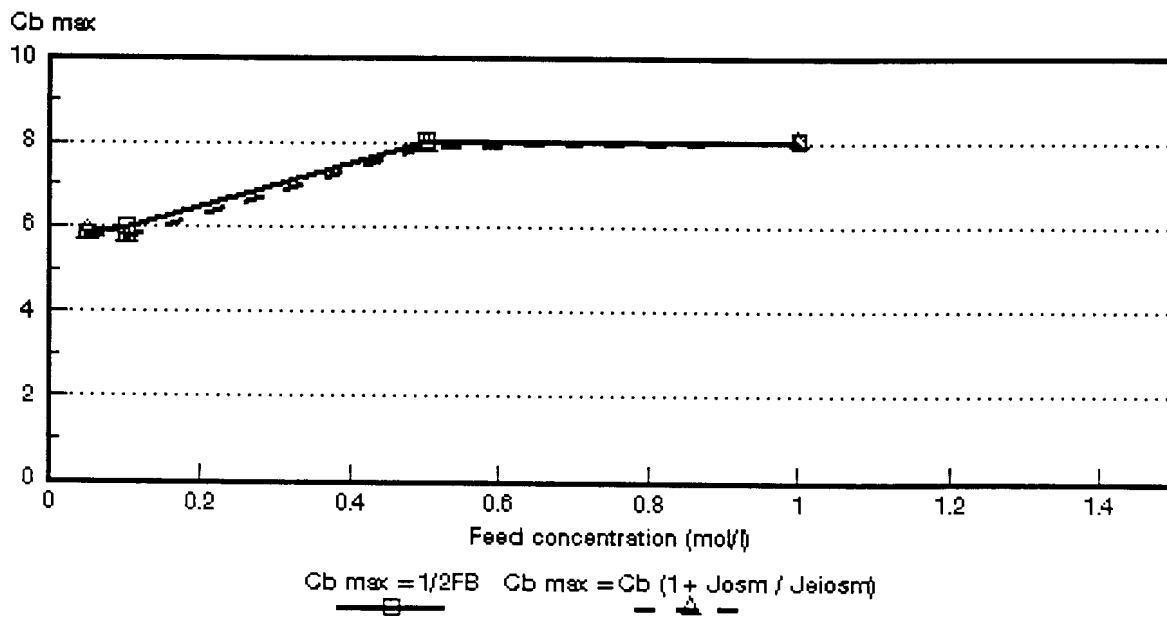


Figure 7.8: Maximum acid brine concentration as a function of feed concentration for different HCl feed concentrations. *ABM-3* and *Selemion CHV* membranes.

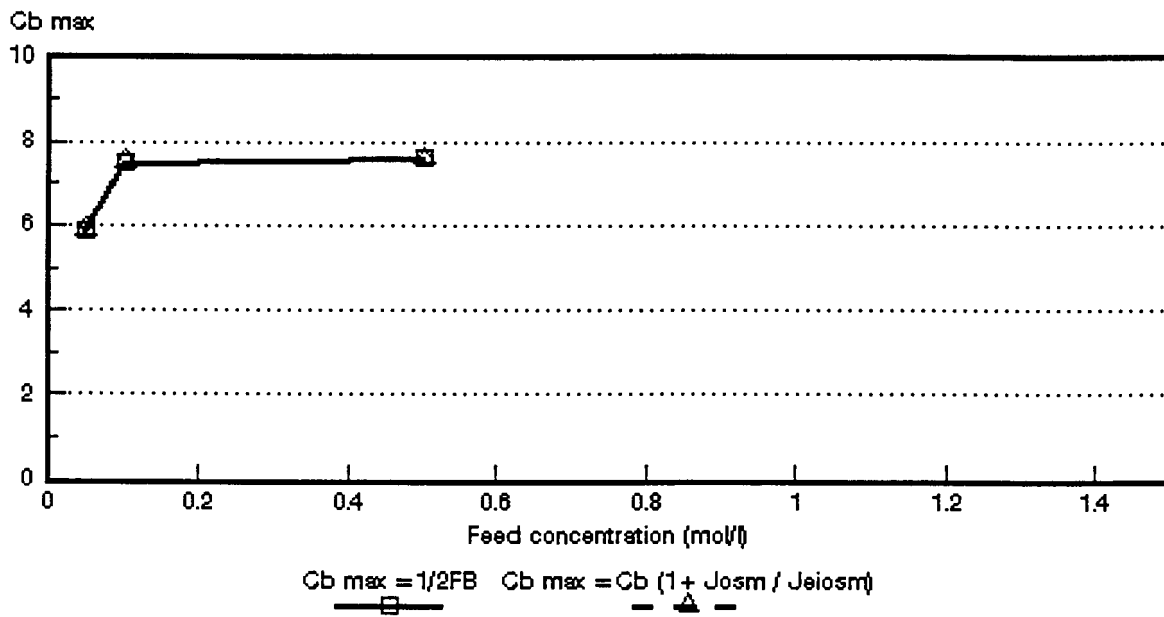


Figure 7.9: Maximum acid brine concentration as a function of feed concentration for different HCl feed concentrations. ABM-2 and *Selemion* CHV membranes.

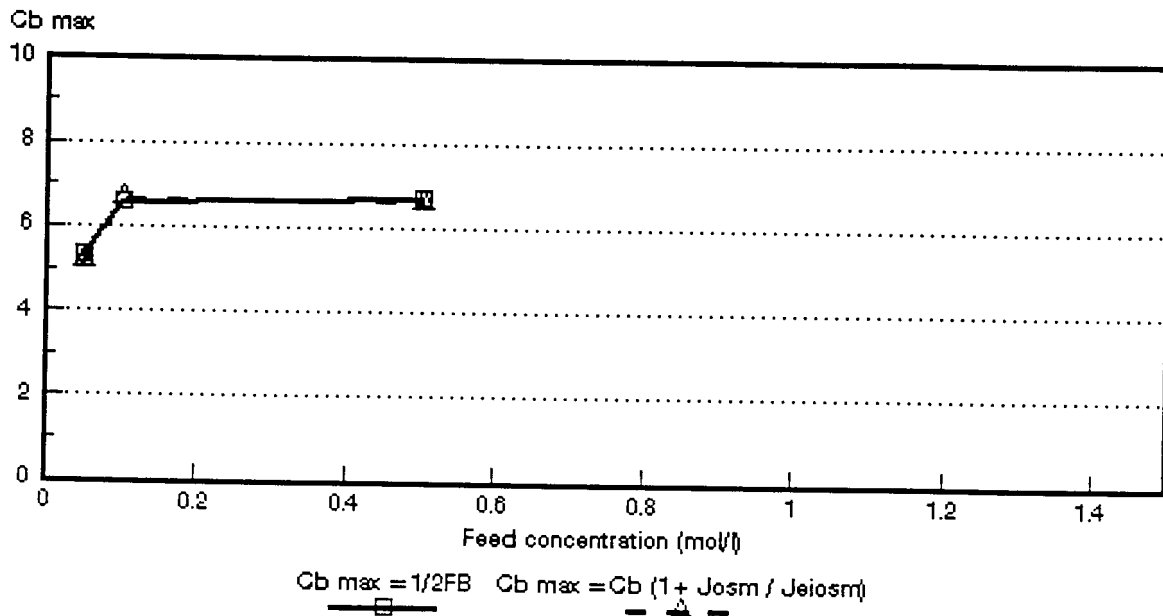


Figure 7.10: Maximum acid brine concentration as a function of feed concentration for different HCl feed concentrations. ABM-1 and *Selemion* CHV membranes.

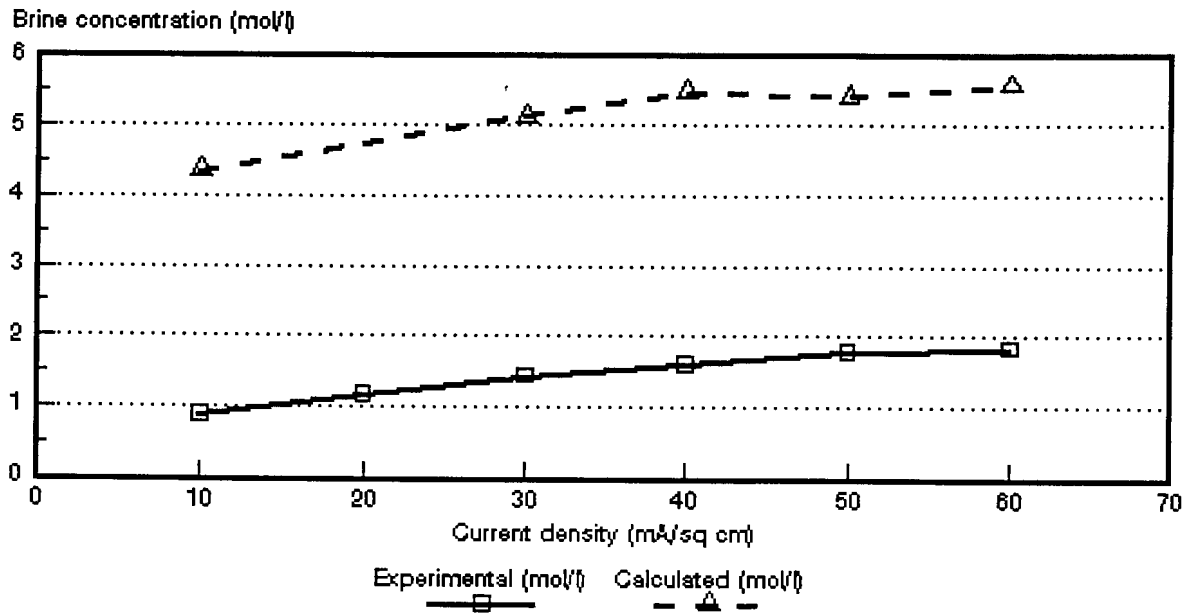


Figure 7.11: Experimental and calculated acid brine concentrations as a function of current density for 0,1 mol/l HCl feed solution. *Selemion* AMV and CMV membranes.

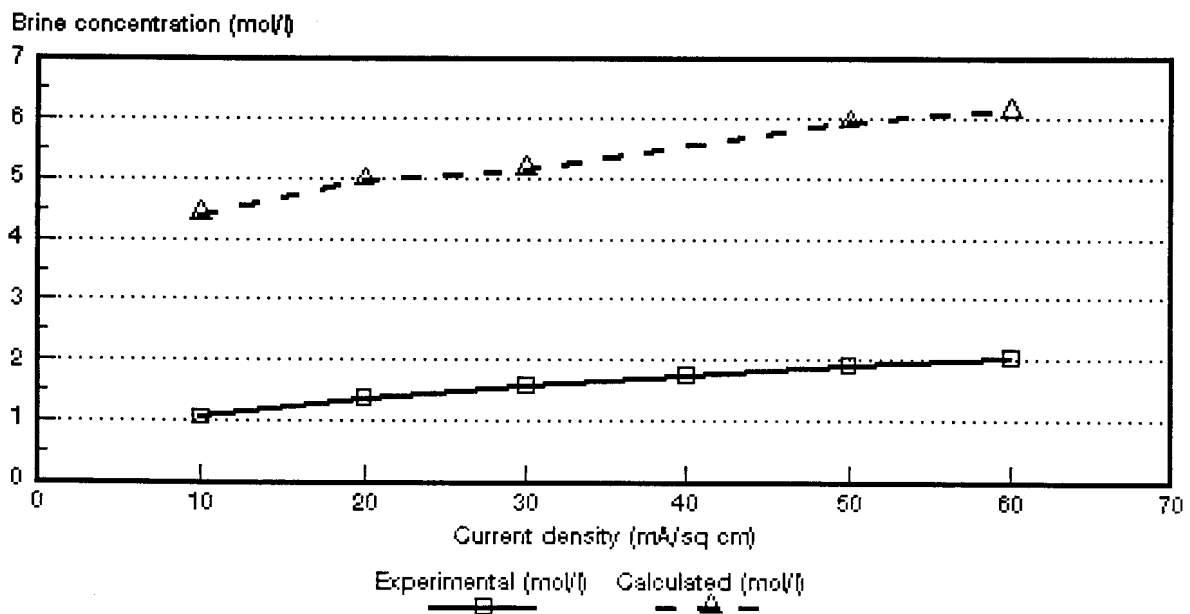


Figure 7.12: Experimental and calculated acid brine concentrations as a function of current density for 0,54 mol/l HCl feed solution. *Selemion* AMV and CMV membranes.

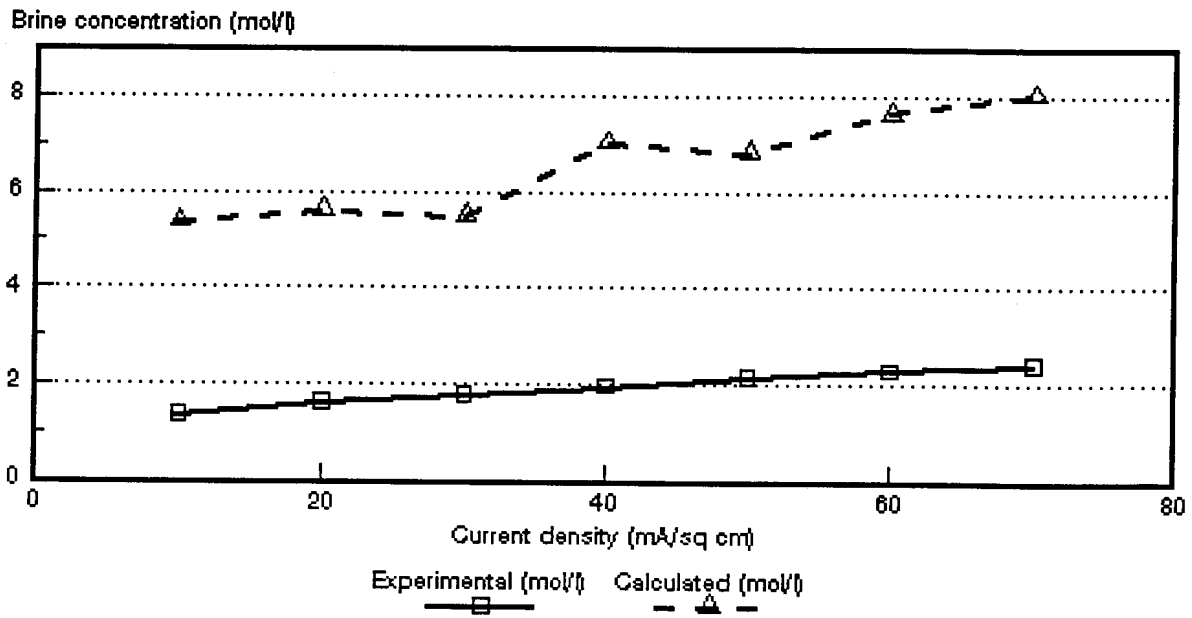


Figure 7.13: Experimental and calculated acid brine concentrations as a function of current density for 1,0 mol/l HCl feed solution. *Selemion AMV* and *CMV* membranes.

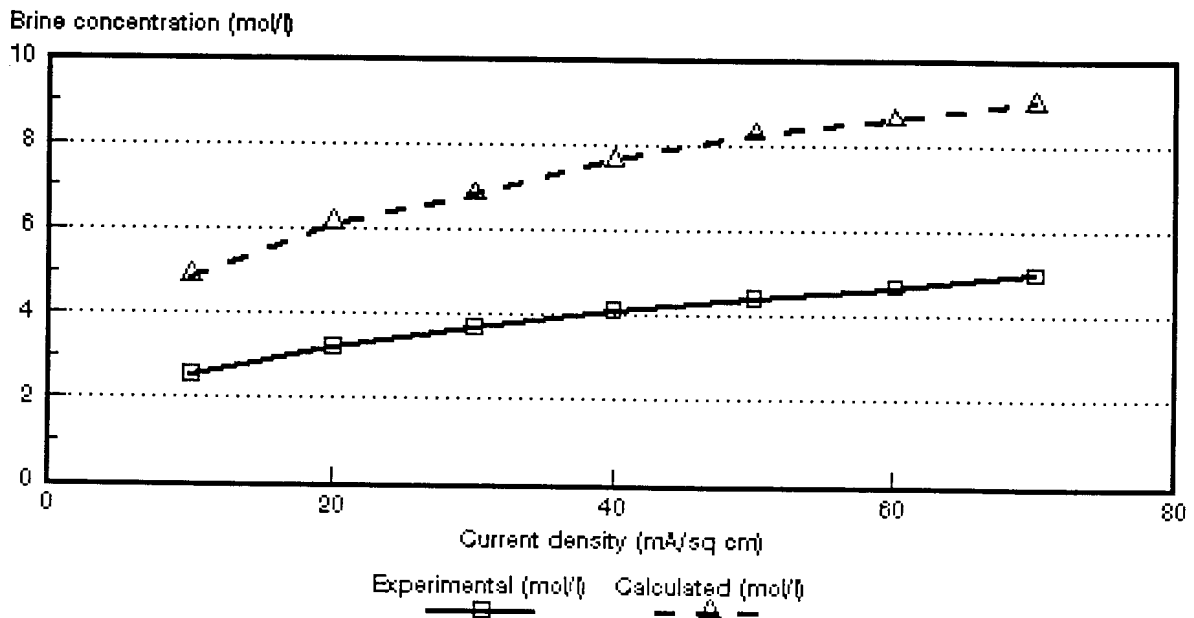


Figure 7.14: Experimental and calculated acid brine concentrations as a function of current density for 0,05 mol/l HCl feed solution. *Selemion AAV* and *CHV* membranes.

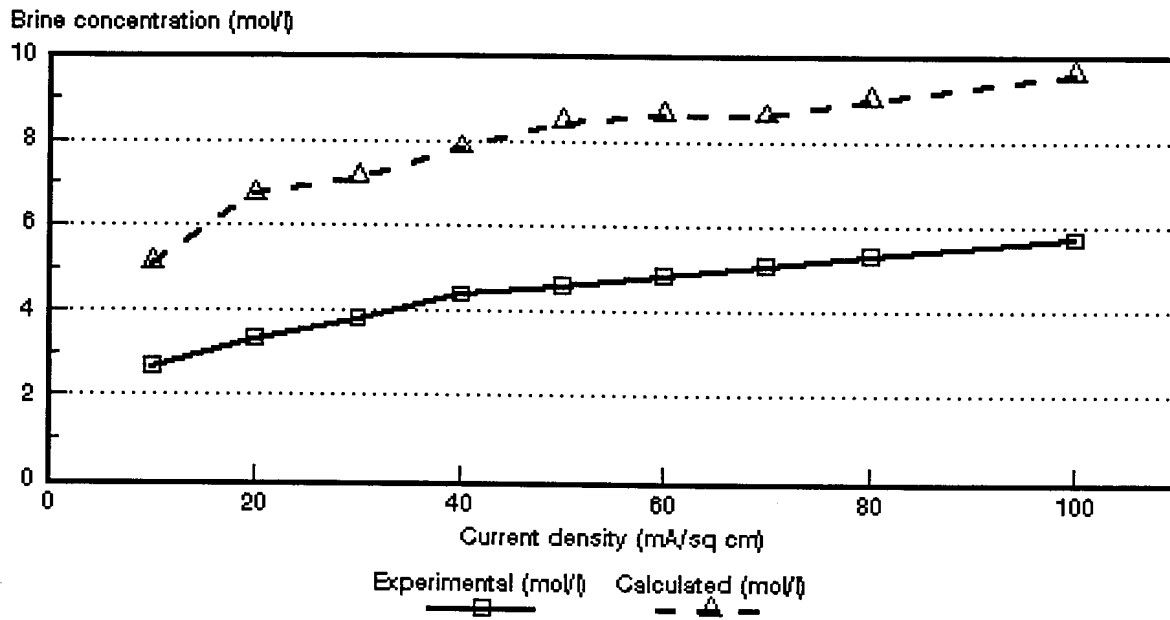


Figure 7.15: Experimental and calculated acid brine concentrations as a function of current density for 0,1 mol/l HCl feed solution. *Selemion AAV* and *CHV* membranes.

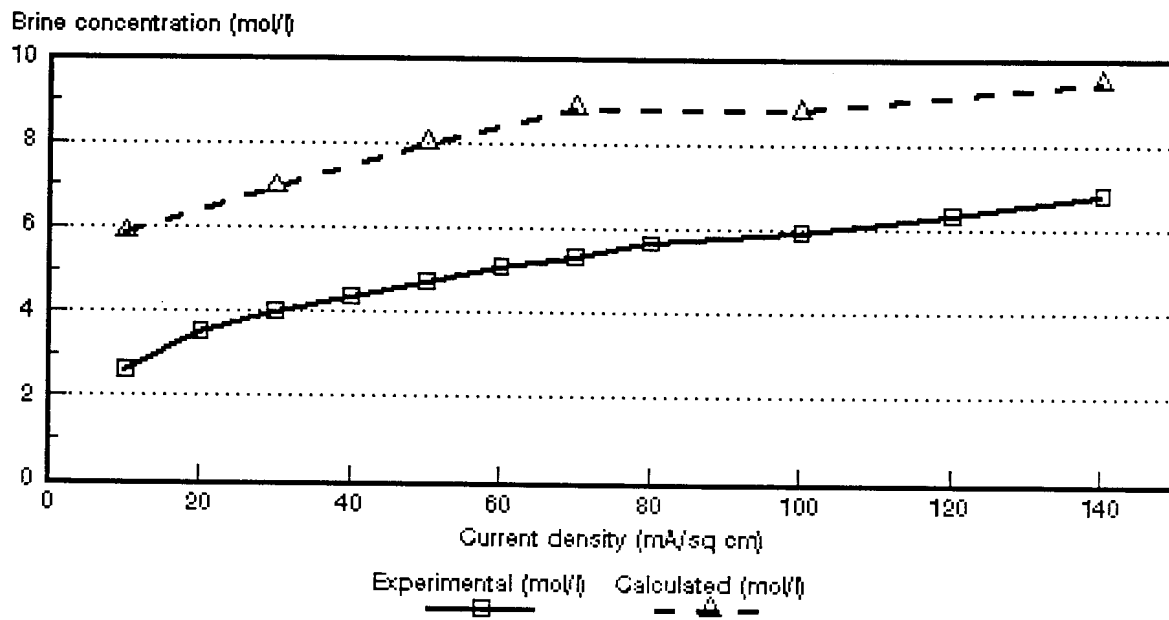


Figure 7.16: Experimental and calculated acid brine concentrations as a function of current density for 0,5 mol/l HCl feed solution. *Selemion AAV* and *CHV* membranes.

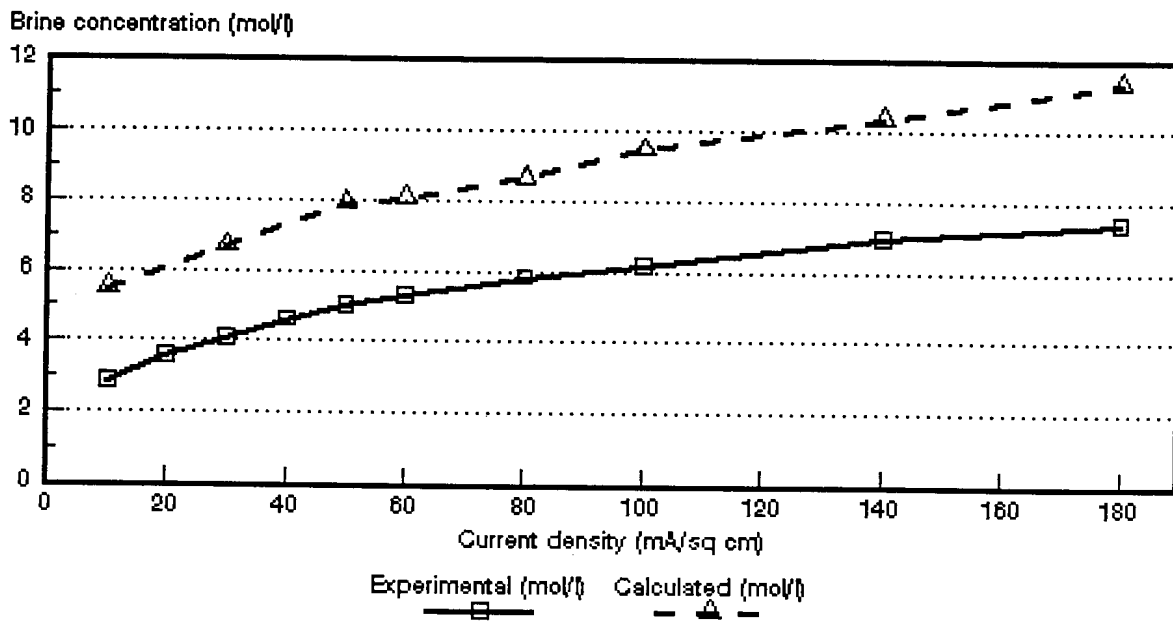


Figure 7.17: Experimental and calculated acid brine concentrations as a function of current density for 1,0 mol/l HCl feed solution. *Selemlon* AAV and CHV membranes.

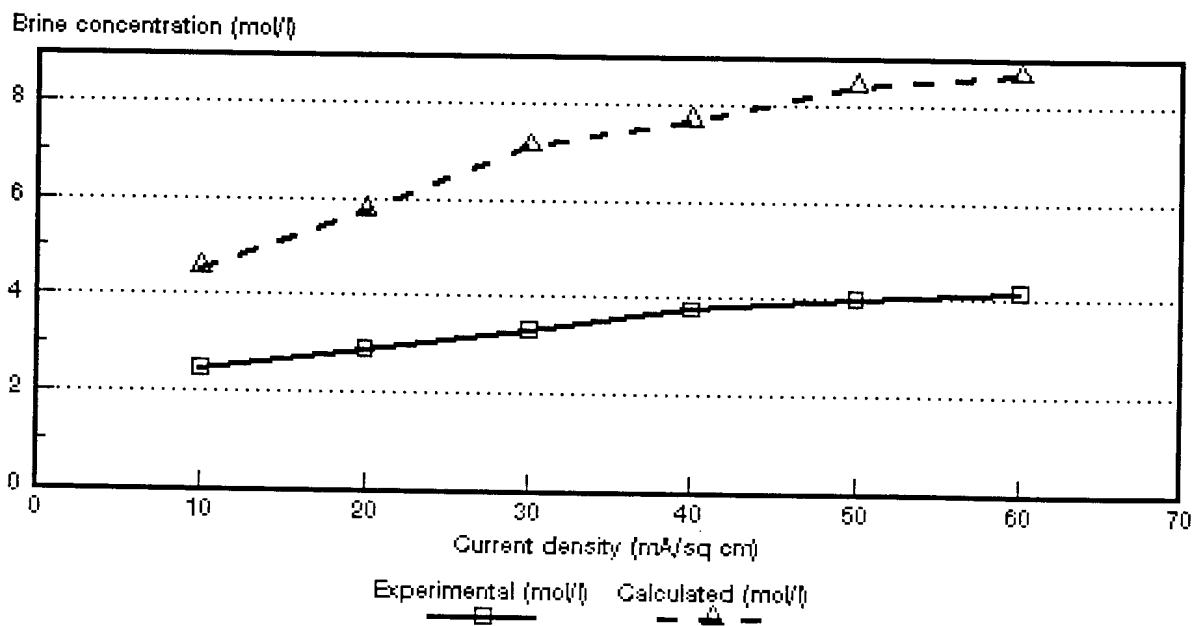


Figure 7.18: Experimental and calculated acid brine concentrations as a function of current density for 0,05 mol/l HCl feed solution. ABM-3 and CHV membranes.

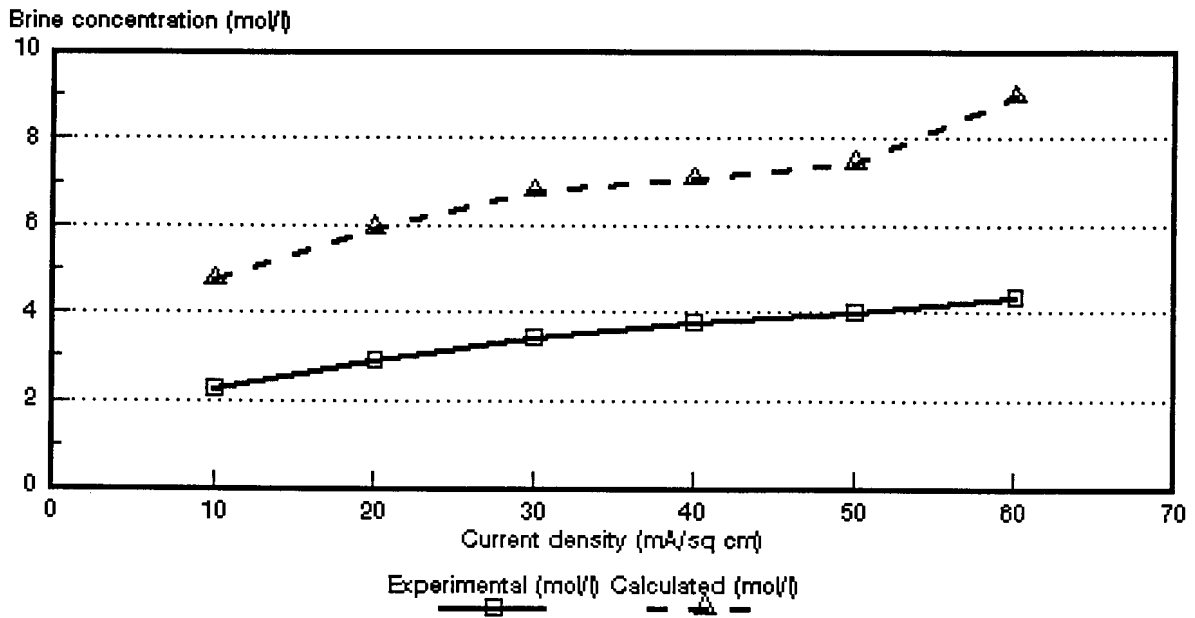


Figure 7.19: Experimental and calculated acid brine concentrations as a function of current density for 0,1 mol/l HCl feed solution. ABM-3 and CHV membranes.

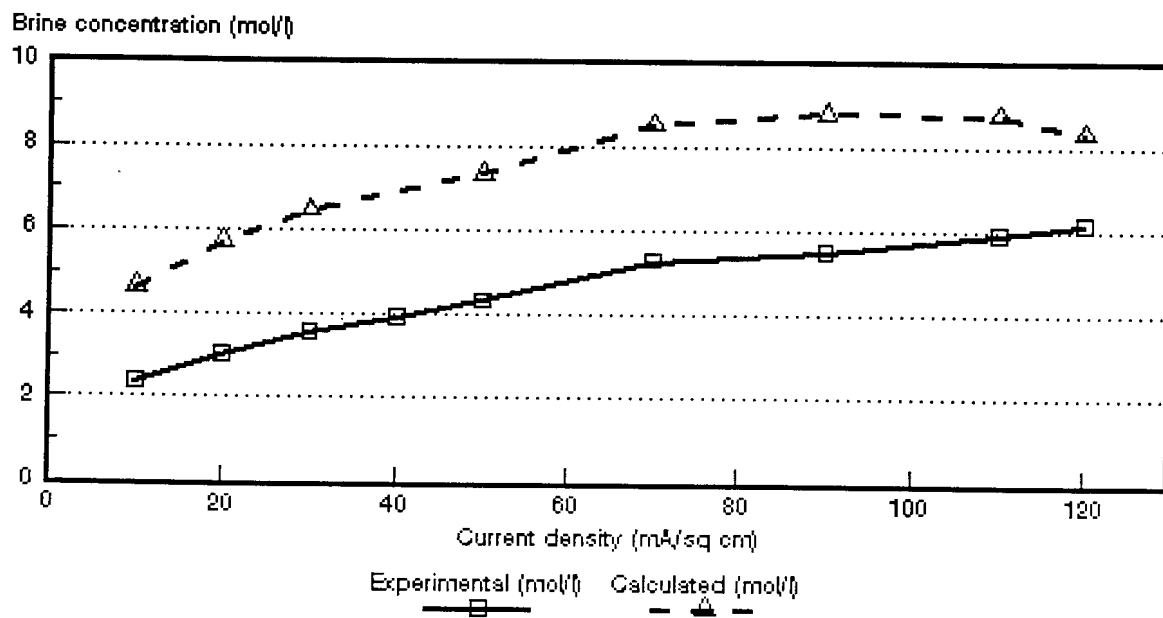


Figure 7.20: Experimental and calculated acid brine concentrations as a function of current density for 0,5 mol/l HCl feed solution. ABM-3 and CHV membranes.

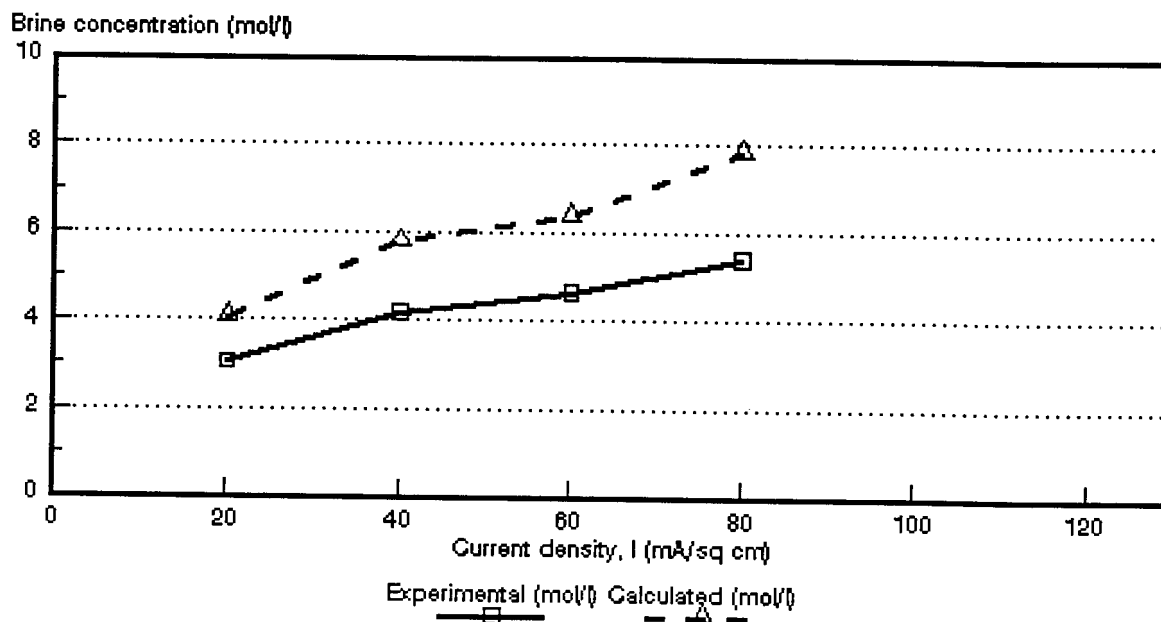


Figure 7.21: Experimental and calculated acid brine concentrations as a function of current density for 1,0 mol/l HCl feed solution. ABM-3 and CHV membranes.

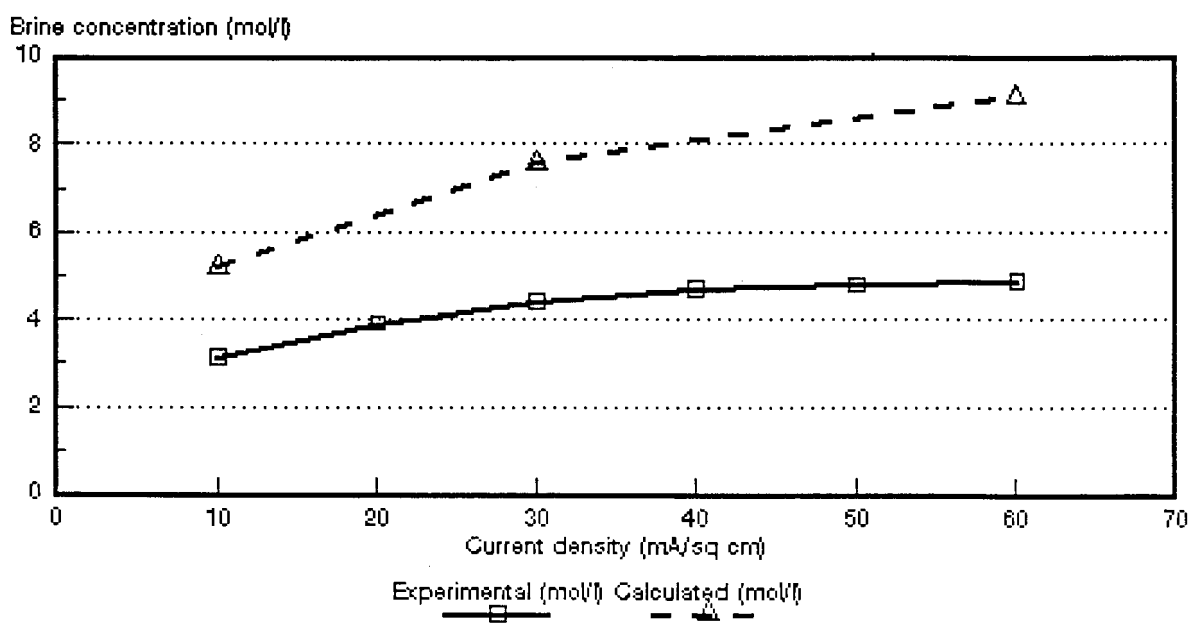


Figure 7.22: Experimental and calculated acid brine concentrations as a function of current density for 0,05 mol/l HCl feed solution. ABM-2 and CHV membranes.

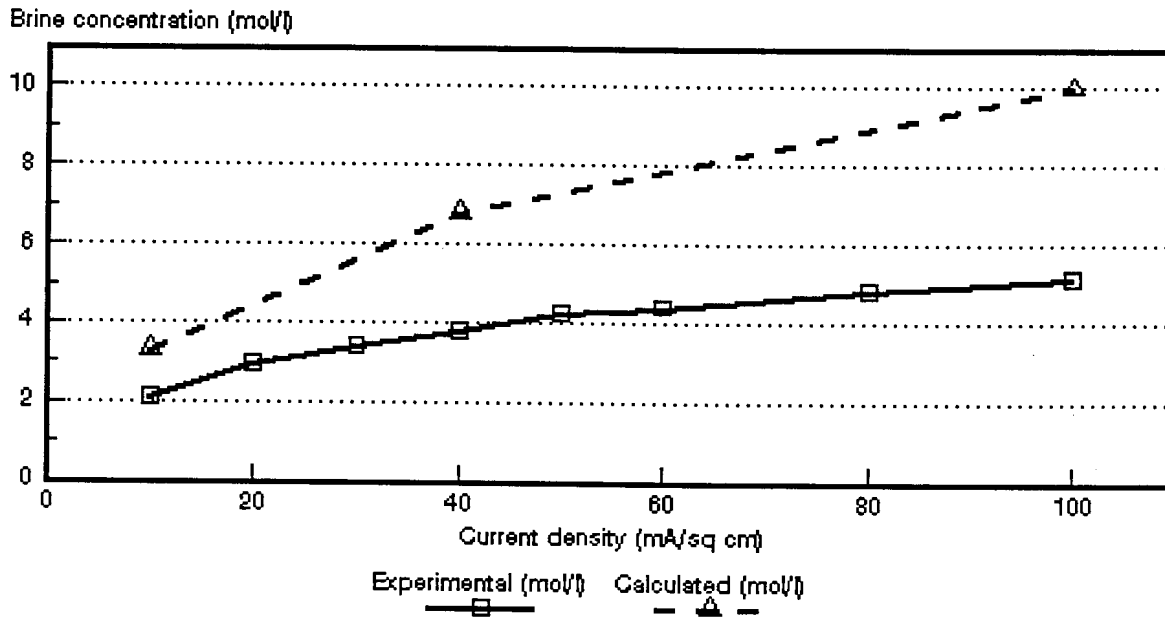


Figure 7.23: Experimental and calculated acid brine concentrations as a function of current density for 0,1 mol/l HCl feed solution. ABM-2 and CHV membranes.

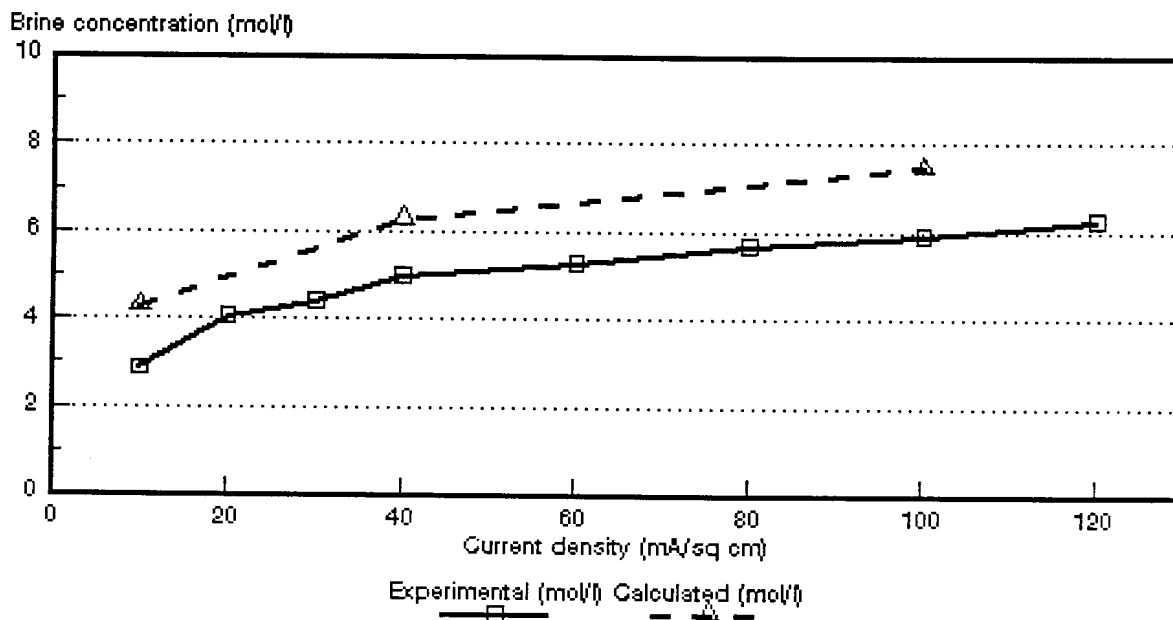


Figure 7.24: Experimental and calculated acid brine concentrations as a function of current density for 0,5 mol/l HCl feed solution. ABM-2 and CHV membranes.

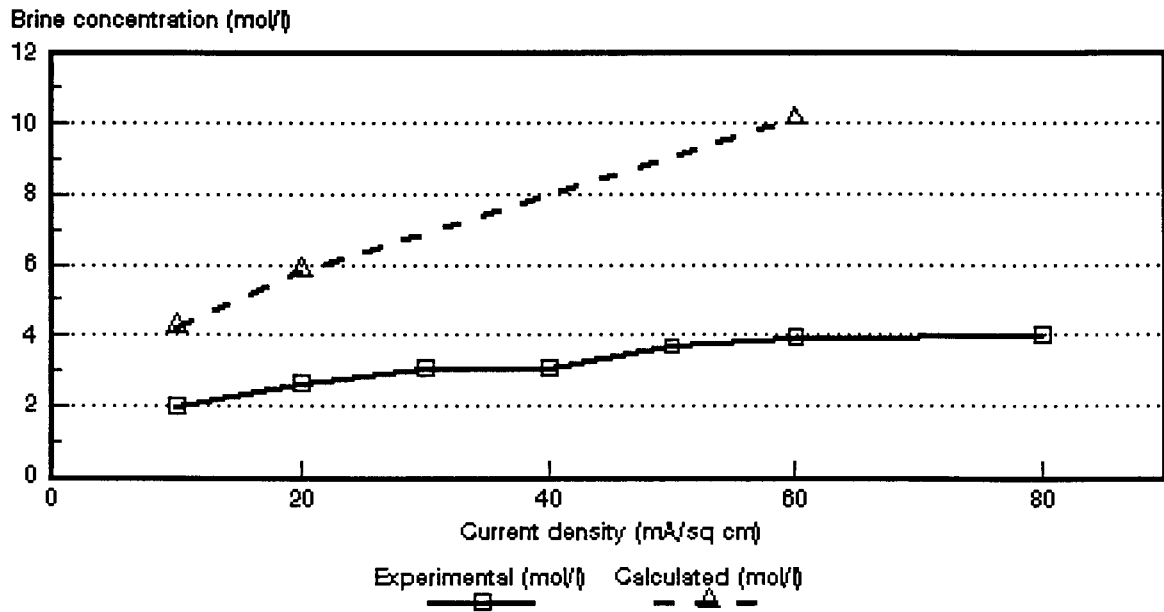


Figure 7.25: Experimental and calculated acid brine concentrations as a function of current density for 0,05 mol/l HCl feed solution. ABM-1 and CHV membranes.

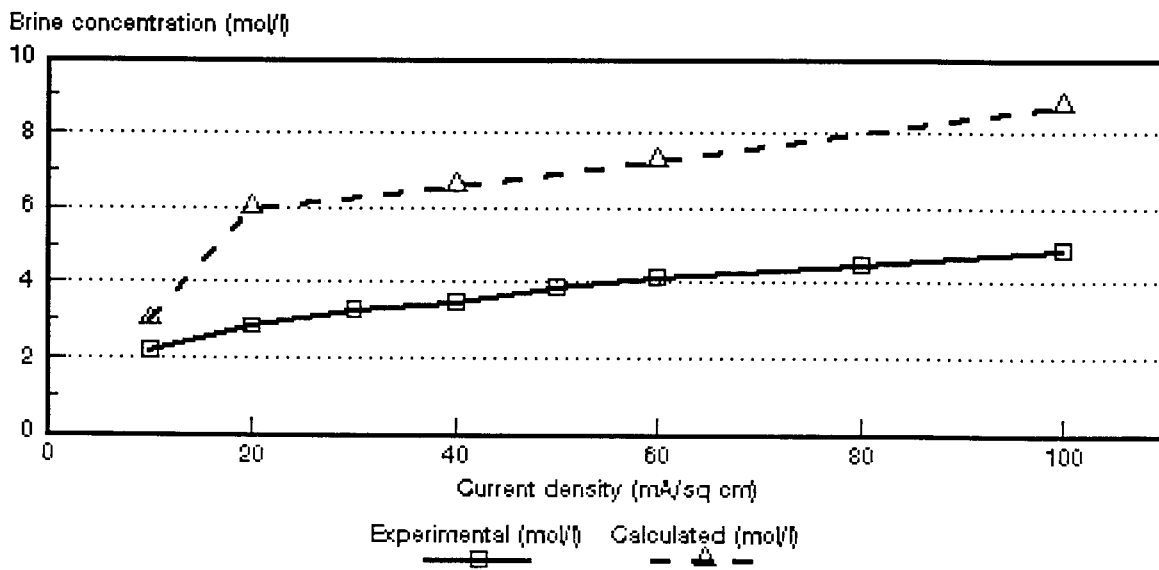


Figure 7.26: Experimental and calculated acid brine concentrations as a function of current density for 0,1 mol/l HCl feed solution. ABM-1 and CHV membranes.

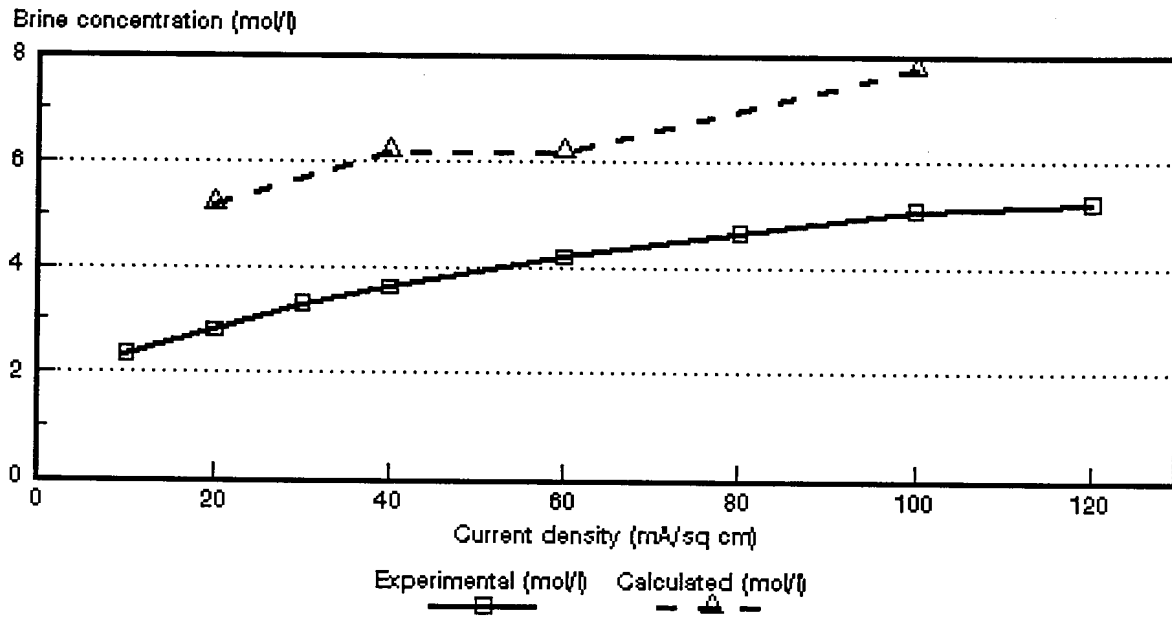


Figure 7.27: Experimental and calculated acid brine concentrations as a function of current density for 0,5 mol/l HCl feed solution. ABM-1 and CHV membranes.

Tabel 7.20: Correlation between calculated (c_{bcalc}) and experimentally (c_{bexp}) determined acid brine concentrations.

Current Density mA/cm ²	c_{bcalc}/c_{bexp}																			
	Selemion AMV & CMV Concentration, mol/l				Selemion AAV & CHV Concentration, mol/l				Israeli & Selemion ABM-3 & CHV Concentration, mol/l				Israeli & Selemion ABM-2 & CHV Concentration, mol/l				Israeli & Selemion ABM-1 & CHV Concentration, mol/l			
	0,05	0,1	0,5	1,0	0,05	0,1	0,5	1,0	0,05	0,1	0,5	1,0	0,05	0,1	0,5	1,0	0,05	0,1	0,5	1,0
10		4,95	4,13	3,96	1,88	1,91	2,24	1,91	1,84	2,10	1,93		1,65	1,57	1,49		2,12	1,36		
20		3,99	3,64	3,48	1,89	2,01			2,00	2,05	1,88	1,33					2,21	2,11	1,86	
30		3,54	3,27	3,08	1,85	1,87	1,72	1,63	2,14	1,99	1,80		1,73							
40		3,39	3,05	3,57	1,86	1,78			2,03	1,88		1,39		1,78				1,89	1,71	
50		3,05	3,12	3,17	1,86	1,83	1,70	1,59	2,11	1,87	1,69				1,25					
60		2,86	3,00	3,34	2,05	1,78		1,52	2,09	2,05		1,38	1,86				2,57	1,69	1,48	
70				3,32	1,80	1,69	1,65				1,61									
80						1,69		1,48				1,46								
90											1,60									
100						1,68	1,48	1,53							1,26			1,79	1,53	
110											1,47			1,93						
120											1,35									
130																				
140							1,40	1,49												
150																				
160																				
170																				
180								1,53												

7.2 Current Efficiency

Current efficiency (ϵ_p) determined during EOP experiments as a function of current density is shown in Figures 7.28 to 7.32. Current efficiency was determined to be very low (approximately 13 to 16%) for the *Selemion* AMV and CMV membranes (Fig. 7.28). This low current efficiency can be ascribed to the low permselectivity of the *Selemion* AMV membranes for chloride ions (proton leakage) (Tables 7.1 to 7.3). The permselectivity (Δt^a) of the *Selemion* AMV membrane was shown to vary between 0,3 and 0,02 at 0,1 mol/l acid feed concentration at different concentration gradients in the current density range from 10 to 60 mA/cm². Permselectivities varied from 0,15 to 0,08 and from 0,09 to 0,18 at 0,54 and 1,0 mol/l acid feed concentration, respectively. Therefore, the *Selemion* AMV membrane has a very low permselectivity for chloride ions.

Current efficiencies obtained with the *Selemion* AAV and CHV membranes were much higher than current efficiencies obtained with the *Selemion* AMV and CMV membranes (Fig. 7.29). Current efficiency of the *Selemion* AAV and CHV membranes was determined at approximately 40%. The apparent transport numbers of the anion-exchange membrane were much higher in this case (Table 7.4 to 7.7) than in the case of the *Selemion* AMV membrane. The apparent transport numbers for the AAV anion-exchange membrane (Δt^a) varied between 0,67 and 0,49 at 0,05 mol/l feed concentration (Table 7.4). Approximately the same values were obtained for the apparent transport number of the *Selemion* AAV membrane in the 0,1 to 1,0 mol/l feed concentration range. Current efficiencies obtained for the ABM-3 and CHV membranes were slightly lower than that obtained for the *Selemion* AAV and CHV membranes in the 0,05 to 0,5 mol/l feed concentration range (Fig. 7.30). Current efficiency was determined at approximately 37%. However, current efficiency for the ABM-3 and CHV membranes was much higher at 1,0 mol/l feed concentration. Current efficiency varied between 60 and 47%. Current efficiency for the ABM-2 and CHV membranes was initially higher than 40% (Fig. 7.31) but then decreased to between 30 and 40%. Current efficiency for the ABM-1 and CHV membranes was determined at between 25 and 40%. It is interesting to note that current efficiency has increased with increasing acid feed concentration in the case of the ABM and CHV membranes.

Current efficiency remained almost constant with increasing current density and increasing acid feed concentration in the case of the *Selemion* AMV and CMV and

Selemion AAV and CHV membranes (Figs. 7.28 and 7.29). However, current efficiency decreased somewhat with increasing current density in the case of the ABM-3, ABM-2 and ABM-1 membranes (Fig's. 7.30 to 7.32). This was more pronounced at the lower acid feed concentrations. Therefore, it appeared that the limiting current density was exceeded. However, current efficiency remained approximately constant at the higher acid feed concentrations (0,5 mol/l) at high current densities showing that polarization was absent.

The apparent transport numbers ($\bar{\Delta}t$, Δt^a and Δt^c) for a concentration difference similar to that obtained in the EOP experiments are shown in Figures 7.33 to 7.49. The current efficiencies (e_p) as determined by the EOP method and shown in Figures 7.28 to 7.32 are also shown in Figures 7.33 to 7.49. The correlation between the apparent transport numbers ($\bar{\Delta}t$, Δt^a , Δt^c) and current efficiency is shown in Tables 7.21 to 7.23.

The apparent transport numbers ($\bar{\Delta}t$'s) were much higher than the current efficiencies (e_p 's) as determined by the EOP method (Tables 7.21 to 7.23 and Figs. 7.33 to 7.49). The apparent transport numbers were from 3 to 5 times higher than the current efficiencies in the case of the *Selemion* AMV and CMV membranes in the acid feed concentration and current density ranges investigated (Table 7.21). In the case of the *Selemion* AAV and CHV membranes the apparent transport numbers were 1,5 to 2 times higher than the current efficiencies. Much the same results were found for the ABM and CHV membranes. Therefore, it appears that a simple membrane potential measurement cannot be used effectively in the case of acids to predict membrane performance accurately. The reason for the big difference between the apparent transport number and the current efficiency may be ascribed to backdiffusion of acid during EOP of acids.

It is interesting to note that much better correlations have been obtained between the apparent transport numbers of the anion membranes (Δt^a) and current efficiencies (Table 7.22). The apparent transport numbers were approximately 1,3 to 1,4 times higher than the current efficiencies in the case of the *Selemion* AAV and CHV membranes in the current density range from 30 to 70 mA/cm² (0,5 mol/l feed). An even better correlation was obtained at 1,0 mol/l feed concentration in the current density range from 40 to 140 mA/cm². The apparent transport numbers were from 1,05 to 1,19 times higher than current efficiencies in this range. The ratio between apparent transport number and current efficiency ($\Delta t^a/e_p$) varied between 1,22 and 0,86 for the ABM-3 and CHV membranes in the current density range from 30 to 70

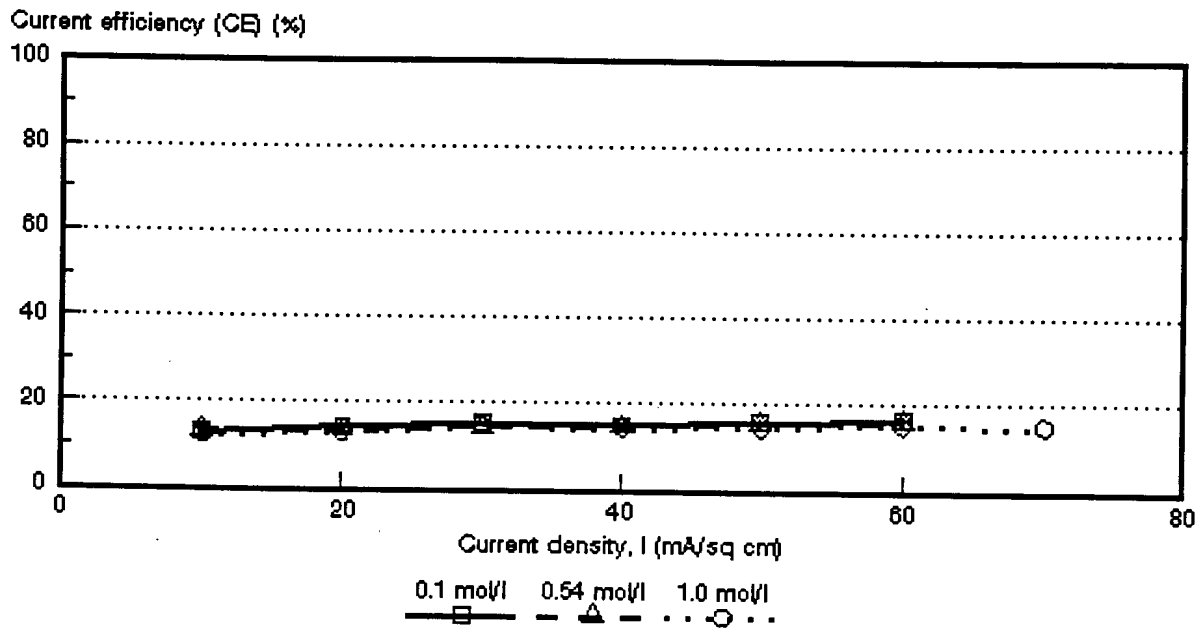


Figure 7.28: Current efficiency (e_p) as a function of current density for 3 different HCl feed concentrations. *Selemion AMV and CMV membranes.*

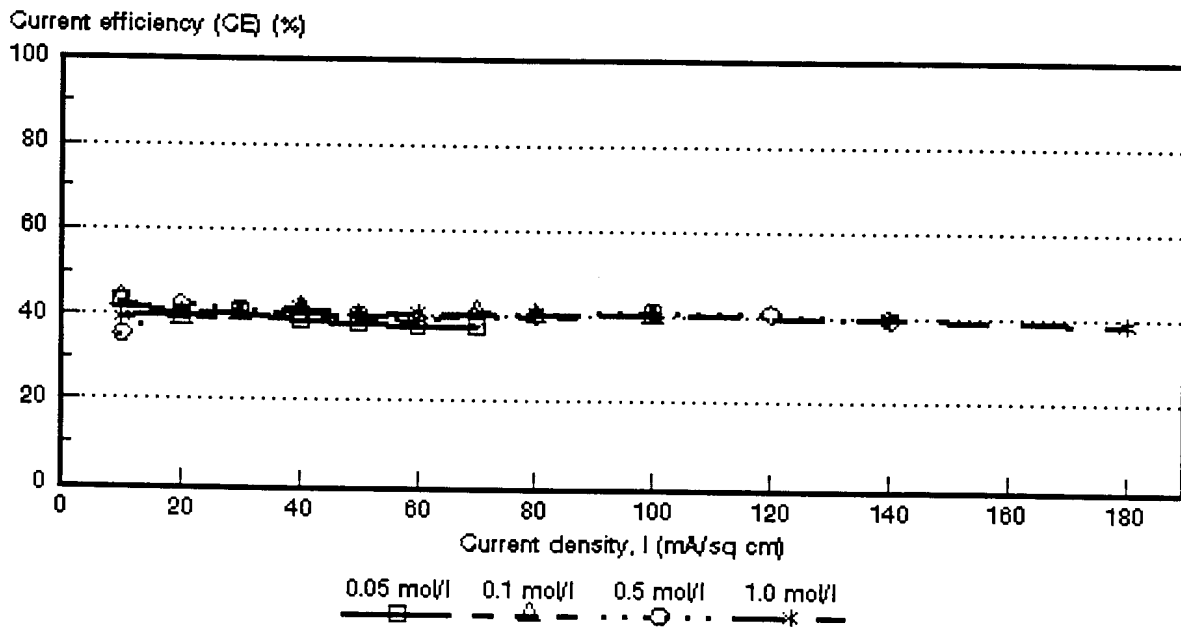


Figure 7.29: Current efficiency (e_p) as a function of current density for 4 different HCl feed concentrations. *Selemion AAV and CHV membranes.*

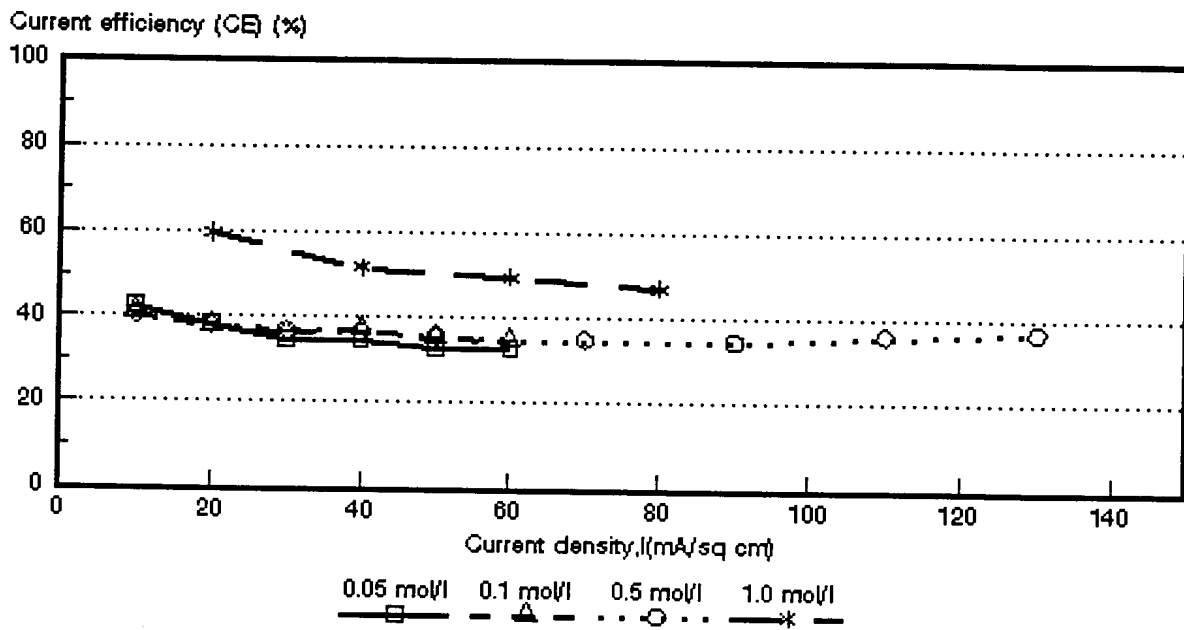


Figure 7.30: Current efficiency (e_p) as a function of current density for 4 different HCl feed concentrations. ABM-3 and *Selemion* CHV membranes.

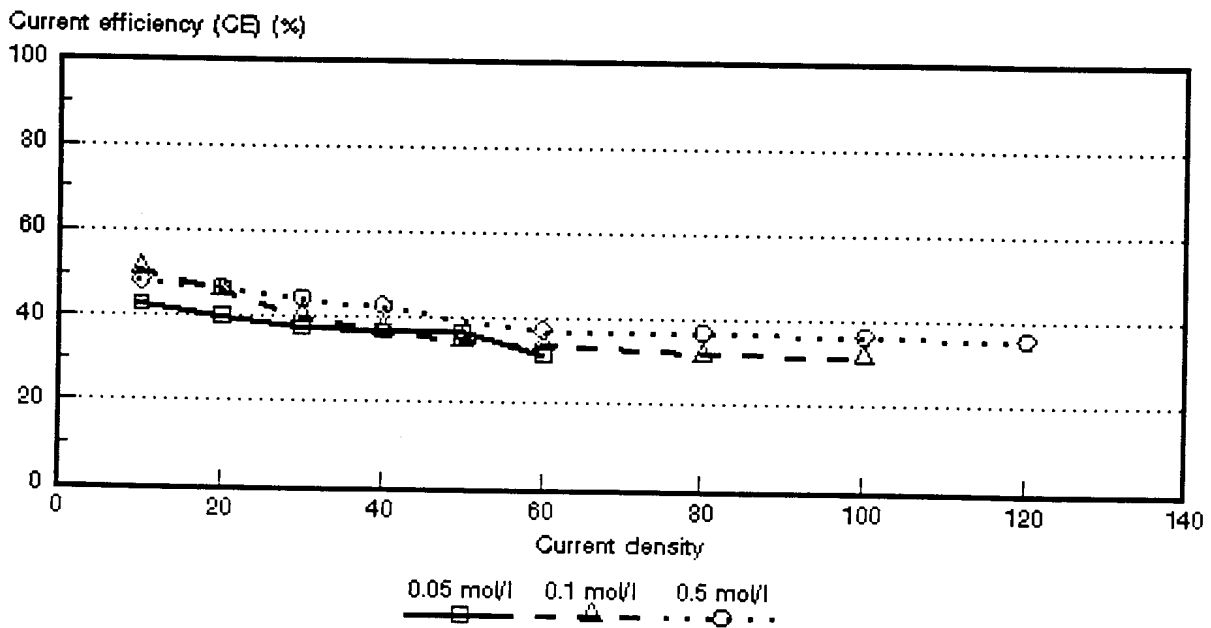


Figure 7.31: Current efficiency (e_p) as a function of current density for 3 different HCl feed concentrations. ABM-2 and *Selemion* CHV membranes.

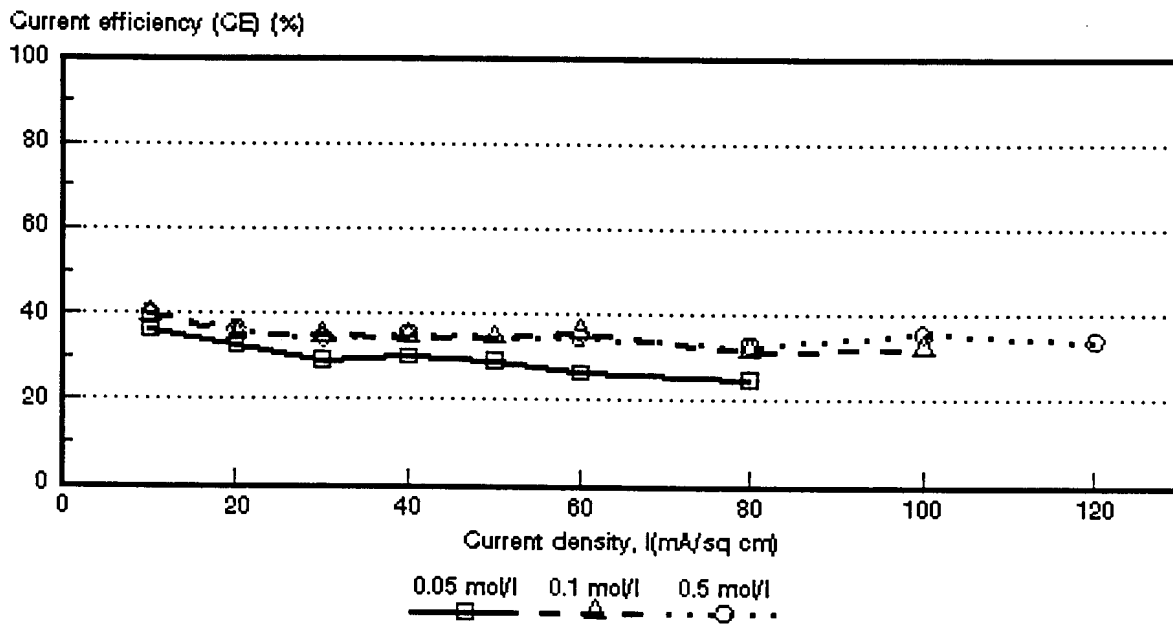


Figure 7.32: Current efficiency (e_p) as a function of current density for 3 different HCl feed concentrations. *ABM-1* and *Selmemion CHV* membranes.

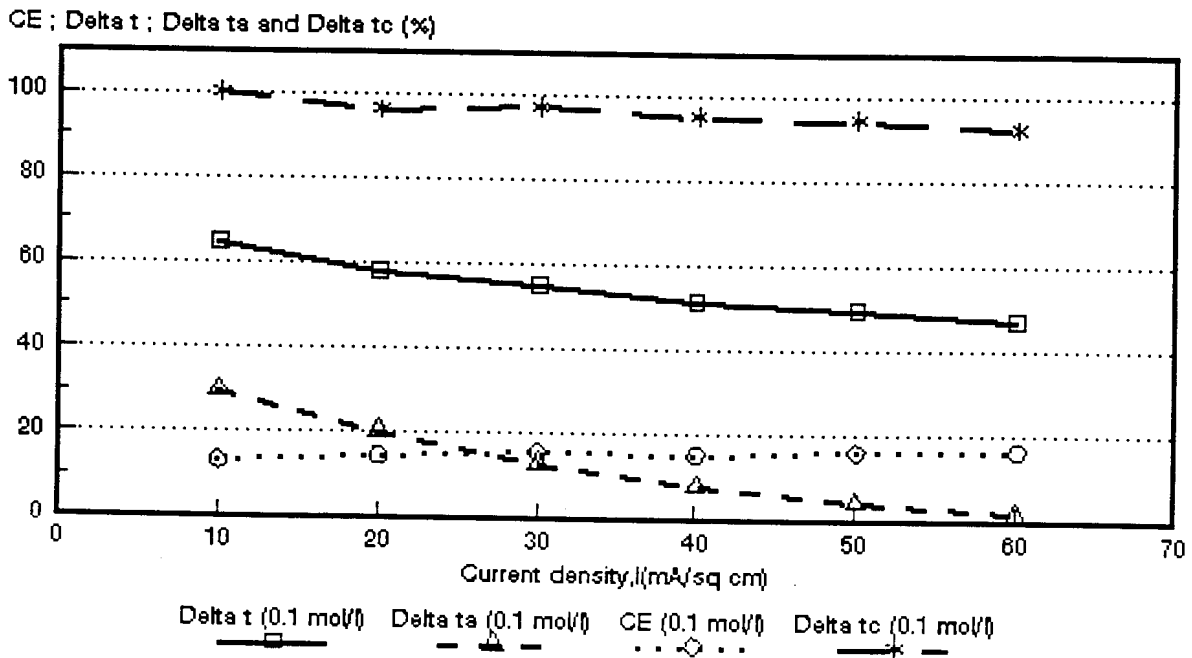


Figure 7.33: Current efficiency ($CE = e_p$) as a function of current density for 0,1 mol/l HCl feed. *Selmemion AMV* and *CMV* membranes. $\Delta t = \bar{\Delta}t$; $\Delta t_a = \Delta t^a$; $\Delta t_c = \Delta t^c$

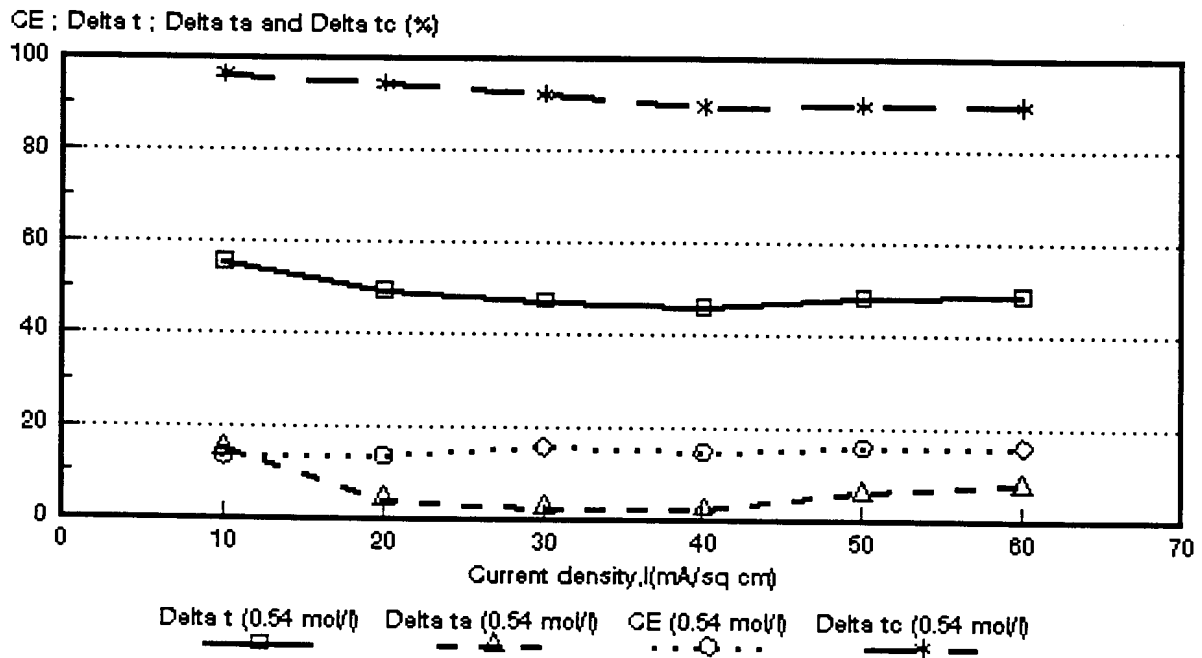


Figure 7.34: Current efficiency ($CE = \epsilon_p$) as a function of current density for 0,54 mol/l HCl feed. *Selemion* AMV and CMV membranes. $\Delta t = \bar{\Delta}t$; $\Delta t_a = \Delta t^a$; $\Delta t_c = \Delta t^c$

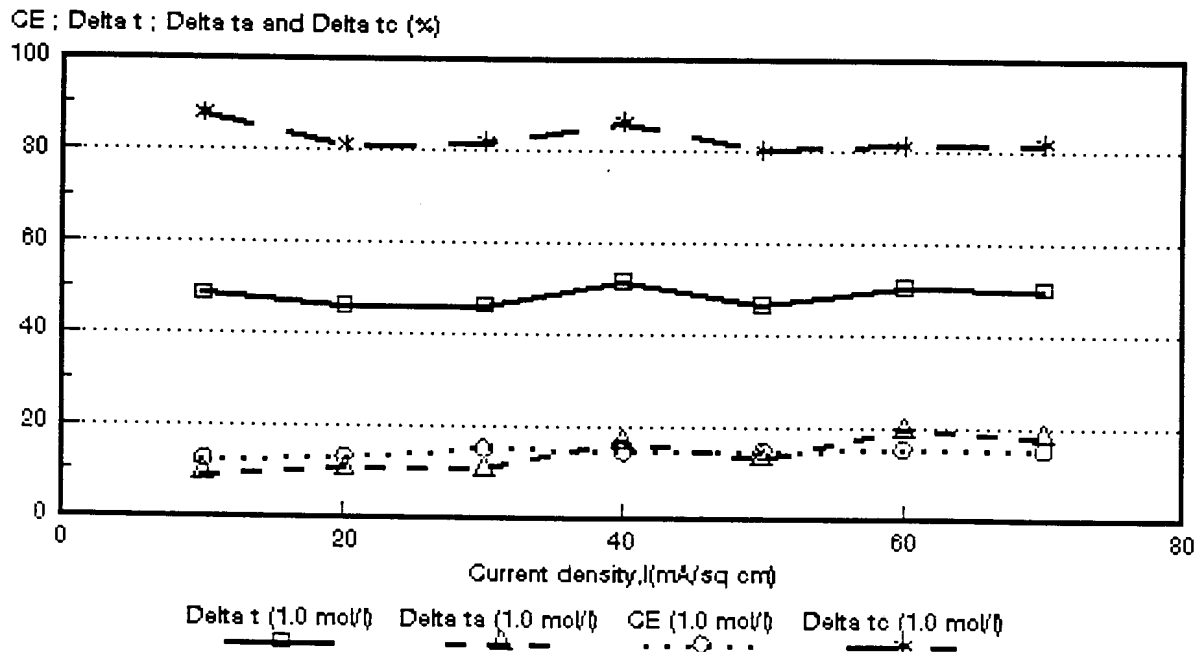


Figure 7.35: Current efficiency ($CE = \epsilon_p$) as a function of current density for 1,0 mol/l HCl feed. *Selemion* AMV and CMV membranes. $\Delta t = \bar{\Delta}t$; $\Delta t_a = \Delta t^a$; $\Delta t_c = \Delta t^c$

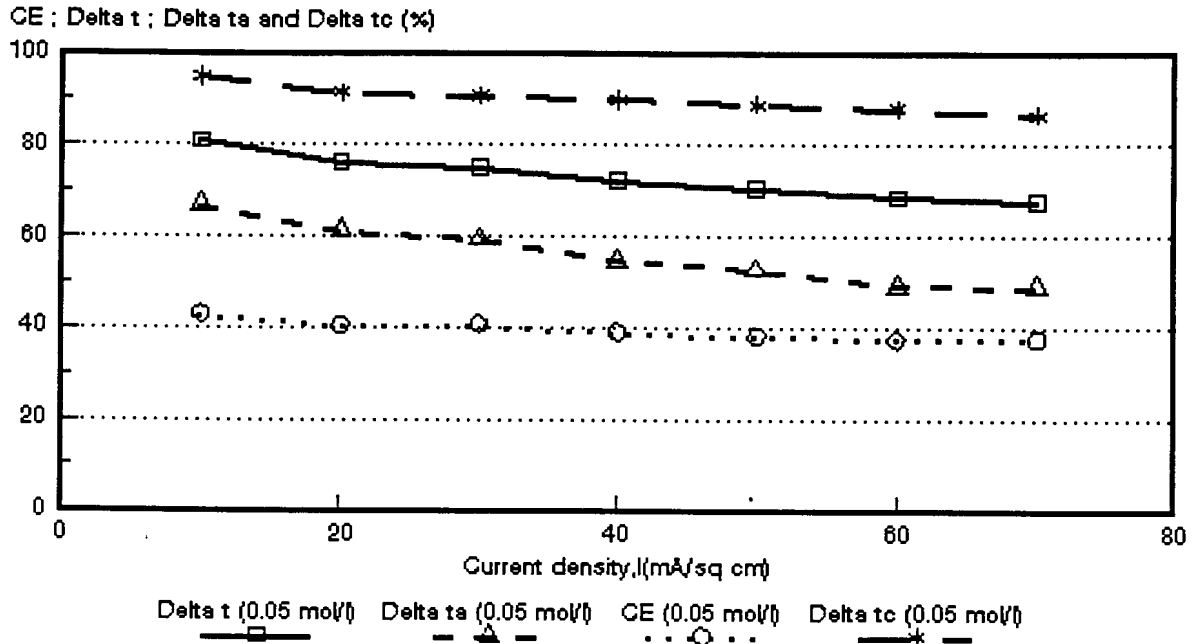


Figure 7.36: Current efficiency ($CE = \epsilon_p$) as a function of current density for 0,05 mol/l HCl feed. *Selemion AMV* and *CMV* membranes. $\Delta t = \bar{\Delta}t$; $\Delta t_a = \Delta t^*$; $\Delta t_c = \Delta t^c$

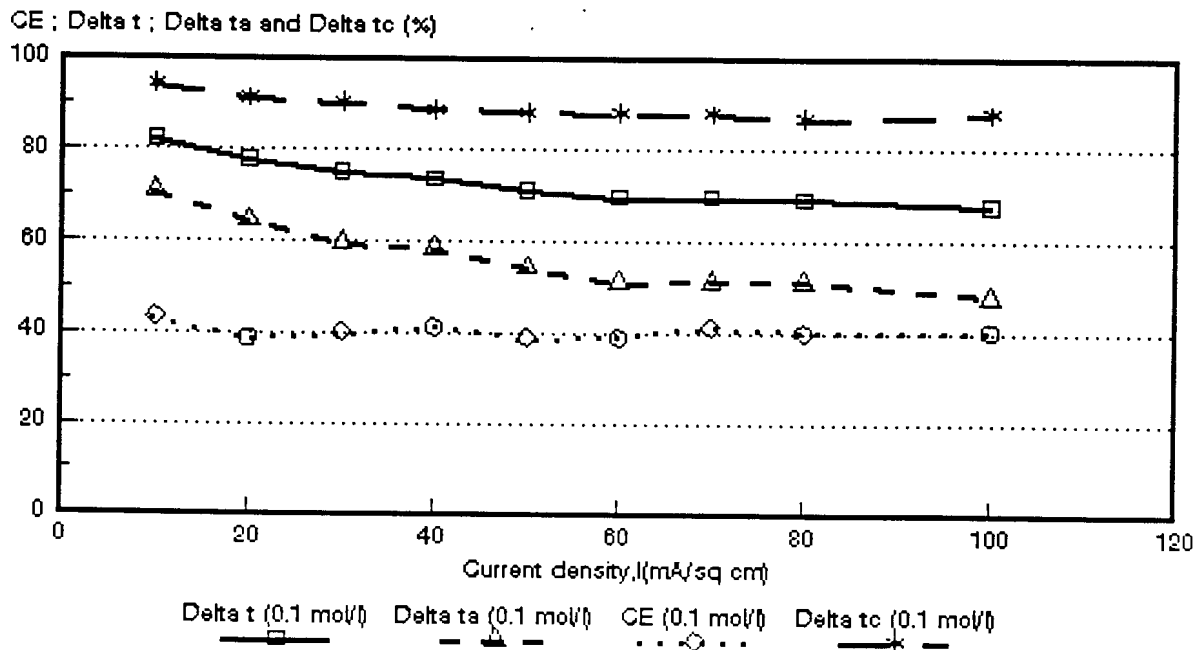


Figure 7.37: Current efficiency ($CE = \epsilon_p$) as a function of current density for 0,1 mol/l HCl feed. *Selemion AAV* and *CHV* membranes. $\Delta t = \bar{\Delta}t$; $\Delta t_a = \Delta t^*$; $\Delta t_c = \Delta t^c$

CE ; Delta t ; Delta ta and Delta tc (%)

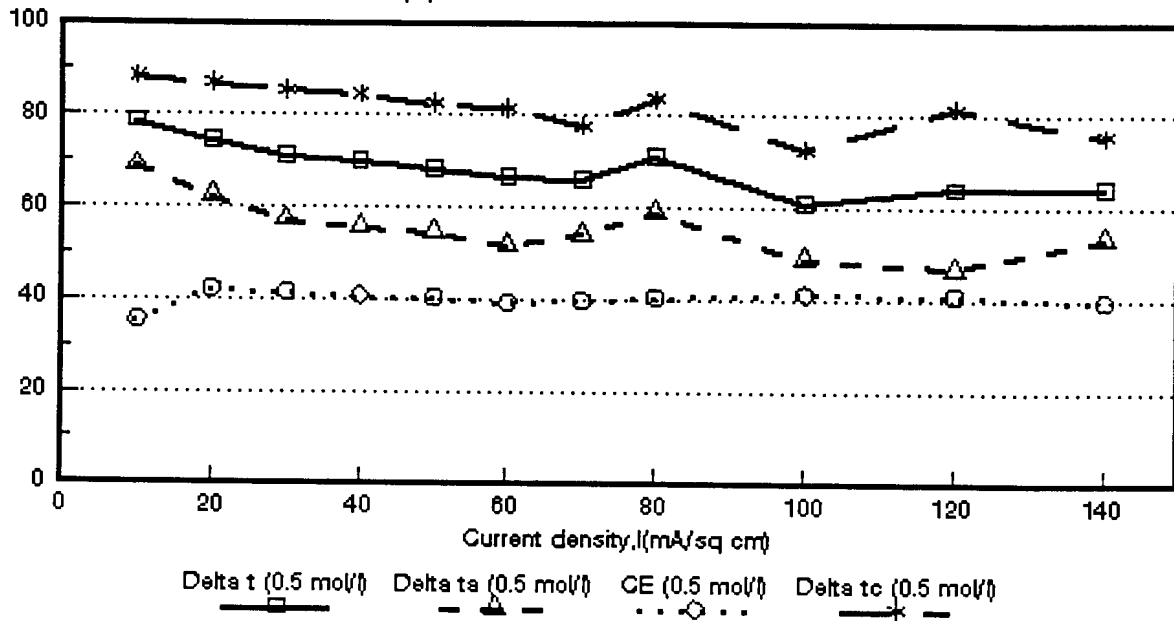


Figure 7.38: Current efficiency ($CE = \epsilon_p$) as a function of current density for 0,5 mol/l HCl feed. *Selemion AAV* and *CHV* membranes. $\Delta t = \bar{\Delta}t$; $\Delta t_a = \Delta t^a$; $\Delta t_c = \Delta t^c$

CE ; Delta t ; Delta ta and Delta tc (%)

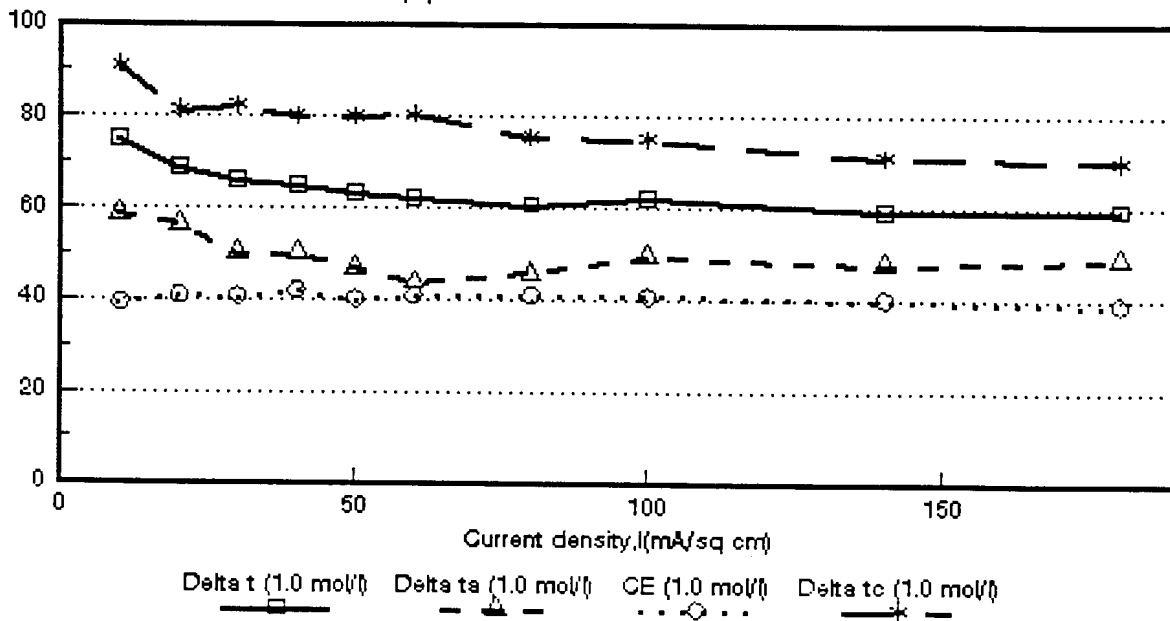


Figure 7.39: Current efficiency ($CE = \epsilon_p$) as a function of current density for 1,0 mol/l HCl feed. *Selemion AAV* and *CHV* membranes. $\Delta t = \bar{\Delta}t$; $\Delta t_a = \Delta t^a$; $\Delta t_c = \Delta t^c$

CE ; Delta t ; Delta ta and Delta tc (%)

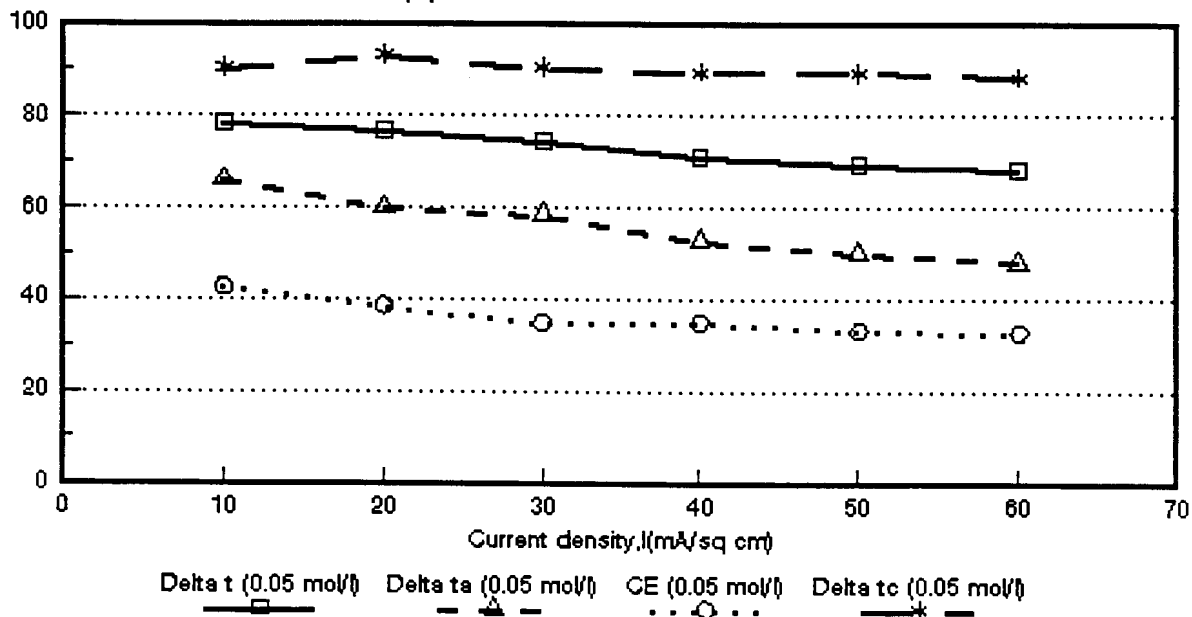


Figure 7.40: Current efficiency ($CE = \epsilon_p$) as a function of current density for 0,05 mol/l HCl feed. *Selemon* ABM-3 and CHV membranes. $\Delta t = \bar{\Delta}t$; $\Delta t_a = \Delta t^a$; $\Delta t_c = \Delta t^c$

CE ; Delta t ; Delta ta and Delta tc (%)

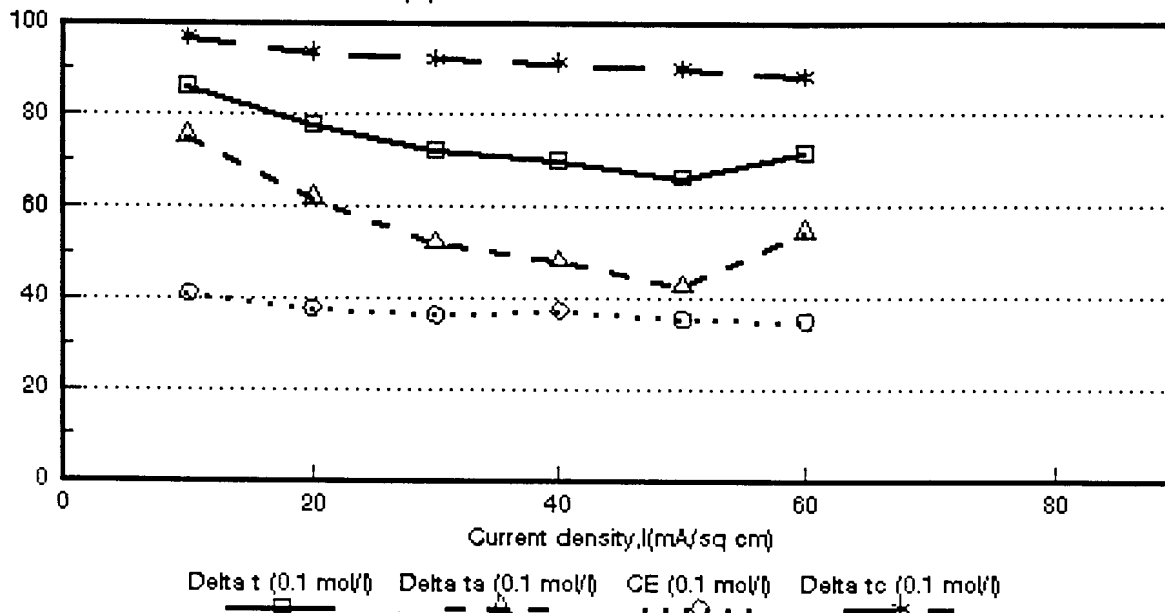


Figure 7.41: Current efficiency ($CE = \epsilon_p$) as a function of current density for 0,1 mol/l HCl feed. ABM-3 and *Selemon* CHV membranes. $\Delta t = \bar{\Delta}t$; $\Delta t_a = \Delta t^a$; $\Delta t_c = \Delta t^c$

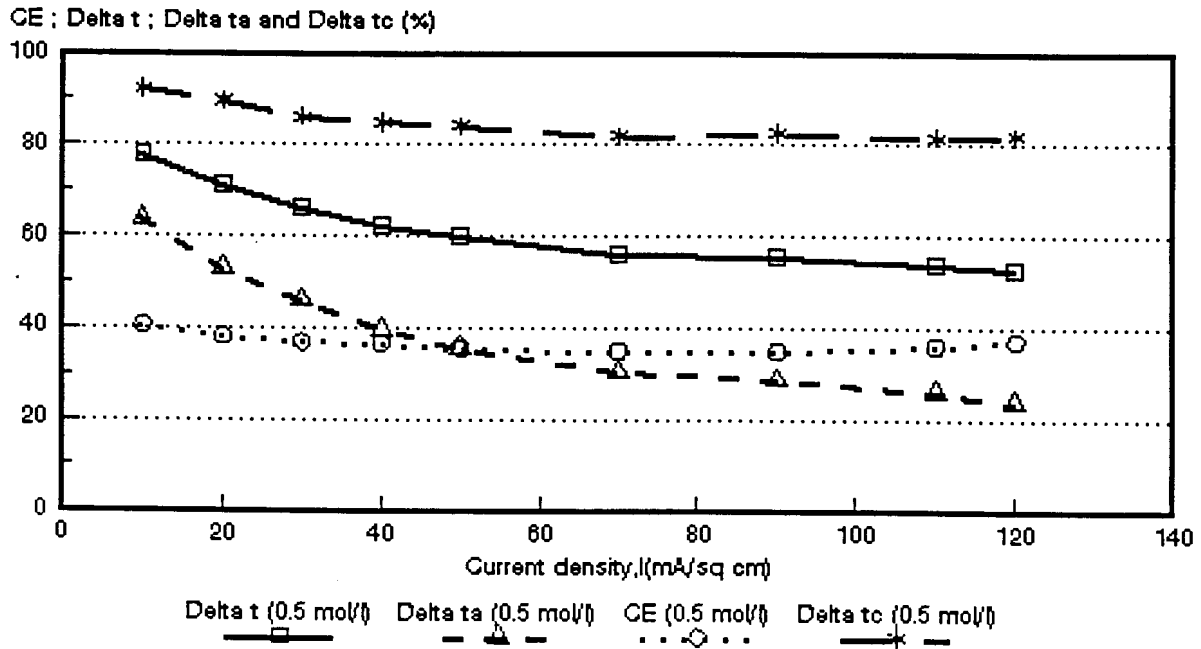


Figure 7.42: Current efficiency ($CE = e_p$) as a function of current density for 0,5 mol/l HCl feed. *Selemion* ABM-3 and CHV membranes. $\Delta t = \bar{\Delta}t$; $\Delta t_a = \Delta t^a$; $\Delta t_c = \Delta t^c$

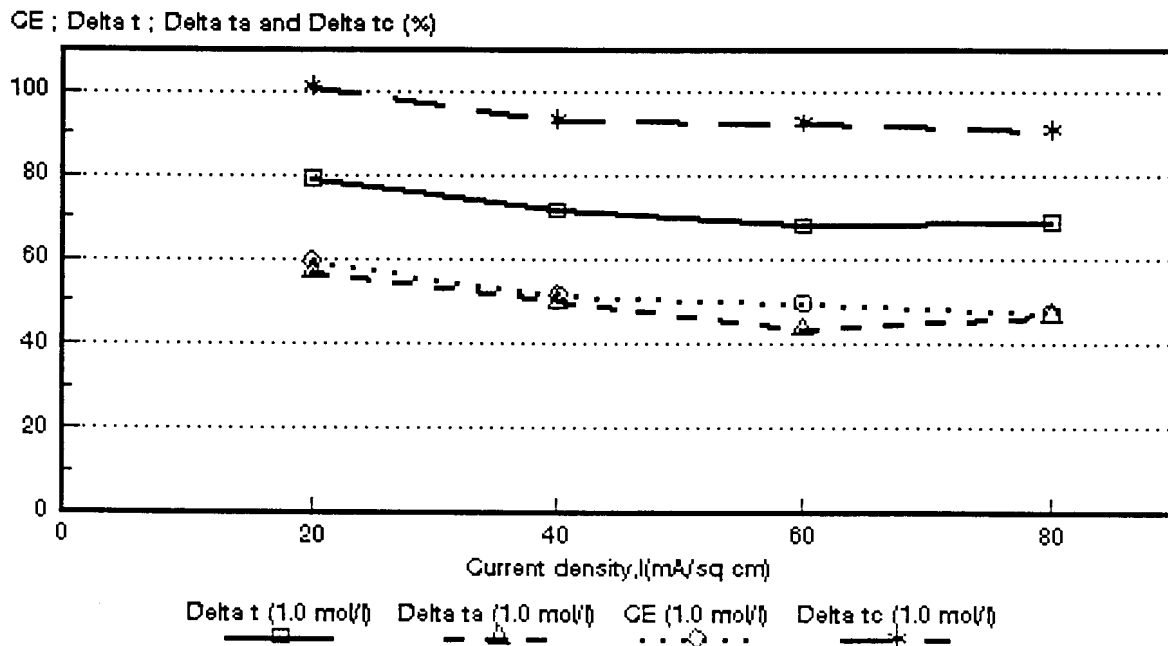


Figure 7.43: Current efficiency ($CE = e_p$) as a function of current density for 1,0 mol/l HCl feed. ABM-3 and *Selemion* CHV membranes. $\Delta t = \bar{\Delta}t$; $\Delta t_a = \Delta t^a$; $\Delta t_c = \Delta t^c$

CE ; Delta t ; Delta ta and Delta tc (%)

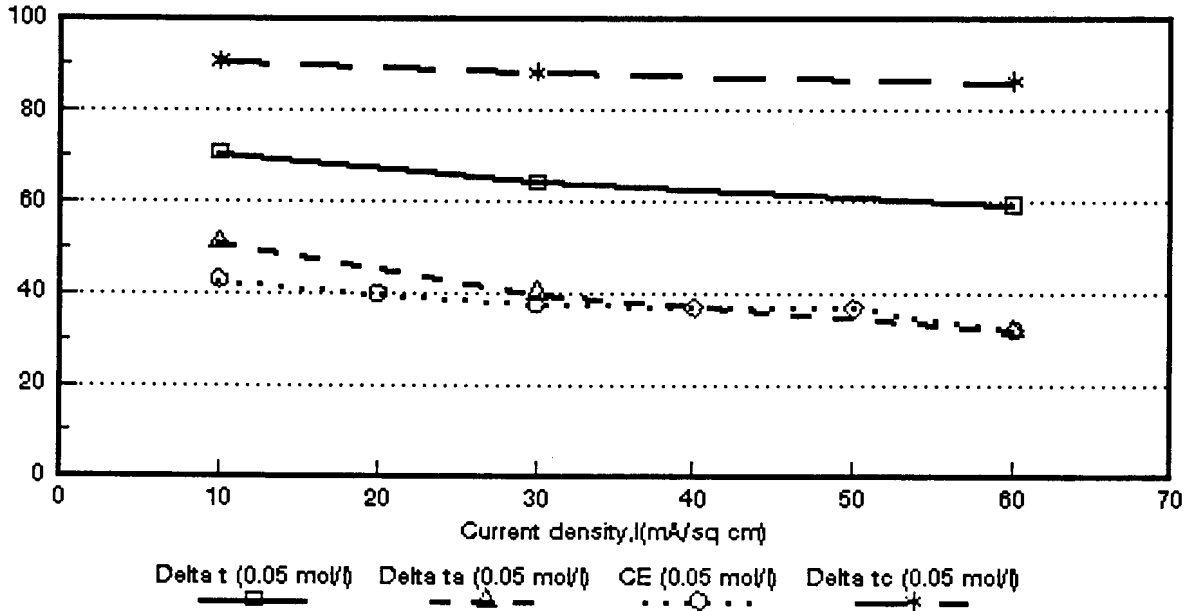


Figure 7.44: Current efficiency ($CE = \epsilon_p$) as a function of current density for 0,05 mol/l HCl feed. ABM-2 and *Selemion* CHV membranes. $\Delta t = \bar{\Delta}t$; $\Delta t_a = \Delta t^a$; $\Delta t_c = \Delta t^c$

CE ; Delta t ; Delta ta and Delta tc (%)

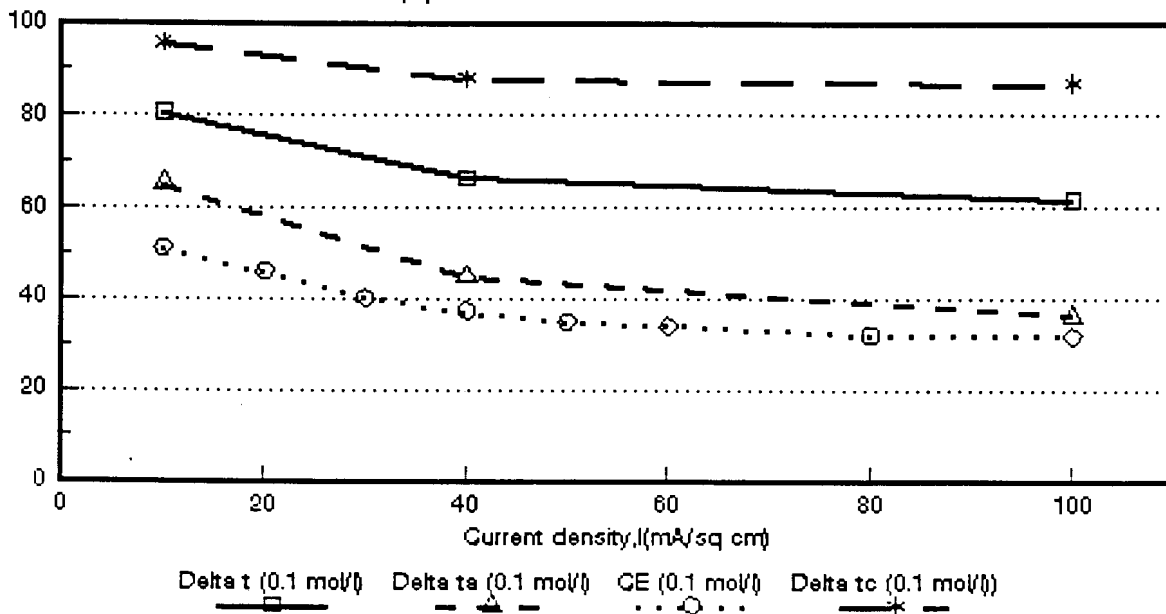


Figure 7.45: Current efficiency ($CE = \epsilon_p$) as a function of current density for 0,1 mol/l HCl feed. ABM-2 and *Selemion* CHV membranes. $\Delta t = \bar{\Delta}t$; $\Delta t_a = \Delta t^a$; $\Delta t_c = \Delta t^c$

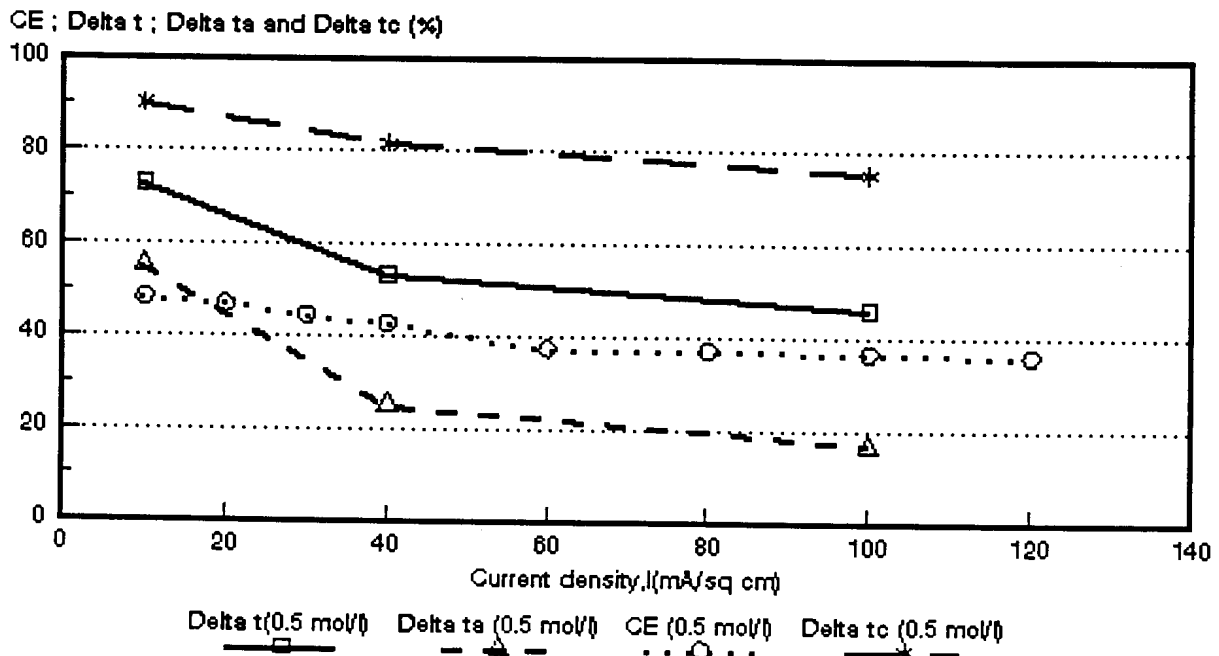


Figure 7.46: Current efficiency ($CE = \epsilon_p$) as a function of current density for 0,5 mol/l HCl feed. ABM-2 and *Selemion* CHV membranes. $\Delta t = \bar{\Delta}t$; $\Delta t_a = \Delta t^a$; $\Delta t_c = \Delta t^c$.

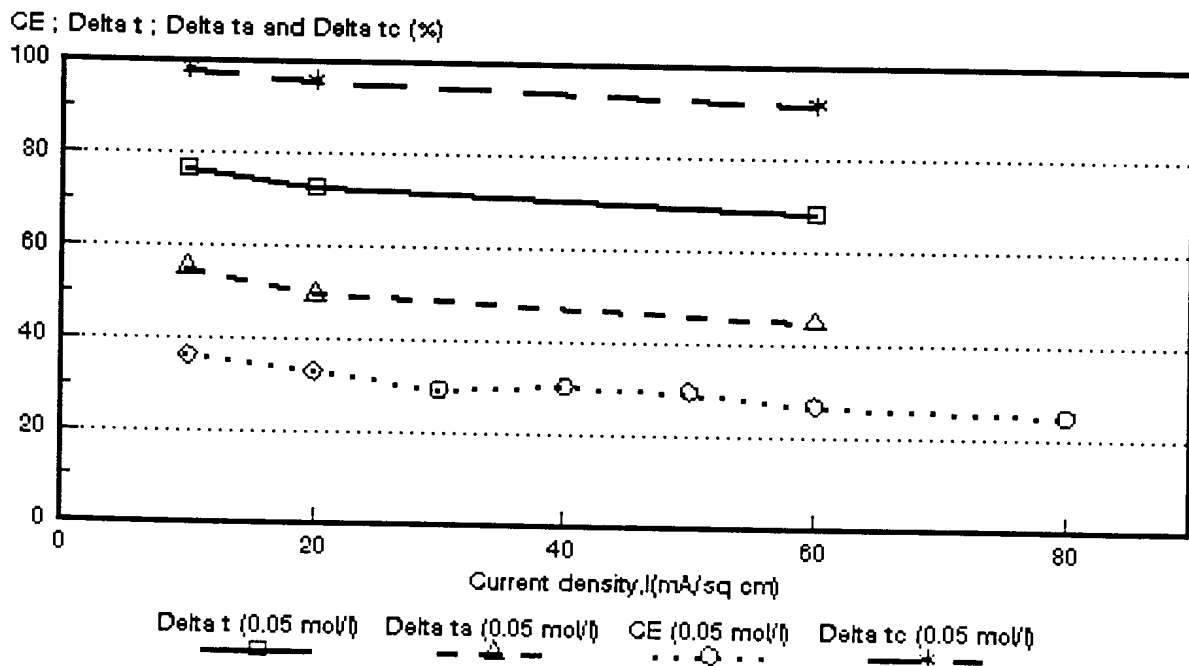


Figure 7.47: Current efficiency ($CE = \epsilon_p$) as a function of current density for 0,05 mol/l HCl feed. ABM-1 and *Selemion* CHV membranes. $\Delta t = \bar{\Delta}t$; $\Delta t_a = \Delta t^a$; $\Delta t_c = \Delta t^c$.

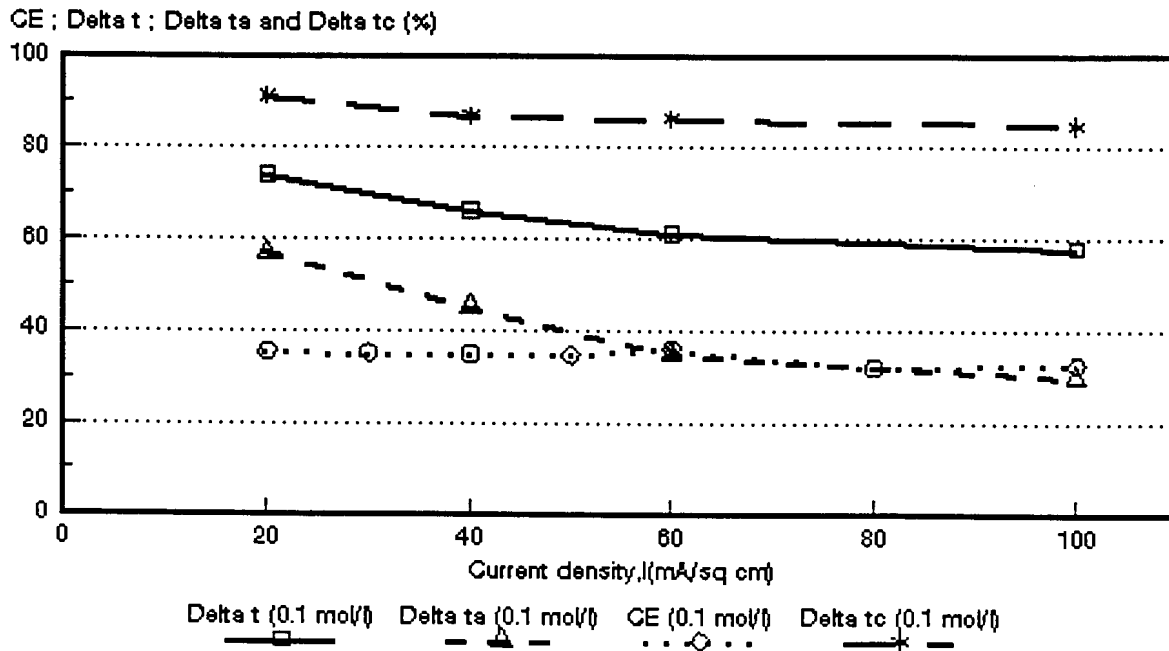


Figure 7.48: Current efficiency ($CE = \epsilon_p$) as a function of current density for 0,1 mol/l HCl feed. ABM-1 and *Selemion* CHV membranes. $\Delta t = \bar{\Delta}t$; $\Delta t_a = \Delta t^a$; $\Delta t_c = \Delta t^c$.

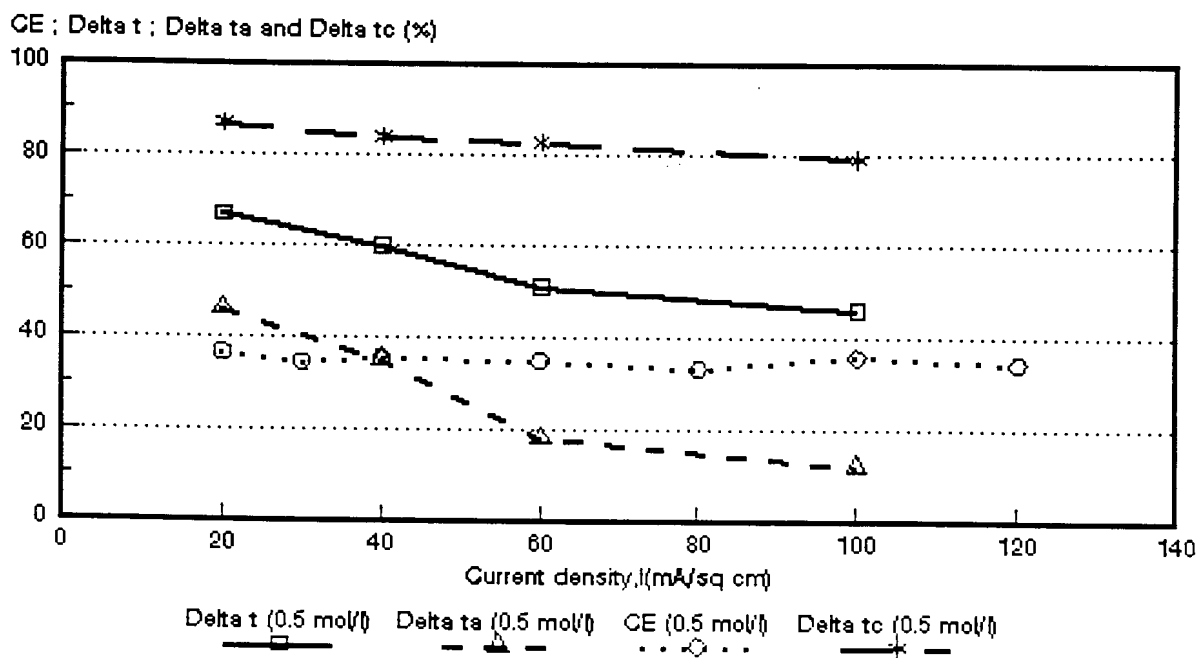


Figure 7.49: Current efficiency ($CE = \epsilon_p$) as a function of current density for 0,5 mol/l HCl feed. ABM-1 and *Selemion* CHV membranes. $\Delta t = \bar{\Delta}t$; $\Delta t_a = \Delta t^a$; $\Delta t_c = \Delta t^c$.

Tabel 7.21: Correlation between apparent transport number of the membrane pair ($\bar{\Delta}t$) and current efficiency (ϵ_p).

Current Density mA/cm ²	$\bar{\Delta}t/\epsilon_p$																			
	Selemion AMV & CMV Concentration, mol/l				Selemion AAV & CHV Concentration, mol/l				Israeli & Selemion ABM-3 & CHV Concentration, mol/l				Israeli & Selemion ABM-2 & CHV Concentration, mol/l				Israeli & Selemion ABM-1 & CHV Concentration, mol/l			
	0,05	0,1	0,5	1,0	0,05	0,1	0,5	1,0	0,05	0,1	0,5	1,0	0,05	0,1	0,5	1,0	0,05	0,1	0,5	1,0
10		4,92	4,18	3,87	1,89	1,89	2,20	1,88	1,84	2,10	1,91		1,66	1,57	1,49		2,10	1,36		
20		3,97	3,68	3,41	1,88	1,98	1,75	1,69	1,98	2,04	1,86	1,33					2,19	2,11	1,84	
30		3,53	3,01	3,07	1,84	1,85	1,71	1,63	2,13	1,98	1,79		1,71							
40		3,42	3,13	3,52	1,85	1,76	1,72	1,55	2,03	1,85	1,69	1,37		1,77	1,24			1,90	1,70	
50		3,09	3,02	3,13	1,83	1,83	1,69	1,57	2,08	1,86	1,66						2,28			
60		2,85	3,04	3,36	1,82	1,76	1,68	1,52	2,08	2,03		1,37	1,85				2,56	1,69	1,47	
70				3,31	1,79	1,67	1,63				1,60									
80						1,72	1,75	1,47				1,44								
90											1,59									
100						1,68	1,45	1,52						1,91	1,26			1,78	1,29	
110											1,47									
120							1,56				1,40									
130																				
140							1,61	1,47												
150																				
160																				
170																				
180								1,52												

Tabel 7.22: Correlation between apparent transport number of the anion membrane (Δt^*) and current efficiency (e_p).

Current Density mA/cm ²	$\Delta t^* / e_p$																			
	Selemion AMV & CMV Concentration, mol/l				Selemion AAV & CHV Concentration, mol/l				Israeli & Selemion ABM-3 & CHV Concentration, mol/l				Israeli & Selemion ABM-2 & CHV Concentration, mol/l				Israeli & Selemion ABM-1 & CHV Concentration, mol/l			
	0,05	0,1	0,5	1,0	0,05	0,1	0,5	1,0	0,05	0,1	0,5	1,0	0,05	0,1	0,5	1,0	0,05	0,1	0,5	1,0
10		2,27	1,12	0,73	1,54	1,61	1,92	1,48	1,55	1,83	1,56		1,19	1,27	1,14		1,52			
20		1,37	0,29	0,83	1,51	1,65	1,47	1,37	1,56	1,61	1,36	0,94					1,49	1,61	1,26	
30		0,83	0,13	0,73	1,45	1,47	1,37	1,23	1,67	1,43	1,22		1,07							
40		0,53	0,14	1,17	1,38	1,40	1,35	1,19	1,49	1,29	1,06	0,97		1,18	0,56			1,30	0,99	
50		0,25	0,38	0,88	1,36	1,39	1,34	1,15	1,51	1,19	0,99									
60		0,12	0,50	1,25	1,31	1,30	1,30	1,05	1,47	1,55		0,87	1,00				1,65	0,97	0,52	
70				1,19	1,28	1,23	1,35				0,86									
80						1,27	1,46	1,10				0,97								
90											0,81									
100						1,19	1,19	1,20						1,23	0,44			0,92	0,34	
110											0,69									
120							1,12				0,62									
130																				
140							1,33	1,17												
150																				
160																				
170																				
180								1,26												

Tabel 7.23: Correlation between apparent transport number of the cation membrane (Δt^c) and current efficiency (ϵ_p).

Current Density mA/cm ²	$\Delta t^c/\epsilon_p$																			
	Selemon AMV & CMV Concentration, mol/l				Selemon AAV & CHV Concentration, mol/l				Israeli & Selemon ABM-3 & CHV Concentration, mol/l				Israeli & Selemon ABM-2 & CHV Concentration, mol/l				Israeli & Selemon ABM-1 & CHV Concentration, mol/l			
	0,05	0,1	0,5	1,0	0,05	0,1	0,5	1,0	0,05	0,1	0,5	1,0	0,05	0,1	0,5	1,0	0,05	0,1	0,5	1,0
10		7,58	7,16	7,10	2,21	2,17	2,48	2,32	2,12	2,37	2,28		2,10	1,86	1,86		2,71	2,31		
20		6,58	6,99	6,14	2,25	2,34	2,06	1,98	2,42	2,46	2,34	1,68					2,92	2,57	2,38	
30		6,22	5,90	5,47	2,21	2,24	2,05	2,02	2,59	2,53	2,33		2,35							
40		6,25	6,12	6,00	2,31	2,13	2,06	1,90	2,55	2,44	2,29	1,80		2,36	1,89			2,50	2,38	
50		5,86	5,66	5,51	2,30	2,26	2,03	2,00	2,69	2,54	2,37									
60		5,58	5,59	5,39	2,35	2,25	2,06	1,96	2,69	2,52		1,85	2,73				3,46	2,39	2,39	
70				5,43	2,29	2,13	1,93				2,32									
80						2,16	2,05	1,83				1,90								
90											2,36									
100						2,17	1,74	1,84						2,73	2,05			2,62	2,21	
110											2,24									
120							1,97				2,18									
130																				
140							1,88	1,77												
150																				
160								1,80												
170																				
180																				

mA/cm^2 (0,1 mol/l feed). The correlation was even better at 1,0 mol/l feed concentration and varied between 0,97 and 0,84 in the 20 to 80 mA/cm^2 current density range.

A satisfactory correlation was obtained between the apparent transport number (Δt^a) and current efficiency at 0,05 mol/l feed concentration in the case of the ABM-2 and CHV membranes (30 to 60 mA/cm^2). The ratio of $\Delta t^a/e_p$ varied between 1,07 and 1,0. The ratio was approximately 1,18 at 0,1 mol/l feed concentration in the same current density range. A very poor correlation, however, was obtained at 0,5 mol/l feed concentration for the same membranes.

The ABM-1 and CHV membranes showed the best correlation (0,92 to 0,97) at 0,1 mol/l feed concentration in the current density range from 60 to 100 mA/cm^2 . A poor correlation, however, was obtained with the Selemion AMV and CMV membranes.

The correlations between the apparent transport numbers of the cation membrane (Δt^c) and current efficiencies (Table 7.23) were not as good as the correlations obtained between the apparent transport numbers of the membrane pair ($\bar{\Delta t}$) (Table 7.21) and that of the anion membrane (Δt^a) and current efficiency (Fig. 7.22). It therefore seems that the best correlation between transport numbers and current efficiency for acid can be obtained from the apparent transport number of the anion membrane. It also seems that the apparent transport number of the anion membrane gives the best approximate estimation of the performance of membranes for acid concentration/desalination. However, accuracy of performance depends on the acid feed concentration used. The performance of a membrane for acid concentration should be estimated with an accuracy of approximately 20% from the apparent transport number of the anion membrane, depending on the acid feed concentration used.

7.3 Water Flow

Water flow (J) through the membranes as a function of current density and acid feed water concentration is shown in Figures 7.50 to 7.54. Water flow (J) through the membranes relative to the flow at $J_{0,5 \text{ mol/l}}$ is shown in Table 7.24. Water flow through the membranes decreased significantly with increasing acid feed concentration in the case of the *Selemion* AMV and CMV membranes. A slight decrease in water flow was also experienced in the case of the *Selemion* AAV and CHV membranes. Therefore, there appeared to be no support (water flow) to improve current efficiency as had been experienced with the sodium chloride solutions (see Figs. 7.28 and 7.29 and Figs. 6.43 to 6.49). However, a definite increase in water flow was observed for the ABM-3 and CHV membranes, especially at the highest feed concentration (Table 7.24) and an increase in current efficiency was experienced for this membrane type at 1,0 mol/l feed concentration (see Fig. 7.30). Increase in water flows were also experienced for the ABM-2, ABM-1 and CHV membranes with increasing acid feed concentration. Current efficiency also increased slightly in these cases (see Figs. 7.31 and 7.32). The high water flow that was experienced with the ABM-2 membranes at 0,1 mol/l feed concentration may be ascribed to membrane leakage due to a partially torn membrane.

Water flow (J) through the membranes as a function of effective current density, i_{eff} , and feed water concentration are shown in Figures 7.55 to 7.59. Straight lines were obtained at higher values of i_{eff} as were experienced with the sodium chloride solutions. The slope of these lines corresponds to the combined electro-osmotic coefficient (2β) of a membrane pair. The electro-osmotic coefficients decreased as a function of increasing acid feed concentration in the feed concentration range from 0,05 to 1,0 mol/l (Figs. 7.60 to 7.64). The electro-osmotic coefficient of the *Selemion* AMV and CMV membranes remained almost constant in the 0,1 to 0,5 mol/l feed concentration range and then decreased more significantly to a lower value at 1,0 mol/l feed concentration (Fig. 7.60). The electro-osmotic coefficient of the *Selemion* AAV and CHV membranes remained constant in the 0,05 to 0,1 mol/l feed range (Fig. 7.61) and then decreased somewhat to remain almost constant in the 0,5 to 1,0 mol/l feed concentration range. The electro-osmotic coefficients of the ABM-3 and CHV membranes decreased significantly in the 0,05 to 0,5 mol/l feed concentration range and then remained constant (Fig. 7.62). Both the ABM-2 and ABM-1 membranes showed a reduction in the electro-osmotic coefficient in the 0,05 to 0,1 mol/l feed concentration ranges and then remained constant in the 0,1 to 0,5 mol/l feed

concentration range (Figs. 7.62 to 7.63). It, therefore, appears that the membranes deswell somewhat with increasing acid feed concentration.

The effect of the electro-osmotic coefficient on the maximum acid brine concentration c_b^{\max} , is shown in Table 7.25. Maximum acid brine concentration increases with decreasing electro-osmotic coefficient. The electro-osmotic coefficients of the *Selemion* AMV and CMV membranes were much higher than that of the other membranes. The electro-osmotic coefficients of the *Selemion* AMV and CMV membranes were determined at 0,357 and 0,371 $\ell/\text{Faraday}$ at 0,1 and 0,54 mol/ ℓ feed concentration, respectively. The electro-osmotic coefficients of the *Selemion* AAV and CHV; ABM-3 and CHV; ABM-2 and CHV and ABM-1 and CHV were determined at 0,141 and 0,126 $\ell/\text{Faraday}$; 0,166 and 0,124 $\ell/\text{Faraday}$; 0,133 and 0,131 $\ell/\text{Faraday}$ and 0,152 and 0,149 $\ell/\text{Faraday}$ under the same feed water conditions as above, respectively. Consequently, much higher acid brine concentrations could be obtained with these membranes.

Approximately 7 to 8 mol H₂O per Faraday passed through the *Selemion* AAV and CHV membranes in the acid feed concentration range from 0,1 to 0,5 mol/ ℓ (Table 7.25). Approximately 7 to 9; 7 and 8 mol H₂O/Faraday passed through the ABM-3 and CHV; ABM-2 and CHV and ABM-1 and CHV membranes under the same feed conditions as above, respectively. Therefore, the newly developed Israeli ABM membranes compare favourably with the commercially available *Selemion* AAV and CHV membranes for acid concentration.

The osmotic water flow (J_{osm}) relative to the total water flow (J) through the membranes as a function of current density, is shown in Table 7.26. The osmotic flow (J_{osm}) relative to the total flow (J) decreases with increasing current density. Osmotic water flow contributes to approximately 50% of the total water flow through the membranes at a current density of 30 mA/cm² at 0,1 mol/ ℓ feed concentration. However, the osmotic water flow contribution relative to the total water flow was much less at high current densities. Approximately 21% of the total water flow through the membranes was caused by osmosis in the case of the *Selemion* AAV and CHV membranes at a current density of 100 mA/cm² (0,1 mol/ ℓ feed). The osmotic water flow contribution in the case of the ABM-3 and *Selemion* CHV membranes comprised 29,4% of the total water flow at a current density of 60 mA/cm² (0,1 mol/ ℓ feed).

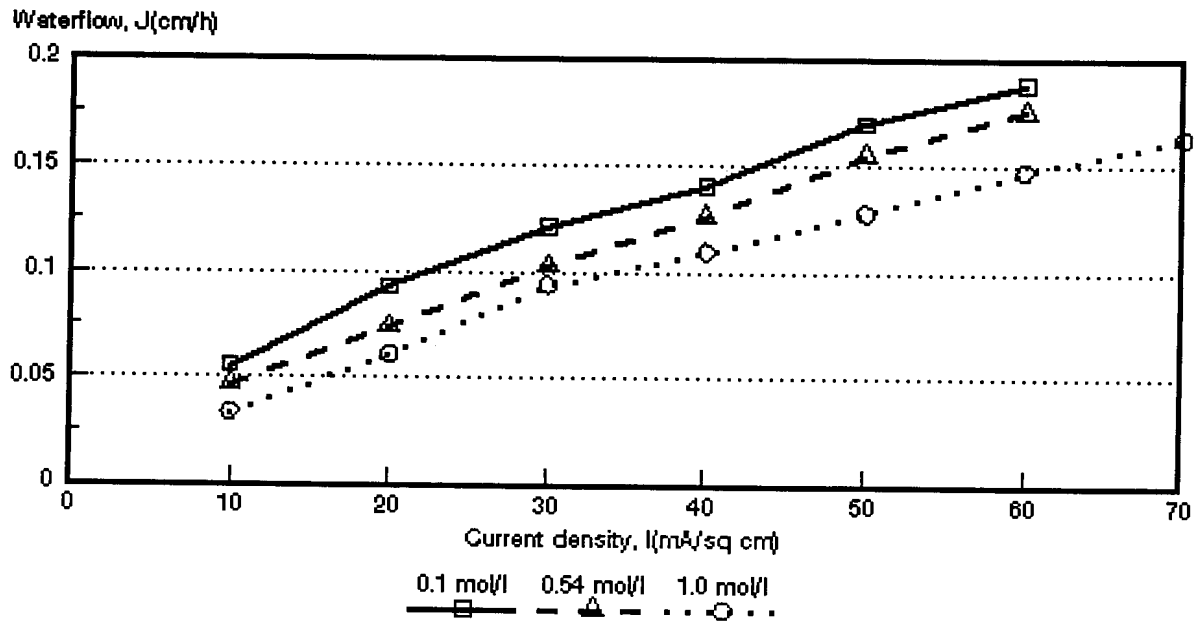


Figure 7.50: Water flow through the membranes as a function of current density and feed water concentration. *Selemion AMV and CMV membranes.*

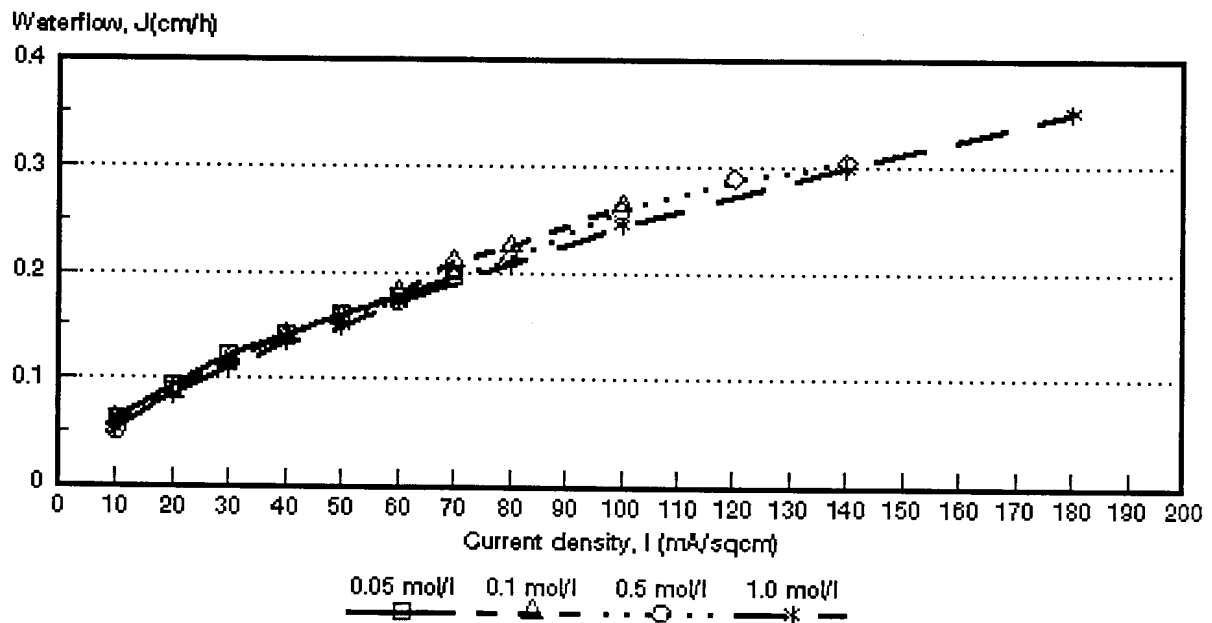


Figure 7.51: Water flow through the membranes as a function of current density and feed water concentration. *Selemion AAV and CHV membranes.*

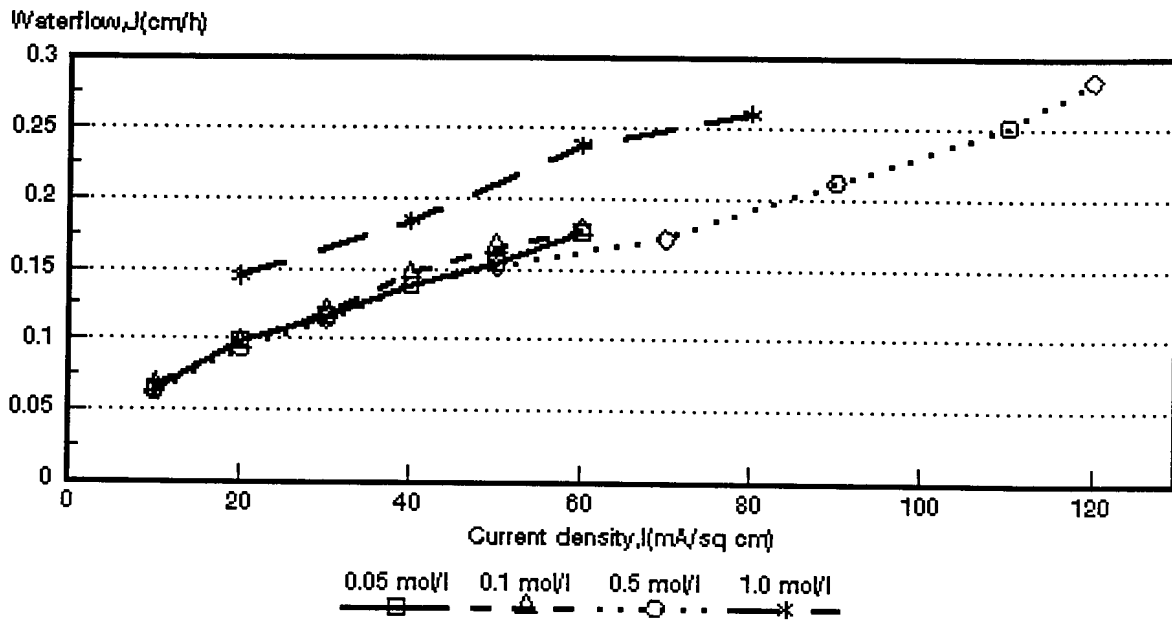


Figure 7.52: Water flow through the membranes as a function of current density and feed water concentration. ABM-3 and *Selemion* CHV membranes.

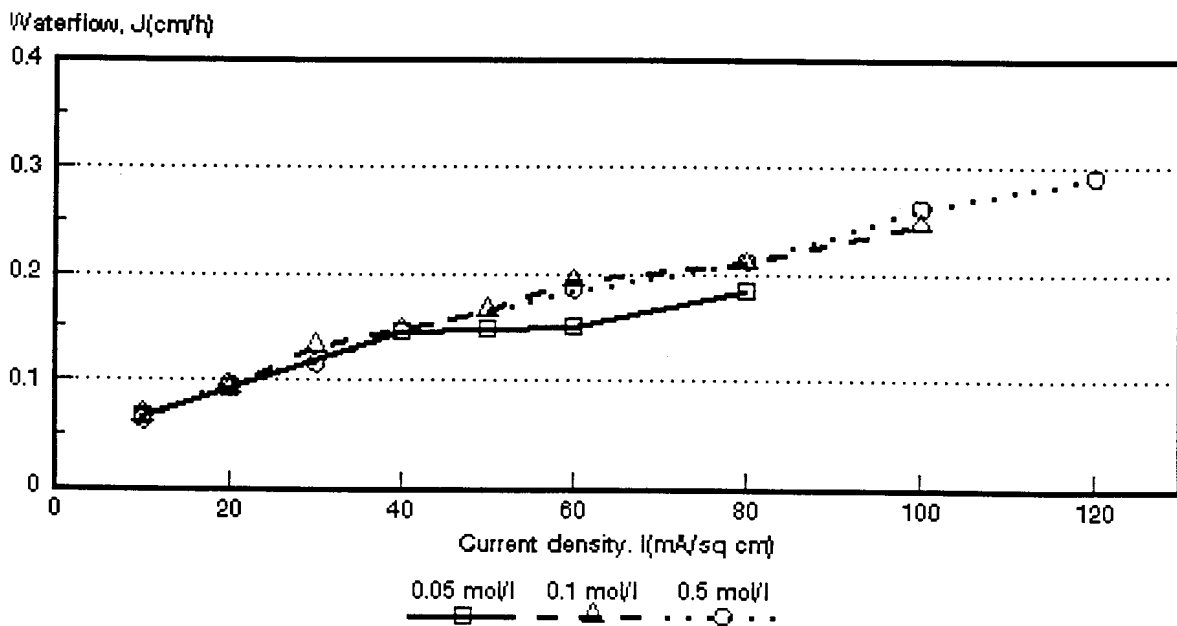


Figure 7.53: Water flow through the membranes as a function of current density and feed water concentration. ABM-2 and *Selemion* CHV membranes.

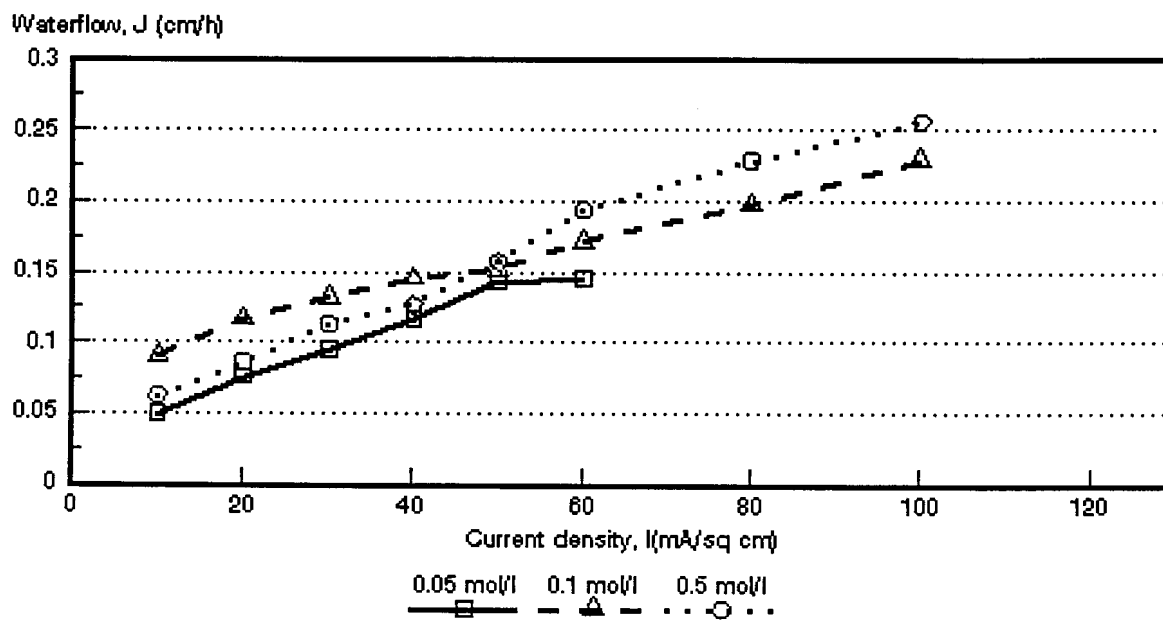


Figure 7.54: Water flow through the membranes as a function of current density and feed water concentration. ABM-1 and *Selemion* CHV membranes.

Tabel 7.24: Water flow (J_i) through the membranes relative to the flow at $J_{0,5 \text{ mol/l}}$

Current Density mA/cm ²	$J/J_{0,5 \text{ mol/l}}$																			
	Selemion AMV & CMV Concentration, mol/l				Selemion AAV & CHV Concentration, mol/l				Israëli & Selemion ABM-3 & CHV Concentration, mol/l				Israëli & Selemion ABM-2 & CHV Concentration, mol/l				Israëli & Selemion ABM-1 & CHV Concentration, mol/l			
	0,05	0,1	0,5	1,0	0,05	0,1	0,5	1,0	0,05	0,1	0,5	1,0	0,05	0,1	0,5	1,0	0,05	0,1	0,5	1,0
10		1,18	1,0	0,71	1,24	1,20	1,0	1,02	1,03	1,09	1,0		0,79	1,45	1,0		1,06	1,06	1,0	
20		1,26	1,0	0,82	1,05	0,97	1,0	0,96	1,05	1,05	1,0	1,56	0,88	1,35	1,0		0,95	0,95	1,0	
30		1,17	1,0	0,91	1,07	1,02	1,0	0,97	1,03	1,04	1,0		0,84	1,17	1,0					
40		1,11	1,0	0,87	1,02	1,01	1,0	0,98	1,00	1,07	1,0	1,33	0,91	1,14	1,0		1,00	1,02	1,0	
50		1,09	1,0	0,83	1,00	0,98	1,0	0,93	1,01	1,09	1,0				1,0				1,0	
60		1,07	1,0	0,84	1,03	1,04	1,0	0,99					0,92	1,09	1,0		0,81	1,05	1,0	
70					1,01	1,08	1,0								1,0				1,0	
80						1,06	1,0	0,98						1,02	1,0		0,87	0,99	1,0	
90							1,0								1,0				1,0	
100						1,02	1,0	0,95						1,00	1,0			0,95	1,0	
110																				
120																				
130																				
140								0,98												
150																				
160																				
170																				
180																				

$i = 0,05; 0,1 \text{ and } 1,0 \text{ mol/l}$

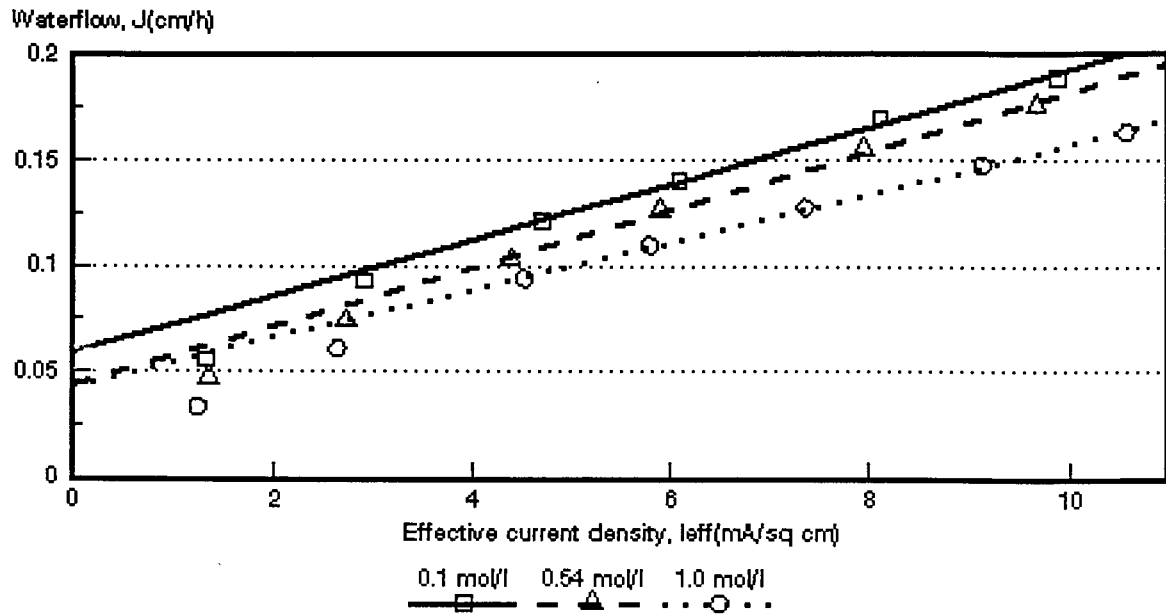


Figure 7.55: Water flow through the membranes as a function of effective current density and HCl feed water concentration. *Selemion AMV and CMV membranes.*

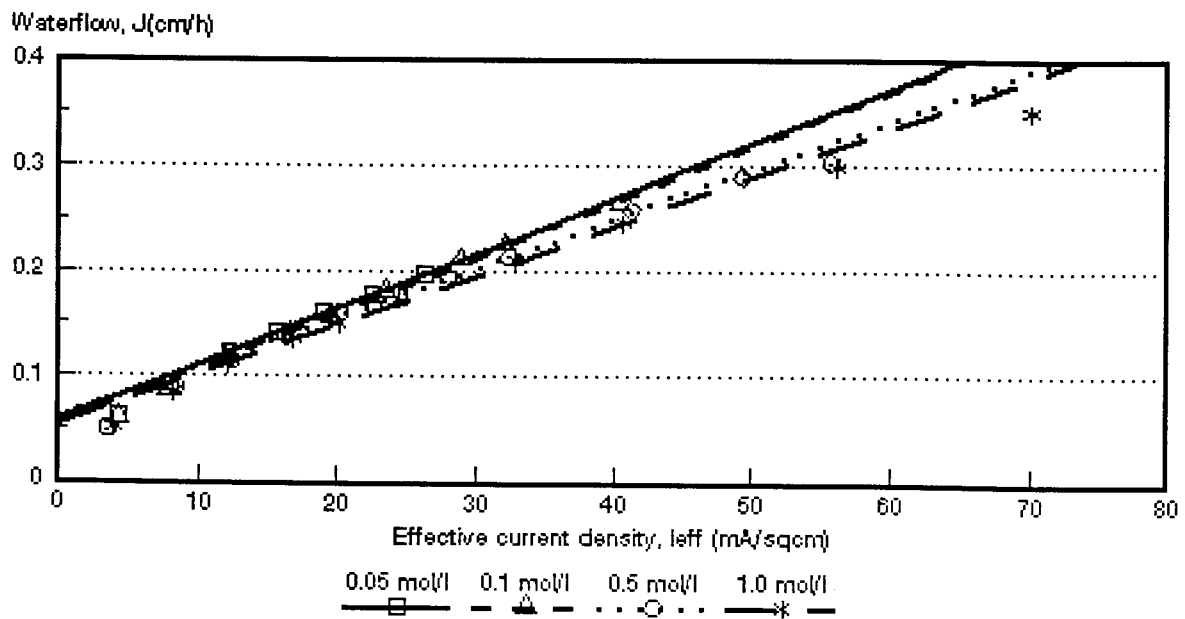


Figure 7.56: Water flow through the membranes as a function of effective current density and HCl feed water concentration. *Selemion AAV and CHV membranes.*

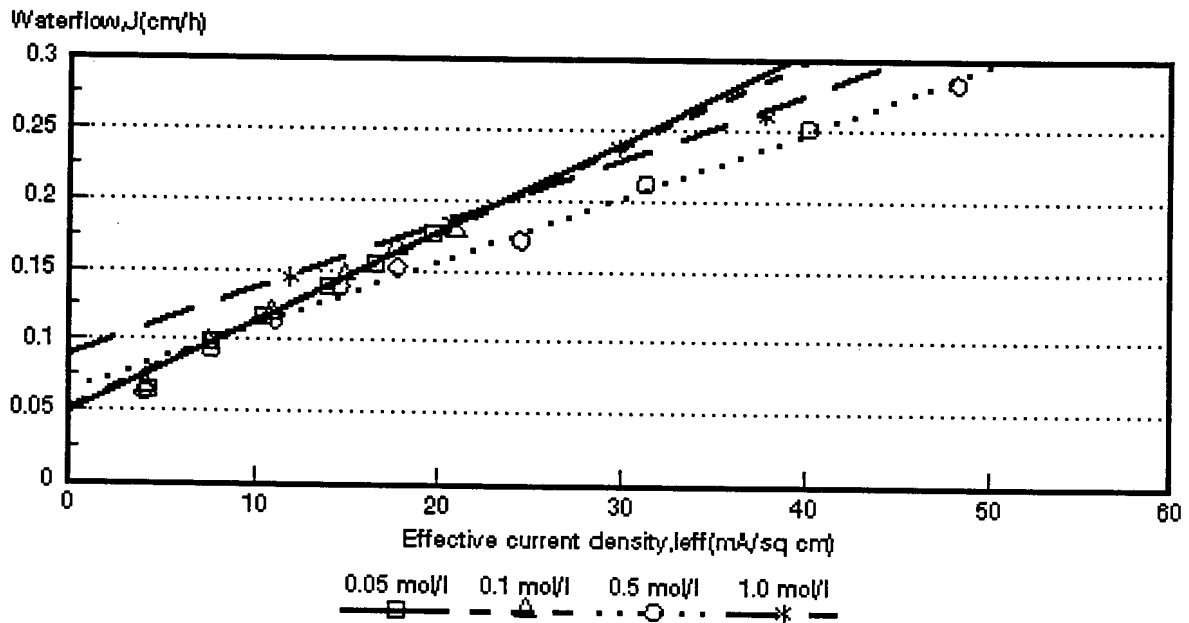


Figure 7.57: Water flow through the membranes as a function of effective current density and HCl feed water concentration. ABM-3 and *Selemion* CHV membranes.

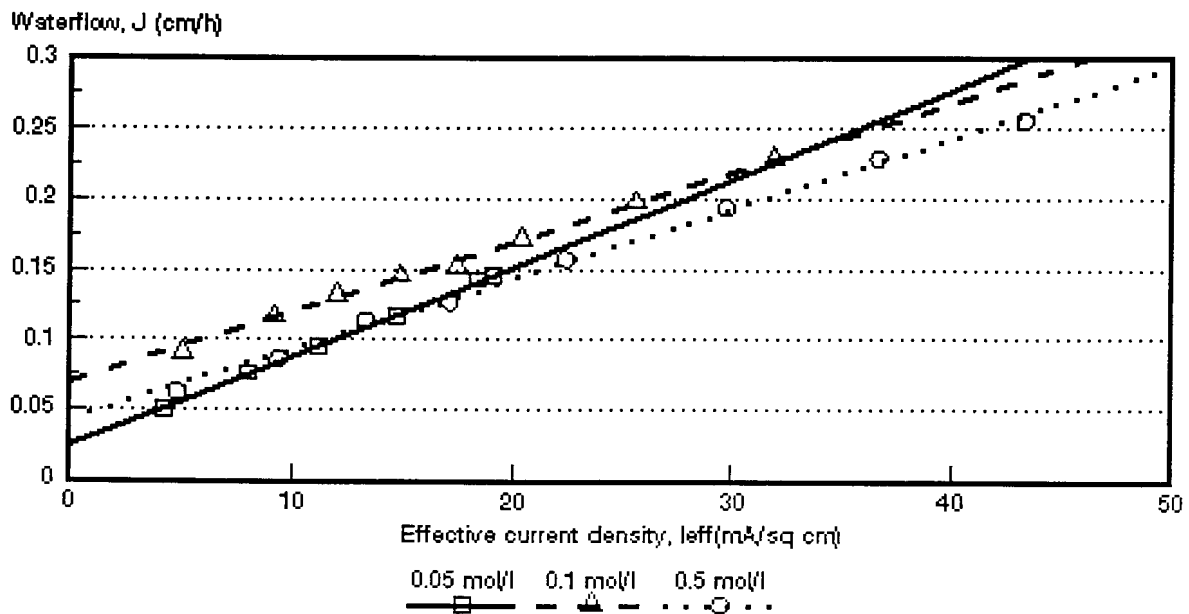


Figure 7.58: Water flow through the membranes as a function of effective current density and HCl feed water concentration. ABM-2 and *Selemion* CHV membranes.

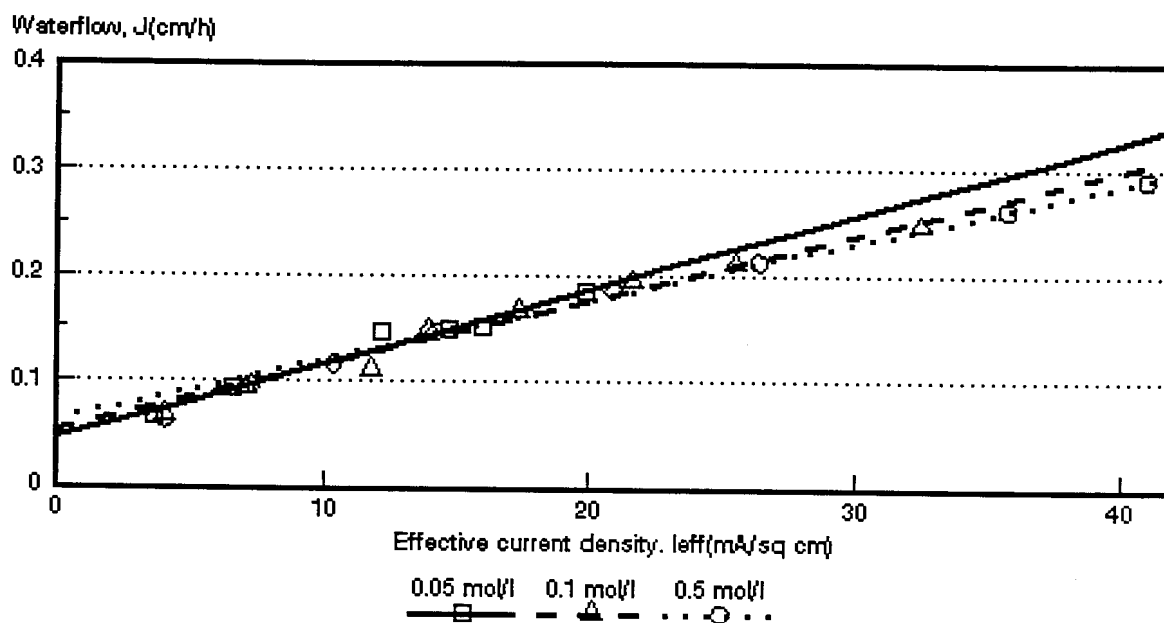


Figure 7.59: Water flow through the membranes as a function of effective current density and HCl feed water concentration. *ABM-1* and *Selemion CHV* membranes.

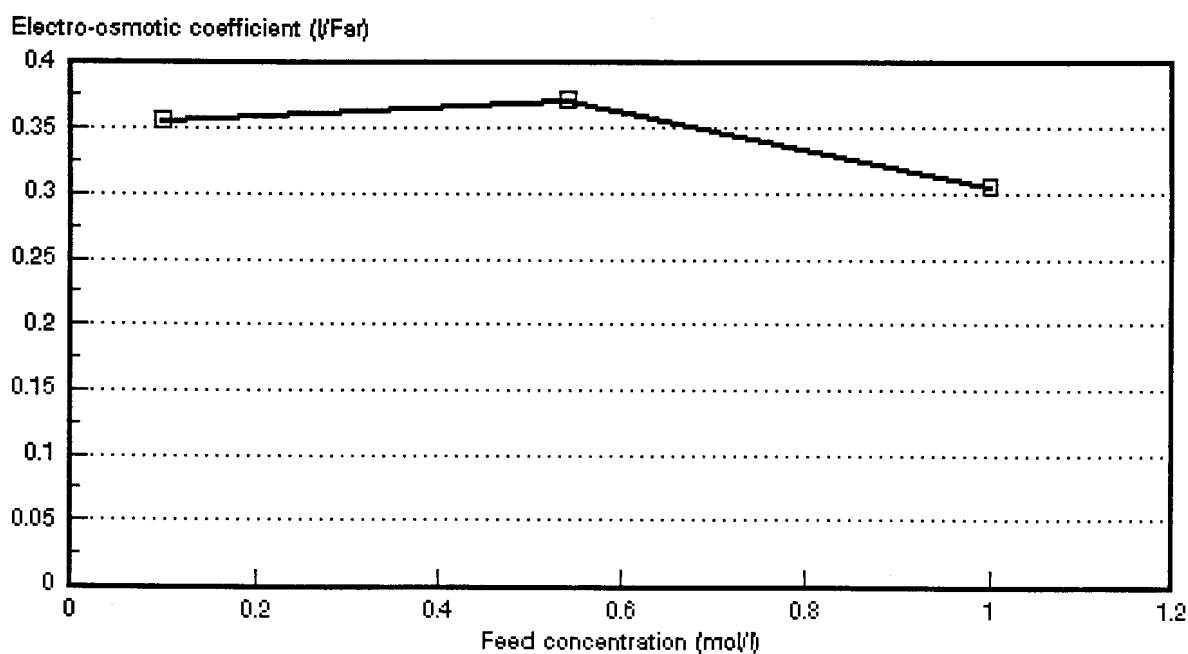


Figure 7.60: Electro-osmotic coefficient as a function of HCl feed water concentration. *Selemion AMV* and *CMV* membranes.

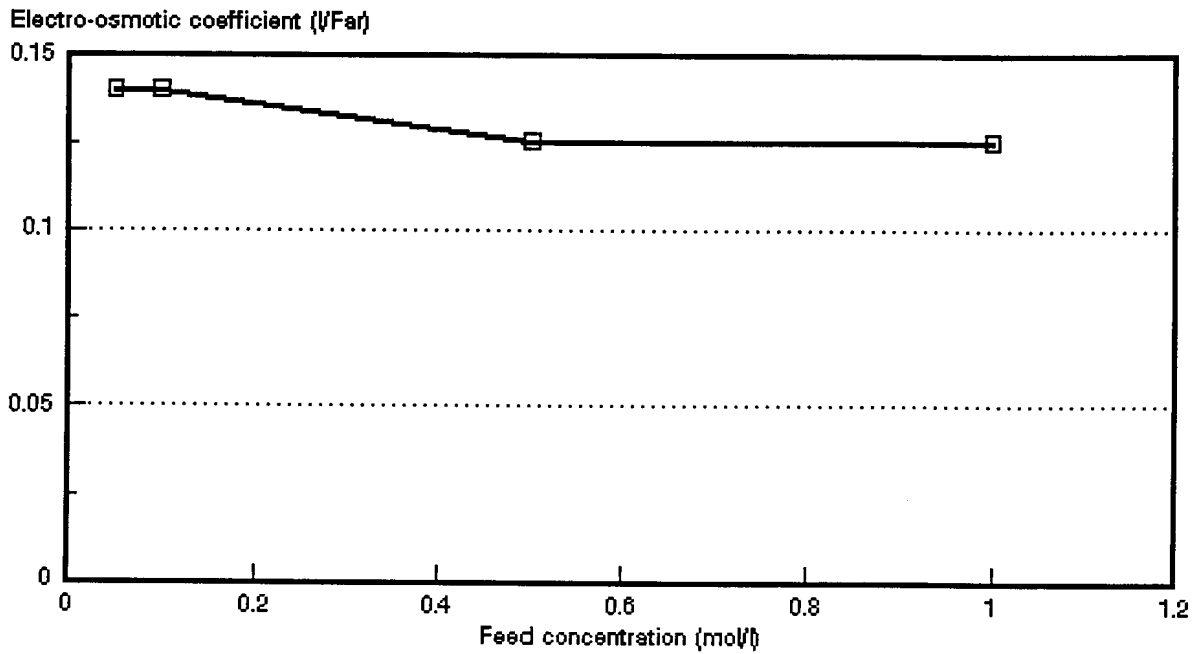


Figure 7.61: Electro-osmotic coefficient as a function of HCl feed water concentration. *Selemion AAV* and *CHV* membranes.

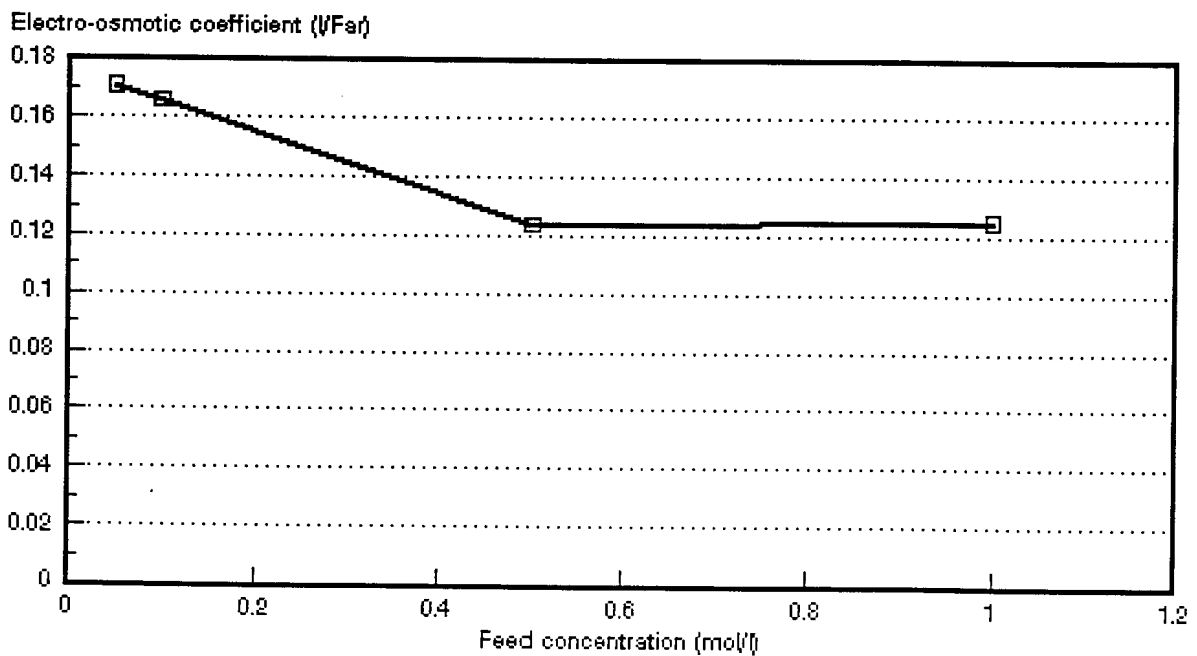


Figure 7.62: Electro-osmotic coefficient as a function of HCl feed water concentration. *ABM-3* and *Selemion CHV* membranes.

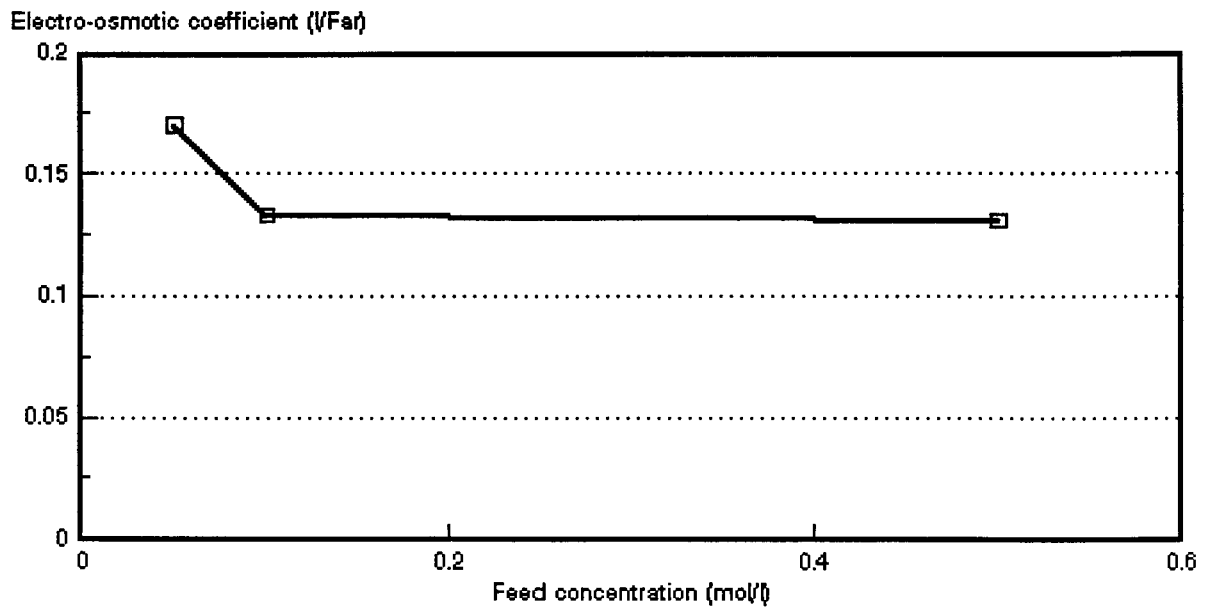


Figure 7.63: Electro-osmotic coefficient as a function of HCl feed water concentration. ABM-2 and *Selemion* CHV membranes.

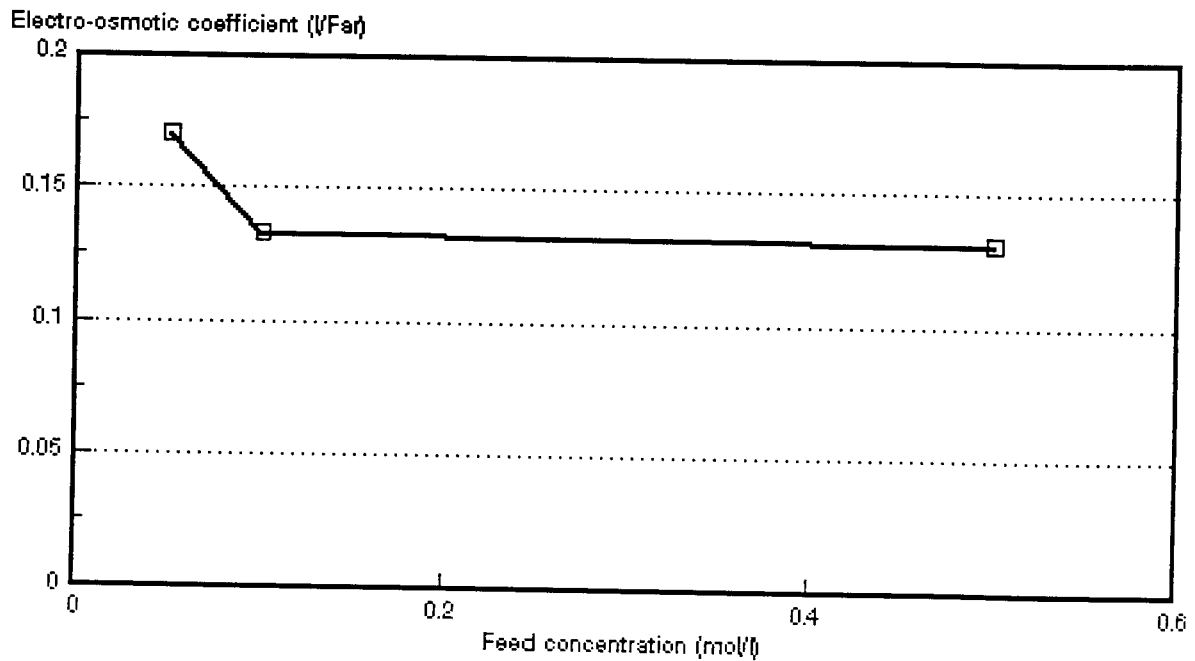


Figure 7.64: Electro-osmotic coefficient as a function of HCl feed water concentration. ABM-1 and *Selemion* CHV membranes.

Table 7.25: Effect of the electro-osmotic coefficient (EOC)* on the maximum acid brine concentration, c_b^{max} .

Membranes	Feed Concentration mol/l	EOC l/Faraday	c_b^{max} mol/l	mol H ₂ O/Faraday
Selemion	0,1	0,357	2,80	19,8
AMV & CMV	0,54	0,371	2,70	20,6
	1,0	0,306	3,27	17,0
Selemion	0,05	0,140	7,14	7,8
AAV & CHV	0,10	0,141	7,09	7,8
	0,50	0,126	7,93	7,0
	1,0	0,125	8,00	7,9
Israeli	0,05	0,171	5,85	9,5
ABM-3 &	0,10	0,166	6,02	9,2
Selemion CHV	0,50	0,124	8,06	6,9
	1,0	0,125	8,03	6,9
Israeli	0,05	0,170	5,88	9,4
ABM-2 &	0,10	0,133	7,51	7,4
Selemion CHV	0,50	0,131	7,6	7,3
Israeli	0,05	0,188	5,32	10,4
ABM-1 &	0,10	0,152	6,58	8,4
Selemion CHV	0,50	0,149	6,71	8,3

* Data from Tables 7.1 to 7.17.

Table 7.26: Osmotic flow* (J_{osm}) relative to the total flow (J) through the membranes as a function of current density.

Membranes	Current Density mA/cm ²	J_{osm}/J (%)			
		Feed Concentration (mol/l)			
		0,05	0,10	0,5	1,0
Selemon AMV & CMV	10		107,6	92,9	128,9
	20		63,8	58,9	71,2
	30		49,1	42,4	46,1
	40		42,4	34,6	39,6
	50		34,9	28,1	33,8
	60		31,4	24,8	26,6
Selemon AAV & CHV	10	96,1	91,9	123,5	109,0
	20	64,1	64,1	69,4	65,4
	30	48,5	47,1	53,7	50,1
	40	42,3	39,4	44,8	41,1
	50	37,3	35,1	38,6	37,3
	60	33,5	30,6	35,7	32,3
	70	30,4	26,1	31,7	
	80		24,5	29,0	26,6
	100		20,9	23,9	22,7
	120			21,4	
	140			20,3	18,6
	180				15,8
Israeli ABM-3 & Selemon CHV	10	77,4	77,5	103,8	
	20	50,5	53,6	69,2	
	30	42,3	44,0	56,4	
	40	35,9	35,6	46,6	
	50	31,1	31,5	42,4	
	60	28,1	29,4		
	70			37,4	
	90			30,4	
	110			25,5	
	120			22,7	
Israeli ABM-2 & Selemon CHV	10	49,1	77,5	74,4	
	20	32,3	60,2	54,1	
	30	25,8	53,4	41,2	
	40	21,0	48,3	36,6	
	50	17,2	46,4		
	60	16,9	41,0	29,5	
	80		35,6	24,0	
	100		30,6	20,3	
	120			18,1	
Israeli ABM-1 & Selemon CHV	10	69,0	102,6	102,0	
	20	50,2	74,7	66,7	
	30	34,9	52,3	55,6	
	40	32,0	46,7	44,5	
	50	31,4	41,9		
	60	30,9	35,7	34,9	
	80	25,1	32,8	30,6	
	100		28,0	24,8	
	120			22,3	

* Data from Tables 7.1 to 7.17.

7.4 Membrane Permselectivity

Membrane permselectivities (from potential measurements) as a function of acid brine concentration for different acid feed concentrations are shown in Figures 7.65 to 7.69. Membrane permselectivity decreased with increasing acid brine concentration and increasing acid feed concentration in the case of *Selemion* AMV and CMV; *Selemion* AAV and CHV; ABM-2 and CHV and ABM-1 and CHV membranes. However, a higher permselectivity was obtained at the highest feed concentration (1,0 mol/l feed) in the case of the ABM-3 and CHV membranes.

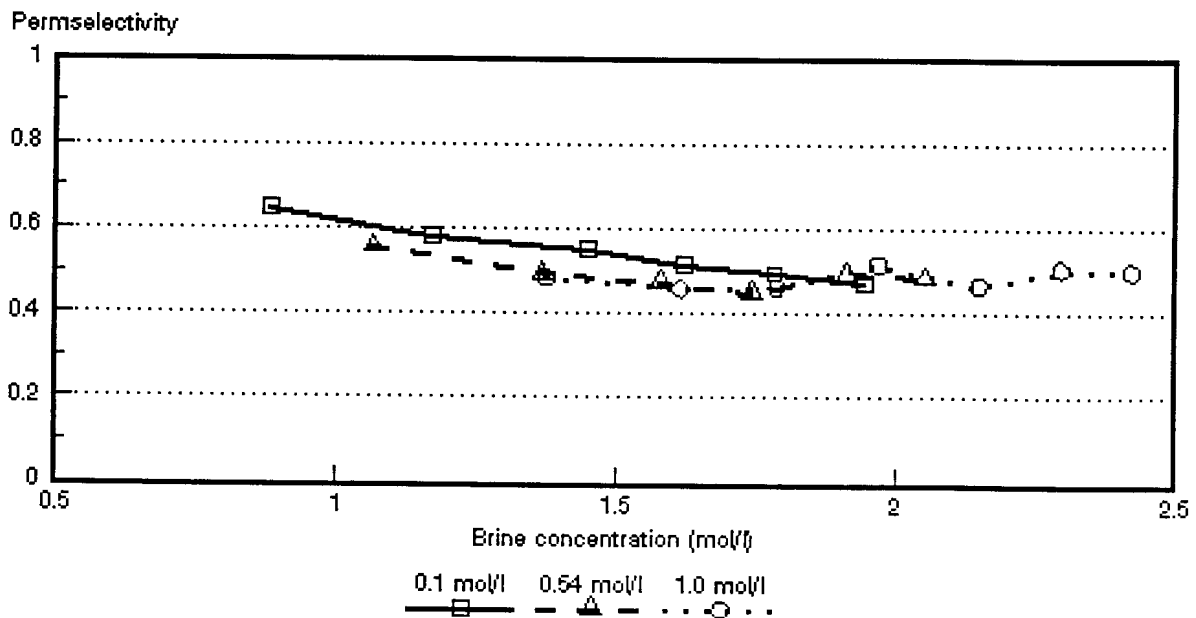


Figure 7.65: Membrane permselectivity (Δt) as a function of acid brine concentration for different HCl feed concentrations. *Selemion* AMV and CMV membranes.

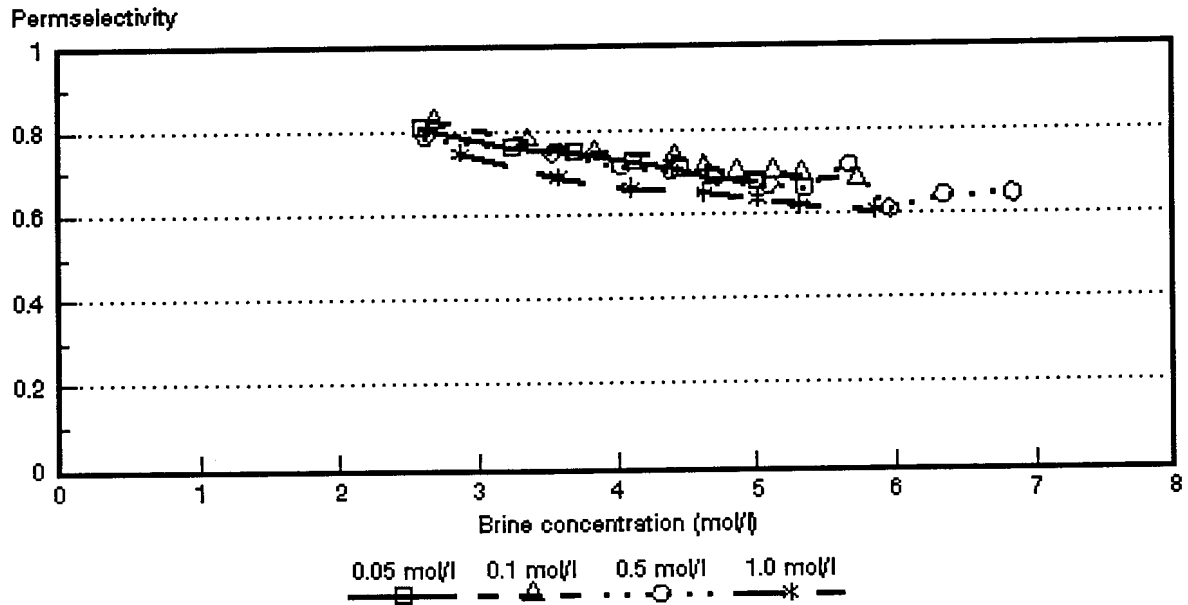


Figure 7.66: Membrane permselectivity ($\bar{\Delta}t$) as a function of acid brine concentration for different HCl feed concentrations. *Selemion AAV* and *CHV* membranes.

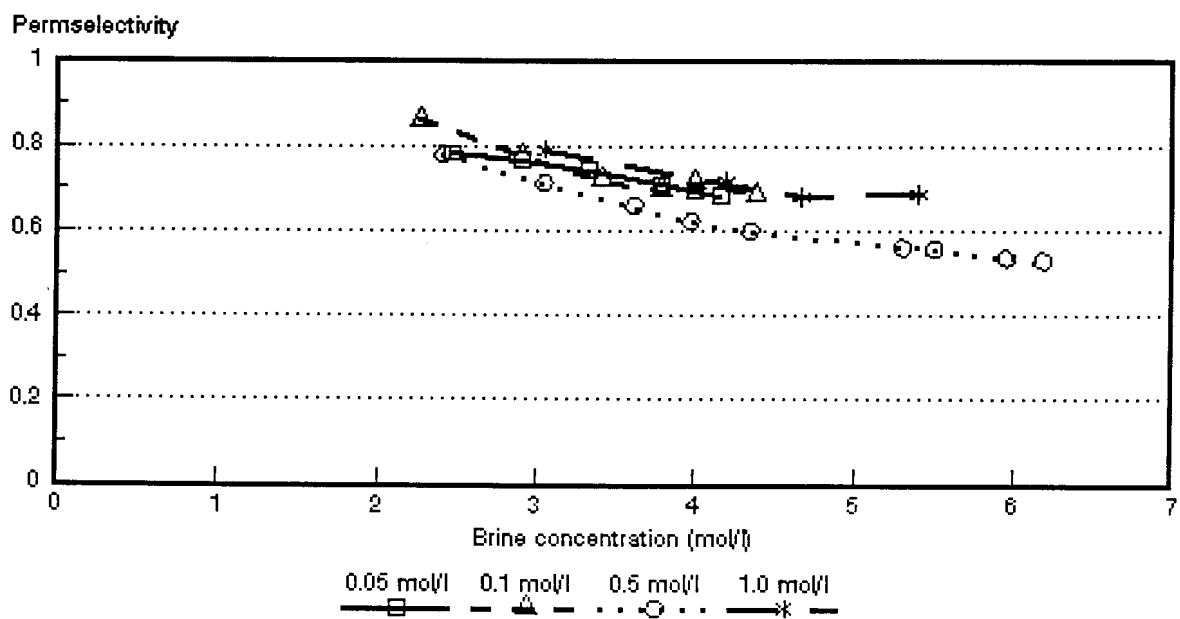


Figure 7.67: Membrane permselectivity ($\bar{\Delta}t$) as a function of acid brine concentration for different HCl feed concentrations. *ABM-3* and *Selemion CHV* membranes.

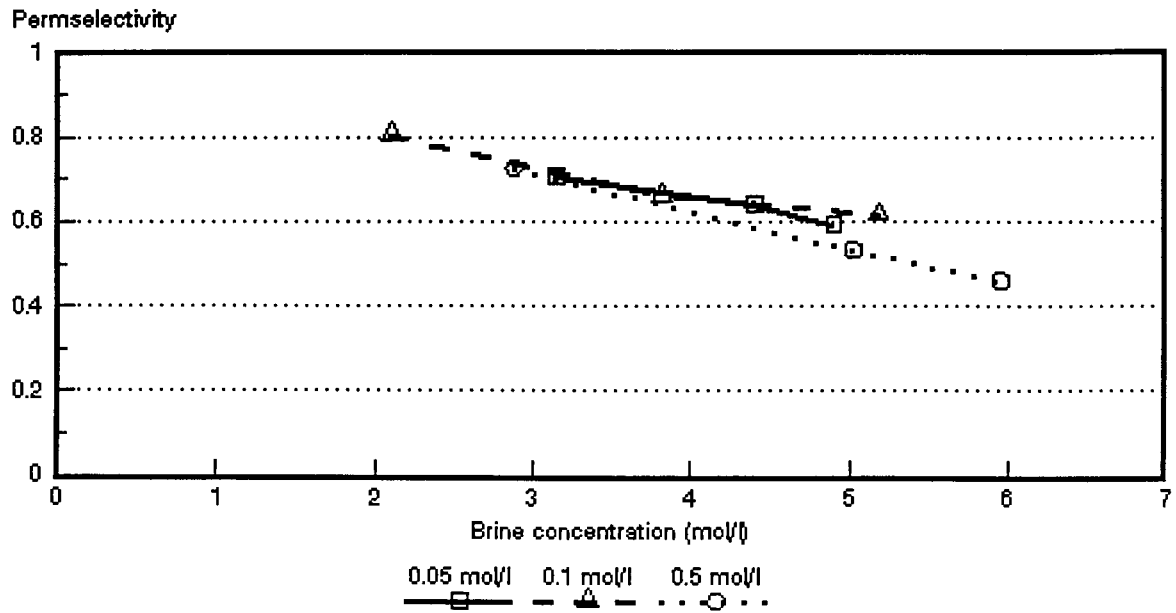


Figure 7.68: Membrane permselectivity ($\bar{\Delta}t$) as a function of acid brine concentration for different HCl feed concentrations. ABM-2 and *Selemion* CHV membranes.

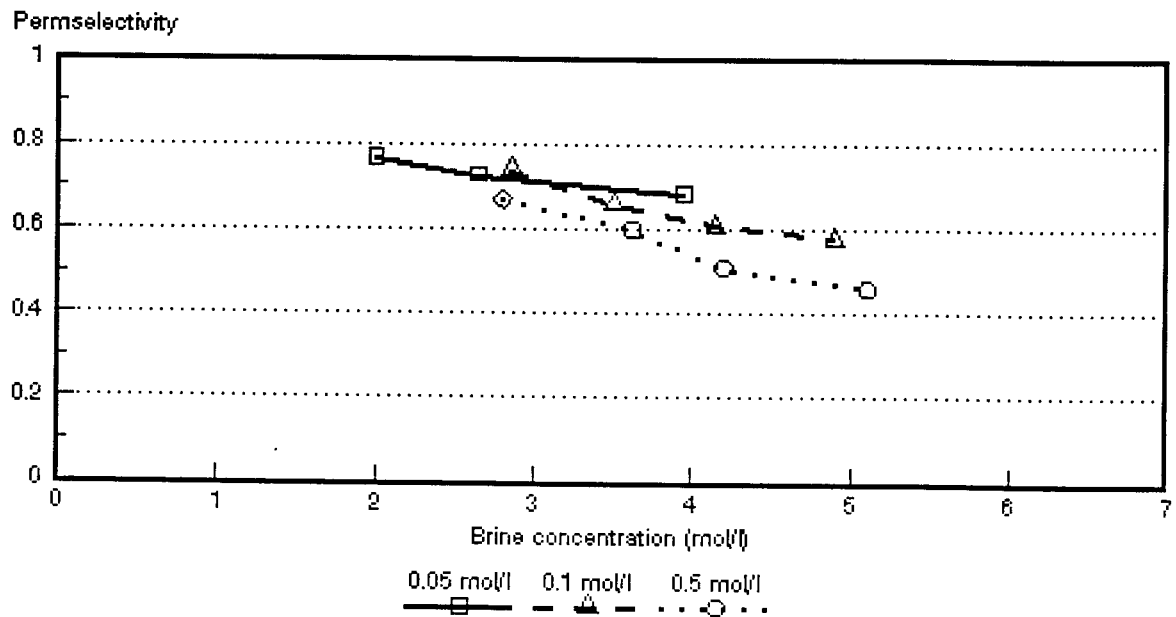


Figure 7.69: Membrane permselectivity ($\bar{\Delta}t$) as a function of acid brine concentration for different HCl feed concentrations. ABM-1 and *Selemion* CHV membranes.

7.5 Acid and Salt Diffusion through Membranes

The diffusion rate of sodium chloride and hydrochloric acid solutions through *Selemion* AMV and AAV membranes was determined in an attempt to explain the difference that was obtained between the apparent transport numbers as determined by the potential method and the current efficiencies as determined by the EOP method. Salt and acid solutions of different concentrations were separated by the membranes and the change in diluate concentration as a function of time was determined. The rate of concentration change per unit time was determined from the results. The results are shown in Table 7.27.

Table 7.27: Change of concentration rate of sodium chloride and hydrochloric acid solutions through Selemion AMV and AAV membranes.

Initial Feed Concentration mol/l	Initial Brine Concentration mol/l	Rate of Concentration Change (ge/h)*			
		Selemion AMV		Selemion AAV	
		Salt Diluate	Acid Diluate	Salt Diluate	Acid Diluate
0,05	2	0,000568	0,005872	0,000165	0,000494
0,05	4	0,000390	0,002800	0,000145	0,002805

* gram equivalents per hour.

The rate of concentration increase in the more dilute compartment was much higher for the acid than for the salt solutions for both membrane types. Consequently, backdiffusion of acid from the brine into the diluate compartment will cause the current efficiency to decrease much more in the case of acids than in the case of salt solutions.

7.6 Membrane Characteristics

7.6.1 Membrane resistance

Membrane resistances are summarized in Table 7.28.

Table 7.28: Membrane resistances of the membranes used for EOP of hydrochloric acid solution.

Membrane	Resistance - ohm·cm ²	
	0,1 mol/l	0,5 mol/l HCl
Selemion AMV	7,4	2,0
Selemion CMV	0,8	0,8
Selemion AAV	8,7	5,2
Selemion CHV	0,6	1,5
ABM-3	48,3	34,7
ABM-2	75,7	47,0
ABM-1	30,6	12,4

7.6.2 Gel water contents and ion-exchange capacities of membranes used for EOP of hydrochloric acid solutions.

The gel water contents and ion-exchange capacities of the membranes used for EOP of hydrochloric acid solutions are shown in Table 7.29.

Table 7.29: Gel water contents and ion exchange capacities of the membranes used for EOP of hydrochloric acid solutions.

Membrane	Gel Water Content %	Ion-Exchange Capacity me/dry g
Selemion AMV	18,4	1,26
Selemion CMV	22,7	2,4
Selemion AAV	9,1	0,48
Selemion CHV	13,4	1,98

7.6.3 Permselectivities of the membranes used for EOP of hydrochloric acid solutions

The permselectivities of the membranes at different hydrochloric acid concentration gradients are summarized in Table 7.30.



Table 7.30: Membrane permselectivities of the membranes used for EOP of hydrochloric acid solutions at different acid concentration gradients

Membrane	$\Delta t(1)^*$	$\Delta t(2)^{**}$	$\Delta t(3)^{***}$
Selemion AMV	0,74	0,46	0,13
Selemion CMV	1,00	0,88	0,88
Selemion AAV	0,97	0,83	0,54
Selemion CHV	0,99	0,87	0,87
ABM-3	0,88	0,63	0,44
ABM-2	0,92	0,77	0,49
ABM-1	0,84	0,60	0,40

(1)* : 0,1 / 0,2 mol/l HCl
(2)** : 0,5 / 1,0 mol/l HCl
(3)*** : 0,1 / 4,0 mol/l HCl

8. ELECTRO-OSMOTIC PUMPING OF CAUSTIC SODA SOLUTIONS WITH DIFFERENT ION-EXCHANGE MEMBRANES

Caustic soda brine concentrations, water flows and current efficiencies were determined at different current densities for different caustic soda feed water concentrations. Membrane permselectivities (apparent transport numbers) were measured at the same concentrations differences as encountered during EOP experiments. The EOP results are summarized in Tables 8.1 to 8.11.

8.1 Brine Concentration

Caustic soda brine concentration (c_b) as a function of current density (I) is shown in Figures 8.1 to 8.3. Initially caustic soda brine concentration increases rapidly and then levels off at higher current densities similar to the results that have been obtained with sodium chloride and hydrochloric acid solutions. Brine concentration increases with increasing current density and increasing feed water concentration. Caustic soda brine concentrations obtained at the highest current densities studied are shown in Table 8.12.

Table 8.12: Caustic soda brine concentrations obtained at the highest current densities investigated for different caustic soda feed water concentrations.

Feed Concentration mol/l	Brine Concentration* (%)		
	Selemion AMV & CMV	Selemion AMP & CMV	Ionac MA-3475 & MC-3470
0,05	14,3	15,4	15,7
0,1	17,7	19,9	18,0
0,5	20,1	22,4	21,7
1,0	24,2	-	16,0

* Data obtained from Tables 8.1 to 8.11.

Very high caustic soda brine concentrations were obtained for all the membranes investigated. Caustic soda brine concentrations of 17,7; 19,9 and 18,0% could be obtained from a 0,1 mol/l caustic soda feed solution with *Selemion* AMV and CMV; *Selemion* AMP and CMV and *Ionac* MA-3475 and MC-3470 membranes, respectively. It is known from the literature that there is presently not an anion-exchange membrane commercially available that is stable at high caustic soda concentrations for long periods⁽¹¹⁴⁾. The *Selemion* AMP anion-exchange membrane is claimed by the manufacturers to be more resistant to caustic soda solutions than other commercially

Table 8.1: Electro-osmotic pumping experimental conditions and results for 0,05 mol/l caustic soda (Selemion AMV and CMV).

Current Density I , mA/cm ²	Brine concentration c_b , mol/l		Water flow J , cm/h	Current Efficiency e_p , %	Effective Current Density I_{eff} , mA/cm ²	Transport Numbers				
	$c_{b, exp.}$	$c_{b, calc.}$				Δt^c	Δt^a	$\bar{\Delta}t$	\bar{i}_1^c	\bar{i}_2^a
10	2,30	3,15	0,0953	58,79	5,88	0,73	0,88	0,80	0,86	0,94
20	2,88	4,08	0,1413	54,43	10,89	0,68	0,87	0,77	0,84	0,94
30	3,18	4,59	0,1854	52,61	15,78	0,65	0,87	0,76	0,82	0,94
40	3,20	5,04	0,2251	48,29	19,31	0,65	0,87	0,76	0,83	0,93
50	3,58	5,50	0,2472	47,39	23,69	0,59	0,87	0,73	0,79	0,94

Electro-osmotic coefficient (2β) = 0,228 μ /F (slope = 0,0085120 ml/mAh)
 $J_{os,m}$ = y-intercept = 0,054571 cm/h
 c_b^{max} = 4,39 mol/l
 $\Delta t^c = t_1^c - t_2^c$

$\Delta t^a = t_2^a - t_1^a$
 $\bar{\Delta}t$ = Average transport number of membrane pair
 \bar{i}_1^c = Transport number of cation through cation membrane
 \bar{i}_2^a = Transport number of anion through anion membrane.

Table 8.2: Electro-osmotic pumping experimental conditions and results for 0,1 mol/l caustic soda (Selemion AMV and CMV)

Current Density I , mA/cm ²	Brine concentration c_b , mol/l		Water flow J , cm/h	Current Efficiency e_p , %	Effective Current Density I_{eff} , mA/cm ²	Transport Numbers				
	$c_{b, exp.}$	$c_{b, calc.}$				Δt^c	Δt^a	$\bar{\Delta}t$	\bar{i}_1^c	\bar{i}_2^a
10	2,16	2,67	0,1147	66,46	6,65	0,78	0,86	0,82	0,89	0,93
20	2,78	3,46	0,1721	64,04	12,81	0,74	0,85	0,80	0,87	0,93
30	3,45	4,31	0,1960	60,43	18,13	0,67	0,84	0,75	0,83	0,92
40	3,50		0,2578	60,48	24,19	0,68	0,84	0,76	0,84	0,92
50	3,69	4,63	0,2966	58,69	29,35	0,64	0,84	0,74	0,82	0,92
60	3,82		0,3108	53,04	31,83	0,67	0,81	0,74	0,83	0,90
80	4,33	5,59	0,3567	51,70	41,36	0,62	0,80	0,71	0,81	0,90
100	4,43	6,21	0,4203	49,85	49,85	0,60	0,80	0,70	0,80	0,90

Electro-osmotic coefficient (2β) = 0,179 μ /F (slope = 0,0066710 ml/mAh)
 $J_{os,m}$ = y-intercept = 0,0898921 cm/h
 c_b^{max} = 5,59 mol/l
 $\Delta t^c = t_1^c - t_2^c$

$\Delta t^a = t_2^a - t_1^a$
 $\bar{\Delta}t$ = Average transport number of membrane pair
 \bar{i}_1^c = Transport number of cation through cation membrane
 \bar{i}_2^a = Transport number of anion through anion membrane.

Table 8.3 : Electro-osmotic pumping experimental conditions and results for 0,5 mol/l caustic soda (Selemion AMV and CMV).

Current Density I , mA/cm ²	Brine concentration c_b , mol/l		Water flow J , cm/h	Current Efficiency e_p , %	Effective Current Density I_{eff} , mA/cm ²	Transport Numbers				
	$c_{b, exp.}$	$c_{b, calc.}$				Δt^c	Δt^a	$\bar{\Delta}t$	\bar{i}_1^c	\bar{i}_2^a
10	2,2	2,02	0,1457	66,39	6,64	0,78	0,80	0,79	0,89	0,90
20	2,33	3,32	0,1748	66,20	13,23	0,77	0,78	0,78	0,89	0,89
30	3,36	3,96	0,2120	63,62	19,89	0,73	0,77	0,75	0,87	0,88
40	3,56		0,2560	61,09	24,28	0,70	0,78	0,74	0,85	0,89
50	3,96	4,97	0,2649	56,24	28,12	0,65	0,76	0,71	0,83	0,88
60	4,13		0,2825	52,07	31,24	0,62	0,77	0,70	0,81	0,89
70	4,39	5,80	0,3072	51,65	36,16	0,59	0,78	0,68	0,79	0,89
80	4,53		0,3355	50,87	40,70	0,60	0,77	0,68	0,80	0,88
100	4,83	6,31	0,3920	50,71	50,71	0,57	0,76	0,66	0,79	0,88
120	5,03	6,40	0,459	51,54	61,85	0,58	0,73	0,66	0,79	0,87

Electro-osmotic coefficient (2β) = 0,152 μ /F (slope = 0,0056728 ml/mAh)
 $J_{os,m}$ = y-intercept = 0,1059033 cm/h
 c_b^{max} = 6,58 mol/l
 $\Delta t^c = t_1^c - t_2^c$

$\Delta t^a = t_2^a - t_1^a$
 $\bar{\Delta}t$ = Average transport number of membrane pair
 \bar{i}_1^c = Transport number of cation through cation membrane
 \bar{i}_2^a = Transport number of anion through anion membrane.

Table 8.4: Electro-osmotic pumping experimental conditions and results for 1 mol/l NaOH (Selemion AMV and CMV)

Current Density I , mA/cm ²	Brine concentration c_b , mol/l		Water flow J , cm/h	Current Efficiency e_p , %	Effective Current Density I_{eff} , mA/cm ²	Transport Numbers				
	$c_{b, exp}$	$c_{b, calc}$				Δt^c	Δt^a	$\bar{\Delta}t$	\bar{i}_1^c	\bar{i}_2^c
30	4,4	3,5	0,1943	76,37	22,91	0,57	0,75	0,66	0,78	0,87
50	5,2	4,55	0,2649	73,84	36,92	0,56	0,74	0,65	0,77	0,86
70	5,8	5,3	0,3046	67,66	47,36	0,50	0,74	0,62	0,75	0,86
90	6,05	6,3	0,3310	59,66	53,69	0,49	0,75	0,62	0,74	0,87

Electro-osmotic coefficient (2β) = 0,118 μ F (slope = 0,0044119 ml/mAh)
 J_{osm} = y-intercept = 0,0962310 cm/h
 c_b^{max} = 8,46 mol/l
 $\Delta t^c = t_1^c - t_2^c$

$\Delta t^a = t_2^a - t_1^a$
 $\bar{\Delta}t$ = Average transport number of membrane pair
 \bar{i}_1^c = Transport number of cation through cation membrane
 \bar{i}_2^c = Transport number of anion through anion membrane.

Table 8.5 : Electro-osmotic pumping experimental conditions and results for 0,05 mol/l caustic soda (Selemion AMP and CMV)

Current Density I , mA/cm ²	Brine concentration c_b , mol/l		Water flow J , cm/h	Current Efficiency e_p , %	Effective Current Density I_{eff} , mA/cm ²	Transport Numbers				
	$c_{b, exp}$	$c_{b, calc}$				Δt^c	Δt^a	$\bar{\Delta}t$	\bar{i}_1^c	\bar{i}_2^c
10	1,92	2,55	0,118	61,07	6,11	0,74	0,87	0,81	0,87	0,93
20	2,48	3,64	0,172	57,06	11,41	0,82	0,86	0,84	0,91	0,93
30	2,76	3,58	0,235	57,92	17,38	0,67	0,85	0,75	0,84	0,92
40	3,16	3,94	0,268	56,66	22,66	0,57	0,84	0,71	0,79	0,92
50	3,44	4,61	0,293	54,06	27,03	0,61	0,84	0,72	0,80	0,92
60	3,84	5,31	0,297	50,90	30,54	0,59	0,82	0,71	0,79	0,91

Electro-osmotic coefficient (2β) = 0,176 μ F (slope = 0,0065825 ml/mAh)
 J_{osm} = y-intercept = 0,1094348 cm/h
 $\bar{\Delta}t$ = Average transport number of membrane pair
 c_b^{max} = 5,68 mol/l

$\Delta t^a = t_2^a - t_1^a$
 $\Delta t^c = t_1^c - t_2^c$
 \bar{i}_1^c = Transport number of cation through cation membrane
 \bar{i}_2^c = Transport number of anion through anion membrane.

Table 8.6 : Electro-osmotic pumping experimental conditions and results for 0,1 mol/l caustic soda (Selemion AMP and CMV)

Current Density I , mA/cm ²	Brine concentration c_b , mol/l		Water flow J , cm/h	Current Efficiency e_p , %	Effective Current Density I_{eff} , mA/cm ²	Transport Numbers				
	$c_{b, exp}$	$c_{b, calc}$				Δt^c	Δt^a	$\bar{\Delta}t$	\bar{i}_1^c	\bar{i}_2^c
10	2,14	2,53	0,117	67,34	6,73	0,76	0,83	0,79	0,88	0,91
20	2,88	3,33	0,169	65,00	13,00	0,70	0,81	0,76	0,85	0,91
30	3,35	3,69	0,221	66,21	19,86	0,65	0,80	0,73	0,83	0,90
40	3,62		0,248	60,12	24,05	0,59	0,80	0,70	0,80	0,90
50	3,90	4,63	0,282	59,04	29,52	0,59	0,81	0,70	0,80	0,90
60	4,38		0,298	58,32	34,99	0,58	0,79	0,69	0,79	0,89
70	4,41	5,24	0,333	56,20	39,34	0,54	0,79	0,67	0,77	0,90
80	4,61		0,366	56,41	45,13	0,54	0,78	0,66	0,77	0,89
90	4,67	5,61	0,396	55,08	49,57	0,53	0,79	0,66	0,77	0,89
100	4,97	5,82	0,404	53,82	53,82	0,48	0,78	0,63	0,74	0,89

Electro-osmotic coefficient (2β) = 0,155 μ F (slope = 0,0057673 ml/mAh)
 J_{osm} = y-intercept = 0,1036958 cm/h
 c_b^{max} = 6,45 mol/l
 $\Delta t^c = t_1^c - t_2^c$

$\Delta t^a = t_2^a - t_1^a$
 $\bar{\Delta}t$ = Average transport number of membrane pair
 \bar{i}_1^c = Transport number of cation through cation membrane
 \bar{i}_2^c = Transport number of anion through anion membrane.

Table 8.7 : Electro-osmotic pumping experimental conditions and results for 0,50 mol/l caustic soda (Selemon AMP and CMV)

Current Density I , mA/cm ²	Brine concentration c_b , mol/l		*Water flow J , cm/h	Current Efficiency e_p , %	Effective Current Density I_{eff} , mA/cm ²	Transport Numbers				
	$c_{b, exp.}$	$c_{b, calc.}$				Δt^c	Δt^a	$\bar{\Delta}t$	\bar{i}_1^c	\bar{i}_2^a
10	2,29	2,62	0,110	67,75	6,78	0,76	0,79	0,77	0,88	0,89
20	3,02	3,36	0,159	64,33	12,87	0,66	0,78	0,72	0,83	0,89
30	3,57	4,05	0,196	62,63	18,79	0,65	0,77	0,71	0,83	0,88
40	3,98		0,236	62,99	25,20	0,56	0,77	0,67	0,78	0,88
50	4,12	4,71	0,265	58,58	29,29	0,60	0,74	0,67	0,80	0,88
60	4,43	5,02	0,295	58,42	35,05	0,58	0,74	0,66	0,79	0,87
70	4,89		0,282	52,83	36,98	0,47	0,75	0,61	0,74	0,87
80	4,83	5,67	0,331	53,59	42,87	0,53	0,72	0,63	0,77	0,86
100	5,19	5,59	0,399	55,46	55,46	0,48	0,72	0,60	0,74	0,86
120	5,59	6,29	0,419	52,76	63,31	0,47	0,70	0,59	0,74	0,85

Electro-osmotic coefficient (2β) = 0,137 μ F (slope = 0,0051179 ml/mAh)

J_{osm} = y-intercept = 0,1068910 cm/h

c_b^{max} = 7,30 mol/l

$\Delta t^c = t_1^c - t_2^c$

$\Delta t^a = t_2^a - t_1^a$

$\bar{\Delta}t$ = Average transport number of membrane pair

\bar{i}_1^c = Transport number of cation through cation membrane

\bar{i}_2^a = Transport number of anion through anion membrane.

Table 8.8 : Electro-osmotic pumping experimental conditions and results for 0,05 mol/l caustic soda (Ionac MA-3475 and MC-3470)

Current Density I , mA/cm ²	Brine concentration c_b , mol/l		Water flow J , cm/h	Current Efficiency e_p , %	Effective Current Density I_{eff} , mA/cm ²	Transport Numbers				
	$c_{b, exp.}$	$c_{b, calc.}$				Δt^c	Δt^a	$\bar{\Delta}t$	\bar{i}_1^c	\bar{i}_2^a
10	2,77	2,79	0,0927	68,8	0,8196	0,57	0,82	0,69	0,78	0,91
20	3,4	3,61	0,1391	63,37	12,6	0,55	0,80	0,67	0,77	0,90
30	3,76	3,96	0,1854	62,29	18,6	0,51	0,80	0,66	0,76	0,90
40	3,92	4,14	0,2344	61,59	24,63	0,51	0,79	0,65	0,75	0,90

Electro-osmotic coefficient (2β) = 0,212 μ F (slope = 0,0079229 ml/mAh)

J_{osm} = y-intercept = 0,0388302 cm/h

c_b^{max} = 4,72 mol/l

$\Delta t^c = t_1^c - t_2^c$

$\Delta t^a = t_2^a - t_1^a$

$\bar{\Delta}t$ = Average transport number of membrane pair

\bar{i}_1^c = Transport number of cation through cation membrane

\bar{i}_2^a = Transport number of anion through anion membrane.

Table 8.9 : Electro-osmotic pumping experimental conditions and results for 0,1 mol/l caustic soda (Ionac MA-3475 and MC-3470)

Current Density I , mA/cm ²	Brine concentration c_b , mol/l		* Water flow, J , cm/h	Current Efficiency e_p , %	Effective Current Density I_{eff} , mA/cm ²	Transport Numbers				
	$c_{b, exp.}$	$c_{b, calc.}$				Δt^c	Δt^a	$\bar{\Delta}t$	\bar{i}_1^c	\bar{i}_2^a
10	2,63	2,58	0,1033	72,22	7,22	0,61	0,81	0,71	0,81	0,91
20	3,4	3,38	0,1522	69,38	13,88	0,57	0,80	0,69	0,79	0,90
30	3,71	3,69	0,200	66,77	20,03	0,52	0,80	0,66	0,76	0,90
40	4,1		0,247	67,93	27,17	0,48	0,79	0,64	0,74	0,89
50	4,26	4,04	0,279	64,50	32,25	0,43	0,78	0,60	0,71	0,89
60	4,15		0,318	58,93	35,35					
70	4,45	4,37	0,371	63,19	44,23	0,45	0,79	0,62	0,73	0,89
75	4,51		0,371	59,71	44,78	0,43	0,79	0,61	0,71	0,89

Electro-osmotic coefficient (2β) = 0,193 μ F (slope = 0,0071947 ml/mAh)

J_{osm} = y-intercept = 0,0529144 cm/h

c_b^{max} = 5,18 mol/l

$\Delta t^c = t_1^c - t_2^c$

$\Delta t^a = t_2^a - t_1^a$

$\bar{\Delta}t$ = Average transport number of membrane pair

\bar{i}_1^c = Transport number of cation through cation membrane

\bar{i}_2^a = Transport number of anion through anion membrane.



Table 8.10 : Electro-osmotic pumping experimental conditions and results for 0,5 mol/l caustic soda (Ionac MA-3475 and MC-3470)

Current Density i , mA/cm ²	Brine concentration c_b , mol/l		Water flow J , cm/h	Current Efficiency e_p , %	Effective Current Density i_{eff} , mA/cm ²	Transport Numbers				
	$c_{b, exp.}$	$c_{b, calc.}$				Δt^*	Δt^*	$\bar{\Delta}t$	\bar{i}_1^*	\bar{i}_2^*
10	2,63	2,13	0,0993	70,56	7,06	0,37	0,76	0,57	0,68	0,88
20	3,40	2,86	0,1378	62,77	12,55	0,32	0,73	0,53	0,66	0,87
30	3,98	3,14	0,1854	65,86	19,76	0,32	0,72	0,52	0,66	0,86
40	4,33	3,35	0,2296	66,65	26,66	0,22	0,72	0,47	0,61	0,86
50	4,50		0,2560	61,77	30,88	0,20	0,72	0,46	0,60	0,86
60	4,55		0,3178	64,62	38,77					
70	4,98	3,50	0,3443	65,67	45,97	0,22	0,70	0,46	0,61	0,85
80	5,00		0,3921	65,68	52,55					
90	5,23	3,71	0,4132	64,31	57,88	0,21	0,70	0,46	0,61	0,85
100	5,20		0,4503	62,77	62,77					
110	5,43		0,14768	63,04	69,34					

Electro-osmotic coefficient (2β) = 0,176 μ F (slope = 0,0065599 m³/mAh)
 J_{osm} = y-intercept = 0,0526844 cm/h
 c_b^{max} = 5,68 mol/l
 $\Delta t^* = t_1^* - t_2^*$

$\Delta t^* = t_2^* - t_1^*$
 $\bar{\Delta}t$ = Average transport number of membrane pair
 \bar{i}_1^* = Transport number of cation through cation membrane
 \bar{i}_2^* = Transport number of anion through anion membrane.

Table 8.11: Electro-osmotic pumping experimental conditions and results for 1,0 mol/l caustic soda (Ionac MA-3475 and MC-3470)

Current Density i , mA/cm ²	Brine concentration c_b , mol/l		Water flow J , cm/h	Current Efficiency e_p , %	Effective Current Density i_{eff} , mA/cm ²	Transport Numbers				
	$c_{b, exp.}$	$c_{b, calc.}$				Δt^*	Δt^*	$\bar{\Delta}t$	\bar{i}_1^*	\bar{i}_2^*
10	2,75	1,80	0,0971	71,60	7,16	0,20	0,73	0,47	0,60	0,87
20	3,44	2,50	0,1378	63,51	12,70	0,21	0,71	0,46	0,61	0,86
30	3,84	2,70	0,1854	63,62	19,09	0,20	0,68	0,44	0,60	0,84
40	4,02	3,40	0,1986	53,52	21,4	0,18	0,73	0,46	0,59	0,87

Electro-osmotic coefficient (2β) = 0,193 μ F (slope = 0,0072079 m³/mAh)
 J_{osm} = y-intercept = 0,0459504 cm/h
 c_b^{max} = 5,18 mol/l
 $\Delta t^* = t_1^* - t_2^*$

$\Delta t^* = t_2^* - t_1^*$
 $\bar{\Delta}t$ = Average transport number of membrane pair
 \bar{i}_1^* = Transport number of cation through cation membrane
 \bar{i}_2^* = Transport number of anion through anion membrane.

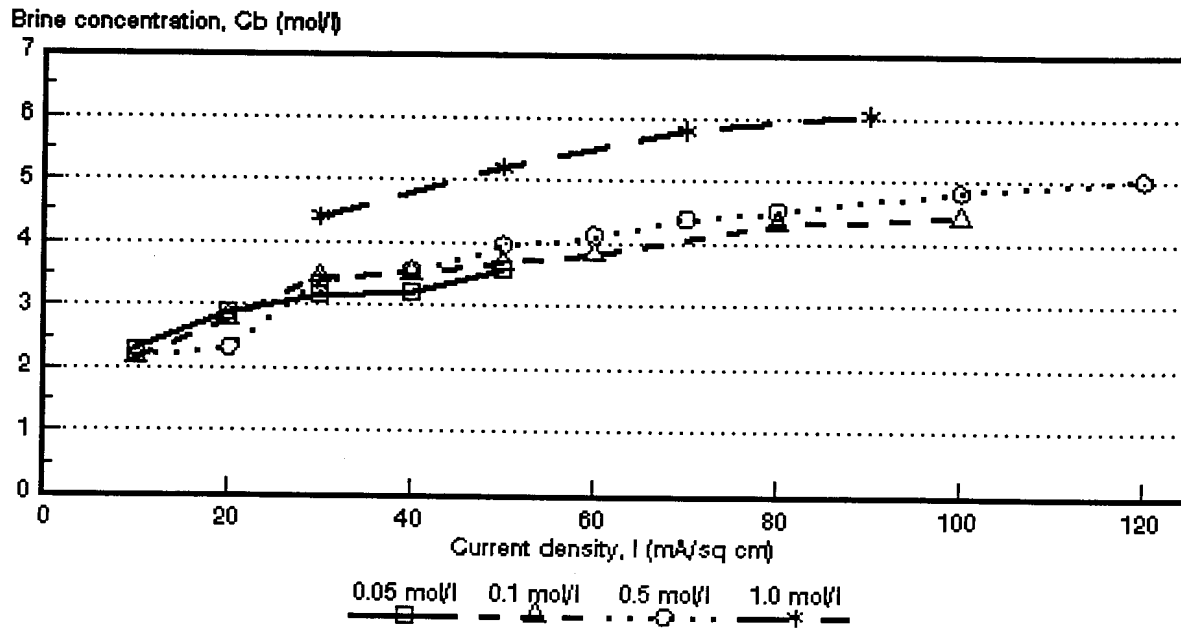


Figure 8.1: Caustic soda concentration as a function of current density for 4 different NaOH feed water concentrations. *Selemon* AMV and CMV membranes.

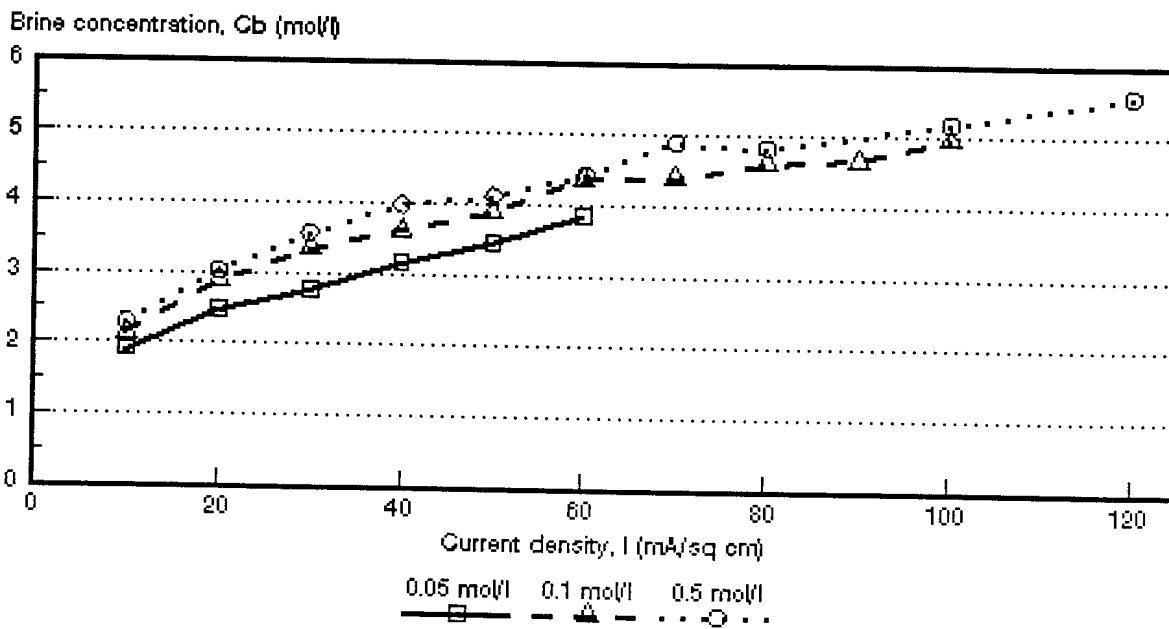


Figure 8.2: Caustic soda concentration as a function of current density for 3 different NaOH feed water concentrations. *Selemon* AMP and CMV membranes.

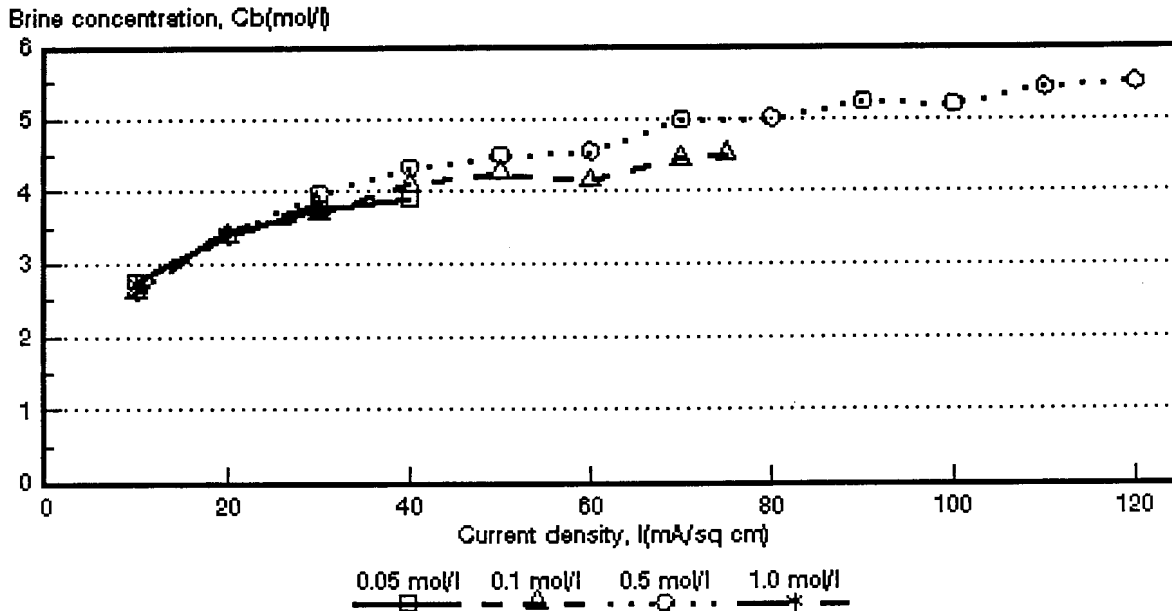


Figure 8.3: Caustic soda concentration as a function of current density for 4 different NaOH feed water concentrations. *Ionac* MA-3475 and MC-3470 membranes.

available anion-exchange membranes. Consequently, membrane life time will be a problem when caustic soda solutions are electrolyzed with conventional ion-exchange membranes. However, the value of the product recovered by ED might be of such a nature that a relatively short membrane life time could be tolerated.

It appears that the caustic soda brine concentration will reach a maximum value, c_b^{\max} , as has been experienced with sodium chloride and hydrochloric acid solutions. This maximum value, however, was not reached even at the lowest caustic soda feed concentrations that were used (Figs. 8.1 to 8.3). It appears, however, that the maximum caustic soda brine concentration will be reached at relatively low current densities at the lowest feed water concentrations used. Maximum caustic soda brine concentration for higher caustic soda feed concentrations (0,1 to 1,0 mol/l) will be reached at high current densities.

Maximum caustic soda brine concentration, c_b^{\max} , was calculated from the same relationships as used in 6.1. The results are shown in Tables 8.13 and Figures 8.4 to 8.6. Maximum caustic soda brine concentration depends somewhat on feed concentration. The *Selemion* AMV and CMV membranes showed an increase in the maximum brine concentration as a function of feed concentration in the feed

Table 8.13: Maximum caustic soda brine concentration, c_b^{\max} , calculated from $c_b^{\max} = 1/2 F\beta^*$ and $c_b^{\max} = c_b (1 + J_{osm}/J_{eliosm})^{}$**

Feed Concentration mol/l	Maximum Brine Concentration, c_b^{\max}					
	AMV and CMV		AMP and CMV		MA-3475 and MC-3470	
	1	2	1	2	1	2
0,05	4,4	4,6	5,7	5,8	4,7	4,7
0,10	5,6	5,4	6,5	6,4	5,2	5,2
0,50	6,6	6,5	7,3	7,2	5,7	5,7
1,0	8,5	8,5			5,2	5,2

- 1 : $c_b^{\max} = 1/2 F\beta$
 2 : $c_b^{\max} = c_b (1 + J_{osm}/J_{eliosm})$
 * : Calculated from electro-osmotic coefficients (Tables 8.1 - 8.11)
 ** : Calculated from $J_{eliosm} = J - J_{osm}$ (y-intercept and the corresponding c_b values) (Tables 8.1 - 8.11).

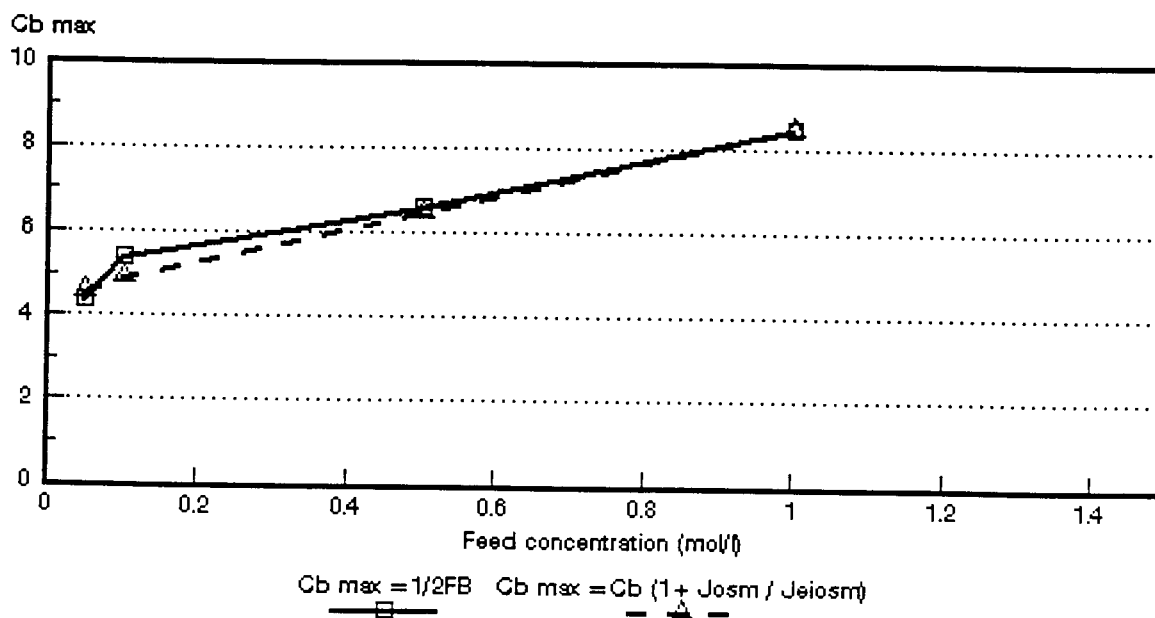


Figure 8.4: Maximum caustic soda brine concentration as a function of feed concentration for different NaOH feed water concentrations. *Selemion* AMV and CMV membranes.

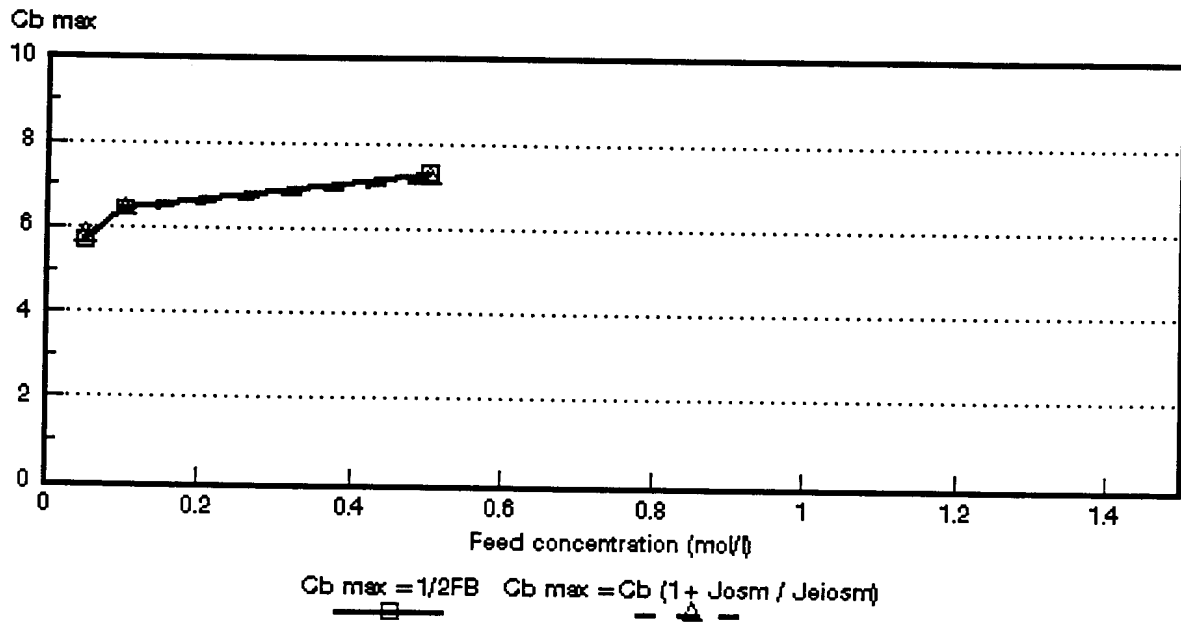


Figure 8.5: Maximum caustic soda brine concentration as a function of feed concentration for different NaOH feed water concentrations. *Selemion* AMP and CMV membranes.

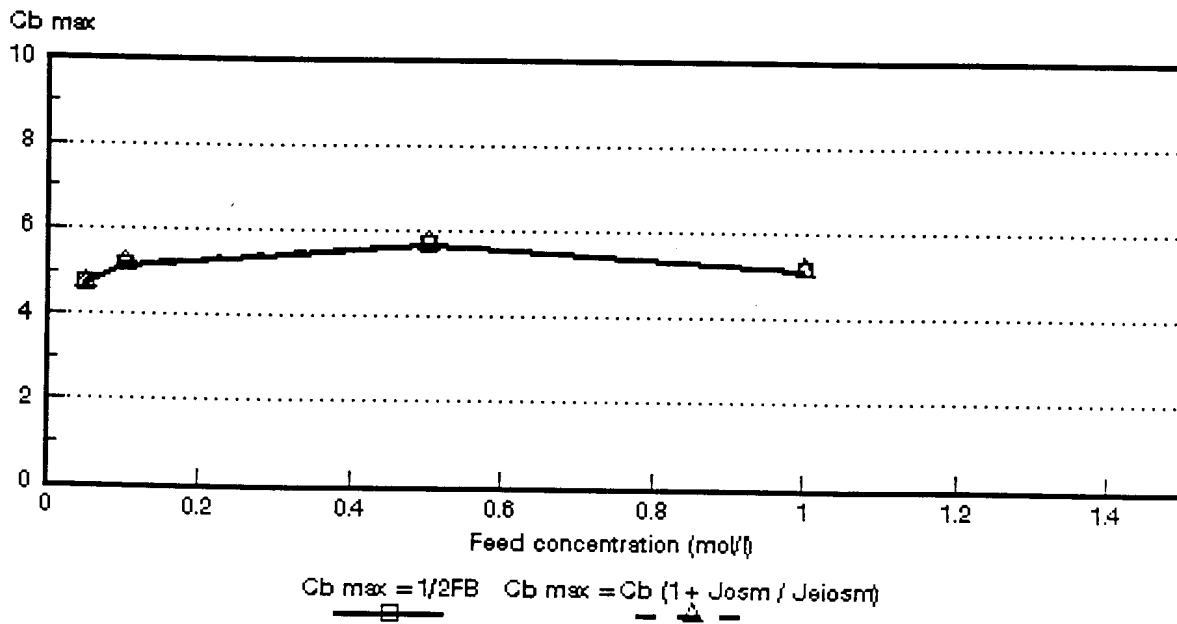


Figure 8.6: Maximum caustic soda brine concentration as a function of feed concentration for different NaOH feed water concentrations. *Ionac* MA-3475 and MC-3470 membranes.

concentration range from 0,05 to 1,0 mol/l (Fig. 8.4). A similar trend was observed for the *Selemion* AMP and CMV membranes (Fig. 8.5) while the *Ionac* membranes first showed an increase and then a slight decrease in c_b^{\max} at high feed concentration (Fig. 8.6). A very good correlation was again obtained by the two methods that were used to calculate the maximum caustic soda brine concentration (Table 8.13).

Caustic soda brine concentrations obtained at different current densities and feed water concentrations were predicted from measured transport numbers and volume flows (J) with the same relationship as used in 6.1. The experimental and calculated caustic soda brine concentrations are shown in Tables 8.1 to 8.11. and Figures 8.7 to 8.17. The calculated caustic soda brine concentrations were determined from the average value of the apparent transport number of a membrane pair ($\bar{\Delta}t$) and from water flows. The correlations between the calculated and experimentally determined brine concentrations, expressed as the ratio $c_{b\text{calc}}/c_{b\text{exp}}$, are shown in Table 8.14.

The calculated caustic soda brine concentrations were significantly higher than the experimentally determined brine concentrations at a caustic soda feed concentration of 0,05 mol/l in the case of the *Selemion* AMV and CMV and *Selemion* AMP and CMV membranes (Table 8.14). The calculated caustic soda brine concentration was from 1,36 to 1,54 times higher than the experimentally determined brine concentration in the case of the *Selemion* AMV and CMV membranes and from 1,25 to 1,47 higher in the case of the *Selemion* AMP and CMV membranes. However, a much better correlation was obtained at 0,1 and 0,5 mol/l caustic soda feed concentration for both membrane pairs. The ratio $c_{b\text{calc}}/c_{b\text{exp}}$ varied between 1,23 and 1,25 (10 to 50 mA/cm², 0,1 mol/l feed) and between 0,92 and 1,25 (10 to 50 mA/cm², 0,5 mol/l feed) for the *Selemion* AMV and CMV membranes. The same ratio for the *Selemion* AMP and CMV membranes varied between 1,10 and 1,19 (10 to 50 mA/cm², 0,1 mol/l feed) and between 1,11 and 1,14 (10 to 50 mA/cm², 0,5 mol/l feed). Therefore, a higher estimation of caustic soda brine concentration can be obtained from measured transport numbers and water flows in this case.

A very good correlation was obtained between the calculated and experimentally determined caustic soda brine concentrations in the case of *Ionac* membranes at 0,05 and 0,1 mol/l feed concentration. The ratio $c_{b\text{calc}}/c_{b\text{exp}}$ varied between 1,01 and 1,06 (10 to 40 mA/cm², 0,05 mol/l feed) and between 0,95 and 0,99 (10 to 70 mA/cm², 0,1 mol/l feed). Therefore, an excellent correlation was obtained. However, the correlations at 0,5 and 1,0 mol/l feed for the same membranes were not very good (Table 8.14).

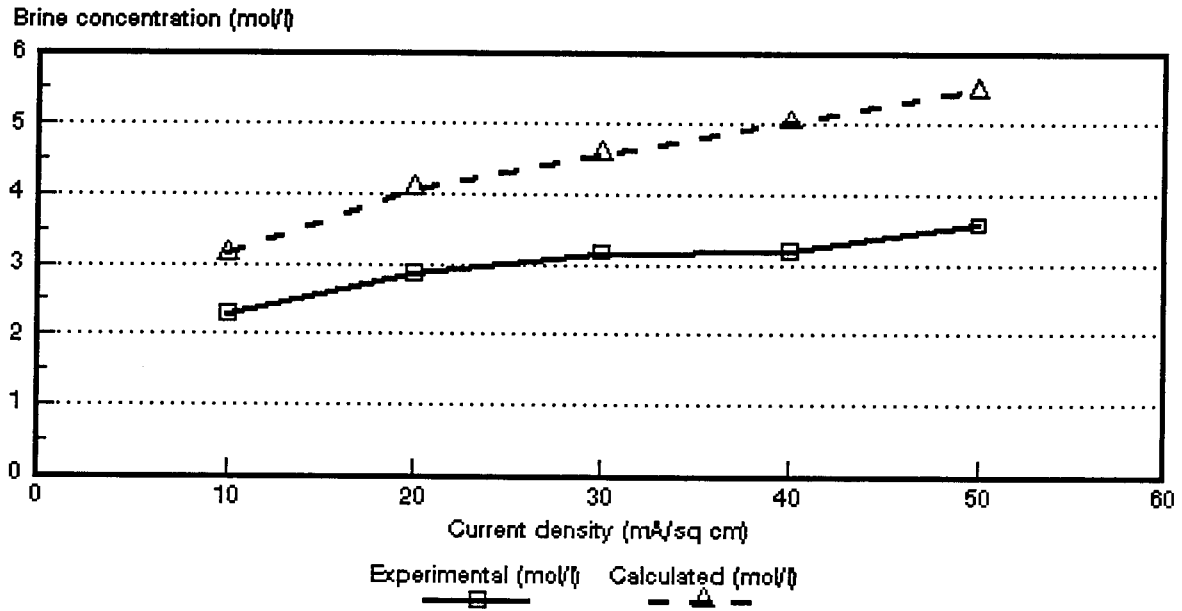


Figure 8.7: Experimental and calculated caustic soda brine concentrations as a function of current density for 0,05 mol/l NaOH feed solution. *Selemion* AMV and CMV membranes.

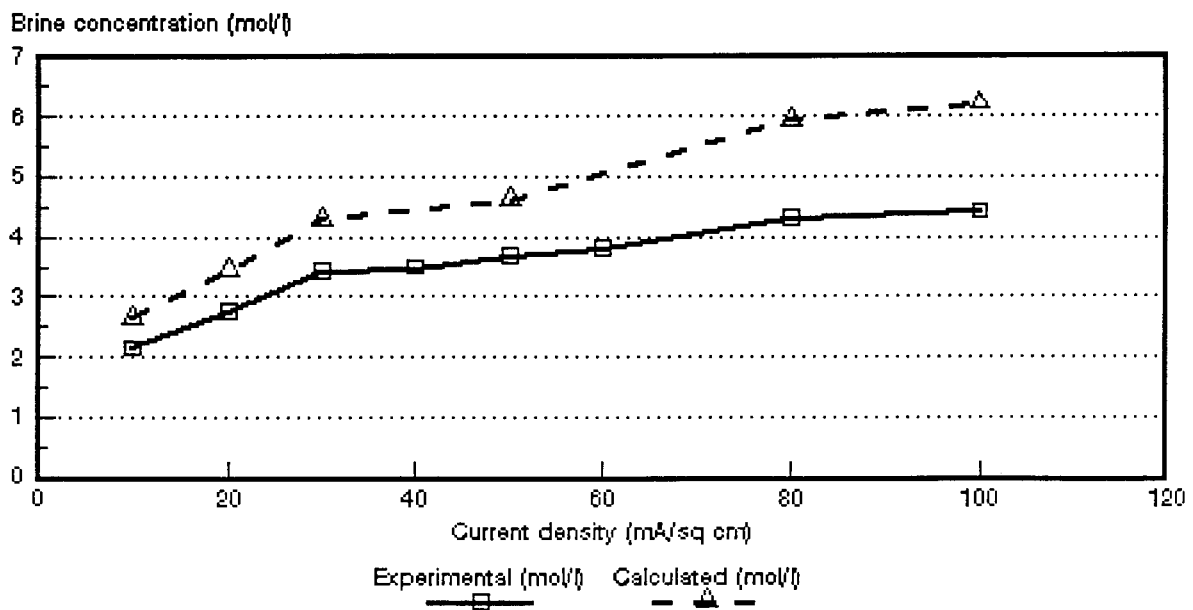


Figure 8.8: Experimental and calculated caustic soda brine concentrations as a function of current density for 0,1 mol/l NaOH feed solution. *Selemion* AMV and CMV membranes.

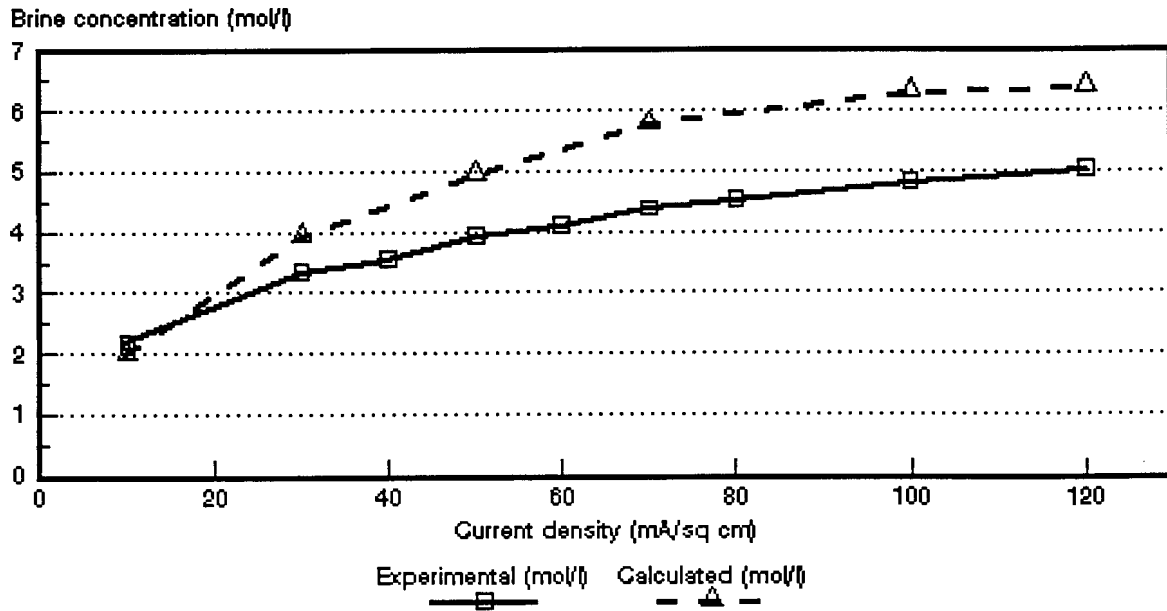


Figure 8.9: Experimental and calculated caustic soda brine concentrations as a function of current density for 0,5 mol/l NaOH feed solution. *Selemion* AMV and CMV membranes.

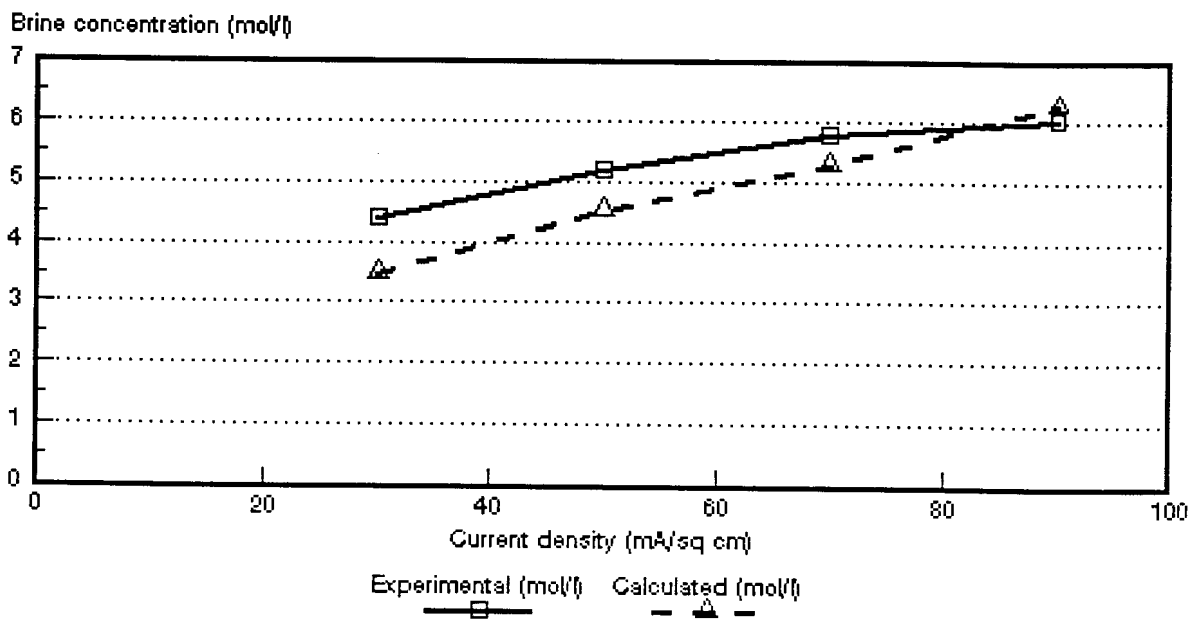


Figure 8.10: Experimental and calculated caustic soda brine concentrations as a function of current density for 1,0 mol/l NaOH feed solution. *Selemion* AMV and CMV membranes.

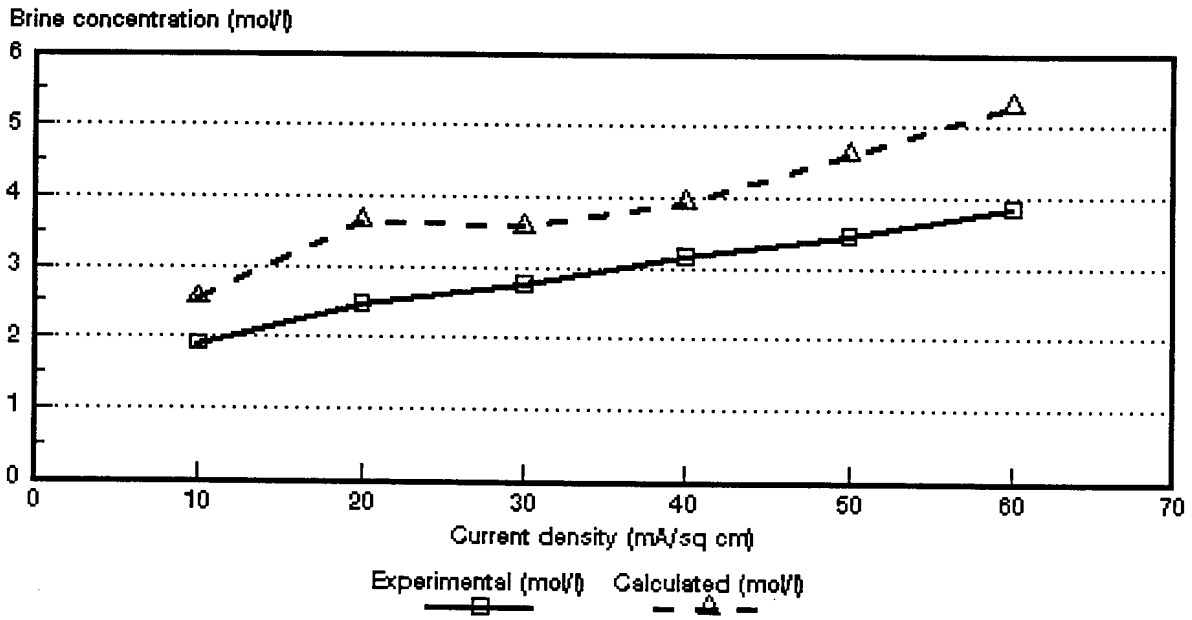


Figure 8.11: Experimental and calculated caustic soda brine concentrations as a function of current density for 0,05 mol/l NaOH feed solution. *Selemion* AMP and CMV membranes.

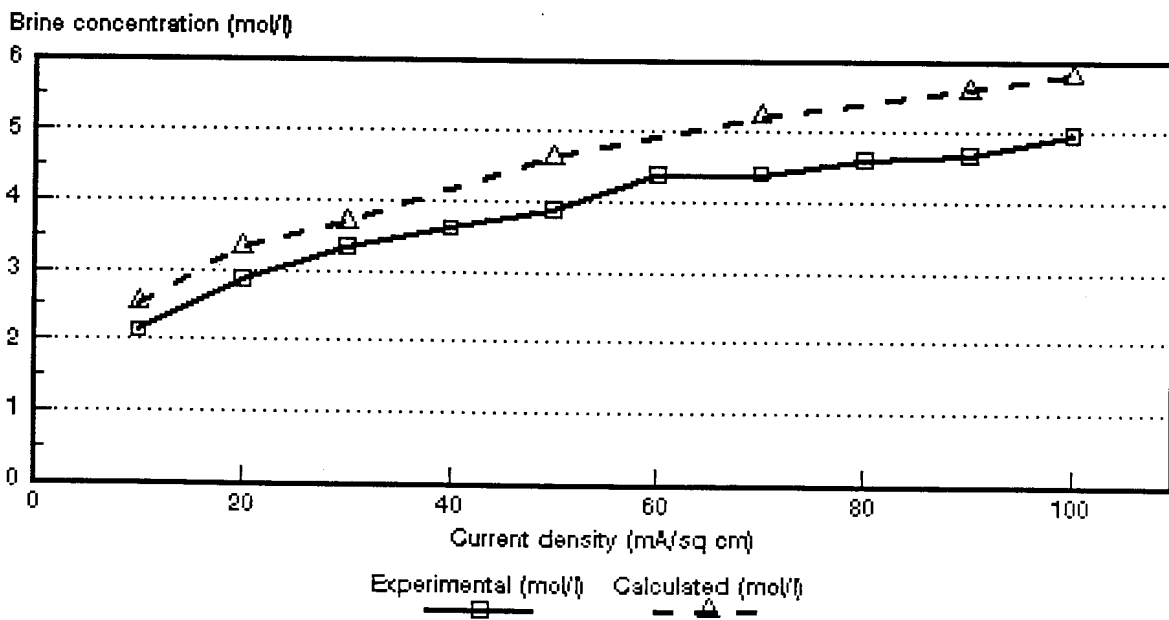


Figure 8.12: Experimental and calculated caustic soda brine concentrations as a function of current density for 0,1 mol/l NaOH feed solution. *Selemion* AMP and CMV membranes.

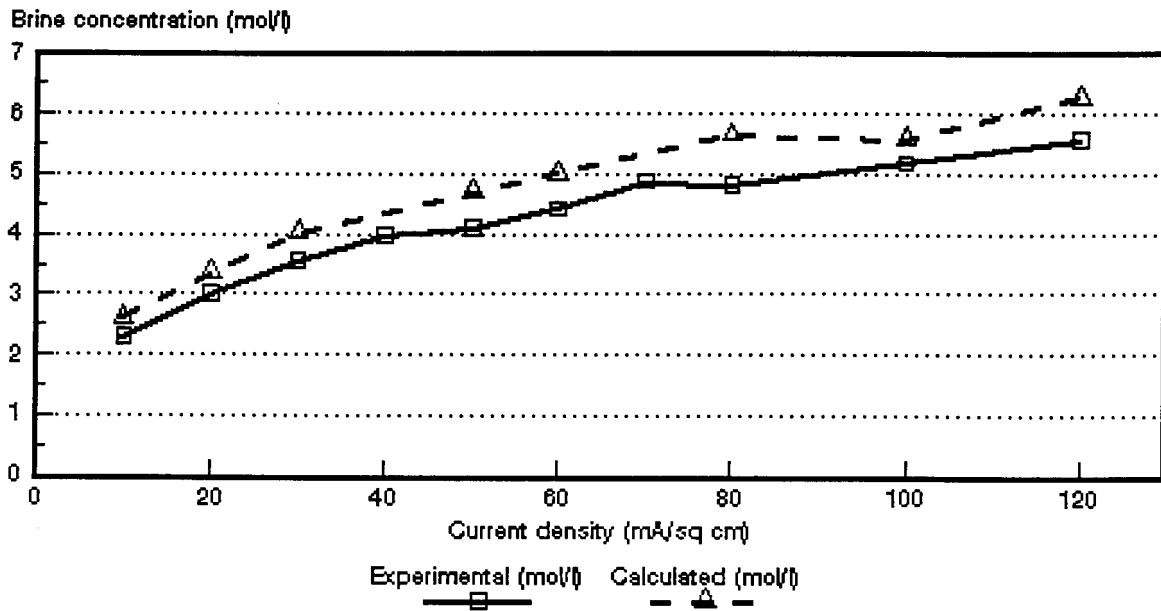


Figure 8.13: Experimental and calculated caustic soda brine concentrations as a function of current density for 0,5 mol/l NaOH feed solution. *Selemion* AMP and CMV membranes.

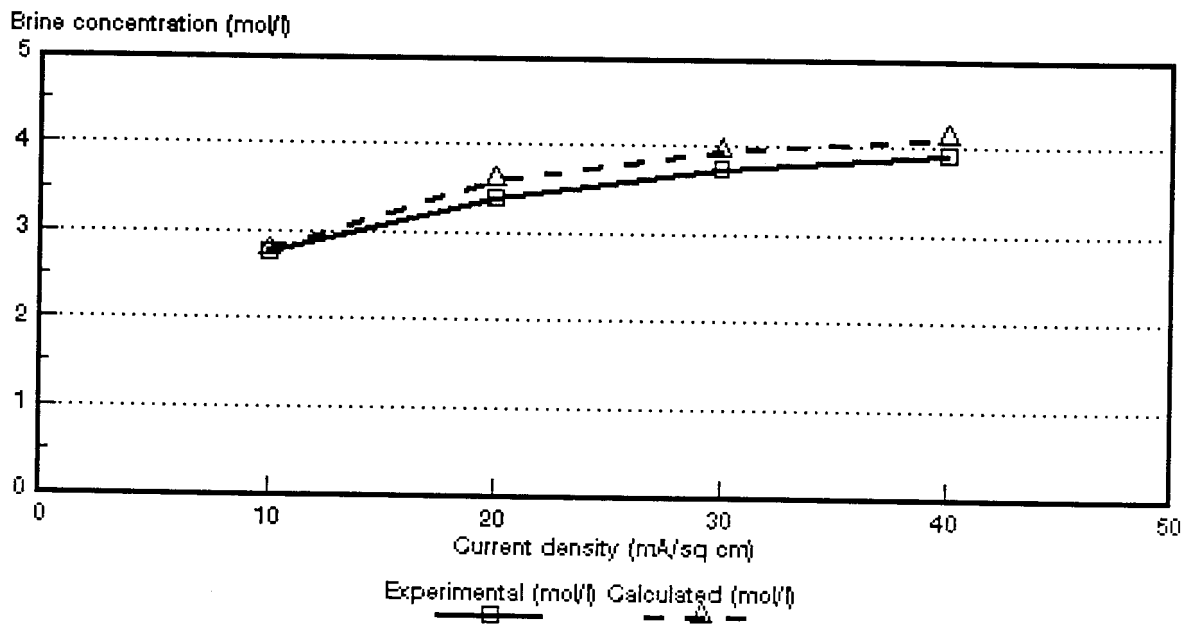


Figure 8.14: Experimental and calculated caustic soda brine concentrations as a function of current density for 0,05 mol/l NaOH feed solution. *Ionac* MA-3475 and MC-3470 membranes.

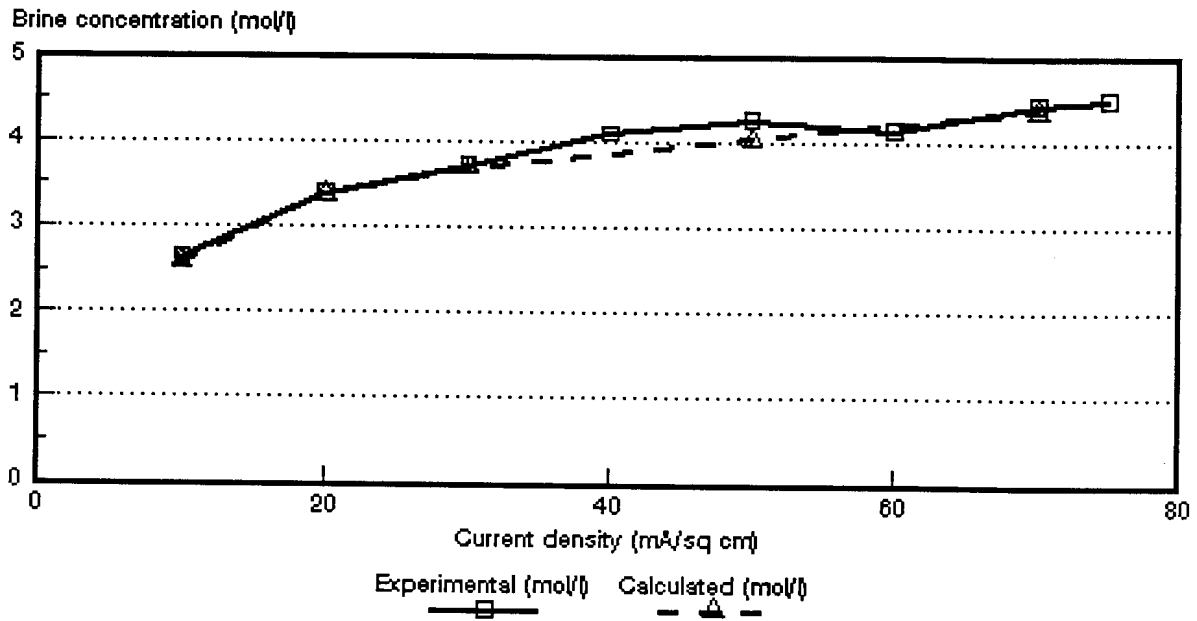


Figure 8.15: Experimental and calculated caustic soda brine concentrations as a function of current density for 0,1 mol/l NaOH feed solution. *Ionac* MA-3475 and MC-3470 membranes.

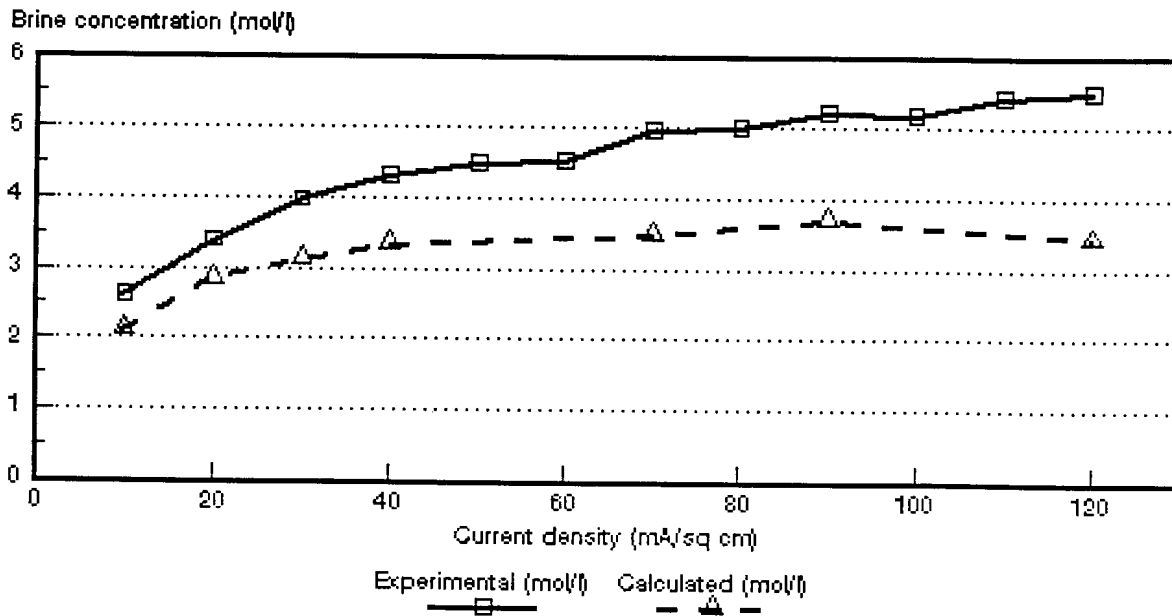


Figure 8.16: Experimental and calculated caustic soda brine concentrations as a function of current density for 0,5 mol/l NaOH feed solution. *Ionac* MA-3475 and MC-3470 membranes.

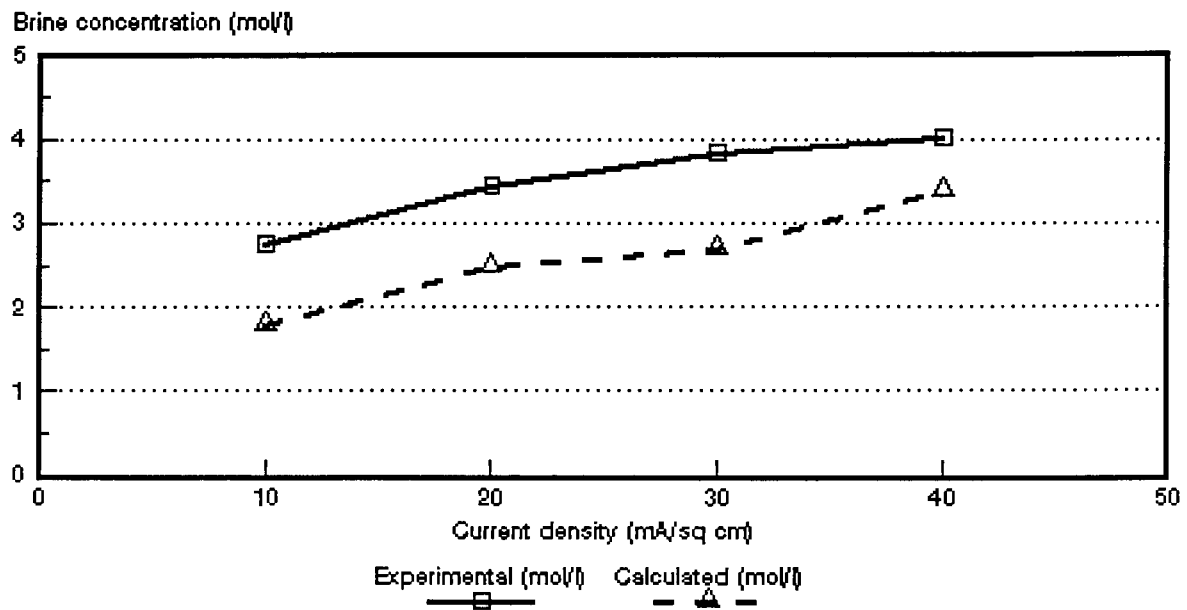


Figure 8.17: Experimental and calculated caustic soda brine concentrations as a function of current density for 1,0 mol/l NaOH feed solution. *Ionac* MA-3475 and MC-3470 membranes.

Table 8.14: Correlation between calculated (c_{bcalo}) and experimentally (c_{bexp}) determined brine concentrations.

Current Density mA/cm ²	c_{bcalo}/c_{bexp}										
	Selemion AMV & CMV Concentration, mol/ℓ				Selemion AMP & CMV Concentration, mol/ℓ			Ionac MA-3475 & MC-3470 Concentration, mol/ℓ			
	0,05	0,1	0,5	1,0	0,05	0,1	0,5	0,05	0,1	0,5	1,0
10	1,36	1,23	0,92		1,33	1,18	1,14	1,01	0,98	0,81	0,65
20	1,42	1,24	1,42		1,47	1,16	1,11	1,06	0,99	0,84	0,73
30	1,44	1,25	1,18	0,80	1,30	1,10	1,13	1,05	0,99	0,79	0,70
40	1,58				1,25			1,06		0,77	0,85
50	1,54	1,25	1,25	0,88	1,34	1,19	1,14		0,95		
60					1,38		1,13				
70			1,32	0,91		1,19			0,98	0,70	
75											
80		1,29					1,17				
90				1,04		1,20				0,71	
100		1,40	1,30			1,17	1,08				
110											
120							1,13				

8.2 Current Efficiency

Current efficiency (ϵ_p) determined during the EOP experiments as a function of current density and caustic soda feed water concentration is shown in Figures 8.18 to 8.20. Current efficiency increases with increasing feed water concentration in the caustic soda feed concentration range from 0,05 to 1,0 mol/l. However, very little difference in current efficiency was experienced in the 0,1 to 0,5 mol/l feed concentration range. Current efficiency was significantly higher at 1,0 mol/l caustic soda feed concentration in the case of the *Selemion* AMV and CMV membranes (Fig. 8.18). This phenomena was not observed in the case of the *Selemion* AMP and CMV (Fig. 8.19) and the *Ionac* membranes (Fig. 8.20).

Current efficiency decreased slightly with increasing current density. This was observed even at the highest caustic soda feed concentration (1,0 mol/l) in the case of the *Selemion* AMV and CMV membranes (Fig. 8.18). Current efficiency, however, appeared to remain reasonably constant in the 0,1 to 0,5 mol/l feed water concentration range for all the membranes investigated.

The apparent transport numbers ($\bar{\Delta}t$, Δt^a and Δt^c) for a concentration difference similar to that obtained in the EOP experiments are shown in Figures 8.21 to 8.31. The current efficiencies (ϵ_p) as determined by the EOP method and shown in Figures 8.18 to 8.20 are also shown in Figures 8.21 to 8.31. The correlation between the apparent transport numbers ($\bar{\Delta}t$, Δt^a , Δt^c) and the current efficiency is shown in Tables 8.15 to 8.17.

The apparent transport numbers ($\bar{\Delta}t$) were significantly higher than the current efficiencies in the case of the *Selemion* AMV and CMV and *Selemion* AMP and CMV membranes at 0,05 mol/l feed concentration (Table 8.15). The apparent transport numbers were from 1,37 to 1,57 times higher than the current efficiency for the *Selemion* AMV and CMV membranes in the 10 to 40 mA/cm² current density range (0,05 mol/l feed). The apparent transport numbers were from 1,30 to 1,48 times higher than current efficiency for the *Selemion* AMP and CMV membranes in the 10 to 60 mA/cm² current density range (0,05 mol/l feed). However, better correlations were obtained in the 0,1 and 0,5 mol/l feed concentration range for both membrane types. The apparent transport numbers were approximately 1,2 times higher than the current efficiency in the 0,1 and 0,5 mol/l feed concentration range for the *Selemion* AMV and CMV membranes (10 to 50 mA/cm²) while the ratio $\bar{\Delta}t/\epsilon_p$ was approximately 0,9 at 1,0

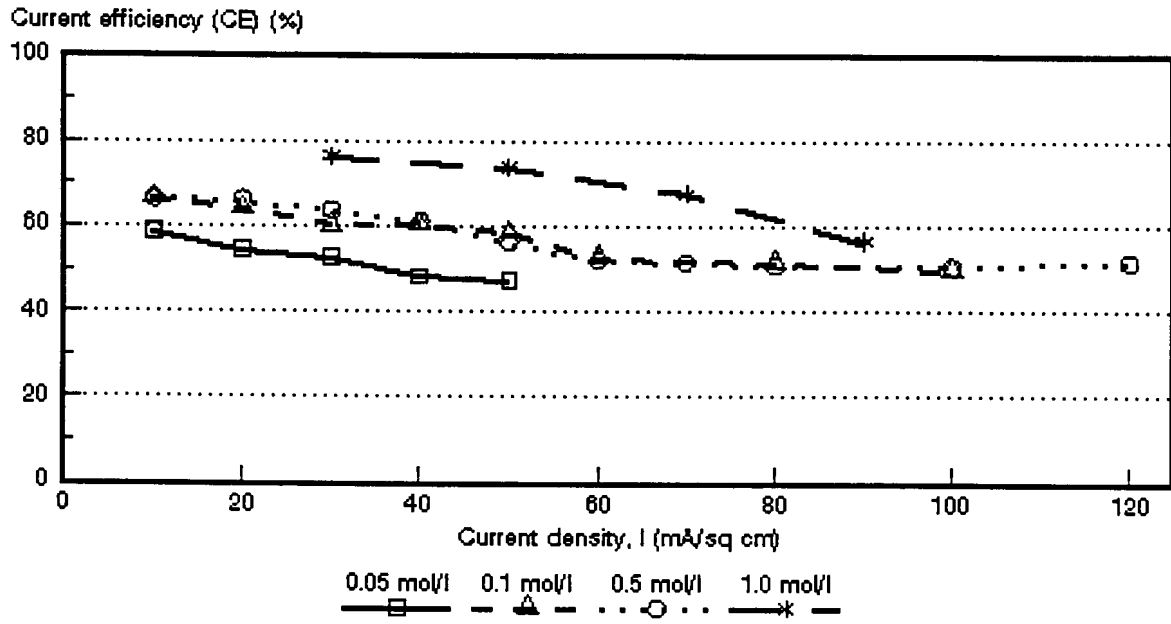


Figure 8.18: Current efficiency (e_p) as a function of current density for 4 different NaOH feed water concentrations. *Selemion AMV* and *CMV* membranes.

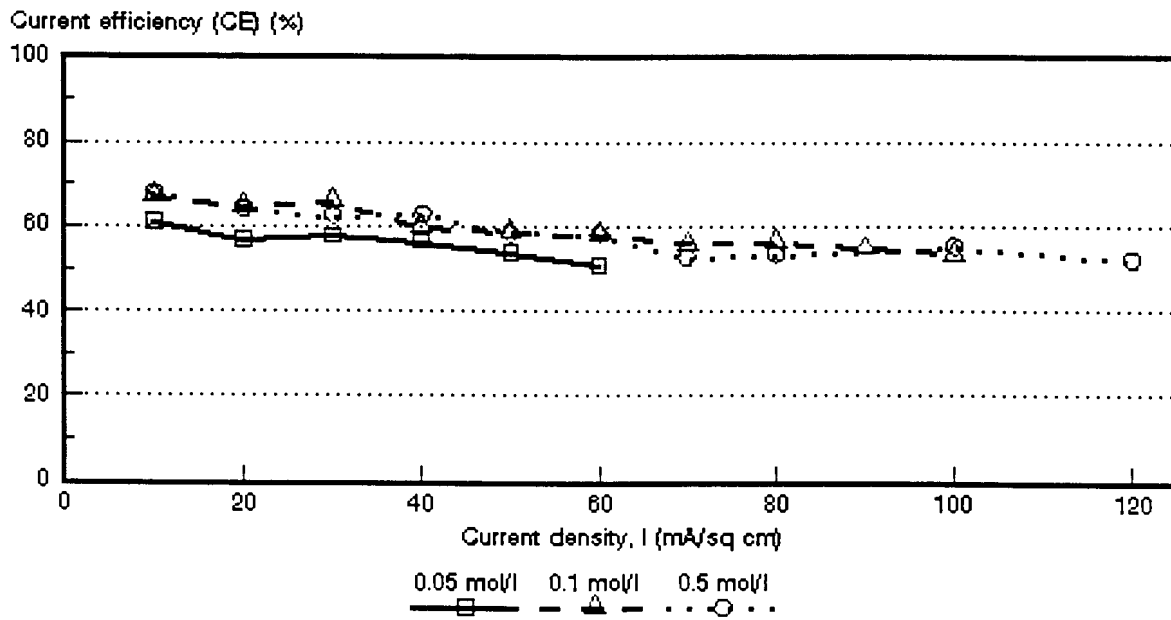


Figure 8.19: Current efficiency (e_p) as a function of current density for 3 different NaOH feed water concentrations. *Selemion AMP* and *CMV* membranes.

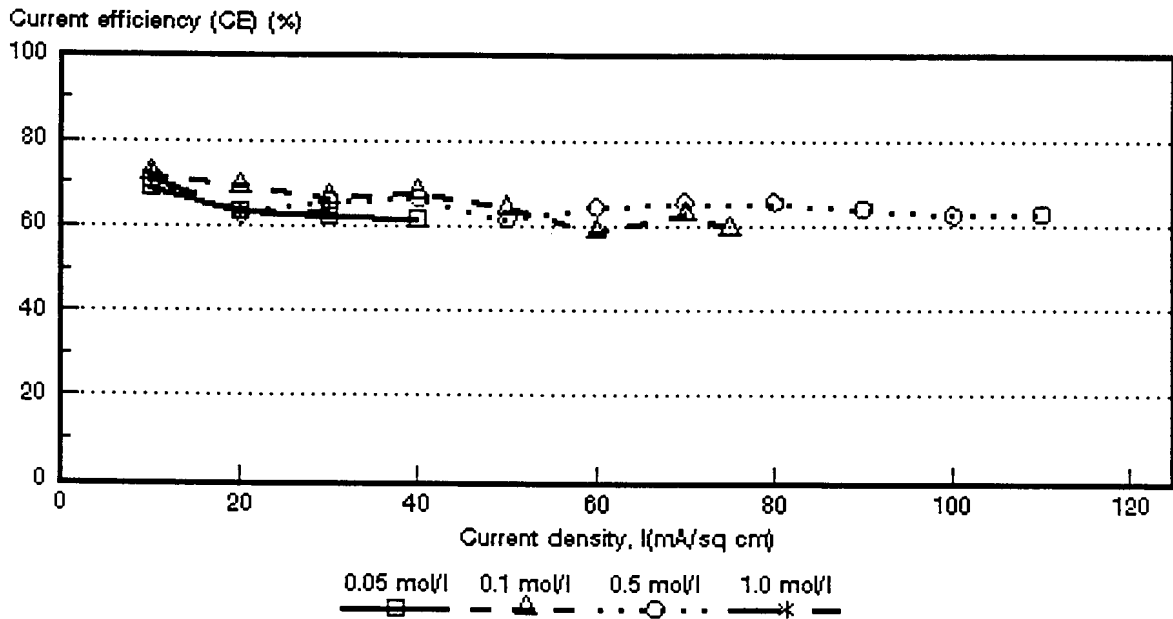


Figure 8.20: Current efficiency (e_p) as a function of current density for 4 different NaOH feed water concentrations. *Ionac MA-3475* and *MC-3470* membranes.

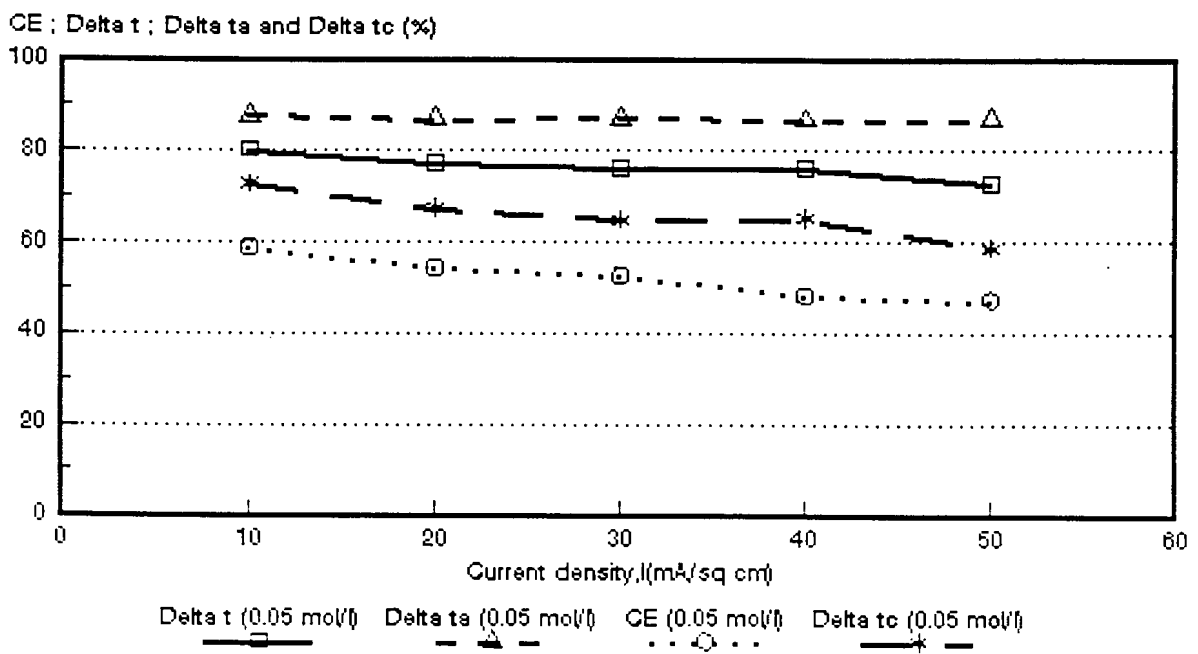


Figure 8.21: Current efficiency ($CE = e_p$) as a function of current density for 0,05 mol/l NaOH feed. *Selemion AMV* and *CMV* membranes. $\Delta t = \bar{\Delta t}$; $\Delta t_a = \Delta t^a$; $\Delta t_c = \Delta t^c$.

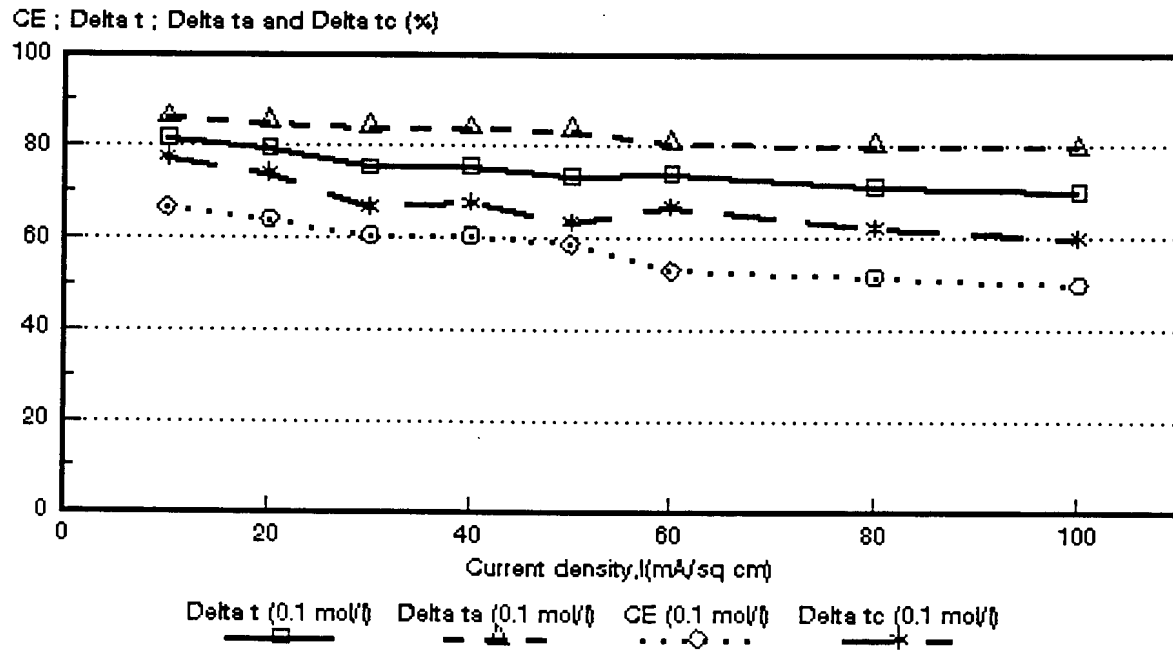


Figure 8.22: Current efficiency ($CE = \epsilon_p$) as a function of current density for 0,1 mol/l NaOH feed. *Selemion* AMV and CMV membranes. $\Delta t = \bar{\Delta}t$; $\Delta t_a = \Delta t^a$; $\Delta t_c = \Delta t^c$.

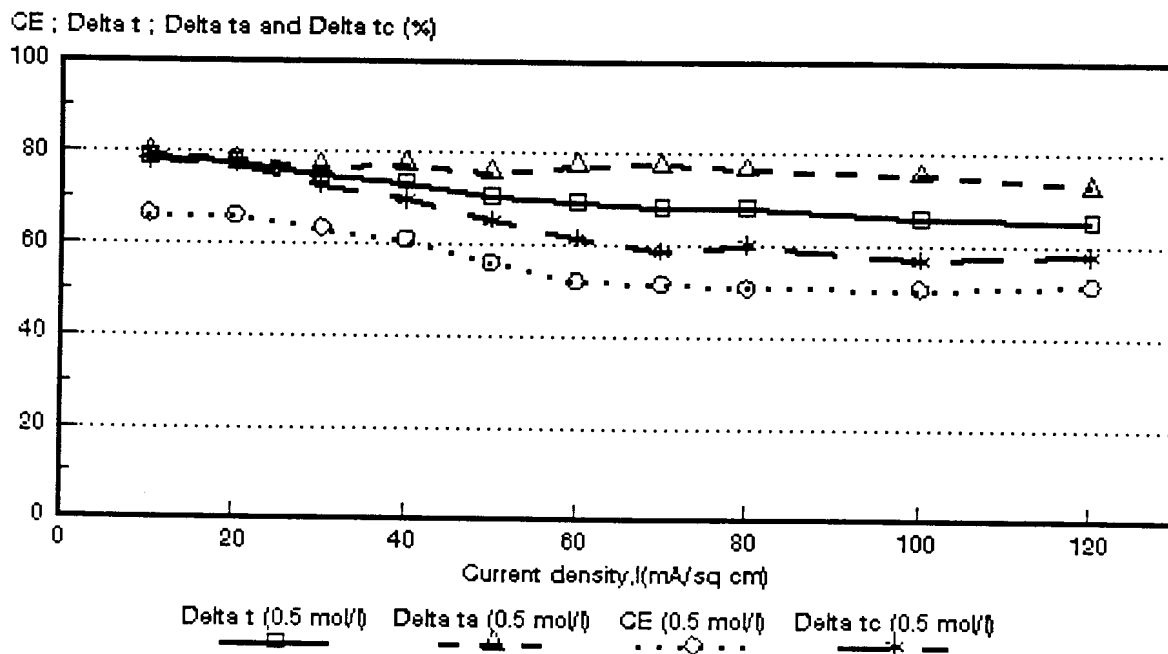


Figure 8.23: Current efficiency ($CE = \epsilon_p$) as a function of current density for 0,5 mol/l NaOH feed. *Selemion* AMV and CMV membranes. $\Delta t = \bar{\Delta}t$; $\Delta t_a = \Delta t^a$; $\Delta t_c = \Delta t^c$.

CE ; Delta t ; Delta ta and Delta tc (%)

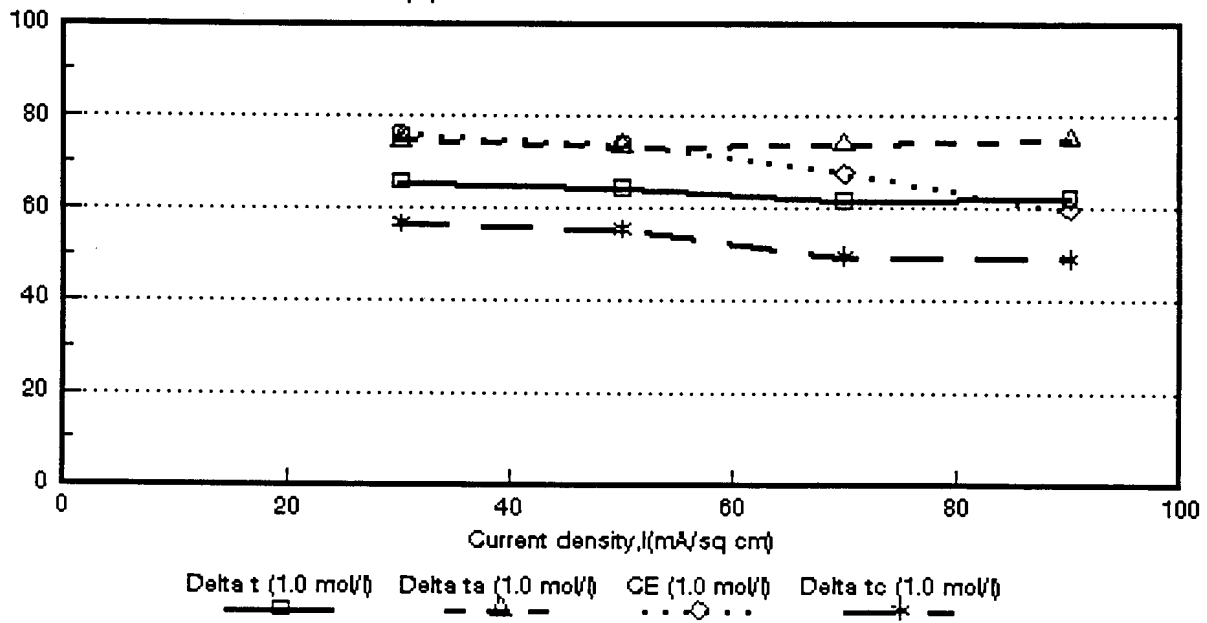


Figure 8.24: Current efficiency ($CE = e_p$) as a function of current density for 1,0 mol/l NaOH feed. *Selemion AMV* and *CMV* membranes. $\Delta t = \bar{\Delta}t$; $\Delta t_a = \Delta t^a$; $\Delta t_c = \Delta t^c$.

CE ; Delta t ; Delta ta and Delta tc (%)

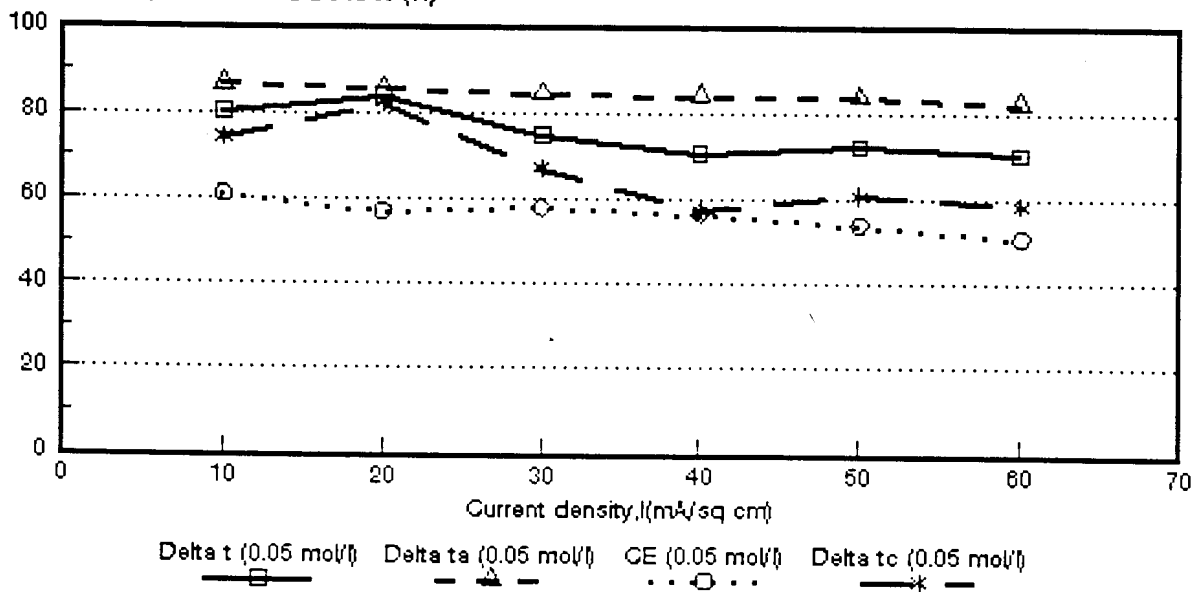


Figure 8.25: Current efficiency ($CE = e_p$) as a function of current density for 0,05 mol/l NaOH feed. *Selemion AMP* and *CMV* membranes. $\Delta t = \bar{\Delta}t$; $\Delta t_a = \Delta t^a$; $\Delta t_c = \Delta t^c$.

CE ; Delta t ; Delta ta and Delta tc (%)

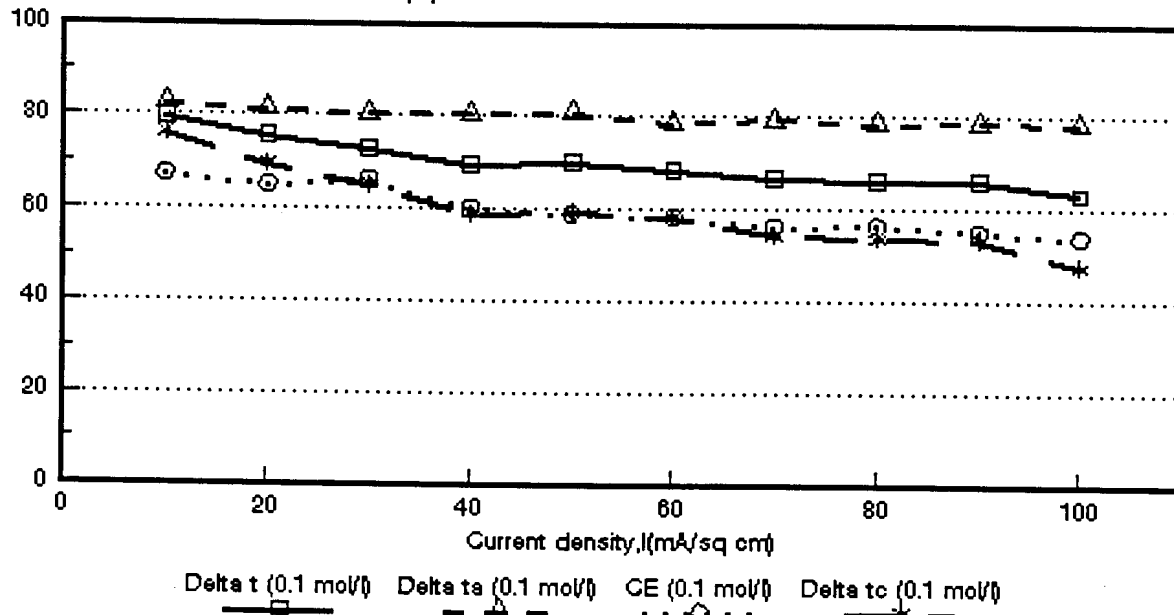


Figure 8.26: Current efficiency ($CE = \epsilon_p$) as a function of current density for 0,1 mol/l NaOH feed. *Selemion* AMP and CMV membranes. $\Delta t = \bar{\Delta}t$; $\Delta t_c = \Delta t^c$; $\Delta t_a = \Delta t^a$.

CE ; Delta t ; Delta ta and Delta tc (%)

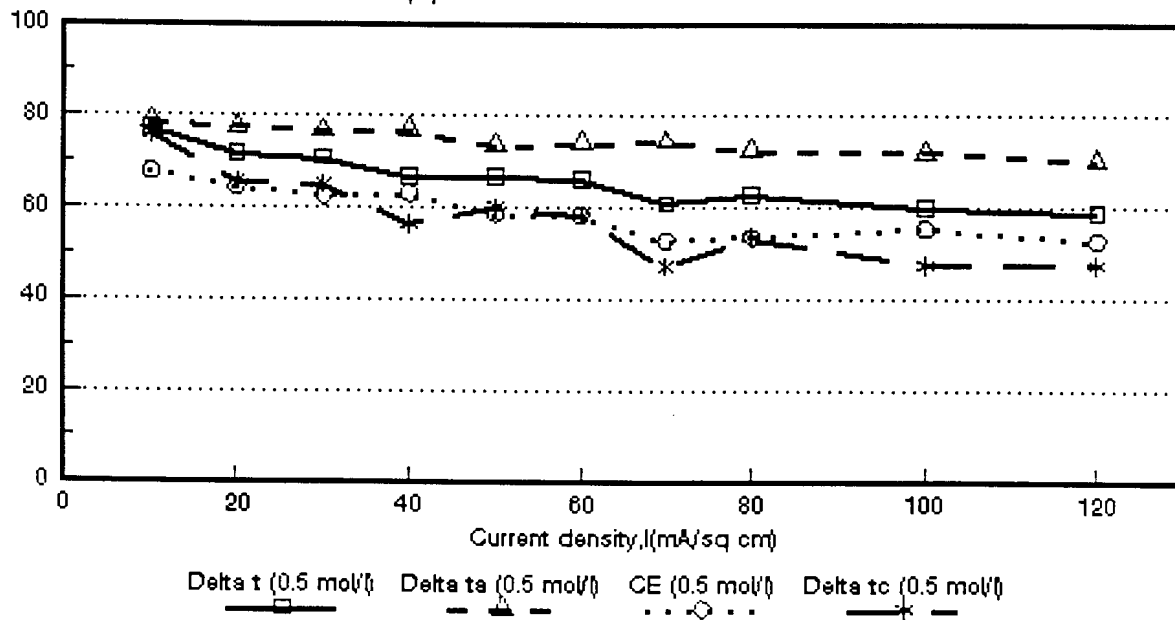


Figure 8.27: Current efficiency ($CE = \epsilon_p$) as a function of current density for 0,5 mol/l NaOH feed. *Selemion* AMP and CMV membranes. $\Delta t = \bar{\Delta}t$; $\Delta t_c = \Delta t^c$; $\Delta t_a = \Delta t^a$.

CE ; Delta t ; Delta ta and Delta tc (%)

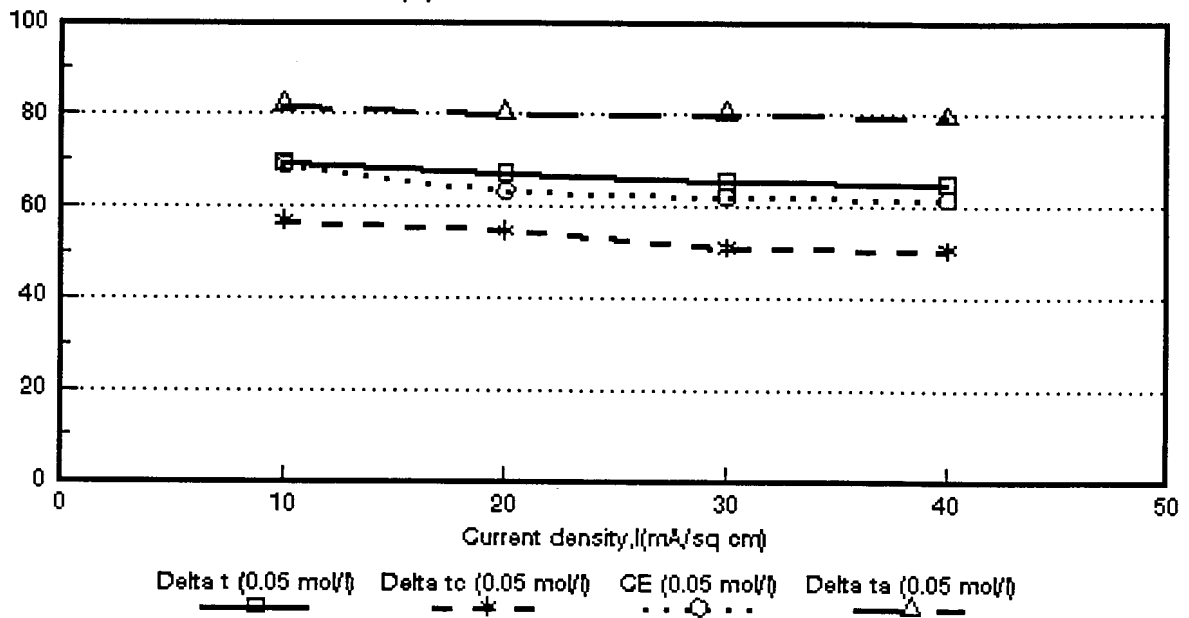


Figure 8.28: Current efficiency ($CE = e_p$) as a function of current density for 0,05 mol/l NaOH feed. *Ionac* MA-3470 and MC-3475 membranes. $\Delta t = \bar{\Delta}t$; $\Delta t_c = \Delta t^c$; $\Delta t_a = \Delta t^a$.

CE ; Delta t ; Delta ta and Delta tc (%)

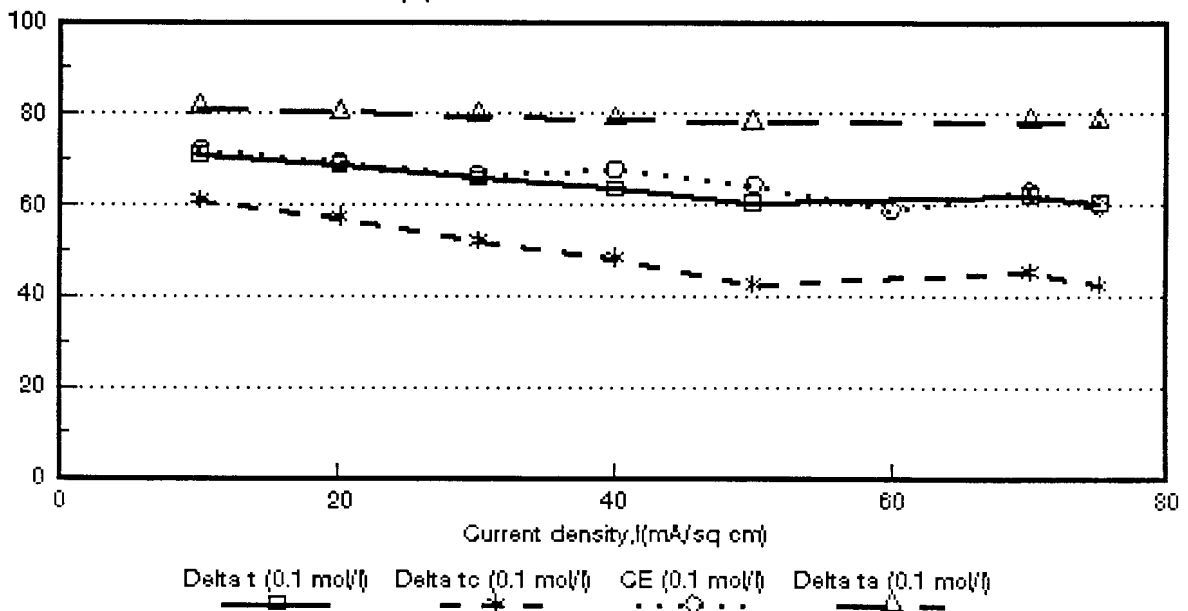


Figure 8.29: Current efficiency ($CE = e_p$) as a function of current density for 0,1 mol/l NaOH feed. *Ionac* MA-3470 and MC-3475 membranes. $\Delta t = \bar{\Delta}t$; $\Delta t_c = \Delta t^c$; $\Delta t_a = \Delta t^a$.

CE ; Delta t ; Delta ta and Delta tc (%)

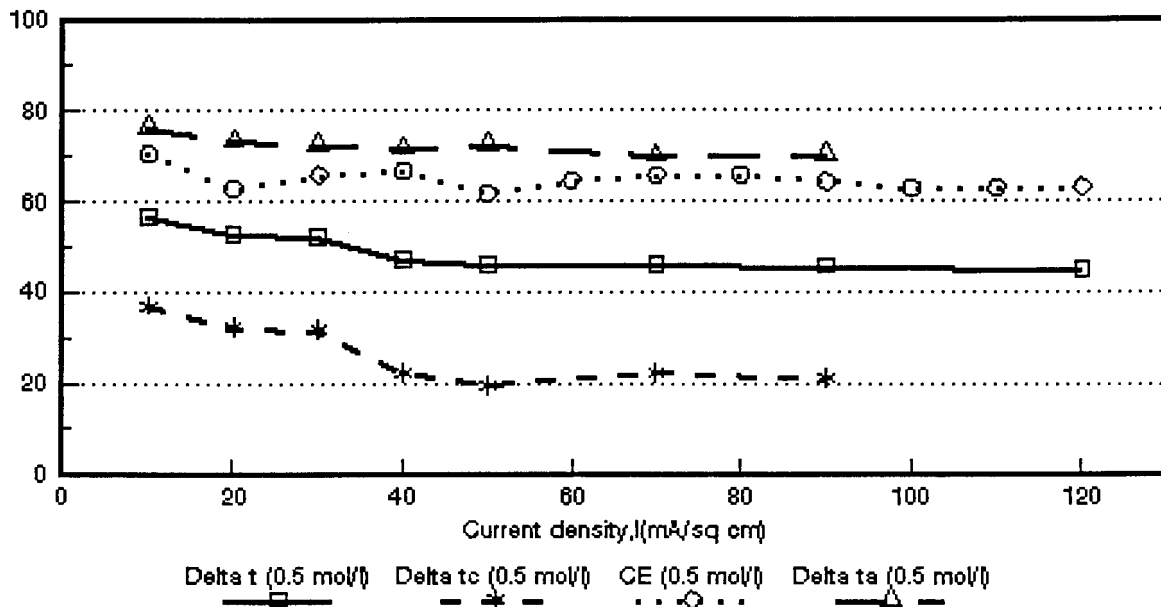


Figure 8.30 Current efficiency ($CE = \epsilon_p$) as a function of current density for 0,5 mol/l NaOH feed. *Ionac* MA-3470 and MC-3475 membranes. $\Delta t = \bar{\Delta}t$; $\Delta t_c = \Delta t^c$; $\Delta t_a = \Delta t^a$.

CE ; Delta t ; Delta ta and Delta tc (%)

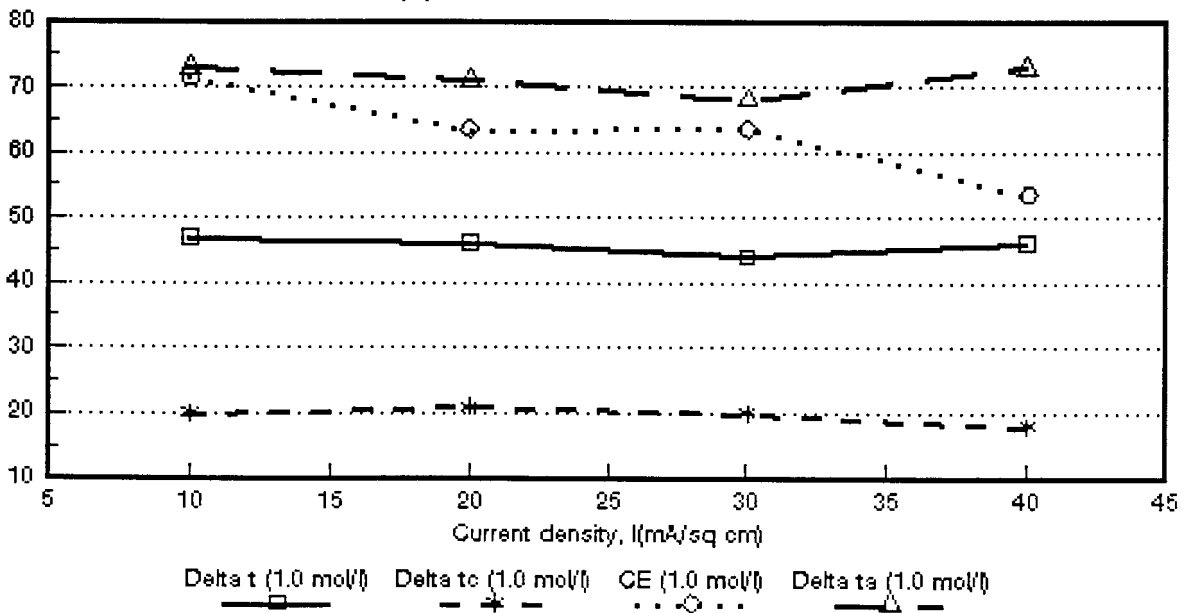


Figure 8.31 Current efficiency ($CE = \epsilon_p$) as a function of current density for 0,1 mol/l NaOH feed. *Ionac* MA-3470 and MC-3475 membranes. $\Delta t = \bar{\Delta}t$; $\Delta t_c = \Delta t^c$; $\Delta t_a = \Delta t^a$.

Table 8.15: Correlation between apparent transport number of a membrane pair ($\bar{\Delta}t$) and current efficiency (e_p).

Current Density mA/cm ²	$\bar{\Delta}t/e_p$										
	Selemion AMV & CMV Concentration, mol/l				Selemion AMP & CMV Concentration, mol/l			Ionac MA-3475 & MC-3470 Concentration, mol/l			
	0,05	0,1	0,5	1,0	0,05	0,1	0,5	0,05	0,1	0,5	1,0
10	1,37	1,23	1,19		1,31	1,17	1,14	1,00	0,98	0,81	0,65
20	1,42	1,23	1,16		1,47	1,15	1,10	1,06	0,98	0,84	0,72
30	1,45	1,24	1,16	0,85	1,30	1,09	1,12	1,06	0,97	0,79	0,69
40	1,57	1,24	1,19		1,48	1,15	1,05	1,06	0,93	0,71	0,84
50		1,24	1,24	0,87	1,33	1,17	1,13		0,93	0,74	
60		1,38	1,32		1,37	1,17	1,13				
70			1,32	0,90		1,17	1,14		0,98	0,70	
75									1,01		
80		1,37	1,34			1,17	1,16				
90				1,04		1,20				0,70	
100		1,38	1,30			1,17	1,06				
110											
120			1,26				1,10				

Table 8.16: Correlation between apparent transport number of the cation membrane (Δt°) and current efficiency (ϵ_p).

Current Density mA/cm ²	$\Delta t^\circ/\epsilon_p$										
	Selemion AMV & CMV Concentration, mol/l				Selemion AMP & CMV Concentration, mol/l			Ionac MA-3475 & MC-3470 Concentration, mol/l			
	0,05	0,1	0,5	1,0	0,05	0,1	0,5	0,05	0,1	0,5	1,0
10	1,24	1,17	1,17		1,21	1,13	1,12	0,83	0,84	0,52	0,29
20	1,25	1,16	1,16		1,43	1,06	1,03	0,87	0,82	0,51	0,33
30	1,23	1,11	1,15	0,73	1,16	0,98	1,04	0,82	0,78	0,47	0,31
40	1,34	1,12	1,13		1,01	0,98	0,89	0,81	0,70	0,33	0,34
50	1,24	1,09	1,16	0,75	1,11	1,00	1,02		0,65	0,31	
60		1,26	1,17		1,14	0,99	0,99				
70			1,12	0,72		0,96	0,89		0,71	0,33	
75									0,70		
80		1,19	1,18			0,94	0,99				
90				0,82		0,96				0,33	
100		1,20	1,12			0,87	0,85				
110											
120			1,13				0,89				

Table 8.17: Correlation between apparent transport number of the anion membrane (Δt^*) and current efficiency (e_p).

Current Density mA/cm ²	$\Delta t^*/e_p$										
	Selemion AMV & CMV Concentration, mol/l				Selemion AMP & CMV Concentration, mol/l			Ionac MA-3475 & MC-3470 Concentration, mol/l			
	0,05	0,1	0,5	1,0	0,05	0,1	0,5	0,05	0,1	0,5	1,0
10	1,49	1,29	1,19		1,41	1,22	1,17	1,19	1,12	1,08	1,02
20	1,60	1,32	1,18		1,49	1,24	1,20	1,26	1,15	1,16	1,12
30	1,65	1,39	1,21	0,97	1,45	1,21	1,21	1,28	1,18	1,09	1,07
40	1,80	1,39	1,26		1,48	1,33	1,21	1,28	1,15	1,08	1,36
50	1,84	1,43	1,35	0,99	1,53	1,36	1,25		1,21	1,17	
60		1,53	1,48		1,61	1,34	1,27				
70			1,49	1,08		1,41	1,40		1,23	1,06	
75									1,31		
80		1,55	1,49			1,38	1,34				
90				1,26		1,42				1,09	
100		1,58	1,48			1,45	1,30				
110											
120			1,42				1,33				

mol/l feed (30 to 50 mA/cm²). The ratio $\bar{\Delta}t/\epsilon_p$ for the *Selemion* AMP and CMV membranes varied between 1,1 and 1,2 (0,1 mol/l feed, 10 to 70 mA/cm²) and was 1,1 at 0,5 mol/l feed concentration (10 to 70 mA/cm²). Therefore, satisfactory correlations were obtained between the apparent transport numbers and current efficiency in the 0,1 to 0,5 mol/l feed concentration ranges.

Very satisfactory correlations were obtained between $\bar{\Delta}t/\epsilon_p$ in the 0,05 to 0,1 mol/l feed concentration range for the *Ionac* membranes (Fig's 8,28 and 8,29). The ratio $\bar{\Delta}t/\epsilon_p$ varied between 1 and 1,1 (10 to 40 mA/cm², 0,05 mol/l) and between 0,9 and 1,0 (10 to 70 mA/cm², 0,1 mol/l feed). The correlation, however, at 0,5 and 1,0 mol/l feed concentration was not satisfactory. The ratio $\bar{\Delta}t/\epsilon_p$ varied between 0,7 and 0,8 at 0,5 mol/l feed concentration and between 0,7 and 0,8 at 1,0 mol/l feed concentration. Therefore, it should be possible to predict membrane performance for caustic soda concentration/desalination with ED with an accuracy of approximately 20% from the apparent transport numbers of the membrane pair. However, the accuracy of the predictions will depend on the feed concentration used.

Satisfactory correlations were obtained between the apparent transport numbers of the cation membrane (Δt^c) and current efficiency in the case of the *Selemion* and *Ionac* membranes (Table 8.16). The ratio between $\Delta t^c/\epsilon_p$ varied between 1,1 and 1,2 in the 0,1 to 0,5 mol/l feed concentration range (10 to 120 mA/cm²) for the *Selemion* AMV and CMV membranes (Table 8.16). The same correlation was approximately 1,2 at 0,5 mol/l feed concentration (10 to 50 mA/cm²) and varied between 0,7 and 0,8 at 1,0 mol/l feed concentration (30 to 90 mA/cm²). The ratio between $\Delta t^c/\epsilon_p$ varied between 1,1 and 1,2 (0,05 mol/l feed; 10 to 60 mA/cm²); 1,0 and 1,1 (0,1 mol/l feed; 10 to 90 mA/cm²) and between 0,9 and 1,1 (0,5 mol/l feed; 10 to 80 mA/cm²) for the *Selemion* AMP and CMV membranes. The ratio $\Delta t^c/\epsilon_p$ was approximately 0,8 (0,5 mol/l feed; 10 to 40 mA/cm²) and varied between 0,7 and 0,8 (0,1 mol/l feed; 10 to 70 mA/cm²) in the case of the *Ionac* membranes. However, a much poorer correlation was obtained at 0,5 and 1,0 mol/l feed concentration as a result of the low selectivity of the cation membrane for sodium ions as a result of the high mobility of the hydroxyl ion⁽³⁰⁾ (Table 8.16). Therefore, it appears that membrane performance for caustic soda concentration/desalination can also be predicted from the apparent transport number of the cation membrane with an accuracy of approximately 20%.

Satisfactory correlations were obtained between the apparent transport number of the anion membrane (Δt^a) and current efficiency in the case of the *Selemion* AMV and CMV

- (1,0 mol/l feed) and *Ionac* membranes (1,0 mol/l feed) (Table 8.17). The ratio $\Delta t^a/\epsilon_p$ varied between approximately 1 and 1,1 in the case of the *Selemion* AMV and CMV membranes (30 to 70 mA/cm²). The ratio $\Delta t^a/\epsilon_p$ varied between 1 and 1,1 in the case of the *Ionac* membranes (10 to 30 mA/cm²). Poorer correlations of $\Delta t^a/\epsilon_p$ were obtained at the other feed concentrations (Table 8.17). Consequently, it should be possible to predict membrane performance for caustic soda concentration/desalination applications with an accuracy of approximately 10% from the apparent transport number of the anion membrane at high (1,0 mol/l) feed concentration.

8.3 Water Flow

Water flow (J) through the membranes as a function of current density and feed water concentration is shown in Figures 8.32 to 8.34. Water flow (J) through the membranes relative to the flow at $J_{0,5 \text{ mol/l}}$ is shown in Table 8.18. Water flow through the membranes increases as a function of current density. Volume flow through the *Selemion* AMV and CMV membranes increased in the 0,05 to 0,1 mol/l feed concentration range (Table 8.18). However, volume flow decreased slightly in the 0,1 to 0,5 mol/l feed concentration range at higher current densities and volume flow remained approximately constant at 1,0 mol/l feed concentration. Current efficiency increased significantly in the 0,05 to 0,1 mol/l feed concentration range (Fig. 8.18) as a result of the increased water flow. Current efficiency, however, was significantly higher at 1,0 mol/l feed concentration (Fig. 8.18) than at 0,01 and 0,5 mol/l feed, despite a slightly lower volume flow.

Volume flow decreased in the case of the *Selemion* AMP and CMV membranes in the feed concentration range from 0,05 to 0,5 mol/l (Table 8.18). Current efficiencies, however, were approximately the same especially at the two higher feed concentrations (Fig. 8.19).

Volume flow was slightly higher at 0,1 mol/l feed concentration in the case of the *Ionac* membranes in the beginning of the run. It is interesting to note that current efficiency has also been slightly higher at this feed concentration (Fig. 8.20). However, current efficiency was approximately the same in the feed concentration range from 0,05 to 1,0 mol/l. Nevertheless, it also appears with caustic soda solutions as has been the case with sodium chloride solutions that increasing water flow can cause an increase in current efficiency.

Water flow (J) through the membranes as a function of effective current density, i_{eff} , and feed concentration is shown in Figures 8.35 to 8.37. Straight lines were obtained at higher values of i_{eff} . The slope of these lines corresponds to the combined electro-osmotic coefficient (2β) of a membrane pair. The electro-osmotic coefficients as a function of caustic soda feed water concentration is shown in Figures 8.38 to 8.40. The electro-osmotic coefficients decreased sharply with increasing feed concentration in the case of the *Selemion* AMV and CMV membranes (Figs. 8.38). It is interesting to note that the electro-osmotic coefficients have decreased over the entire feed concentration range from 0,05 to 1,0 mol/l. A similar effect was observed with the *Selemion* AMP

and CMV membranes but the decrease in the electro-osmotic coefficients were far less (Fig. 8.39). These membranes, therefore, deswell less than the *Selemion* AMV and CMV membranes with increasing feed concentration. The *Ionac* membranes also showed less deswelling than the *Selemion* AMV and CMV membranes (Fig. 8.40).

The effect of the electro-osmotic coefficient on the maximum caustic soda brine concentration, c_b^{\max} , is shown in Table 8.19. Maximum caustic soda brine concentration increases with decreasing electro-osmotic coefficient. The electro-osmotic coefficient of the *Selemion* AMP and CMV membranes were lower than that of the *Selemion* AMV and CMV and *Ionac* membranes. The electro-osmotic coefficient of the *Selemion* AMP and CMV membranes were determined at 0,155 ℓ /Faraday at 0,1 mol/ ℓ feed concentration. The coefficients for the *Selemion* AMV and CMV and *Ionac* membranes at the same feed concentration were 0,179 and 0,193 ℓ /Faraday, respectively. Therefore, higher caustic soda brine concentrations could be obtained with the *Selemion* AMP and CMV membranes.

Approximately 8 to 9 mol H₂O/Faraday passed through the *Selemion* AMP and CMV membranes in the feed concentration range between 0,1 and 0,5 mol/ ℓ (Table 8.19). Approximately 8 to 10 and 10 to 11 mol H₂O/Faraday passed through the membranes in the case of the *Selemion* AMV and CMV and *Ionac* membranes, respectively (0,1 to 0,5 mol/ ℓ feed).

The osmotic flow (J_{osm}) relative to the total flow (J) through the membranes as a function of current density is shown in Table 8.20. The osmotic water flow through the membranes decreases with increasing current density. Osmotic water flow represented 45,9; 46,9 and 26,5% of the total flow through the membranes at a current density of 30 mA/cm² in the case of the *Selemion* AMV and CMV; *Selemion* AMP and CMV and *Ionac* membranes, respectively. Therefore, osmosis makes a significant contribution to water flow through the membranes at relative low current density. The osmotic contribution to total flow through the membranes (*Selemion* AMV and CMV and *Selemion* AMP and CMV) at a current density of 100 mA/cm² (0,1 mol/ ℓ feed) was 21,4 and 25,7%, respectively. The osmotic contribution to the total flow in the case of the *Ionac* membranes at a current density of 70 mA/cm² (0,1 mol/ ℓ feed) was 14,2%. Therefore, the contribution of osmotic water flow to total water flow through the membranes is much lower at high current density.

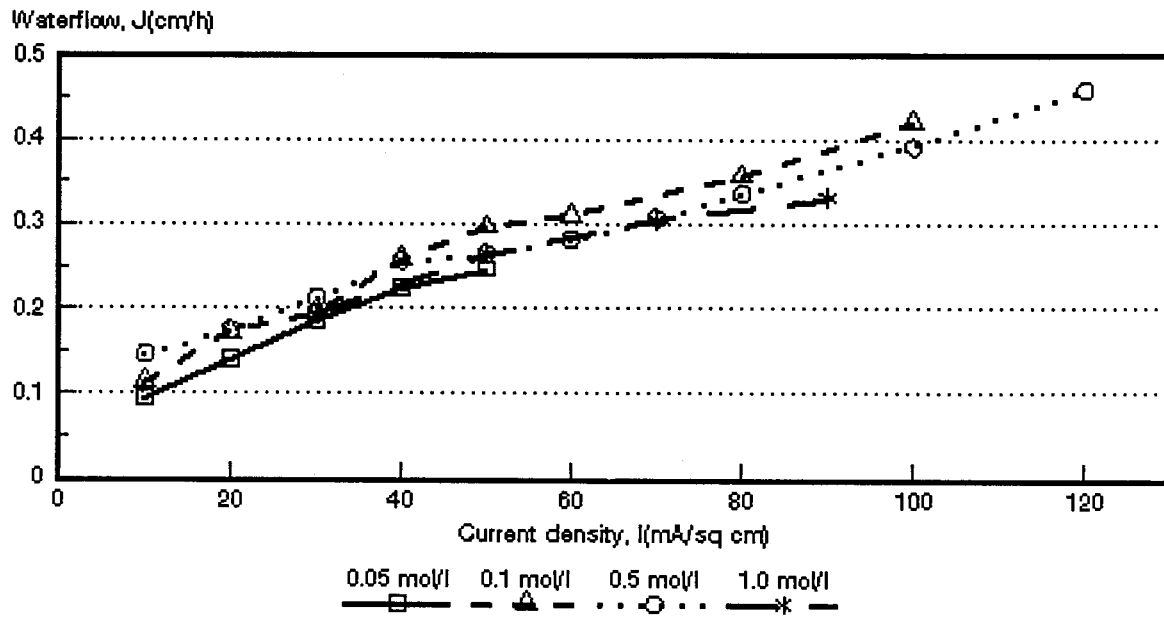


Figure 8.32 Water flow through the membranes as a function of current density and feed water concentration. *Selemion* AMV and CMV membranes.

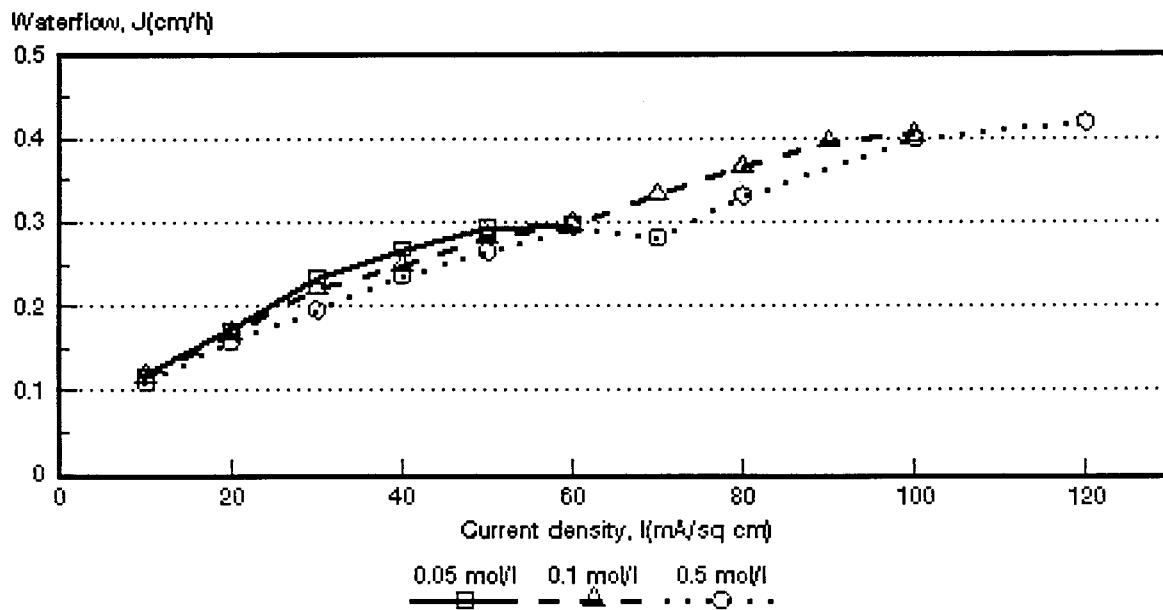


Figure 8.33: Water flow through the membranes as a function of current density and feed water concentration. *Selemion* AMP and CMV membranes.

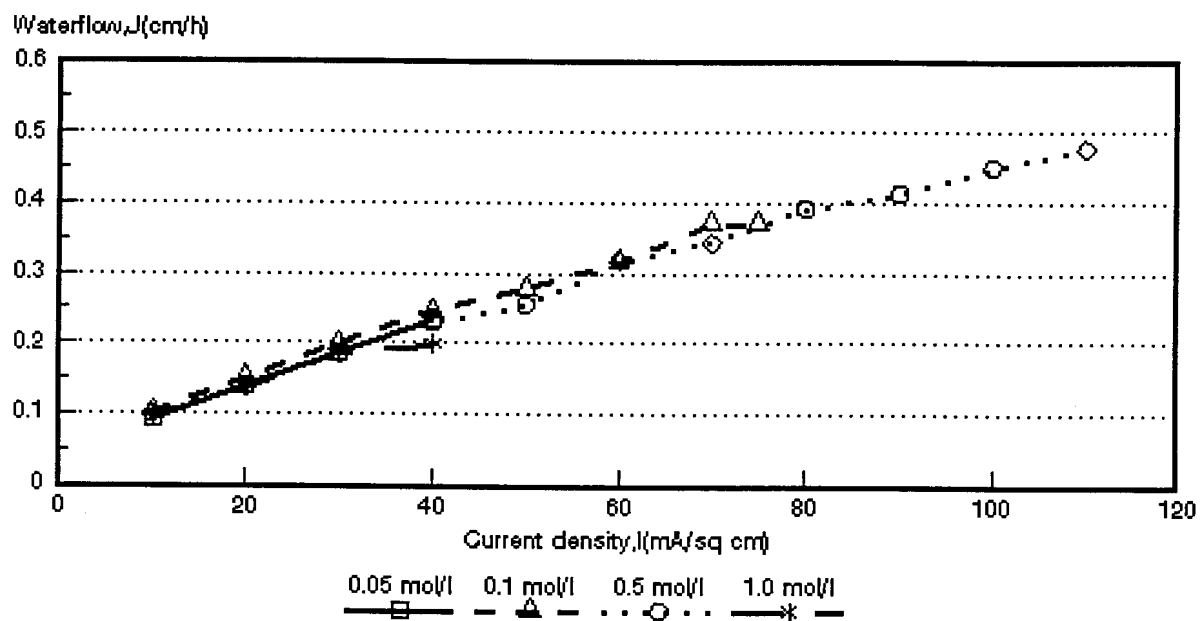


Figure 8.34: Water flow through the membranes as a function of current density and feed water concentration. *Ionac* MA-3475 and MC-3470 membranes.

Table 8.18: Water flow (J) through the membranes relative to the flow at $J_{0,5 \text{ mol/l}}$

Current Density mA/cm ²	$J/J_{0,5 \text{ mol/l}}$										
	Selemion AMV & CMV Concentration, mol/l				Selemion AMP & CMV Concentration, mol/l			Ionac MA-3475 & MC-3470 Concentration, mol/l			
	0,05	0,1	0,5	1,0	0,05	0,1	0,5	0,05	0,1	0,5	1,0
10	0,65	0,79	1,0		1,07	1,06	1,0	0,93	1,04	1,0	0,98
20	0,81	0,98	1,0		1,08	1,06	1,0	1,01	1,10	1,0	1,00
30	0,87	0,92	1,0	0,92	1,20	1,13	1,0	1,00	1,08	1,0	1,00
40	0,88	1,01	1,0		1,14	1,05	1,0	1,02	1,08	1,0	0,86
50	0,93	1,12	1,0	1,0	1,11	1,06	1,0		1,00	1,0	
60		1,10	1,0		1,01	1,01	1,0		1,08	1,0	
70		1,06	1,0	0,99		1,18	1,0				
75		1,07	1,0				1,0				
80						1,11	1,0				
90							1,0				
100						1,01	1,0				
110											
120											

$i = 0,05; 0,1 \text{ and } 1,0 \text{ mol/l}$

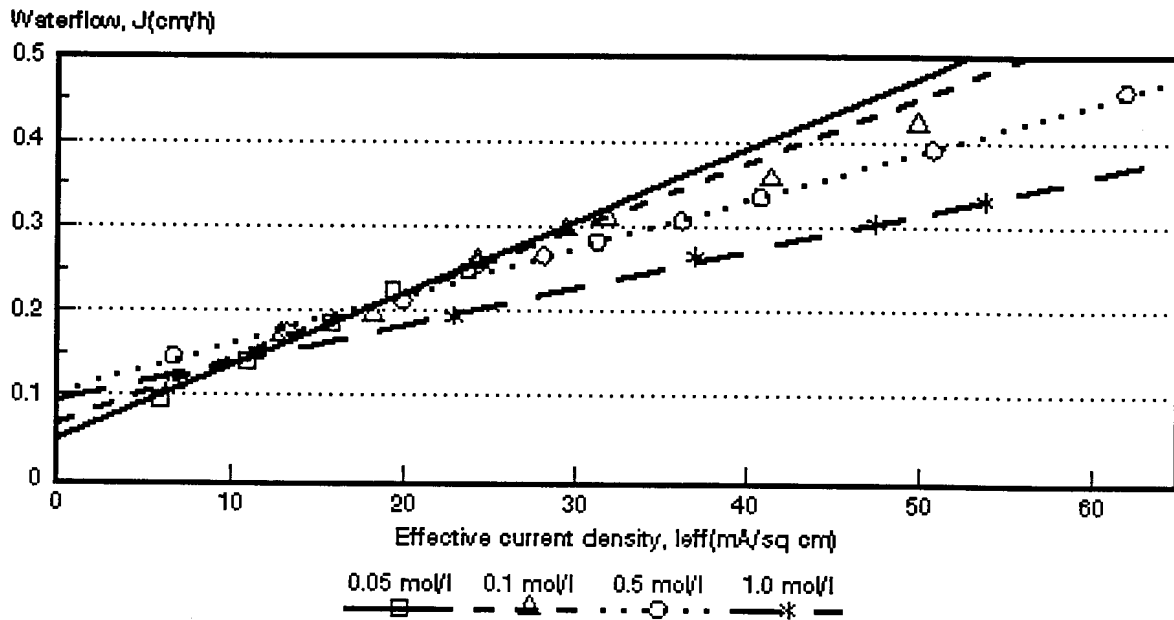


Figure 8.35: Water flow through the membranes as a function of effective current density and feed water concentration. *Selemion* AMV and CMV membranes.

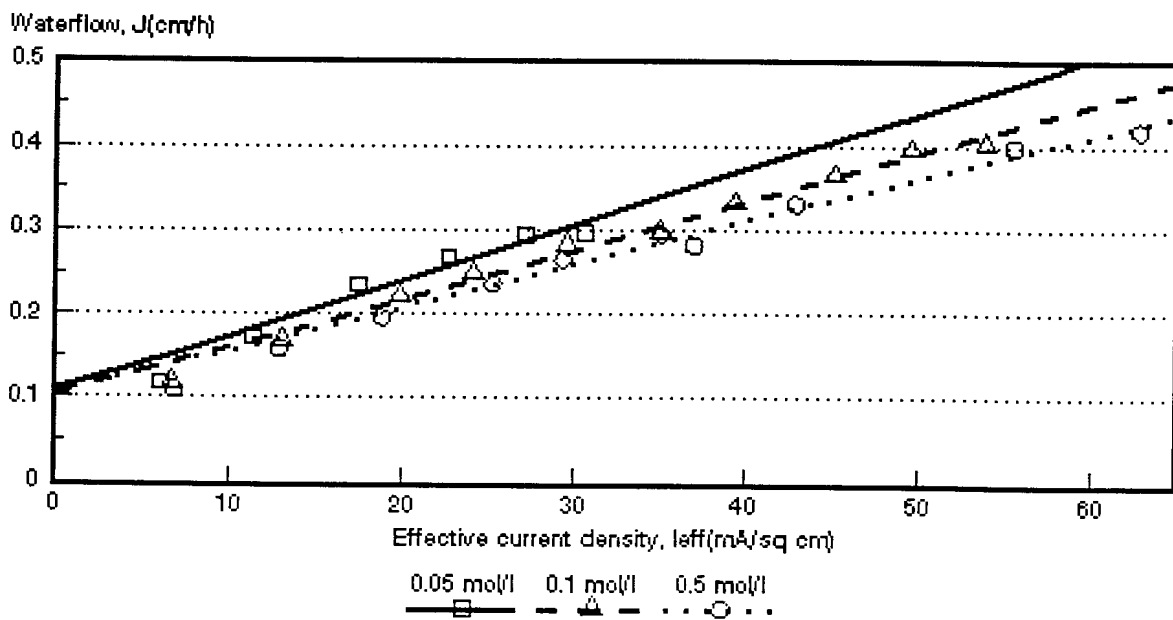


Figure 8.36: Water flow through the membranes as a function of effective current density and feed water concentration. *Selemion* AMP and CMV membranes.

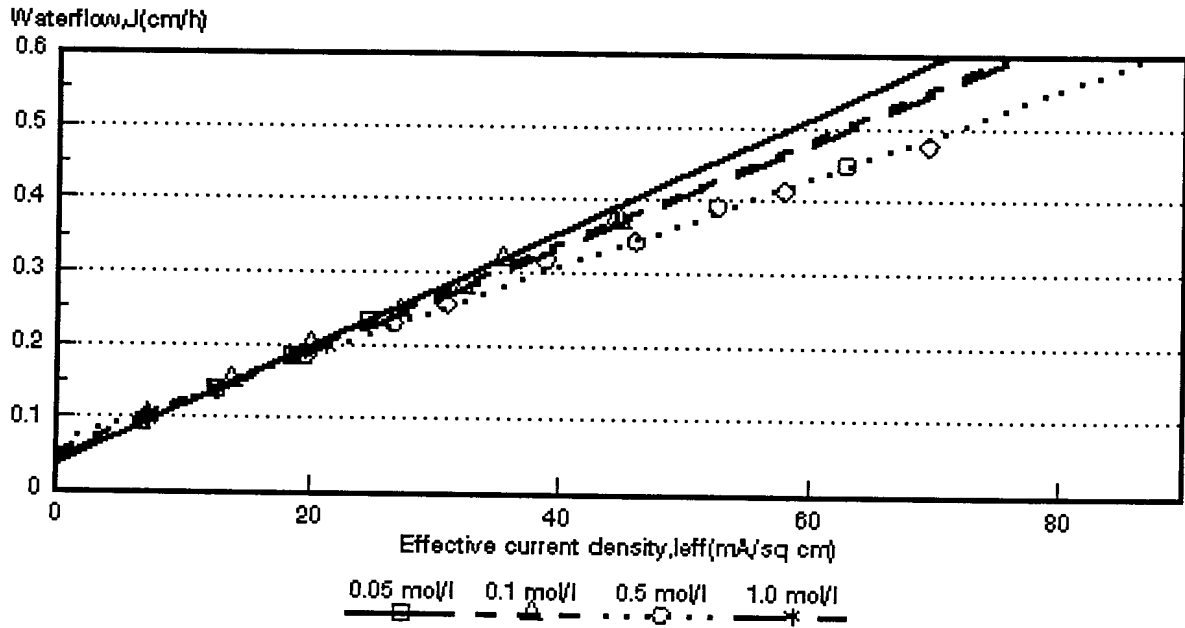


Figure 8.37: Water flow through the membranes as a function of effective current density and feed water concentration. *Ionac* MA-3475 and MC-3470 membranes.

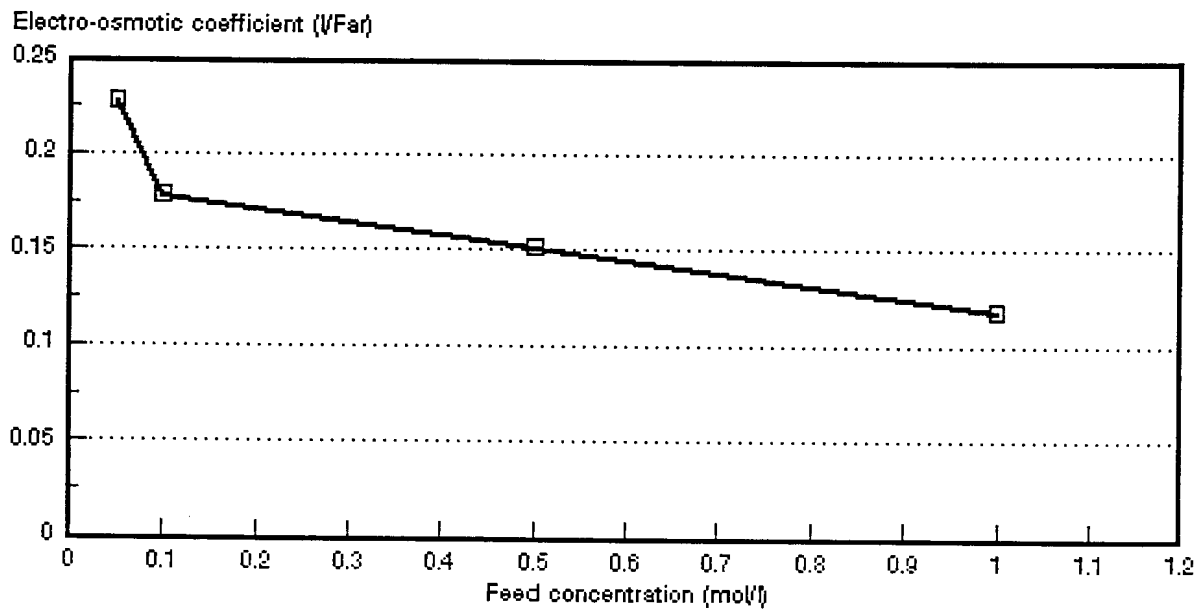


Figure 8.38: Electro-osmotic coefficient as a function of NaOH feed concentration. *Selemion* AMV and CMV membranes.

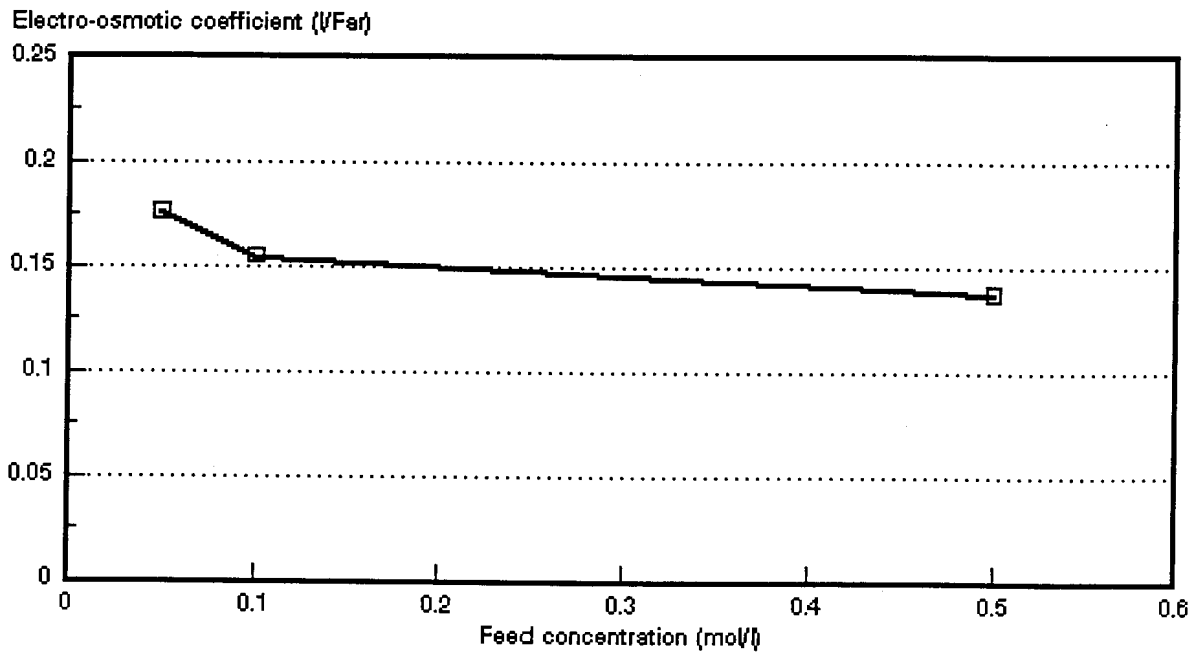


Figure 8.39: Electro-osmotic coefficient as a function of NaOH feed concentration. *Selemion AMP and CMV membranes.*

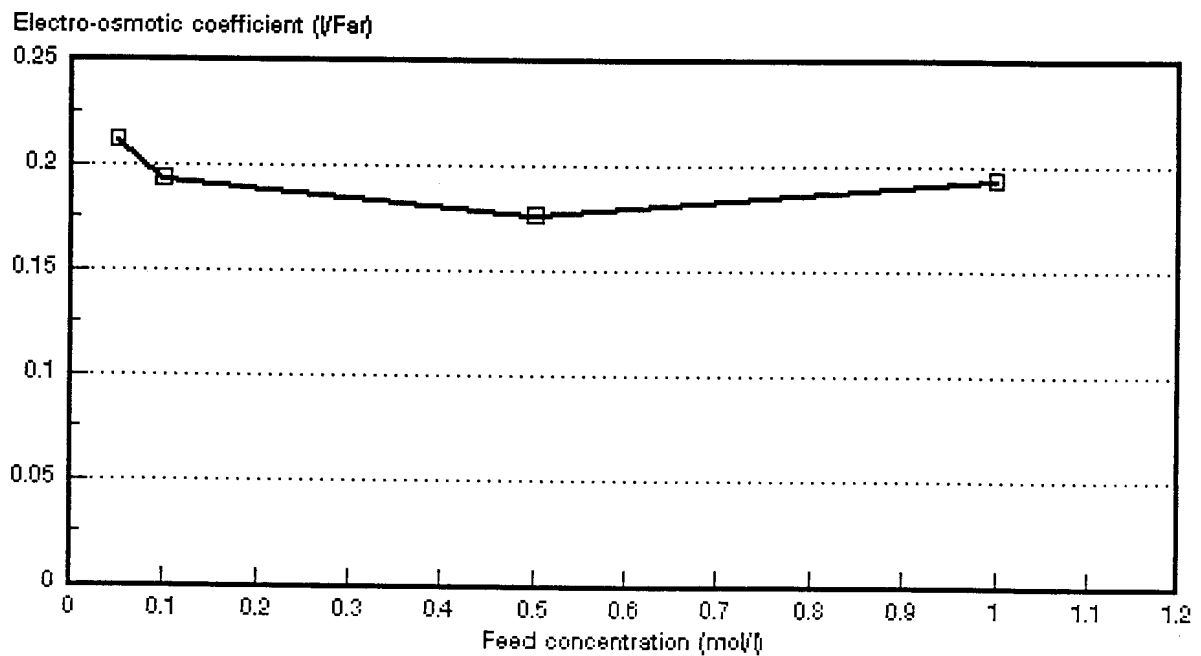


Figure 8.40: Electro-osmotic coefficient as a function of NaOH feed concentration. *Ionac MA-3475 and MC-3470 membranes.*

Table 8.19: Effect of the electro-osmotic coefficient (EOC)* on the maximum caustic soda brine concentration, c_b^{max} .

Membranes	Feed Concentration mol/l	EOC l/Faraday	c_b^{max} mol/l	mol H ₂ O/Faraday
Selemin AMV & CMV	0,05	0,228	4,39	12,7
	0,10	0,179	5,59	9,9
	0,50	0,152	6,58	8,4
	1,0	0,118	8,46	6,6
Selemin AMP & CMV	0,05	0,176	5,68	9,8
	0,10	0,155	6,45	8,6
	0,5	0,137	7,30	7,6
Ionac MA-3470 & MC-3475	0,05	0,212	4,72	11,8
	0,10	0,193	5,18	10,7
	0,50	0,176	5,68	9,8
	1,0	0,193	5,18	10,7

* Data from Tables 8.1 to 8.11.

Table 8.20: Osmotic flow* (J_{osm}) relative to the total flow (J) through the membranes as a function of current density.

Membranes	Current Density mA/cm ²	J_{osm}/J (%)			
		Feed concentration (mol/l)			
		0,05	0,1	0,5	1,0
Selemin AMV & CMV	10	57,3	78,4	72,7	49,5
	20	38,6	52,23	60,6	
	30	29,4	45,9	50,0	
	40	24,2	34,9	41,4	
	50	22,1	30,3	40,0	
	60		28,9	37,5	
	70				
	80		25,2	31,6	
	90				
	100		21,4	27,0	
Selemin AMP & CMV	10	92,7	88,6	97,1	29,07
	20	63,6	61,4	67,2	
	30	46,6	46,9	54,5	
	40	40,8	41,8	45,3	
	50	37,3	36,8	40,3	
	60	36,8	37,8	36,2	
	70		31,1		
	80		28,3	32,3	
	90		26,2		
	100		25,7	26,7	
Ionac MA-3475 & MC-3470	10	41,9	51,2	53,1	47,3
	20	27,9	34,8	38,2	
	30	20,9	26,5	28,4	
	40	16,6	21,4	22,9	
	50		18,9	20,6	
	60		16,6	16,6	
	70		14,2	15,3	
	80			13,4	
100			11,7		

* Data from Tables 8.1 to 8.11.

8.4 Membrane Permselectivity

Membrane permselectivity (from membrane potential measurements) as a function of brine concentration at different initial feed water concentrations is shown in Figures 8.41 to 8.43. Membrane permselectivity decreases with increasing caustic soda brine concentration and increasing feed water concentration. It is interesting to note that membrane permselectivity has not been much effected by increasing brine concentration in the case of the *Selemion* AMP and CMV membranes at 0,1 mol/l feed concentration.

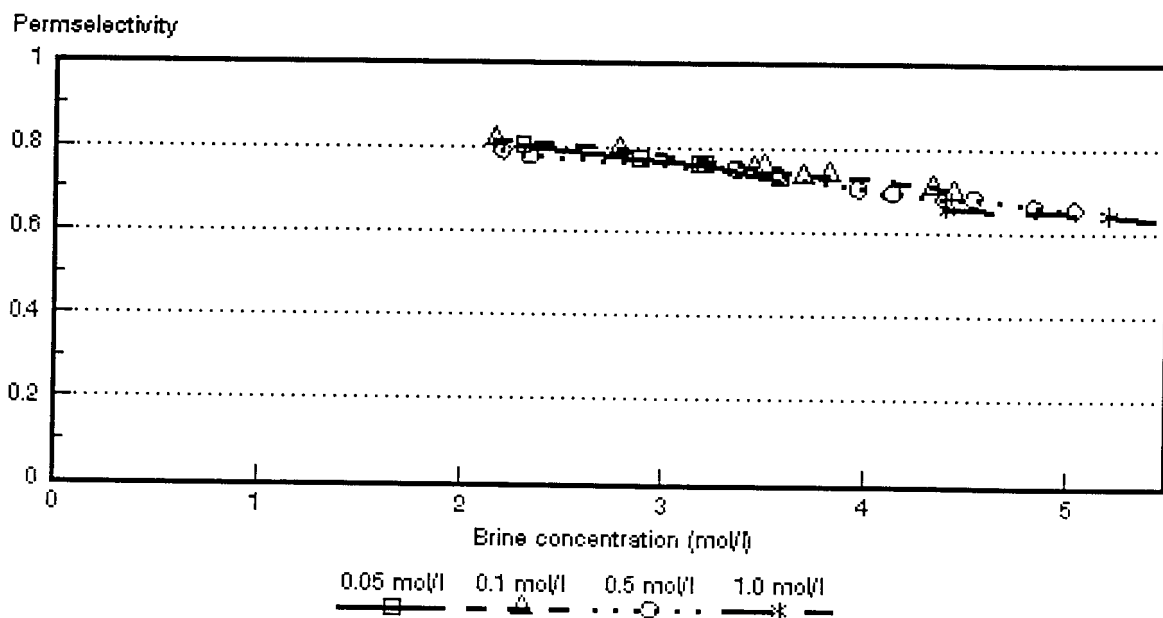


Figure 8.41: Permselectivity ($\bar{\Delta}t$) as a function of brine concentration for different NaOH feed concentrations. *Selemion* AMV and CMV membranes.

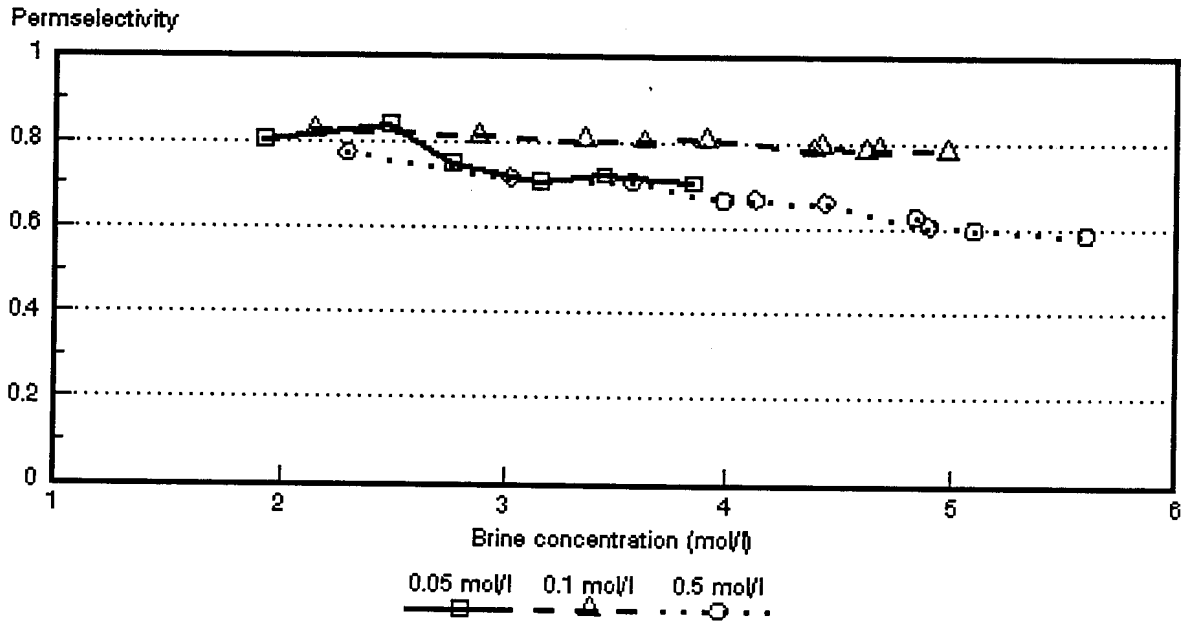


Figure 8.42: Permselectivity ($\bar{\Delta}t$) as a function of brine concentration for different NaOH feed concentrations. *Selemion AMP* and *CMV* membranes.

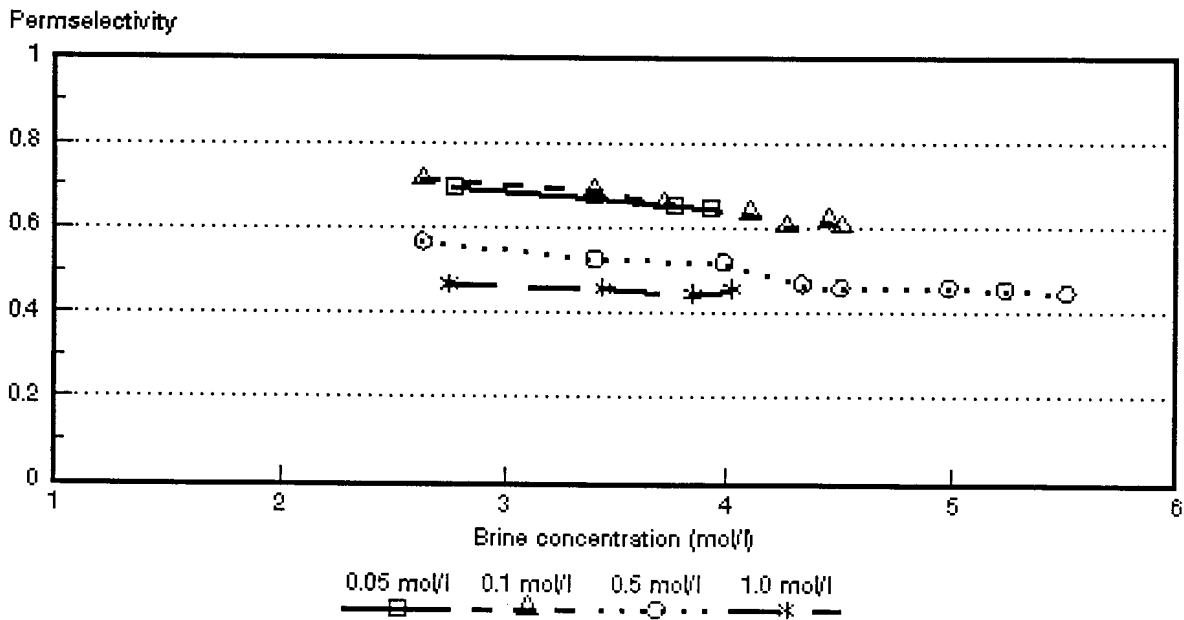


Figure 8.43: Permselectivity ($\bar{\Delta}t$) as a function of brine concentration for different NaOH feed concentrations. *Ionac MA-3475* and *MC-3470* membranes.

8.5 Membrane Characteristics

8.5.1 Membrane resistances of membranes used for EOP of caustic soda solutions

Membrane resistances of the membranes used for EOP of caustic soda solutions are summarized in Table 8.21.

Table 8.21: Membrane resistances of the membranes used for EOP of caustic soda solutions.

Membrane	Resistance - ohm-cm ²	
	0,1 mol/l	0,5 mol/l
Selemion AMV	4,1	0,5
Selemion AMP	9,6	1,5
Selemion CMV	5,1	1,2
Ionac MA-3475	15,7	7,1
Ionac MC-3470	26,9	15,7

8.5.2 Gel water contents and ion-exchange capacities of the membranes used for EOP of caustic soda solutions.

Gel water contents and ion-exchange capacities of the membranes used for EOP of caustic soda solutions are shown in Table 8.22.

Table 8.22: Gel water contents and ion-exchange capacities of the membranes used for EOP of caustic soda solutions.

Membrane	Gel Water Content	Ion-exchange Capacity
	%	me/dry g
Selemion AMV	18,4	1,3
Selemion CMV	22,7	2,3
Selemion AMP	17,6	1,1
Ionac MA-3475	17,8	1,1
Ionac MC-3470	18,5	1,8

8.5.3 Permselectivities of the membranes used for EOP of caustic soda solutions.

Permselectivities of the membranes used for EOP of caustic soda solutions are shown in Table 8.23.

Table 8.23: Membrane permselectivities of the membranes used for EOP of caustic soda solutions at different salt gradients.

Membrane	$\Delta t(1)^*$	$\Delta t(2)^{**}$	$\Delta t(3)^{***}$
Selemion AMV	0,87	0,87	0,83
Selemion CMV	0,98	0,83	0,65
Selemion AMP	0,93	0,87	0,81
Ionac MA-3475	0,87	0,82	0,79
Ionac MC-3470	0,92	0,61	0,46

(1)* : 0,1 / 0,2 mol/l NaOH

(2)** : 0,5 / 1,0 mol/l NaOH

(3)*** : 0,1 / 4,0 mol/l NaOH

9. ELECTRO-OSMOTIC PUMPING OF SODIUM CHLORIDE-, HYDROCHLORIC ACID- AND CAUSTIC SODA SOLUTIONS IN A CONVENTIONAL ELECTRODIALYSIS STACK

9.1 Concentration/Desalination of Sodium Chloride Solutions with *Ionac* MA-3475 and MC-3470 Membranes.

The concentration/desalination results of different sodium chloride feed water concentrations at different cell pair voltages are summarized in Table 9.1.

9.1.1 Brine and dialysate concentrations

Dialysate and brine concentrations as a function of time and cell pair voltage for different initial feed water concentrations are shown in Figures 9.1 to 9.8. Brine concentration as a function of feed water concentration and cell pair voltage is shown in Figure 9.9. A typical example of current as a function of time and cell pair voltage for an approximately 3 000 mg/ℓ feed water solution is shown in Figure 9.10.

Desalination/concentration rate increased with increasing cell pair voltage (Figs. 9.1 to 9.8 and 9.10). Brine concentration increased as a function of feed water concentration and cell pair voltage (Table 9.1 and Fig. 9.9). Brine concentrations of 2,1 to 14,0% could be obtained in the feed water concentration range from 1 000 to 10 000 mg/ℓ and cell pair voltage range from 0,5 to 4 volt per cell pair (Table 9.1). Product water concentrations of less than 500 mg/ℓ could be obtained in the same feed water concentration and cell pair voltage range.

The concentration factors (brine/feed) were relatively low (Table 9.1). This could be ascribed to the small volume of feed water (12 ℓ) that was used. Concentration factors decreased with increasing feed concentration. This shows that there is a limit to the brine concentration that can be obtained with ED. Brine concentration that can be obtained with ED depends inter alia on the permselectivity of the ion-exchange membranes and current density used and on the feed water concentration^(6, 7). Ion-exchange membranes tend to lose some of their permselectivity at high concentration.

9.1.2 Brine volume and water recovery

Low brine volume and high water recoveries were obtained (Table 9.1). Brine volume varied between 1,5 and 4% of the treated water volume in the feed water concentration

Table 9.1: Concentration/desalination results of sodium chloride solutions at different feed concentrations and cell pair voltages using Ionac MA-3475 and MC-3470 membranes.

V _{cp}	c _f mg/l	c _p mg/l	c _b mg/l	CF	CE %	WR %	BV %	EEC kWh/m ³	OP m ³ /m ² ·d	d _{eff} mm	R _{op} ohm·cm ²
0,5	992	212	21 981	22,2	93,6	98,1	1,9	0,192	0,37		
	2 906	488	73 460	25,3	84,3	97,1	2,9	0,662	0,28	4,23	49,2
1,0	933	193	30 814	33	81,8	98,5	1,5	0,417	0,45		
	3 224	503	82 025	25,4	81,1	97,2	2,8	1,55	0,35	6,76	80,2
	5 132	451	99 786	19,4	91,4	96,0	4,0	2,358	0,30	6,56	69,2
1,5	1 033	196	42 805	41,4	75,2	98,5	1,5	0,769	0,48		
	3 349	435	83 738	25,0	79,9	97,3	2,7	2,52	0,37	11,83	62,9
	3 045	450	86 893	28,5	81,3	97,6	2,4	2,21	0,55*	5,66	99,75
	3 058	433	104 475	34,16	83,01	97,6	2,4	2,18	0,67**	4,81	75,5
2	4 959	372	107 630	21,7	78,9	96,3	3,7	5,35	0,36	10,18	77,1
	10 709	548	136 933	12,8	93,3	93,7	6,3	10,03	0,32	12,11	31,8
3	3 515	430	100 868	28,7	69,4	97,3	2,7	6,14	0,51	11,95	128,8
	5 388	407	112 589	20,9	76,3	96,2	3,7	9,02	0,41	13,86	91,1
	10 364	487	139 637	13,5	86,90	94,2	6,8	15,7	0,36	15,22	50,3
4	10 364	409	139 637	13,5	77,6	94,0	6,0	23,6	0,38	15,49	79,7

*: 2,1 cm/s linear flow velocity; **: 2,73 cm/s linear flow velocity; other experiments conducted at a linear flow velocity approximately 1 cm/s

CF = concentration factor

CE = current efficiency

BV = brine volume

OP = output (yield)

WR = water recovery

EEC = electrical energy consumption

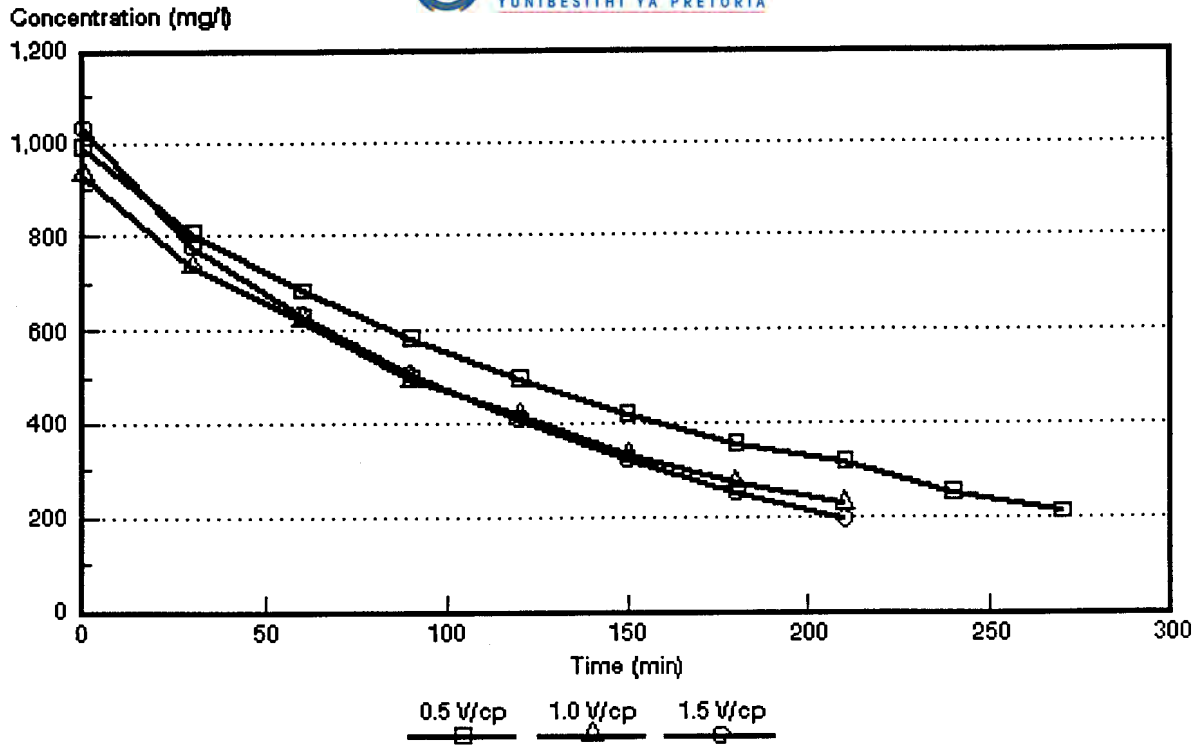


Figure 9.1: Dialysate concentration as a function of time and cell pair voltage for an approximately 1 000 mg/l sodium chloride feed solution.

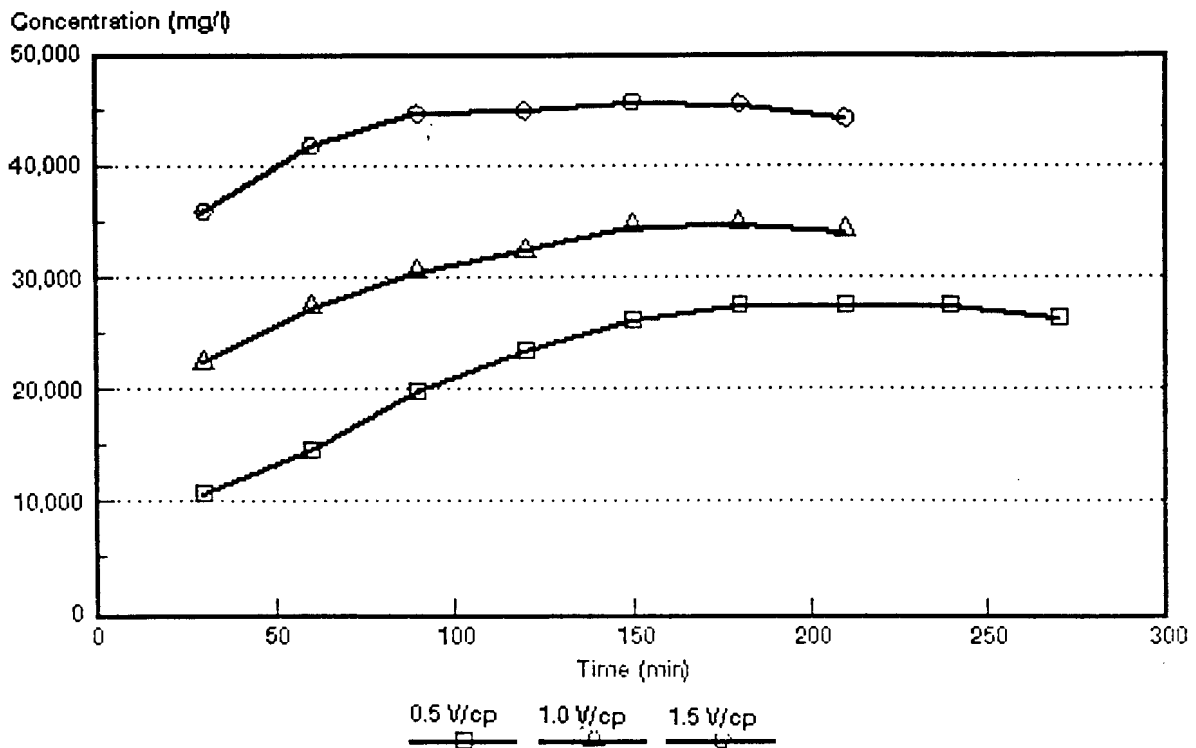


Figure 9.2: Brine concentration as a function of time and cell pair voltage for an approximately 1 000 mg/l sodium chloride feed solution.

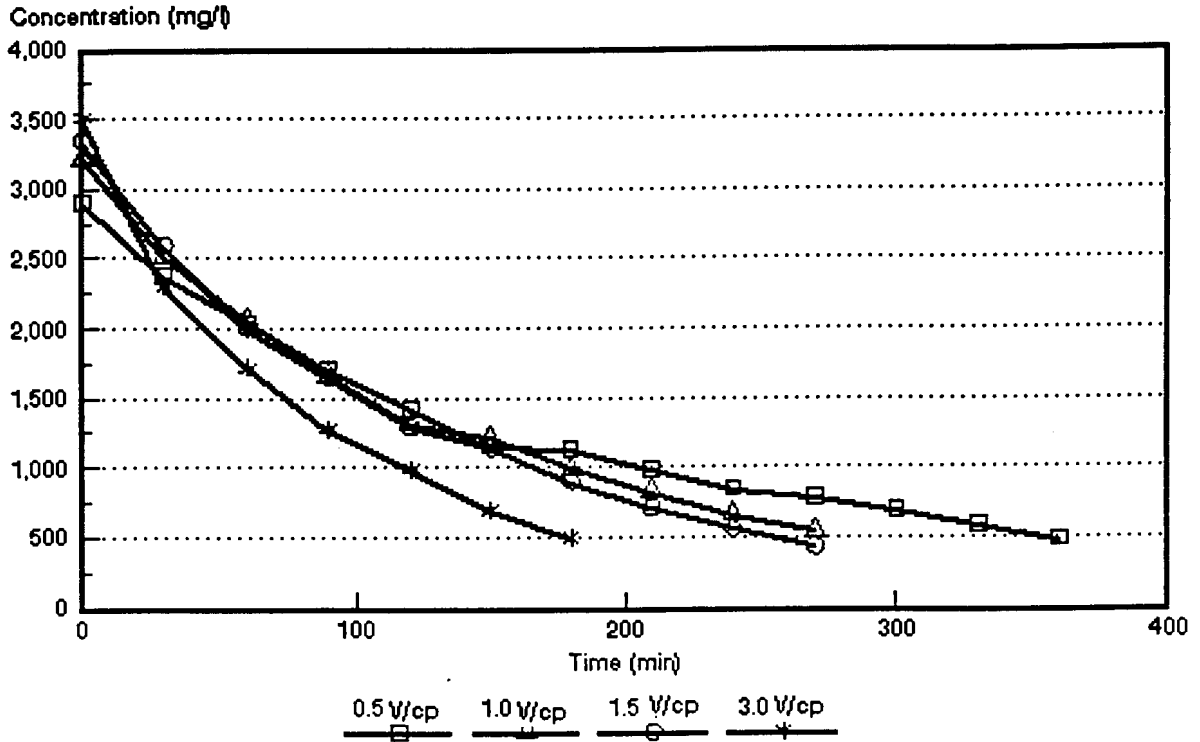


Figure 9.3: Dialysate concentration as a function of time and cell pair voltage for an approximately 3 000 mg/l sodium chloride feed solution.

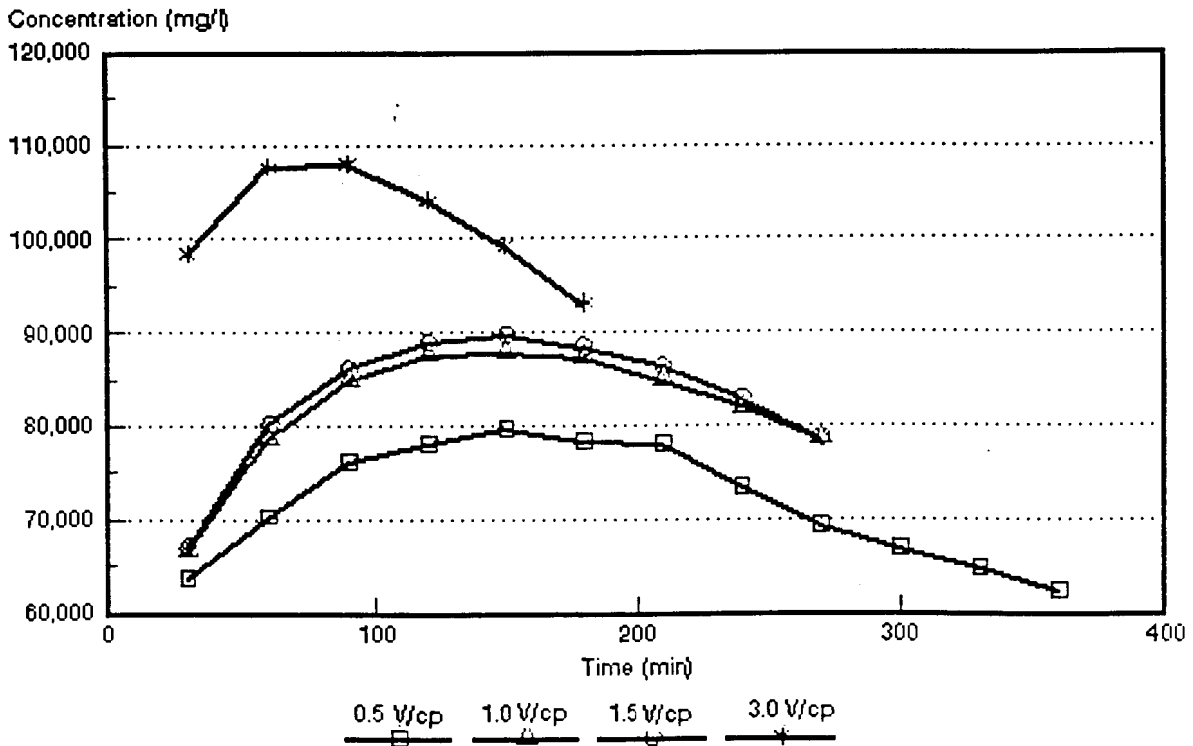


Figure 9.4: Brine concentration as a function of time and cell pair voltage for an approximately 3 000 mg/l sodium chloride feed solution.

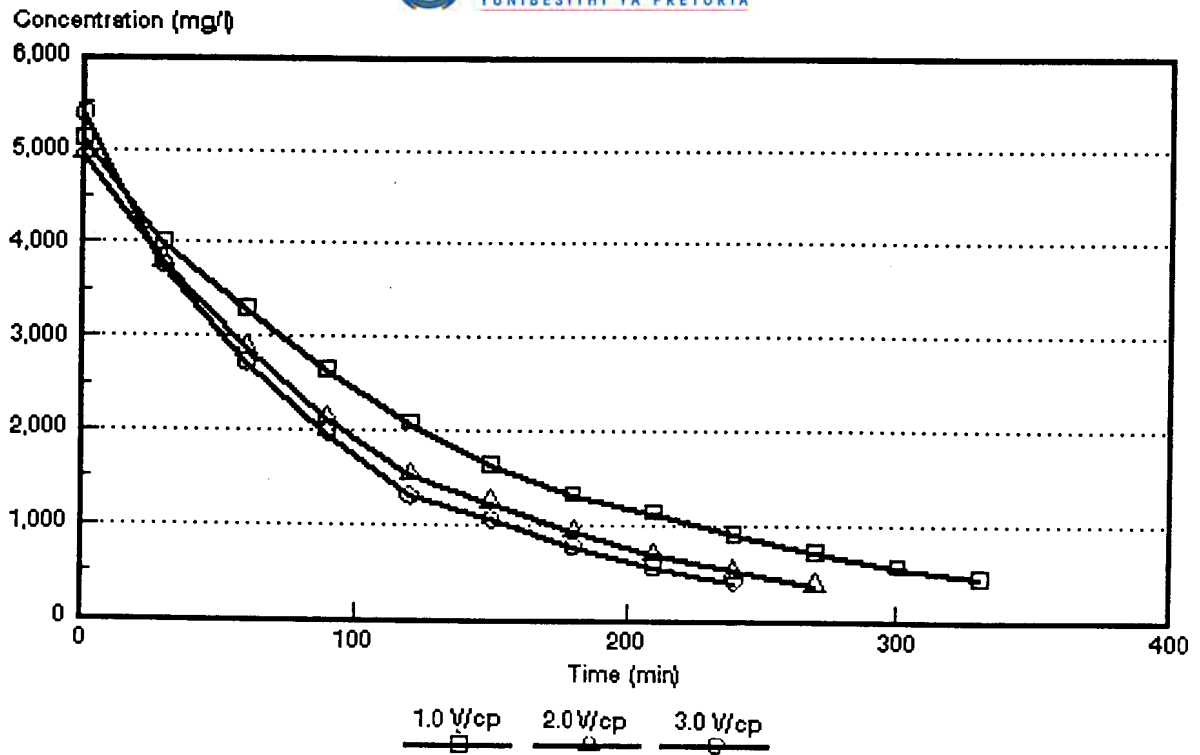


Figure 9.5: Dialysate concentration as a function of time and cell pair voltage for an approximately 5 000 mg/l sodium chloride feed solution.

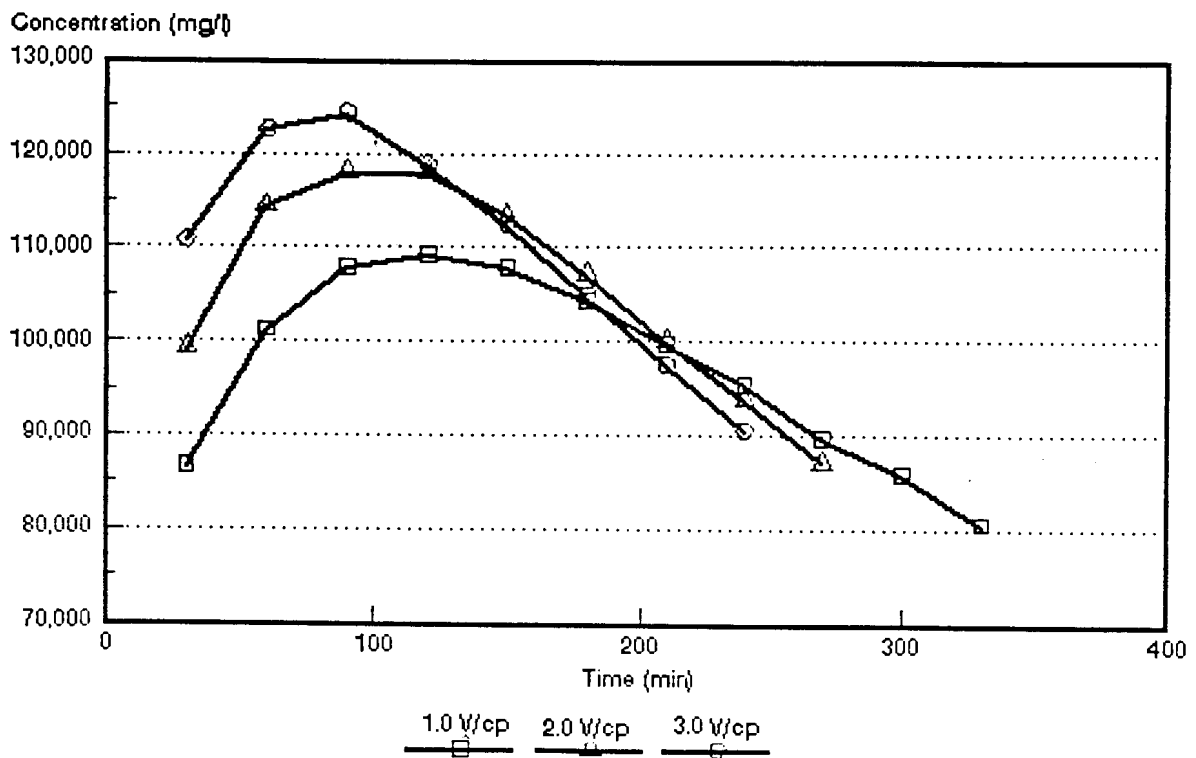


Figure 9.6: Brine concentration as a function of time and cell pair voltage for an approximately 5 000 mg/l sodium chloride feed solution.

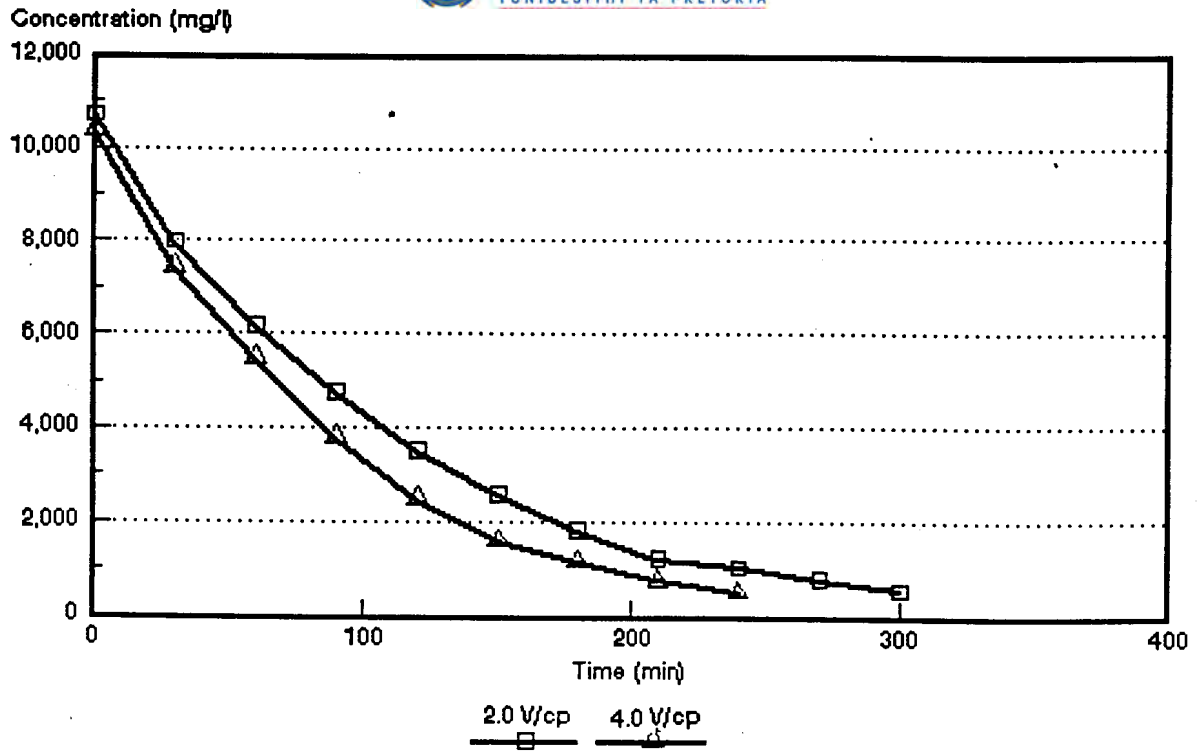


Figure 9.7: Dialysate concentration as a function of time and cell pair voltage for an approximately 10 000 mg/l sodium chloride feed solution.

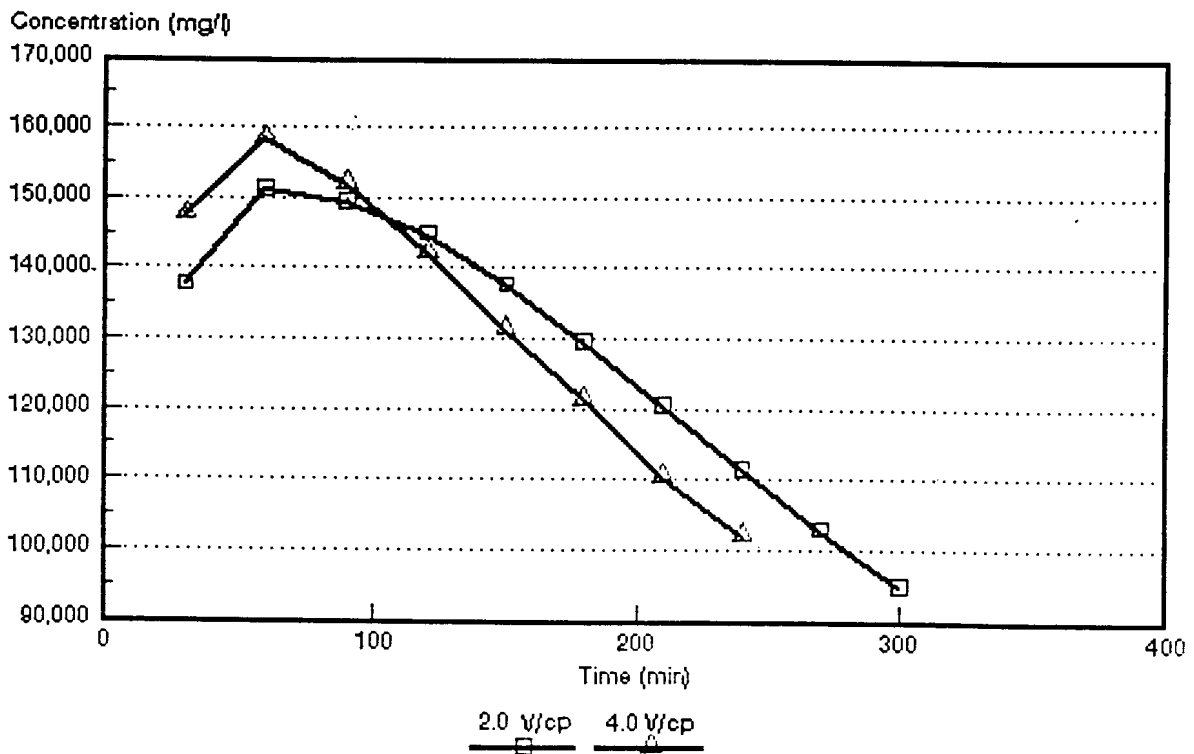


Figure 9.8: Brine concentration as a function of time and cell pair voltage for an approximately 10 000 mg/l sodium chloride feed solution.

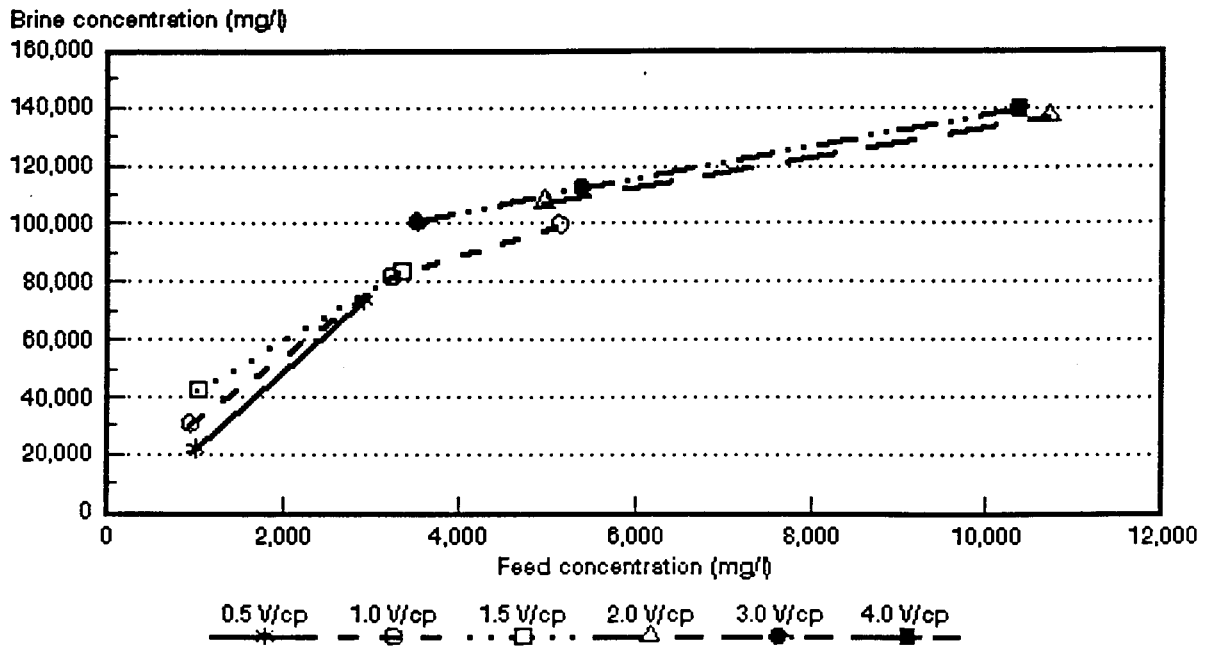


Figure 9.9: Brine concentration as a function of sodium chloride feed water concentration and cell pair voltage.

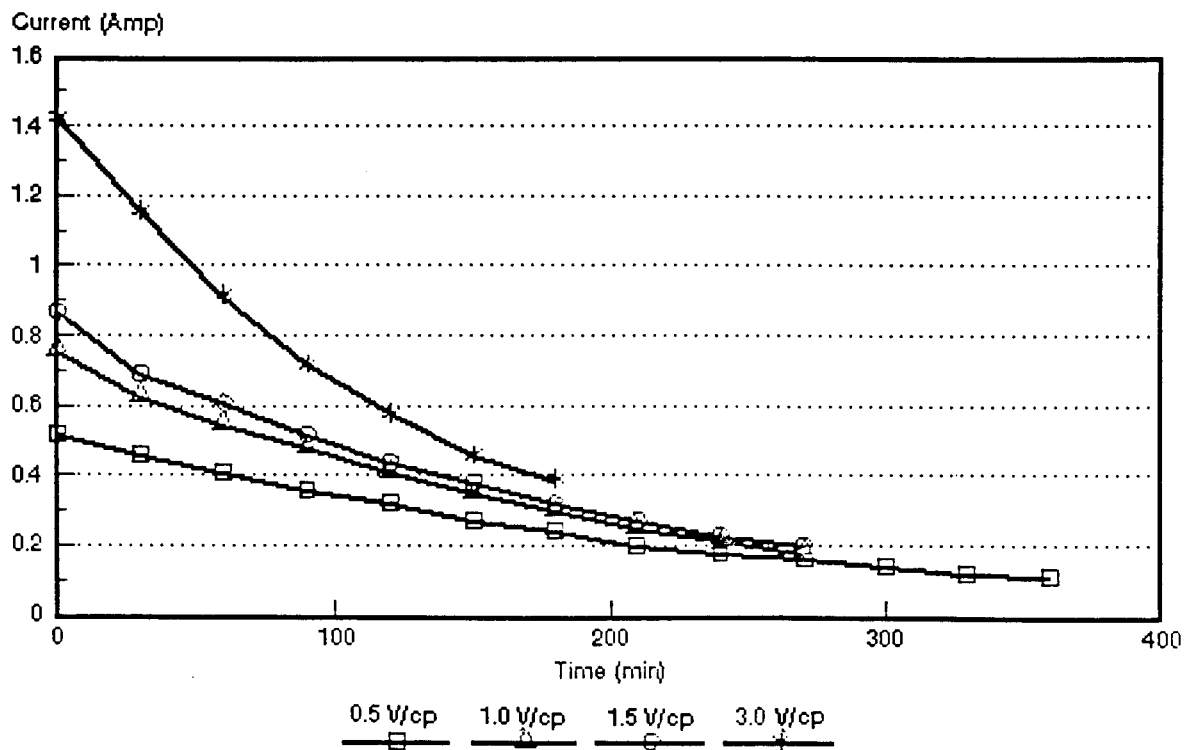


Figure 9.10: Electrical current as a function of time and cell pair voltage during desalination of an approximately 3 000 mg/l sodium chloride solution.

range from 1 000 to 5 000 mg/ℓ (0,5 to 1,5 V/cp). Brine volume increased with increasing feed water concentration (Table 9.1) and a brine volume of 6,8% was obtained at a feed water concentration of approximately 10 000 mg/ℓ (3 V/cp). Water recoveries of approximately 96% were obtained in the feed water concentration range from 1 000 to 5 000 mg/ℓ. The lowest water recovery that was obtained was 93,7% (at approximately 10 000 mg/ℓ). Therefore, high water recoveries and low brine volumes could be obtained with EOP-ED.

9.1.3 Current efficiency

Current efficiency increased with increasing feed water concentration, especially at the higher cell pair voltages (Table 9.1 and Figure 9.11). This could be ascribed to an increasing flow of water through the membranes with increasing feed water concentration. Current efficiencies of 75,2 and 93,6% were obtained in the feed water and cell pair voltage ranges of 1 000 to 5 000 mg/ℓ and 0,5 to 1,5 V/cp, respectively. (Table 9.1). Current efficiencies of 69,4 to 86,9% were obtained in the feed water and cell pair voltage ranges of 3 000 to 10 000 mg/ℓ and 2 to 4 V/cp, respectively. Current efficiency further decreased with increasing cell pair voltage. This could be ascribed to increasing polarization that was taking place at the higher cell pair voltages.

9.1.4 Electrical energy consumption

Electrical energy consumption obtained during EOP-ED was low. Electrical energy consumption of less than 2,5 kWh/m³ product water was obtained in the cell pair voltage and feed water concentration ranges of 0,5 to 1,5 V/cp (1 000 to 3 000 mg/ℓ)(Table 9.1), respectively. Electrical energy consumption further increased with increasing cell pair voltage and increasing feed water concentration (Fig. 9.12). Electrical energy consumption was 10 and 23,6 kWh/m³ product water at 2 and 4 volt per cell pair, respectively (approximately 10 000 mg/ℓ feed). (Note: electrical energy consumption was only determined for ion transport).

9.1.5 Product water yield

Product water yield was low (Table 9.1). Product water yield varied between 0,28 and 0,67 m³/m²-d in the cell pair voltage and feed water concentration ranges studied. Water yield decreased as a function of feed water concentration and cell pair voltage (Table 9.1). A linear flow velocity of approximately 1 cm/s was used for most of the

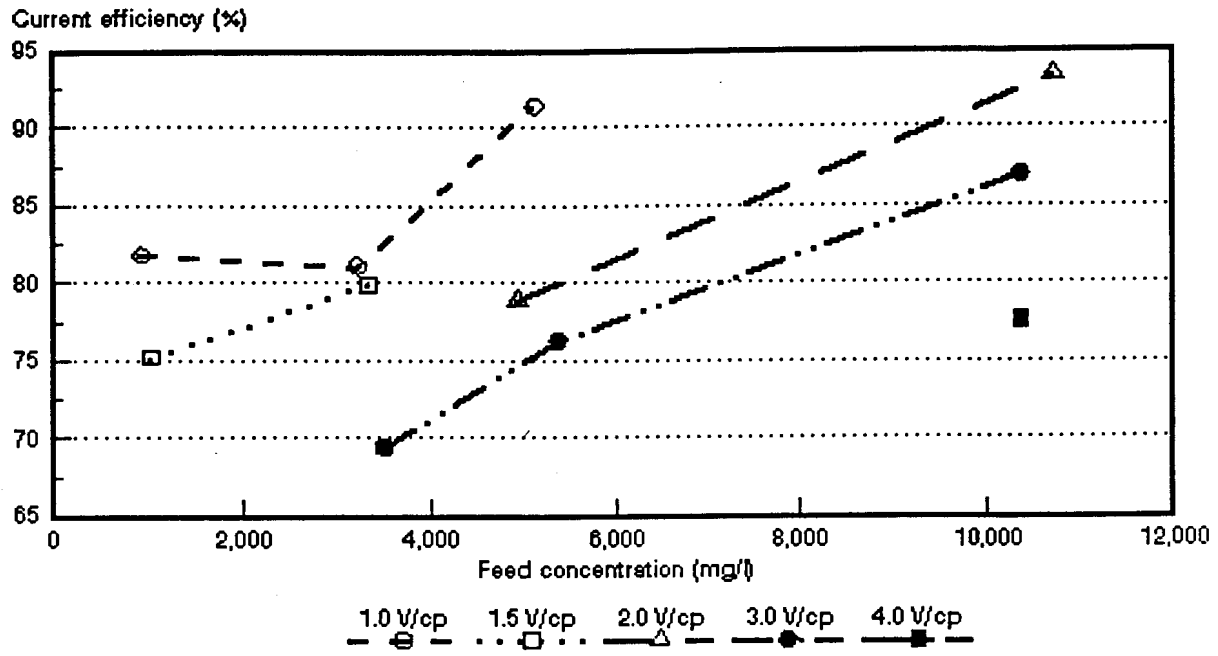


Figure 9.11: Current efficiency as a function of sodium chloride feed concentration and cell pair voltage.

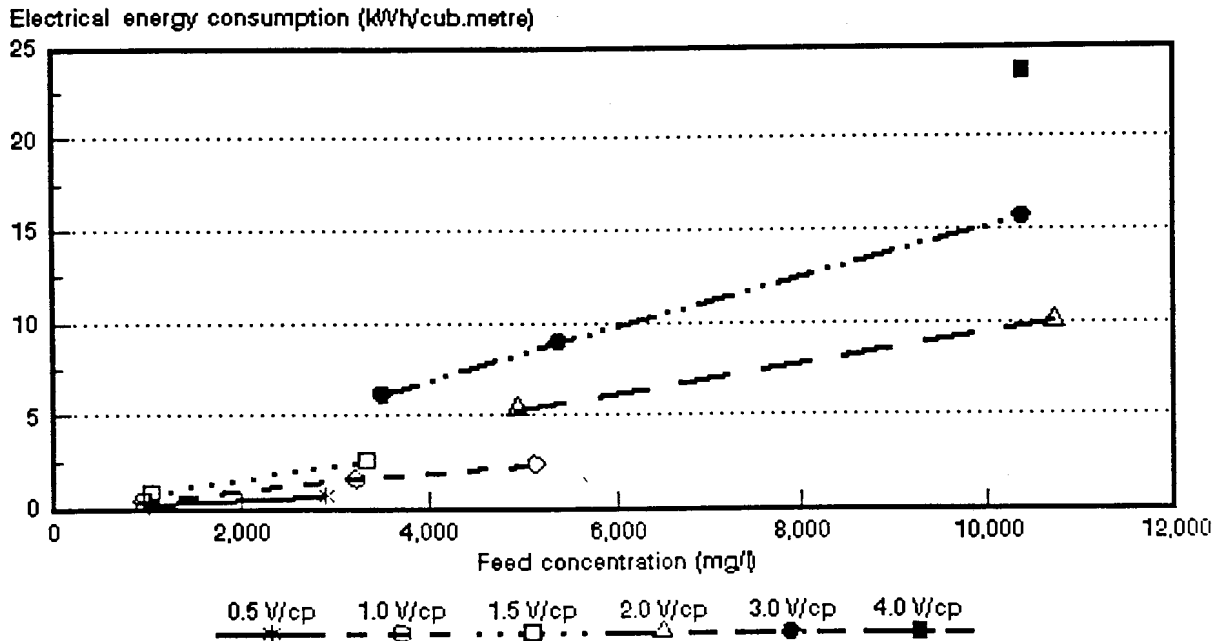


Figure 9.12: Electrical consumption as a function of sodium chloride feed concentration and cell pair voltage.

runs. However, linear flow velocity was increased to 2,1 cm/s and 2,7 cm/s at 3 000 mg/l feed water concentration (1,5 V/cp)(Table 9.1). Product water yield was significantly increased when the linear flow velocity was increased.

9.1.6 Effective cell pair thickness and cell pair resistance

An example of cell pair resistance (R_{cp}) as a function of the specific resistance of the dialysate and cell pair voltage is shown in Figure 9.13. (Approximately 3 000 mg/l feed). The lines through the linear region and extrapolation to the y-axis gives the cell pair resistance. The slope of the linear region gives the effective cell pair thickness, d_{eff} . The lines, however, deviate from linearity towards the end of the runs when the current is low and polarization is less. The effective cell pair thickness, d_{eff} , increased with increasing cell pair voltage and increasing feed water concentration. (Table 9.1). Cell pair resistance, R_{cp} , decreased with increasing feed water concentration and increased with increasing cell pair voltage (Table 9.1). The cell pair resistance increased slower than the specific resistance of the dialysate towards the end of the run because polarization is less. The effective thickness of the cell pair decreased significantly when the linear flow velocity was increased (Table 9.1).

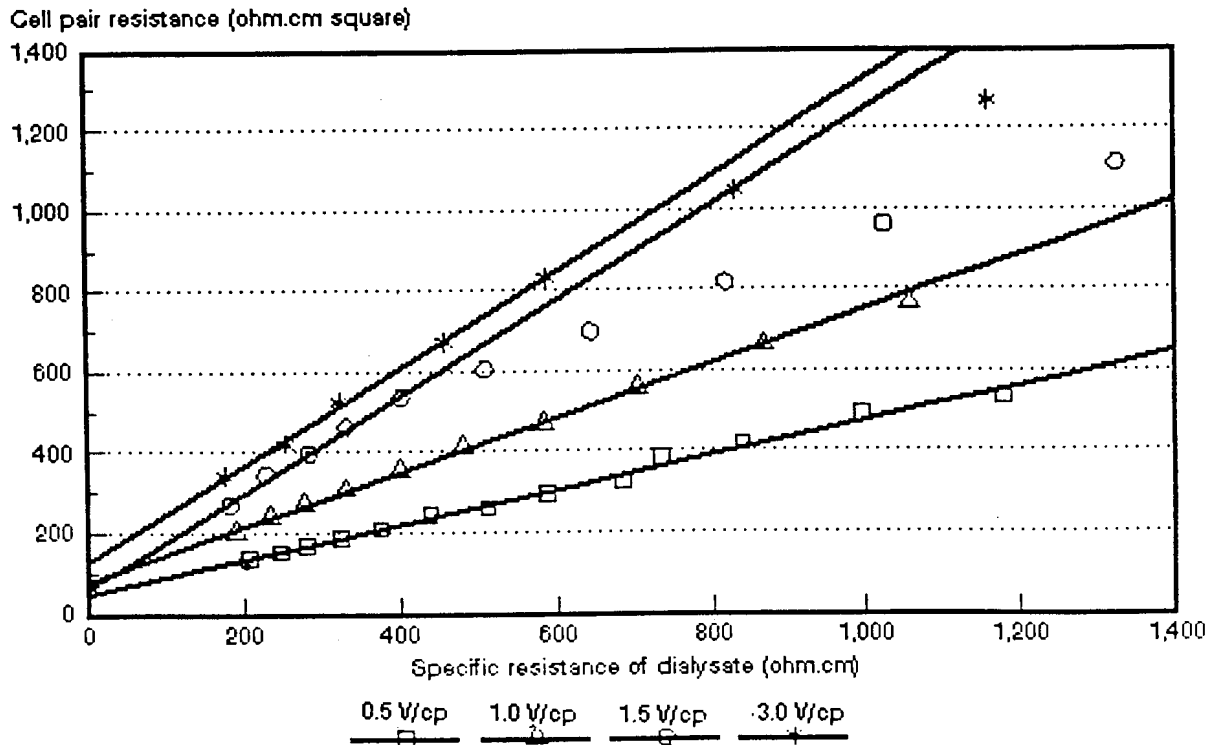


Figure 9.13: Cell pair resistance as a function of the specific resistance of the dialysate at different cell pair voltages (approximately 3 000 mg/l sodium chloride feed).

9.2 Concentration/Desalination of Hydrochloric Acid Solutions with *Selemion* AAV and CHV Membranes

The concentration/desalination results of different hydrochloric acid feed water concentrations at different cell pair voltages are summarized in Table 9.2.

9.2.1 Acid brine and dialysate concentration

Dialysate and acid brine concentration as a function of time and cell pair voltage for different initial acid feed concentrations are shown in Figures 9.14 to 9.19. Acid brine concentration as a function of hydrochloric acid feed concentration and cell pair voltage is shown in Figure 9.20. Electric current as a function of time during concentration/desalination of an approximately 3 000 mg/l hydrochloric acid feed solution is shown in Figure 9.21.

Faster and better acid removal was obtained at the higher cell pair voltages (Figs. 9.14, 9.16 and 9.18). Not much difference was experienced in the highest acid brine concentrations that could be obtained at the different cell pair voltages (Figs. 9.15, 9.17 and 9.19). Acid brine concentrations of 3,6 to 8,7% were obtained in the acid feed concentration range from approximately 1 000 to 5 000 mg/l and cell pair voltage range from 0,5 to 4,0 volt per cell pair. Acid brine concentration further increased with increasing feed water concentration and increasing cell pair voltage (Fig. 9.20). Acid product water concentrations of less than 500 mg/l could be obtained in the acid feed concentration and cell pair voltage range studied (Table 9.2).

Concentration factors were low. Concentration factors decreased as a function of acid feed concentration (Table 9.2).

9.2.2 Acid brine volume and water recovery

Low brine volumes and high water recoveries were obtained. Brine volume varied between 2,4 and 7,8% of the treated water volume in the acid feed concentration range of 1 000 to 5 000 mg/l (0,5 to 4,0 V/cp) (Table 9.2). Brine volume also increased with increasing acid feed concentration and the highest acid brine concentration was obtained at an acid feed concentration of 5 000 mg/l (1 V/cp). Water recovery was high. Water recovery of approximately 97% was obtained at an acid feed concentration of approximately 1 000 mg/l (0,5 to 1 V/cp). The lowest water recovery obtained was 92,2% at an acid feed concentration of approximately 5 000 mg/l (1,0

Table 9.2: Concentration/desalination results of hydrochloric acid solutions at different feed concentrations and cell pair voltages using Selemion AAV and CHV membranes.

Vcp	cf mg/l	cp mg/l	c _b mg/l	CF	CE %	WR %	BV %	EEC kWh/m ³	OP m ³ /m ² ·d	d _{eff} mm	Rcp ohm·cm ²
0,5	1 130	197	36 460	32,3	37,8	97,1	2,9	0,182	0,33	5,1	15,1
0,5*	2 989	452	56 513	18,9	46,3	93,6	6,4	2,18	0,64	5,0	
1,0	1 021	175	36 460	35,7	29,2	97,6	2,4	2,14	0,39	7,90	58,4
1,0	3 281	452	67 451	20,6	35,6	94,6	5,4	5,90	0,36	13,80	1,9
1,0*	2 989	379	61 982	20,7	35,7	94,0	6,0	5,5	0,64	8,1	-1,6
1,0	5 032	510	85 681	17,0	32,0	92,2	7,8	10,5	0,31	13,50	
1,5	1 167	175	38 283	32,8	34,3	97,5	2,5	3,2	0,41	11,97	112,1
2,0	3 318	419	69 274	20,9	32,7	94,3	5,7	13,2	0,38	25,9	4,8
2,0*	3 099	510	43 752	14,12	38,6	92,5	7,5	10,83	0,70	21,4	-1,2
2,0	5 213	496	85 681	16,4	31,6	92,3	7,7	22,1	0,33	25,6	
3,0	3 354	467	72 920	21,7	33,9	94,6	5,4	18,99	0,43	37,3	3,5
3,0*	3 537	496	69 274	19,6	33,80	93,75	6,25	21,33	0,80	25,9	1,2
3,0	5 287	481	87 504	16,6	32,2	92,5	7,5	33,17	0,35	35,9	
4,0	3 208	423	72 920	22,7	33,3	94,9	5,1	24,76	0,46	46,8	13,2
4,0	4 958	467	85 681	17,2	31,3	92,8	7,2	42,58	0,40	44,9	3,9

* Linear flow velocity \approx 5 cm/s. Other experiments conducted at a linear flow velocity of 1 cm/s.

CF = concentration factor

CE = current efficiency

BV = brine volume

OP = output (yield)

WR = water recovery

EEC = electrical energy consumption

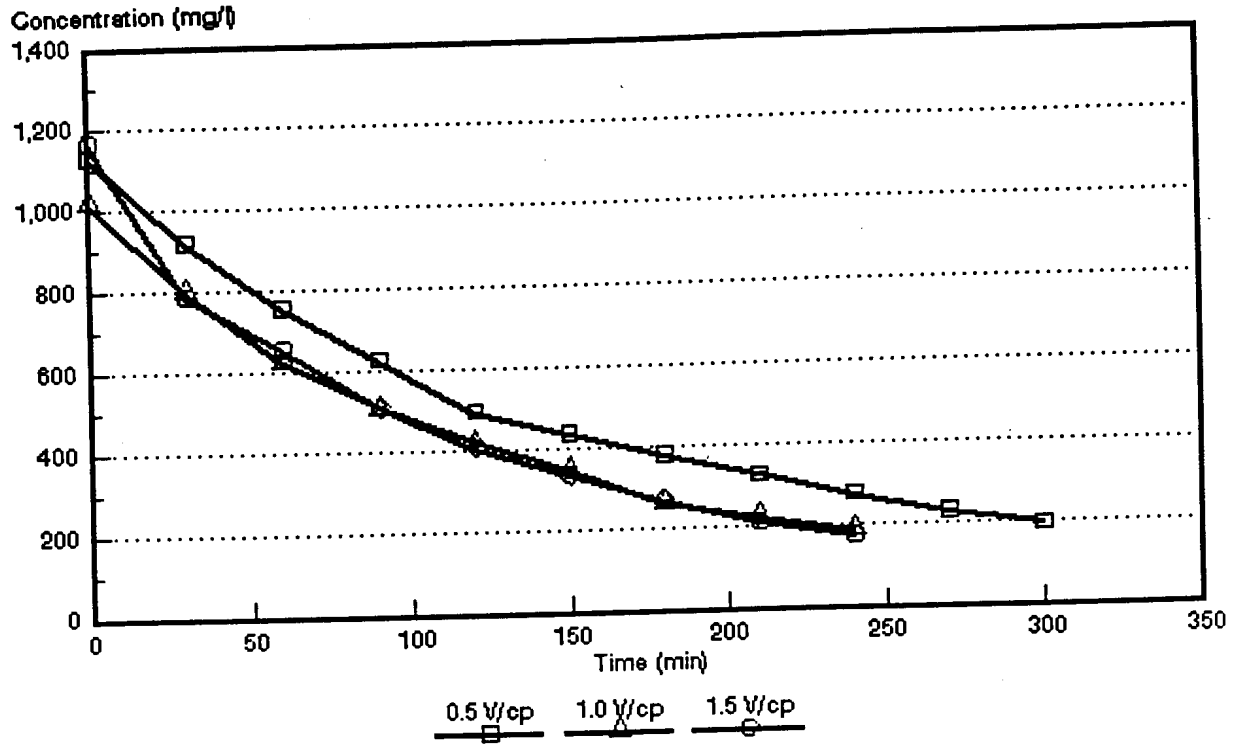


Figure 9.14: Dialysate concentration as a function of time and cell pair voltage for approximately 1 000 mg/l hydrochloric acid solutions.

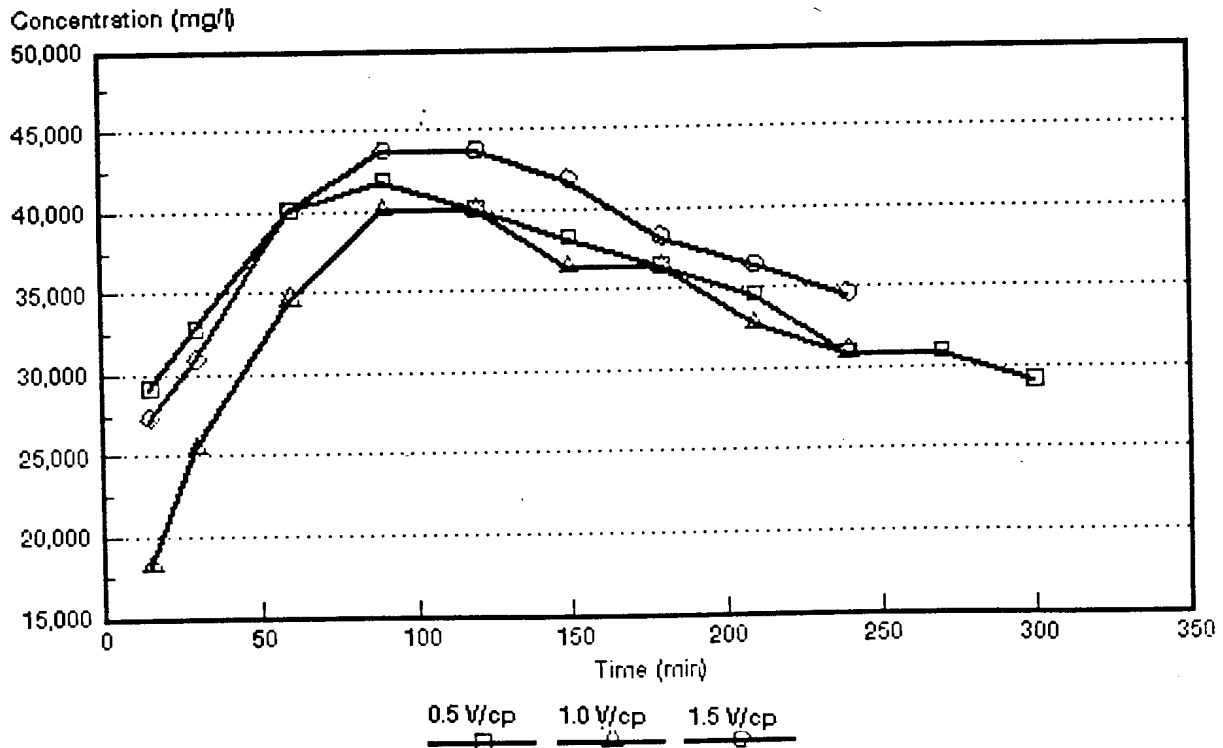


Figure 9.15: Brine concentration as a function of time and cell pair voltage for approximately 1 000 mg/l hydrochloric acid solutions.

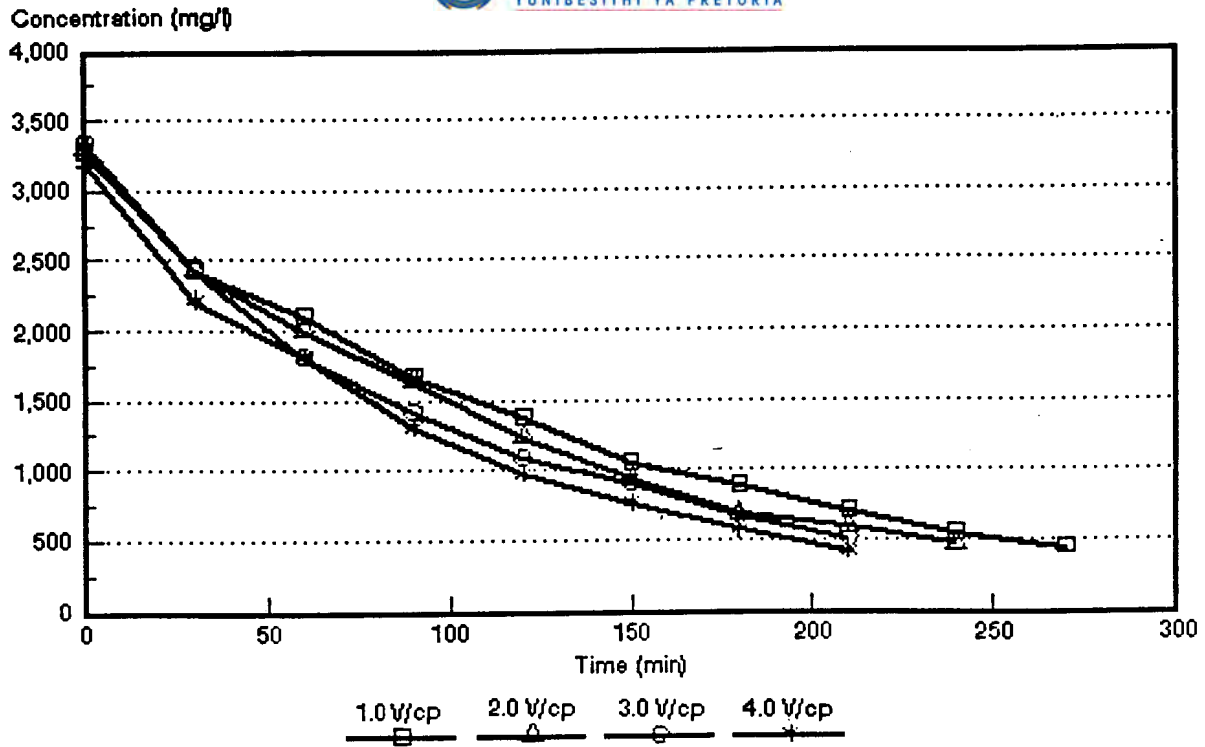


Figure 9.16: Dialysate concentration as a function of time and cell pair voltage for approximately 3 000 mg/l hydrochloric acid solutions.

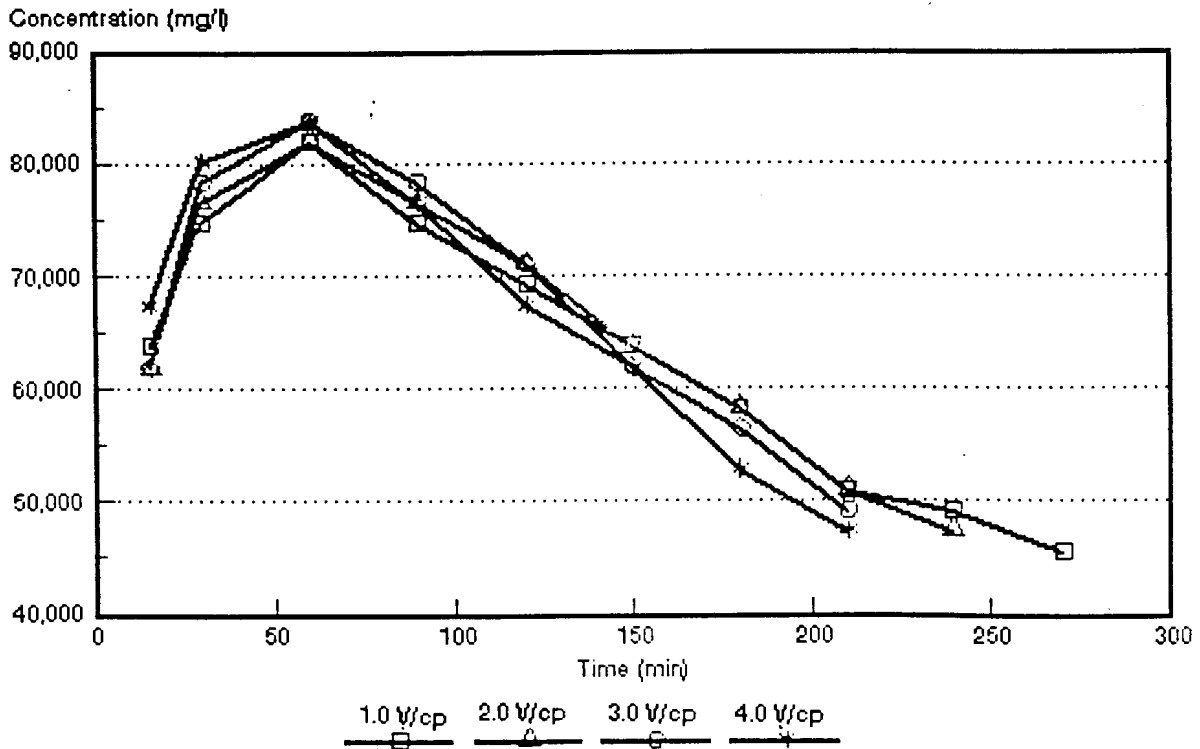


Figure 9.17: Brine concentration as a function of time and cell pair voltage for approximately 3 000 mg/l hydrochloric acid solutions.

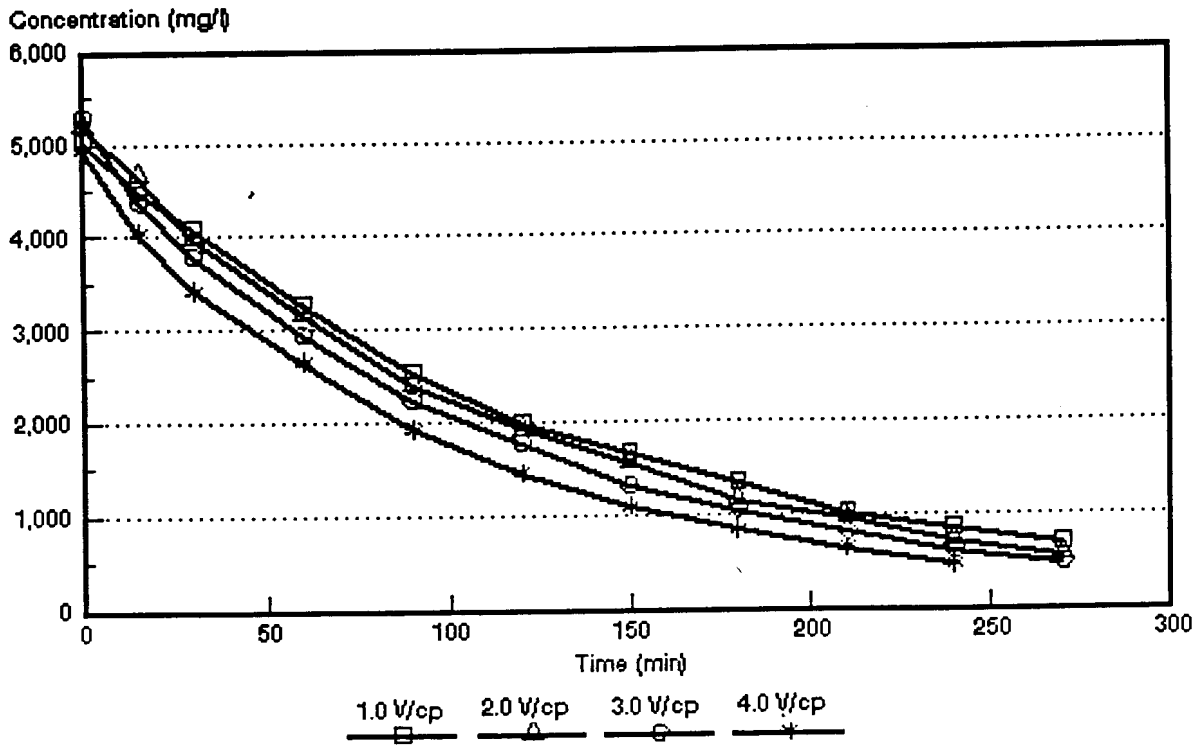


Figure 9.18: Dialysate concentration as a function of time and cell pair voltage for approximately 5 000 mg/l hydrochloric acid solutions.

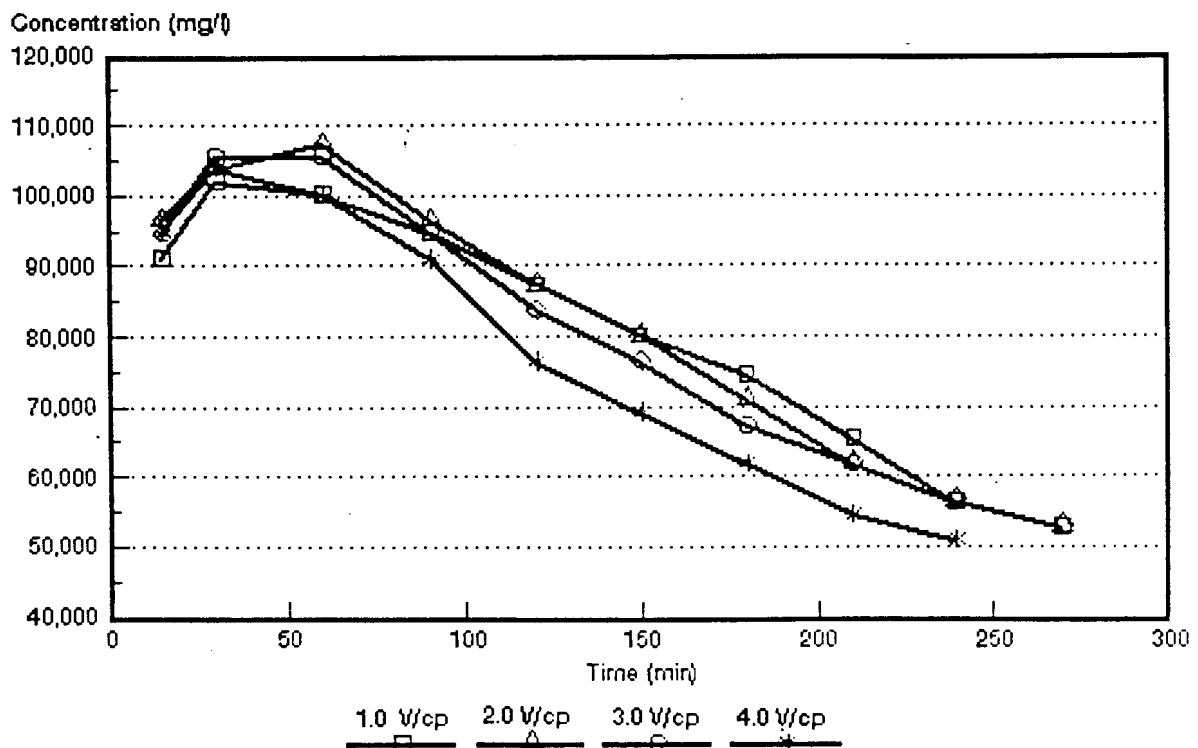


Figure 9.19: Brine concentration as a function of time and cell pair voltage for approximately 5 000 mg/l hydrochloric acid solutions.

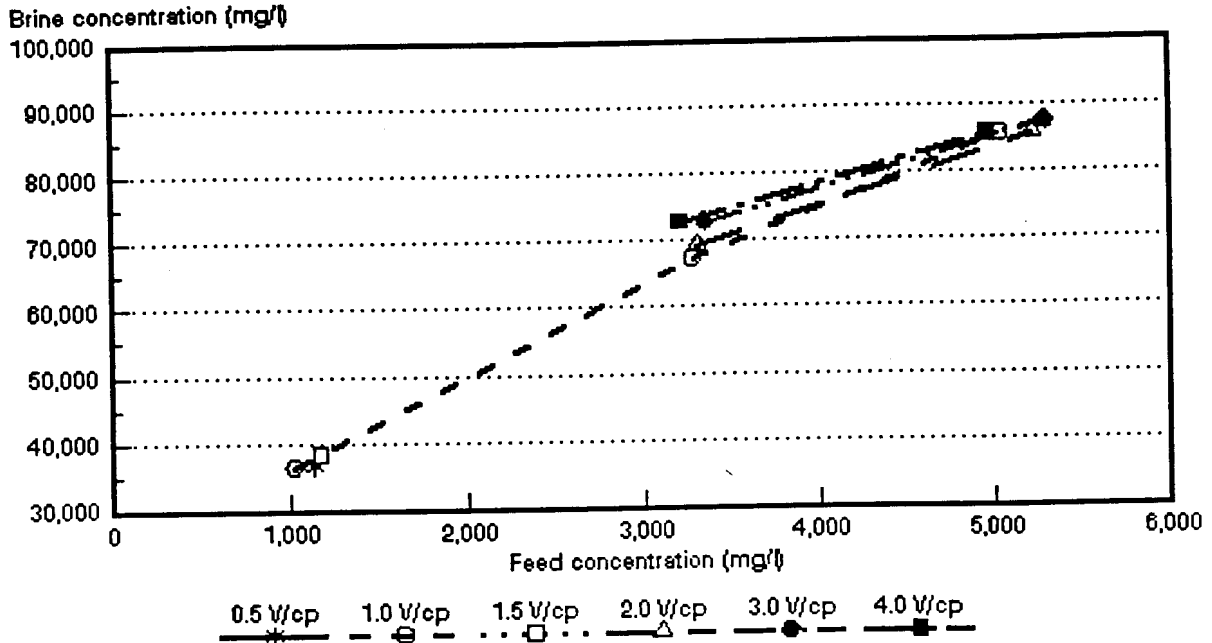


Figure 9.20: Brine concentration as a function of hydrochloric acid feed concentration and cell pair voltage.

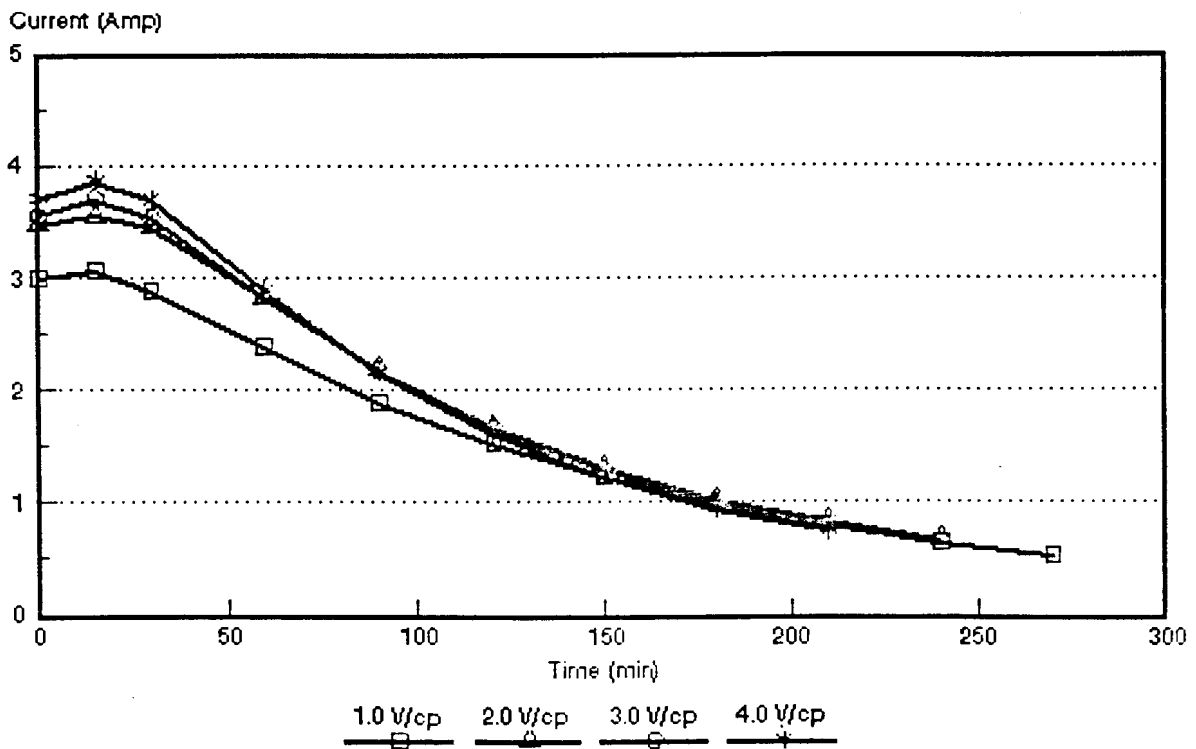


Figure 9.21: Electric current as a function of time and cell pair voltage during concentration/desalination of approximately 3 000 mg/l hydrochloric acid solutions.

V/cp). Therefore, high water recoveries and low acid brine volumes could be obtained with EOP-ED of acidic solutions.

9.2.3 Current efficiency

Current efficiencies were low (Table 9.2). Current efficiency varied between 46,3 and 29,2% in the acid feed concentration and cell pair voltage ranges studied. Current efficiency did not change with increasing cell pair voltage and decreased with increasing feed water concentration especially at the higher acid feed concentrations (Fig. 9.22). This is contrary to what has been experienced during EOP-ED of sodium chloride solutions and can be ascribed to less water that permeates through the membranes at higher feed concentration. The low current efficiencies that were obtained with the acid solutions could be ascribed to the inability of the anion membranes to resist the passage of hydrogen ions. However, the permselectivity of the *Selemion* AAV membranes for hydrogen ions is much better than that of other membranes normally used for ED of saline solutions.

9.2.4 Electrical energy consumption

Electrical energy consumption increased with increasing cell pair voltage and increasing acid feed concentration (Table 9.2 and Fig. 9.23). Low electrical energy consumption was obtained at low cell pair voltages and low acid feed concentrations. Electrical energy consumptions of 0,2 to 3,2 kWh/m³ product were obtained in the acid feed and cell pair voltage range of approximately 1 000 mg/l and 0,5 to 1,5 V/cp, respectively. However, electrical energy consumption increased rapidly with increasing feed concentration and cell pair voltage. The electrical energy consumption at 2,0; 3,0 and 4,0 V/cp of an approximately 3 000 mg/l hydrochloric acid solution was determined at 13,2; 18,9 and 24,8 kWh/m³ product water, respectively.

9.2.5 Product water yield

Product water yield (output) increased with increasing cell pair voltage and decreased with increasing acid feed concentration (Table 9.2). Output also increased significantly with increasing linear flow velocity through the stack. Output was determined at 0,38 m³/m²-d at a linear flow velocity of 1 cm/s (2,0 V/cp). At a linear flow velocity of 5 cm/s, output was determined at 0,7 m³/m²-d (Table 9.2). Therefore, it would be advantageous to operate an EOP-ED stack at the highest possible linear flow velocity.

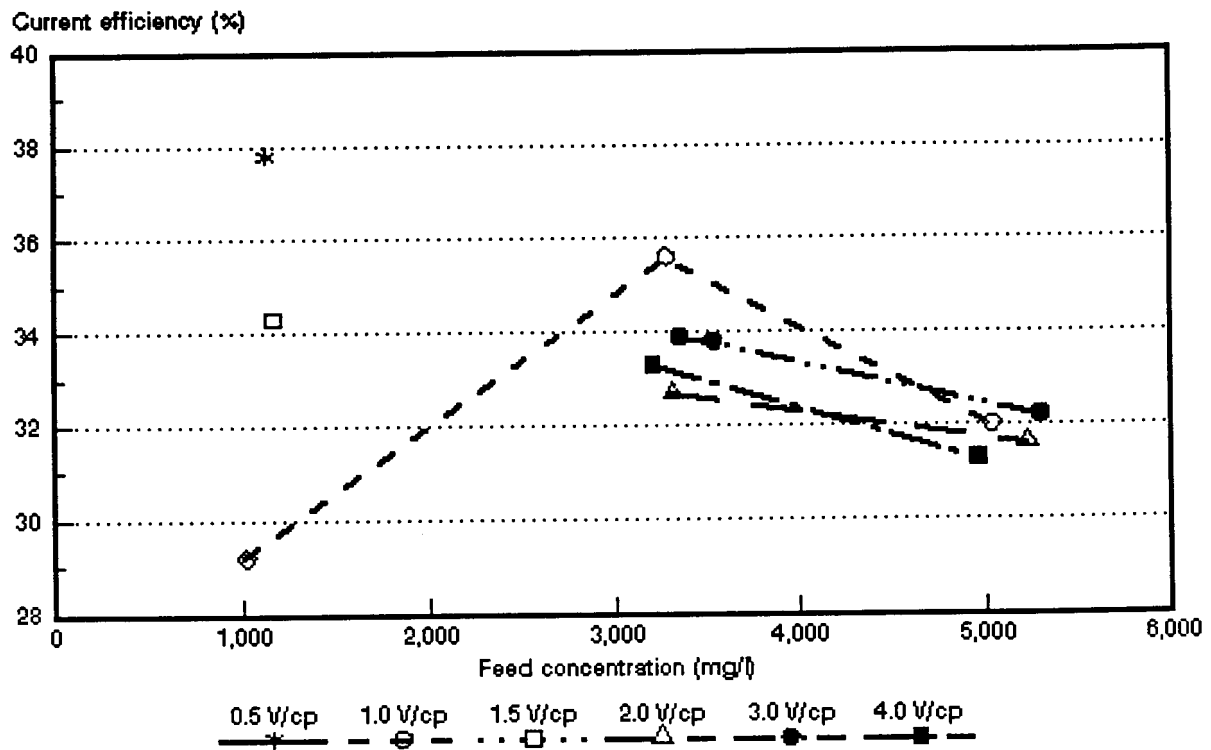


Figure 9.22: Current efficiency as a function of hydrochloric acid feed concentration and cell pair voltage.

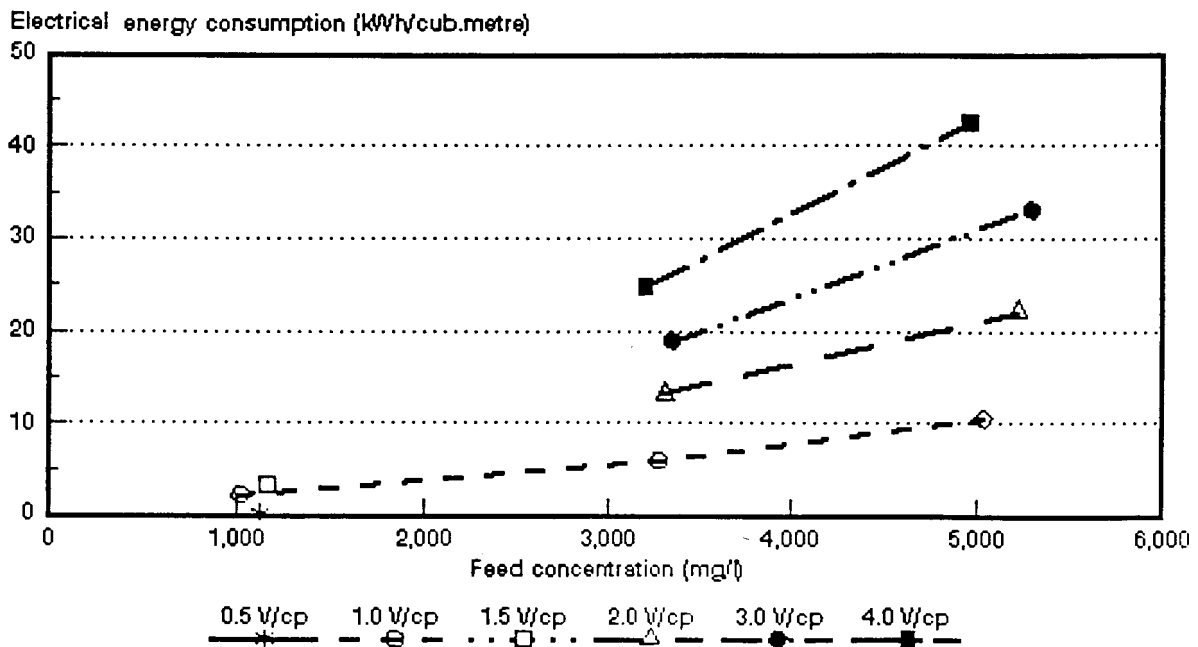


Figure 9.23: Electrical energy consumption as a function of hydrochloric acid feed concentration and cell pair voltage.

9.2.6 Effective cell pair thickness and cell pair resistance

An example of cell pair resistance (R_{cp}) as a function of the specific resistance of the dialysate and cell pair voltage is shown in Figure 9.24 for an approximately 5 000 mg/l hydrochloric acid feed solution. Straight lines were obtained over the cell pair voltage range studied. The slope of the lines increased with increasing cell pair voltage as was experienced with sodium chloride solutions. However, the slopes of the lines were much steeper in the case of the acid especially at the higher cell pair voltages.

The effective cell pair thickness, d_{eff} , was determined at 13,5; 25,6; 35,9 and 44,9 mm at 1; 2; 3 and 4 V/cp, respectively (5 000 mg/l feed) (Table 9.2). Effective cell pair thickness decreased significantly with increasing linear flow velocity. The effective cell pair thickness decreased from 13,8 mm to 8,1 mm at 1 V/cp (3 000 mg/l feed).

Cell pair resistance, R_{cp} , decreased with increasing feed concentration and decreasing cell pair voltage. The negative cell pair resistances reported in Table 9.2 could be ascribed to experimental error due to the very low resistance of the cell pair.

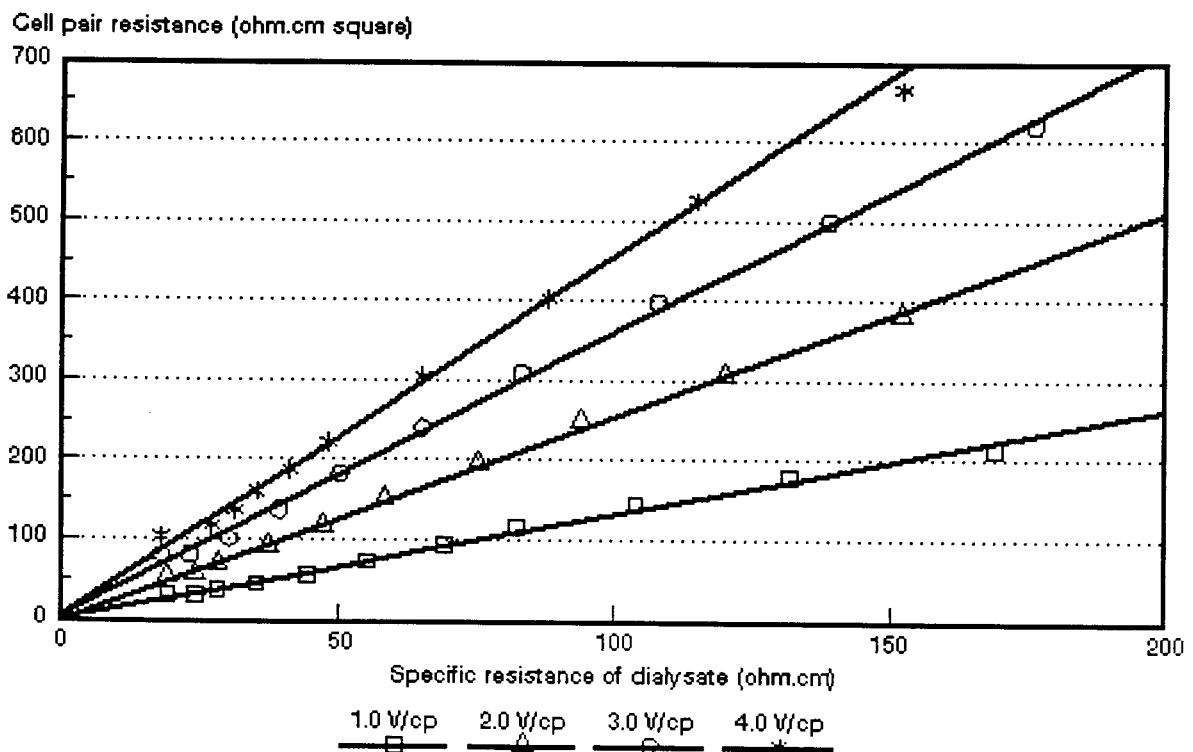


Figure 9.24: Cell pair resistance as a function of specific resistance of the dialysate and cell pair voltage for approximately 5 000 mg/l hydrochloric acid solutions.

9.3 Concentration/Desalination of Caustic Soda Solutions with *Selemion* AMV and CMV Membranes

The concentration/desalination results of different caustic soda feed water concentrations at different cell pair voltages are summarized in Table 9.3.

9.3.1 Brine and dialysate concentration

Dialysate and brine concentrations as a function of time and cell pair voltage for different initial feed water concentrations are shown in Figs. 9.25 to 9.30. Caustic soda brine concentration as a function of feed concentration and cell pair voltage is shown in Figure 9.31. A typical example of electric current as a function of time and cell pair voltage for an approximately 5 000 mg/ℓ caustic soda feed solution is shown in Figure 9.32.

Desalination/concentration rate increased with increasing cell pair voltage (Figs. 9.25 to 9.30 and Fig. 9.32). Brine concentration increased as a function of feed concentration and cell pair voltage (Table 9.3 and Fig. 9.31). Caustic soda brine concentrations of 2,8 to 9,8% were obtained in the feed and cell pair voltage ranges of approximately 1 000 to 10 000 mg/ℓ and 0,5 to 3,0 V/cp, respectively.

Product water with a concentration of less than 400 mg/ℓ caustic soda could be produced (Table 9.3) from caustic soda feed waters in the feed and cell pair voltage ranges of 1 000 to 10 000 mg/ℓ and 0,5 to 3,0 V/cp, respectively. It was possible to produce a product water with a concentration of less than 100 mg/ℓ caustic soda.

Concentration factors increased with increasing cell pair voltage and decreased with increasing feed concentration as was experienced with sodium chloride and hydrochloric acid solutions.

9.3.2 Brine volume and water recovery

Low brine volumes and high water recoveries were again obtained (Table 9.3). Brine volume varied between 2,3 and 7,3% in the caustic soda feed water and cell pair voltage ranges of 1 000 to 5 000 mg/ℓ and 0,5 to 3 V/cp, respectively. Brine volume further increased with increasing caustic soda feed water concentration in the feed concentration range from 1000 to 10 000 mg/ℓ. The highest brine volume of 11,7%

Table 9.3: Concentration/desalination results of caustic soda solutions at different feed concentrations and cell pair voltages using Selemion AMV and CMV membranes.

Vcp	c_i mg/l	c_p mg/l	c_b mg/l	CF	CE %	WR %	BV %	EEC kWh/m ³	OP m ³ /m ² ·d	d_{eff} mm	Rcp ohm cm ²
0,5	1 008	168	30 000	29,8	75,1	97,7	2,3	0,77	0,42	6,03	56,1
1,0	1 056	120	28 000	26,5	68,96	97,55	2,45	0,91	0,44	11,6	54,8
	2 920	400	60 000	20,6	77,96	96,8	3,2	2,18	0,47		
	5 480	224	64 000	11,7	77,80	92,7	7,3	4,54	0,33		
	10 640	400	90 000	8,5	73,3	88,3	11,7	9,40	0,33	12,64	0,15
1,5	1 104	96	30 000	27,2	71,98	97,6	2,4	1,41	0,51	11,99	146,8
2,0	3 400	400	80 000	23,5	81,2	96,9	3,1	4,97	0,73	13,59	7,1
	4 960	85	76 000	15,3	78,1	93,75	6,25	8,38	0,43		
	10 880	320	98 000	9,0	73,1	90,0	10,0	19,42	0,56		
3,0	3 200	384	84 000	26,3	79,2	97,0	3,0	7,18	1,27		
	5 560	256	86 000	15,5	78,36	94,6	5,4	13,64	0,92		

Linear flow velocity 1 cm/s.

CF = concentration factor

CE = current efficiency

BV = brine volume

OP = output (yield)

WR = water recovery

EEC = electrical energy consumption

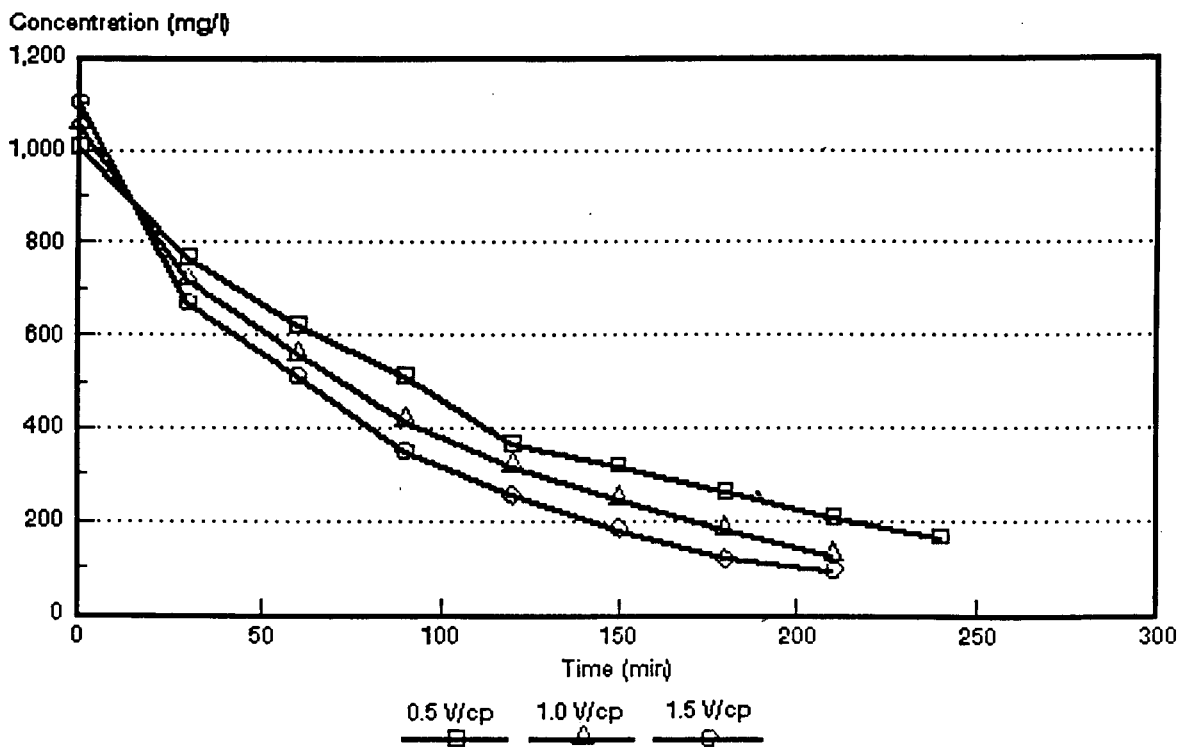


Figure 9.25: Dialysate concentration as a function of time and cell pair voltage for an approximately 1 000 mg/l caustic soda feed solution.

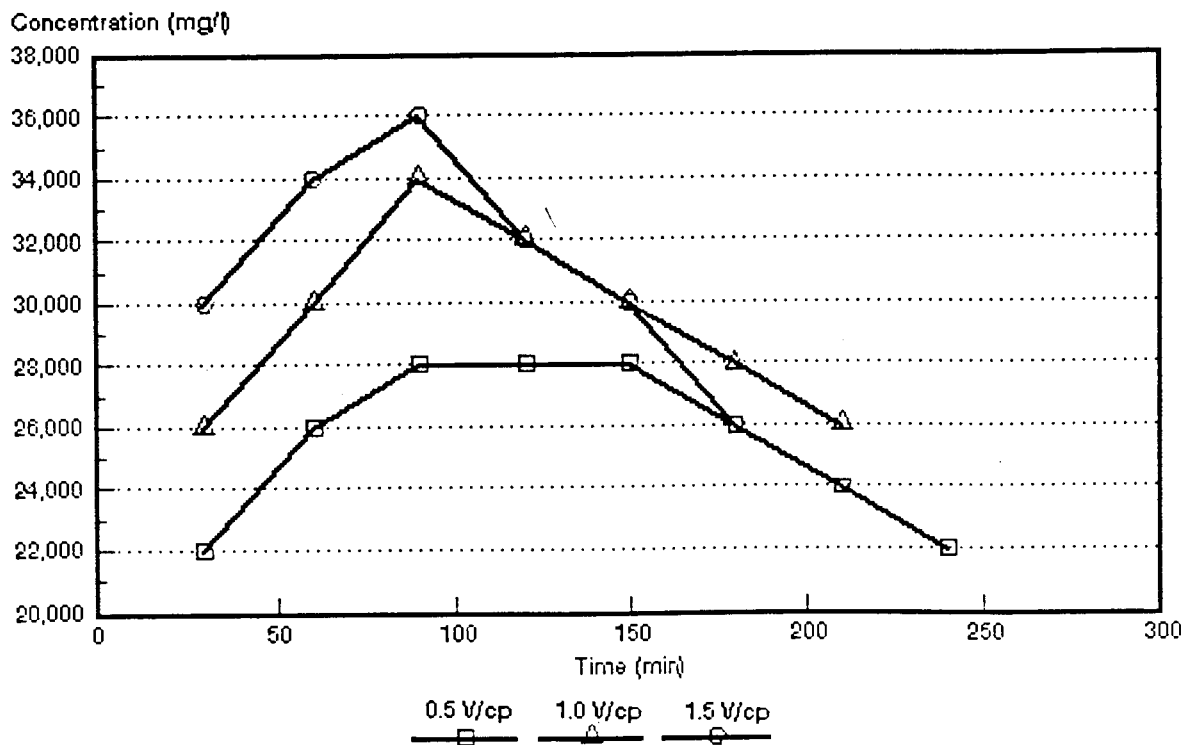


Figure 9.26: Brine concentration as a function of time and cell pair voltage for an approximately 1 000 mg/l caustic soda feed solution.

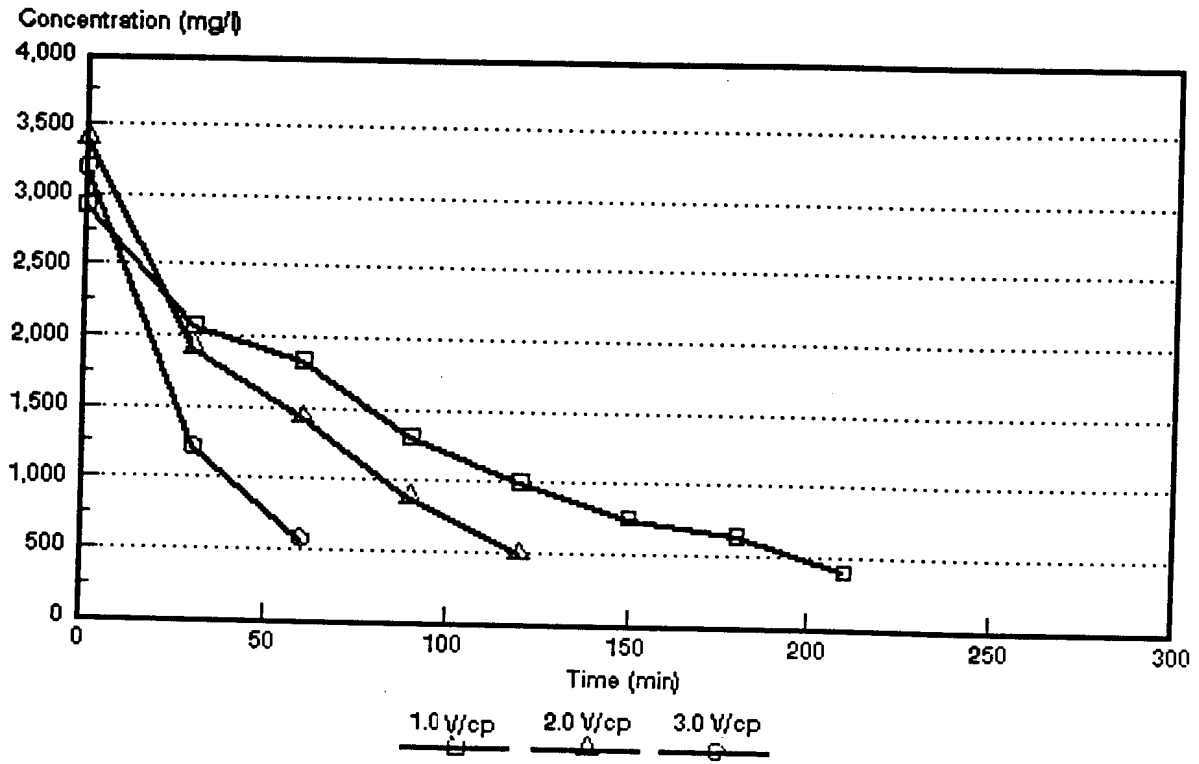


Figure 9.27: Dialysate concentration as a function of time and cell pair voltage for an approximately 3 000 mg/l caustic soda feed solution.

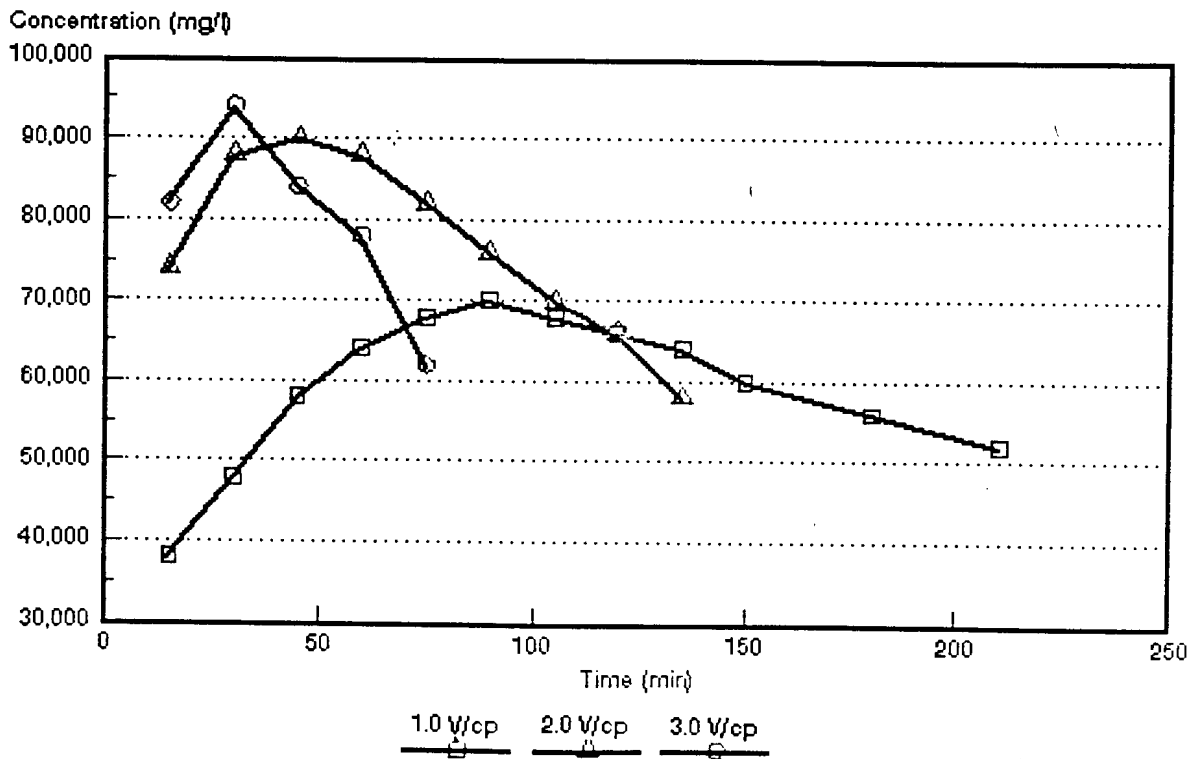


Figure 9.28: Brine concentration as a function of time and cell pair voltage for an approximately 3 000 mg/l caustic soda feed solution.

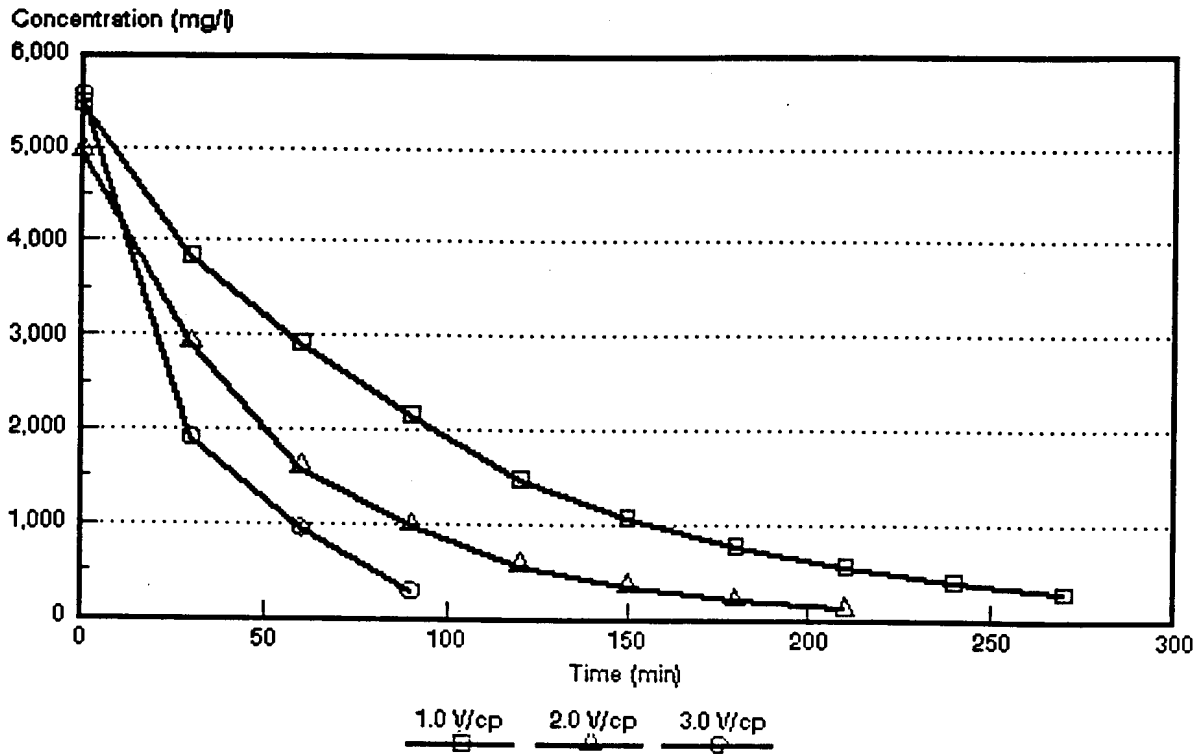


Figure 9.29: Dialysate concentration as a function of time and cell pair voltage for an approximately 5 000 mg/l caustic soda feed solution.

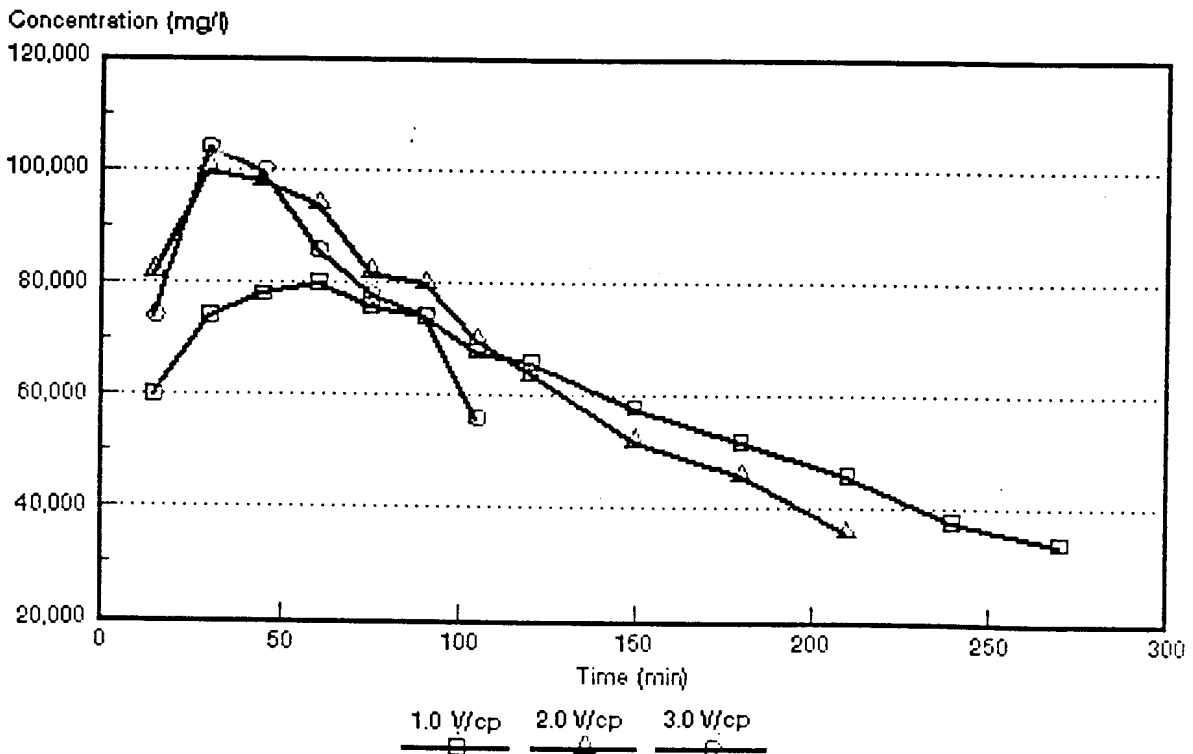


Figure 9.30: Brine concentration as a function of time and cell pair voltage for an approximately 5 000 mg/l caustic soda feed solution.

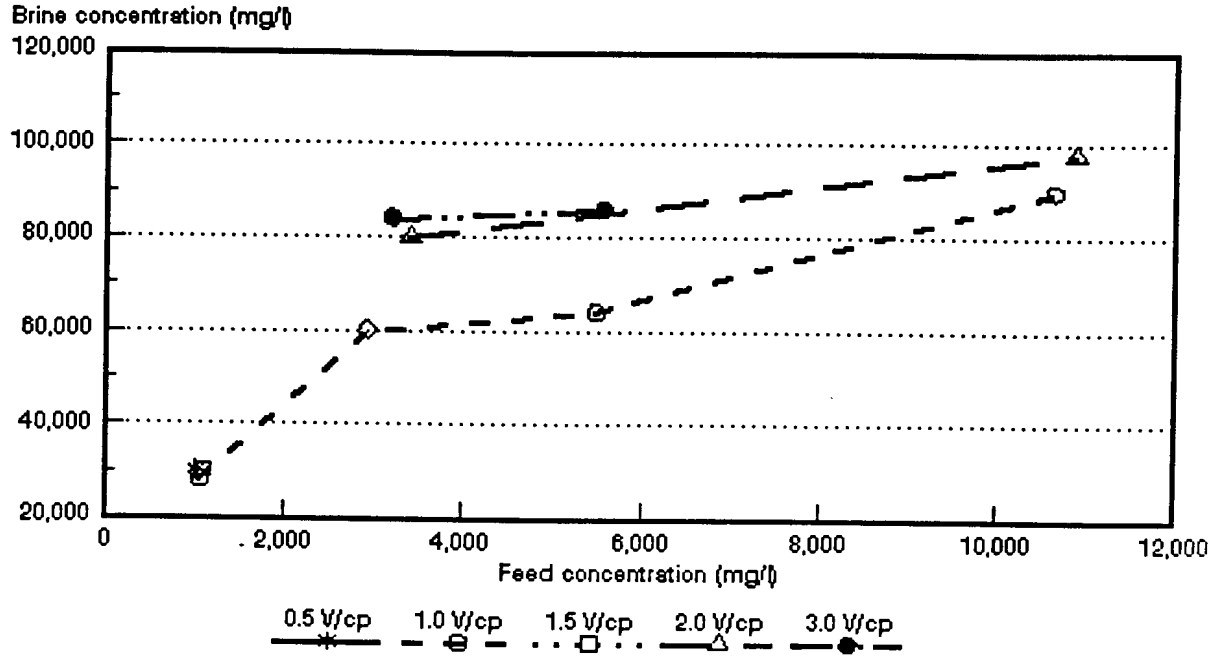


Figure 9.31: Brine concentration as a function of sodium hydroxide feed concentration and cell pair voltage.

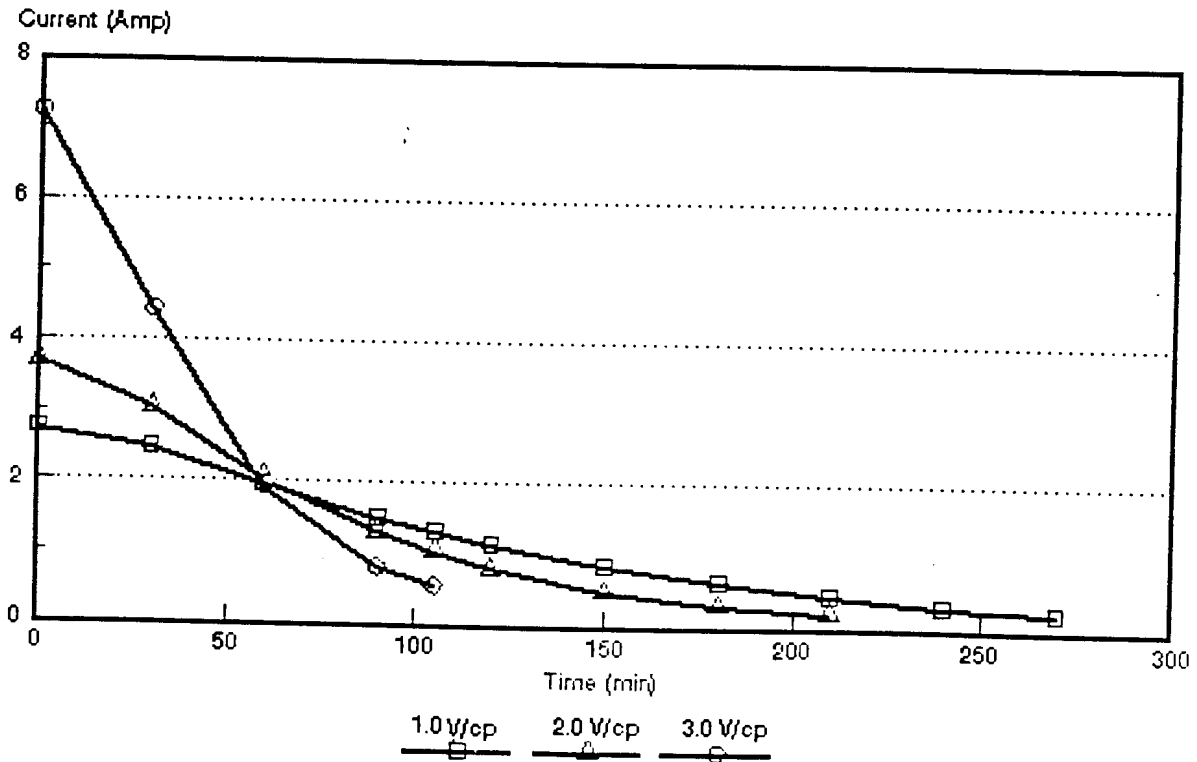


Figure 9.32: Current as a function of time and cell pair voltage for an approximately 5 000 mg/l caustic soda solution.

was obtained at a caustic soda feed water concentration of approximately 10 000 mg/ℓ (1,0 V/cp). Water recoveries were high. Water recoveries of 93 to 97,5% were obtained in the caustic soda feed water concentration range from 1 000 to 5 000 mg/ℓ.

9.3.3 Current efficiency

Current efficiency increased with increasing caustic soda feed water concentration at 1,0 V/cp (Table 9.3 and Fig. 9.33). However, current efficiency slightly decreased with increasing caustic soda feed water concentration at the other cell pair voltages. Current efficiency did not decrease significantly with increasing cell pair voltage.

Current efficiencies of 73,3 to 77,9% were obtained in the caustic soda feed water and cell pair voltage ranges of 1 000 to 10 000 mg/ℓ and 0,5 to 1,5 V/cp, respectively. Current efficiencies of 73,1 to 81,2% were obtained in the caustic soda feed water and cell pair voltage ranges of 3 000 to 10 000 mg/ℓ and 2,0 to 3,0 V/cp, respectively.

9.3.4 Electrical energy consumption

Electrical energy consumption increased with increasing caustic soda feed water concentration and increasing cell pair voltage (Table 9.3 and Fig. 9.34). Electrical energy consumption was low at low cell pair voltages (0,5 to 1,5) and low feed concentrations (1 000 to 3 000 mg/ℓ). Electrical energy consumption varied between 0,4 and 2,2 kWh/m³ product water in this range. However, electrical energy consumption became higher at higher cell pair voltages and caustic soda feed water concentrations. An electrical energy consumption of 19,4 kWh/m³ product water was obtained at a cell pair voltage of 2,0 and a caustic soda feed water concentration of approximately 11 000 mg/ℓ.

9.3.5 Product water yield

Product water yield increased with increasing cell pair voltage and decreased with increasing feed concentration (Table 9.3).

9.3.6 Effective cell pair thickness and cell pair resistance

An example of cell pair resistance (R_{cp}) as a function of the specific resistance of the dialysate and cell pair voltage is shown in Figure 9.35 (approximately 1 000 mg/ℓ

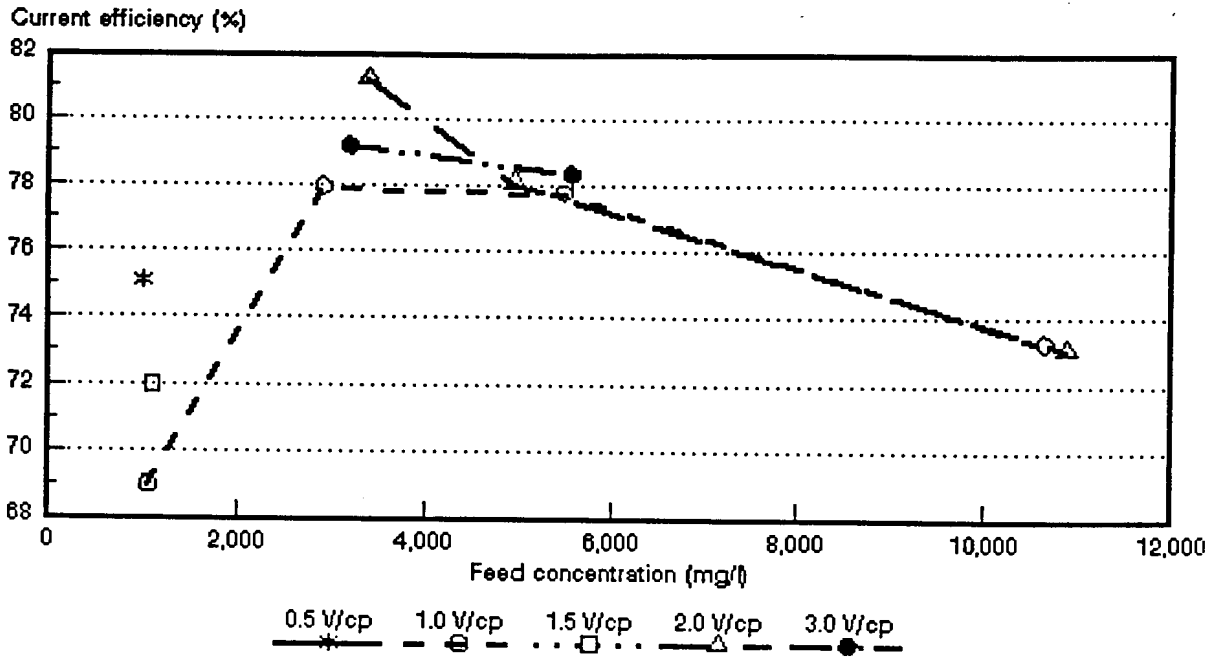


Figure 9.33: Current efficiency as a function of sodium hydroxide feed concentration and cell pair voltage.

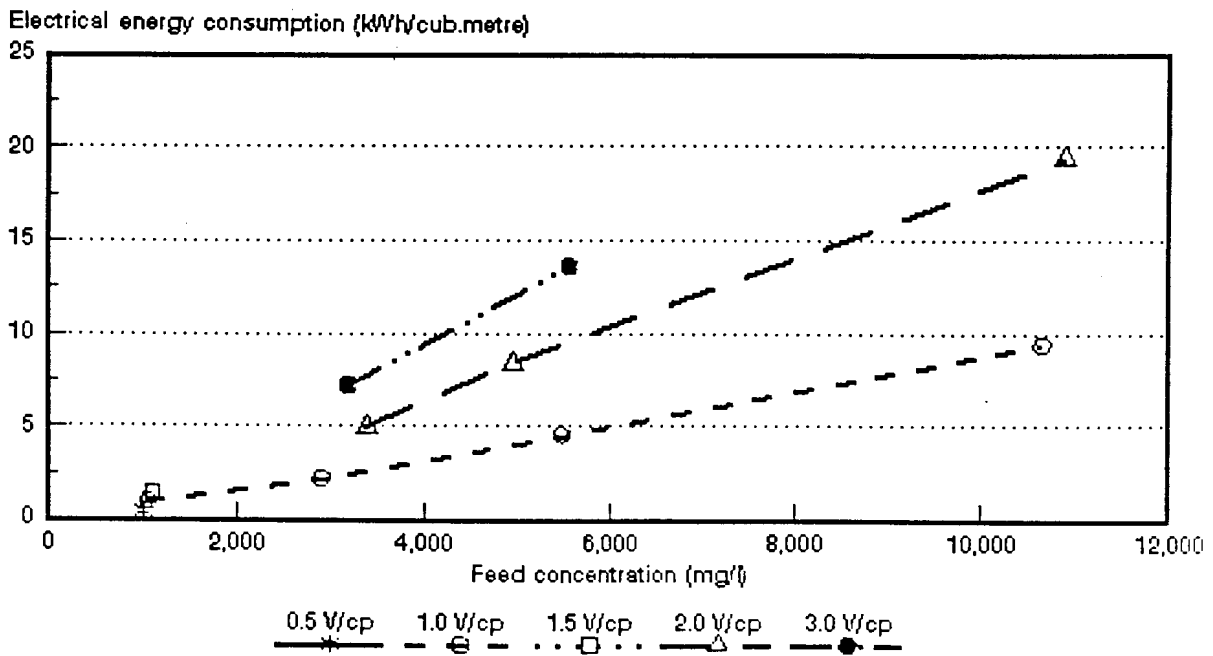


Figure 9.34: Electrical energy consumption as a function of sodium hydroxide feed concentration and cell pair voltage.

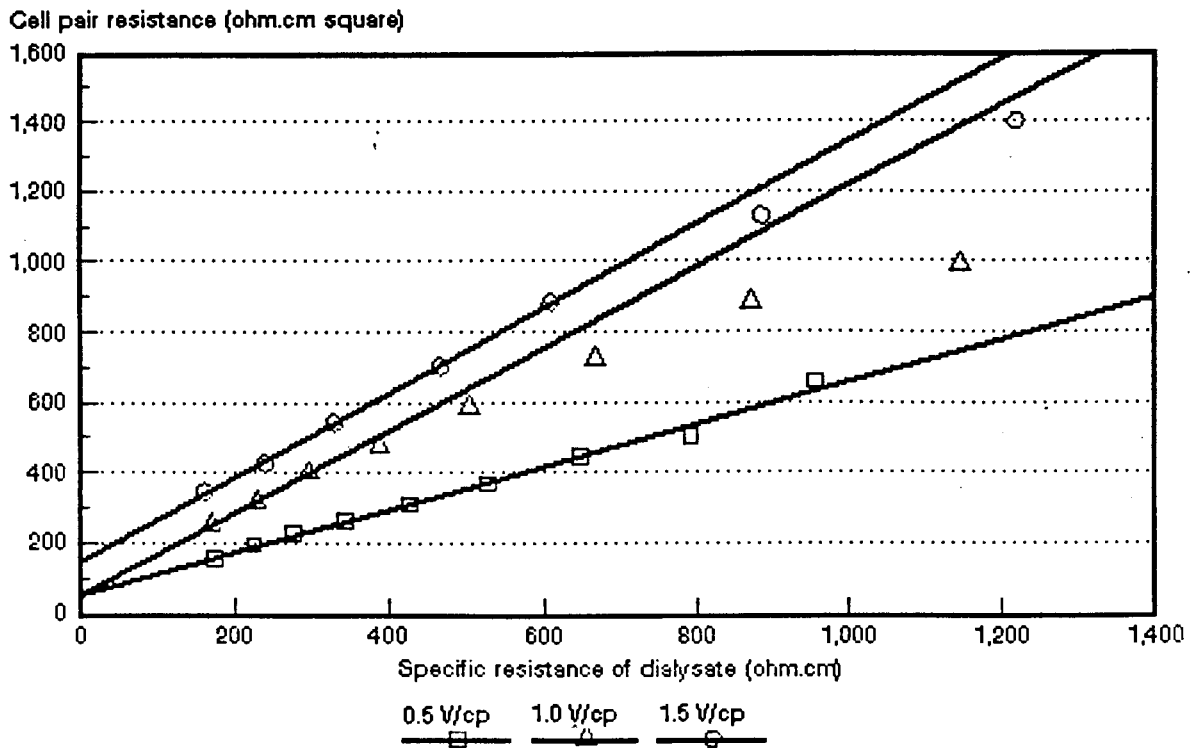


Figure 9.35: Cell pair resistance as a function of specific resistance of the dialysate and cell pair voltage for approximately 1 000 mg/l caustic soda solution.

caustic soda feed). Polarization increased with increasing cell pair voltage in the cell pair voltage range from 0,5 to 1,0 V/cp. The effective cell pair thickness, d_{eff} , was determined at 6,03 mm at 0,5 V/cp (1 000 mg/l feed). Cell pair thickness was 11,6 at 1,0 V/cp (1 000 mg/l feed) and 11,99 at 1,5 V/cp (1 000 mg/l feed). This showed that polarization was approximately the same at 1,0 and 1,5 V/cp.

Cell pair resistance decreased with increasing feed concentration (Table 9.3). A cell pair resistance of only 0,15 ohm·cm² was obtained at 10 000 mg/l caustic soda feed concentration (1,0 V/cp).

10. CONCENTRATION/DESALINATION OF SALT SOLUTIONS AND INDUSTRIAL EFFLUENTS WITH SCED

10.1 Concentration of salt solutions

A summary of the concentration/desalination results of the different salt solutions is shown in Tables 10.1 to 10.5.

10.1.1 Desalination rate, product and brine concentration

Examples of the desalination/concentration of sodium chloride, ammonium nitrate and sodium sulphate solutions as a function of time at constant cell pair voltage are shown in Figures 10.1 to 10.3. The effect of increasing cell pair voltage on desalination/concentration of an approximately 1 000 mg/l sodium sulphate solution is shown in Figure 10.4.

Desalination rate decreased with decreasing feed concentration (Figs. 10.1 to 10.3) and decreasing cell pair voltage (Figure 10.4). However, approximately the same initial desalination rate was obtained at 1,18 and 1,76 V/cp (Figure 10.4). The optimum cell pair voltage for desalination regarding polarization and electrical energy consumption should be determined for each feed concentration, because this information is required to operate an ED stack under optimum conditions. This, however, was not the main purpose of this investigation. The main purpose of this investigation was to evaluate the performance of the SCED unit for concentration/desalination of saline solutions at cell pair voltages normally applied in ED.

All the different salt solutions could be easily desalinated from approximately 10 000 mg/l to 300 mg/l and less (Figs. 10.1 to 10.3 and Tables 10.1 to 10.5). Product concentrations of less than 100 mg/l could be obtained with ease in some cases. Therefore, SCED appears to be effective for the production of low TDS water.

Brine concentration increased with increasing feed concentration and increasing cell pair voltage (Tables 10.1 to 10.5 and Figure 10.5). Sodium chloride, ammonium nitrate, sodium sulphate, sodium nitrate and calcium chloride brine concentrations of 2,2 to 16,1%; 4,9 to 15%; 7,8 to 16,3%; 6,0 to 12,5% and 3,8 to 7,5% could be obtained, in the feed concentration and cell pair voltage range of 0,1 to 1% and 0,59 to 1,76 V/cp, respectively. Therefore, relatively high brine concentrations could be obtained

Table 10.1: Concentration/Desalination Results of Sodium Chloride Solutions at different cell pair voltages.

Vcp	Cf mg/l	Cp mg/l	Cb mg/l	CF	CE %	WR %	BV %	EEC kWh/m ³	OP m ³ /m ² .d	d _{eff} mm	Rcp ohm-cm ²
0,59	1010	282	22 450	22,20	72,20	96,00	4,00	0,34	1,22	0,95	38,8
1,18	950	35	31 000	35,40	66,70	96,30	3,70	0,77	1,53	1,01	39,2
	1 900	40	53 500	28,10	73,70	96,50	3,50	1,41	1,36	0,91	35,1
	3 400	125	72 000	21,20	56,40	96,40	3,60	3,26	1,36	0,97	21,3
	5 400	65	82 000	15,20	78,60	94,80	5,20	3,86	1,20	0,88	18,2
	10 200	195	161 000	15,80	67,90	93,50	6,50	8,04	1,19	0,87	14,4
1,76	985	25	37 000	37,70	63,90	96,70	3,30	1,25	1,75	1,09	46,5
	1 700	25	53 500	31,10	67,80	96,40	3,60	2,07	1,53	1,08	32,9
	2 700	48	72 000	27,40	55,20	96,50	3,50	3,74	1,75	1,05	26,7
	4 850	25	82 000	17,40	69,60	94,60	5,40	5,82	1,20	0,90	21,8
	9 400	120	161 000	18,10	71,90	94,00	6,00	11,10	1,49	0,95	15,1

Vcp = cell pair voltage
 Cf = feed concentration
 Cp = product concentration
 Cb = brine concentration
 CF = concentration factor
 CE = current efficiency
 WR = water recovery
 BV = brine volume
 EEC = electrical energy consumption
 OP = output
 d_{eff} = thickness of dialysate
 Rcp = cell pair resistance

Table 10.2: Concentration/Desalination Results of Ammonia Nitrate Solutions at different cell pair voltages

Vcp	Cf mg/l	Cp mg/l	Cb mg/l	CF	CE %	WR %	BV %	EEC kWh/m ³	OP m ³ /m ² .d	d _{eff} mm	Rcp ohm-cm ²
0.59	580	240	58 000	100,00	29,70	99,30	0,70	0,23	1,58	0,97	25,6
	1 010	230	80 000	79,60	43,50	98,90	1,10	0,35	1,26	0,97	24,6
1.18	435	50	49 000	112,60	28 70	99,30	0,70	0,54	1,58	0,67	68,2
	1 100	55	87 500	79,60	51,80	98,80	1,20	0,80	1,39	0,84	38,6
	1 800	90	82 500	45,80	45,80	98,30	1,70	1,50	1,39	0,80	38,2
	3 100	125	117 630	30,70	48,20	98,00	2,00	2,45	1,38	0,75	20,2
	4 950	190	100 000	20,20	47,20	97,20	2,80	4,09	1,37	0,79	14,5
9 100	320	146 000	16,00	49,40	95,30	4,70	7,37	1,21	0,85	14,7	
1.76	420	42	64 500	153,50	22,40	99,00	1,00	1,00	1,58	0,85	45,3
	1 300	60	78 000	60,00	36,30	98,70	1,30	2,05	1,57	1,14	35,6
	1 800	35	120 000	66,70	41,70	98,50	1,50	2,54	1,39	0,87	28,8
	2 800	35	150 000	53,60	47,20	98,10	1,90	3,55	1,24	1,02	19,0
	4 525	45	136 500	30,20	47,20	97,30	2,70	6,78	1,24	1,06	12,8
	9 800	70	130 000	13,30	46,50	94,70	5,30	13,09	1,20	0,87	11,2

Table 10.3: Concentration/Desalination Results of Sodium Sulphate Solutions at different cell pair voltages.

Vcp	Cf mg/t	Cp mg/t	Cb mg/t	CF	CE %	WR %	BV %	EEC kWh/m ³	OP m ³ /m ² .d	d _{av} mm	Rcp ohm-cm ²
0.59	1 110	165	78 500	70,70	79,30	98,90	1,10	0,27	1,40	0,84	65,6
1.18	1 100	50	81 000	73,60	71,90	98,70	1,30	0,66	1,57	0,99	57,2
	2 100	70	120 000	57,10	71,70	98,50	1,50	1,28	1,39	0,99	47,7
	3 400	95	132 000	38,80	76,20	98,10	1,90	1,97	1,25	0,75	37,2
	5 350	445	133 000	24,80	62,30	97,50	2,50	3,59	1,24	1,02	32,3
	9 700	1 500	156 000	16,08	63,20	96,50	3,50	6,01	1,23	0,89	28,6
1.76	1 050	30	89 000	84,80	52,70	98,30	1,70	1,31	1,56	1,11	59,0
	1 900	35	123 000	64,60	63,40	98,50	1,50	1,99	1,39	1,25	42,8
	3 000	77	136 000	45,50	76,20	98,20	1,80	3,20	1,25	1,14	45,6
	4 950	65	134 000	27,10	62,30	97,50	2,50	4,75	1,24	1,25	29,9
	9 525	180	163 000	17,11	63,20	96,10	3,90	13,85	1,23	1,17	23,2

Table 10.4: Concentration/Desalination Results of Sodium Nitrate Solutions at different cell pair voltages

Vcp	Cf mg/t	Cp mg/t	Cb mg/t	CF	CE %	WR %	BV %	EEC kWh/m ³	OP m ³ /m ² .d	d _{av} mm	Rcp ohm-cm ²
0,59	1 100	465	65 000	59,30	41,50	98,90	1,10	0,28	1,57	1,01	28,8
1.18	1 000	90	63 500	63,3	47,0	98,6	1,40	0,73	1,57	0,99	32,1
	1 950	100	71 000	36,5	65,0,	98,4	1,60	1,07	1,39	1,01	30,4
	2 800	100	82 000	29,3	63,2	98,1	1,90	1,61	1,38	0,83	29,7
	5 000	140	102 000	20,5	56,67	97,3	2,70	3,29	1,24	0,86	19,3
	10 100	530	123 000	12,2	53,1	96,0	4,00	6,98	1,22	1,02	10,2
1.76	1 000	70	60 500	60,30	40,70	98,50	1,50	1,30	1,57	1,16	33,6
	2 100	60	69 500	33,10	51,30	98,20	1,80	2,25	1,39	1,12	28,3
	2 800	50	81 000	29,00	53,80	98,00	2,00	2,90	1,38	1,06	25,3
	5 200	90	117 000	22,50	55,00	97,10	3,90	5,34	1,23	1,27	17,0
	9 800	150	125 000	12,80	51,80	95,60	4,40	10,85	1,21	1,27	10,7

Table 10.5: Concentration/Desalination Results of Calcium Chloride Solutions at different cell pair voltages.

Vcp	Cf mg/l	Cp mg/l	Cb mg/l	CF	CE %	WR %	BV %	EEC kWh/m ³	OP m ³ /m ² .d	deff mm	Rcp ohm-cm ²
0,59	1 100	310	42 000	38,20	47,80	98,70	1,30	0,48	1,57	0,93	40,3
1.18	970	50	41 200	42,50	45,70	98,50	1,50	1,17	1,56	1,05	36,4
	2 100	110	51 000	24,30	49,70	97,80	2,20	2,34	1,38	1,15	27,5
	2 950	160	57 000	19,30	46,30	97,20	2,80	3,53	1,37	1,19	19,9
	5 000	230	75 000	14,00	45,70	95,80	4,20	6,21	1,22	1,19	15,4
	10 300	940	75 000	7,30	44,30	92,70	7,30	13,06	1,18	1,12	9,6
1.76	840	20	38 500	45,80	36,50	98,50	1,50	1,94	1,56	1,18	34,7
	2 000	35	45 500	22,80	48,10	97,80	2,20	3,57	1,38	1,32	28,2
	3 000	85	54 500	18,20	43,40	97,00	3,00	5,91	1,37	1,37	22,9
	5 050	65	73 000	14,50	43,20	95,60	4,40	10,31	1,22	1,31	14,0

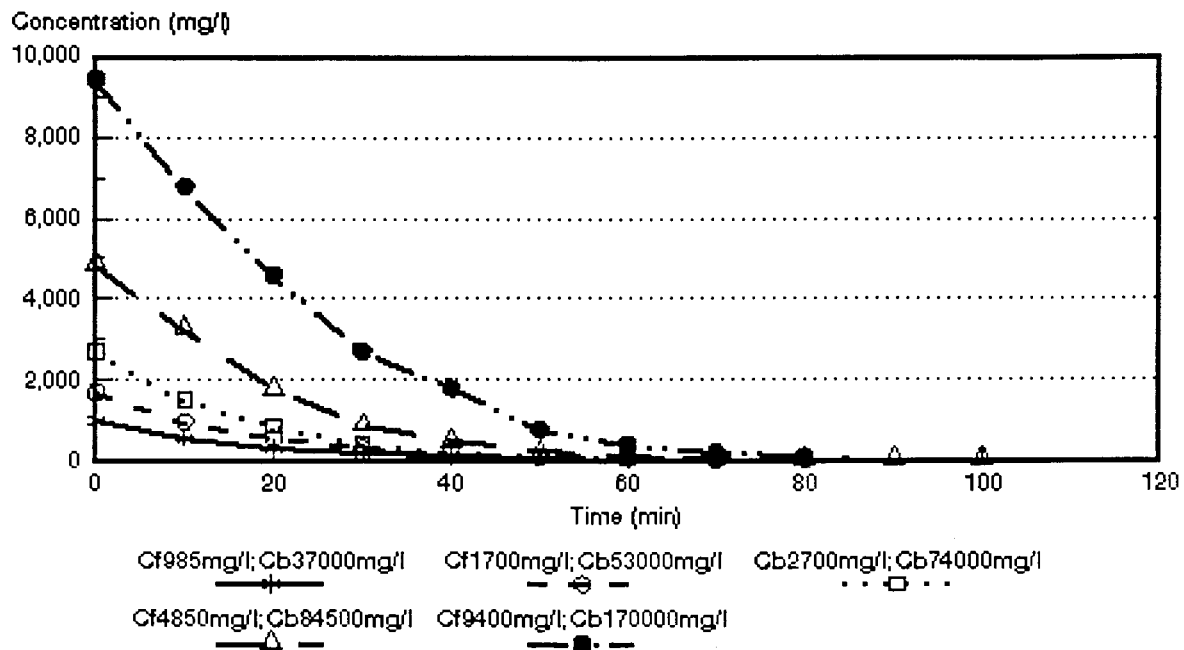


Figure 10.1: Concentration/desalination of different sodium chloride feed concentrations at 1,76 V/cp.

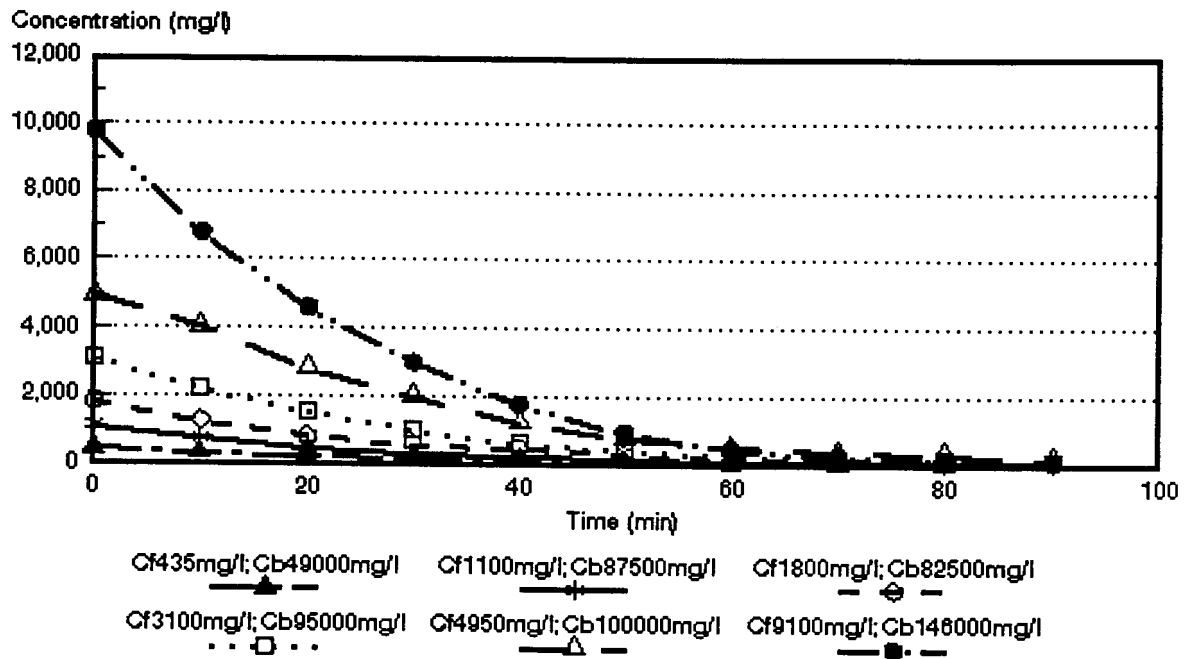


Figure 10.2: Desalination/concentration of different ammonium nitrate feed concentrations at 1,18 V/cp.

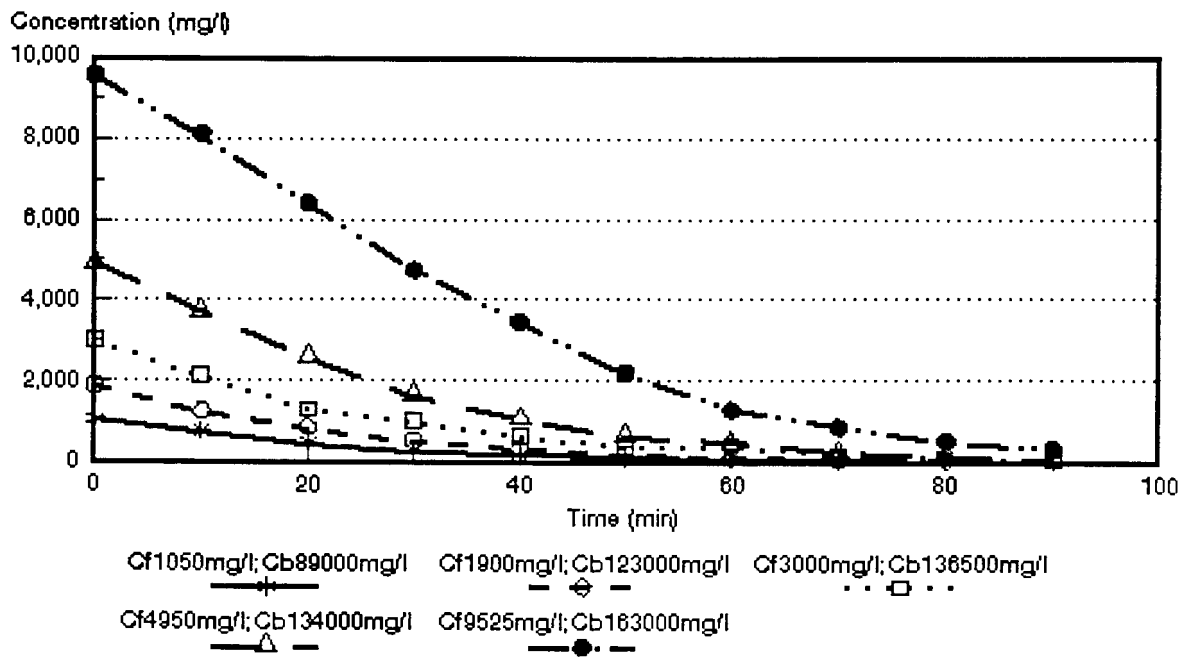


Figure 10.3: Desalination/concentration of different sodium sulphate feed concentrations at 1,76 V/cp.

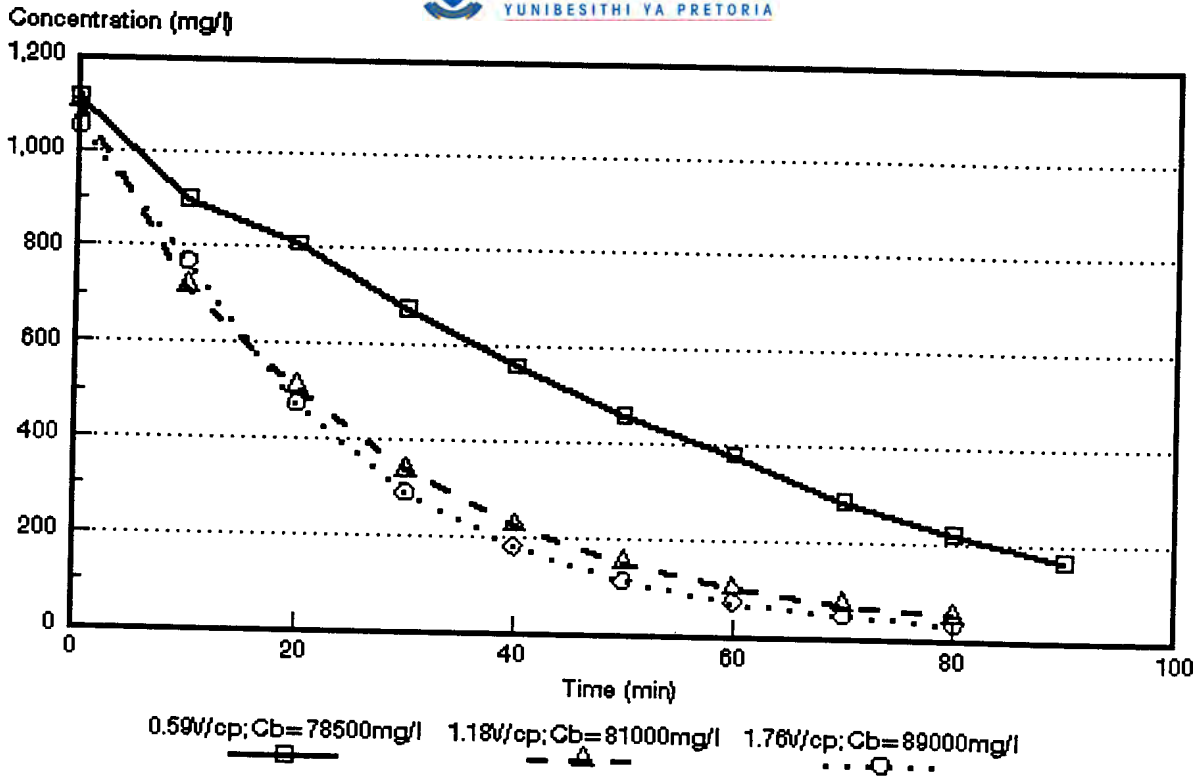


Figure 10.4: Desalination/concentration of sodium sulphate solutions at different cell pair voltages.

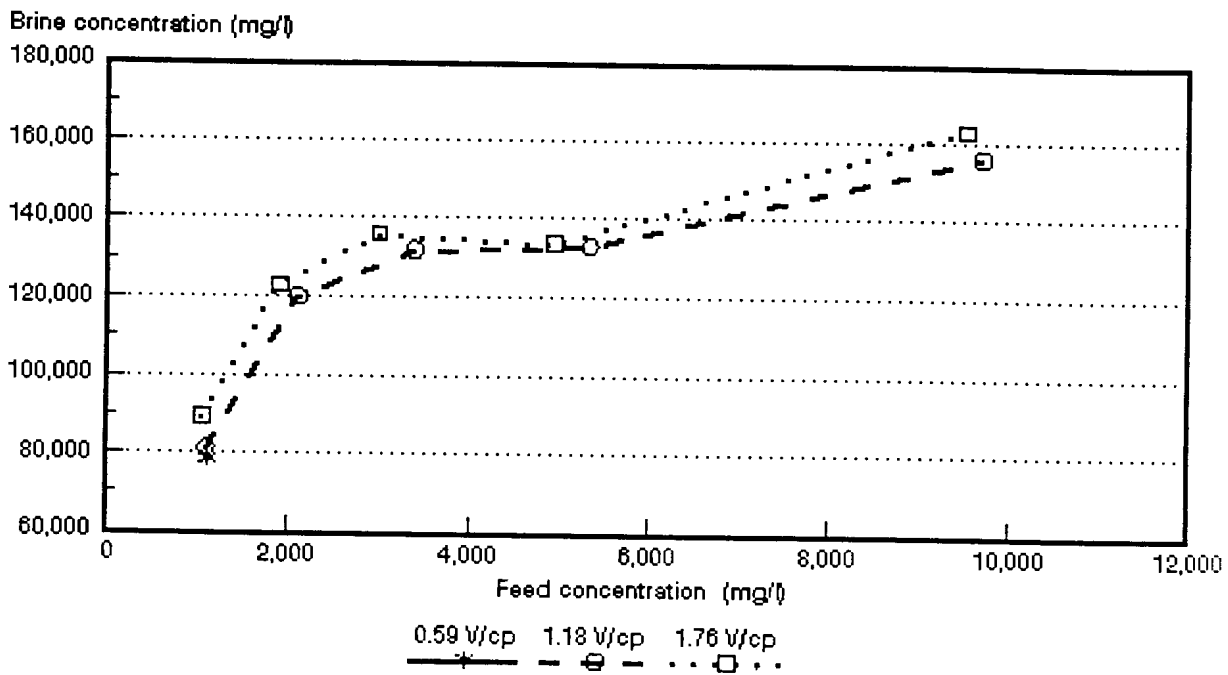


Figure 10.5: Brine concentration as a function of sodium sulphate feed concentration and cell pair voltage.

which would make the SCED technique suitable for concentration/desalination of industrial effluents. It is interesting to note that relatively low brine concentrations have been obtained with calcium chloride solutions (Table 10.5) in comparison with the other ions. However, the low current efficiency obtained with calcium chloride solutions explained the low brine concentrations that were obtained.

Concentration factors (brine/feed) decreased with increasing feed concentration (Tables 10.1 to 10.5). Therefore, there is a limit to the brine concentration that can be achieved. The brine concentration that can be obtained depends *inter alia* on the permselectivity of the ion-exchange membranes, feed concentration and current density used^(6, 115). Ion-exchange membranes tend to lose their permselectivity at high concentration due to backdiffusion of salt with the result that there is a limit to the brine concentration that can be achieved.

10.1.2 Current efficiency

Current efficiency increased with increasing feed concentration and decreasing cell pair voltage (Tables 10.1 to 10.5 and Figure 10.6). Current efficiency, however, decreased slightly at higher feed concentrations due to the lower permselectivity of the ion-exchange membranes at high feed concentration. Increasing current efficiency with increasing feed concentration may be ascribed to a higher flow of electro-osmotic water through the membranes at increasing feed concentration.

Current efficiencies of 55 to 74%; 30 to 52%; 53 to 79%; 42 to 65% and 37 to 50% were obtained with sodium chloride, ammonium nitrate, sodium sulphate, sodium nitrate and calcium chloride solutions, respectively, in the concentration and cell pair voltage ranges studied. Relatively low current efficiencies were obtained with ammonium nitrate and calcium chloride solutions. This shows that the ion-exchange membranes used do not have a very high permselectivity for ammonium nitrate and calcium chloride solutions.

10.1.3 Water recovery and brine volume

High water recovery and low brine volume were obtained at low to moderately high feed (1 000 to 3 000 mg/l) concentrations (Tables 10.1 to 10.5). Brine volumes between 3 and 4%; 1 and 2%; 1 and 2%; 1 and 2% and 1 and 3% were obtained with sodium chloride, ammonium nitrate, sodium sulphate, sodium nitrate and calcium

chloride solutions, respectively. Higher brine volumes (3 to 7%), however, were obtained at higher feed concentrations (5 000 to 10 000 mg/ℓ). Therefore, very low brine volumes could be obtained with SCED. This low brine volume that is produced with SCED can reduce brine disposal cost significantly especially where brine is to be trucked away for disposal.

Excellent water recoveries were obtained. Water recoveries of approximately 96% were obtained in the feed concentration range of 1 000 to 3 000 mg/ℓ and of approximately 94% in the feed concentration range from 5 000 to 10 000 mg/ℓ. These high water recoveries and low brine volumes are significantly better than water recoveries of approximately 80% which is normally obtained with conventional electrodialysis.

10.1.4 Electrical energy consumption

Electrical energy consumption increased with increasing feed concentration and cell pair voltage (Figure 10.7 and Tables 10.1 to 10.5). Very low electrical energy consumptions (0,27 to 0,48 kWh/m³ product water) were obtained at a cell pair voltage of 0,59 in the 1 000 mg/ℓ feed concentration range. Electrical energy consumptions of 0,66 to 5,91 kWh/m³ were obtained in the feed concentration range of 1 000 to 3 000 mg/ℓ (1,18 to 1,76 V/cp range). Higher electrical energy consumption (3,29 to 13,06 kWh/m³) was encountered in the feed concentration range from 5 000 to 10 000 mg/ℓ.

Electrical energy consumption was determined for ion transport only. The voltage drop across the electrode compartments was not taken into consideration because it is usually insignificant in a large membrane stack containing many membrane pairs (300 membrane pairs or more)⁽⁷⁾. The electrical energy consumption obtained during SCED usage would give a good indication of the operational cost that could be expected with SCED applications.

10.1.5 Product water yield

Product water yield (output) increased with increasing cell pair voltage and decreased with increasing feed concentration (Tables 10.1 to 10.5). Product water yield is a very important engineering design parameter because the membrane area required for a certain flow rate can be calculated from this figure.

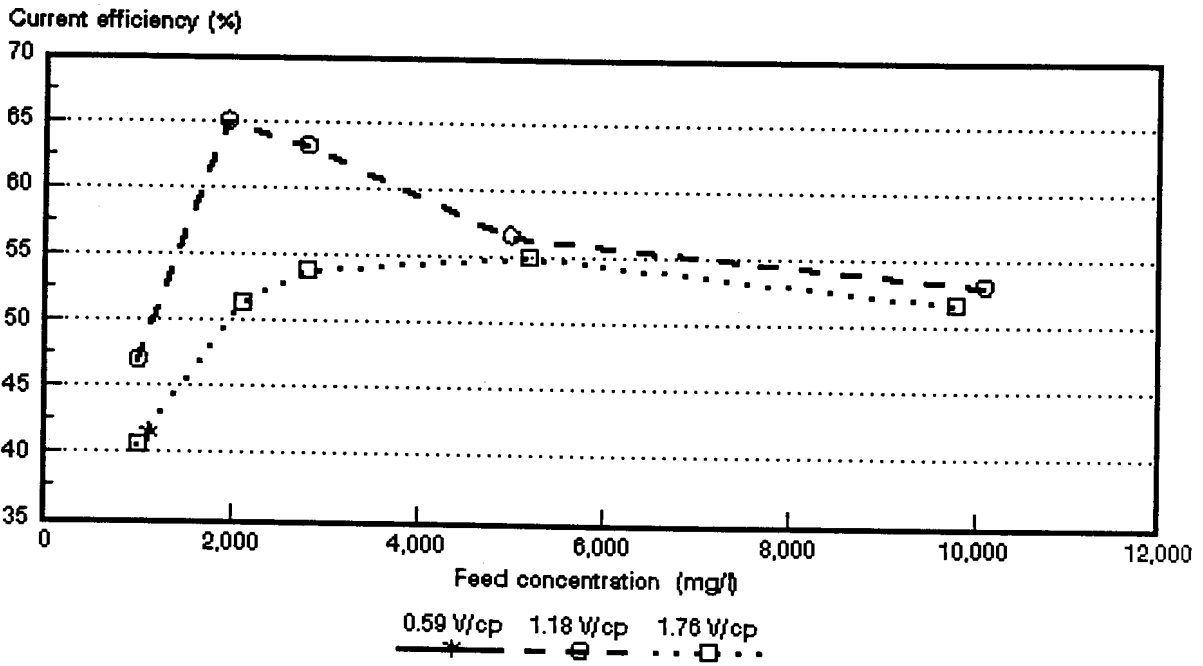


Figure 10.6: Current efficiency as a function of sodium nitrate feed concentration and cell pair voltage.

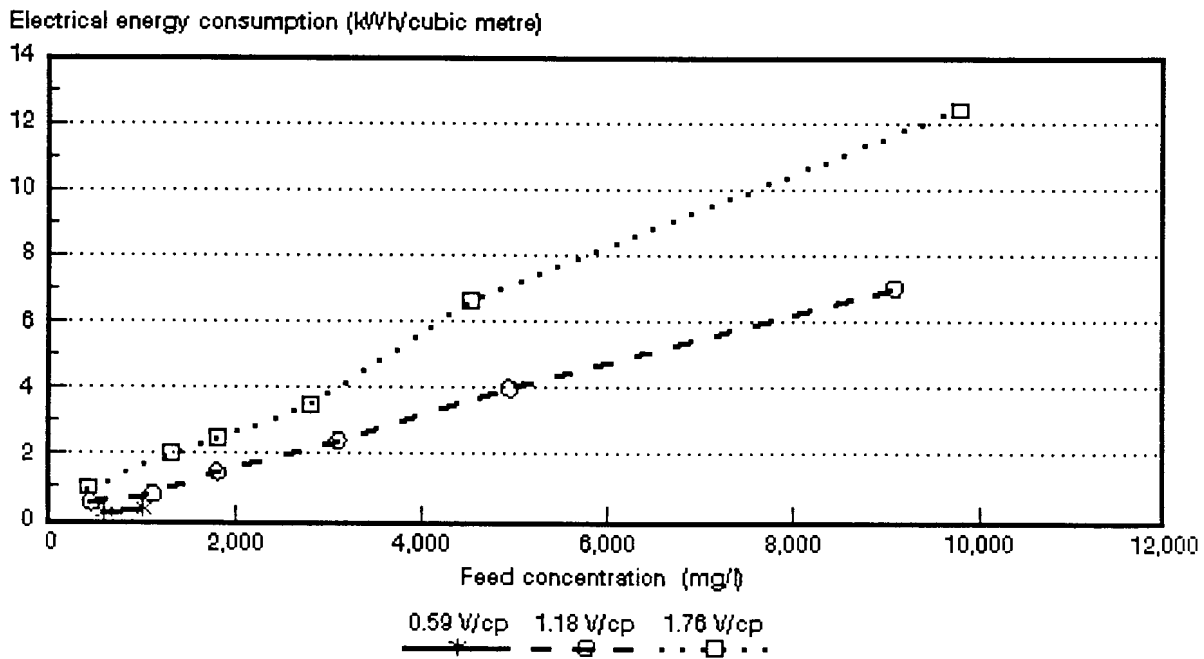


Figure 10.7: Electrical energy consumption as a function of ammonium nitrate feed concentration and cell pair voltage.

10.1.6 Cell pair resistance (R_{cp}) and effective thickness (d_{eff}) of the dialysate compartment

Cell pair resistance as a function of the specific resistance of the dialysate for sodium sulphate solutions at different cell pair voltages is shown in Figure 10.8. Similar graphs were obtained for the other salt solutions. The lines consist of a linear region followed by a curved region⁽¹¹⁶⁾. The line starts to curve when the specific resistance of the dialysate becomes very high. Linear regression through the linear region of the lines gives d_{eff} (slope) and the cell pair resistance (R_{cp}) (y-intercept). The lines show that polarization and hence effective thickness of the dialysate compartment depends on cell pair voltage. The effective thickness of the dialysate compartment increased from 0,84 (at 0,59 V/cp), 0,99 mm (at 1,18 V/cp) to 1,11 mm (at 1,76 V/cp). Membrane resistance (R_m) for the sum of the anion- and cation-exchange membranes was determined at 65,6 - (0,59 V/cp), 57,2 - (1,18 V/cp) and 59,0 ohm·cm² (at 1,76 V/cp). It was further found that R_{cp} decreased with increasing feed concentration (Tables 10.1 to 10.5). The cell pair resistance at 1,18 V/cp and an initial ammonium nitrate feed concentration of 9 100 mg/ℓ was determined at only 14,7 ohm·cm² (Table 10.2).

The model $R_{cp} = R_m + \rho d_{eff}$ is applicable not only to sodium chloride solutions but also to ammonium nitrate, sodium sulphate, sodium nitrate and calcium chloride solutions. However, care must be taken to use the linear portion of the curve (R_{cp} vs specific resistance) in the determination of R_{cp} and d_{eff} . This is also a method that can be used for the determination of cell pair resistance. Cell pair resistance, however, depends on the initial feed concentration. Therefore, feed concentration must be specified when cell pair resistance is given.

10.2 Concentration/Desalination of Industrial Effluents

10.2.1 Treatment of runoff from a fertilizer factory terrain with SCED

Runoff from an ammonium nitrate fertilizer factory terrain is presently stored in evaporation ponds. This runoff contains, amongst other ions, ammonium, nitrate and phosphate ions which have the potential to pollute the environment. Water and chemicals can also be recovered from the effluent for reuse. Sealed-cell ED was therefore investigated for treatment of this effluent⁽¹¹⁶⁾.

The concentration/desalination results of the relatively dilute runoff are shown in Table 10.6.

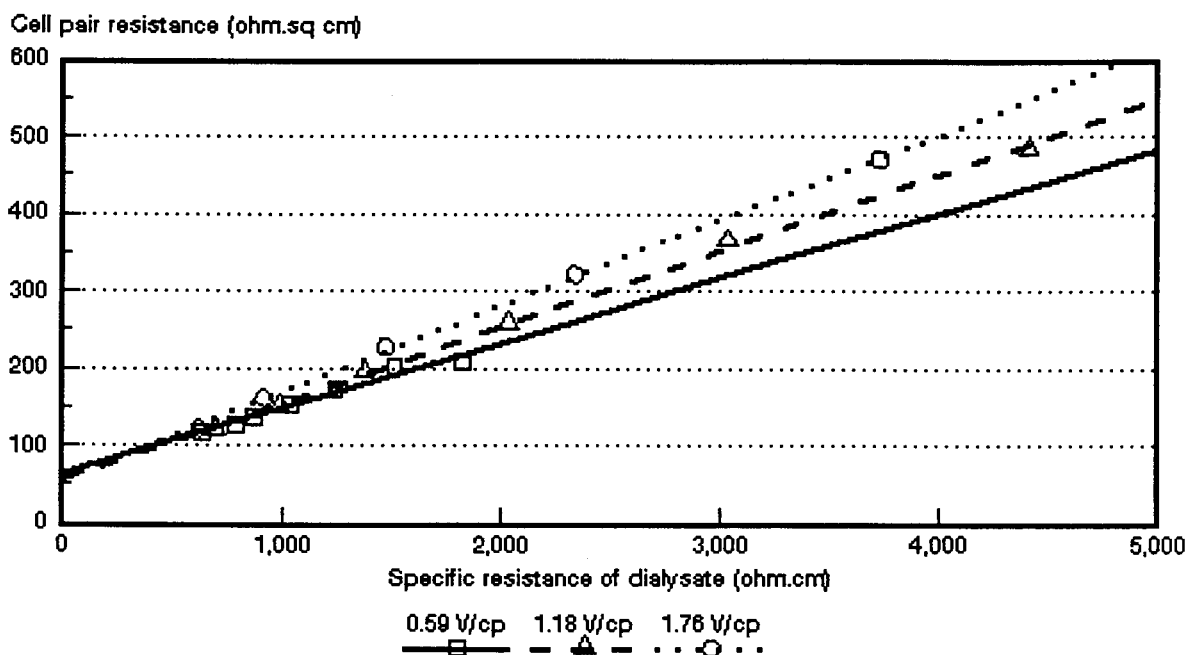


Figure 10.8: Cell pair resistance as a function of specific resistance of dialysate at different cell pair voltages for approximately 1 000 mg/l Na_2SO_4 feed solutions.

Table 10.6: Concentration/desalination results of fertilizer run-off at different cell pair voltages

V_{cp}	C_1 mS/m	C_p mS/m	C_b mS/m	% Conductivity Removal	CE %	WR %	BV %	EEC kWh/m ³	OP m ³ /m ² .d
1,18	545	29,8	10 724	94,5	56,9	97,2	2,8	2,7	1,03
0,88	556	48,9	10 312	91,2	63,3	97,2	2,8	2,0	0,77
0,59	520	53,3	8 830	89,7	-	96,9	3,1	1,24	0,54

Excellent salinity removals were obtained at the three cell pair voltages investigated. Salinity removal of 94,5% was obtained at a cell pair voltage of 1,18. Salinity removal decreased to only 89,7% at 0,59 V/cp.

Feed water conductivity was reduced from 545 mS/m to 29,8 mS/m at an electrical energy consumption of 2,7 kWh/m³ (1,18 V/cp). Brine volume comprised only 2,8% of the initial feed volume. Effluent volume could therefore be reduced significantly.

The chemical composition of feed, product and brine is shown in Table 10.7.

Table 10.7: Chemical composition of feed, product and brine

Constituent	Feed mg/ℓ	Product mg/ℓ	Brine mg/ℓ	% Removal
Sodium	111	25	3 758	77,50
Potassium	34	5	1 035	85,30
Calcium	93	24	3 404	74,20
Magnesium	64	8	2 121	87,50
Ammonium	621	30	16 638	95,20
Nitrate	1 936	73	63 783	96,30
Silica	7,70	4,60	54,40	40,30
Sulphate	299	48	8 469	83,90
Ortho-phosphate (P)	73,80	20,80	1 143	71,80
Chloride	187	14	5 371	92,50
Alkalinity (CaCO ₃)	22	3	24	86,40
COD	219	19	587	91,30
Manganese	0,409	<0,025	18,90	42,90
Iron	<0,025	<0,025	0,91	
Fluoride	1,66	0,35	3,70	78,90
TDS (calculated)	3 602	296	108 114	91,80
pH	5,7	4,3	4,4	

TDS was reduced from 3 602 mg/ℓ to 296 mg/ℓ (1,18 V/cp) with ease. Therefore, a very good quality product water could be produced which might be reused at the factory. Very good ammonium (95,2%) and nitrate (96,3%) removals were obtained. Ammonium and nitrate were reduced from 621 and 1 936 mg/ℓ in the feed to 30 and 73 mg/ℓ in the product, respectively.

The brine had a TDS of 10,8%. Brine volume comprised only about 3% of the initial feed volume. Therefore, brine volume could be reduced significantly which means that smaller evaporation ponds would be required, or that the present ponds could last much longer. Ammonium and nitrate values may also be recovered from the brine for reuse. Potential pollution problems will therefore be reduced significantly.

The ion-exchange membranes used in the SCED unit performed well for treatment of the fertilizer runoff. However, membrane fouling or scaling in the long term may affect the process adversely. Therefore, membrane fouling and cleaning studies over an extended time period will be necessary to determine the effectiveness of SCED for this application.

10.2.2 Treatment of a concentrated Ammonium Nitrate Type effluent with SCED

The treatment of a more concentrated ammonium nitrate type effluent from a fertilizer manufacturing plant was also investigated with SCED. The pH of the effluent was approximately 11 and the effluent was neutralized with sulphuric acid prior to SCED treatment⁽¹¹⁶⁾. Concentration/desalination of the ammonium sulphate effluent was conducted in stages because of the high concentration of the effluent (13 230 mS/m or 123 700 mg/l TDS). The product water after the first desalination stage was used as feed for the next concentration/desalination stage. The concentration/desalination results are shown in Table 10.8.

Table 10.8: Concentration/desalination results of ammonium sulphate effluent

Vcp	Cf mS/m	Cp mS/m	Cb mS/m	% Conductivity Removal	CE %	WR %	BV %	EEC kWh/m ³	OP m ³ /m ² ·d
0,53	13 230	8 452	26 313	36,1	43,1	84,7	15,3	23,3	0,448
0,53	8 751	2 437	18 952	72,2	-	78,8	21,2	28,9	0,318
1,18	2 424	6,2	17 416	99,8	46,9	91,6	8,4	17,9	0,282

Feed (13 230 mS/m) was first desalinated to 8 452 mS/m. Desalination rate was low due to the low cell pair voltage (0,53 V/cp) that could be applied as a result of excessive current that was drawn by the high conductivity of the feed solution⁽¹¹⁶⁾. It was only at the third desalination stage that a higher cell pair voltage could be applied.

The chemical composition of the feed, product and brine after the third desalination/concentration stage is shown in Table 10.9.

Table 10.9: Chemical composition of feed, product and brine (3rd stage desalination)

Constituent	Feed mg/ℓ	Product mg/ℓ	Brine mg/ℓ	% Removal
Sodium	268	12	2 787	95,52
Potassium	3	1	17	66,67
Calcium	7	1	60	85,71
Magnesium	1	4	13	
Kjeldahl-N	3 340	17	38 199	99,49
Ammonium	4 179	10	48 214	99,76
Nitrate	2 215	17	25 473	99,23
Silica	9,50	3,90	40,10	58,95
Sulphate	9 762	10	113 184	99,90
Total phosphate (P)	3,20	0,20	28,20	93,75
Chloride	103	28	1 167	72,82
COD	41	19	163	53,66
TDS (Calculated)	16 557	88	191 208	99,47
pH	3,6	4,9	2,9	

Very good ion removals were obtained. TDS was reduced from 16 557 mg/ℓ to 88 mg/ℓ, a 99,5% removal. Ammonium and nitrate removals were both approximately 99%. Brine with a TDS of 19,1% was obtained. Brine volume comprised 8,4% of the initial feed volume. Electrical energy consumption was determined at 17,9 kWh/m³ in this case. This energy consumption is high. However, an excellent quality product water was obtained which could be reused. This demonstrates that SCED may be effective for the treatment of relatively high TDS waters although the electrical energy consumption is high.

10.2.3 Treatment of an effluent saturated with Calcium Sulphate with SCED

Hydrochloric acid is used for extraction of calcium from activated carbon which is used for gold extraction by a gold recovery company. At times the effluent contains high concentrations of calcium (3 800 mg/ℓ), chloride (7 000 mg/ℓ) and sulphate (600 mg/ℓ). Sealed-cell ED was attempted for treatment of this high concentration calcium

sulphate effluent (TDS 23 000 mg/ℓ) for chloride recovery⁽¹¹⁶⁾. However, a white precipitate of calcium sulphate formed in the membrane bags shortly after the experiment was started. Therefore, calcium sulphate should be reduced to low levels to prevent calcium sulphate scaling during SCED treatment. This was done by treating another effluent sample (TDS 4 500 mg/ℓ) with barium carbonate. Sulphate was reduced from 339 mg/ℓ to 5 mg/ℓ.

The concentration/desalination results are summarized in Table 10.10.

Table 10.10: Concentration/desalination results of calcium chloride effluent

V_{cp}	C_i mS/m	C_p mS/m	C_b mS/m	% Conductivity Removal	CE %	WR %	BV %	EEC kWh/m ³
1,18	1 182	362	13 548	69,4	32,5	97,0	3	6,4
1,18	383	51	9 609	86,7	28,8	97,7	2,3	3,1

Concentration/desalination was conducted in two stages. Conductivity was first reduced from 1 182 mS/m to 362 mS/m and then from 362 mS/m to 51 mS/m. Very low current efficiencies were obtained for the first (32,5%) and second (28,8%) desalination stages. Brine volume comprised approximately 3% (1st stage) and 2,3% (2nd stage) of the feed water volume and electrical energy consumption was determined at 6,4 and 3,1 kWh/m³ for the first and second desalination stages, respectively.

The chemical composition of the feed, product and brine for the second desalination stage is shown in Table 10.11.

Table 10.11: Chemical composition of feed, product and brine (2nd stage desalination)

Constituent	Feed mg/ℓ	Product mg/ℓ	Brine mg/ℓ	% Removal
pH	8,1	8,1	6,7	
Conductivity (mS/m)	383	51	9 609	86,7
Sodium	191	77	4 862	59,7
Potassium	9	3	162	66,7
Calcium	278	10	17 045	96,4
Magnesium	5	4	7	20,0
Ammonium	27	7	447	274,1
Nitrate	4	2	241	50,0
Sulphate	3	4	3	-
Chloride	783	113	46 412	85,6
Alkalinity (CaCO ₃)	139	65	338	53,2
TDS (calculated)	1 469	299	102 180	79,6

A very good quality product water was obtained after the second desalination stage. TDS was reduced from 1 469 mg/ℓ to 299 mg/ℓ at an electrical energy consumption of 3,1 kWh/m³.

Chloride was effectively concentrated. The chloride concentration in the brine was 4,6%. This chloride may be converted into hydrochloric acid in an electrochemical cell. The recovered hydrochloric acid can then be used for removal of calcium from the spent activated carbon. This matter, however, warrants further investigation.

The high calcium concentration in the brine may cause scaling problems. However, no sign of scaling was detected during the laboratory tests. Membrane fouling and cleaning tests, however, should be conducted over an extended period of time to determine the practical feasibility of the process.

11. GENERAL DISCUSSION

11.1 Requirements for ED Membranes

The customary requirements for ED membranes are:

- a) low electrical resistance⁽⁶⁾ ($< 20 \text{ ohm} \cdot \text{cm}^2$);
- b) high permselectivity⁽⁶⁾ ($> 0,9$);
- c) low electro-osmotic coefficient⁽⁷⁾ ($< 12 \text{ mol H}_2\text{O/Faraday}$);
- d) good chemical and dimensional stability⁽¹¹⁴⁾; and
- e) satisfactory polarization characteristics⁽⁷⁾.

These requirements are also necessary for ED membranes for use in EOP. However, an additional requirement for EOP-ED is finite transport of water through the membranes. It has been shown that increasing flow of water through the membranes causes an increase in current efficiency.

It was shown by Narebska and Koter⁽¹⁸⁾ that ion-water coupling became higher in more concentrated solutions (approximately $0,5 \text{ mol/l}$). At higher concentrations ($> 0,5 \text{ mol/l}$), the amount of free water in the membrane, the water transport number and the osmotic flow decrease. Effects originating from the deswelling of the membrane at high external concentration, may result in the observed decrease of the electro-osmotic flow and the increased coupling between ions and the amount of water, crossing the membrane⁽¹⁸⁾.

It has been found by Narebska *et al.*⁽³¹⁾ that the resistance against flowing anions in a cation membrane is imposed by water; the lower the amount of water in the membrane, the higher the resistance. Consequently, increased ion-water coupling causes increased resistance to the penetration of co-ions into the membrane matrix. The result is an increase in current efficiency. It is therefore not necessary for ED membranes for use in EOP to have very high permselectivities, because permselectivity will be increased with increasing flow of water through the membranes. This was especially observed for the more porous heterogeneous membranes at high feed concentration (1 mol/l). Consequently, membranes with a relatively low permselectivity (approximately $0,6$) should be suitable for concentration of salt solutions with EOP-ED.

11.2 Permselectivity with Acids and Bases

An increasing amount of water flowed through the membranes with an increase in feed water concentration during EOP of salt solutions. However, a decrease in water flow was experienced with an increase in feed concentration during EOP of acid solutions. The anion membranes used for acid EOP had a very low permselectivity for chloride ions due to the very high mobility of the protons in the membrane⁽¹¹⁾. Consequently, the protons which flowed in the opposite direction to the flow of water would inhibit water flow through the membranes. Therefore, very little water will pass through the anion membrane in the case of acid EOP.

The cation membranes used for acid EOP, on the other hand, had a very high permselectivity for protons ($> 0,9$). Back diffusion should be very low in this case because back diffusion would be inhibited by the opposite flow of protons⁽¹⁹⁾. Osmotic flow, however, can be high through the cation membrane⁽¹⁹⁾.

The cation membranes had a lower current efficiency than the anion membranes during EOP of caustic soda solutions. This is due to the high mobility of the hydroxyl ion⁽³⁰⁾. It was shown by Koter and Narebska⁽³²⁾ that hydroxide ions impeded cations, particularly at high external concentration, much more than chloride ions. This can be attributed to the higher partial friction between sodium and hydroxyl ions.

The resistance imposed by a membrane matrix on the permeating hydroxyl ions is much lower than that for chloride ions according to Narebska *et al.*⁽³⁰⁾. Three factors contributing to this effect, viz: the friction imposed by the cation (f_{21}), water (f_{2w}); and the polymer matrix (f_{2m}) - influence the flow of hydroxyl and chloride ions to different degrees. Chloride ions are hindered mainly by water, especially at increasing sorption. The flow of hydroxyl ions in diluted solution is hindered by the matrix and at high concentration by the cation and then by water⁽³⁰⁾.

11.3 Brine Concentration, Electro-Osmotic and Osmotic Flows

Brine concentration increases with increasing feed water concentration and current density. This happens because the membranes become increasingly dewatered at high current density. Consequently, the electro-osmotic coefficient decreases.

The osmotic flow relative to the total flow through the membranes decreased with

increasing current density. Consequently, the relative amount of electro-osmotic flow through the membranes, increased as a function of current density. Osmotic flow, however, appears to contribute significantly to the total flow in EOP. The osmotic flow through the *Ionac* membranes at a current density of 20 mA/cm² (0,1 mol/l feed) comprised 33,9% of the total flow through the membranes. Osmotic flow was reduced to 19,0% of the total flow at a current density of 50 mA/cm² (0,1 mol/l feed). Osmotic flow through the *Selemion* AAV and CHV membranes contributed 64,1% to the total flow at a current density of 20 mA/cm² (0,1 mol/l feed). Osmotic flow decreased to 20,9% at a current density of 100 mA/cm² (0,1 mol/l feed). Osmotic flow through the *Selemion* AMP and CMV membranes contributed 61,4% to the total flow through the membranes at a current density of 20 mA/cm² (0,1 mol/l feed). Osmotic contribution decreased to 25,7% at a current density of 100 mA/cm² (0,1 mol/l).

Approximately 7 mol H₂O/Faraday permeated through the *Selemion* AAV and CHV membranes in the feed concentration range from 0,5 to 1,0 mol/l. It is known that little water (< 1 mol/Faraday) can permeate acid blocking anion membranes⁽⁴⁸⁾. Therefore, the water could have entered the membranes only through the cation membrane.

Osmotic flow increased with increasing feed water concentration. It was also observed that the osmotic flow decreased in some cases at the highest feed concentrations. This can be ascribed to stronger back diffusion at the highest feed water concentrations. It was also interesting to note that a decrease in osmotic flow had taken place with increasing feed water concentration in the case of the more hydrophobic *Ionac* and WTPS membranes. The osmotic flow also increased through the Israeli ABM and *Selemion* membranes with increasing feed concentration and higher current efficiencies were experienced.

11.4 **Discrepancy between Transport Numbers Derived from Potential Measurements and Current Efficiency Actually Obtained**

The correct relationships to be used when measuring membrane potential for the prediction of desalting in ED, are as follows:

$$[J/I]_{\Delta\mu_s; j_v = 0} = \Delta t/F$$

(see eqs. 3.2.23 and 3.2.24)

$$= -[\Delta\Psi/\Delta\mu_s]_{j_v = 0}$$

The correct Onsager relationship for potential measured is at zero current and at zero volume flow, and for the transport number, at zero concentration gradient and zero volume flow⁽¹¹⁷⁾. In practical ED, measurements are conducted at zero pressure and in presence of concentration gradients and volume flows. These factors will influence the results considerably in all systems in which volume flow is important and where the concentration factor is high as is encountered in EOP. In the measurement of membrane potential, the volume flow is against the concentration potential and in general will decrease the potential. In ED water flow helps to increase current efficiency, but the concentration gradient acts against current efficiency.

In the case of sodium chloride solutions, the apparent transport number of the membrane pair ($\bar{\Delta}t$) was higher than current efficiency (e_p) at low feed water concentrations (approximately 0,05 mol/l). This was predicted with the following relationship:

$$\eta < \frac{|\Delta\Psi_m^c + \Delta\Psi_m^a|}{|2\Delta\Psi_l|} \quad (\text{see eq. 3.11.12})$$

Equation (3.11.12) is valid if the influence of volume flow is negligible.

The apparent transport number ($\bar{\Delta}t$) decreased with increasing feed water concentration. Current efficiency, however, increased with increasing feed water concentration as a result of increasing water flow. Consequently, current efficiency became higher than the apparent transport number at higher feed water concentrations (0,5 to 1 mol/l). Current efficiency, however, decreased at very high feed concentrations as a result of back diffusion. Similar results were obtained with EOP of caustic soda solutions.

Current efficiency was much lower than $\bar{\Delta}t$ during EOP of acid solutions. This can be ascribed to back diffusion of acid through the membranes during EOP which reduces current efficiency significantly.

Garza and Kedem⁽²⁾ have found that the apparent transport number of a membrane

pair ($\bar{\Delta}t$) gave a good lower estimate of the actual Coulomb efficiency of the EOP process in the case of sodium chloride solutions (0,1 mol/l feed) using *Selemion* AMV and CMV and polyethylene based membranes. However, it was found in this study that the apparent transport number of a membrane pair gave a higher estimate of the Coulomb efficiency of the EOP process in the 0,05 to 0,1 mol/l feed concentration range. The apparent transport number of a membrane pair gave a lower estimation of the actual current efficiency in the feed water concentration range from approximately 0,5 to 1,0 mol/l. However, the apparent transport number of a membrane pair gave a much too high estimation of current efficiency of the EOP process for hydrochloric acid concentration. The apparent transport number of the anion membrane, however, gave a much better estimation of current efficiency.

11.5 Current Efficiency and Energy Conversion in ED

The effects which diminish current efficiency in ED are the following⁽¹⁷⁾:

- a) electric transport of co-ions;
- b) diffusion of solute;
- c) electro-osmotic flow; and
- d) osmotic water flows.

The imperfect selectivity, \bar{t}_2 , assumed to be one of the most important characteristics of a membrane can produce up to 8% (NaCl) and 35% (NaOH) of the current efficiency losses at $\tilde{m} = 2$ ⁽¹⁷⁾. Similar to \bar{t}_2 , the effect of electro-osmotic flow of water (\bar{t}_w) increases with m . It plays a significant role in the system with sodium chloride where it diminishes current efficiency up to 30% according to Koter and Narebska⁽¹⁷⁾. However, it was found in this study that electro-osmotic flow of water increased current efficiency significantly in the 0,05 to 1,0 mol/l feed concentration range.

Depending on the working conditions, i.e. on the concentration ratio m'/m'' and current density, the decrease in current efficiency due to osmotic and diffusion flows can be larger than that caused by electric transport of co-ions and water. This effect is especially seen at the higher mean concentrations where the current efficiency can be reduced to zero⁽¹⁷⁾.

Efficiency of energy conversion in ED consists of the following two terms, viz., η_{IE} (ion-current coupling) and η_{WE} (ion-water coupling) according to Narebska and Koter⁽¹⁸⁾. The first term expresses the storage of energy in producing a concentration difference

in the permeant. The second term corresponds to the transport of water, which acts opposite to the separation of the components. It causes a waste of energy by decreasing the concentration difference. This water flow has a negative effect on energy conversion in ED. However, electro-osmosis can also have a positive effect on ED by increasing current efficiency as has been demonstrated in this study.

11.6 Water Flow, Concentration Gradient and Permselectivity

Salt flux (S^c) through a cation-exchange membrane can be predicted with the following relationship:

$$S^c = \frac{J_1^c + J_2^c}{2} = c_s(1 - \sigma)J_v^c + \bar{P}\Delta C + \frac{\Delta t^c}{2} I/F \quad (\text{see eq. 3.11.1})$$

Salt flux (both cation and anion) through ion-exchange membranes depends on water flow (J_v) through the membranes, concentration gradient (ΔC) across the membrane and membrane permselectivity ($\bar{\sigma}$). It was shown that increasing water flow through the membranes increased current efficiency. It was also shown that an increasing concentration gradient (ΔC) across the membranes decreased current efficiency. Current efficiency or salt flux was also low when the permselectivity of the membranes was low. The experimental data for salt, acid and base EOP can therefore be satisfactorily described by eq. (3.11.1).

Back diffusion through ion-exchange membranes in presence (at zero pressure) and absence of water flow can be predicted with the following relationship according to Kedem⁽¹⁵⁾:

$$\left[\frac{J_s}{X_s C_s} / \frac{J_1 - J_2}{X_1} \right]_{\Delta p = 0} < \left[\frac{J_s}{X_s C_s} / \frac{J_1 - J_2}{X_1} \right]_{J_v = 0} \quad (\text{see eq. 3.3.45})$$

Back diffusion of salt through a membrane is less when water flows from the opposite side (l.h.s. of eq. 3.3.45). However, back diffusion of salt is more in the absence of volume flow (r.h.s. of eq. 3.3.45). Therefore, current efficiency will be higher when salt diffusion is lower and this will occur when water flows through the membrane. This was illustrated especially during EOP of sodium chloride solutions.

A decreasing amount of water permeated the membranes during acid EOP with increasing acid feed water concentration. It was also found that back diffusion was

high during acid EOP. Therefore, the right hand side of equation (3.3.45) is applicable to the experimental data that have been observed with EOP of hydrochloric acid solutions.

11.7 Prediction of Brine Concentration

Maximum brine concentration, c_b^{\max} was predicted with the following two relationships:

$$c_b^{\max} = \frac{1}{2FB} \quad (\text{see eq. 3.10.28})$$

and

$$c_b^{\max} = c_b(1 + J_{\text{osm}}/J_{\text{elosm}}) \quad (\text{see eq. 3.10.31})$$

Brine concentration (salt, acid or base) at high current density, c_b^{\max} , appeared to attain a constant value, independent of current density and dependent on the feed water concentration. Maximum brine concentration was more dependent on feed concentration where the membranes deswelled more with increasing feed water concentration.

Maximum brine concentration could be predicted accurately with equations (3.10.28) and (3.10.31). Therefore, any one of these two methods can be used to predict c_b^{\max} .

Brine concentration, c_b , was predicted from the water flow through the membranes and the apparent transport of the membrane pair ($\bar{\Delta}t$) with the following relationship:

$$c_b = \frac{I\bar{\Delta}t}{2FJ} \quad (\text{see eq. 3.10.17})$$

Brine concentration could be predicted more accurately in the case of sodium chloride and caustic soda solutions than in the case of hydrochloric acid solutions. This can be explained by back diffusion of acid that has been experienced during EOP of the hydrochloric acid solutions. However, a much better prediction of acid brine concentration should be obtained by using the apparent transport number of the anion membrane (Δt^a) in the above equation.

The permselectivity of the membranes ($\bar{\Delta}t$'s) decreased with increasing feed water concentration. Brine concentration, on the other hand, increased with increasing feed water concentration. Therefore, the ratio $c_{b \text{ calc}}/c_{b \text{ exp}}$ decreased with increasing feed

concentration. The accuracy of prediction of brine concentration will therefore depend on the feed concentration used for the determination of the apparent transport number.

11.8 Membranes for Sodium Chloride, Hydrochloric Acid and Caustic Soda Concentration

The *Selemion* and *Ionac* membranes performed satisfactorily for concentration of sodium chloride solutions. The *Raipore* membranes, however, did not perform well, due to the high water transport that was experienced with this membrane type. Consequently, lower concentrations and efficiencies were obtained. The *Ionics*, WTPS, WTPVC and WTPST membranes all gave good results in terms of brine concentration and current efficiency. However, serious polarization was experienced with the WTPS membranes and ways to improve the polarization characteristics of these membranes should be investigated.

The presently commercially available anion-exchange membranes are not stable for long periods when exposed to high pH values⁽¹¹⁴⁾. Consequently, the membranes that were evaluated for caustic soda concentration would have a relatively short life time when treating caustic soda effluents. Nevertheless, satisfactory results were obtained with the *Selemion* and *Ionac* membranes that were used for caustic soda concentration. Membrane life time studies, however, should be conducted to determine the effectiveness of these membranes for caustic soda concentration.

The newly developed Israeli ABM membranes compared favourably with the *Selemion* AAV membrane for acid concentration. The *Selemion* AAV membranes were specially designed for acid concentration. It was shown that the *Selemion* AAV membrane adsorbed a substantial amount of acid⁽⁴⁸⁾. The low dissociation of sorbed acid in the membrane was shown to be a factor which was responsible for the decrease in proton leakage of this anion membrane.

A high degree of ion-coupling will be observed in the case of charged hydrophobic membranes when acid is absorbed by the membrane. It was shown that the flux of chloride ions from the anode to the cathode steadily increased as the amount of sorbed acid was increased⁽⁴⁸⁾. This result showed that chloride ions are associated with the movement of positively charged species. This may be due to the formation of an aggregate form such as $(\text{CH}_3\text{OC})^+$ resulting from the solvation of a proton by a water and an hydrochloric acid molecule⁽⁴⁸⁾. This shows that ion association is taking

place inside the membrane.

11.9 Conventional EOP-ED Stack

It was demonstrated that a conventional ED stack can be used as an EOP-ED stack for concentration of sodium chloride, hydrochloric acid and caustic soda solutions using commercially available ion-exchange membranes. Relatively high brine concentrations and low brine volumes were obtained. Electrical energy consumption was also low at low cell pair voltages.

An advantage of using a conventional ED stack as an EOP-ED stack is that the membranes can be taken out of the stack for cleaning purposes if it should be required. It is not possible to open sealed-cell ED membranes for cleaning. A disadvantage of using a conventional ED stack as an EOP-ED stack is that the membrane utilization factor will be low (approximately 80%). However, it should be possible to improve the membrane utilization factor with improved gasket design and this matter needs further investigation.

11.10 Sealed-Cell Electrodialysis

The sealed-cell ED unit performed satisfactorily for concentration/desalination of salt solutions and industrial effluents. High brine concentrations and low brine volumes were obtained. Low electrical energy consumptions were also obtained at low feed concentrations. Electrical energy consumptions obtained with the conventional EOP-ED stack were comparable to the electrical energy consumptions obtained with the sealed-cell ED stack.

The effective thickness of the dialysate compartment, d_{eff} , was much lower in the case of the sealed-cell ED unit than in the case of the EOP-ED stack. This can be ascribed to the thinner dialysate compartments that have been used in the sealed-cell unit and to the higher linear flow velocities used.

The advantages and disadvantages of SCED are as follows: The capital cost of SCED equipment should be less than that of a conventional plate-and-frame ED stack, because of the simpler construction of the SCED stack. The membrane utilization factor in the membrane bags is approximately 95% compared to approximately 80% for membranes in conventional ED stacks. Higher current densities can be used in

SCED than in conventional sheet flow ED because higher linear flow velocities can be obtained with ease. The higher current densities will result in higher water production rates. Brine volumes produced by SCED are smaller than those obtained with conventional ED. Therefore, the brine disposal problem will be reduced.

More electrical energy per unit of product water produced, will be used in the SCED stack due to the higher current densities used. However, the increased cost for electrical energy should be off-set by a decrease in capital cost. Scale may form more readily in the membrane bags because the SCED stack does not have a built-in self cleaning device such as encountered in the EDR system⁽⁹⁾. It will be difficult to remove scale from the membrane bags once it has formed because the bags cannot be opened for cleaning. Therefore, scale forming chemicals should be removed by ion-exchange or nanofiltration prior to SCED treatment. This will affect the economics of the process adversely, especially if large flows are involved.

Scale-up of a laboratory size SCED unit (100 cm²/cp) to a pilot or full-scale plant would be possible. It would be possible to manufacture large-scale membrane bags commercially and the bags would be robust. An advantage of the membranes that were used in the SCED stack was that they could be stored dry. This is usually not the case with ion-exchange membranes normally used in conventional ED. The successful application of SCED technology seems to depend on the need to apply this technology in preference to conventional ED for specific applications where high brine concentrations and small brine volumes are required.

12. SUMMARY AND CONCLUSIONS

Salts, acids and bases frequently occur in industrial effluents. These effluents usually have a large pollution potential. Often the effluents also contain valuable chemicals and water that can be recovered for reuse. Effluent disposal cost can be high, especially where effluents must be trucked away for safe disposal. However, it would be possible to reduce disposal cost significantly if effluent volume could be reduced to a significant extent.

Electro-osmotic pumping ED has the potential to be applied for industrial effluent treatment. Preliminary work has indicated that small brine volumes and high brine concentrations could be achieved with EOP-ED at attractive electrical energy consumptions. However, it was determined that the following needs still existed regarding the application of EOP-ED for industrial effluent treatment:

- a) to consider and document the relevant EOP-ED and ED theory properly;
- b) to study the EOP-ED characteristics (transport numbers, brine concentration, current efficiency, current density, electro-osmotic coefficient, etc.) of commercially available and other ion-exchange membranes in a single cell pair with the aim to identify membranes suitable for EOP-ED;
- c) to develop a simple method and to evaluate existing models with which membrane performance for salt, acid and base EOP-ED, can be predicted; and
- d) to evaluate the EOP-ED process for industrial effluent treatment.

The following conclusions can be drawn as a result of this investigation:

- A conventional ED stack which was converted into an EOP-ED stack performed satisfactorily for concentration/desalination of sodium chloride, hydrochloric and caustic soda solutions. Dialysate concentrations of less than 500 mg/l could be obtained in the feed water and cell pair voltage ranges from 1 000 to 10 000 mg/l and 0,5 to 4 V/cp, respectively. Brine concentrations of 2,1 to 14,0%; 3,6% to 8,7% and 2,3% to 7,3% were obtained for sodium chloride, hydrochloric acid and caustic soda solutions, respectively.

Current efficiency increased with increasing feed water concentration during EOP-ED of sodium chloride and caustic soda solutions. This is in contrast to what is usually happening. Increasing feed water concentration causes increasing water flow through the membranes which inhibits co-ion invasion. Therefore, higher current efficiency is obtained. This supported the results that were obtained in a single cell pair. Current

efficiencies varied between 75,2 and 93,6%; 29,2 and 46,3% and 68,9 and 81,2% for sodium chloride (1 000 to 5 000 mg/ℓ feed; 0,5 to 1,5 V/cp); hydrochloric acid (1 000 to 5 000 mg/ℓ feed; 0,5 to 4,0 V/cp); and caustic soda solutions (1 000 to 10 000 mg/ℓ feed; 0,5 to 3 V/cp), respectively.

Low brine volumes and high water recoveries were obtained. Brine volume increased with increasing feed water concentration and decreased with increasing cell pair voltage. Brine volume varied between 1,5 and 4,0% for sodium chloride (1 000 to 5 000 mg/ℓ feed; 0,5 to 1,0 V/cp); between 2,4 and 7,8% for hydrochloric acid (1 000 to 5 000 mg/ℓ feed; 0,5 to 1,5 V/cp); and between 2,3 to 7,3% for caustic soda solutions (1 000 to 5 000 mg/ℓ feed; 0,5 to 1,5 V/cp).

Electrical energy consumption was low at low feed water concentrations and low cell pair voltages. Electrical energy consumption increased with increasing feed water concentration and increasing cell pair voltage. Electrical energy consumption of less than 2,5 kWh/m³ product water was obtained for sodium chloride (0,5 to 1,5 V/cp; 1 000 to 3 000 mg/ℓ feed); between 0,2 and 3,2 kWh/m³ product for hydrochloric acid (0,5 to 1,5 V/cp; approximately 1 000 mg/ℓ feed); and between 0,4 and 2,2 kWh/m³ product for caustic soda solutions (0,5 to 1,5 V/cp; 1 000 to 3 000 mg/ℓ feed).

Water yield increased with increasing cell pair voltage and decreased with decreasing feed water concentration. Water yield was 0,38 m³/m².d at a linear flow velocity of 1 cm/s through the stack when hydrochloric acid was concentrated (2 V/cp; 3 000 mg/ℓ feed). Water yield was increased to 0,7 m³/m².d when linear flow velocity was increased to 5 cm/s. A higher linear flow velocity will also depress polarisation. Therefore, it would be advantageous to operate an EOP-ED stack at the highest possible linear flow velocity.

- Sealed-cell ED should be effective for concentration/desalination of relatively dilute (500 to 3 000 mg/ℓ TDS) non-scaling forming salt solutions. Product water with a TDS of less than 300 mg/ℓ could be produced in the feed water concentration range from 500 to 10 000 mg/ℓ TDS. Electrical energy consumption of 0,27 to 5,9 kWh/m³ product was obtained (500 to 3 000 mg/ℓ feed range). Brine volume comprised approximately 2% of the initial feed water volume. Therefore, brine disposal costs should be significantly reduced with this technology.

Sealed-cell ED became less efficient in the 5 000 to 10 000 mg/ℓ TDS feed water

concentration range due to high electrical energy consumption (3,3 to 13,0 kWh/m³ product). However, SCED may be applied in this TDS range depending on the value of the products that can be recovered.

Treatment of scale forming waters will affect the process adversely because scale will precipitate in the membrane bags which cannot be opened for cleaning. Membrane scaling may be removed by current reversal or with cleaning solutions. However, this matter needs further investigation. Scale-forming waters, however, should be avoided or treated with ion-exchange or nanofiltration prior to SCED.

It was demonstrated that a relatively dilute ammonium nitrate effluent (TDS 3 600 mg/ℓ) could be successfully treated in the laboratory with SCED. Brine volume comprised only 2,8% of the treated water volume. Electrical energy consumption was determined at 2,7 kWh/m³ product. Both the brine and the treated water could be reused. Membrane fouling or scaling, however, may affect the process adversely and this matter needs further investigation.

It was difficult to concentrate/desalinate a concentrated ammonium sulphate effluent (approximately 13 200 mS/m or 123 700 mg/ℓ TDS) with SCED. Concentration/desalination was conducted in stages. Nevertheless, it was possible to desalinate the effluent to 6,2 mS/m (88 mg/ℓ TDS). However, electrical energy consumption was high (59 kWh/m³ product). Brine volume comprised 45% of the treated volume. A very high brine concentration (approximately 26 300 mS/m or 332 000 mg/ℓ TDS) could be obtained after the first desalination stage. However, a more dilute (16 557 mg/ℓ TDS) ammonium sulphate effluent (3rd stage) could be more easily concentrated/desalinated to 88 and 191 208 mg/ℓ TDS product water and brine, respectively, at water recovery and electrical energy consumption of 91,6% and 17,9 kWh/m³, respectively. Therefore, SCED could also be effectively applied for the desalination/concentration of relatively high TDS waters.

It was not possible to concentrate/desalinate an effluent saturated with calcium sulphate with SCED due to membrane scaling which took place. However, it was possible to concentrate/desalinate the effluent effectively after sulphate removal by chemical precipitation. It was possible to concentrate/desalinate the effluent from 1 182 mS/m (4 461 mg/ℓ TDS) to 51 mS/m (299 mg/ℓ TDS) at an electrical energy consumption of 9,5 kWh/m³ product. Brine volume comprised 5,3% of the treated feed. The cost effectiveness of these procedures need to be evaluated.

The ion-exchange membranes used in the SCED stack performed very well for ammonium and nitrate removal. Ammonium and nitrate ions were removed from 4 179 and 2 215 mg/ℓ in one case to 10 - (99,8% removal) and 17 mg/ℓ (99,2% removal), respectively.

Capital cost of SCED equipment should be less than that of conventional ED due to the simpler design of the SCED stack. The membrane utilization factor of 95% is much higher than in conventional (approximately 80%) ED.

Sealed-cell ED has potential for treatment of relatively dilute (< 3 000 mg/ℓ TDS) non-scaling waters for water and chemical recovery for reuse. However, high TDS (up to 16 000 mg/ℓ) waters can also be treated depending on the value of the products that can be recovered.

Studies in a single cell pair have shown the following:

- Brine concentration increased with increasing current density and increasing feed water concentration. Brine concentration appeared to attain a constant value at high current density dependent on the electro-osmotic coefficients of the membranes.
- Current efficiencies were nearly constant in a wide range of current densities (0 to 70 mA/cm²) and feed water concentrations (0,05 to 1,0 mol/ℓ) in the case of the *Selemion* and *Raipore* membranes used for sodium chloride concentration. The same phenomenon was observed for the *Selemion* membranes used for acid concentration. However, all the other membranes showed a slight decrease in current efficiency with increasing current density. This showed that the limiting current density was exceeded and that polarization was taking place. Significant polarization took place with the WTPS membranes at relatively low current density (> 20 mA/cm²).
- Water flow through the membranes increased with increasing current density. Water flow through the membranes also increased with increasing feed water concentration, especially for the membranes that were used for salt and caustic soda concentration. This increasing water flow improved current efficiency and water flow can therefore also have a positive effect on ED. However, water flow decreased through the *Selemion* membranes that were used for acid concentration when feed water concentration was increased and no increase in current efficiency was observed. Current efficiency,

however, increased through the Israeli ABM membranes when water flow increased.

The electro-osmotic coefficients were determined to be a function of feed water concentration. The coefficients decreased with increasing feed water concentration until a constant value was obtained at high current density. The decrease in electro-osmotic coefficients with an increase in feed water concentration can be ascribed to deswelling of the membranes with increasing feed water concentration or to a reduction in membrane permselectivity when the feed water concentration is increased.

Osmotic flow in EOP decreases relative to the total flow with increasing current density while the electro-osmotic flow increases relative to the osmotic flow. Osmotic flow, however, contributes significantly to the total water flow in EOP. Osmotic flow through the *Selemion* AAV and CHV membranes contributed 64,1% of the total flow through the membranes at a current density of 20 mA/cm² (0,1 mol/l feed). Osmotic flow was 20,9% of the total flow at a current density of 100 mA/cm² (0,1 mol/l feed).

- Membrane permselectivity decreased with increasing brine and feed water concentration and increasing concentration gradient across the membranes.
- *Selemion* AMV and CMV and *Ionac* membranes performed satisfactorily for concentration of sodium chloride solutions. Salt brine concentrations of 19,3%; 25,1%; 27,2% and 29,8% were obtained at feed water concentrations of 0,05; 0,1; 0,5 and 1,0 mol/l, respectively, with the *Selemion* AMV and CMV membranes. Current efficiency in this feed water concentration range varied from 62 to 91%. Performance of the *Ionics* and WTPS membranes were poorer while the poorest results were obtained with the WTPVC, WTPST and *Raipore* membranes.

Satisfactory results were obtained with the *Selemion* AAV and CHV and newly developed Israeli ABM-3 and ABM-2 membranes for hydrochloric acid concentration. Acid brine concentrations of 18,3%; 20,9%; 25,0% and 27,2% were obtained at 0,05; 0,1; 0,5 and 1,0 mol/l feed water concentration, respectively, for the *Selemion* AAV and CHV membranes. Current efficiency varied between 35 and 42%. Higher current efficiencies, however, were obtained with the Israeli ABM-3 membranes. Current efficiency varied between 34 and 60% in the same feed water concentration range.

Selemion AMV and CMV, *Selemion* AMP and CMV and *Ionac* membranes performed well for caustic soda concentration. Caustic soda brine concentrations of 14,3%;

17,7%; 20,1% and 24,4% were obtained at high current density at 0,05; 0,1; 0,5 and 1,0 mol/l feed water concentration, respectively, with the *Selemion* AMV and CMV membranes. Current efficiency varied from 47 to 76%.

Membrane current efficiency in EOP increased with increasing water flow through the membranes. This was especially observed for the more porous heterogeneous membranes at high feed water (1,0 mol/l) concentration. It will therefore not be necessary for membranes to have very high ($> 0,9$) permselectivities for use in EOP-ED.

- It has been found that a simple potential measurement can be used effectively to predict membrane performance for salt, acid and base concentration with ED. The ratio between the apparent transport number ($\bar{\Delta}t$) and current efficiency (ϵ_p), however, depends on the feed concentration and current density used. Ratio's of $\bar{\Delta}t/\epsilon_p$ varied between 1,0 and 1,07 (0,1 mol/l feed, *Selemion* AMV and CMV, salt concentration); 0,95 to 1,09 (0,5 mol/l feed, *Ionac*); 1,02 and 1,05 (0,5 mol/l feed, *Raipore*); 0,95 and 1,02 (0,5 mol/l, *Ionics*). Consequently, it should be possible to predict current efficiency for concentration of sodium chloride solutions with an accuracy of approximately 10% and better from the apparent transport number of the membrane pair.

Correlations obtained between the apparent transport number ($\bar{\Delta}t$) and current efficiency for membranes used for acid concentration, were unsatisfactory. The apparent transport number of the membrane pair ($\bar{\Delta}t$) was from 1,5 to 4 times higher than current efficiency in the feed acid concentration range from 0,05 to 1,0 mol/l. Back diffusion of hydrochloric acid through the membranes caused the lower current efficiency. However, the apparent number of the anion membrane (Δt^a) gave a much better indication of membrane performance for acid concentration. Ratio's of $\Delta t^a/\epsilon_p$ of 1,1 to 1,2 (1,0 mol/l, *Selemion* AAV); 0,97 to 0,84 (1,0 mol/l, ABM-2); 0,92 to 0,97 (0,1 mol/l, ABM-1) were obtained. Consequently, it should be possible to predict current efficiency for concentration of hydrochloric acid solutions with an accuracy of approximately 20% and better from the apparent transport number of the anion membrane.

Correlations obtained between the apparent transport number ($\bar{\Delta}t$) and current efficiency of the membranes investigated for caustic soda concentration were satisfactory. Ratio's of $\bar{\Delta}t/\epsilon_p$ of 1,0 to 1,1 (0,05 mol/l, *Ionac*); 0,9 to 1,0 (0,1 mol/l, *Ionac*); 0,9 (1,0 mol/l, *Selemion* AMV and CMV); 1,1 to 1,2 (0,1 mol/l, *Selemion* AMP

and CMV); 1,1 (0,5 mol/ℓ, *Selemion* AMP and CMV) were obtained. Therefore, it should be possible to predict current efficiency for concentration of caustic soda solutions with an accuracy of approximately 20% and better from the apparent transport number of the membrane pair. Good correlations were also obtained between the apparent transport number of the cation membrane (Δt^c) and current efficiency. Consequently, it should also be possible to predict current efficiency with an accuracy of approximately 20% and better from the apparent transport number of the cation membrane.

- The correct Onsager relationships to be used for potential measurement ($\Delta\Psi$) and for the transport number (JF/l) are at zero current and zero volume flow, and at zero concentration gradient and zero volume flow, respectively. In practical ED, measurements are conducted at zero pressure and in the presence of concentration gradients and volume flows. These factors will influence the results considerably in all systems in which volume flow is important and where the concentration factor is high as is encountered in EOP. In measurement of membrane potential, the volume flow is against the concentration potential and in general will decrease potential. In ED, water flow helps to increase current efficiency, but the concentration gradient is against current efficiency.
- Brine concentration can be predicted from apparent transport numbers ($\bar{\Delta t}'s$) and water flows through the membranes. The ratio $c_{b\text{calc}}/c_{b\text{exp}}$ decreased with increasing feed concentration.
- Maximum brine concentration, c_b^{max} , can be predicted from two simple models. A very good correlation was obtained by the two methods. Maximum brine concentration increased with increasing feed concentration and appeared to level off at high feed concentration (0,5 to 1,0 mol/ℓ).
- Models described the system satisfactorily for concentration of sodium chloride, hydrochloric acid and caustic soda solutions with commercially available membranes. Brine concentration approached a limiting value (plateau) at high current density dependent on the electro-osmotic coefficients of the membranes. A constant slope (electro-osmotic coefficient) was obtained when water flow was plotted against current density. Straight lines were obtained when cell pair resistance was plotted against the specific resistance of the dialysate. Current efficiency increased with increasing flow of water, decreased when back diffusion was high and transport numbers were low.

13. **NOMENCLATURE**

Sections 2.1 and 2.2

c_b^{\max}	-	Maximum brine concentration (mol/l)
ϵ_p, η_c	-	current efficiency (%)
J	-	volume flow through membranes (cm/h)
I_{eff}	-	effective current density (Coulomb efficiency x current density)
C_b	-	brine concentration (mol/l)
β	-	electro-osmotic coefficient (l/Faraday)
F	-	Faraday's constant (96 500 Coulomb/ge)
J_{osm}	-	osmotic water flow (cm/h)
J_{elosm}	-	electro-osmotic water flow (cm/h) ($J = J_{\text{osm}} + J_{\text{elosm}}$)
C_f	-	feed concentration (mg/l)
C_p	-	product concentration (mg/l)
d_{eff}	-	effective thickness of dialysate compartment (mm) (polarisation factor)
V_{cp}	-	cell pair voltage (volt)
R_{cp}	-	cell pair resistance ($\Omega \cdot \text{cm}^2$)
ρ	-	specific resistance of dialysate ($\Omega \cdot \text{cm}$)
a	-	anion membrane
c	-	cation membrane
$\Delta \Psi_m$	-	membrane potential (mV)
$\bar{\Delta}t$	-	apparent transport number of membrane pair

Section 2.3

r_{ik}	-	phenomenological resistance coefficient
f_{ik}	-	phenomenological friction coefficient
f_{21}	-	friction imposed by cation (1) on anion
f_{2w}	-	friction imposed by water (w) on anion (2)
f_{2m}	-	friction imposed by polymer matrix (m) on anion (2)
r_{ii}	-	straight resistance coefficients
m_{ext}	-	external concentration
$2m$	-	anion-polymer frictional force
$2w$	-	anion-water frictional force
$\bar{\Delta}t$	-	apparent transport number of membrane pair

Section 2.4

\bar{a}_w	-	water activity in interior of membrane
a_w	-	water activity outside membrane
Π	-	membrane internal osmotic pressure
R	-	gas constant
T	-	absolute temperature
V_w	-	partial molar volume of internal water component of membrane
n_o	-	equilibrium water content

Section 2.5

E	-	membrane potential
E_{\max}	-	maximum membrane potential
\bar{t}_+	-	transport number
$\bar{t}_{+(\text{app})}$	-	apparent transport number
a'	-	activity on one side of the membrane
a''	-	activity on the other side of the membrane
F	-	Faraday's constant
I	-	electric current
J_i	-	ion flux of species i
\bar{t}_i	-	transport number of species i inside the membrane

Sections 3.1.1 and 3.1.2

J_i	-	Flux density of i ($\text{mol}/\text{cm}^2\text{s}^{-1}$)
C_i	-	concentration of i (mol cm^{-3})
μ_i	-	electrochemical potential of i
x	-	distance from reference plane in membrane
R	-	gas constant
T	-	absolute temperature
γ_i	-	activity coefficient of i
V_i	-	partial molar volume of i
p	-	pressure
z_i	-	number of positive charges per ion (valency)
F	-	Faraday's number
ψ	-	electrical potential

D_i	-	diffusion coefficient of i
u_i	-	absolute mobility of i
v	-	velocity of local center of mass
L_{ik}	-	phenomenological conductance coefficient
X_k	-	force on k per mole
σ	-	rate of entropy production, reflection coefficient
ϕ	-	dissipation function
n	-	number of components
J_D	-	exchange flow
π_s	-	osmotic pressure
L_p	-	phenomenological coefficient
L_{pD}	-	phenomenological coefficient
L_D	-	phenomenological coefficient
J_v	-	total volume flux density (cm^3/s^1)
ω	-	solute permeability
R_{ik}	-	phenomenological resistance coefficient
A_{ik}	-	minor of L_{ik} in $ L $
$ L $	-	determinant of L_{ik}
μ_s	-	chemical potential of electrolyte
I	-	electric current density (amp/cm^2)
E	-	electromotive force

Section 3.1.3

C_i	-	concentration of i ($\text{mol}\cdot\text{cm}^{-3}$)
F	-	Faraday's number
F_{ik}	-	frictional force of k on i per mol of i
f_{ik}	-	molar frictional coefficient of i with k
J_i	-	flux density of i ($\text{mol}\cdot\text{cm}^{-2}\cdot\text{s}^{-1}$)
k	-	specific electrical conductance
v_i	-	mean velocity of i
X_i	-	force on i per mol

Section 3.2

J_1	-	flow of cation J_1
J_2	-	flow of anion J_2

$\Delta \tilde{\mu}_i$	-	difference in electrochemical potential
L_i	-	phenomenological coefficient
$\Delta \mu_s$	-	chemical potential
I	-	electric current
Z_1	-	valance of cation
Z_2	-	valance of anion
F	-	Faraday's constant
E	-	electromotive force
J_v	-	volume flow
Δt	-	apparent transport number
$\Delta \Psi$	-	potential difference across the membrane

Section 3.3

a	-	$a = X^*/X_t$
c_2^t	-	total concentration of salt in membrane
c_s^*	-	salt concentration in the aqueous solution
c_s^{av}	-	average concentration of salt in the two solutions adjacent to the membrane
c_1^*, c_2^*	-	concentration of the free counter- and co-ions in the membrane
c_s	-	concentration of associated salt in the membrane
E	-	electromotive force
F	-	Faraday's constant
f_{ij}	-	frictional coefficient
f_{12}	-	frictional coefficient between co- and counter-ions
I	-	electrical current
J_i	-	flow of species i
J_1, J_2	-	stoichiometric flows of counter-ions and co-ions, respectively
J_s	-	flow of salt
J_1^*, J_2^*	-	flow of free counter-ions and co-ions, respectively
k	-	distribution coefficient of salt between membrane and aqueous phases
K_d^s	-	dissociation constant of salt in the membrane
K_d^f	-	dissociation constant of fixed group in the membrane
L_p	-	filtration coefficient
m	-	$m = K_d^s/K_d^f$
Δp	-	pressure difference
P_E	-	electro-osmotic pressure measured at zero volume flow and the absence of salt gradients

q^2	-	degree of coupling
R_{11}^*	-	straight resistance coefficients for transport of counter-ions, co-ions
R_{22}^*, R_s	-	and salt, respectively
R_{12}	-	coupling resistance coefficient between flows of ion 1 and 2
R	-	universal gas constant
T	-	absolute temperature
X_i	-	driving force for species i
X_1, X_2, X_s	-	driving forces for transport of counter-ions, co-ions and salt, respectively
X_t	-	total concentration of fixed groups in the membrane
X^*	-	concentration of dissociated fixed groups in the membrane
Xc_1	-	associated fixed groups in the membrane
z_i	-	valency of ion i
α	-	$\alpha = K_d^s kc_s^{-2}$
β	-	electro-osmotic permeability measured at zero pressure and salt gradient
t_1, t_2	-	transport number of counter-ions and co-ions, respectively
ψ, ψ'	-	electric potential in aqueous and membrane phases
$\mu_i^0, \mu_i^{0'}$	-	standard chemical potential of species i in membrane and aqueous solution, respectively
$\tilde{\mu}_1, \tilde{\mu}_2$	-	electrochemical potential of counter-ion 1 and of co-ion 2 in membrane, respectively
$\Delta \tilde{\mu}_i$	-	difference in electrochemical potential of species i
$\tilde{\mu}_1', \tilde{\mu}_2'$	-	electrochemical potential of counter-ion 1 and of co-ion 2 in aqueous solution, respectively
μ_s	-	chemical potential of salt in membrane
$\Delta \tilde{\mu}_i$	-	difference in electrochemical potentials of species i
κ	-	membrane conductance measured in the absence of salt gradient and volume flow
κ'	-	membrane conductance measured in the absence of a pressure gradient
ω_s	-	salt permeability defined for $J_v = 0$
ω_s'	-	salt permeability defined for $\Delta p - \Delta \pi = 0$ and $I = 0$
ω_s''	-	salt permeability defined for $\Delta p = 0$ and $I = 0$
$\frac{\omega_s c_s^{av}}{\kappa F^2}$	-	leak conductance (LC) ratio defined for $J_v = 0$
σ	-	reflection coefficient

Section 3.5

Δc^0	-	concentration difference across membrane at time $t = 0$
$c^{\circ'}$	-	concentration at one side of the membrane at time $t = 0$
$c^{\circ''}$	-	concentration at other side of membrane at time $t = 0$
Δc^t	-	concentration difference across membrane after time t
J_1	-	total counter-ions
J_w	-	water flux
\bar{t}_2	-	co-ion transport number
\bar{t}_w	-	water transport number
\bar{t}_1	-	counter-ion transport number
\bar{t}_1^r	-	reduced transport number of counter-ions
\bar{m}	-	mean molality
J_s, J_w^{os}	-	diffusion and osmotic fluxes
I	-	electric current
ω	-	-1 for cation-exchange membrane; +1 for anion-exchange membrane
$f(L_{ik}, \bar{m})$	-	combination of the phenomenological conductance coefficient L_{ik} and the mean mobility, \bar{m} , of a solute
$\Delta \mu_s$	-	chemical potential difference of the solute
I	-	electric current
$\Delta c_a^t, \Delta c_c^t$	-	concentration changes of anolyte and catholyte after time Δt
\bar{c}^0	-	mean concentration of anolyte and catholyte at time $t = 0$, $\bar{c}^0 = (c_a^0 + c_c^0)/2$
η_E	-	efficiency of energy conversion
J_1^w	-	$J_1/v_1 - 0,018 \bar{m} J_w$
ΔE	-	difference of electrical potential measured with electrodes reversible to co-ions

Section 3.6

c_i	-	concentration of species i , mol.m ⁻³
E	-	potential difference. V
I	-	current density, A.m ⁻²
J_i	-	flux density of species i , mol.m ⁻² .s ⁻¹
L_{ik}	-	conductance coefficients
m_{ext}	-	external molality of NaCl
q, q_{ik}	-	coupling coefficients
\bar{t}_w	-	transport number of water, mol per Faraday
X_i	-	thermodynamic force

x	-	force ratio
Z	-	square route of the straight conductance coefficients
η	-	efficiency of energy conversion
μ_i	-	chemical potential of species i, J.mol ⁻¹
π	-	osmotic pressure, Pa
ϕ	-	dissipation function
1	-	sodium ions
s	-	solute
w	-	water

Section 3.7

J_w	-	osmotic flow of water
J_s	-	diffusion flow of solute
$\Delta\mu_s, \Delta\mu_w$	-	differences of chemical potential of solute and water, respectively
L_{ik}	-	phenomenological conductance coefficient
J'_w	-	flow of water against the flow of solute conjugated to the concentration part of the chemical potential difference of water, $\Delta\mu_w^c$
J_v	-	total volume flow conjugated to the difference of pressure in the compartments on the opposite side of the membrane, Δp
ϕ	-	dissipation function
η	-	efficiency of energy conversion
q	-	coupling coefficient
$\Delta\pi$	-	difference in osmotic pressure
σ	-	reflection coefficient

Section 3.8

Π	-	osmotic swelling pressure
\bar{a}_w	-	water activity in membrane
a_w	-	water activity outside membrane
R	-	gas constant
T	-	absolute temperature
\bar{C}	-	internal equilibrium electrolyte concentration
C	-	concentration mol/l
v_w	-	partial molar volume of the internal water component

Section 3.9

E	-	total electromotive force of membrane cell
M	-	molecular mass of solvent
m	-	concentration
\bar{t}_w	-	water transport number
\bar{t}_i	-	transport number
R	-	gas constant
T	-	absolute temperature
F	-	Faraday
a	-	activity
$t_{+(app)}$	-	apparent transport number
t_+	-	true transport number
\bar{X}	-	fixed charge density (equivalent per unit volume of swollen membrane)
\bar{s}	-	equivalent of co-ions per equivalent of fixed group present in the membrane
u 's	-	mobilities of ions
\bar{k}'	-	specific conductance of membrane
β	-	volume of water flowing per Coulomb
V	-	volume of water flowing per second (millilitre)
i	-	current in amperes
k_i	-	specific conductance of pore liquid
A	-	pore area
ϕ_w	-	volume fraction of water in the membrane
\bar{X}_v	-	equivalent of fixed groups per unit volume of interstitial water
ΔV_c	-	volume decrease at anode due to water transport
ΔV_o	-	observed volume change
\bar{V}	-	partial molar volume

Sections 3.10 and 3.11

a_i	-	activity of species i (mol/l)
A_m	-	effective membrane area (cm ²)
c_i	-	concentration of species i (mol/l)
F	-	Faraday's constant - 96 500 (amp.sec/mol)
F_i	-	driving force acting on species i
I	-	electric current density (amp/cm ²)
I_{eff}	-	effective current density (amp/cm ²)

j_i	-	flux of species i through a membrane ($\text{mol}/(\text{sec} \cdot \text{cm}^2)$)
J	-	volume flow through a membrane ($\text{cm}/\text{sec} = \text{cm}^3/\text{cm}^2 \cdot \text{sec}$)
L_p	-	filtration coefficient
P	-	solute permeability
Q	-	amount of feed solution entering a diluate channel per unit time
R	-	universal gas constant
s^c	-	salt flux (cation)
s^a	-	salt flux (anion)
t_i	-	transport number of ionic species i
\bar{t}_i	-	effective transport number of the ionic species i
Δt	-	difference between counter-ion and co-ion effective transport members
$\bar{\Delta t}$	-	effective transport number of a membrane pair
T	-	absolute temperature, $^\circ\text{K}$
V_w	-	water flow through a membrane (cm/s)
V	-	volume of solution that enters a membrane bag per unit area
\bar{V}	-	molar volume of species i
Δx	-	membrane thickness
β_i	-	drag coefficients associated with the ionic species i
γ_i	-	activity coefficient of species i
δ	-	thickness of the unstirred layer next to a solid surface
e_c	-	overall current efficiency
e_p	-	Coulomb efficiency (current efficiency)
e_w	-	efficiency associated with water transport through membranes
Δ	-	degree of demineralization
μ_i	-	chemical potential of ionic species i
$\tilde{\mu}_i$	-	electrochemical potential of ionic specie i
$\Delta \Psi_m$	-	electrical potential difference between reversible electrodes, due to a difference of concentration at both sides of the membrane
π	-	osmotic pressure
σ	-	reflection coefficient
ω	-	salt permeability
η	-	current efficiency
a	-	anion-exchange membrane
c	-	cation-exchange membrane
F	-	Faraday's constant ($\text{Coulomb equiv}^{-1}$)
I	-	current density, amp cm^{-2}
J	-	molar flux, $\text{mol cm}^{-2} \text{ sec}^{-1}$

J_v	-	volume flux, $\text{cm} \cdot \text{sec}^{-1}$
L_p	-	hydraulic permeability $\text{cm} \cdot \text{sec}^{-1}$ per unit pressure
P	-	local solute permeability, $\text{cm}^2 \cdot \text{sec}^{-1}$
R	-	universal gas constant
R_{cp}	-	apparent resistance of cell pair $\text{ohm} \cdot \text{cm}^2$
R_m	-	resistance of membrane pair $\text{ohm} \cdot \text{cm}^2$
S	-	rate of salt removal, $\text{mol}/\text{cm}^2 \cdot \text{s}$
T	-	absolute temperature
V_{cp}	-	voltage per cell pair, volts
c_s	-	salt concentration, mol/cm^3
c_b, c_f	-	concentration of brine, feed, product
c_p	-	respectively, mol/cm^3
d_{eff}	-	effective thickness of dialysate cell, mm
β	-	electro-osmotic coefficient, $\text{cm}^3 \text{Coulomb}^{-1}$
γ_{\pm}	-	activity coefficient
μ_i	-	thermodynamic potential
$\bar{\mu}_i$	-	electrochemical potential
η, η_c	-	efficiency, current efficiency
π	-	osmotic pressure
ρ	-	specific resistance of dialysate, $\text{ohm} \cdot \text{cm}$
t	-	transport number
ψ	-	potential, volt
ω	-	Permeability coefficient

Section 3.12

t_1	-	transport number of cations in solution
t_2	-	transport number of anions in solution
\bar{t}_1^c	-	transport number of cations in CPM
\bar{t}_2^c	-	transport number of anions in CPM
\bar{t}_1^a	-	transport number of cations in APM
\bar{t}_2^a	-	transport number of anions in APM
T_{DC}	-	apparent diffusion transport number of anion near cation membrane
T_{DA}	-	apparent diffusion transport number of cation near anion membrane
N	-	number of membrane pairs
F	-	Faraday's constant
R	-	gas constant

T	-	absolute temperature
E_m	-	membrane potential
T_D	-	flux of salt from the diluate channel
d	-	desalting rate (equiv cm ² .s ⁻¹)
p^c	-	permselectivity of cation membrane
p^a	-	permselectivity of anion membrane
P	-	power required to drive cell pair
i	-	current density
V_{cp}	-	cell pair voltage
δ	-	thicknes of boundary layer
R_d	-	resistance 1 cm ² cross section, d.
κ	-	conductivity (ohm/cm) ⁻¹
C_d	-	concentration of diluate stream (equiv/cm ³)
C_c	-	brine concentration (equiv/cm ³)
C_c/C_d	-	C = non-dimentsional concentration ratio term
Λ	-	equivalent conductivity in cm ² /ohm equiv.
R_{BC}	-	boundary layer resistance at cation membrane
R_{BA}	-	boundary layer resistance at anion membrane
C_w	-	solute concentration at membrane/diluate interface
C_{w1}	-	bulk concentration of concentrated salt on one side of membrane
C_{w2}	-	bulk concentration of dilute salt solution on other side of membrane
C_{wbc}	-	concentration-polarized membrane/boundary layer concentration at brine side of cation membrane
C_{wdc}	-	concentration-polarization membrane/boundary layer concentration at diluate side of anion membrane
Ud	-	flow rate
λ	-	cell to boundary layer thickness ratio
D	-	diffusion coefficient (cm ² /s)
R	-	gas constnt
β	-	$\frac{F^2D}{\Delta t_2 RT}$

14. LITERATURE

1. Garza, G. (1973): Electrodialysis by Electro-Osmotic Pumping and Ion Separation with Charged Membranes. Thesis submitted to the Weizmann Institute of Science, Rehovot, Israel.
2. Garza, G., and Kedem, O. (1976): Electro-Osmotic Pumping in Unit-Cells. 5th International Symposium on Fresh Water from the Sea, 13, 79-87.
3. Kedem, O., Tanny, G. and Maoz, G. (1978): A simple Electrodialysis Stack. *Desalination*, 24, 313-319.
4. Kedem, O., and Cohen, J. (1983): EDS-Sealed-Cell Electrodialysis. *Desalination*, 46, 291-299.
5. Kedem, O., and Bar-On, Z. (1986): Electro-Osmotic Pumping in a Sealed-Cell ED Stack. AIChE Symposium Series, Industrial Membrane Processes, 248, 82, 19-27.
6. Nishiwaki, T. (1972): Concentration of Electrolytes prior to Evaporation with an Electromembrane Process, In: R.E. Lacey and S. Loeb (Ed.), Industrial Processing with Membranes, Wiley-Inter-Science, New York.
7. Wilson, J.R. (1960): Demineralization by Electrodialysis, London, Butterworth Scientific Publications.
8. U.S.A.I.D. Desalination Manual (1980). CH & M, International Corporation, 7201 NW, 11th Place, Gainesville, Florida, USA, 32601.
9. Meares, P., Thain, J.F., and Dawson, D.G. (1972): Transport Across Ion-Exchange Resin Membranes: The Frictional Model of Transport, In: Eisenmann, G. (Ed), Membranes, A Series of Advances, Volume 1, Macroscopic Systems and Models, Marcel Dekker, Inc. New York.
10. Teorell, T. (1953): Transport Processes and Electrical Phenomena in Ionic Membranes. *Progr. Biophys. Biophys. Chem.*, 3, 305.
11. Helfferich, F. (1962): *Ion-Exchange*, McGraw-Hill, New York, 344.

12. Staverman, A.J. (1952): Non-Equilibrium Thermodynamics of Membrane Processes. *Trans. Faraday soc.*, 48, 176.
13. Catchalsky, A., and Curren, P.F. (1965): Non-Equilibrium Thermodynamics In Biophysics, Harvard University Press, Cambridge Mass.
14. Kedem, O., and Katchalsky, A. (1963): Permeability of Composite Membranes. *Trans. Faraday Soc.*, 59, 1918, 1931, 1941.
15. Kedem, O. (1983): A Simple Procedure for Estimating Ion Coupling from Conventional Transport Coefficients. *Journal of Membrane Science*, 14, 249-262.
16. Johnstone, B.L. (1987): Lecture on Basic Principles of Electrodialysis.
17. Koter, S., and Narebska, A. (1989/90): Current Efficiency and Transport Phenomena in Systems with Charged Membranes. *Separation Science and Technology*, 24, (15), 1337-1354.
18. Narebska, A., and Koter, S. (1987): Irreversible Thermodynamics of Transport Across Charged Membranes. Part III - Efficiency of Energy Conversion in Separation Processes with Nafion 120 Membrane from Phenomenological Transport Coefficients. *Journal of Membrane Science*, 30, 141 - 152.
19. Narebska, A., koter, S., and Kujowski, W. (1990): Conversion of Osmotic Energy in Systems with Charged Membranes. *Journal Non-Equilibrium Thermodynamics*, 15, 1 - 10.
20. Brydges, T.G., and Lorimer, J.W. (1983): The Dependence of Electro-Osmotic Flow on Current Density and Time. *Journal of Membrane Science*, 13, 291-305.
21. Kruissink, C.H.A. (1983): The effect of Electro-Osmotic Water Transport on Current Efficiency and Cell Performance in Chlor-Alkali Membrane Electrolysis. *Journal of Membrane Science*, 14, 331-366.
22. Hidalgo-Alvarez, R., de las Nieves, F.J. and Pardo, G. (1984): Anamalous Electro-Osmotic Flow through a Heteroporous Ion-Exchange Membrane - A Test Based upon the Reciprocity Relations. *Journal of Non-Equilibrium Thermodynamics*, 9, 157-1643.

23. Ceynowa, Josef (1983): Electro-Osmosis in the System Ion-Exchange Membrane-Sulphuric Acid Solution. *Die Angewandte Makromolekulare Chemie*, 116, 165-174 (No 1824).
24. Tombalakion, A.S., Barton, H.J., Graydon, W.F. (1962): *Journal Physical Chemistry*, 66, 1006.
25. Rueda, C., Ruiz-Bauza, C., and Agular, J. (1977): Electro-Osmotic Permeability of Cellulose Acetate Membranes. *Journal Physical Chemistry*, 61, 789.
26. Tasaka, Masayasu., Tamura, Staoski., and Takemura, Naota (1982): Concentration Dependence of Electro-Osmosis and Streaming Potential across Charged Membranes. *Journal of Membrane Science*, 12, 169-182.
27. Oda, Goshio., and Yawataya, Tadaski (1957): On the Distribution and Behaviour of Water in Cation-Exchange Resin Membranes. *Bulletin of the Chemical Society of Japan*, 30, (3), 213.
28. Narebska, A., Koter, S., and Kujowski, W. (1984): Ions and Water Transport Across Charged Nafion Membranes. Irreversible Thermodynamic Approach. *Desalination*, 51, 3 - 17.
29. Narebska, A. and Koter, S. (1987): Conductivity of Ion-Exchange Membranes - Convection Conductivity and Other Components. *Electro-Chimica Acta*, 32, (3), 449 - 453.
30. Narebska, A., Kujowski, W., and Koter, S. (1987): Irreversible Thermodynamics of Transport Across Charged Membranes, Part II - Ion-Water Interactions in Permeation of Alkali. *Journal of Membrane Science*, 30, 125 - 140.
31. Narebska, A., Koter, S., and Kujowski, W. (1985): Irreversible Thermodynamics of Transport Across Charged Membranes. 1. Macroscopic Resistance Coefficients for a System with Nafion 120 Membrane. *Journal of Membrane Science*, 25, 153 - 170.
32. Koter, S., and Narebska, A. (1987): Conductivity of Ion-Exchange Membranes. *Electrochimica Acta*, 32, (3), 455 - 458.
33. Kononov, A.N., Ponomarev, M.I., Shkaraputa, L.N., Grebenyuk, V.D., and Sklyar, V.T. (1984): Removal of Hydrochloric Acid from Waste Waters Containing Organic Synthesis Products. *Khimiya i Teckhnologiya Vody*, 6, (1), 66-68.

34. Korngold, E. (1978): Concentration of sulphuric and Hydrochloric Acids. *Electrodialysis in Advanced Waste Water Treatment*, 24, 129-139.
35. Laskorin, B.M., Smirnova, N.M., Tisov, Y., Gorina, G.N., and Borisov, A.V. (1973): Use of Electro dialysis with Ion-Selective Membranes for Concentrating Carbonate Solutions. *Zhurnal Prikladnoi Khimii*, 46, (9), 2117-2119.
36. Smagin, V.N., and Chukkin, V.A. (1975): Concentration of Brines of Desalination Plants with Electro dialysis. *5th International symposium on Fresh Water from the Sea*, 3, 139-148.
37. Urano, K., Ase, T., and Naito, Y. (1984): Recovery of Acid from Wastewater by Electro dialysis. *Desalination*, 51, 213-226.
38. Itoi, S., Nakamura, I., and Kawahara, T. (1980): Recovery of Metals from Plating Rinse Waters. *Desalination*, 32, 383.
39. Schoeman, J.J. (1985): The Status of Electro dialysis Technology for Brackish and Industrial Water Treatment. *Water SA*, 11, (2), 79-86.
40. Lakshminarayanan, N. (1962): Electro-Osmotic Permeability of Ion-Exchange Resin Membranes. *Proceedings Indian Academy, Sci.*, A55, 200.
41. Demarty, M., Maurel, A., and Selegny, E. (1974). *Journal Chim. Phys., Phys. Chim. Biol.*, 71, 811.
42. Mauritz, K.A., and Hopfinger, A.J. (1982): Structural Properties of Membrane Ionomers, In: *Modern Aspects of Electrochemistry*, 14, J.O.M. Bockris, B.E. Conway, and R.E. White, Eds., Plenum Publishing Corp., Ch.6.
43. Narebska, A., and Wodzki, R. (1982): Swelling Equilibria and Structure Variations of Nafion and Polyethylene (Polystyrene Sulphonic Acid) Membranes at High Electrolyte Concentrations and Increased Temperature. *Die Angewandte Makromolekulare Chemie*, 107, 51 - 60 (No. 1679).
44. Narebska, A., Wodzki, R., and Erdmann, K. (1983): Properties of Perflurosulphonic Acid Membranes in Concentrated Sodium Chloride and Sodium Hydroxide Solutions. *Die Angewandte Makromolekulare Chemie*, 111, 85 - 95 (No. 1711).

45. Lakshminarayanaiah, N. (1969): *Transport Phenomena In Membranes*. Academic Press, Inc. 111 Fifth Avenue, New York, New York 10003.
46. Kressman, T.R.E., and Tye, F.L. (1956): *Discussions Farady Soc.* 21, 185.
47. Lakshminarayanaiah, N., and Subrahmanyam, V. (1964): *J Polymer Sci. Pt. A* 2, 4491.
48. Boudet-Dumy, M., Lindheimer, A., and Gavach, C. (1991): Transport Properties of Anion-Exchange Membranes In Contact with Hydrochloric Acid Solutions. Membranes for Acid Recovery by Electrodialysis. *Journal of Membrane Science*, 57, 57-68.
49. Cherif, A.T., and Gavach, C. (1988): Sulphuric Acid Concentration with an Electrodialysis Process, *Hydrometallurgy*, 21, 191.
50. Huang, T.C., and Juang, R.S. (1986): Recovery of Sulphuric Acid with Multi-Compartment Electrodialysis. *Ind. Eng. Chem. Processes Des. Dev.*, 25, 537.
51. Nott, B.R. (1981): Electrodialysis for Recovering Acid and Caustic from Ion-Exchange Regeneration Wastes. *Ind. Eng. Chem. Prod. Res. Dev.*, 20, 170.
52. Grebenyuk, V.D., Penkalo, I.I., and Chalaya, L.M. (1986): Desalination of Water with Simultaneous Production of Alkali and Acid. *Khim. Teknol. Vody*, 8, 76.
53. Leitz, F.B. (1976): Electrodialysis for Industrial Water Clean-Up. *Environ. Sci. Technol.*, 10, 136.
54. Eisenmann, J.L. (1979): Membrane Processes for Metal Recovery from Electroplating Rinse Water. Second Conference on Advanced Pollution Control for the Metal Finishing Industry, E.P.A., Cincinnati, OH, 99.
55. Hanley, T.R., Chiu, H.K., and Urban, R.J. (1985): Phosphoric Acid Concentration by Electrodialysis. *AIChE Symp. Ser.*, 82, 121.
56. McRae, W.A. (1983): In *Desalination Technology, Developments and Practice* (A. Porteous, ed), *Applied Science*, Chapter 8.

57. Iaconelli, W.B. (1973): The Use of Electrodialysis in the Food Industry, Paper presented at the IFT Annual Meeting.
58. Reed, P.B., (1984): *Chem. Eng. Prog.*, 47.
59. Barney, J.J., and Hendrik, J.L., (1878): *Chem. Prod. Res. Dev.*, 17, 17.
60. Bhagat (1980): *Water Pollution Control*, 11, 118.
61. Melzer, J., and Van Deventer, D. (1983): Electrodialysis Used for Desalination of Waste Water in an Eskom Power Station. -- Presented at a Symposium on Desalination: New Developments and Industrial Application, CSIR Conference Centre, Pretoria, 27 October 1983.
62. Gering, K.L., and Scamehorn, J.F. (1988): Use of Electrodialysis to Remove Heavy Metals from Water. *Separation Science and Technology*, 23, (14 & 15), 2231-2267.
63. Goldman, D.E. (1943): Potential, Impedance and Rectification in Membranes. *J. Gen. Physiol.*, 27, 37.
64. Kirkwood, J.G. (1954): In *Ion Transport Across Membranes* (H.T. Clarke, ed), Academic, New York, 119.
65. Miller, D.G. (1960): Thermodynamics of Irreversible Processes. *Chem. Rev.*, 60, 15.
66. Kedem, O., and Katchalsky, A. (1958): Thermodynamic Analysis of the Permeability of Biological Membranes to Non-Electrolytes. *Biochim. Biophys. Acta.* 27, 229.
67. Krämer, H., and Meares, P. (1969): Correlation of Electrical and Permeability Properties of Ion-Selective Membranes. *Biophys. J.*, 9, 1006.
68. Kedem, O., and Essig, A. (1965): Isotope Flows and Flux Ratios in Biological Membranes. *J. Gen. Physiol.*, 48, 1047.
69. Coster, H.G.L. and George, E.P. (1968): A Thermodynamic Analysis of Fluxes and Flux-Ration in Biological Membranes. *Biophys. J.*, 8, 457.

70. Mazur, P. and Overbeek, J.T. (1951): On Electro-Osmosis and Streaming-Potentials in Diaphragms. *Rec. Trav. Chim.*, 70, 83.
71. Spiegler, K.S. (1958): *Trans. Faraday Soc.*, 54, 1408.
72. Kedem, O. and Caplan, S.R. (1965): Degree of Coupling and its Relation to Efficiency of Energy Conversion. *Trans. Faraday Soc.*, 61, (9), 1897.
73. Kedem, O., and Perry, M. (1977): Proc. Symp. on the Behaviour of Ions in Macromolecular and Biological Systems, Colston, England, 134.
74. Caplan, S.R. (1965): The Degree of Coupling and Efficiency of Fuel Cells and Membrane Desalination Processes. *J. Phys. Chem.*, 69, 3801.
75. Lee, K.H., Baker, R.W., and Lonsdale, H.K. (1981): Membranes for Power Generation by Pressure Retarded Osmosis. *Jour. Membrane Science*, 8, 141.
76. Donnan, F.G. (1924): *Chem Rev.* 1, 73.
77. Hale, D.K., and McCauley, D.J. (1961): *Trans. Faraday Soc.* 57, 135.
78. Lakshminarayanaiah, N. (1965): *Chem. Rev.* 65, 531.
79. Lakshminarayanaiah, N. (1969): *J. Phys. Chem.* 73, 97.
80. Oda, Y., and Yawataya, T. (1956): *Bull. Chem. Soc. Japan.* 29, 673.
81. Harned, H.S., and Owen, B.B. (1958): "The Physical Chemistry of Electrolytic Solutions", 3rd ed., p. 359. Reinhold, New York.
82. Spiegler, K.S., and Kedem, O. (1966): Thermodynamics of Hyperfiltration (Reverse Osmosis): Criteria for Efficient Membranes. *Desalination*, 1, 311-326.
83. Ionics Pamphlet on EDR (1987).

84. Katz, W.E. (1977): The Electrodialysis Reversal (EDR) Process. Presented at the International Congress on Desalination and Water Reuse, Tokyo, November/December 1977. Published by Ionics, Inc., 65 Grove Street, Watertown, MA, USA 02172 (Bulletin TP. 307).
85. Leitz, F.B. and Eisenmann, J.L. (1981): Electrodialysis as a Separation Process. A.I.Ch.E. Symposium Series 77, 204-209.
86. Tani, Y. (1981): Energy Saving Electrodialyzer for Seawater Desalination. Technical Proceedings, Ninth Annual Conference, National Water Supply Improvement Association, Washington, D.C. Published by NIWSA, 26 Newbury Road, Ipswich, NA, USA, 01938.
87. Urano, K. (1977): Present Status of Electrodialysis Process in Japan. *Desalination*, 20, 365.
88. Wirth, J.R. and Westbrook, G. (1977): Cooling Water Salinity and Brine Disposal Optimized with Electrodialysis Water Recovery/Brine Concentration System. *Combustion*, May, 33-37.
89. Lakshminarayanan, N. (1965): *Chem. Revs.* 65, 494.
90. Friedlander, H.Z. and Rickles, R.N. (1966): *Anal. Chem.* 37, 27A.
91. Molau, G.E. (1981): Heterogeneous Ion-Exchange Membranes. *Journ. of Membrane Science*, 8, 309-330.
92. Korngold, E., De Körösy, F., Rahav, R. and Taboch, M.F. (1970): Fouling of Anion-Selective Membranes in Electrodialysis. *Desalination*, 8, 195.
93. Van Duin, P.J. (1973): Poisoning of Electrodialysis Membranes. Proceedings of 4th International Symposium on Fresh Water from the Sea, 3, 253-259.
94. Katz, W.E. (1982): Desalination by ED and EDR-State-of-the-Art in 1981. *Desalination*, 42, 129.
95. Fraivillig, J.B. (1983): Reverse Osmosis/Electrodialysis Reversal Comparison. Permasep Products (Du Pont), Maylands Avenue, Hemel Hempstead, Herts, HP2-7DP.

96. Miva, T. (1977). Desalting by Electrodialysis. *Desalination*, 20, 375.
97. Song, Shi and Pei-Qi Chem (1983): Design and Field Trials of a 200 m³/day Seawater Desalination by Electrodialysis. *Desalination*, 46, 191.
98. Parsi, E.J., Prato, T.A. and P'Donoghue, K. (1980): Status of High Temperature Electrodialysis. Presented at the Eighth Annual Conference of the National Water Supply Improvement Association, San Francisco, 6-10 July.
99. Brown, D.R. (1981): Desalting High Salinity Water Using 10-Stage EDR. Proceedings of the Ninth Annual Conference and International Trade Fair of the National Water Supply Association, 2.
100. Elyanow, D., Parent, R.G. and Mahoney, J. (1980): Parametric Tests of an Electrodialysis Reversal System with Aliphatic Anion Membranes. Report to WRT, US Department of the Interior (Contract No. 14-34-0001-9510), Washington, D.C.
101. Katz, W.E. (1971): Electrodialysis for Low TDS Waters. *Ind. Water Engng.*, June/July (Bulletin TP.301).
102. Highfield, W.H. (1980): Electrodialysis in Industrial Water Treatment. Presented at the 41st Annual Meeting of the International Water Conference, Pittsburgh, Pennsylvania, October, 1980. (Bulletin TP.316).
103. Itoi, S. (1979): Electrodialysis of Effluents from Treatment of Metallic Surfaces. *Desalination* 28, 193.
104. Trivedi, D.S., and Prober, R. (1972): On the Feasibility of Recovering Nickel from Plating Wastes by Electrodialysis. *Ion Exch. Membr.*, 1, 37.
105. Eisenmann, J.T. (1977): Recovery of Nickel from Plating Bath Rinse Waters by ED. *Plat. Surf. Finish.*, 64 (11), 34.
106. Jordan, D.R., Bearden, M.D. and Mclhenny, W.R. (1975): Blowdown Concentration by Electrodialysis. *Chem. Engineering. Prog.*, 71(7), 77.

107. Jordan, D.R., Mclhenny, W.F., and Westbrook, G.T. (1976): Cooling Tower Effluent Reduction by Electrodialysis. American Power Conference.
108. Westbrook, G.T. and Wirth, L.F. Jr. (1976): Water Reuse by Electrodialysis. *Ind. Water Engng.*, April/May 8.
109. Smirnova, N.M., Laskorin, B.N., Mishukova, J.S. and Borisov, A.V. (1983): The Application of Electrodialysis with Ion-Exchange Membranes for Treatment of Sodium Sulphate Solutions. *Desalination*, 46, 197.
110. Nott, B.R. (1981): Electrodialysis for Recovering Acid and Caustic Soda from Ion-Exchange Regeneration Wastes. *Ind. Engng. Chem. Product Des. and Dev.*, 20, (1).
111. Schoeman, J.J. and Botha, G.R. (1981): Behandeling van Industriële Uitvloeisels met Elektrodialise. Presented at a Symposium on Industrial Effluents, 23 November, Pretoria.
112. Oren, G. and Litan, J. (1974): The State of the Solution Membrane Interface during Ion Transport Across and Ion-Exchange Membrane. *Journ. Physical Chemistry*, 78, 1805.
113. Simon, G.P. and Calmon, C. (1986): Experimental Mehtods for the Determination of Non-Transport Properties of Membranes. *Desalination*, 59, 106, 103.
114. Kneifel, K., and Hattenbach, K. (1980): Properties and Long-Term Behaviour of Ion-Exchange Membranes. *Desalination*, 34, 77.
115. Schoeman, J.J., Hill, E., Enslin, G.M. and MacLeod, H. (1990): Electro-Osmotic Pumping of Salts, Acids and Bases. Contract Report to the Water Research Commission.
116. Schoeman, J.J. and Enslin, G.M. (1989): Evaluation of Sealed-Cell Electrodialysis for Industrial Effluent Treatment. Contract Report to the Water Research Commission.
117. Kedem, O. (1992): Private Communication.

APPENDIX A

1. DEFINITION OF TRANSPORT NUMBERS

- a) Transport number of ion i , t_i :

$$t_i = (z_i J_i F / I)_{\Delta C = 0}, \quad i = 1, 2 \quad (\text{A1})$$

where I is the electric current, J_i is the flux of species i , z_i is its charge, and F is the Faraday constant.

- b) Reduced transport number of species i (6), t_i^r .

For ions ($i = 1, 2$):

$$t_i^r = \frac{1}{z_i} t_i = \left(\frac{F J_i}{I} \right)_{\Delta C = 0}$$

For water:

$$t_w^r = t_w = \left(\frac{F J_w}{I} \right)_{\Delta C = 0} \quad (\text{A2})$$



APPENDIX B

1. **DERIVATION OF THE FORMULA FOR THE CURRENT EFFICIENCY (Eq. 3.5.3, Fig. 3.5.1)**

At $t = 0$ the concentrations of the anode ($i = a$) and the cathode ($i = c$) solutions are

$$c_i^{\circ} = n_i^{\circ}/V^{\circ}, \quad i = a, c \quad (\text{B1})$$

where n_i° is the number of moles of an electrolyte in the "i" solution. The volumes of both solutions are equal and denoted by V° . After passing the current I during time Δt , the concentrations in both compartments change to

$$c_i^t = (n_i^{\circ} + \Delta n_i) / (V^{\circ} + \Delta V_i), \quad i = a, c \quad (\text{B2})$$

where Δn_i and ΔV_i are the changes of the amount of an electrolyte and of the volume in the "i" compartment, respectively. Assuming $\Delta V_i \ll V^{\circ}$, from eqs. (B1) and (B2) we obtain

$$\Delta c_c^t - \Delta c_a^t = (\Delta n_c - \Delta n_a - c_c^{\circ} \Delta V_c + c_a^{\circ} \Delta V_a) / V^{\circ} \quad (\text{B3})$$

For the standard system (Fig. 3.5.1), the changes of ΔV_i and Δn_i are as follows:

Real membrane:

$$\begin{aligned} \Delta n_i &= z_i(\Delta n^m + \Delta n^{\text{mid}}) \\ &= z_i \omega J_i / v_i \Delta t \quad (\text{moles of } A v_1 B v_2) \end{aligned} \quad (\text{B4})$$

$$\begin{aligned} \Delta V_i &= z_i(\Delta V^m + \Delta V^{\text{mid}}) \\ &= z_i \omega (\bar{v}_s J_i / v_i + \bar{v}_w J_w) \Delta t, \quad i = a \text{ or } c \end{aligned} \quad (\text{B5})$$

where $z_a = 1$, $z_c = -1$

Δn^m and ΔV^m denote changes in the amounts of ions and of volume due to the transport across the investigated membrane, respectively

$$\Delta n^m = \omega J_1 \Delta t / v_1 (A v_1 B v_2) + x / |z_2| \quad (\text{B6})$$

$$\Delta V^m = \left(\omega \bar{v}_s J_1 / v_1 + \bar{v}_w J_w + \frac{\bar{v}_2}{|z_2|} \frac{I}{F} \right) \Delta t \quad (\text{B7})$$

Δn^{mid} and ΔV^{mid} denote analogical effects of transport across ideal membranes surrounding the investigated membrane

$$\Delta n^{\text{mid}} = -x/|z_2|(B^{z_2}) \quad (\text{B8})$$

$$\Delta V^{\text{mid}} = -\frac{\bar{v}_2}{|z_2|} x \quad (\text{B9})$$

$$x = |A\Delta t/F| \quad (\text{B10})$$

$$J_1 = -\omega \bar{t}_1^r I/F + v_1 J_s \quad (\text{B11})$$

$$J_w = -\omega \bar{t}_w I/F + J_w^{\text{os}} \quad (\text{B12})$$

Ideal membrane ($\bar{t}_2, \bar{t}_w, J_s, J_w^{\text{os}} = 0$):

Equations (B4) and (B5) are simplified to

$$\Delta n_1 = -z_1 \frac{1}{z_1 v_1} x \quad (\text{B13})$$

$$\Delta V_1 = -z_1 \frac{\bar{v}_s}{z_1 v_1} x \quad (\text{B14})$$

By substituting eqs. (B13), (B14) and (B3) into eq. (5), we obtain :

$$(\Delta c^t - \Delta \bar{c}^o)_{\text{ideal}} = \frac{2(1 - \bar{v}_s \bar{c}^o)x}{z_1 v_1 V^o} \quad (\text{B15})$$

By substituting eqs. (B4) and (B5) through eqs. (B3) and (B15) in the formula defining the current efficiency (eq. 3.5.1), we obtain:

$$\text{CE} = \frac{z_1 v_1 F}{I} \left[\frac{J_1}{v_1} - \frac{c^o \bar{v}_w}{1 - \bar{v}_s \bar{c}^o} J_w \right] \quad (\text{B16})$$

By introducing eqs. (B11) and (B12) into eq. (B16), we finally obtain:

$$CE = z_1 v_1 \left[\frac{\bar{t}_1^r}{v_1} - \left(\frac{\bar{c}_s}{\bar{c}_w} \right) \bar{t}_w - \omega \left(J_s - \left(\frac{\bar{c}_s}{\bar{c}_w} \right) J_w^{os} \right) \frac{F}{I} \right] \quad (B16a)$$

where

$$\left(\frac{\bar{c}_s}{\bar{c}_w} \right) = \frac{\bar{v}_w \bar{c}^\circ}{1 - \bar{v}_s \bar{c}^\circ} = 0,018 \tilde{m} \quad (B17)$$

$$\bar{c}^\circ = (c_a^\circ + c_k^\circ)/2 \quad (B18)$$

2. THE SYSTEM WITH ELECTRODE REACTIONS

In practice, in any system there are electrodes and electrode reactions which cause additional variations in the concentrations in mol/dm³ of the solutions. Consequently, the differences Δn_i^{cor} and ΔV_i^{cor} will appear:

$$\Delta n_i^{mid} = z_i \Delta n^{mid} = \Delta n_i^{el} + \Delta n_i^{cor}, \quad i = a, c \quad (B19)$$

$$\Delta V_i^{mid} = z_i \Delta V^{mid} = \Delta V_i^{el} + \Delta V_i^{cor}, \quad i = a, c \quad (B20)$$

where Δn_i^{el} and ΔV_i^{el} denote changes of amount of ions and volume due to electrode reactions.

By substituting eqs. (B19) and (B20) through eqs. (B3) and (B5) into eq. (6), we obtain:

$$CE = \frac{z_1 v_1}{2(1 - \bar{v}_s \bar{c}^\circ)} \left[\frac{V^\circ F}{I} \left(\frac{\Delta c_c^t}{\Delta t} - \frac{\Delta c_a^t}{\Delta t} \right)^{pract} + \frac{\Delta \bar{n}_c^{cor} - \Delta \bar{n}_a^{cor} - c_c^\circ \Delta \bar{V}_c^{cor} + c_a^\circ \Delta \bar{V}^{cor}}{\text{correction}} \right] \quad (B21)$$

where $\Delta \bar{n}_i^{cor} = \omega \Delta n_i^{cor}/x$; $\Delta \bar{V}_i^{cor} = 1 - \omega \Delta V_i^{cor}/x$, $i = a, c$

$\Delta \bar{n}_i^{cor}$ and $\Delta \bar{V}_i^{cor}$ for some systems are presented in Table 1. Substitution in the right-hand term of eq. (B21) gives the necessary corrections⁽¹⁷⁾.



Table 1: Δn_i^{cor} and ΔV_i^{cor} for different electrode/electrolyte/membrane systems (eq. B21).

Electrode	Cation-exchange membrane		Anion-exchange membrane ($z_2 = z$)	
	$i = a, c; z_s = 1; z_c = -1$			
	$\Delta \bar{n}_i^{\text{cor}}$	ΔV_i^{cor}	Δn_i^{cor}	ΔV_i^{cor}
Ag/AgCl Solute: MeCl_z	0	$z_i(\bar{v}_{\text{Ag}} - \bar{v}_{\text{AgCl}})$	z/z_2	$z_i(\bar{v}_s/z_2 + \bar{v}_{\text{Ag}} - \bar{v}_{\text{AgCl}})$
Pt Solute: Me(OH)_z	0	c: \bar{v}_w a: $-0.5\bar{v}_w$	z/z_2	c: $-\bar{v}_s/z_2 + \bar{v}_w$ a: $\bar{v}_s/z_2 - 0.5\bar{v}_w$
Pt Solute: H_2SO_4	$-z/2$	c: $0.5\bar{v}_s$ a: $-0.5(\bar{v}_s - \bar{v}_w)$	0	c: 0 a: $0.5\bar{v}_w$



UNIVERSITEIT VAN PRETORIA
UNIVERSITY OF PRETORIA
YUNIBESITHI YA PRETORIA

APPENDIX C

Table 1: Electrodialysis desalination/concentration results of an approximately 1 000 mg/ℓ NaCl solution with Ionac MA-3475 and MC-3470 membranes at 0,5 V/cp (4 v/8 cp; 10V total).

Time min	Current amp	Cf mS/m	Cf mg/ℓ	Cb mS/m	Cb mg/ℓ	pH feed	pH brine
0	0,18	170	992			7,1	
15	0,17	151	880	1 197	7 855	6,6	7,2
30	0,16	139	809	1 610	10 709	6,8	7,3
45	0,15	128	744	1 980	11 429	7,0	7,3
60	0,14	118	685	2 340	14 675	7,4	7,3
75	0,13	109	632	2 660	17 560	7,5	7,1
90	0,12	101	585	2 910	19 814	7,5	7,0
105	0,11	93,6	542	3 180	22 248	7,6	6,9
120	0,10	86,3	499	3 320	23 511	7,6	6,8
135	0,09	79,0	456	3 500	25 133	7,8	7,1
150	0,09	73,1	420	3 610	26 125	7,8	6,8
165	0,08	68,2	392	3 720	27 117	7,6	6,9
180	0,08	62,2	357	3 760	27 478	7,7	6,8
195	0,07	58,5	335	3 770	27 568	7,5	6,8
210	0,07	55,5	317	3 770	27 568	7,6	6,9
225	0,06	48,0	273	3 760	27 478	7,4	6,9
240	0,06	44,3	251	3 760	27 478	7,5	6,9
255	0,05	41,5	235	3 760	27 478	7,3	7,0
270	0,05	37,6	212	3 640	26 396	7,0	7,0

Cross sectional area of diluating chamber is:

$$13 \text{ cm} \times 0,2 \text{ cm} = 2,6 \text{ cm}^2$$

For a linear flow rate of 1 cm/s:

$$2,6 \text{ cm}^2 \times 1 \text{ cm/s} = 2,6 \text{ cm}^3/\text{s} \text{ (flow rate)}$$

Therefore, for 10 diluating chambers, the flow rate must be 1 560 ml/min.



Flow rate used	:	1 350 ml/min
∴ Linear flow velocity	:	0,87 cm/s
Feed volume (beginning)	:	12 l
Product volume (end)	:	11,25 l
Brine volume (end)	:	230 ml
Brine conductivity	:	3 150 mS/m
Brine concentration	:	21 981 mg/l

$$\begin{aligned}
 \int f(x) dx &= 15/2 (l_1 + 2 (l_2 + l_3 + \dots + l_{n-1}) + l_n) \\
 &= 7,5 (3,69) \\
 &= 27,675 \text{ amp.min} \\
 &= 1660,5 \text{ amp.s (coulombs)}.
 \end{aligned}$$

Salt equivalents removed:

$$\begin{aligned}
 \text{Beginning: } 12 \text{ l} \times 992 \text{ mg/l} &= 11\,904 \text{ mg} \\
 &\underline{11\,904} \\
 \text{i.e. } &58,44 = 203,7 \text{ me}
 \end{aligned}$$

$$\begin{aligned}
 \text{End : } 11,77 \times 212 \text{ mg/l} &= 2\,495,24 \text{ mg} \\
 &\underline{2\,495,24} \\
 \text{i.e. } &58,44 = 42,7
 \end{aligned}$$

$$\begin{aligned}
 \therefore \text{ me removed} &= 161 \text{ me} \\
 &= 0,161 \text{ ge}
 \end{aligned}$$

$$\begin{aligned}
 \text{Current efficiency (\%)} &= \frac{96\,500 \text{ C} \times 0,161 \text{ ge} \times 100}{\text{ge}} \\
 &= \frac{10 \text{ cp} \times 1660,5 \text{ C}}{96\,500 \text{ C}} \\
 &= 93,57\%
 \end{aligned}$$

Electrical energy consumption:

$$\begin{aligned}
 p &= V \times I \times h \text{ (across membranes only)} \\
 &= 5 \times \frac{27,675}{60} \\
 &= 2,306 \text{ wh} \\
 &= 0,002306 \text{ kwh}
 \end{aligned}$$

$$\begin{aligned}
 \text{Energy consumption/m}^3 &= \frac{0,00231}{0,012} \\
 &= 0,19219 \text{ kwh/m}^3 \text{ feed}
 \end{aligned}$$

$$\begin{aligned}
 \% \text{ water recovery} &= \frac{11,77 \times 100}{12} \\
 &= 98,08 \%
 \end{aligned}$$

$$\begin{aligned}
 \% \text{ Brine volume} &= \frac{0,23 \times 100}{12} \\
 &= 1,92 \%
 \end{aligned}$$

$$\begin{aligned}
 \text{Concentration factor} &= \frac{21\,981}{992} \\
 &= 22,16
 \end{aligned}$$

$$\begin{aligned}
 \text{Water yield} &= 0,01177 \text{ m}^3 \times 1\,440 \text{ min} \\
 &\quad 0,169 \text{ m}^2 \times 270 \text{ min} \quad \text{d} \\
 &= 0,369 \text{ m}^3/\text{m}^2\text{-d}
 \end{aligned}$$

(Note: membrane area is 169 cm², but there are 10 membrane pairs, therefore total membrane area is 0,169 m²).

Table 2: Electro dialysis concentration/desalination results of an approximately 3 000 mg/ℓ HCl solution with Selemium AAV and CHV membranes at 2 V/cp (16 V/8 cp).

Time min	Current amp	Vo V	Cf M	Cf mg/ℓ	Cb M	Cb mg/ℓ	V-Vo 10 cp	CD mA/cm ²	Rcp	Specific resistance ohm-cm
0	3,48	1,08	0,091	3318			1,892	20,6	91,9	28
15	3,56	1,65	0,076	2771	1,7	61982	1,835	21,1	87,1	32
30	3,46	1,38	0,067	2463	2,1	76566	1,862	20,5	91,0	35
45	3,18	1,39	0,061	2224	2,2	80212	1,861	18,8	98,9	40
60	2,83	1,32	0,055	2005	2,25	82035	1,868	16,8	112	44
75	2,49	1,21	0,047	1714	2,25	82035	1,879	14,7	128	49
90	2,19	1,20	0,045	1641	2,1	76566	1,880	13,0	145	53
105	1,92	1,23	0,036	1313	2,0	72920	1,877	11,4	165	63
120	1,68	1,27	0,034	1240	1,95	71097	1,874	9,9	189	69
135	1,49	1,28	0,029	1057	1,85	67451	1,872	8,8	212	80
150	1,32	1,32	0,026	948	1,75	63805	1,868	7,8	239	85
165	1,16	1,42	0,022	802	1,65	60159	1,858	6,9	271	99
180	1,03	1,62	0,019	692	1,60	58336	1,838	6,1	302	111
195	0,93	1,86	0,018	656	1,50	54690	1,814	5,5	330	126
210	0,84	1,73	0,017	602	1,40	51044	1,827	5,0	368	139
225	0,75	1,83	0,014	510	1,35	49221	1,812	4,4	409	156
240	0,67	2,13	0,013	474	1,30	47398	1,787	4,0	451	174
255	0,61	2,13	0,012	419	1,2	43752	1,787	3,6	495	193

Linear flow velocity : 0,87 cm/s

Feed volume (beginning) : 12 ℓ

Product Volume (end) : 11,32 ℓ

Brine Volume (end) : 680 ml

Brine molarity : 1, 9 M

$$\begin{aligned}
 \int f(x) dx &= 15/2 (I_1 + 2 (I_2 + I_3 + \dots + I_{n-1}) + I_n) \\
 &= 7,5 (63,09) \\
 &= 473,175 \text{ amp}\cdot\text{min} \\
 &= 28390, 5 \text{ amp}\cdot\text{s (coulombs)}
 \end{aligned}$$



Acid equivalents removed:

$$\begin{aligned} \text{Beginning} & : 12 \text{ l} \times 3318 \text{ mg/l} = 39816 \text{ mg} \\ \text{i.e.} & \quad \quad \quad \frac{39816}{36,46} = 1092,05 \text{ me} \end{aligned}$$

$$\begin{aligned} \text{End} & : 11,32 \text{ l} \times 419 \text{ mg/l} = 4743,08 \text{ mg} \\ \text{i.e.} & \quad \quad \quad \frac{4743,08}{36,46} = 130,09 \text{ me} \end{aligned}$$

$$\begin{aligned} \therefore \text{me removed} & = 1092,05 - 130,09 \\ & = 961,96 \text{ me} \\ & = 0,96196 \text{ ge} \end{aligned}$$

$$\begin{aligned} \text{Current efficiency (\%)} & = \frac{96500 \text{ C} \times 0,96196 \text{ ge} \times 100}{\text{ge}} \\ & \quad \quad \quad \frac{10 \text{ cp} \times 28390,5 \text{ C}}{32,7} \\ & = 32,7 \% \end{aligned}$$

$$\begin{aligned} \text{Energy Consumption (P)} & = V \times I \times h \\ & = \frac{20 \times 473,175}{60} \\ & = 157,725 \text{ Wh} \\ & = 0,157725 \text{ kwh} \end{aligned}$$

$$\begin{aligned} \therefore \text{Energy Consumption/m}^3 & = \frac{0,157725}{0,012} \\ & = 13,15 \text{ kwh/m}^3 \text{ feed} \end{aligned}$$

$$\begin{aligned} \% \text{ Water recovery} & = \frac{11,32 \times 100}{12} \\ & = 94,3\% \end{aligned}$$

$$\begin{aligned} \% \text{ Brine volume} & = \frac{0,68 \times 100}{12} \\ & = 5,7 \% \end{aligned}$$



$$\begin{aligned}\text{Concentration factor} &= \frac{69274}{3318} \\ &= 20,9\end{aligned}$$

$$\begin{aligned}\text{Water yield} &= \frac{0,01132 \times 1440}{0,169 \times 255} \\ &= 0,38 \text{ m}^3/\text{m}^2\text{-d}\end{aligned}$$



APPENDIX D

PUBLICATIONS BY J J SCHOEMAN

(a) Full length articles in specialist journals

Author(s)	Title	Year	Detailed reference
Schoeman, J J	Ontsouting van brakwaters en konsentring van industriële uitvloeiels deur middel van elektrodialise	1983	Die Suid-Afrikaanse Tydskrif vir Natuurwetenskap en Tegnologie, <u>2</u> (4)
Schoeman, J J and Botha, G R	An evaluation of the activated alumina process for fluoride removal for drinking water and some factors influencing its performance	1985	Water S.A. <u>11</u> (1)
Schoeman, J J	The status of electro dialysis technology for brackish and industrial water treatment	1985	Water S.A. <u>11</u> (2)
Schoeman, J J	An evaluation of a South African clinoptilolite for ammonia-nitrogen removal from an underground mine water	1986	Water S.A. <u>12</u> (2)
Schoeman, J J	Rapid determination of the fouling of Electro dialysis membranes by industrial effluents	1987	Water S.A. <u>12</u> (12)
Schoeman, J J	An investigation of the performance of two newly installed defluoridation plants in South Africa and some factors affecting their performance	1987	Water Sci. Tech. <u>19</u>
Schoeman, J J	The effect of particle size and interfering ions on fluoride removal by activated alumina	1987	Water S.A. <u>13</u> (4)
Schoeman, J J Buys, I J M Schutte, I B and McLeod, H	Pilot investigation on the treatment of fertilizer manufacturing process effluent using lime and electro dialysis reversal	1988	Desalination, <u>70</u>
Schoeman, J J and Van Staden, J F	Evaluation of sealed-cell electro dialysis for industrial effluent treatment	1991	Water S.A. <u>17</u> (4)
Schoeman, J J, Van Staden, J F, Saayman, H M and Vorster, W A	Evaluation of reverse osmosis for electroplating effluent treatment	1992	Submitted for publication to Water Sci. Tech.
Schoeman, J J and Van Staden, J F	Electro-osmotic pumping of salts, acids and bases in a conventional electro dialysis stack	1992	Submitted for publication to Water S.A.